Targeting the Unfolded Protein Response as a Novel Therapeutic Approach in Haematological Malignancies

Linsey Ida Madadi, MPharm, MRPharmS, MSc
Cancer Pharmacology Group
Centre for Haemato-Oncology
Barts Cancer Institute
Barts and the London School of Medicine and Dentistry
Queen Mary University of London

Supervised by
Dr Simon Joel
Dr Heather Oakervee

Thesis submitted for the degree of Doctor of Philosophy of the University of London

April 2012

DECLARATION

I undertake that the material contained in this thesis is my own work, and any material from others has been duly acknowledged in the thesis text.

Signed: _____ **Date: _____**

ACKNOWLEDGEMENTS

Thank you to all those in the Cancer Pharmacology Lab for your support, particularly my supervisor Dr Simon Joel.

Special thanks to Dr Hashem Madadi, for his enduring support and encouragement in all my academic pursuits.

This work is dedicated to the memory of Yalda Madadi.

ABSTRACT

The unfolded protein response (UPR) is a complex signalling pathway activated in response to endoplasmic reticulum stress. In recent years, the UPR has been implicated in cancer and chemosensitivity, particularly in solid tumours. This thesis investigated the potential value of targeting the UPR as a novel therapeutic approach in haematological malignancies using a panel of cell lines representing AML, lymphoma and myeloma. The UPR was constitutively active in these haematological cancer cell lines, with differential activation of key UPR proteins both in the panel and between the panel, peripheral blood mononuclear cells and the colorectal cancer cell line HT-29. A number of strategies were used to modulate the UPR and study chemosensitivity. Minimally toxic concentrations of the ER stress inducer thapsigargin protected cells from cytotoxic agents, with a reduction in antiproliferative drug effect. The activity of the novel small molecule versipelostatin, reported to downregulate the ER molecular chaperones GRP78 and GRP94, was also investigated, with the downregulation previously reported in solid tumour cell lines (Park *et al*. 2004) confirmed in HT-29 cells, but not observed in the haematological cell lines studied (although versipelostatin was an effective cytotoxic agent at low micromolar concentration). Combination experiments with the chemical chaperone 4-phenylbutyric acid (PBA) resulted in a small increase in apoptosis when PBA was combined with ER stress inducers. However, PBA also showed HDAC inhibitory activity at the concentrations used. Finally, siRNA mediated silencing of GRP78 and GRP94 in THP1 (AML) and U266 (myeloma) cells resulted in a decrease in the targeted protein, but showed only minimal effects on chemosensitivity. In conclusion, the UPR is activated in these haematological cancer cell lines and plays a complex role in chemosensitivity. In contrast to previous reports in solid tumour cells, modulating the UPR in these haematological malignancies had only a modest effect on chemosensitivity.

TABLE OF CONTENTS

LIST OF FIGURES

LIST OF TABLES

LIST OF ABBREVIATIONS

Abbreviation	
17-AAG	17-allylamino, 17-demethoxygeldanamycin; tanespimycin
2-DG	2-deoxyglucose
4-HC	4-hydroperoxycyclophosphamide
AML	Acute myeloid leukaemia
ASK1	Apoptosis signal-regulating kinase 1
ATF4	Activating transcription factor 4
ATF6	Activating transcription factor 6
BAK	BCL-2 antagonist/killer
BAX	BCL-2-associated X protein
BCL-2	B-cell leukaemia/lymphoma 2
BCL-X_L	Basal cell lymphoma-extra large
BiP	Immunoglobulin heavy-chain binding protein (see GRP78)
Bort	Bortezomib
bZIP	Basic leucine zipper
CHOP	C/EPB homologous protein (see GADD153)
CLL	Chronic lymphocytic leukaemia
COX-2	Cyclooxygenase-2
DLBCL	Diffuse large B-cell lymphoma
DNA	Deoxyribonucleic acid
Dox	Doxorubicin
eIF2α	Eukaryotic translation initiation factor 2 alpha
EC	Effective concentration
ER	Endoplasmic reticulum
ERAD	Endoplasmic reticulum associated degradation
ERK	Extracellular signal-regulated kinase

GADD153	Growth arrest- and DNA damage-inducible gene 153 (see CHOP)
GRP78	Glucose related protein 78 (see BiP)
GRP94	Glucose related protein 94
HDAC	Histone deacetylase
HIF	Hypoxia-inducible factor
HIV	Human immunodeficiency virus
HSP	Heat shock protein
IGF-1	Insulin-like growth factor-1
IL	Interleukin
IRE1	Inositol-requiring enzyme 1
JNK	Jun N-terminal kinase
MAPK	Mitogen-activated protein kinase
MEK	Mitogen-activated protein kinase kinase
MM	Multiple myeloma
mRNA	Messenger ribonucleic acid
MTOC	Microtubule organising centre
NHL	Non-Hodgkin lymphoma
NSAID	Non-steroidal anti-inflammatory drug
PBA	4-phenylbutyric acid (see 4-PBA)
PCR	Polymerase chain reaction
PDI	Protein disulphide isomerase
PEK	Pancreatic eukaryotic initiation factor 2 alpha-subunit kinase (see PERK)
PERK	PKR-like endoplasmic reticulum kinase (see PEK)
PKR	RNA-dependent protein kinase
RNA	Ribonucleic acid
RNAi	RNA interference
RT-PCR	Reverse transcription polymerase chain reaction

SAHA	Suberoylanilide hydroxamic acid; Vorinostat
siRNA	Small interfering RNA
TG	Thapsigargin
TM	Tunicamycin
TNF	Tumour necrosis factor
TRAF2	TNF receptor-associated factor 2
UPR	Unfolded protein response
VEGF	Vascular endothelial growth factor
VST	Versipelostatin
XBP1	X-box binding protein 1
XBP1s	Spliced X-box binding protein 1
XBP1u	Unspliced X-box binding protein 1

1. Introduction

1.1 Haematological malignancies

1.1.1 – Classification of Haematological Malignancies

Cancer or malignancy are terms used to describe many different diseases characterised by uncontrolled growth. Similarly, the term haematological malignancies refers to a number of histologically and prognostically distinct types of cancer of the haematopoeitic system. There are a number of classification systems that have been developed to describe the various haematological malignancies. The main distinction between haematological cancer subtypes is based on whether the tumour is of myeloid or lymphoid origin. The myeloid malignancies are commonly classified using the French American British (FAB) classification (Bennett *et al.*, 1976b), whilst lymphoid malignancies are commonly classified using the Revised European American Lymphoma (REAL) classification (Harris *et al.*, 1994). More recently, the World Health Organisation has published the World Health Organization Classification of Neoplastic Diseases of the Hematopoietic and Lymphoid Tissues (Harris *et al.*, 1999). The WHO classification is based on both the FAB and REAL classifications with some significant differences, such as the incorporation of cytogenetic features in the classification of myeloid disorders.

1.1.2 – Acute Myeloid Leukaemia

The leukaemias are relatively rare, accounting for two percent of all cancers in the UK. In 2007 there were just over 7000 new cases of leukaemia in the UK, with a five year survival of around 40 percent. Acute myeloid leukemia (AML) is the most common acute leukaemia in adults and incidence increases with age (CancerResearchUK, 2010a). AML,

also known as acute myelogenous leukemia, is characterized by the rapid proliferation of myeloblasts (immature precursor myeloid cells) which accumulate in the bone marrow and interfere with the production of normal blood cells (Abeloff, 2004).

The FAB classification system divides AML into 8 subtypes, designated M0 to M7. based on morphologic and genetic factors (Bennett *et al.*, 1976). The more recent WHO classification of AML aims to provide more clinically useful prognostic information than the FAB criteria (Harris *et al.*, 1999). The four subtypes of AML in the WHO classification system are:

1. AML with characteristic genetic abnormalities
2. AML with multilineage dysplasia
3. AML and myelodysplastic syndromes (MDS), therapy-related
4. AML not otherwise categorized

AML is typically detected as an abnormal result on a full blood count, which may show an increased level of abnormal white blood cells or the presence of leukaemic blasts. Bone marrow aspiration and biopsy are usually necessary for a definitive diagnosis. If AML is left untreated most patients will die within a few months of diagnosis. However, the disease is potentially curable, although the proportion of patients cured with current treatments is small. Treatment consists of induction chemotherapy (aiming to induce disease remission) followed by consolidation chemotherapy (aiming to eliminate any minimal residual disease and maintain remission) (Abeloff, 2004).

1.1.3 – Multiple Myeloma

Multiple myeloma (MM) is a malignant disease of plasma cells, characterised by the production of abnormal intact monoclonal immunoglobulin (known as paraprotein or

monoclonal (M) protein) or monoclonal free light chains (known as Bence Jones Protein). The disease can have wide reaching effects, manifesting as bone lesions, fractures, myelosuppression, renal failure and other symptoms. MM often develops from an asymptomatic premalignant stage of clonal plasma cell proliferation called monoclonal gammopathy of undetermined significance (MGUS) (Abeloff, 2004). Myeloma accounts for approximately ten percent of all malignancies of the haematopoeitic system (Kyle and Rajkumar, 2008). In the UK, MM is a relatively rare disease accounting for one percent of all cancers. Incidence of the disease increases with advancing age and is extremely rare in people below the age of 30. In 2007, just over 4000 new cases of multiple myeloma were registered and 5 year survival is currently less than 30 percent (CancerResearchUK, 2010b).

The Durie-Salmon staging system for myeloma was introduced in 1975 (Durie and Salmon, 1975), however this system has now been superseded by the International Staging System (ISS) for MM published by the International Myeloma Working Group in 2005. The ISS assigns three stages of disease: stage I (serum β_2-microglobulin <3.5 mg/L, serum albumin ≥3.5 g/dL), stage II (disease that is neither stage I or stage III), and stage III (serum β_2-microglobulin ≥5.5 mg/L) (Greipp *et al.*, 2005).

The first step in treatment of patients with symptomatic disease is combination chemotherapy. The choice of regimen is primarily dependent on whether or not the patient is a candidate for haematopoeitic stem cell transplantation (Kyle and Rajkumar, 2008).

1.1.4 – Non-Hodgkin Lymphoma

Non-Hodgkin lymphoma (NHL), as the name suggests, is the name used to describe the many (and varied) malignant disorders of the lymphoid system other than Hodgkin lymphoma. These diseases are often grouped in terms of whether they are aggressive (high

grade) tumours or less aggressive (low grade) tumours. NHL is the fifth most common cancer in the UK, with over 10000 new cases in 2007. Current five year survival rates are over 50 percent (CancerResearchUK, 2010c).

As mentioned previously, lymphoid malignancies are classified according to the WHO Classification of Neoplastic Diseases of the Hematopoietic and Lymphoid Tissues, which followed on from the earlier REAL classification system. In the WHO classification system diffuse large B-cell lymphoma (DLBCL) is a subtype of B-cell neoplasms (Harris *et al.*, 1999). DLBCL is the most common lymphoid malignancy in adults and accounts for over 30 percent of all NHL cases (The Non-Hodgkin's Lymphoma Classification Project 1997). Other types of B-cell NHL include follicular lymphoma (the most prevalent indolent lymphoma, which transforms to DLBCL in 20 to 30 percent of patients, depending on age), Burkitt's lymphoma (highly aggressive; c-myc translocation associated; common lymphoma in HIV patients), and mantle cell lymphoma (rare, aggressive tumour; characterised by translocation t(11:14); very poor prognosis) (Canellos *et al.*, 2006).

1.2. Endoplasmic Reticulum Stress

1.2.1 – The Endoplasmic Reticulum

The endoplasmic reticulum (ER) was first described by Porter and colleagues in 1945, who used electron microscopy in order to visualise cellular structures that had not previously been seen (Porter *et al*. 1945). The ER is an organelle consisting of an interconnected network of tubules, vesicles, and sacs that is present in all eukaryotic cells. This interconnected network forms a continuous phospholipid ER membrane around the cisternal space (known as the ER lumen) and functions to separate the ER lumen from the cytosol. The ER has a number of functions, which include production of proteins and lipids,

protein folding and protein secretion. The ER is the first compartment in the secretory pathway, to which proteins translocate for correct folding before delivery to the appropriate sites within the cell. Proper functioning of the ER is essential for most cellular activities and survival.

There are three types of endoplasmic reticulum: rough ER, smooth ER and sarcoplasmic reticulm (SR). The rough ER is covered with membrane bound ribosomes, which are the sites of protein synthesis. Unlike rough ER, smooth ER does not have bound ribosomes. Smooth ER contains exit sites, enabling transport vesicles carrying newly synthesised proteins and lipids to travel out of the ER and transfer to the Golgi apparatus. Sarcoplasmic reticulum is a specialised smooth ER responsible for pumping calcium into the ER lumen from the cytosol via a calcium-ATPase. Both the amount of ER and the particular type of ER within an individual cell is determined by the specific cell type and functions to enable that cell type to carry out its specialised role and meet cellular demands. For example, in comparison to other cell types, muscle cells contain an abundant sarcoplasmic reticulum which is necessary for the release and reuptake of calcium during the process of muscle contraction and relaxation (Alberts, 2002). Another example of differences in ER between cell types is seen in plasma cells, which contain more ER than other cell types in order to carry out their functions as secretory cells (Yoshida, 2009).

1.2.2 – Protein Folding in the Endoplasmic Reticulum

The main stages involved in the production of proteins are transcription, translation and maturation. Many proteins in the ER lumen are in transit to other sites, such as the golgi or mitochondria. ER resident proteins contain an ER retention signal of 4 amino acids at their carboxyl terminus (Lys-Asp-Glu-Leu (KDEL)) that distinguishes them from proteins bound elsewhere and prevents their secretion (Munro and Pelham, 1987). Selected proteins

from the cytosol are captured by the ER as they are being synthesised. Secretory proteins (water soluble) translocate across the ER membrane and undergo folding in the ER lumen, whereas transmembrane proteins only partially pass through the ER membrane and remain attached to ribosomes on the cytosolic ER surface. Folding of proteins can occur even as the protein is still being synthesised, i.e. it is a co-translational process (Alberts, 2002). Protein folding in the ER is shown in figure 1.1.

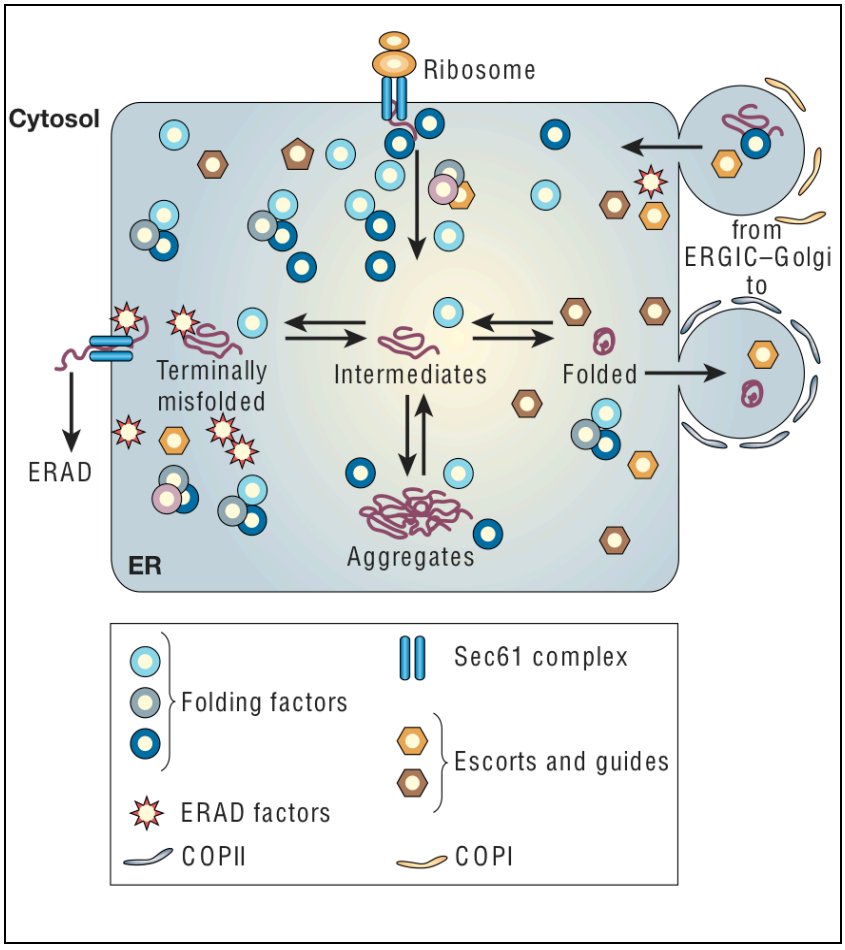

Figure 1.1. Protein folding in the ER.
Proteins enter the ER from the ribosome through the Sec61 complex, where ER chaperones and folding enymes (folding factors) facilitate correct folding. The ER also contains escorts and guides that mediate transport downstream in the secretory pathway. COPI and COPII are coat protein complexes involved in protein transport.
Terminally misfolded proteins are targeted for endoplasmic reticulum associated degradation (ERAD), with ERAD factors mediating transport to the proteasome for degradation.
Reproduced from Sitia and Braakman (2003).

Translocation to the ER membrane is initiated by the binding of an ER signal sequence on the protein to a signal recognition particle (SRP) and a signal recognition particle receptor in the ER membrane. The SRP and its receptor have been shown to be present in all cells and evolutionarily conserved (Keenan *et al.*, 2001). One end of the SRP binds to the ER signal sequence on the polypeptide chain as it emerges from the ribosome during synthesis, whilst the other end blocks the elongation factor binding site at the interface between the large and small ribosomal subunits. It is thought that the resulting translational pause allows time for the ribosome to bind to the ER membrane ensuring that the protein is not released into the cytosol. The SRP-ribosome complex then binds to the SRP receptor and reaches a protein translocator in the ER membrane. The SRP and SRP receptor are released and the polypeptide chain transferred across the ER membrane through an aqueous pore in the translocator. At the core of the translocator is the Sec61 complex, which is built from three units evolutionarily conserved from bacteria to eucaryotic cells. The translocation of proteins across the ER membrane is usually co-translational, however post-translational transport into the ER can also occur. Once the protein has been released into the cytosol it binds to chaperone proteins (to prevent folding) and accessory proteins (associated with the Sec61 complex) that span the ER membrane and direct the ER chaperone protein GRP78 on to the polypeptide chain as it emerges from the pore into the ER lumen (Alberts, 2002, Keenan *et al.*, 2001).

During maturation, the unfolded protein undergoes conformational changes that enable it to achieve its most energetically favourable state (Ellgaard and Helenius, 2003). This folding of the protein is essential to enable the protein to reach its target site within the cell. Studies on smaller proteins have shown that the interaction of a small number of amino acid residues on the polypeptide chain results in the formation of a folding nucleus and that the lowest energy overall structure then forms around this by means of trial and error (Fersht, 2000). In mammalian cells proteins are folded in the ER or the cytosol. There are a number of differences between protein folding in the ER and the cytosol, for example, the ER is a

more oxidising environment than the cytosol and is also the main area of calcium storage (Schroder and Kaufman, 2005b).

The ER also contains molecular chaperones and enzymes that function to aid correct protein folding. There are several families of molecular chaperones and different family members function in different organelles, for example heat shock protein (HSP) 70 family chaperones bind to a string of hydrophobic amino acids before the protein has left the ribosome, whereas the cytosolic HSP60 family chaperones isolate proteins in a barrel-like structure that provides a favourable environment for correct folding (Alberts, 2002). ER resident molecular chaperones include the HSP70 (e.g. GRP78) and HSP90 (e.g. GRP94) families, the lectins calnexin and calreticulin, and the HSP40 family of co-chaperones. HSPs have an affinity for and bind to exposed hydrophobic patches on unfolded proteins that would ordinarily be buried in the interior of the structure, using hydrolysis of ATP to provide the energy required to carry out their chaperone function. HSPs often require many cycles of ATP hydrolysis in order to fold a single polypeptide chain correctly (Ellgaard and Helenius, 2003, Alberts, 2002, Ma and Hendershot, 2004a). Folding enzymes include the thiol-disulphide oxidoreductase family, one example of which is the enzyme protein disulphide isomerase (PDI). PDI catalyses the formation of disulphide bonds in the ER via oxidation of free sulfhydryl (SH) groups on cysteines; this reaction is very rarely found in the cytosol due to its reducing environment (Ellgaard and Helenius, 2003, Braakman *et al.*, 1992).

Nascent polypeptide chains are subject to numerous post translational modifications in the ER, such as N-linked glycosylation, disulphide-bond formation, signal sequence cleavage and addition of glycosylphosphatidylinositol anchors. These modifications are essential for correct protein folding and only occur in the ER (Ellgaard and Helenius, 2003). Two of the most important translational modifications in the ER are N-linked glycosylation and disulphide bond formation (catalysed by the enzyme PDI) (Schroder and Kaufman, 2005b). Both of these processes act to enable unfolded proteins to achieve their final folded

conformation. Modifications such as these continue to take place in the ER until the final folded state of the protein has been reached, at which point the protein is marked for export from the ER.

1.2.3 – Endoplasmic Reticulum Associated Degradation

A large number of proteins fail to achieve their desired three-dimensional conformation due to the many intermediate stages involved in folding and the resulting opportunities for errors to occur. Errors in the folding process may also occur for other reasons, such as genetic mutations and errors during transcription or translation. It has been reported that as many as a third of all newly synthesised proteins are destroyed during, or within minutes of, their synthesis (Schubert *et al.*, 2000). The folding machinery can also be affected by the physiological conditions within the cell, for example, temperature, redox state or exposure to external toxins (Vembar and Brodsky, 2008). In addition to affecting the production of new proteins, these cellular conditions can also cause mature proteins to become defective (Hirsch *et al.*, 2009). The resulting aberrant proteins must be dealt with in order to prevent build up of unfolded or misfolded proteins that may overwhelm the ER protein folding machinery and impair normal cellular function. It is therefore imperative that the ER has a means of monitoring protein folding and dealing with any problems that may arise in the folding machinery. This system is known as ER quality control and is mediated by the ER molecular chaperones. This quality control mechanism detects unfolded or misfolded proteins and will either attempt to further facilitate correct folding or will target the protein for a process known as ER associated degradation (ERAD) (McCracken and Brodsky, 1996).

Work by the Klausner group in the late 1980s led to the discovery of the ERAD pathway (Lippincott-Schwartz *et al.*, 1988). Later work by Sommer and Jentsch linked

ERAD with the ubiquitin-proteasome pathway by showing that targeted ER proteins are degraded in the cytoplasm by the 26S proteasome (Sommer and Jentsch, 1993). As illustrated in figure 1.2, there are five steps in the ERAD pathway: recognition of damaged or misfolded proteins by molecular chaperones such as PDI and HSP70 family members, targeting, retrotranslocation, ubiquitylation, and proteasomal degradation (Vembar and Brodsky, 2008). In addition to targeting defective proteins, ERAD is also exploited by some pathogenic viruses and bacterial toxins in order to infect host cells (Meusser *et al.*, 2005, Lord *et al.*, 2005). It has also been discovered that turnover of ER resident enzymes utilises ERAD, as illustrated by regulation of the sterol synthesis pathway. When sterol production needs to be halted, the rate-limiting enzyme HMG-CoA reductase is targeted for regulated degradation via the ERAD pathway (Hampton, 2002).

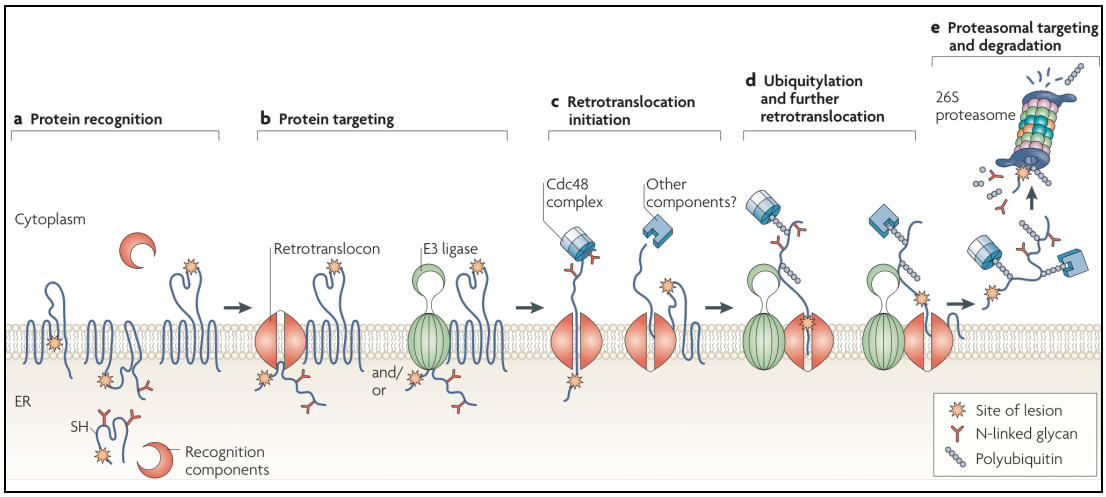

Figure 1.2. The stages involved in endoplasmic reticulum associated degradation (ERAD). Reproduced from Vembar and Brodsky (2008).

The exact mechanism of a misfolded protein being targeted as a substrate for ERAD is not known (although in recent years more details of this targeting mechanism have been elucidated for a very small number of individual substrates). ER molecular chaperones recognise and bind to hydrophobic polypeptide motifs on misfolded proteins that would normally be buried within the folded protein structure and therefore not available for

chemical interaction. One theory suggests that prolonged binding of a molecular chaperone to an ERAD substrate leads to recruitment of an E3 ubiquitin ligase and polyubiquitination of the substrate (Denic *et al.*, 2006).

In order to further understand the process of substrate recognition and targeting for ERAD, it is necessary to look in more detail at the way unfolded/misfolded proteins are processed in the ER and the role of N-linked glycosylation. Glycosylation is one of the most important post translational modifications of proteins that occurs in the ER. Glycosylation is the covalent addition of sugars to proteins and around half of all eucaryotic proteins are glycosylated. Glycosylation is one of the major biosynthetic functions of the ER and most proteins synthesised in the ER are glycosylated, compared to very few proteins in the cytosol. A preformed precursor oligosaccharide ($glucose_3$-$mannose_9$-N-$acetylglucosamine_2$) is transferred to the side chain NH_2 group of an asparagine amino acid of the protein in a process termed N-linked glycosylation. The oligosaccharide transfer is catalysed by a membrane bound enzyme complex (an oligosaccharide transferase) which has its active site exposed on the luminal side of the ER membrane (this explains why cytosolic proteins are not glycosylated in this manner). The original precursor oligosaccharide is later modified to form the mature glycoprotein. Cycles of glucose trimming and glucose addition take place in the ER until the final folded state of the protein has been reached, at which point the protein is marked for exit from the ER. The pattern of this N-linked glycosylation indicates the extent of protein folding and provides an indication of the amount of time a protein has been in the ER. Glucose trimming by ER glucosidases I and II labels the protein as actively being folded and allows association of the chaperones calnexin and calreticulin to aid folding. The folding process continues with further modifications, and where necessary glucose addition by UDP-glucose:glycoprotein glucosyl transferase (UGGT) allows re-association of the protein with calnexin and calreticulin thereby facilitating further attempts at correct folding. If correct protein conformation cannot be reached within a given time frame, ER mannosidase I and the mannosidase-like proteins EDEM1, EDEM2 and EDEM3

initiate mannose trimming and subsequent ERAD (Vembar and Brodsky, 2008, Alberts, 2002, Hirsch *et al.*, 2009, Buchberger *et al.*, 2010, Helenius, 1994). However, it should be noted that the exact mechanism of de-mannosylation and the initiation of ERAD in mammalian cells is still unclear, although a number of theories have been proposed and are currently being investigated (Aebi *et al.*, 2010).

The process discussed here relates to ERAD initiation for misfolded glycosylated proteins, although it should be mentioned that not all ER proteins are glycosylated. Therefore, it is logical to assume that a concurrent system exists to recognise and target misfolded non-glycosylated proteins for degradation. It is thought that in this simpler system ERAD is initiated by binding and association of molecular chaperones and folding catalysts. To date, ERAD initiation for non-glycosylated proteins has not received much attention, as opposed to the extensive study of glycosylated protein systems (Buchberger *et al.*, 2010).

After an incorrectly folded protein has been recognised and targeted by molecular chaperones in the ER, it is exported back into the cytosol (retrotranslocation or dislocation) in a similar way to other modes of translocation, although the exact mechanism is unknown. Once in the cytosol the oligosaccharide chain is removed from glycoproteins by an N-glycanase. The protein is directed to membrane bound ligases on the cytosolic side of the ER membrane. The protein is then ubiquitinated by an E3 ubiquitin ligase (a catalytic RING-finger protein). A ligase complex then forms, consisting of an E3 ligase plus ubiquitin-conjugating enzymes (E2) and other co-factors. The polyubiquitinated protein is then transported to the 26S proteasome for degradation. Prior to proteasomal degradation, the ubiquitin chain is removed by deubiquitinating enzymes and the free ubiquitin released for reuse (Vembar and Brodsky, 2008, Hirsch *et al.*, 2009).

1.2.4 – The Endoplasmic Reticulum Stress Response

Correct folding of proteins is essential to maintain normal cellular function. In the cytosol, accumulation of unfolded or misfolded proteins activates the heat shock response, leading to transcription of cytosolic chaperones in an attempt to further aid protein folding (Alberts, 2002). A similar process occurs in the ER. Various physiological stresses alter the ability of the ER to function normally and result in the accumulation of misfolded or unfolded proteins - a situation referred to as ER stress. The term ER stress describes an imbalance between the demand on ER function and the ER capacity of the cell (Ron, 2002, Schroder and Kaufman, 2005b). There are many factors that can provoke ER stress (Schroder and Kaufman, 2005a).

Redox disturbances due to hypoxia, oxidising agents or reducing agents can interfere with the process of disulphide bond formation in the ER lumen leading to misfolded protein accumulation. Similarly, conditions that interfere with N-linked glycosylation lead to ER stress, such as glucose deprivation. Alterations in ER calcium homeostasis also cause ER stress and many of the ER resident molecular chaperones are calcium dependent (Schroder and Kaufman, 2005a). These physiological stressors result in accumulation of unfolded or misfolded proteins thereby provoking an ER stress response and activation of a complex signalling pathway known as the unfolded protein response (Wu and Kaufman, 2006).

1.2.5 Pharmacological Induction of Endoplasmic Reticulum Stress

In addition to normal cellular stresses, a number of pharmacological agents have been discovered to induce ER stress and trigger the ER stress response, thereby activating the unfolded protein response. Some examples of ER stress inducing agents are discussed below.

Tunicamycin is a mixture of homologous antibiotics produced from the bacteria *Streptomyces iysosuperficus*. Tunicamycin inhibits N-linked glycosylation by inhibiting the N-acetylglucosamine transferases, thereby preventing glycosylation of newly synthesised proteins. This leads to accumulation of proteins in the ER and ER stress (Heifetz *et al.*, 1979). Tunicamycin has been shown to cause apoptosis in both plant and mammalian cells by inducing ER stress (Crosti *et al.*, 2001, Fujita *et al.*, 2002). It has been reported in the literature that induction of ER stress with tunicamycin can increase the activity of cytotoxic drugs in multidrug resistant cancer cell lines (Hiss *et al.*, 1996, Hiss *et al.*, 2007). However, clinical relevance of these studies are limited by the high tunicamycin concentrations used, which would be expected to exhibit significant toxicity even as single agents. Also, these studies only investigated the effect of simultaneous exposure to the two drugs. Treatment with tunicamycin has been shown to enhance tumour necrosis factor-related apoptosis-inducing ligand (TRAIL)-induced apoptosis of endometrial cells (Hasegawa *et al.*, 2008) and to sensitise melanoma cells to TRAIL-induced apoptosis in vitro (Jiang *et al.*, 2007a). More recently, one study reported that treatment with tunicamycin induced resistance to the cytotoxic agents camptothecin and etoposide in hepatocellular carcinoma cells. The authors suggested that this decreased cytotoxicity was due to both GRP78 induction and an independent arrest of the cell cycle in the G1 phase (Hsu *et al.*, 2009). Interestingly, these findings taken together suggest that the role of tunicamycin mediated ER stress may be more complex than initially thought.

Thapsigargin is a sesquiterpene lactone extracted from the plant, *Thapsia garganica*. It is an effective inhibitor of sarcoplasmic endoplasmic reticulum calcium ATPases (known as SERCA pumps). This inhibition leads to release of intracellular calcium, resulting in ER stress (Kijima *et al.*, 1991). Inhibition of the sarcoplasmic endoplasmic reticulum calcium ATPase by thapsigargin has been shown to occur at concentrations as low as 10^{-10}M (Sagara and Inesi, 1991). Along with tunicamycin, thapsigargin is commonly used by researchers to induce ER stress in order to study such stress and the resultant unfolded protein response.

Like tunicamycin, thapsigargin has been shown to sensitise melanoma cells to TRAIL-induced apoptosis by inducing ER stress and the unfolded protein response (Chen *et al.*, 2007). It has been reported that multidrug resistant cells deficient in the proapoptotic Bcl-2 family members Bax and Bak are sensitive to ER stress mediated cell death (caspase independent) following treatment with thapsigargin (Janssen *et al.*, 2009). Another interesting area of research is the development of prodrugs of thapsigargin to inhibit SERCA pumps as a novel targeted treatment strategy in prostate cancer. The thapsigargin prodrug (thapsigargin coupled to a targeting peptide) is activated by the proteolytic enzyme prostate specific antigen (PSA) and has been shown to be selectively toxic to prostate cancer cells in preclinical studies *in vitro* and *in vivo* (Christensen *et al.*, 2009, Denmeade and Isaacs, 2005). If this approach proves succesful it would provide a solution to the important issue of thapsigargin cytotoxicity to normal cells and it may eventually be possible to apply this targeted strategy to other tumour types.

Heat shock protein 90 (HSP90) inhibitors are a novel class of compound currently in development, with several compounds now in clinical trials. These agents are being investigated for their anticancer activity (Neckers and Neckers, 2002). HSP90 is a molecular chaperone involved in protein stabilisation, preventing protein aggregation, and in the trafficking and activation of many client proteins (Hartl and Hayer-Hartl, 2002). In recent years there has been considerable focus on HSP90 inhibition as a novel treatment approach in cancer therapy. HSP90 chaperones a number of oncoproteins that are degraded when HSP90 is inhibited (Goetz *et al.*, 2003, Neckers, 2002). Although early trials of HSP90 inhibitors were hampered by a number of stability and toxicity issues, progress is being made, with new formulations and compounds now in clinical trials (Trepel *et al.*, 2010). It is thought that HSP90 as a therapeutic target may exhibit selectivity for cancer cells. A high-affinity activated form of HSP90 that forms a complex with high ATPase activity has been identified in tumours, whereas HSP90 in normal cells is in an uncomplexed (inactive) form that has low ATPase activity (Kamal *et al.*, 2003). HSP90 inhibitors have been shown to be

effective in both *in vitro* and *in vivo* models of multiple myeloma (Mitsiades *et al.*, 2006). The HSP90 inhibitor 17-AAG (tanespimycin) has been shown to cause multiple myeloma cell death via a mechanism involving induction of ER stress and UPR pathways (Davenport *et al.*, 2007). It is now becoming clear this class of compound exert their anticancer activity in part by provoking ER stress and may also play a role in treatment of cancers not dependent on the main HSP90 client proteins (Mitsiades *et al.*, 2006). These findings provide a link between HSP90 inhibition, ER stress and the unfolded protein response in cancer therapeutics, highlighting the potential for future work in this area.

Proteasome inhibitors have emerged over the last few years as a novel class of anticancer agent. The first in class proteasome inhibitor bortezomib (Velcade®, Millenium Pharmaceuticals) is currently licensed in the UK for treatment of multiple myeloma, and is also licensed for the treatment of mantle cell lymphoma in the USA (Orlowski and Kuhn, 2008). Investigations are ongoing in other tumour types, including solid tumours, non-hodgkin lymphoma and leukaemia (Richardson *et al.*, 2006, Vink *et al.*, 2006). As discussed previously, the proteasome is involved in maintaining cellular homeostasis by degrading polyubiquitinated substrate proteins and is an integral component of the ERAD pathway (Sommer and Jentsch, 1993). Inhibition of the proteasome has wide reaching effects on a number of pathways involved in cancer. Mechanisms of action of this class of compound are thought to include inhibition of NF-κB signalling, induction of cell cycle arrest, and induction of apoptosis (Orlowski and Kuhn, 2008). It has also been discovered that proteasome inhibition induces ER stress and activates the unfolded protein response in multple myeloma cells, and that this may be related to their function as secretory cells (Obeng *et al.*, 2006). More recently, it has been shown that bortezomib preferentially targets hypoxic tumour cells causing cell death and that this effect is due to ER stress and activation of the unfolded protein response in the hypoxic tumour cells (Fels *et al.*, 2008). Following on from bortezomib, second generation proteasome inhibitors are now in clinical development (Dick and Fleming, 2010). Much like HSP90 inhibitors, ER stress induction

and unfolded protein response activation have now been implicated in the anticancer activity of proteasome inhibitors.

1.3 The Unfolded Protein Response

1.3.1 – Discovery of the Glucose Related Proteins

The glucose related proteins (GRPs) were first identified in the 1970s. The discovery of the proteins p78 and p94 by induction in RNA tumour virus transformed cells led to further work by Ira Pastan's group at the National Cancer Institute, NIH, Maryland. Pastan's group discovered that induction of the two proteins was not a direct result of cell transformation, but was in fact due to rapid depletion of glucose from the growth medium of transformed tumour cells. Due to their relation with glucose these proteins were designated glucose related proteins; GRP78 and GRP94 (Shiu *et al.*, 1977). In addition to the discovery by the Pastan group, GRP78 was independently identified by another research group. In 1983, a group led by Haas identified an ER protein that bound to free immunoglobulin heavy chains and inhibited secretion in the absence of light chains. They named the protein immunoglobulin heavy-chain binding protein, BiP (Haas and Wabl, 1983). In a 1986 paper in the journal *Cell*, Munro and Pellam established that GRP78 and BiP were the same protein (Munro and Pelham, 1986). It was later discovered that GRP78/BiP bound to various unfolded proteins in the ER and prevented their transport and secretion (Bole *et al.*, 1986). Further studies on the regulatory mechanisms resulting in increased transcription of genes encoding the GRPs were carried out by Lee and colleagues (Lee, 1987).

GRP78 and GRP94 are both molecular chaperones. GRP78 is a member of the HSP70 family and GRP94 is member of the HSP90 family of heat shock proteins (Lee, 2007). GRP78 recognises hydrophobic residues on unfolded or misfolded proteins and binds

to them, thereby preventing their interaction with other molecules (Bole *et al.*, 1986). GRP94 is the ER resident isoform of cytosolic HSP90, however in contrast to HSP90 (which has a very large number of client proteins), GRP94 appears to have a very limited number of client proteins. GRP94 has been shown to be involved in B-cell differentiation and is also involved in the immune response (Ni and Lee, 2007, Liu and Li, 2008).

1.3.2 – Discovery of the Unfolded Protein Response

ER stress and the unfolded protein response (UPR) first came to light due to the work of two independent research groups in the late 1980s. Randal Kaufman's research group at the University of Michigan Medical Centre and Joseph Sambrook's group at Cold Spring Harbour Laboratory, New York both observed that the accumulation of unfolded or misfolded proteins in the ER led to the induction of the GRPs, which were known to be involved in the folding of proteins (Dorner *et al.*, 1987, Kozutsumi *et al.*, 1988). In a paper by Gething and Sambrook it was suggested that the induction of GRPs by unfolded proteins in the ER functioned to upregulate chaperone expression in an attempt to prevent accumulation of unfolded proteins and maintain normal ER function. This signalling pathway then became known as the unfolded protein response (UPR) (Gething and Sambrook, 1992). At this stage the link between unfolded proteins and the induction of molecular chaperones had been clearly established, however details of the signalling pathway involved remained unknown.

In 1992, work in the Sambrook lab revealed a 22 bp *cis*-acting element in the yeast BiP promoter was sufficient to induce the yeast KAR2 (BiP) gene in response to the accumulation of unfolded proteins (Mori *et al.*, 1992). This crucial finding was utilised by both the Sambrook group, and the Walter group at the University of California, San Francisco, and led to the identification of IRE1 (inositol-requiring enzyme 1); a novel ER

serine/threonine kinase (Cox *et al.*, 1993, Mori *et al.*, 1993). A further series of papers published by the Walter lab elucidated the UPR signalling pathway in yeast; the critical finding being the splicing of *HAC1* mRNA mediated by IRE1 upon UPR activation, which produces a more active HAC transcription factor than the unspliced mRNA protein product (Kaufman, 1999). It was discovered that whilst only three gene products are needed to provoke the UPR in yeast, almost 400 genes are subsequently affected to varying degrees (Patil and Walter, 2001). In 1998, mammalian IRE1α and IRE1β were independently identified by the groups of Ron and Kaufman. The IRE1α homolog was shown to be ubiquitously expressed, whereas the IRE1β homolog is only expressed in intestinal epithelium. A number of features of the UPR were shown to have been conserved between yeast and mammals, although no mammalian homolog of the yeast *HAC1* gene was found (Tirasophon *et al.*, 1998, Wang *et al.*, 1998).

In 1999, a second mammalian UPR kinase was isolated in the ER by both the Ron group and the Wek group independently, designated PERK and PEK respectively. PERK/PEK is a member of the eIF2α family of kinases and when activated causes phosphorylation of eIF2α and subsequent inhibition of general protein translation (Shi *et al.*, 1998, Harding *et al.*, 1999). At around the same time the group led by Mori showed that ATF6 (a basic leucine zipper (bZIP) transcription factor previously identified by Prywes and colleagues) was the third ER stress sensor. Upon activation of the UPR, ATF6 protein is transported to the Golgi apparatus where it is cleaved by site 1 and site 2 proteases. Cleaved ATF6 then travels to the nucleus and activates transcription of UPR target genes (Yoshida *et al.*, 1998, Ma and Hendershot, 2001).

So by this point the PERK and ATF6 signalling branches of the UPR had been described, however, as no mammalian homolog of the *HAC1* gene had been discovered there was no explanation as to why IRE1 had been evolutionarily conserved. The final piece of the puzzle fell into place in 2001 when the Kaufman and Mori labs reported that XBP1 (an

X-box binding protein) undergoes IRE1 mediated mRNA splicing in a similar manner to *HAC1* mRNA. This unconventional splicing in *C.elegans* and mammals excises an XBP1 mRNA fragment of 23 base pairs and 26 base pairs respectively, and the resulting protein product is a highly active transcription factor able to activate UPR target genes. These experiments also provided a link, via XBP1, between the IRE1 and ATF6 signalling pathways (Shen *et al.*, 2001, Yoshida *et al.*, 2001). This unconventional splicing of XBP1 mRNA has recently been confirmed to occur in the cytoplasm, rather than conventional mRNA splicing which only occurs in the nucleus (Uemura *et al.*, 2009, Yanagitani *et al.*, 2009).

There has been a succession of discoveries over the last 20 years that have provided knowledge of the UPR, starting in yeast, progressing to *C.elegans*, followed by the characterisation of the mammalian UPR. The three UPR signalling pathways and how they relate to one another are depicted in figure 1.3.

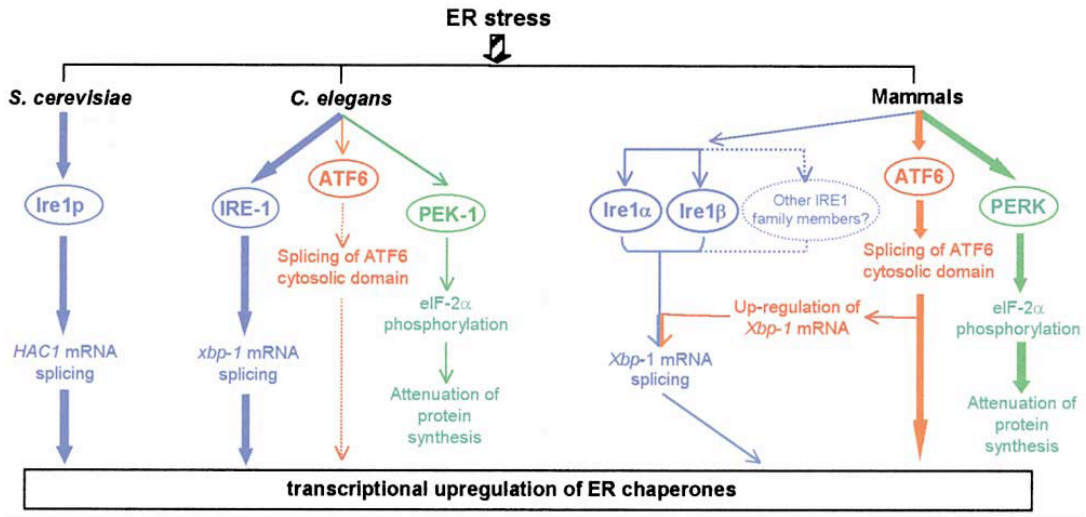

Figure 1.3. Comparison of the UPR signalling pathways in *S.cerevisiae*, *C.elegans* and mammals. Broad lines represent the pathways dominant for UPR activation, narrow lines represent functional UPR pathways, and dotted lines represent pathways not required for activation of molecular chaperones during the UPR.
Reproduced from Ma and Hendershot (2001).

1.3.3 – The Mammalian Unfolded Protein Response

Under normal physiological conditions, GRP78 is bound to the three ER transmembrane stress sensors PERK, IRE1, and ATF6 thereby keeping them in an inactive form. During ER stress GRP78 dissociates from the receptors allowing their phosphorylation and activation of the three pathways of the UPR (Lee, 2001). The UPR has a number of protective functions: to increase the folding capacity of the ER, reduce protein translation, increase the amount of ER within the cell, and promote degradation of misfolded proteins via ERAD pathways. It is thought that these UPR functions are particularly relevant in the normal physiology of highly secretory cells, such as plasma cells, intestinal epithelial cells and pancreatic β cells where there is an increased ER workload. In situations where ER stress is prolonged, or the UPR is unable to restore normal ER function, the UPR initiates apoptosis (programmed cell death). Thus the UPR has complex and conflicting functions within the cell (Bernales *et al.*, 2006). The mammalian UPR is illustrated in Figure 1.4. Since 2006, when figure 1.2 was published, the importance of the ER molecular chaperone GRP94 in the UPR has become apparent and continues to be investigated. The activation of each of the three branches of the UPR is discussed individually below.

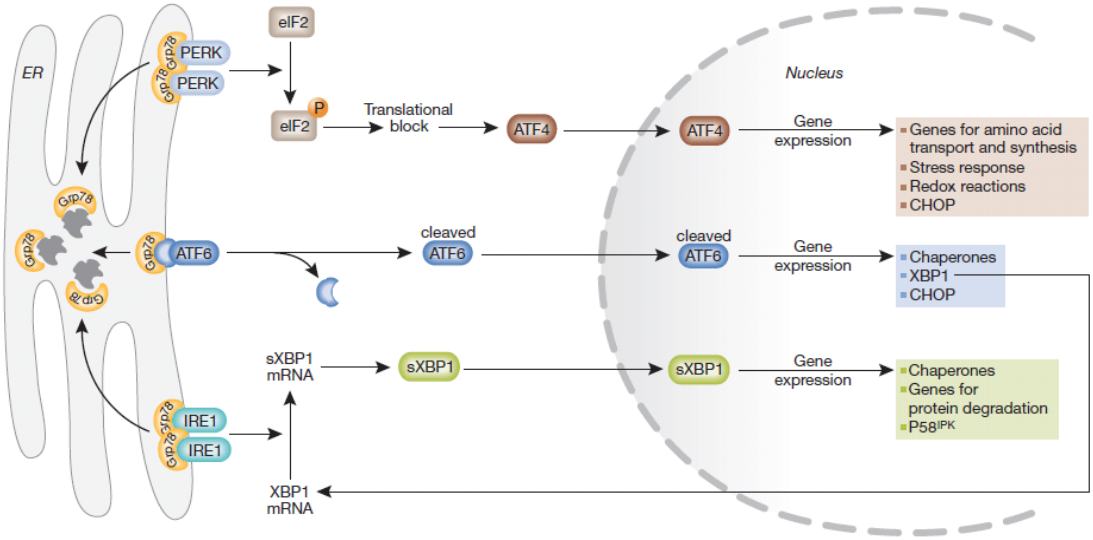

Figure 1.4. The mammalian unfolded protein response.
Reproduced from Szegezdi *et al.* (2006).

PERK: Dissociation of GRP78 from PERK allows receptor dimerisation and autophosphorylation of the kinase domain of the receptor. This activated PERK phosphorylates eIF2α which causes an inhibition of general protein translation, thereby reducing the protein load in the ER (Harding *et al.*, 2000ba). This inhibition of protein translation has been shown to occur immediately after the onset of ER stress, whereas UPR gene activation occurs one to two hours after stress onset (Harding *et al.*, 2000ab, Harding *et al.*, 2000ba). Some proteins escape this translational block, such as activating transcription factor 4 (ATF4); a basic leucine zipper (bZIP) transcription factor. ATF4 induces a number of genes with protective functions for the ER, however one of the genes induced by ATF4 is the pro-apoptotic transcription factor C/EPB homologous protein (CHOP, also called GADD153) (Harding *et al.*, 2000ab). The role of CHOP in apoptosis has been shown to occur in response to ER stress (Zinszner *et al.*, 1998). It has been discovered that a negative feedback loop exists that is mediated by GADD34 and leads to dephosphoryation of eIF2α. This dephosphorylation of eIF2α removes the block on general protein translation and is thought to promote recovery once the cellular stress has subsided (Novoa *et al.*, 2001, Ma and Hendershot, 2003). So it has been established that the PERK pathway has both protective effects (by decreasing general protein synthesis) and pro-apoptotic effects (via induction of CHOP).

IRE1: IRE1 is a transmembrane kinase/endoribonuclease and dissociation from GRP78 leads to autophosphorylation of the kinase domain and activation of the endoribonuclease domain, resulting in splicing of XBP1 mRNA. This XBP1 splice variant encodes a highly active (and more efficient) transcription factor, which induces UPR target genes such as molecular chaperones. It has been shown that activation of the kinase domain of IRE1 is required for its RNase activity and splicing of XBP1 *in vivo*, and that this autophosphorylation can be blocked by the use of ATP-competitive tyrosine kinase inhibitors (Ali *et al.*, 2011, Korennykh *et al.*, 2008). XBP1 has been shown to be involved in B-cell differentiation and plasma cell development (Reimold *et al.*, 2001, Gass *et al.*, 2004,

Gass *et al.*, 2008, Iwakoshi *et al.*, 2003). Knockout mouse models have provided valuable insight into the role of IRE1 and XBP1 in B cell development. IRE1α knockout mice exhibit embryonic lethality (Urano *et al.*, 2000, Lee *et al.*, 2002), as do XBP1 knockout mice (Reimold *et al.*, 2001). IRE1 (via its cytoplasmic domain) has been shown to be required in the first stage of B cell lymphopoiesis, and ire1α-/- B cells were unable to differentiate into antibody secreting plasma cells (Zhang *et al.*, 2005). XBP1 has also been shown to be necessary for the development of antibody secreting plasma cells, with xbp1-/- plasma cells unable to differentiate into antibody secreting plasma cells *in vivo* (Reimold *et al*., 2001). Microarray analysis of gene expression has revealed differential expression of XBP1 between normal plasma cells, MGUS plasma cells, and myeloma plasma cells, as well as different expression ratios of spliced to unspliced XBP1 (Davies *et al.*, 2003). Another gene expression study in a patient with multiple myeloma and the patient's identical twin reported an approximately 15-fold upregulation in XBP1 expression in the patient myeloma cells compared to the normal twin plasma cells (Munshi *et al.*, 2004). The XBP1 splice variant has also been shown to trigger ER expansion during the UPR (Sriburi *et al.*, 2004). Another target of spliced XBP1 is $P58^{IPK}$. $P58^{IPK}$ is a member of the HSP40 family and acts to inhibit PERK causing a negative feedback loop, which in turn removes the PERK induced block in protein translation (Yan *et al.*, 2002, van Huizen *et al.*, 2003). This negative feedback loop is thought to be a late effect of PERK pathway activation, suggested to occur several hours after phosphorylation of eIF2α (Szegezdi *et al.*, 2006). It has also been reported that $P58^{IPK}$ is present in the ER lumen in association with GRP78 and functions as a cochaperone (Rutkowski *et al.*, 2007). Levels of spliced XBP1 have been reported to effect outcome in multiple myeloma patients, with increased overall survival in those patients with lower XBP1 spliced to XBP1 unspliced ratios and increased response to treatment with thalidomide containing therapy compared to conventional chemotherapy in these patients (Bagratuni *et al.*, 2010). This study suggests a role for spliced XBP1 as both a prognostic factor and a predictor of response to treatment in multiple myeloma. In addition to its importance in plasma cells and myeloma, XBP1 is also of significance in other types of

secretory cells. XBP1 deletion in intestinal epithelial cells resulted in intestinal inflammation in mouse models and was associated with human inflammatory bowel disease (Kaser *et al.*, 2008). The IRE1/XBP1 pathway has been shown to be involved in inflammatory responses in macrophages and in innate immunity under both stress and non-stress conditions (Martinon and Glimcher, 2011, Martinon *et al.*, 2010). Previously, it was thought that binding or dissociation of GRP78 to the three ER stress inducers was responsible for turning off or switching on the UPR. However, a recent study has proposed that contrary to this idea of simply turning the UPR on or off, binding of GRP78 to inactive IRE1 receptor molecules is involved in preventing activation, stabilising and deactivating the UPR once favourable protein folding conditions have been reached (Pincus *et al.*, 2010).

ATF6: ATF6 is a transmembrane protein that encodes a bZIP transcription factor in its cytosolic domain. ATF6 exists as a 90kDa membrane bound isoform under normal physiological conditions. Under ER stress conditions, GRP78 dissociates from the receptor and the cytoplasmic portion of ATF6 translocates to the Golgi apparatus where it is cleaved by site 1 and site 2 proteases to its 50kDa active form. Cleaved (active) ATF6 then travels to the nucleus and induces target genes with an ER stress response element (ERSE) in their promoter, such as molecular chaperones, XBP1 and CHOP (Haze *et al.*, 1999, Yoshida *et al.*, 1998, Yoshida *et al.*, 2001). During the UPR, activated ATF6 has a critical role in ER expansion (a physical increase in the size of the ER), thereby allowing further capacity for the ER to correct the perturbations in the protein folding machinery. It has been shown that this ER expansion occurs independently of any XBP1 mediated ER expansion (Bommiasamy *et al.*, 2009). It has been suggested that ATF6 is retained in the ER due to interaction of its oligosaccharide chain with the lectin chaperone calreticulin (Schroder and Kaufman, 2005b). Work by Shen and colleagues has revealed that contrary to earlier theory, GRP78 binds to ATF6 in a stable manner and dissociation of GRP78 during the UPR is regulated rather than being due to competitive binding of GRP78 to unfolded proteins during such stress conditions (Shen *et al.*, 2005). There are two mammalian isoforms of ATF6;

ATF6α and ATF6β. Knockdown of ATF6α in mice has shown that whilst it is not required for development or basal chaperone expression, ATF6α function is required for recovery from acute and chronic cellular stress. This is in spite of fully functioning PERK and IRE1 branches of the UPR existing in these animals (Wu *et al.*, 2007). In another study, mice with a knockdown of either isoform of ATF6 were found to develop normally, however, dual knockdown of both ATF6 isoforms caused embryonic lethality. The same study reported that ATF6α isoform was required for transcription of molecular chaperones during the UPR and that ATF6α forms a heterodimer with XBP1 leading to transcription of proteins involved in ERAD (Yamamoto *et al.*, 2007). More recently, it has been reported that ATF6 is involved in the survival of dormant cancer cells. In an *in vivo* study of squamous cell carcinoma, it was shown that ATF6 mediated the survival of dormant tumour cells via upregulation of Rheb and activation of mTOR in an AKT independent manner (Schewe and Aguirre-Ghiso, 2008). This research suggests that the prosurvival functions of ATF6 activation during the UPR can be exploited by cancer cells.

There are still a number of questions and controversies surrounding the activation of the UPR and the regulation of the conflicting pro-survival and pro-apoptotic signalling. The debate surrounds how these complex signalling cascades interact with one another to determine the fate of the ER stressed cell. Previously some authors suggested that the three UPR branches are activated in turn; PERK first, followed by ATF6, then finally IRE1 (Szegezdi *et al.*, 2006). It has been shown that when IRE1 and PERK are individually activated in the absence of misfolded proteins for an equal duration of time, PERK activation results in decreased proliferation and cell death, whereas IRE1 activation increased cell proliferation resulting in cellular survival (Lin *et al.*, 2009b). Whilst these results are interesting in examining the individual roles of PERK and IRE1 activation, they deal with activation of one arm of the UPR in absence of the others. This is unlikely to accurately reflect the complex situation under conditions of cellular stress, where the three branches of

the UPR interact with one another. Another study discovered that when PERK function was suppressed, compensatory activation of the IRE1 and ATF6 pathways of the UPR occurred (Yamaguchi *et al.*, 2008). In a 2007 paper in the journal *Science*, the Walter lab has provided valuable insight into signalling and cell fate during the UPR. The paper reports that in human cells exposed to persistent ER stress all three branches of the UPR were simultaneously activated, however there were considerable differences in the length of time each branch remained active after the onset of stress. The researchers discovered that IRE1 responses were attenuated within eight hours of stress onset, even in the presence of persistent stress. ATF6 showed a delay in attenuation in comparison to IRE1, however the PERK pathway was found to be active as long as 30 hours after the initial onset of stress. These results are represented in figure 1.5. The authors went on to show that this attenuation of IRE1 activity is an important factor in allowing cell death after UPR activation (Lin *et al.*, 2007). A later study by the same research group confirmed that even under prolonged stress conditions, attenuation of IRE1 signalling occurs, as evidenced by dephosphorylation of the kinase domain and decreased RNase activity (Li *et al.*, 2010). This data provides an insight into how cells may make the decision to allow survival or initiate apoptosis when confronted with ER stress.

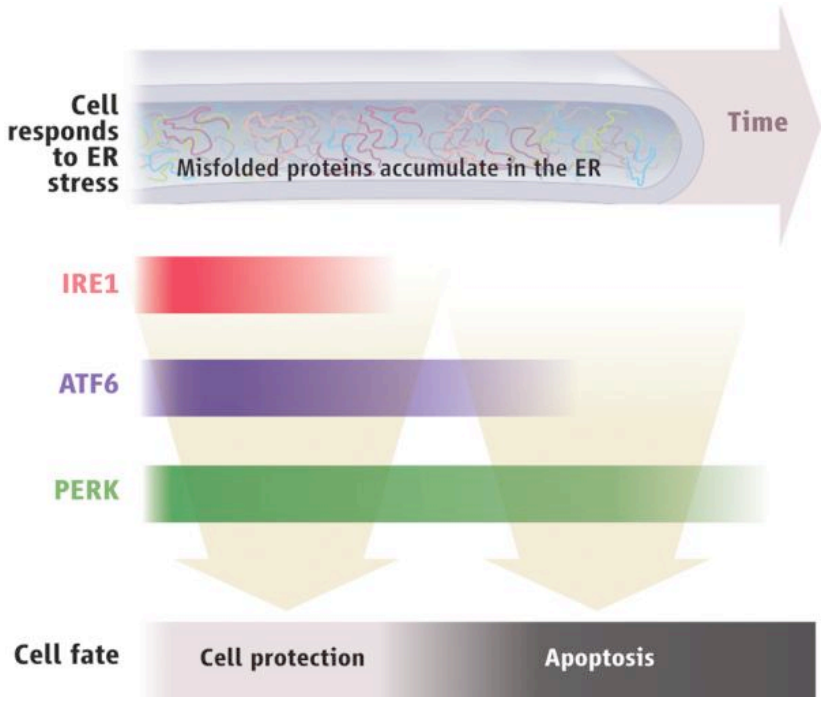

Figure 1.5. Time course for activation of the three branches of the UPR. Reproduced from Lin *et al.* (2007).

1.3.4 – Endoplasmic Reticulum Stress Induced Cell Death

Some of the key mediators in ER stress induced cell death are shown in figure 1.4 and discussed below. Whilst it has been recognised for some time that if the UPR is unable to restore ER homeostasis it can trigger apoptotic cell death, it is now becoming clear that the UPR is also involved in other cell death pathways.

Both the IRE1 and PERK branches of the UPR have been implicated in ER stress induced apoptosis. In contrast, the ATF6 pathway appears to have only protective functions (Thuerauf *et al.*, 2007, Szegezdi *et al.*, 2006). IRE1 is known to bind to TRAF2 (tumour necrosis factor receptor associated factor 2) leading to activation of ASK1 and JNK (Urano *et al.*, 2000). Interestingly, it has also been shown that IRE1α physically interacts with the pro-apoptotic BCL-2 family proteins BAX and BAK, providing a link between the UPR and the core apoptotic pathway (Hetz *et al.*, 2006). Another role for IRE1 in cell death comes via activation of caspase 12, an ER localised caspase activated exclusively during the UPR

(Nakagawa *et al.*, 2000). However, the majority of humans lack caspase 12 (due to a mutation in the coding region) and as a result, this pathway is unlikely to be of significance in man. Caspase 4, a pro-inflammatory caspase, is one of the closest relations to rodent caspase 12 and it has been suggested that this caspase may be involved in ER stress induced apoptotic signalling in humans (Hitomi *et al.*, 2004). The PERK pathway is involved in ER stress induced apoptosis via induction of ATF4 and the resultant upregulation of CHOP as discussed previously.

In addition to the accepted mechanism of UPR induced apoptosis, it has been shown that ER stress induced cell death can occur by differing mechanisms and involves both caspase dependent apoptosis and caspase independent cell death or necrosis (Egger *et al.*, 2003). One such mechanism is alteration of ER calcium content, which is the mechanism of action of a number of pharmacological agents known to cause ER stress induced apoptosis. Anti-apoptotic BCL-2 and BCL-X_L proteins have been shown to decrease calcium concentrations in the ER and pro-apoptotic BAX protein has been found to increase ER calcium concentrations (Foyouzi-Youssefi *et al.*, 2000, Jones *et al.*, 2007). Another study reported that cells deficient in BAX and BAK were chemoresistant, however they were still sensitive to ER stress induced apoptosis mediated by thapsigargin treatment (Janssen *et al.*, 2009).

Recently, an increasing role for autophagy in ER induced cell death has become apparent. Autophagy (autophagocytosis) is a cellular process involving lysosomal degradation of cellular components. ER stress has been found to induce autophagy, while the disturbance of autophagy makes cells more vulnerable to ER stress (Ogata *et al.*, 2006). The PERK pathway has been implicated in autophagy in response to ER stress, although the significance of this remains to be determined (Kouroku *et al.*, 2007). Recently it has been reported that GRP78 is required for ER stress induced autophagy to occur (Abramson *et al.*, 2008). Links have also been discovered between ER stress, the ubiquitin-proteasome system

and autophagy. The ubiquitin-proteasome system has been shown to induce autophagy in response to ER stress and it is thought this may be a compensatory mechanism activated when the proteasome is overwhelmed by misfolded proteins (Ding *et al.*, 2007).

Another mechanism by which cells dispose of misfolded or unfolded polyubiquitinated proteins is the aggresome pathway (Garcia-Mata *et al.*, 2002). The incorrectly folded proteins coaggregate into a single aggresomal particle, which then migrates toward the microtubule organising centre (MTOC) and on to the aggresome. These aggresomes recruit chaperones, proteasome subunits and ubiquitination enzymes in an attempt to dispose of the aggregated misfolded proteins. Clearance of the aggresomes is thought to occur via autophagy. Autophagosomes engulf the aggresomes and the proteins are then degraded by lysosomes (Rodriguez-Gonzalez *et al.*, 2008). The aggresome pathway has been implicated in cancer and identified as a possible therapeutic target, particularly in multiple myeloma (Hideshima *et al.*, 2005).

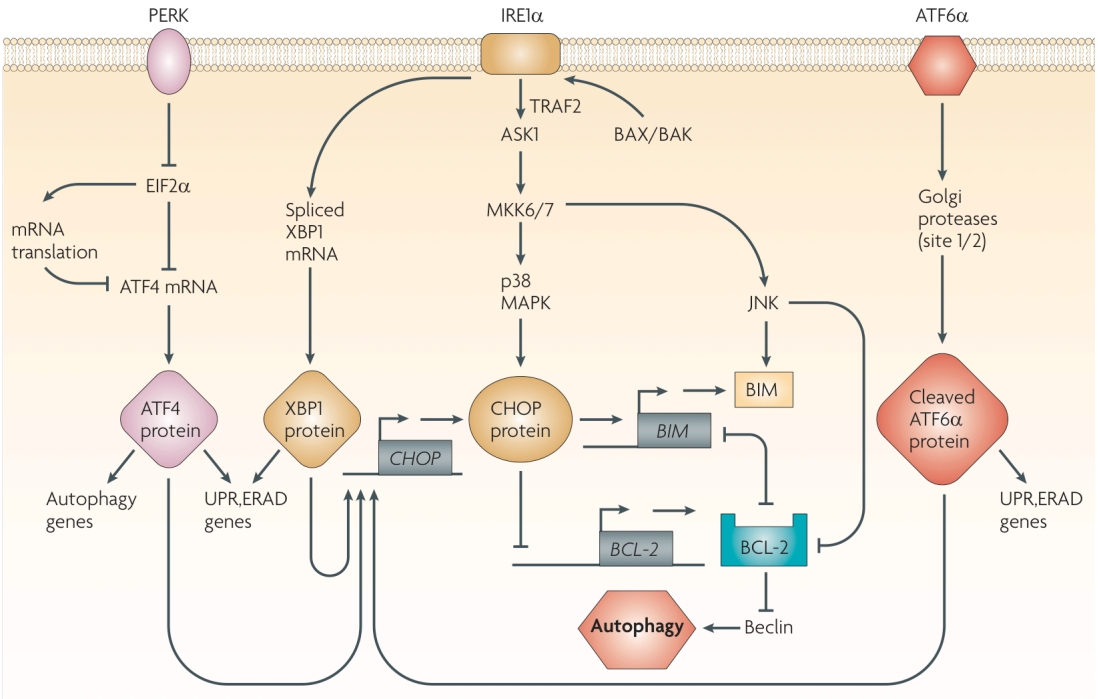

Figure 1.6. The role of the unfolded protein response in cell death. Reproduced from Kim *et al.* (2008).

1.4 The Unfolded Protein Response and Disease

1.4.1 – Classification of Diseases Caused by Impaired Endoplasmic Reticulum Function

ER stress and the UPR have been linked to a number of diverse clinical disorders, such as neurodegenerative diseases, diabetes, stroke, vascular injury, kidney disease, viral pathogenesis and cancer (Kaufman, 2002). Based on the classification of ER storage diseases by Kim and Arvan, Schroder and Kaufman have classified diseases caused by impaired ER and UPR function (Schroder and Kaufman, 2005b). These ER related diseases are designated class I to class IV:

- Class I diseases are caused by a mutation in secretory client proteins and alter folding of the affected protein. Class I diseases include cystic fibrosis and diabetes.
- Class II diseases are caused by mutations in the protein trafficking machinery and loss of function at the target site of the protein. Class II diseases include the blood coagulation disorder combined coagulation factor V and VIII deficiency.
- Class III diseases occur as a result of impaired UPR signalling. Examples of class III diseases include IRE1/XBP1 related colitits and the infant diabetic syndrome Wollcott-Rallison Syndrome, caused by mutations in the PERK kinase domain.
- Class IV diseases are those diseases in which UPR signalling is functional, however the protective responses of the UPR are impaired. This is seen in a number of neurodegenerative diseases, such as Huntington's disease, where the proteasome is poisoned by cytosolic polyglutamine repeats.

Most cancers would fall into class III or class IV diseases, and the mechanisms underlying class III and IV diseases are utilised in the drug treatment of cancer (particularly diseases derived from secretory cells). For example, proteasome inhibition as a therapeutic strategy in multiple myeloma (Schroder and Kaufman, 2005b).

1.4.2 – The Role of the Unfolded Protein Response in Disease

While the UPR is now implicated in a number of diseases, the underlying mechanisms remain to be fully uncovered. Also, it is not always clear whether the UPR is the primary cause in the pathogenesis of a particular disease, or a secondary response that may, for example, contribute to disease severity (Zhao and Ackerman, 2006). Whilst a number of clinical disorders where the UPR is involved have now been identified, there is currently a distinct lack of treatments that utilise or target the UPR or UPR components.

One group of disorders where the UPR is implicated in disease pathogenesis are the neurodegenerative diseases. It has been reported that the neuronal loss in both inherited and sporadic forms of neurodegenerative diseases can occur alongside aggregation of misfolded or mutant proteins (Selkoe, 2003). The UPR has been linked to both Alzheimer's disease and Parkinson's disease, as well as other neurodegenerative disorders such as Huntington's disease and spongiform encephalopathy (Zhao and Ackerman, 2006).

Gene mutations associated with Alzheimer's disease (e.g. presenilin-1 mutations in familial Alzheimer's and presenilin-2 in sporadic Alzheimer's) have been reported to downregulate UPR signalling via IRE1, PERK and ATF6, thereby increasing vulnerability to ER stress (Katayama *et al.*, 2001, Sato *et al.*, 2001). Downregulation of GRP78 has also been observed in the presence of these mutations *in vitro*, consistent with the finding that levels of the molecular chaperones GRP78 and GRP94 are decreased in the brains of Alzheimer's patients compared with age-matched controls (Katayama *et al.*, 1999). In cells with amyloid beta peptides or overexpression of presenilin-1 mutations associated with Alzheimer's disease, ER calcium homeostasis is impaired leading to neuronal toxicity and apoptosis (Mattson *et al.*, 1993, Guo *et al.*, 1997, Mattson *et al.*, 2000).

Parkin is an E3 ubiquitin ligase involved in the degradation of unfolded or misfolded proteins. Mutations in the parkin gene have been found to protect cells from UPR associated cell death and have been linked to Parkinson's disease (Shimura *et al.*, 2000, Imai *et al.*, 2000). It has also been shown that transient cerebral ischaemia activates the UPR, as indicated by XBP1 mRNA splicing (Paschen *et al.*, 2003), phosphorylation of PERK (Kumar *et al.*, 2001) and expression of UPR genes (Paschen, 2004).

ER stress and the UPR have also been linked to both type I and type II diabetes (Eizirik *et al.*, 2008). For example, a mutation in the EIF2AK3 gene (encoding human PEK/PERK) causes Wolcott-Rallison syndrome; a rare disease characterised by insulin dependent diabetes occurring in early infancy (with further symptoms such as osteoporosis, cardiovascular problems, mental and growth retardation occurring at a later age) (Delepine *et al.*, 2000). ER stress has also been found to play a role in the apoptosis of pancreatic islet β-cells in type II diabetes (Laybutt *et al.*, 2007). Recently, it has been suggested that ER stress and the UPR may provide the link between obesity, insulin resistance, and the resulting type II diabetes (Ozcan *et al.*, 2004, Boden *et al.*, 2008).

Other diseases where the UPR is now known to have some sort of involvement include cardiovascular disease (Toth *et al.*, 2007), kidney disorders (Kitamura, 2008) and musculoskeletal disorders (Acosta-Alvear *et al.*, 2007).

1.4.3 – The Unfolded Protein Response in Cancer

Cancer is one of the many diseases in which the UPR is proposed to be a factor. The vast majority of work done to date on the role of the UPR in cancer is in the area of solid tumours, particularly in relation to tumour hypoxia. As a tumour grows, increasing demands are placed on the microenvironment, eventually leading to glucose starvation, low pH, poor

vascular supply and hypoxia (Ma and Hendershot, 2004b). Whilst the hypoxia-inducible factor (HIF) pathway in hypoxia has been known for some time, more recently a role for the UPR in relation to hypoxia has become apparent (Wouters and Koritzinsky, 2008). Koumenis and colleagues showed that both moderate and severe hypoxia were sufficient to activate the PERK branch of the UPR and that this activation was important for survival during hypoxia (Koumenis *et al.*, 2002). Tumour hypoxia has also been reported to activate the IRE1 branch of the UPR, indicated by XBP1 mRNA splicing, and again this activation was found to be necessary for survival during hypoxia and continued tumour growth (Romero-Ramirez *et al.*, 2004). Questions remain regarding the mechanisms underlying UPR activation by hypoxia, including whether there is any involvement of the ATF6 pathway. Further work is being done in this area to fully elucidate the interaction between tumour hypoxia and the UPR.

Other areas of tumour development where the UPR has been implicated include tumour angiogenesis and metastasis. Drogat and colleagues reported that activation of the IRE1 signalling pathway of the UPR in response to tumour hypoxia resulted in upregulation of vascular endothelial growth factor A (VEGF-A). They also showed that in IRE1α-null mouse embryonic fibroblasts there was no upregulation of VEGF-A in response to either oxygen or glucose deprivation, and that this correlated with decreased tumor angiogenesis and growth in vivo (Drogat *et al.*, 2007). In a model of human glioma, it was shown that IRE1α inhibition led to a reduction in tumour angiogenesis, indicating a possible role for IRE1 in tumour invasiveness (Auf *et al.*, 2010). IRE1α has also been shown to be required for vascularisation and placental development in mice, with IRE1α deletion causing embryonic lethality (Iwawaki *et al.*, 2009). A study in human pancreatic adenocarcinomas found that XBP1 was required for angiogenesis during early tumour growth and that the proangiogenic effects of XBP1 occur independent of VEGF (Romero-Ramirez *et al.*, 2009).

Involvement of the UPR in a number of different solid tumour types has been shown. In hepatocellular carcinoma GRP78 has been identified as a transformation associated gene, along with activation of the ATF6 and IRE1/XBP1 pathways (Shuda *et al.*, 2003). In colon cancer, GRP78 has been shown to be upregulated in colon cancer tissue and increased cytoplasmic GRP78 expression was associated with the transformation from normal tissue to adenoma and then carcinoma (Xing *et al.*, 2006). GRP78 has also been shown to be overexpressed in malignant breast tumours, but there was no overexpression seen in benign breast tumours (Fernandez *et al.*, 2000). Both GRP78 and GRP94 have been shown to be overexpressed in lung cancer tissues (Wang *et al.*, 2005), and GRP94 overexpression has been reported in oesophageal adenocarcinomas (Chen *et al.*, 2002). Activation of the UPR has also been shown in prostate cancer (Misra *et al.*, 2006) and GRP78 has been linked to prostate cancer metastasis. GRP78 has been shown to be weakly expressed in normal prostate tissue, however it is highly expressed in the bone metastases of prostate cancer patients (Mintz *et al.*, 2003). In another study in prostate cancer it was found that the intensity of GRP78 expression in prostate tissue was associated with survival and clinical recurrence (Daneshmand *et al.*, 2007). The antiapoptotic BCL-2 family protein MCL-1 has also been implicated in ER stress and cancer. It has been reported that melanoma cells are resistant to ER stress induced apoptosis and that this increased survival is due to an upregulation of MCL-1 (Jiang *et al.*, 2007b). This finding suggests that inhibition of MCL-1 could be used as a therapeutic strategy to increase sensitivity to agents causing cell death via ER stress and the UPR. Another finding of note from work in solid tumours is the discovery that alterations in genes encoding the sarcoplasmic endoplasmic reticulum calcium pumps have been found in squamous cell head and neck carcinoma (Korosec *et al.*, 2008). This has interesting implications with respect to the modulation of ER calcium as a therapeutic strategy.

A large amount of work has been done on the UPR in solid tumours, however, comparatively little work has been done thus far on the role of the UPR in haematological

malignancies. The work that has been done has focused primarily on activation of the UPR resulting from various therapeutic strategies in multiple myeloma, which will be discussed in further sections.

1.5 The Unfolded Protein Response and Drug Resistance in Cancer

A number of years before the elucidation of the mammalian UPR pathways and the vital role played by molecular chaperones such as GRP78, it was already known that the glucose related proteins were involved in resistance of tumours to treatment with traditional DNA-damaging chemotherapy drugs. In 1987, it was shown that exposure of chinese hamster ovary (CHO) cells to conditions that induced GRPs (e.g. glucose deprivation and anoxia) induced resistance to the topoisomerase II poison doxorubicin (Shen *et al.*, 1987). These researchers then went on to attempt to identify a mechanism for this resistance. They found that following exposure of CHO cells to GRP inducing conditions (also including tunicamycin treatment) there was a rapid and selective depletion of topoisomerase II from the nucleus of these cells and associated cell cycle effects (Shen *et al.*, 1989).

Other investigators also reported that upregulation of GRP78 led to downregulation of topoisomerase II and resistance to topoisomerase II inhibitors, including etoposide (Yun *et al.*, 1995, Gosky and Chatterjee, 2003). However, further studies indicated that the downregulation of topoisomerase II and induction of drug resistance attributed solely to GRP78 in these early studies was actually due to UPR activation (Reddy *et al.*, 2003, Gray *et al.*, 2005). It was shown that in the absence of ER stress inducers, overexpression of GRP78 did not result in depletion of topoisomerase or arrest in G1 phase of the cell cycle (Reddy *et al.*, 2003). This was confirmed by a later study which reported that a cell line overexpressing GRP78, which was unable to activate the UPR, did not show topoisomerase II depletion or increased resistance to etoposide in response to stress conditions. The authors

of this study attributed the decrease in topoisomerase II levels and the induction of resistance to topoisomerase II targeting drugs to activation of the UPR in general (including the resulting upregulation of GRP78), as opposed to it being a direct effect of GRP78 (Gray *et al.*, 2005). Another proposed mechanism for this drug resistance came from the identification of a sequence on topoisomerase IIα that induces its proteasomal degradation in response to glucose deprivation and activates an UPR (Yun *et al.*, 2004).

In contrast to the relation between expression of GRP78 and resistance to topoisomerase II poisons, it has been shown that increased expression of GRP78 can actually sensitise tumours to other DNA damaging agents (Chatterjee *et al.*, 1997). Clonogenic assay experiments showed that overexpression of GRP78 was associated with an increased sensitivity to DNA cross-linking agents, including melphalan and cisplatin (Chatterjee *et al.*, 1997). The authors concluded that overexpression of GRP78 decreased the ability of these cells to repair DNA cross-links, resulting in increased cytotoxicity (Chatterjee *et al.*, 1997).

The role of GRP78 in resistance of tumours to drug treatment is now being studied further. Due to the vital role this molecular chaperone plays in UPR activation there is strong mechanistic rationale for targeting it. This rationale was confirmed by Lee and colleagues in a 2006 study in breast cancer (Lee *et al.*, 2006). This retrospective cohort study analysed tumour specimens from 127 breast cancer patients and concluded that GRP78 was a predictor of response to chemotherapy. The authors reported that high GRP78 expression was associated with a shorter time to disease recurrence after doxorubicin containing chemotherapy. High tumour GRP78 expression was also associated with a shorter time to disease recurrence following mastectomy in this study (Lee *et al.*, 2006). This was the first report to build on the earlier *in vitro* work and shed light on the role of GRP78 in patient tumours. In parallel to this work, a study reporting immunohistochemistry results from prostate cancer patient samples revealed an association between GRP78 expression and the development of castration resistance, which may have important

prognostic implications for prostate cancer patients (Pootrakul *et al.*, 2006). Building on this work in breast and prostate cancers, the Lee group focused on GRP78 in malignant gliomas; a tumour type known to have poor chemosensitivity. It was shown that GRP78 is overexpressed in human malignant glioma cell lines compared to normal adult brain. The expression of GRP78 was reported to correlate with the rate of tumour cell proliferation. A small interfering RNA (siRNA) approach to down-regulating GRP78 decreased glioma cell proliferation and decreased resistance to the chemotherapeutic agent temozolomide used in this tumour type, whereas overexpression of GRP78 induced temozolomide resistance. This siRNA mediated down-regulation of GRP78 also sensitised cells to the chemotherapetic agents fluorouracil and irinotecan (Pyrko *et al.*, 2007b). This study highlighted the possibility of targeting the UPR via GRP78 in order to increase sensitivity to current chemotherapy treatments and reported that overexpression of GRP78 appears to be associated with increased chemoresistance.

A study by Zhang and colleagues provided a link between the UPR and the mitogen-activated protein kinase (MAPK) pathway mediated by the IRE1 pathway. The authors found that in gastric cancer cells GRP78 is a target of the MEK/ERK pathway and is responsible for protection against ER stress induced apoptosis (Zhang *et al.*, 2008). This study also suggested a role for GRP78 in decreasing chemosensitivity of tumours and highlighted the potential in targeting GRP78 as an adjunct to cancer chemotherapy.

It has been reported that GRP78 is involved in resistance to the proteasome inhibitor bortezomib in solid tumours. By studying a number of bortezomib resistant cell lines, it was discovered that these tumour cell lines were able to secrete GRP78 into the cell supernatant and that this was responsible for resistance to bortezomib treatment. Interestingly, the investigators found that this effect was only seen in solid tumour cell lines and did not occur in multiple myeloma cell lines (Kern *et al.*, 2009). Another study in mantle cell lymphoma has linked upregulation of GRP78 to bortezomib resistance. These investigators found that

downregulation of GRP78 either by knockdown or pretreatment with the HSP90 inhibitor IPI-504 lead to an increase in apoptosis following bortezomib treatment (Roue *et al.*, 2011)

Whilst there is some conflicting information on the role of GRP78 in drug sensitivity from the *in vitro* studies, the general consensus amongst investigators is that GRP78 has a protective effect in cancer cells and represents a valid therapeutic target in cancer.

Although most of the work concerning the UPR and drug resistance in cancer has investigated the role of GRP78, other components of the UPR have also been shown to be involved. It has been reported that activation of the phosphoinositide-3-kinase (PI3K) pathway and Akt, mediated by the XBP-1 (IRE1) pathway of the UPR, is implicated in the resistance of melanoma cells to the chemotherapy agents docetaxel and vincristine (Jiang *et al.*, 2009). PERK activation and the subsequent phosphorylation of eIF2α has been linked to control of the cell cycle by inhibiting translation of cyclin D1 and causing cell cycle arrest in G1 phase (Brewer and Diehl, 2000). This PERK mediated cell cycle arrest has been implicated in the survival and drug resistance of dormant tumour cells (Ranganathan *et al.*, 2006, Ranganathan *et al.*, 2008). However, it has so far not been demonstrated that PERK is solely responsible for this effect and other eIF2α kinases, such as GCN2, also appear to be involved (Hamanaka *et al.*, 2005). One study has suggested that both PERK and PKR lead to cell cycle arrest by increasing proteasomal degradation of cyclin D1 in cells where eIF2α is phosphorylated (Raven *et al.*, 2008). These interesting results provide scope for future work in this area and may eventually lead to new drug targets, enabling successful treatment of dormant or slowly proliferating tumour cells and reversal of drug resistance.

1.6 The Unfolded Protein Response and Modulating Chemosensitivity in Cancer

Due to the wide ranging involvement of the UPR reported in cancer, the role of the UPR in modulating chemosensitivity has recently begun to be investigated. The rationale for this is that as cancer cells have been shown to have a constitutively active UPR (to varying extents) (Ma and Hendershot, 2004b), provoking further ER stress will result in increased cell death via the UPR machinery, while leaving normal (unstressed) cells able to adapt and therefore unaffected.

Many drugs have been identified where the UPR is implicated in their mechanism of action to some extent. In order to facilitate discussion of these agents and their effect on chemosensitivity of tumours, I have grouped them according to mechanism of action. This approach results in the creation of four distinct groups: drugs that affect molecular chaperones involved in the UPR, drugs with direct effects on UPR transmembrane receptors and downstream signalling pathways, drugs that interfere with ERAD or cell death pathways, and drugs acting by other mechanisms. These groups of agents are discussed in detail below.

1.6.1 – Drugs acting on UPR molecular chaperones

The two molecular chaperones with the most direct effect on UPR activation and UPR signalling are GRP78 and GRP94. The role of these chaperones in the UPR has been discussed in detail in earlier sections. However, there are also other molecular chaperones that are involved in the UPR which are being investigated in terms of their effect on sensitivity of tumours to chemotherapeutic agents. It has been shown that the sensitivity of cells to apoptosis correlated with expression of HSP70 in AML cells *in vitro* (Chant *et al.*, 1996). This may have implications for chemosensitivity of these leukaemic cells.

Interestingly, it has been reported that inhibition of protein sulphide isomerases with the PDI inhibitor bacitracin increased apoptosis in response to ER stress inducing treatment in melanoma cells. This study provided very promising results and proof of principle *in vitro*, however the authors note that this strategy would be limited *in vivo* by the nephrotoxicity and low membrane permeability of bacitracin (Lovat *et al.*, 2008). The development of potent and specific small molecule inhibitors of PDI is eagerly awaited.

Based on earlier siRNA studies (Pyrko *et al.*, 2007b) inhibition of GRP78 has emerged as another possible method of modulating the UPR in order to increase chemosensitivity of tumours. The only small molecule inhibitor of GRP78 that has been described to date is versipelostatin; a natural product identified by a cell based screen for agents that would affect molecular chaperones (Park *et al.*, 2002). In a 2004 article Park and colleagues investigated the effect of this drug on UPR activation in response to glucose deprivation or other ER stress inducing agents. They also investigated the antitumour activity of versipelostatin *in vivo* (Park *et al.*, 2004). Versipelostatin selectively inhibited expression of both GRP78 and GRP94 in response to ER stress induced by glucose deprivation (but not tumicamycin induced ER stress). XBP1 splicing and ATF4 expression were both decreased by versipelostatin during glucose deprivation, indicating UPR suppression. In a mouse xenograft model, the *in vivo* cytotoxic effect of versipelostatin was comparable to that of single agent cisplatin treatment, and the drug was well tolerated (Brough *et al.*, 2008). This work provided encouraging early results for this novel compound.

Other strategies for targeting GRP78 are being explored, for example, the use of the cytokine interleukin-24 (IL-24 – also known as melanoma differentiation-associated gene-7 or MDA-7); a member of the interleukin-10 family of cytokines (Jiang *et al.*, 1995, Dent *et al.*, 2005). One of the effects of IL-24 is to cause ER stress through generation of reactive oxygen species. IL-24 also directly interacts with GRP78 in the ER and has been shown to

suppress tumour growth, or cause apoptosis, in cell lines and mouse models of cancer (Gupta *et al.*, 2006). A recent study has shown that in prostate carcinoma cells, IL-24 causes apoptosis via inhibition of the antiapoptotic BCL-2 family protein MCL-1 (Dash *et al.*, 2010). Another recent study reported that IL-24 treatment in AML cell lines resulted in ER stress induction and subsequent apoptosis (Rahmani *et al.*, 2010). Research is continuing into the use of this cytokine in cancer therapy, and has progressed into clinical trials (phase I and II). IL-24 treatment is a gene therapy product and is delivered *in vivo* by recombinant MDA-7/IL-24 adenovirus. Treatment with IL-24 has also been studied in glioma, leukaemia and ovarian cancers (Yacoub *et al.*, 2010a, Yacoub *et al.*, 2010b, Yang *et al.*, 2010). IL-24 therapy was well tolerated in phase I clinical trials and evidence of efficacy has already been seen (Inoue *et al.*, 2006, Lebedeva *et al.*, 2007).

Another group of drugs that have recently been linked with the ER chaperone proteins and UPR activation are histone deacetylase (HDAC) inhibitors. HDAC inhibitors are novel anticancer agents, with the first in class inhibitor suberoylanilide hydroxamic acid (SAHA; vorinostat (Zolinza®)) approved by the FDA in the United States for the treatment of cutaneous T-cell lymphoma in 2006. A second HDAC inhibitor romidepsin (Istodax®) was also approved by the United States FDA in 2009 for the treatment of cutaneous T-cell lymphoma. Histone proteins are involved in the packing of DNA into nucleosomes. Epigenetic modifications of histone proteins, such as acetylation and methylation, are involved in a number of important processes, including gene regulation and DNA repair. HDACs and histone acetyl transferases (HATs) are together responsible for the modification of histones and regulation of target gene expression. HATs mediate histone acetylation thereby facilitating gene expression, whilst HDACs mediate removal of acetyl groups (deacetylation) resulting in repression of transcription (Lane and Chabner, 2009, Bolden *et al.*, 2006).

Eight classes of HDACs have been identified (based on homology with HDACs in yeast) and HDAC inhibitors can act on one or more of these classes. The hydroxamic acid derived HDAC inhibitors, such as SAHA, are pan-HDAC inhibitors acting on class I, II and IV HDACs (Bolden *et al.*, 2006, Lane and Chabner, 2009). HDAC inhibitors have recently been linked to GRP78 and the UPR. It has been known for some time that HSP90 is a non-histone substrate of HDAC enzymes (Yu *et al.*, 2002) and a 2009 recent study published in the journal Science has identified other chaperones that are non-histone HDAC substrates, including HSPA5 (GRP78) and HSP90B1 (GRP94). It has been suggested that lysine acetylation on HSP90 may contribute to the anticancer activity of HDAC inhibitors, although recent knowledge of the roles of the ER molecular chaperones (GRP78 in particular) suggests an additional possible role for these proteins in mediating HDAC inhibitor activity (Choudhary *et al.*, 2009). Another study reported that the GRP78 promoter is repressed by HDAC1 and that HDAC inhibitors specifically induce GRP78 expression. These investigators also report that overexpression of GRP78 results in resistance to HDAC inhibitor induced apoptosis (in 293T renal epithelial cells), whilst GRP78 knockdown sensitised cells to HDAC inhibitor activity (in the colorectal HCT116 and melanoma MDA-MB-435 cell lines) (Baumeister *et al.*, 2009). GRP78 and UPR activation have also been reported to contribute to the anticancer activity of SAHA. Studies in a panel of glioblastoma and prostate cell lines showed that SAHA treatment resulted in GRP78 acetylation and subsequent activation of PERK (with eIF2α phosphorylation, ATF4 and CHOP expression), although the authors comment that this UPR activation was specific to certain cell lines. Knockdown of PERK using siRNA lead to an increase in cytotoxicity following SAHA treatment in the U251 glioblastoma cell line (Kahali *et al.*, 2010). Whilst these studies have reported an association between HDAC inhibition, GRP78 induction and UPR activation, a causal link has not yet been established.

In recent years it has been discovered that a number of drugs widely used in clinical practice have other, previously unknown, off target effects linked to the unfolded protein

response. For example, the antidiabetic drug metformin (belonging to the biguanide class) is one of the most common agents prescribed for the treatment of type 2 diabetes. It acts by inhibiting glucose production in the liver, delaying intestinal glucose absorption and increasing insulin sensitivity in muscle. It has been reported that metformin (and the other biguanide drugs buformin and phenformin) modulated the UPR under glucose deprivation conditions in a manner similar to that of versipelostatin (Saito *et al.*, 2009). Whilst a great deal more research is needed as regards metformin for cancer treatment, utilising drugs that are already in widespread clinical use for their UPR targeting effects is a particularly attractive treatment strategy. A drug such as metformin that is taken orally, has been used for many years, is considered safe and has a well-known adverse effect profile would be an ideal therapeutic candidate.

One of the limitations of the agents mentioned above in targeting molecular chaperones is the possible lack of total selectivity for a given chaperone. However, these targets have only recently been identified and it is hoped that with continued research, agents with higher target selectivity (and therefore more potential to pass successfully through the drug development process and into the clinic) will be identified.

1.6.2 – Drugs with direct effects on UPR receptors and downstream signalling

The second group of drugs used to modulate the UPR in cancer treatment are those drugs with direct effects on UPR transmembrane receptors and downstream signalling pathways. A number of different agents have now been linked directly to the UPR sensors PERK, IRE1 and ATF6 or their downstream signalling molecules and these agents are discussed below.

ER stress has been shown to be involved in apoptosis induced by treatment with the non-steroidal anti-inflammatory drug (NSAID) indometacin. Increased GRP78 expression was seen, along with ATF6 and XBP1 activation, and expression of AFT4 and CHOP (Tsutsumi *et al.*, 2004). The cyclooxygenase-2 (COX-2) inhibitors, e.g. celecoxib, are also anti-inflammatory drugs. They selectively inhibit COX-2 and therefore have less gastric adverse effects than traditional NSAIDs (Beers and Merck Research Laboratories., 2006). These drugs have also been found to cause ER stress mediated apoptosis, however in contrast to indometacin the mechanism of this apoptosis is due to effects on intracellular calcium and these drugs are therefore discussed in the next section.

HSP90 inhibitors also interact directly with UPR signalling. As early as 2002 it was shown that HSP90 physically interacts with the ER transmembrane receptors PERK and IRE1, by association with their cytoplasmic kinase domains. In particular, HSP90 modulates the UPR through stabilisation of IRE1 (Marcu *et al.*, 2002). The activity of HSP90 inhibitors in multiple myeloma was reported (Mitsiades *et al.*, 2006) and further work published in 2007 showed that HSP90 inhibition with 17-AAG activated an UPR in multiple myeloma plasma cells, as evidenced by ATF6 activation, XBP1 splicing and induction of CHOP (Davenport *et al.*, 2007). The activity of another novel HSP90 inhibitor, IPI-504, has been shown in multiple myeloma cells, however, in contrast to the UPR activation seen with other HSP90 inhibitors, it has been reported that this agent blocks activation of the UPR (Patterson *et al.*, 2008). IPI-504 has been found to induce apoptosis in diffuse large B-cell lymphomas that are dependent on the HSP90 client protein AKT (Abramson *et al.*, 2008), which may also be a factor in myeloma cytotoxicity. As mentioned in the drug resistance section previously, IPI-504 has also been reported to overcome resistance to bortezomib occurring due to secretion of GRP78 by solid tumour cell lines (Roue *et al.*, 2011). It is worth mentioning that inhibitors of cytosolic HSP90, namely geldanamycin, also bind to both other mammalian isoforms of HSP90; its ER homologue GRP94, and its mitochondrial homologue TRAP1 (Felts *et al.*, 2000, Chavany *et al.*, 1996). This binding is rarely

discussed in the context of HSP90 treatment and is not generally given much significance when considering the mechanism of action of these drugs. It is probable that this is due to the large number of client proteins of HSP90 (many of which are key players in cancer) compared with the very few client proteins of GRP94, of which very little was known about until recently.

Other agents exerting an anticancer effect via UPR receptors and signalling have recently been described. The Ras inhibitor Salirasib (FTS) has been shown to cause ER stress induced apoptosis in cells overexpressing the Myc oncogene via increased GRP78, phosphorylation of PERK receptor and activation of downstream proapoptotic signalling (Yaari-Stark *et al.*, 2010). This finding has implications for potential cancer treatment as a number of different tumour types have been reported to have amplification of the Myc gene. Another compound that has recently been described to act via the UPR is the flavonoid xanthohumol. A study in chronic lymphocytic leukaemia (CLL) found that treatment with xanthohumol induced the chaperones GRP78 and HSP70 as well as leading to sustained eIF2α phosphorylation and activation of proapoptotic UPR signalling (Lust *et al.*, 2009). Other flavonoids have also been reported to act in this way, such as activation of the proapoptotic PERK pathway in leukaemic cell lines by tangeretin (Lust *et al.*, 2010). The natural plant phenol compound resveratrol has also been reported to exert an anticancer effect via PERK pathway mediated cell cycle arrest (Liu *et al.*, 2010). The tyrosine kinase inhibitor sorafenib used in renal cancer has been shown to induce cell death via ER stress and UPR activation in leukaemia cells (Rahmani *et al.*, 2007).

Research has been carried out over recent years to identify specific inhibitors of the UPR receptors, particularly the kinases (and in the case of IRE1, endoribonuclease) PERK and IRE1. Earlier this year two separate research groups published studies of small molecule IRE1 inhibitors. An article by Papandreou and colleagues in the journal Blood describes the novel small molecule compound STF-083010, an inhibitor of IRE1

endoribonuclease activity, after ER stress in both *in vitro* and *in vivo* models of multiple myeloma (Papandreou *et al.*, 2011). In the other paper by Volkmann and colleagues, the Salicylaldehyde analogs were reported to be specific inhibitors of the IRE1 endoribonuclease. These compounds have been shown to bind to IRE1 in a specific, reversible and dose dependent manner in both *in vivo* and *in vitro* models of ER stress (Volkmann *et al.*, 2011). While research is still at an extremely early stage, it is promising that compounds are being developed to target IRE1 and presents a good starting point for future drug development. IRE1 inhibitor therapy has the potential to be particularly efficacious in cancers (or other disorders) where activation of the IRE1/XBP1 pathway has been implicated in disease pathology, for example, multiple myeloma.

1.6.3 – Drugs that interfere with ERAD or cell death pathways

The third group of drugs that modulate ER function act by interfering with ERAD or cell death pathways. The main examples of drugs acting via this mechanism are proteasome inhibitors. As previously discussed, the 26S proteasome is responsible for the degradation of polyubiquinated proteins and degradation of unfolded or misfolded polyubiquitinated proteins via the proteasome is the final stage in ERAD. It is thought that by inhibiting the proteasome, therefore interfering with ERAD, other cell death/degradation pathways will be activated by the resulting ER stress and UPR activation. Proteasome inhibition is already used in myeloma and some lymphomas, and is also being investigated in leukaemia (McConkey and Zhu, 2008, McConkey *et al.*, 2005, Vink *et al.*, 2006, Riccioni *et al.*, 2007). The first in class proteasome inhibitor bortezomib has also been shown to increase the sensitivity of multiple myeloma cells to other chemotherapeutic agents (Ma *et al.*, 2003). Experiments in pancreatic cancer cells showed that bortezomib sensitised the cells to ER stress mediated apoptosis (Nawrocki *et al.*, 2005b). The same researchers then reported that bortezomib inhibited PERK, but increased GRP78 and CHOP expression, and induced

apoptosis as a result of ER stress induction in pancreatic cancer cells (Nawrocki *et al.*, 2005a). It was reported that in multiple myeloma cells bortezomib treatment activated unfolded protein response mediated apoptosis, via activation of the PERK pathway (Obeng *et al.*, 2006). It has also been shown that bortezomib is preferentially cytotoxic to hypoxic tumour cells due to an overactivation of ER stress. Interestingly, whether cell death occurred via apoptosis or autophagy was found to depend on the cell type (Fels *et al.*, 2008).

A number of drugs used to treat HIV have recently been identified as potential anticancer agents, exerting their anticancer effects through ER stress. The HIV protease inhibitors nelfinavir, atazanavir and ritonavir have all been discovered to have anticancer activity (Gills *et al.*, 2007, Pyrko *et al.*, 2007a, Kraus *et al.*, 2008). Ritonavir was shown to increase sensitivity to bortezomib in sarcoma (Kraus *et al.*, 2008). These agents have been found to decrease AKT and inhibit the proteasome, thereby activating the UPR and subsequent apoptosis (Gupta *et al.*, 2007). By inhibiting the proteasome these agents exert their anticancer effects by interfering with ERAD in the same way as bortezomib. The use of these drugs to modulate the UPR has the advantage that they are established drugs used for many years in treatment of patients and their adverse effects are well known. Also, these drugs are taken orally, which is a major advantage in terms of drug administration. For these reasons, HIV protease inhibitor drugs have progressed quickly into clinical trials in cancer patients. A phase I trial of nelfinavir in conjunction with chemoradiation in locally advanced pancreatic cancer has recently been completed, with acceptable toxicity and promising activity reported (Brunner *et al.*, 2008).

The sarcoplasmic endoplasmic reticulum is a specialised smooth ER responsible for pumping calcium into the ER lumen from the cytosol via a calcium-ATPase, (known as SERCA pumps), and inhibition of these pumps leads to leakage of intracellular calcium and ER induced cell death. The pharmacological inducer of ER stress, thapsigargin, acts in this manner. It therefore follows that other agents that disturb ER calcium homeostasis could be

used as potential anticancer agents via their induction of ER stress induced cell death. The COX-2 inhibitors, e.g. celecoxib, are anti-inflammatory drugs used in the treatment of arthritis and pain. They selectively inhibit COX-2 and therefore have less gastric adverse effects than traditional NSAIDs (Beers and Merck Research Laboratories., 2006). Celecoxib has been shown to inhibit SERCA pumps in a similar way to thapsigargin, however it is much less potent. It is thought that this effect on ER calcium may also be responsible for the cardiac adverse effects reported with long-term celecoxib treatment (Johnson *et al.*, 2002). Recently it was discovered that celecoxib causes calcium dependent activation of the PERK-eIF2α-ATF4-CHOP signalling branch of the UPR and an inhibition of general protein synthesis (Tsutsumi *et al.*, 2006, Pyrko *et al.*, 2008). It was later found that this UPR activation was also induced by a non-COX-2 inhibiting analogue of celecoxib (dimethylcelecoxib), therefore the activity is mediated by a COX-2 independent mechanism (Pyrko *et al.*, 2006). Celecoxib or dimethylcelecoxib treatment has also shown increased cytotoxicity to glioblastoma cells when combined with the proteasome inhibitor bortezomib (Kardosh *et al.*, 2008). Celecoxib has been investigated as an adjunct to treatment with the HIV protease inhibitor nelfinavir in drug resistant breast cancer cell lines, resulting in increased ER stress induced toxicity (Cho *et al.*, 2009).

Mitochondrial inhibitors are another group of potential anticancer agents with a mechanism of action linked to ER stress induced cell death. It has been reported that calcium leaked from the ER is delivered back to the mitochondria and it has therefore been suggested that in cells with an abundance of calcium the mitochondria will be of greater importance in calcium homeostasis. Experiments in multiple myeloma cell lines showed that this increased calcium leakage to the mitochondria was present when compared to B-cell leukaemia cell lines. The authors reported that this corresponded to an increased sensitivity to various mitochondrial inhibitors, such as carbonyl cyanide *m*-chloro phenyl hydrazone (CCCP), in the multiple myeloma cell lines (Kurtoglu *et al.*, 2010). This study suggests

another area of interest for cancer research, providing a potential strategy to target highly secretory cells with increased demands on ER function.

Another clinically used drug that has recently been linked to ER stress induced cell death is the calcium channel blocker verapamil. Verapamil is widely used clinically for the treatment of arrhythmias and hypertension. Verapamil is also an inhibitor of the multidrug resistance gene product P-glycycoprotein (Pgp; a drug efflux pump). It was found that the bortezomib mediated UPR activation in myeloma cells was enhanced by verapamil treatment leading to increased cytotoxicity (Meister *et al.*, 2010).

1.6.4 – Drugs acting via other mechanisms

Lastly, there are a number of agents that act via other mechanisms to those discussed above. It has been reported that insulin-like growth factor 1 (IGF-1) protects cells from ER stress induced apoptosis by increasing the adaptive capacity of the ER. It does this by inducing expression of GRP78, stimulating translational recovery, and enhancing ER protein folding capacity (Novosyadlyy *et al.*, 2008). Another agent identified as targeting the ER is the lactone antibiotic brefeldin A. Brefeldin A inhibits transport of proteins from the ER to the Golgi apparatus, resulting in disruption of normal ER protein trafficking and ER stress. In chronic lymphocytic leukaemia (CLL) cells brefeldin A treatment led to Golgi collapse, caspase activation, and cell death, even in cells resistant to the chemotherapeutic agent fludarabine commonly used to treat this disease (Carew *et al.*, 2006). Brefeldin A is currently being investigated further as a potential anticancer treatment. Research has also been conducted into the use of chemical chaperones to modulate the UPR. The chemical chaperone 4-phenylbutyric acid is a butyric acid derivative that has been reported to enhance the adaptive capacity of the ER and reduce the degree of UPR activation (de Almeida *et al.*,

2007). Therefore the use of chemical chaperones could present another potential anticancer strategy in tumours where UPR activation has been implicated.

As can be seen from the many agents discussed above, modulating the UPR in cancer is a thriving research area and many compounds acting via this pathway are currently being investigated as anticancer agents. Many of the drugs shown to have UPR mediated anticancer effects were previously known to have anticancer activity, however their UPR mechanism or involvement was only discovered at a later stage. There is still much work to be done in order to establish druggable UPR targets and develop agents that exhibit high selectivity towards them. Whilst the ultimate aim of such investigation is to identify novel targets for drug treatment in cancer patients, this area of research is complicated by the fact that the UPR is an incredibly complex signalling pathway involved in many cellular processes and under many physiological conditions. As a consequence, modulating UPR components in an attempt to treat cancer may have unexpected consequences when carried out *in vivo*.

In conclusion, the UPR is a complex signalling pathway activated in response to cellular stress that aims to restore normal ER function, or if this is not possible, initiates programmed cell death. The UPR has been implicated in a number of diseases, including cancer, and modulating the UPR represents a potential strategy for novel anticancer drug development.

1.7 Project Aims

This PhD project aims to investigate modulating the UPR as a novel therapeutic approach in haematological malignancies. The role of the UPR in mediating the activity of both novel and established cytotoxic agents will be studied. Various approaches will be utilised to investigate the UPR as a novel target in haematological malignancies. The hypothesis being tested in this work is that modulating the UPR will affect chemosensitivity in haematological cancer cells, and represents a potential strategy for anticancer treatment.

- The basal status of UPR activation in haematological cancers and relation to chemosensitivity will be investigated
- The role of the UPR in mediating the activity of both novel and established cytotoxic agents in haematological malignancies will be studied
- Underlying levels of ER stress, as well as provoking an ER stress response prior to cytotoxic treatment will be studied.
- The effect of modulating the UPR on chemosensitivity will be investigated by gene silencing using RNA interference, as well as specific small molecule approaches.

2. Materials and Methods

2.1 Cell Culture

Ten haematological cancer cell lines were used in the initial panel. Characteristics of each cell line can be found in table 2.1 below.

Cell line	Cancer type	Origin	Growth properties	Morphology
U937	Histiocytic lymphoma	Pleural effusion of 37 year old male with histiocytic lymphoma	Suspension	Monocyte
HL60	Acute myeloid leukaemia	Peripheral blood leukocytes from 36 year old female with acute myeloid leukaemia (AML FAB M2)	Suspension	Myeloblastic
THP1	Acute monocytic leukaemia	Peripheral blood of 1 year old male infant with acute monocytic leukaemia	Suspension	Monocyte
RPMI-8226	Multiple myeloma	Peripheral blood of 61 year old male with multiple myeloma	Semi-adherent	Lymphoblast
U266	Multiple myeloma	Peripheral blood of 53 year old male with multiple myeloma	Suspension	Lymphoblast
MM1.S	Multiple myeloma	Peripheral blood of patient with multiple myeloma	Semi-adherent	Lymphoblast
CRL-2261	B cell lymphoma	Ascites of 52 year old male patient with NHL	Suspension	Lymphoblast
SUD4	B cell lymphoma		Suspension	Lymphoblast
DOHH2	B cell lymphoma	Pleural effusion of a 60 year old male with centroblastic/centrocytic NHL that had transformed into an immunoblastic lymphoma	Suspension	Lymphoblast

Table 2.1. Characteristics of haematological cancer cell lines used in this project.

HL60, THP1, RPMI-8226, U266, CRL-2261, SUD4 and DOHH2 cell lines were obtained from Cancer Research UK Cell Services. MM1.S cell line was obtained from Dana Farber Cancer Institute. The colorectal cancer cell line HT-29 was obtained from Cancer Research UK Cell Services. All cell culture materials were procured from Sigma Aldrich,

UK unless otherwise specified. All suspension cell lines were cultured in RPMI-1640 medium supplemented with 10% foetal calf serum (FCS) and 1% penicillin-streptomycin. The adherent cell line HT-29 was cultured in McCoy's 5A medium (Invitrogen, UK) supplemented with 10% foetal calf serum (FCS), 1% penicillin-streptomycin and 0.22g/L L-glutamine. Cells were passaged every 3-4 days. AML and lymphoma cell lines were set at a concentration of 2 x 10^5 cells/ml in culture and MM cell lines were set at a concentration of 5 x 10^5 cells/ml. All cell culture was performed under sterile conditions. Cells were incubated at 37°C and 5% CO_2 in a humidified atmosphere.

Cell number and viability was assessed by trypan blue exclusion. Cells with a ruptured membrane (i.e. non-viable cells) take up the trypan dye and therefore appear blue when viewed under a microscope. Cells were counted using a haemocytometer. Cell suspensions were removed from culture flasks (MM1.S cells were first trypsinised or gently scraped), and centrifuged for 5 minutes at 150 x *g*. The resulting supernatant was discarded and the cell pellet resuspended in fresh medium. 10µl of cell suspension was mixed with 10µl of trypan blue (Sigma Aldrich, UK) and placed into the chamber of a haemocytometer. Cells were then counted using an inverted microscope. The number and viability of cells contained in one of the large grids (16 small squares) on the outside of the haemocytometer were counted. If cell number was below 35, then all four large outer grids were counted and the mean cell number and viability recorded. From these values the percentage of viable cells and the number of viable cells per ml were calculated.

2.2 Freezing Cells and Thawing from Liquid Nitrogen

Cells were removed from culture flasks and counted as described in the previous section. After centrifugation (5 minutes at 150 x *g*) the cell pellet was resuspended in freezing medium (70% RPMI-1640, 20% FCS and 10% DMSO) at a concentration of 2 to 4

x 10^6 cells/ml, dependent on the cell line. One millilitre aliquots were placed into cryovials and frozen overnight at -80°C before transfer to liquid nitrogen (-196°C).

To thaw cells, cryovials were placed directly into a water bath at 37°C. Once defrosted, the cell suspension was transferred to a falcon tube containing 10 ml fresh culture medium. After 5 minutes centrifugation at 150 x *g*, the supernatant was removed and the cell pellet resuspended in fresh medium before being placed into flasks for culture.

2.3 Preparation of Drug Stocks

Doxorubicin, cytarabine, etoposide, melphalan, tunicamycin, thapsigargin, 17-allylaminogeldanamycin, and 4-phenylbutyric acid were obtained from Sigma Aldrich, UK. 4-hydroperoxycyclophosphamide (the active metabolite of cyclophosphamide) was obtained from Squarix Biotechnology, Germany. Bortezomib (Velcade®) was provided by Millenium Pharmaceuticals, Inc., USA. KW-2478 was provided by Kyowa Hakko Kirin, Japan. Versipelostatin was kindly provided by Dr K Shin-ya, National Institute of Advanced Industrial Science and Technology, Japan. SAHA was synthesised by Professor C Marson, UCL.

All stock solutions were prepared in DMSO under sterile conditions unless otherwise specified. Concentration of DMSO in culture was kept to a minimum and did not exceed 0.05%. Aliquots of stock solutions were stored at 4°C or -20°C until use (dependent on drug stability). All further dilutions of the stock solutions were prepared fresh in culture medium under sterile conditions immediately prior to use. Doxorubicin, 2-deoxyglucose and 4-hydroperoxycyclophosphamide stock solutions were prepared in purified water and used immediately. 17-allylaminogeldanamycin stocks were prepared in methanol.

2.4 Guava ViaCount Assay

The Guava ViaCount assay (Guava Technologies Inc., USA) was used to determine total cell number (total cell number per millilitre) and cell viability (percentage viable cells and percentage dead cells) of each sample. This assay uses the Guava PCA – 96 System allowing measurement of samples in 96 well microplates. Cells are stained with the Guava ViaCount Flex Reagent and their fluorescence was analysed. The assay distinguishes between viable and non-viable cells based on the differential permeabilities of two DNA-binding dyes in the reagent. The nuclear dye stains all nucleated cells, while the viability dye stains only dead/dying cells. This enables the assay software to distinguish between viable, apoptotic, and dead cells. Debris is excluded from the analysis results based on negative staining with the nuclear dye**.** The EasyFit analysis algorithm (Guava Technologies Inc., USA), providing 3-dimensional analysis for more accurate results, was used for all experiments.

Cells in exponential growth phase were plated into 96 well plates (5000 cells per well) and incubated at 37°C and 5% CO_2 in air. Drug was added after 24 hours incubation, then on completion of the experimental incubation, plates were removed from the incubator and 100µl of diluted Guava ViaCount Flex Reagent was added to each well. Plates were then analysed using the Guava PCA™ – 96 System. All samples were run in triplicate and each experiment was repeated on three separate occasions to ensure reproducibility. The mean values and standard deviations of each data set were then calculated and used in subsequent data analysis. For concentration-effect modelling in GraphPad Prism, the mean values for each concentration in each experiment were used.

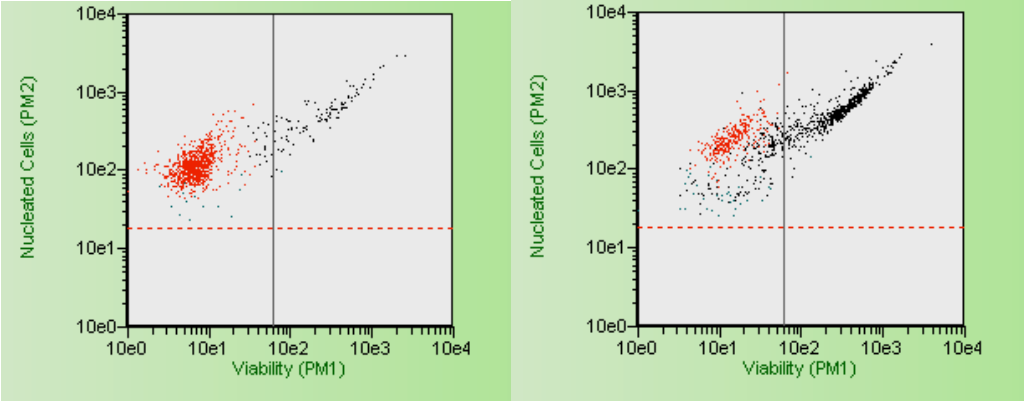

Figure 2.1. Example dot plots generated from Guava Viacount assay. Untreated U266 cells (left) and U266 cells treated with 8nM bortezomib (right) for 48 hours. Viable cells are shown in red, dead cells are shown in black and cellular debris is shown in green.

	EasyFit Results		Manual Results	
	Count	% of Total	Count	% of Total
Viable	906	90.42%	896	89.60%
Dead	96	9.58%	104	10.40%
	Viable	Total	Viable	Total
Cells / mL	1.44e05	1.59e05	1.42e05	1.58e05
Cells in Org. Sample	1.44e05	1.59e05	1.42e05	1.58e05
Debris Index	0.40%		0.60%	

Figure 2.2. Example data from Guava Viacount assay. The EasyFit analysis results can be used for subsequent data analysis (recommended by the manufacturer for more accurate results), or alternatively a gate can be placed around the population of interest manually. EasyFit analysis was used throughout the experiments in this thesis.

2.5 ATP Cytotoxicity Assay

The effect of drug treatment on cell proliferation and viability was investigated using a plate based adenosine triphosphate (ATP) cytotoxicity assay. Cells in exponential growth phase were plated into 96 well plates (5000 cells per well in 100µl medium) and incubated for 24 hours. Varying concentrations of drug were diluted in culture medium and then added to each well to obtain the required final concentration. Single agent treated wells, combination treated wells, and untreated control wells were present on each plate in the

combination experiments. Control wells and single agent treatment wells were topped up with culture medium so that all wells of the plate contained a fixed volume of 120µl. Plates were then incubated for 48 hours at 37°C and 5% CO_2 in air.

48 hours after addition of drug, plates were analysed using the ViaLight HS assay kit (Lonza Group Ltd, Switzerland) and read using a BMG Labtech Polarstar Optima microplate reader (BMG Labtech, Germany). The ViaLight HS kit is a high sensitivity cell proliferation/cytotoxicity assay. This assay uses a bioluminescence method to measure ATP content utilising the enzyme luciferase. All mammalian cells require ATP to remain alive and functional and any kind of cell injury results in a rapid decrease in levels of ATP. Therefore, this assay is used as a measure of cell number and viability. At the end of the incubation period 100µl of Nucleotide Releasing Reagent was added to each well of the plate to extract the ATP from the cells. After 5 minutes 20µl of ATP Monitoring Reagent was added to each well to generate luminescence signal (automated injection using the microplate reader) and the plate was read.

Experiments were repeated at least three times on separate occasions to ensure reproducibility. Effect of drug treatment was calculated from the assay data (expressed as a percentage of the control value). For each drug, the mean values and standard deviations of all experiments were determined for graphical representation. For concentration-effect modelling in GraphPad Prism, the mean values for each concentration in each experiment were used.

2.6 Calculation of EC_{50} values

Drug activity data was fitted using sigmoidal concentration effect curves to derive EC_{50} values (effective concentration 50 – i.e. the concentration required to exert 50% of maximum effect) with 95% confidence intervals, using non linear regression in GraphPad

Prism software (GraphPad Software, San Diego, USA). This was done for cell number and cell viability data. Minimum and maximum values for effect of drug on cell number were set to zero and 100 percent (with respect to control). For the effect of drug on cell viability the minimum effect was set to zero and the maximum was set to the control cell viability for each individual cell line. However, for drugs where the observed effect plateaud above zero, and the correlation coefficient (R_2, a measure of the goodness of fit from nonlinear regression) was less than 0.9, the minimum value was not set to zero and was fitted according to the model.

The GraphPad Prism software fits data according to the following equation,

$$Y = Bottom + (Top - Bottom) / (1 + 10 \wedge ((\log EC_{50} - X) \cdot H)$$

Where, Y = effect

X = log drug concentration

Top = maximum effect

Bottom = minimum effect

H = hillslope

This equation was rearranged algebraically in order to calculate any drug concentration required to give a particular effect (e.g. drug concentration required for an EC_{25} effect). This method was used to calculate equipotent concentrations of drugs for use in subsequent experiments, using the model parameters (top, bottom, H) determined from the initial fits.

2.7 Preparation of whole cell lysates

Whole cell lysates were prepared for use in western blotting experiments. Two million cells were plated out into each well of six-well culture plates and incubated for 24 hours at 37°C and 5% CO_2 in air. Where required, drug dilutions were prepared from stock solutions in fresh culture medium in order to obtain the required molar concentration per

well. Drug dilutions were made in the smallest possible volume, and never to exceed five percent of the total well volume. Cells were then incubated for a further period as specified in each experiment, after which time the cells were harvested and the cell suspension centrifuged for five minutes at 150 x *g*. The supernatant was then discarded and cell pellets were washed twice in Hanks Balanced Salt Solution (Sigma Aldrich, UK). Cells were then centrifuged at 240 x *g* for ten minutes at 4°C and the supernatant was discarded. Cell Lytic lysis buffer (Sigma Aldrich, UK) containing Complete protease inhibitor cocktail (Roche, UK) was added to the samples. PhoStop phosphatase inhibitor cocktail (Roche, UK) was added to samples where phosphorylation status of proteins was to be investigated. Samples were left on ice for 20-30 minutes to allow cell lysis to take place. Cell lysates were then centrifuged for 10 minutes at 20800 x *g* and 4°C, the resulting supernatant harvested and the remaining pellet discarded. The total protein content of each lysate was then measured using the BCA protein assay kit (Pierce, UK) according to the manufacturer's protocol. Samples were used immediately or placed into storage at -80°C until use.

2.8 Western Blotting

Protein samples were electrophoresed in 1 x NuPAGE MOPS SDS Running Buffer on SDS-polyacrylamide gels using the Novex mini/midi gel system (Invitrogen, UK) at 200V for approximately one hour. An equal amount of protein per sample was loaded into each lane of the gel (10µg - 40µg protein as necessary for the experiment). Novex pre-stained protein marker (Invitrogen, UK) was run alongside the samples as a reference for protein migration through the gel. Proteins were transferred onto a PVDF membrane using the i-blot dry transfer system (Invitrogen, UK). Membranes were then blocked with 5% non-fat milk in Tris-buffered saline-Tween 20 (TBS-T) for one hour with gentle shaking (to prevent non-specific protein binding) then washed briefly in TBS-T before incubation with

the primary antibody. 5% bovine serum albumin (BSA) in TBS-T was used as blocking buffer when probing for phosphorylated proteins.

Membranes were incubated with primary antibody either overnight at 4°C or for two hours at room temperature as per the manufacturer's data sheet, then removed and followed by three washes of five minutes each in TBS-T. Secondary antibody (horseradish peroxidase conjugated antibody) was then added for one hour, followed by a further three washes in TBS-T after antibody removal. All primary and secondary antibodies were diluted in TBS-T immediately prior to incubation. Preliminary experiments were carried out in order to optimise the concentration of both primary and secondary antibody for each experiment. Details of primary and secondary antibodies used are given in table 2.2.

Antibody binding was detected using the enhanced chemiluminescence (ECL) detection system (Amersham, UK) and Hyperfilm ECL (Amersham, UK). For experiments in chapters three to six inclusive, film developing was carried out using a manual tray developing method under darkroom conditions. Processing chemicals consisted of film developer, stop bath and fixer used according to manufacturer's instructions (Tetenal, Germany). For experiments in chapters seven to nine inclusive, developing was carried out using a Fuji ImageQuant LAS 4000 camera (FujiFilm, Japan) used according to manufacturer's instructions. Membranes were stripped (Restore Plus Stripping Solution, Pierce, UK) and blocked before probing with new antibodies. GAPDH antibody or α-tubulin antibody were used as a loading control in each experiment.

Primary Antibody	Dilution used	Secondary Antibody	Dilution used
GRP78 (sc-13539, Santa Cruz Biotechnology)	1:1000	Anti-rat	1:3000
GRP94 (sc-32249, Santa Cruz Biotechnology)	1:1000	Anti-rat	1:3000
IRE1 (#3294, Cell Signaling Technology)	1:1000	Anti-rabbit	1:3000
IRE1 (phospho S724) (ab48187, Abcam)	1:1000	Anti-rabbit	1:3000
PERK (ab31373, Abcam)	1:1000	Anti-rabbit	1:3000
p-PERK (Thr 981) (sc-32577, Santa Cruz Biotechnology)	1:1000	Anti-mouse	1:3000
ATF6 (B50090, Stratagene)	1:1000	Anti-mouse	1:3000
ATF4 (ab50983, Abcam)	1:1000	Anti-mouse	1:3000
GADD153 (sc-7351, Santa Cruz Biotechnology)	1:500	Anti-mouse	1:3000
eIF2α (#9722, Cell Signaling Technology)	1:1000	Anti-rabbit	1:3000
p-eIF2α (Ser51) (#9721, Cell Signaling Technology)	1:1000	Anti-rabbit	1:3000
XBP1u (ab79724, Abcam)	1:1000	Anti-rabbit	1:3000
XBP1s (619502, Biolegend)	1:1000	Anti-rabbit	1:3000
HSP90 (sc-69703, Santa Cruz Biotechnology)	1:1000	Anti-mouse	1:3000
HSP70 (#4876, Cell Signaling Technology)	1:1000	Anti-rabbit	1:3000
PDI (sc-30931, Santa Cruz Biotechnology)	1:1000	Anti-goat	1:3000
BCL2 (M0887, Dako)	1:1000	Anti-mouse	1:3000
MCL1 (sc-819, Santa Cruz Biotechnology)	1:1000	Anti-rabbit	1:3000
PARP (#9542, Cell Signaling Technology)	1:1000	Anti-rabbit	1:3000
LC3B (#2775, Cell Signaling Technology)	1:1000	Anti-rabbit	1:3000
α-Tubulin (#2125, Cell Signaling Technology)	1:1000	Anti-rabbit	1:3000
GAPDH (ab9484, Abcam)	1:1000	Anti-mouse	1:3000

Table 2.2. Primary and secondary antibodies used for western blotting. All secondary antibodies were obtained from Dako Ltd., UK.

2.9 Guava Nexin Assay

The Guava Nexin assay (Guava Technologies Inc., USA) is a fluorescence based apoptosis assay using the Guava PCA – 96 System allowing measurement of samples in 96 well microplates. The assay utilises two dyes in order to detect cells undergoing apoptosis; Annexin V and 7-AAD. Annexin V is a calcium-dependent phospholipid binding protein with high affinity for the membrane component phosphatidylserine. Early in the apoptotic pathway, phosphatidylserine molecules are translocated to the outer surface of the cell membrane where Annexin V can bind to them. The cell impermeant dye, 7-AAD, is also used as an indicator of cell membrane structural integrity. 7-AAD is excluded from live, healthy cells as well as early apoptotic cells. Assay results were analysed using the Guava Nexin Analysis Software (Guava Technologies Inc., USA). Results are obtained for four distinct cell populations present within the original sample:

- Viable cells, not undergoing detectable apoptosis (Annexin V-PE (-) and 7-AAD (-))
- Early apoptotic cells (Annexin V(+) and 7-AAD(-))
- Late stage apoptotic and dead cells (Annexin V(+) and 7-AAD(+))
- Nuclear debris (Annexin V-PE (-) and 7-AAD (+))

Cells in exponential growth phase were plated into 96 well plates (10000 cells per well) and incubated at 37°C and 5% CO_2 in air for 24 hours before addition of drug solution. The required amount of each drug was diluted in fresh culture medium and added to each well in order to achieve the desired molar concentration per well. Control wells and single agent treatment wells were topped up with culture medium so that all wells of the plate contained a fixed volume of 120µl. A positive control for apoptosis (doxorubicin 1µM) was included in all experiments. Cells were then returned to the incubator for a further 48 hours. On completion of the 48 hour incubation with drug, plates were removed from the incubator and Guava Nexin Reagent was added to each well. Plates were incubated in the dark at

room temperature for 20 minutes, then analysed using the Guava PCA – 96 System. All samples were run in triplicate and mean values and standard deviations used in subsequent data analysis.

2.10 Histone Deacetylase (HDAC) Activity Assay

Inhibition of histone deacetylases (HDAC) by drug was evaluated using an HDAC Fluorimetric Assay/Drug Discovery Kit (BIOMOL, Enzo Life Sciences, UK) as per manufacturer's protocol. The HeLa nuclear extract included in the kit is rich in HDAC activity and is used as the source of HDAC enzyme in the assay. The potent HDAC inhibitor Trichostatin A was included as a positive control inhibitor. Deacetylation of the substrate sensitises it to the developer, generating a fluorophore, which is excited with 360nm light and the emmited light (460nm) detected using a fluorometric plate reader (BMG Labtech Polarstar Optima, BMG Labtech, Germany). Trichostatin A or test inhibitor was diluted in assay buffer and plated into wells of a 96-well plate. Diluted HeLa extract was added to all wells (except for no enzyme controls). Fluor de Lys Substrate was then added to the wells initiating HDAC reactions. After 30 minutes, Fluor de Lys Developer was added to stop the reactions and the plate was incubated in the dark at room temperature for 15 minutes. Samples were then read using a microplate reader (excitation wavelength 350 to 380nm and emission 440 to 460nm).

2.11 siRNA Transfection

HP Validated siRNA and HiPerFect Transfection Reagent were obtained from Qiagen, UK. The following siRNA duplexes were used: All Stars Negative Control siRNA Alexa Fluor 488 labelled (catalog no. 1027292), GRP78 siRNA (catalog no. SI02780554), GRP94 siRNA (catalog no. SI02663738), GFP siRNA (catalog no. 1022064) and the

positive control MAPK1 siRNA (catalog no. 1022564). Sequences for the siRNA duplexes used are listed below. GRP78 siRNA, sense GGGUGUGUGUUCACCUUCAdTdT, antisense UGAAGGUGAACACACACCCdTdA; GRP94 siRNA, sense GCCUCAGUUUGAACAUUGAdTdT, antisense UCAAUGUUCAAACUGAGGCdGdA; GFP siRNA, sense GCAAGCUGACCCUGAAGUUCAU, antisense GAACUUCAGGGUCAGCUUGCCG; MAPK1 siRNA, sense UGCUGACUCCAAAGCUCUGdTdT, antisense CAGAGCUUUGGAGUCAGCAdTdT.

Transfection was carried out as per the manufacturer's protocol for suspension cell lines. The day before transfection cells in exponential growth phase were seeded in flasks at a density of 3 x 10^5 cells/ml in RPMI-1640 containing 10% foetal bovine serum and 1% penicillin streptomycin. Cells were incubated under normal growth conditions for 24 hours before plating out at 2 x 10^5 cells per well of a 24-well plate in 100µl culture medium containing serum and antibiotics. 100µl of siRNA at a concentration of 200nM (diluted in serum free medium) was added to 3µl of HiPerFect transfection reagent (giving a siRNA to transfection reagent ratio of 500:1), mixed by vortexing and incubated at room temperature for 5 to 10 minutes to allow formation of transfection complexes. The transfection complexes were then added drop-wise onto the cells and mixed by swirling the plate. Cells were incubated under normal growth conditions for a further 6 hours before the addition of 400µl culture medium containing serum and antibiotics. Cells were then returned to the incubator until analysis of transfection efficiency at 24 hours post transfection. Further culture medium was added as required. Positive control siRNA, negative control siRNA, mock transfected (transfection reagent without siRNA) and untransfected controls were included in all experiments.

2.12 Flow Cytometry

The uptake of siRNA into cells was monitored by observation of Alexa Fluor 488 fluorescence after transfection with Alexa Fluor 488 labelled negative control siRNA (Qiagen, UK). The percentage of cells transfected with siRNA from the total cell population (transfection efficiency) was determined at 24 hours post transfection. Transfection was carried out as described in section 2.11, then aliquots of cell samples removed and analysed. Cells were washed twice with PBS, then resuspended in 500µl PBS and run immediately using a BD FacsCalibur flow cytometer with BD CellQuest software used for acquisition (BD Biosciences, UK). Dot blots were created with x set to forward scatter (corresponding to cell size) and y set to side scatter (corresponding to cell granularity), with a gate then applied to include the cell population of interest (all viable cells). Histogram plots were also created with the acquisition parameter being FL1 fluorescence. Samples were run and set to acquire a minimum of 5000 events per sample, dependent on the cell line. Data was analysed using WinMDI version 2.8. Percent positive cells for fluorescence compared with mock transfected controls gave percentage uptake of siRNA, ie. transfection efficiency.

2.13 Real Time Reverse Transcription Polymerase Chain Reaction (RT-PCR)

All reagents for real time reverse transcription polymerase chain reaction (RT-PCR) were obtained from Applied Biosystems, UK. TaqMan Fast Cells-to-CT Kit was used to prepare samples for use in real time RT-PCR according to manufacturer's protocol. Pilot experiments were carried out using the TaqMan Fast Cells-to-CT Kit in conjunction with the TaqMan Cells-to-CT Control Kit in order to optimise the procedure and determine the cell number to be used for each cell line. One x 10^5 cells were washed twice with cold PBS before being incubated with Lysis Solution (containing reagents to inactivate endogenous RNases and DNase I to degrade genomic DNA) at room temperature for 5 minutes. After this time Stop Solution was added to inactivate the lysis reagents. Lysates were then reverse

transcribed to cDNA using RT Enzyme Mix and buffer and run in a thermal cycler (37°C for 60 minutes, then 95°C for 5 minutes to inactivate the RT). Minus RT controls were included to demonstrate that the template for PCR was cDNA, not genomic DNA. Completed RT reactions were either used immediately or stored at -20°C until use.

The cDNA was amplified by fast-cycling real time PCR using Taqman Fast Universal PCR Master Mix and Taqman Gene Expression Assay. PCR Cocktail was added to cDNA samples and run in an Applied Biosystems 7900HD real time PCR instrument using fast settings (enzyme activation at 95°C for 20 seconds, PCR at 95°C for 1 second then 60°C for 20 seconds x 40 cycles). Gene expression assays were used for the target genes GRP78 (Assay ID: Hs00607129_gH) and GRP94 (Assay ID: Hs00427665_g1). Assays were also used for the endogenous control gene actin (Assay ID: Hs03023880_g1) and the positive control gene MAPK1 (Assay ID: Hs00177066_m1). Non-template control samples were included for each assay to ensure that any fluorescent signal generated in the assay was not due to DNA contamination.

2.14 Colony Formation Assay

Cells were transfected as described in section 2.11. Addition of drugs to cells was made at 48 hours post transfection and cells were incubated under normal growth conditions for a further 48 hours. Medium containing drug was then removed and cells resuspended in fresh medium. Cells were counted and viability determined and 500 cells per well were plated into 12-well plates in MethoCult methylcellulose-based media (StemCell Technologies, UK) according to the manufacturer's instructions. All plates contained wells with water only in order to maintain humidity and prevent the methylcellulose from drying out. The cells were then incubated under normal growth conditions and allowed to form colonies for 10 to 14 days. Each drug treated sample was grown in duplicate and each

experiment was performed on two separate occasions. Colonies were visualised for counting using an inverted microscope fitted with a camera. For each well, photographs were taken with the well viewed under 10x magnification from three different (randomly chosen) areas of the well.

2.15 Statistical Analysis

Statistical analysis was performed using Microsoft Excel software, Microsoft Corporation, USA. The data obtained from drug treatment experiments was used to determine mean and standard deviation values for each drug concentration. These values were then used for graphical representation and subsequent statistical analysis. Data was assumed to be normally distributed and parametric tests were therefore used throughout. Pairs were analysed using t-test and a p value of less than 0.05 was considered to be statistically significant. A random sample of results from paired t-test obtained using Microsoft Excel were confirmed using the statistical package GraphPad InStat (GraphPad Software, San Diego, USA) to ensure accuracy.

2.16 Drug Combination Analysis

The effect of two drugs used in combination was calculated using the fractional product method described by Webb (Webb, 1963) in order to determine if the combination effect was additive, supra additive, or antagonistic. The fractional product method calculates the expected effect of a combination of two drugs according to the formula:

$$Fu_{drug1,drug2} = Fu_{drug1} \times Fu_{drug2}$$

where Fu is the fraction of cells unaffected following drug treatment.

The ratio of the observed effect to the expected effect provides a measure of the interaction of two drugs used in a combination. If the ratio of the combination effect is 1 (i.e. the observed effect equals the expected effect), the combination is designated additive. If the ratio is less than 1 (i.e. the observed effect is greater than the expected effect), then the combination is considered to be supra-additive or synergistic. If the ratio is more than 1 (i.e. the observed effect is less than the expected effect), then the combination is said to be antagonistic.

3. Basal Expression of Unfolded Protein Response Proteins in a Panel of Haematological Cell Lines

3.1 Introduction

The UPR in solid tumours has been the focus of considerable research in recent years, however less is known about the role of the UPR in haematological malignancies. The focus of this thesis is the involvement of the UPR in the chemosensitivity of haematological malignancies, however, it is necessary to first understand the basal activity of the UPR in these cells. As discussed in chapter 1, the UPR is a physiological mechanism that exists to protect organisms by maintaining protein homeostasis and preventing damage caused by unfolded or aggregated proteins. This is initially a survival response, however if the damage to a cell becomes too severe then programmed cell death results in order to protect the organism as a whole. Protein misfolding or aggregation has been shown to be involved in a number of diseases, including diabetes, neurodegenerative diseases and cancer (Schroder and Kaufman, 2005b). The importance of the UPR in mediating the response to cytotoxic drug treatments (particularly for solid tumours) has been discussed in chapter 1, however the basal UPR in haematological malignancies has not been described. For this reason, this chapter is concerned with determining the basal UPR activation status of a panel of haematological malignancy cell lines and establishing their sensitivity to treatment with a number of conventional and novel anticancer agents.

The three pathways of the mammalian UPR (PERK, IRE1 and ATF6) have been discussed in detail in Chapter 1. Under normal physiological conditions the ER molecular chaperone GRP78 is bound to the three ER transmembrane stress sensors PERK, IRE1, and ATF6 thereby keeping them in an inactive form. During ER stress GRP78 dissociates from the receptors allowing activation of the three pathways of the UPR (Lee, 2001). The UPR

has a number of protective functions within a cell. It acts to increase the folding capacity of the ER, reduce protein translation, increase the amount of ER within the cell, and promote degradation of misfolded proteins via ERAD pathways. It is thought that these UPR functions are particularly relevant in the normal physiology of highly secretory cells, such as plasma cells, intestinal epithelial cells and pancreatic β cells where there is an increased ER workload (Kim *et al.*, 2008, Bernales *et al.*, 2006). In situations where ER stress is prolonged, or the UPR is unable to restore normal ER function, the UPR initiates apoptosis (Bernales *et al.*, 2006).

In order to further understand the significance of the basal physiological UPR in haematological cancer cells, the role of the UPR in unstressed cells should first be considered. Unstressed (healthy) cells also experience some degree of ER stress and subsequent UPR activation, which is thought to adjust the folding capacity of the ER and regulate ER protein load in the manner classically attributed to the UPR and described above (Schroder and Kaufman, 2005b). However, this physiological UPR has more recently been suggested to play other roles within healthy cells, such as control of nutrient sensing and differentiation mechanisms (Kaufman *et al.*, 2002, Wellen and Thompson, 2010).

In this chapter the basal status of a number of UPR markers were studied in order to establish the extent of the basal physiological UPR in a panel of haematological cancer cell lines. As well as investigating basal protein expression of the three UPR receptors, other markers of the UPR were studied, such as the key ER molecular chaperones GRP78 and GRP94. Based on the results of these initial western blotting experiments, cell lines representative of the basal expression of the UPR markers studied were selected for further study. Prior to moving on to investigate the effect of chemotherapeutic agents commonly used in these cancer types on the UPR, it was necessary to establish the activity of these drugs in the panel of cell lines being studied. Therefore, cytotoxicity experiments were carried out to discover the effect of drug treatment on cell viability and cell proliferation in

these cell lines, and if there was any correlation between chemosensitivity and basal UPR status.

A number of both conventional and novel chemotherapy agents were used in these experiments. Conventional cytotoxic agents used were doxorubicin, cyclophosphamide, melphalan, cytarabine and etoposide. Novel agents used were the proteasome inhibitor bortezomib and the HSP90 inhibitor KW-2478. Two agents known to pharmacologically induce the UPR, tunicamycin and thapsigargin, were also studied in all cell lines in the panel.

Tunicamycin is an inhibitor of N-linked glycosylation that prevents glycosylation of newly synthesised proteins leading to accumulation of proteins in the ER and subsequent ER stress (Heifetz *et al.*, 1979). The activity of tunicamycin has been described in detail in chapter 1.2.5.

Thapsigargin is an inhibitor of sarcoplasmic endoplasmic reticulum calcium ATPases (known as SERCA pumps). This inhibition leads to release of intracellular calcium, resulting in ER stress (Kijima *et al.*, 1991). Thapsigargin is discussed in more detail in chapter 1.2.5.

The first in class proteasome inhibitor bortezomib (Velcade®, Millenium Pharmaceuticals) is currently licensed in the UK for treatment of multiple myeloma. Bortezomib and proteasome inhibition have been discussed in more detail in chapter 1.2.5.

Doxorubicin is an anthracycline antibiotic used in the treatment of a large number of different cancers, including both solid tumours and haematological malignancies. It appears to act by a number of mechanisms, with the main one thought to be binding to and inhibition of the enzyme DNA topoisomerase II, thereby preventing replication (Tannock, 2005).

Both cyclophosphamide and melphalan are alkylating agents (derived from nitrogen mustard). Cyclophosphamide is used to treat many different types of cancer, including haematological malignancies, while melphalan is predominantly used in the treatment of multiple myeloma. They act by directly binding to DNA and forming crosslinks, which prevent cellular DNA replication. The parent drug cyclophosphamide is an inert prodrug and is metabolised in the liver to the active form 4-hydroxycyclophosphamide (4-HC). Cyclophosphamide and melphalan can be clinically administered both orally and intravenously (Tannock, 2005).

Cytarabine (cytosine arabinoside) is an antimetabolite drug used in the treatment of haematological malignancies, particularly leukaemias. Cytarabine binds to the enzyme DNA polymerase and results in arrest of cells in the S-phase of the cell cycle (those actively undergoing DNA synthesis) (Tannock, 2005).

Etoposide is a semi-synthetic plant alkaloid agent (epipodophyllotoxin) and topoisomerase II inhibitor. It is used in the treatment of a number of cancers, such as breast cancer and leukaemia (Tannock, 2005).

KW-2478 is a novel HSP90 inhibitor currently undergoing clinical trials in a number of cancers, including haematological malignancies. HSP90 inhibitors have been discussed in chapter 1.2.5. The ansamycin antibiotics geldanamycin and its derivatives (such as 17-AAG and 17-DMAG) represent the main HSP90 compounds investigated thus far, however the clinical development of these compounds has been complicated by their poor solubility and issues with hepatotoxicity (Neckers, 2002). Other compounds with differing chemical structures are now also being studied. One such compound is the novel HSP90 inhibitor KW-2478 (Kyowa Hakko Kirin, Japan). KW-2478 is a non-ansamycin, non-purine analogue class of HSP90 inhibitor. The chemical and biological activity of this compound has recently been reported, along with its activity in multiple myeloma (Nakashima *et al.*, 2010).

The results of a first in man phase I clinical trial of KW-2478, as well as results from *in vitro* studies in B-cell malignancies carried out in the Cancer Pharmacology Lab, were presented at the American Society of Haematology conference in December 2008 (Cavenagh *et al.*, 2008, Juliger *et al.*, 2008). KW-2478 was therefore included in the drug treatments being investigated for activity in this haematological cancer cell line panel.

The experiments described here provide valuable insight into areas of the UPR activated at a basal level and possible targets for modulating response to drug treatment in these haematological cancer cell lines. The activity of novel and established anticancer agents has been determined, whilst also investigating if any correlation exists between chemosensitivity and basal UPR status in these haematological cell lines. These results provide a foundation for future experiments investigating drug induced activation of the UPR, and targeting the UPR to modulate chemosensitivity.

3.2 Materials and Methods

Untreated cells in exponential growth phase were used to prepare whole cell lysates, as described in section 2.6. Basal expression of UPR proteins was then studied using western blotting (see section 2.7 for details). Equal amounts of protein (10μg or 20μg, dependent on experiment) were loaded per well for each experiment. ER molecular chaperones, as well as markers from all three branches of the unfolded protein response were studied. Three acute myeloid leukaemia (AML) cell lines, three multiple myeloma (MM) and three diffuse large B-cell lymphoma (DLBCL) cell lines were included in the initial panel studied. AML cell lines used were U937, HL-60 and THP1. MM cell lines used were RPMI-8226, U266 and MM1.S. DLBCL cell lines used were CRL-2261, SUD4 and DoHH2. The colorectal cancer cell line HT29 was used as an example of a solid tumour cell line (and was used in subsequent studies with versipelostatin). Peripheral blood mononuclear cells from two healthy donors were used as an example of healthy

haematological cells (kindly provided by Dr S Kassam, Cancer Pharmacology Lab). Ethics committee approval for the use of blood from healthy volunteers for these studies was granted by the East London and City Research Ethics Committee 1 (ELCREC).

Drug dilutions were made as described in section 2.3. Cells in exponential growth phase were plated into 96 well plates (5000 cells per well) and incubated at 37°C and 5% CO_2 in air for 24 hours before addition of drug solution. The required amount of each drug was diluted in fresh culture medium and 10 µl of this solution was added to each well in order to achieve the desired molar concentration per well. Untreated control cells had 10µl fresh medium alone added to the wells. Cells were then returned to the incubator for a further 48 hours after which time 100µl of diluted Guava ViaCount Flex Reagent was added to each well and drug activity was measured using the plate based Guava Viacount® assay (see sections 2.3 and 2.4). This assay provided total cell number and cell viability data after 48 hours incubation with drug.

HL-60 and THP1 cells were treated with doxorubicin, 4-HC (the active metabolite of cyclophosphamide), cytarabine and etoposide. RPMI-8226 and U266 cells were treated with doxorubicin, 4-HC and melphalan. DoHH2 and SUD4 cells were treated with doxorubicin and 4-HC. All cell lines were also treated with the proteasome inhibitor bortezomib and the ER stress inducing drugs tunicamycin (TM; an inhibitor of N-linked glycosylation) and thapsigargin (TG; an inhibitor of sarcoplasmic-endoplasmic reticulum calcium pumps). The AML cell lines were also treated with the novel HSP90 inhibitor KW-2478, with data for the remaining cell lines provided from a separate experiment carried out in our lab by Dr S Juliger (using the same experimental conditions).

Each drug concentration was tested in triplicate plate wells, and each experiment was carried out on three separate occasions. Mean values and standard deviations were calculated for each experiment and used in subsequent data analysis. Non-linear regression

using a sigmoidal concentration-effect curve was carried out and EC_{50}, EC_{25} and EC_5 values were calculated from these results using GraphPad Prism software (see section 2.5). Whilst cell number data was also available from these experiments, the effect of drug on cell viability was considered the most important in the context of cancer chemotherapy; therefore EC_{25} and EC_5 values for cell viability were calculated for use in further experiments.

3.3 Results

Western immunoblotting experiments were carried out in order to ascertain the basal expression of various UPR proteins in a panel of ten haematological cancer cell lines. The results of these western blotting experiments are shown in figure 3.1. This experiment was repeated for low expression proteins, loading 20μg per sample (shown in figure 3.2).

These experiments have revealed a number of differences in UPR protein expression both between, and within, the three haematological tumour types.

The MM cell lines all show higher expression of IRE1 receptor than the other tumour types. The AML cell lines do express IRE1, albeit to a lesser extent, however IRE1 receptor expression was completely absent in the lymphoma cell lines CRL-2261, SUD4 and DOHH2.

The MM cell lines also exhibited the highest expression of the molecular chaperone GRP94, followed by the AML cell lines, then the lymphoma cell lines SUD4 and DHL4. The lymphoma cell lines CRL-2261 and DOHH2 showed considerably lower expression of GRP94 compared with all other cell lines studied.

The AML cell lines U937 and HL-60 were found to have lower levels of PERK receptor than the other cell lines.

The 50kDa isoform of ATF6, only present during ER stress, was visible in all cell lines, but more prominent in some of the AML and MM lines. The 90kDa isoform of ATF6, corresponding to the membrane bound form of the protein, was also present in all cell lines, though at a lower level.

All cell lines expressed the molecular chaperone GRP78. ATF4 protein was expressed in all cell lines to a similar degree. Expression of eIF2α was seen in all cell lines, with the phosphorylated eIF2α protein seen as a very faint band present in all cell lines.

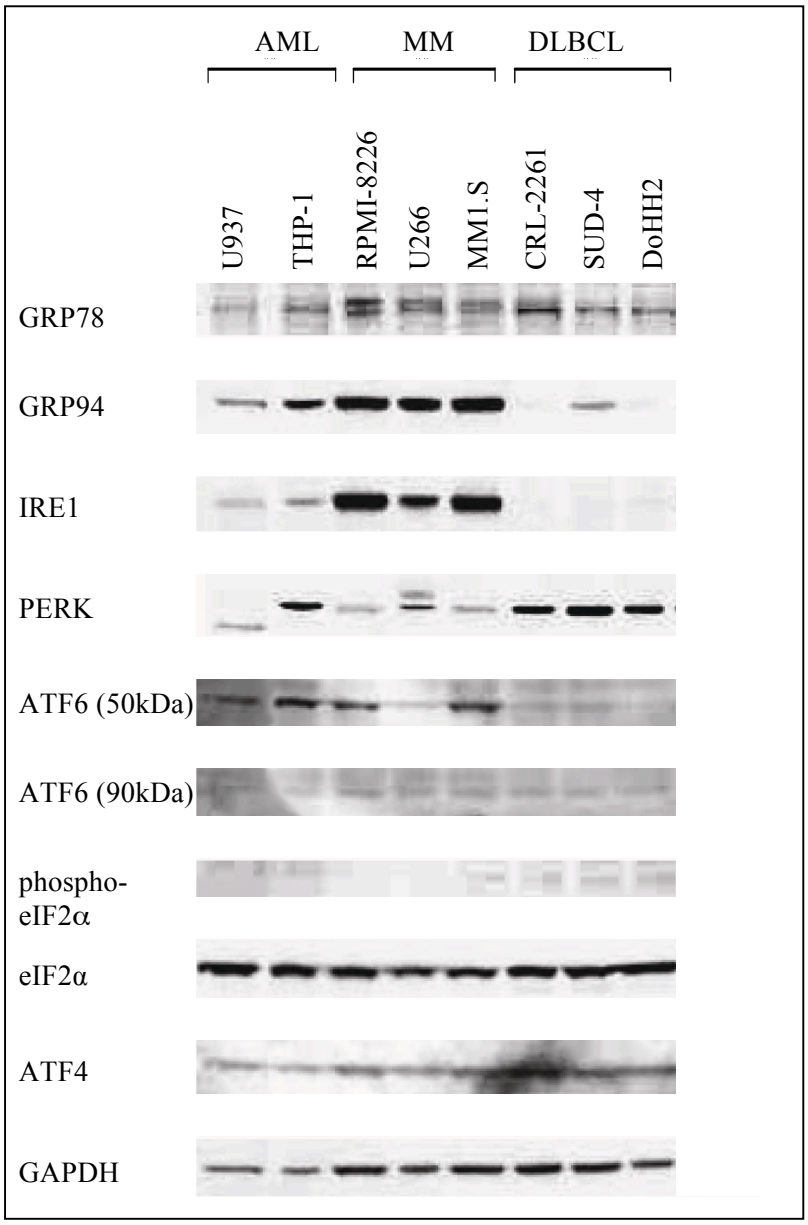

Figure 3.1. Western blotting experiments to show basal expression of UPR markers in a panel of haematological cancer cell lines. GAPDH included as a loading control. 10μg of protein loaded.

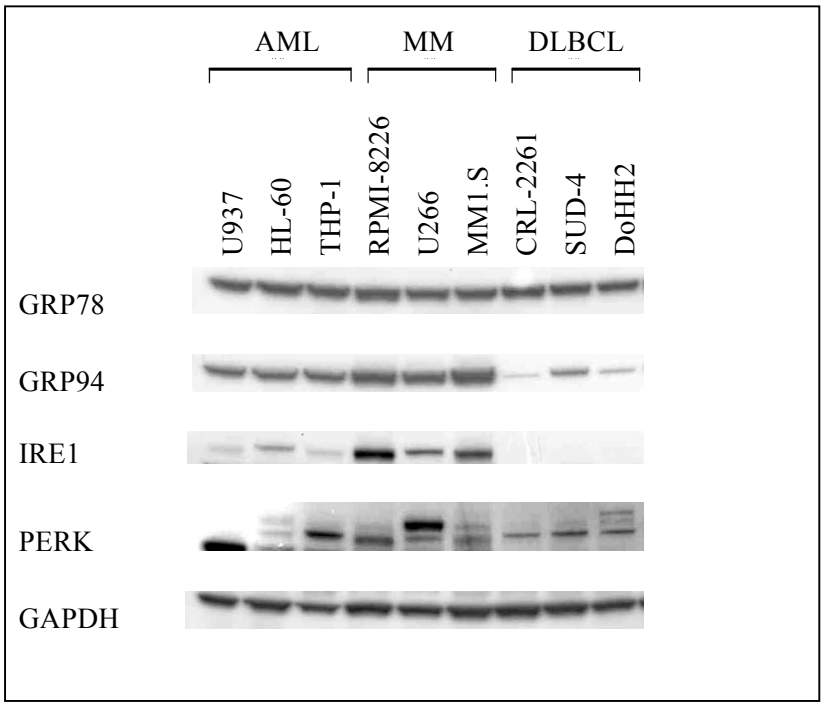

Figure 3.2. Western blotting experiments to show basal expression of UPR markers in a panel of haematological cancer cell lines. GAPDH included as a loading control. 20μg of protein loaded.

Further basal UPR experiments were conducted with the 9 cell line haematological cancer cell line panel, plus the colorectal cancer cell line HT-29 and two samples of peripheral blood mononuclear cells (PBMC) from healthy donors.

The cancer cell lines typically showed increased expression of the molecular chaperone GRP78 compared with the two PBMC samples.

As reported earlier, the AML and MM cell lines showed increased expression of the molecular chaperone GRP94 compared with the lymphoma cell lines. Interestingly, it was found that the level of GRP94 expression in the two PBMC samples was similar to that of the higher expressing AML and MM lines. The solid tumour cell line HT-29 also showed clear GRP78 and GRP94 expression.

Three levels of IRE1 receptor expression were seen in the panel studied. IRE1 was highly expressed in the MM cell lines. AML cell lines, HT-29 and the PBMC samples expressed IRE1 at a low level. IRE1 receptor expression was not seen in the lymphoma cell lines.

PERK receptor was expressed in all the cancer cell lines, with higher expression seen in U266 and DOHH2 cell lines. PERK receptor expression was not seen in the PBMC samples.

The 90kDa isoform of ATF6 was expressed in all cell lines, with a higher level in the PBMC samples and HT-29. The 50kDa cleaved form of ATF6 was also observed in all cancer cell lines, with higher levels in U266, CRL and SUD4 cells. The 50 kDa cleaved form was not observed in the two PBMC samples.

A faint band for phosphorylated eIF2α was seen in all cell lines, with total eIF2α protein expressed in all cancer cell lines. By comparison, total and phosphorylated eIF2α were very low in the two PBMC samples.

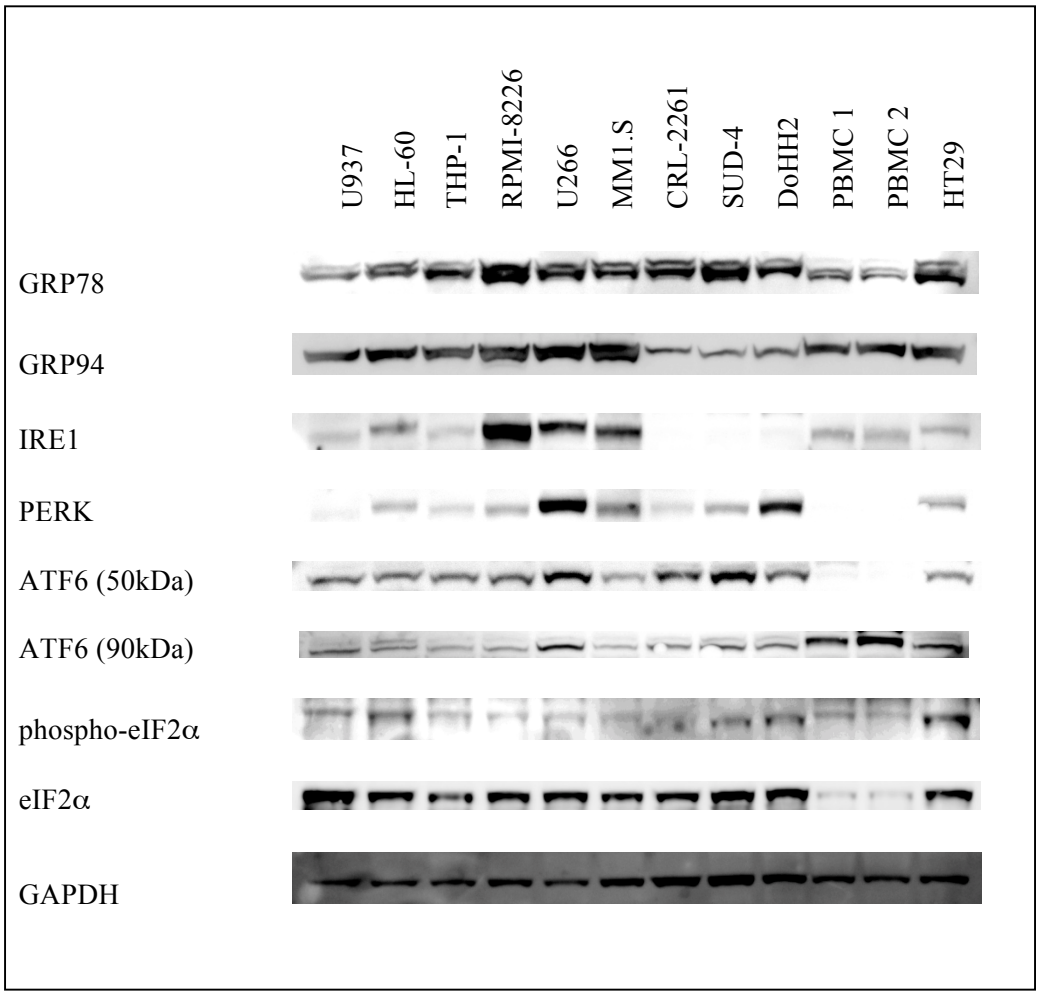

Figure 3.3. Western blotting experiments to show basal expression of UPR markers in a panel of haematological cancer cell lines. GAPDH included as a loading control. Two peripheral blood mononuclear cell (PBMC) samples were included as an example of healthy haematological cells. The colorectal cancer cell line HT29 was included as an example of a solid tumour cell line.

The next experiments in this chapter were conducted in order to establish the activity of a number of conventional and novel anticancer agents in the cell line panel. Tables 3.1 and 3.2 show the results obtained for a single drug (doxorubicin) in a single cell line (HL-60) and illustrated in figure 3.4. This was done for all drugs in each cell line (data tables are shown in appendix 1). The concentration effect plots obtained for the effect of drug on cell number and viability are shown in figures 3.5 to 3.13. The EC_{50} values for cell number and cell viability are also shown, along with EC_5 and EC_{25} values for cell viability.

Cell line	Conc.	Cell no. (% of control)			Average	SD
		Set 1	Set 2	Set 3		
HL-60	**0**	100.0	100.0	100.0	**100.0**	**0.0**
HL-60	**1nM**	83.7	88.3	85.8	**85.9**	**2.3**
HL-60	**10nM**	79.5	81.4	76.5	**79.1**	**2.5**
HL-60	**100nM**	47.2	34.7	41.2	**41.0**	**6.3**
HL-60	**300nM**	45.2	37.0	38.8	**40.3**	**4.3**
HL-60	**1µM**	42.7	34.1	33.7	**36.8**	**5.1**

Table 3.1. Effect of treatment with increasing concentrations of doxorubicin for 48 hours on cell number in the AML cell line HL60

Cell line	Conc.	Cell viability (%)			Average	SD
		Set 1	Set 2	Set 3		
HL-60	**0**	94.0	90.2	85.6	**89.9**	**4.2**
HL-60	**1nM**	80.1	86.3	89.9	**85.4**	**5.0**
HL-60	**10nM**	86.4	85.0	91.2	**87.5**	**3.3**
HL-60	**100nM**	77.0	72.1	67.6	**72.2**	**4.7**
HL-60	**300nM**	11.1	24.6	32.7	**22.8**	**10.9**
HL-60	**1µM**	0.0	8.6	0.0	**2.9**	**5.0**

Table 3.2. Effect of treatment with increasing concentrations of doxorubicin for 48 hours on cell viability in the AML cell line HL60

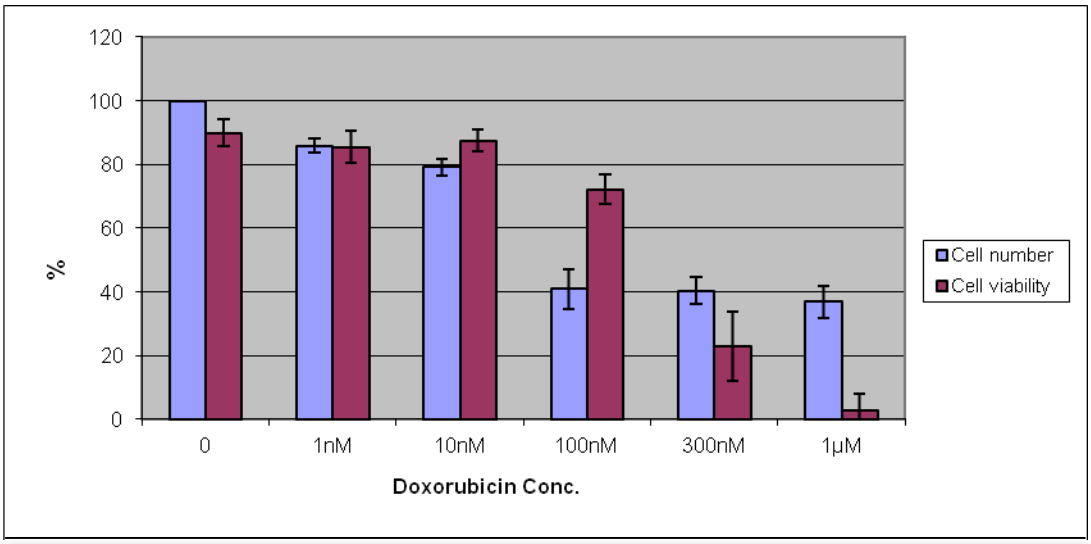

Figure 3.4. Effect of treatment with increasing concentrations of doxorubicin for 48 hours on cell number and viability in the AML cell line HL60. Error bars show mean ± standard deviation (SD)

A

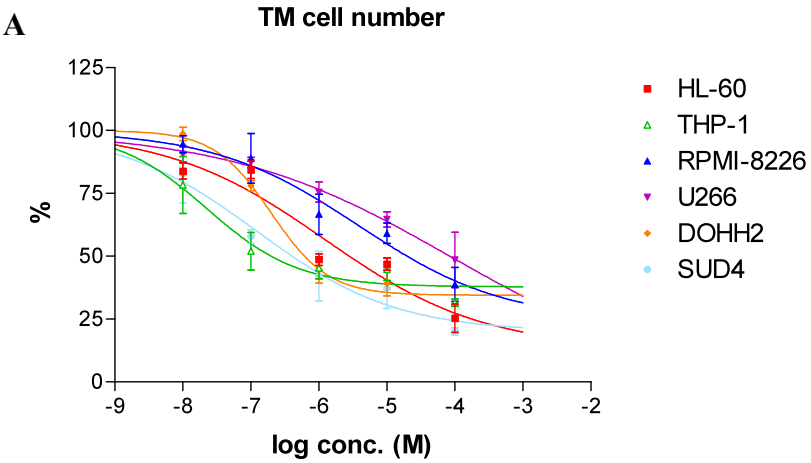

B

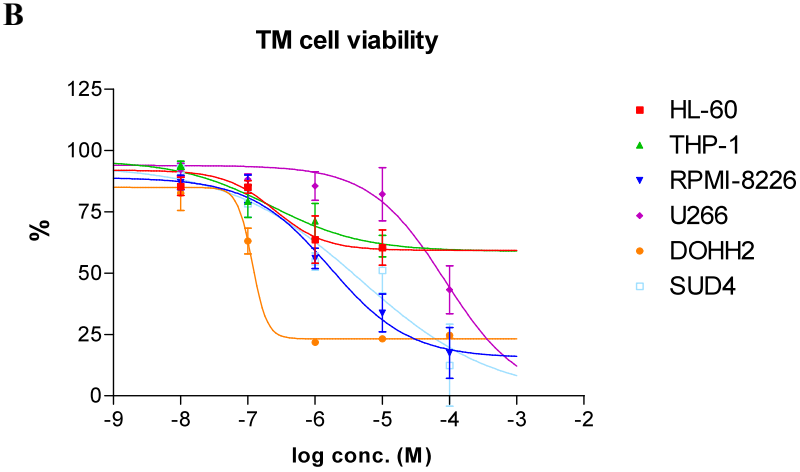

C

Drug	Cell line	EC_{50} cell number	EC_{50} cell viability	EC_{25} cell viability	EC_5 cell viability
TM	HL-60	1.2µM	251.8nM	97.9nM	20.0nM
	THP-1	22.6nM	220.9nM	38.8nM	2.1nM
	RPMI8226	3.9µM	1.7µM	378.5nM	31.1nM
	U266	84.1µM	85.8µM	20.8µM	1.9µM
	DOHH2	198.4nM	116.4nM	88.2nM	55.4nM
	SUD4	122.6nM	4.9µM	399.9nM	6.0nM

Figure 3.5. Effect of tunicamycin (TM) treatment on cell number and viability of six haematological cancer cell lines. **A** – Total cell number against log TM concentration (error bars show mean ± SD). **B** - Viable cell number against log TM concentration (error bars show mean ± SD). **C** - EC_{50} (cell number and viability), EC_{25} and EC_5 (cell viability) values calculated from GraphPad Prism fitted parameters.

A

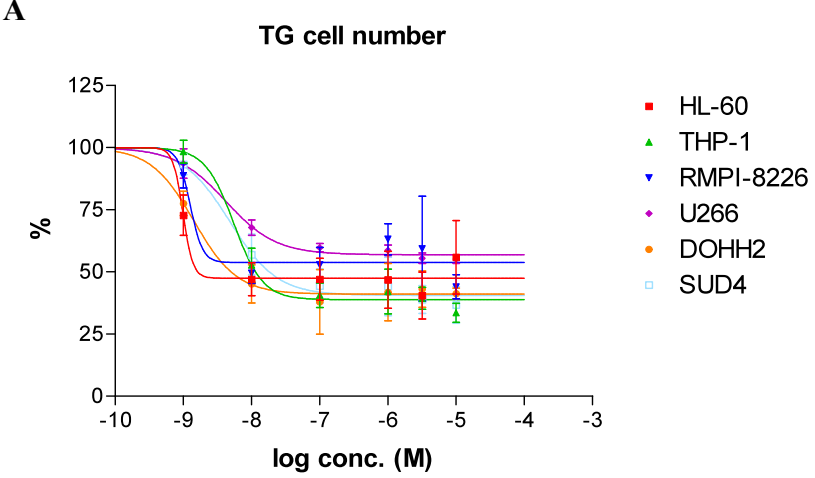

B

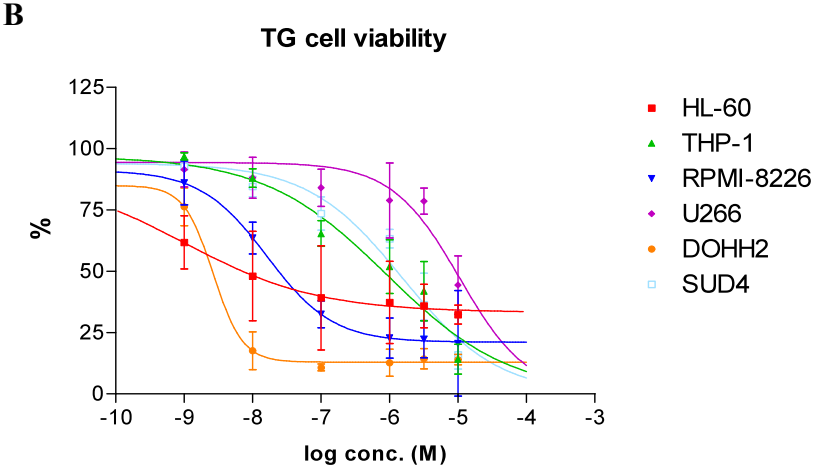

C

Drug	Cell line	EC_{50} cell number	EC_{50} cell viability	EC_{25} cell viability	EC_5 cell viability
TG	HL-60	0.8nM	2.1nM	0.1nM	0.001nM
	THP-1	7.7nM	947.0nM	94.8nM	1.1nM
	RPMI8226	1.2nM	15.3nM	4.8nM	0.6nM
	U266	4.2nM	28.7µM	3.0µM	364.0nM
	DOHH2	1.3nM	3.1nM	1.6nM	0.6nM
	SUD4	4.9nM	1.6µM	272.5nM	14.3nM

Figure 3.6. Effect of thapsigargin (TG) treatment on cell number and viability of six haematological cancer cell lines. **A** - Total cell number against log TG concentration (error bars show mean ± SD). **B** - Viable cell number against log TG concentration (error bars show mean ± SD). **C** - EC_{50} (cell number and viability), EC_{25} and EC_5 (cell viability) values

A

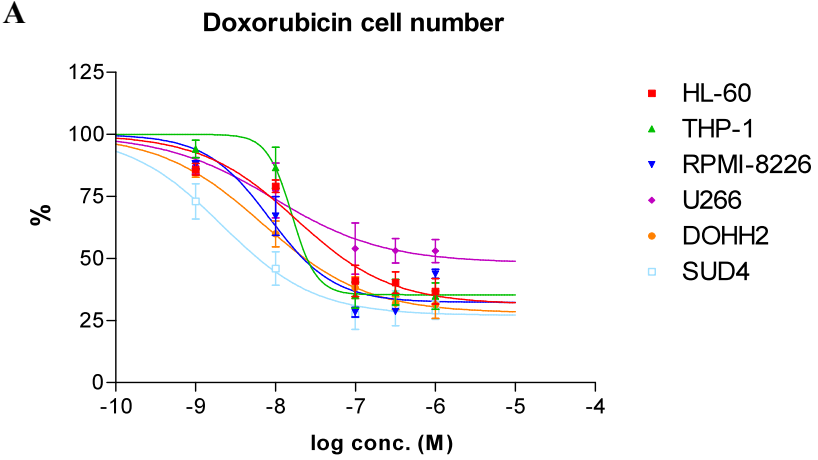

B

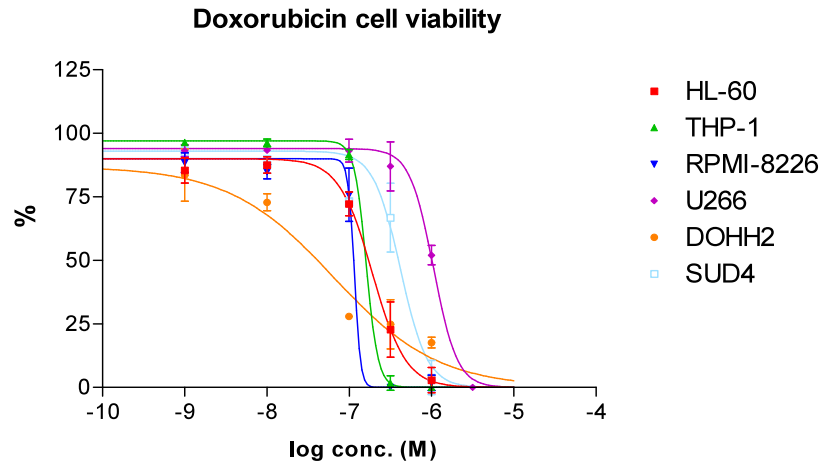

C

Drug	Cell line	EC_{50} cell number	EC_{50} cell viability	EC_{25} cell viability	EC_5 cell viability
Doxorubicin	HL-60	16.5nM	176.2nM	114.6nM	48.4nM
	THP-1	14.0nM	158.0nM	134.0nM	98.3nM
	RPMI8226	4.6nM	115.3nM	105.0nM	89.6nM
	U266	9.6nM	1.1µM	736.0nM	399.2nM
	DOHH2	5.7nM	51.5nM	12.8nM	0.9nM
	SUD4	2.3nM	422.3nM	277.7nM	138.2nM

Figure 3.7. Effect of doxorubicin treatment on cell number and viability of six haematological cancer cell lines. **A** - Total cell number against log doxorubicin concentration (error bars show mean ± SD). **B** - Viable cell number against log doxorubicin concentration (error bars show mean ± SD). **C** - EC_{50} (cell number and viability), EC_{25} and EC_5 (cell viability) values

A

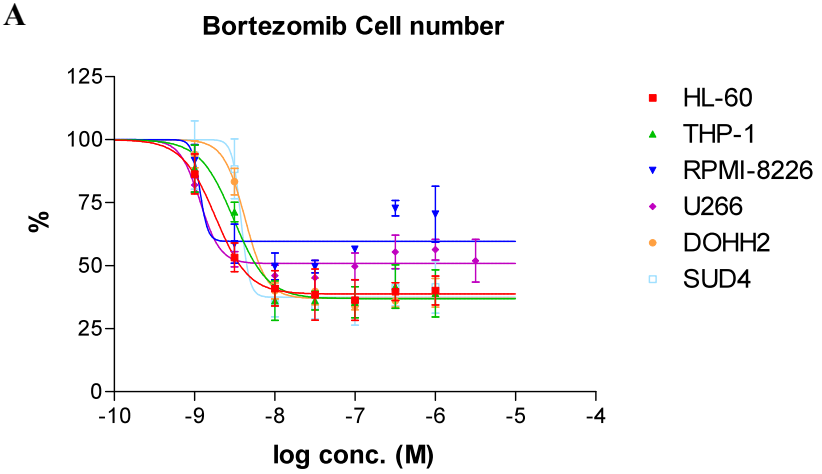

B

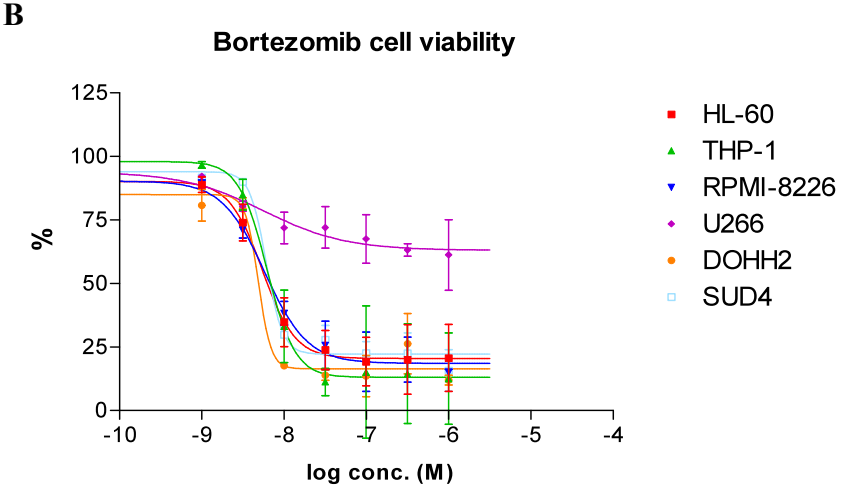

C

Drug	Cell line	EC_{50} cell number	EC_{50} cell viability	EC_{25} cell viability	EC_5 cell viability
Bortezomib	HL-60	1.8nM	5.5nM	3.3nM	1.4nM
	THP-1	3.1nM	6.2nM	4.1nM	2.0nM
	RPMI8226	1.2nM	6.1nM	3.0nM	1.0nM
	U266	1.2nM	6.0nM	1.6nM	0.2nM
	DOHH2	4.3nM	4.7nM	4.0nM	2.9nM
	SUD4	3.9nM	6.1nM	4.7nM	3.1nM

Figure 3.8. Effect of bortezomib treatment on cell number and viability of six haematological cancer cell lines. **A** - Total cell number against log bortezomib concentration (error bars show mean ± SD). **B** - Viable cell number against log bortezomib concentration (error bars show mean ± SD). **C** - EC_{50} (cell number and viability), EC_{25} and EC_5 (cell viability) values

A

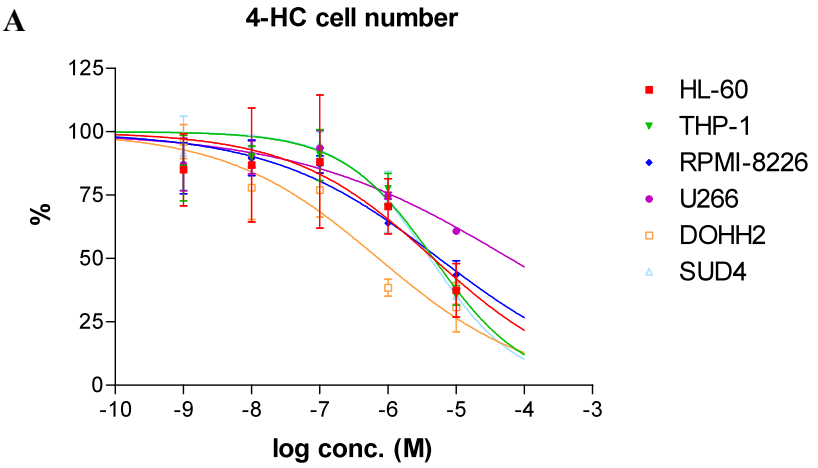

B

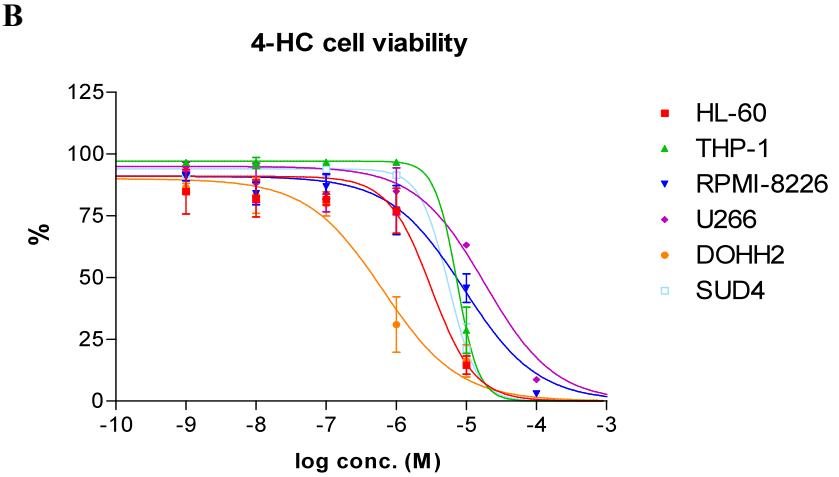

C

Drug	Cell line	EC_{50} cell number	EC_{50} cell viability	EC_{25} cell viability	EC_5 cell viability
4-HC	HL-60	3.2µM	5.4µM	1.5µM	393.6nM
	THP-1	2.7µM	7.2µM	4.9µM	2.5µM
	RPMI8226	1.4µM	12.4µM	2.4µM	257.9nM
	U266	1.1µM	18.4µM	5.2µM	635.4nM
	DOHH2	276.4nM	594.1nM	163.7nM	16.5nM
	SUD4	1.7µM	11.0µM	3.3µM	1.4µM

Figure 3.9. Effect of 4-hydroperoxycyclophosphamide (4-HC) treatment on cell number and viability of six haematological cancer cell lines. **A** - Total cell number against log 4-HC concentration (error bars show mean ± SD). **B** - Viable cell number against log 4-HC concentration (error bars show mean ± SD). **C** - EC_{50} (cell number and viability), EC_{25} and EC_5 (cell viability) values

A

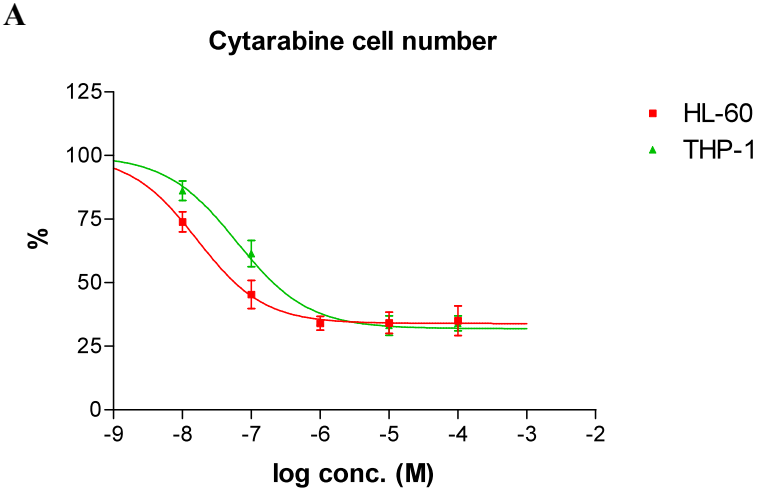

B

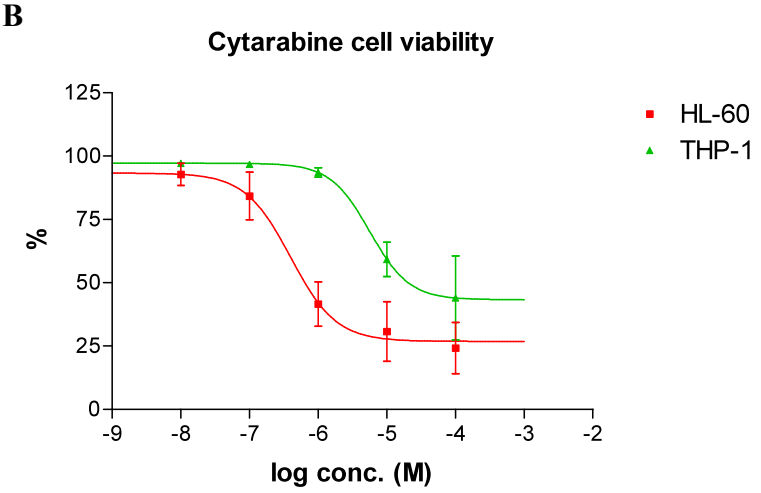

C

Drug	Cell line	EC_{50} cell number	EC_{50} cell viability	EC_{25} cell viability	EC_5 cell viability
Cytarabine	HL-60	16.3nM	396.9nM	171.9nM	42.1nM
	THP-1	62nM	5.6µM	2.7µM	801.1nM

Figure 3.10. Effect of cytarabine treatment on cell number and viability of AML cell lines. **A** - Total cell number against log cytarabine concentration (error bars show mean ± SD). **B** - Viable cell number against log cytarabine concentration (error bars show mean ± SD). **C** - EC_{50} (cell number and viability), EC_{25} and EC_5 (cell viability) values

A

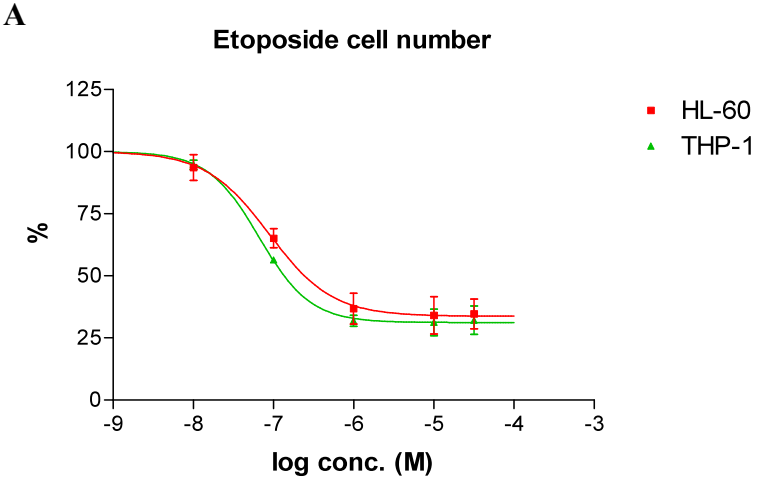

B

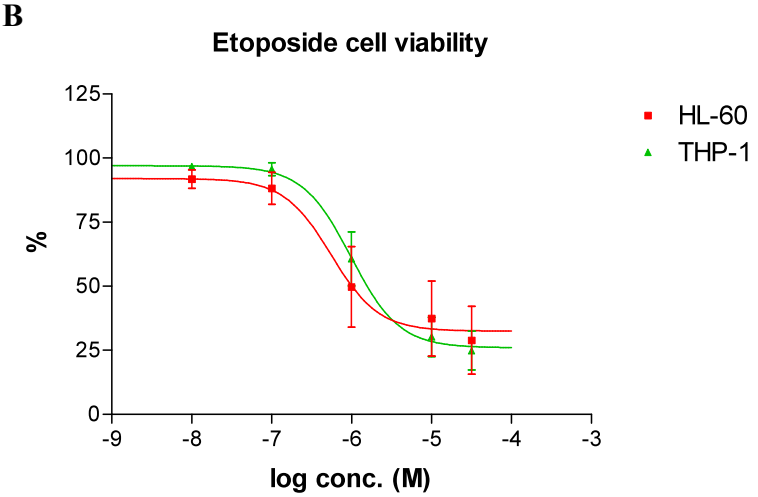

C

Drug	Cell line	EC_{50} cell number	EC_{50} cell viability	EC_{25} cell viability	EC_5 cell viability
Etoposide	HL-60	88.2nM	555.8nM	262.4nM	74.3nM
	THP-1	66.1nM	982.2nM	457.3nM	126.7nM

Figure 3.11. Effect of etoposide treatment on cell number and viability of AML cell lines. **A** - Total cell number against log etoposide concentration (error bars show mean ± SD). **B** - Viable cell number against log etoposide concentration (error bars show mean ± SD). **C** - EC_{50} (cell number and viability), EC_{25} and EC_5 (cell viability) values

A

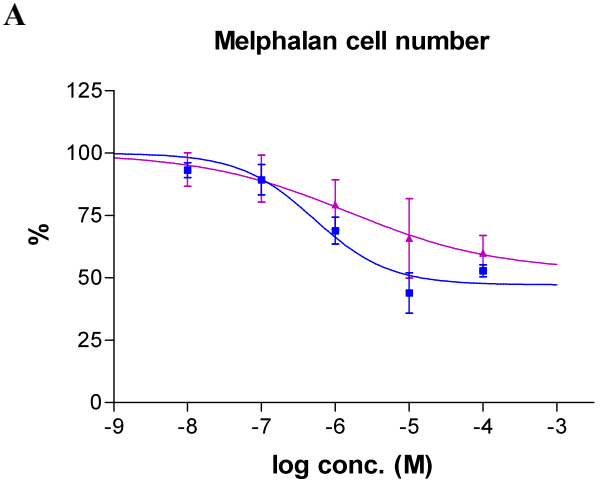

B

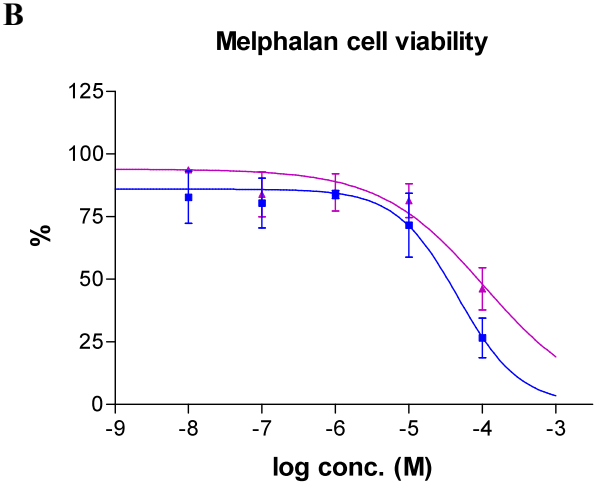

C

Drug	Cell line	EC_{50} cell number	EC_{50} cell viability	EC_{25} cell viability	EC_5 cell viability
Melphalan	RPMI8226	515.1nM	46.2µM	15.9µM	2.6µM
	U266	1.5µM	107.4µM	18.0µM	888.5nM

Figure 3.12. Effect of melphalan treatment on cell number and viability of MM cell lines. **A** - Total cell number against log melphalan concentration (error bars show mean ± SD). **B** - Viable cell number against log melphalan concentration (error bars show mean ± SD). **C** - EC_{50} (cell number and viability), EC_{25} and EC_5 (cell viability) values

A

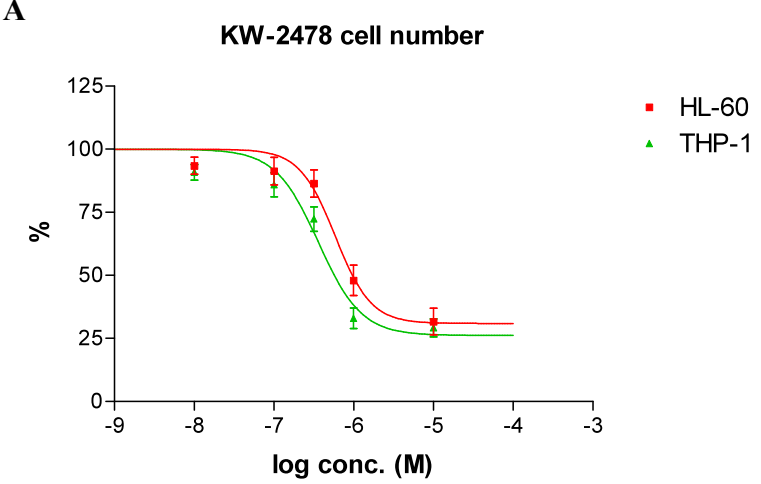

B

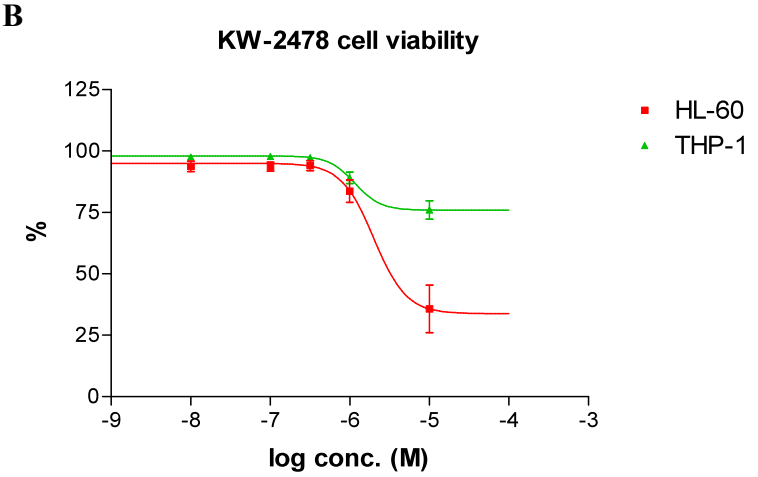

C

Drug	Cell line	EC_{50} cell number	EC_{50} cell viability	EC_{25} cell viability	EC_5 cell viability
KW-2478	HL-60	588.9nM	2.0µM	1.2µM	504.4nM
	THP-1	361.1nM	1.2µM	768.6nM	387.1nM
	RPMI8226*	250.0nM	145.0nM	30.0nM	2.1nM
	U266*	257.0nM	473.0nM	330.6nM	118.5nM
	DOHH2*	251.0nM	350.0nM	175.3nM	54.7nM
	SUD4*	101.0nM	94.1nM	33.0nM	5.7nM

Figure 3.13. Effect of KW-2478 treatment on cell number and viability of AML cell lines. **A** - Total cell number against log KW-2478 concentration (error bars show mean ± SD). **B** - Viable cell number against log KW-2478 concentration (error bars show mean ± SD). **C** - EC_{50} (cell number and viability), EC_{25} and EC_5 (cell viability) values.
* Values calculated from a separate experiment carried out within our lab by Dr S Juliger

The individual cell lines showed differing sensitivities to the drugs studied. The widest range in drug effect was seen when the cells were treated with the two ER stress inducing drugs. Large differences in sensitivity were seen between cell lines, for example, the EC_{50} values for thapsigargin effect on cell viability range from approximately 1nM to 10μM (see figure 3.6). This large difference in sensitivity was seen both within the same tumour type and between tumour types. The DOHH2 cell line proved to be most sensitive cell line to ER stress induction with both tunicamycin and thapsigargin in the panel tested. Whilst the effect of tunicamycin on cell proliferation followed the same pattern in all six cell lines, the effect on viability did not follow the same pattern. In the two AML cell lines viability decreased in a concentration dependent manner initially, however the effect then plateaued just above 60% cell viability.

The conventional cytotoxic agents doxorubicin, 4-HC, cytarabine, etoposide and melphalan all decreased cell proliferation and viability, as would be expected. There were, however, a number of differences in sensitivity to the drugs in the cell line panel studied. The U266 cell line was less sensitive to treatment with doxorubicin in terms of effect on cell viability. DOHH2 cells proved considerably more sensitive to the effect of doxorubicin on cell viability than the other cell lines, whilst the SUD4 cell line was the most sensitive to the anti-proliferative effect of doxorubicin. The DOHH2 cell line also proved to be the most sensitive cell line to treatment with 4-HC. The THP1 cell line was less sensitive to the effect of cytarabine than the HL-60 cell line, however both showed very similar sensitivity to etoposide.

The U266 cell line was less sensitive to treatment with bortezomib and doxorubicin in terms of the effect on cell viability, although sensitivity to melphalan was comparable to that of the other myeloma cell line studied RPMI-8226.

The HSP90 inhibitor KW-2478 inhibited cell proliferation as expected in both AML cell lines, however it did not show a marked effect on the viability of THP-1 cell line, with viability remaining above 75% for the concentration range studied.

3.4 Discussion

The expression of UPR proteins in untreated cells was investigated, using a limited antibody panel, in order to provide an indication of the basal level of UPR activation across the panel of haematological cancer cell lines. The aim of these initial experiments was to establish the full spectrum of UPR activation in the cell line panel. This in turn would allow the selection of representative cell lines for further detailed study.

The first set of experiments, as seen in figure 3.1, provided a number of interesting findings. Whilst all cell lines in the panel exhibited GRP78 protein expression to a similar extent, there were considerable differences in the expression of GRP94 protein. This pattern of GRP94 protein expression mirrored the expression of IRE1 protein seen in the cell line panel, suggesting a potential link between the two. It is thought that IRE1 activity and subsequent spliced XBP1 activity is of particular importance in highly secretory cells (Gass *et al.*, 2004, Kaser *et al.*, 2008), such as myeloma cells. The results observed here also suggest that GRP94 is of increased importance in myeloma cells (and potentially other types of secretory cells). Multiple myeloma cell lines showed the highest expression of both IRE1 receptor and GRP94 proteins, followed by AML cell lines, with the lowest expression in the lymphoma cell lines. These results were confirmed by the further experiments shown in figure 3.2. Another interesting result seen was the level of activated (cleaved) ATF6 protein in the AML and MM cell lines. This result is of note as it shows a degree of basal activation of the ATF6 branch of the UPR in these cell lines. The results in figure 3.1 show that PERK receptor protein expression is higher in the lymphoma cell lines, compared to the other tumour types, suggesting a potential importance of the PERK branch of the UPR in

lymphoma. However, when a larger amount of protein was loaded (see figure 3.2), this pattern was less clear.

The next set of experiments went on to look at the haematological malignancy cell line panel whilst also including a solid tumour sample and two PBMC samples for comparison purposes. The colorectal cancer cell line HT-29 was chosen as it is a widely used and well categorised cell line for *in vitro* research purposes, and will be used in subsequent experiments. Two PBMC samples were obtained from healthy donors and included in the experiments in order to provide a reference for the basal UPR protein expression of healthy haematological cells. This was chosen to be the best approach following previous issues with the proliferation of the NC-NC normal B-cell line. Whilst it would also have been valuable to include a number of primary samples from patients with these tumour types, these samples are limited and in great demand and were therefore not available for these experiments.

As seen in figure 3.3, these experiments both confirmed and expanded upon the results of the previous experiments. They also highlighted a number of key differences in the basal expression of UPR proteins in the haematological cancer cell lines compared to the solid tumour cell line and the healthy haematological cell (PBMC) samples. Whilst all cell lines exhibited GRP78 protein expression, this expression was lower in the PBMC samples. In contrast to this, GRP94 expression was lowest in the lymphoma cell lines, whilst the PBMC samples contained increased GRP94 expression at a level similar to that seen in the other cancer cell lines. This interesting finding suggests GRP94 may be more important in the function of normal healthy cells than previously thought. Another interesting result was the expression of IRE1 receptor protein. As reported in the earlier experiments, IRE1 receptor was highly expressed in the myeloma cell lines, yet expression was undetectable under these experimental conditions in any of the lymphoma cell lines. The solid tumour cell line and PBMC samples showed expression of IRE1 protein at a lower level than the

myeloma cell lines, comparable to the expression seen in the AML cell lines. These results confirm the importance of the IRE1 receptor in myeloma cells, and suggests IRE1 is of little importance in lymphoma cell line basal UPR.

Differences were also seen in the level of ATF6 protein across the samples studied as seen in figure 3.3. The 50kDa active (cleaved) ATF6 protein was present in all the cancer cell lines, with lower levels in the solid tumour HT-29 cell line and the semi-adherent myeloma cell line MM1S. However, it was observed that the two PBMC samples did not express this activated ATF6 protein, indicative of an active UPR. As may be expected, the highest expression of full length ATF6 protein was also seen in these two samples. In line with current knowledge of the UPR, these results suggest that UPR mediated activation of ATF6 is not seen in these healthy haematological cells and that the ATF6 protein in these samples is expressed as the 90kDa membrane bound form.

In terms of PERK pathway proteins, there were also differences seen in PERK receptor protein as well as phosphorylated eIF2α (p-eIF2α) and total eIF2α (a downstream target of PERK receptor). PERK receptor protein expression was seen to some degree in all the cancer cell lines, however protein expression was undetectable under these experimental conditions in the two PBMC samples. PERK protein expression was considerably higher in the U266 myeloma cell line and the DOHH2 lymphoma cell line than in the other cancer cell lines. Similarly, phosphorylated eIF2α expression was seen at the protein level in all cancer cell lines, however it was also expressed at a low level in the PBMC samples. Total eIF2α protein was highly expressed to a similar degree in all cancer cell lines in contrast to the two PBMC samples, which had a low expression of eIF2α compared to the cancer cell lines. Again, these results highlight the clear differences seen in UPR protein expression between unstressed healthy cells and cancer cells in these experiments.

One of the key findings from these experiments of basal UPR protein expression is the difference that was observed in the basal expression of the three UPR receptors IRE1, PERK and ATF6 across the cell line panel studied. Whilst it should be noted that the IRE and PERK results are somewhat limited by the fact that they refer to total receptor protein expression and not specifically phosphorylated protein, a number of notable observations have been reported here. In some cell lines in the panel, expression of these UPR receptors was not detectable in these experiments. This is not to suggest that receptor expression is not present in these cells, but reflects that expression is present at a much lower level than the comparison cell lines in the panel, and as such longer exposure times (and increased protein load) are needed to detect expression using Western blotting. The lack of expression of PERK protein or the activated (cleaved) form of ATF6 protein in the PBMC samples indicate the lack of any basal activation of these pathways of the UPR in healthy cells. However, activation of both these pathways is seen at the protein level in all the cancer cell lines, albeit to differing extents. Another finding of note is the pattern of expression of IRE1 protein. IRE1 protein levels were highly expressed in the myeloma cell lines and expression was also seen in the AML cell lines, solid tumour cell line and both PBMC samples. However, IRE1 protein levels were undetectable in the lymphoma cell lines in these experiments, indicating a possible lack of importance of this pathway in the basal UPR of lymphoma cells. This observation suggests an interesting difference in activation of the fundamental UPR branches between tumour types that has not been reported to date.

In conjunction with the determination of basal UPR activation in these cells lines, it was also important to establish sensitivity to cytotoxic agents across the haematological cell line panel, and any relationship between the two. There are a number of established experimental methods used to investigate the cytotoxicity of a drug *in vitro*. These methods include plate based cytotoxicity assays (such as the widely used MTT assay), clonogenic assay, the study of apoptosis by other methods (such as flow cytometry or TUNEL staining), or the traditional method of trypan blue exlusion. For the experiments in this chapter it was

decided to use the plate based Guava Viacount assay as this assay offered a number of advantages over other methods available (see chapter 2.4 for assay details). This assay was microplate based which was more convenient when studying several drugs across a panel of cell lines. In addition, this assay has the advantage over other methods such as MTT that it provides individual data on both the effect of a drug on cell proliferation and the effect on cell viability. This was considered particularly useful in the study of the novel anticancer agents, where anticancer effects may be due to a cytostatic effect and not only the traditional cytotoxic action seen with conventional chemotherapy drugs.

A number of both conventional and novel chemotherapy agents were used in these experiments. Some drugs are clinically used in only one particular tumour type, for example cytarabine and etoposide in AML or melphalan treatment in myeloma, and as a result their use was also limited to that particular tumour type in these experiments. Other drugs, such as doxorubicin and cyclophosphamide have a role clinically in the treatment of patients with all three tumour types and were therefore used in all cell lines. Novel agents used were the proteasome inhibitor bortezomib and the HSP90 inhibitor KW-2478. Whilst bortezomib is currently only licensed for the treatment of multiple myeloma in the UK, it has recently been linked to the unfolded protein response and was therefore also used in all cell lines being studied. The novel HSP90 inhibitor KW-2478 is currently progressing through clinical trials and is now entered into a phase I/II trial as combination therapy with bortezomib (Clinical Trials.gov identifier: NCT01063907).

As would be expected, there were a number of differences in drug activity across the cell line panel. These differences were seen both within, and between, tumour types. Whilst this in itself is not surprising, there were a number of notable results seen, particularly in response to treatment with the two ER stress inducing agents. Whilst all the conventional cytotoxic drugs exhibited activity in the cell lines studied, the pattern of sensitivity depended

on the drug being used and not the cell line itself. Anti-proliferative effects were seen at lower concentrations than cytotoxic effects, as would be expected with these drugs.

In terms of the novel anticancer drugs used, it was observed that the non-myeloma cell lines were particularly sensitive to the effects of bortezomib, although this drug is only used clinically for the treatment of myeloma. The KW-2478 compound was an effective anti-proliferative agent, whilst it only proved cytotoxic in one of the two leukaemia cell lines studied. Previous work in our lab has established a similar pattern in other cell lines, such as myeloma and mantle cell lymphoma (Juliger, S., personal communication).

The largest difference in drug activity and sensitivity was seen with the two ER stress inducing agents. Interestingly, the response to pharmacological ER stress induction did not appear to be related to either tumour type or sensitivity to other types of anticancer agent. In addition, the cell lines most sensitive to stress induction with tunicamycin were not necessarily the most sensitive to treatment with thapsigargin. This may represent the different mechanisms by which these compounds cause ER stress, or may be due to other as yet undetermined factors. Thapsigargin, in particular, showed a very large range in potency across the cell line panel studied.

Drug sensitivity did not appear to be related to basal UPR activation in the haematological cell line panel studied. The pattern of basal activation of UPR proteins in the cell line panel did not correspond to chemosensitivity. For example, the DLBCL cell lines DOHH2 and SUD4 exhibited similar basal activation of UPR proteins, however sensitivity to drug treatment was varied.

In conclusion, basal expression of UPR proteins across cell lines and tumour types has not previously been described and these studies have provided novel insights into basal UPR activity in the haematological cancer cell line panel. The activity of a number of both

conventional and novel cytotoxic agents were established in these cell lines; characterising the effect on both proliferation and cell viability. This information will be used in investigating the UPR in response to treatment with these agents in the haematological cancer cell lines being studied.

4. Treatment with Minimally Toxic and Cytotoxic Drug Concentrations and Study of Unfolded Protein Response Activation *in vitro*

4.1 Introduction

There have been a number of reports over the years that have linked the UPR, or its individual components, to the response to drug treatment. However, published studies have focused on the change in drug treatment that results after modulating the UPR in some way, for example, overexpression of GRP78 and the subsequent change in activity of a particular drug compared to cells without such forced overexpression. The results of these types of experiments were discussed in chapter 1. The activation of UPR markers in response to drug treatment in a panel of haematological cell lines has not previously been described. This chapter is concerned with determining the extent of UPR activation following treatment with various conventional and novel anticancer agents in the haematological cell line panel being studied.

The mammalian UPR is represented in figure 1.4 (Szegezdi *et al.*, 2006). This figure illustrates the three pathways of the UPR (IRE1, PERK and ATF6), whilst also highlighting key downstream components activated during the UPR. The role of the ER resident molecular chaperone GRP78 in binding to and stabilising the three transmembrane receptors is shown. Another key ER molecular chaperone involved in the UPR, GRP94, is not specifically mentioned, but is one of the chaperones whose transcription is induced upon UPR activation.

The experiments in this chapter aim to establish the extent of UPR activation (if any) in these haematological cancer cells after treatment with a number of established chemotherapy drugs and also novel anticancer agents. The choice of drug treatment used

reflects the clinical treatment of these cancer types, and varies accordingly between the AML, myeloma and DLBCL cell lines studied. The two ER stress inducing agents used in previous experiments have also been included here to establish their effect on individual components of the UPR. Experiments in this chapter will focus on changes in the UPR observed at the translational level, as this was considered to be most relevant to the clinical use of these agents.

4.2 Materials and Methods

Based on the drug activity experiments described in chapter 3, equipotent concentrations (a minimally toxic concentration (EC_5) and cytotoxic concentrations (EC_{25} and EC_{50})) were calculated for each drug used in each cell line (as described in chapter 2.7). The concentrations used are listed in chapter 3.3. Whilst KW-2478 was shown to affect cell number, it did not show a marked effect on cell viability in the majority of cell lines studied. Where this was the case, the maximal effect of the drug as fitted by the model used appeared small, with a correspondingly small EC_{50} value. For this reason it was decided to include a third concentration in the western blotting experiments; the concentration of KW-2478 that resulted in an actual 25% decrease in cell viability from the control viability.

Cells in exponential growth phase were plated into 6-well plates and incubated under normal growth conditions for 24 hours. After this time, drug solutions were prepared for use in fresh culture medium from drug stocks (see section 2.3) and were added to the plates. Cells were incubated with drug for either 6 hours or 24 hours (untreated controls were also included in each experiment) and whole cell lysates prepared, as described in section 2.6. Levels of various UPR markers at the protein level were then studied by western blotting (as described in section 2.7) in order to establish the effect of drug treatments on the UPR. 20μg of protein lysate was loaded into each gel well unless otherwise specified. Considerable

preliminary work was carried out in order to optimise the experimental conditions used, such as amount of lysate, antibody concentrations and antibody incubation times for each cell line being studied. Visualisation of western blots was achieved using chemiluminescence and manual film developing. The manual developing process was first optimised in order to establish optimum conditions. This consisted of developing the film for 2 minutes, immersion into stop solution to inactivate the developer for 30 seconds, immersion in fixer solution for 5 minutes, then a final rinse before allowing the film to air dry. The amount of time the film was placed onto the chemiluminescent membrane was optimised for each individual antibody used in each individual cell line. Experiments were carried out at least once, with experiments repeated to confirm key results.

4.3 Results

Figures 4.1 to 4.4 show protein levels of the UPR markers studied in the AML cell lines after treatment with EC_5 and EC_{25} concentrations of drugs for 6 and 24 hours. Where clear changes in the activation of UPR proteins were seen, relative to the untreated control, such changes are described below. A number of UPR proteins were studied in addition to those shown here, but were not detectable under the experimental conditions used.

Figure 4.1 shows that in the HL-60 cell line, 6 hour exposure to the study drugs resulted in clear changes only in the level of GRP78 protein (relative to control), with an increase seen with all drug treatments except tunicamycin (even allowing for small differences in the intensity of the GAPDH band). GRP78 remained elevated in this cell line after 24 hours of treatment with bortezomib (EC_{25}) and KW-2478 at all concentrations (see figure 4.2). GRP94 protein levels were also increased following 24 hours of drug treatment with tunicamycin (EC_5 and EC_{25}) and thapsigargin (EC_{25}).

In the THP1 cell line, GRP78 protein was increased in response to 6 hours of drug treatment with EC_{25} concentrations of tunicamycin and thapsigargin, as well as with KW-2478 at all concentrations, as shown in figure 4.3. With tunicamycin and thapsigargin (EC_{25}) this was associated with a small increase in GRP94 protein. In addition, an increased level of phosphorylated eIF2α protein can be seen following 6 hours treatment with KW-2478 at the concentration resulting in 25% cell death. After 24 hours of drug treatment, GRP78 protein levels were increased in the bortezomib (EC_{25} only), cytarabine and KW-2478 treated samples, whilst GRP94 protein levels were increased in the thapsigargin (EC_{25} only), cytarabine, etoposide and KW-2478 treated samples (see figure 4.4).

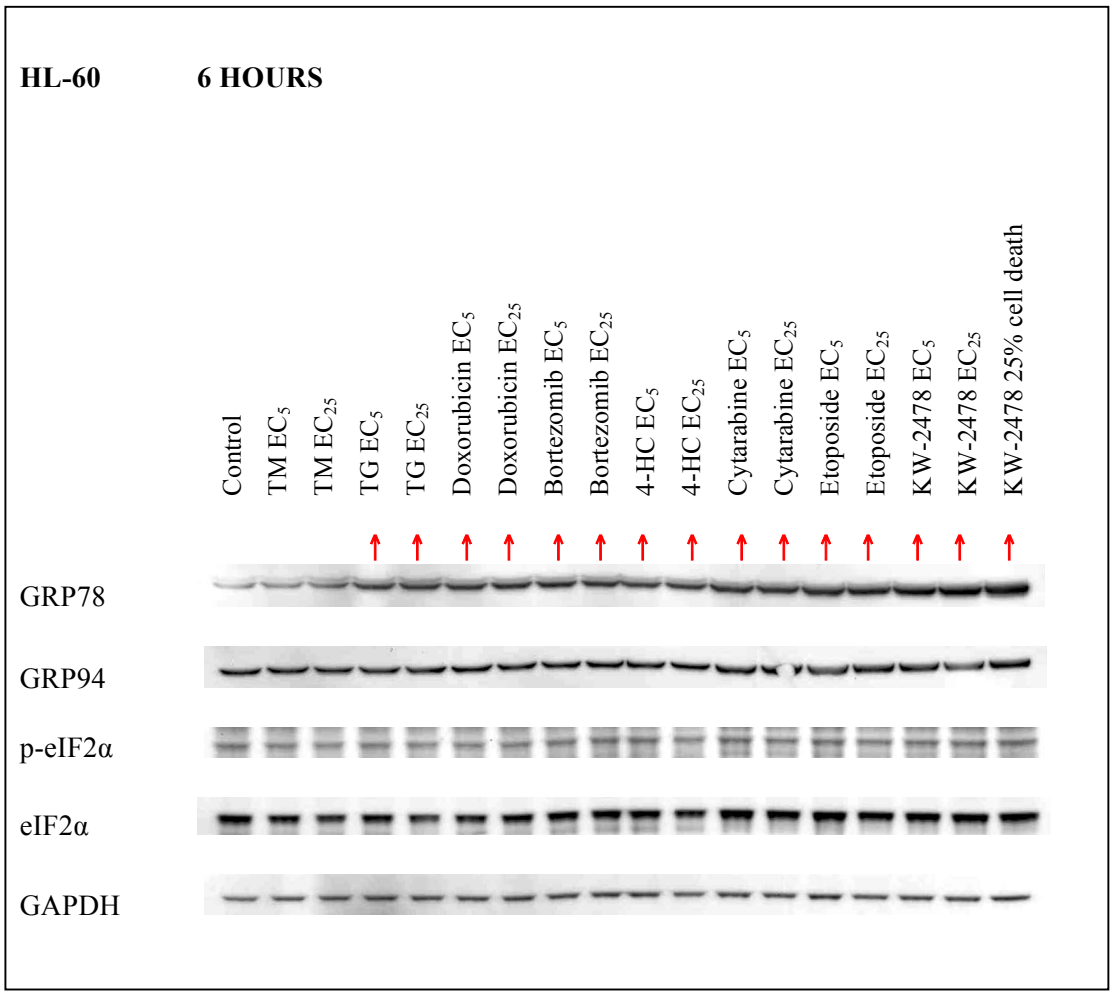

Figure 4.1. Western blotting experiments to investigate activation of unfolded protein response markers in the AML cell line HL-60 after 6 hours of drug treatment. GAPDH is included as a loading control.

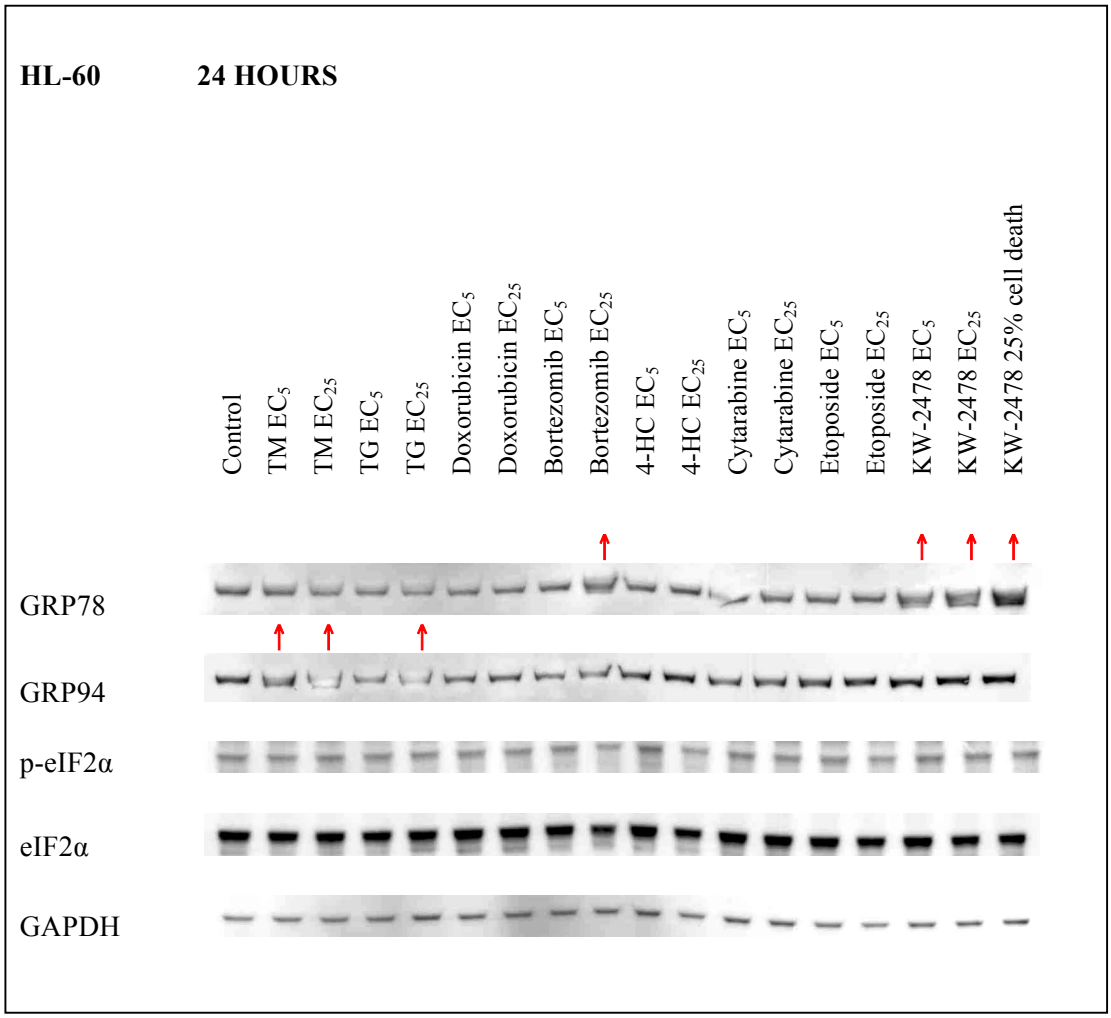

Figure 4.2. Western blotting experiments to investigate activation of unfolded protein response markers in the AML cell line HL-60 after 24 hours of drug treatment. GAPDH is included as a loading control.

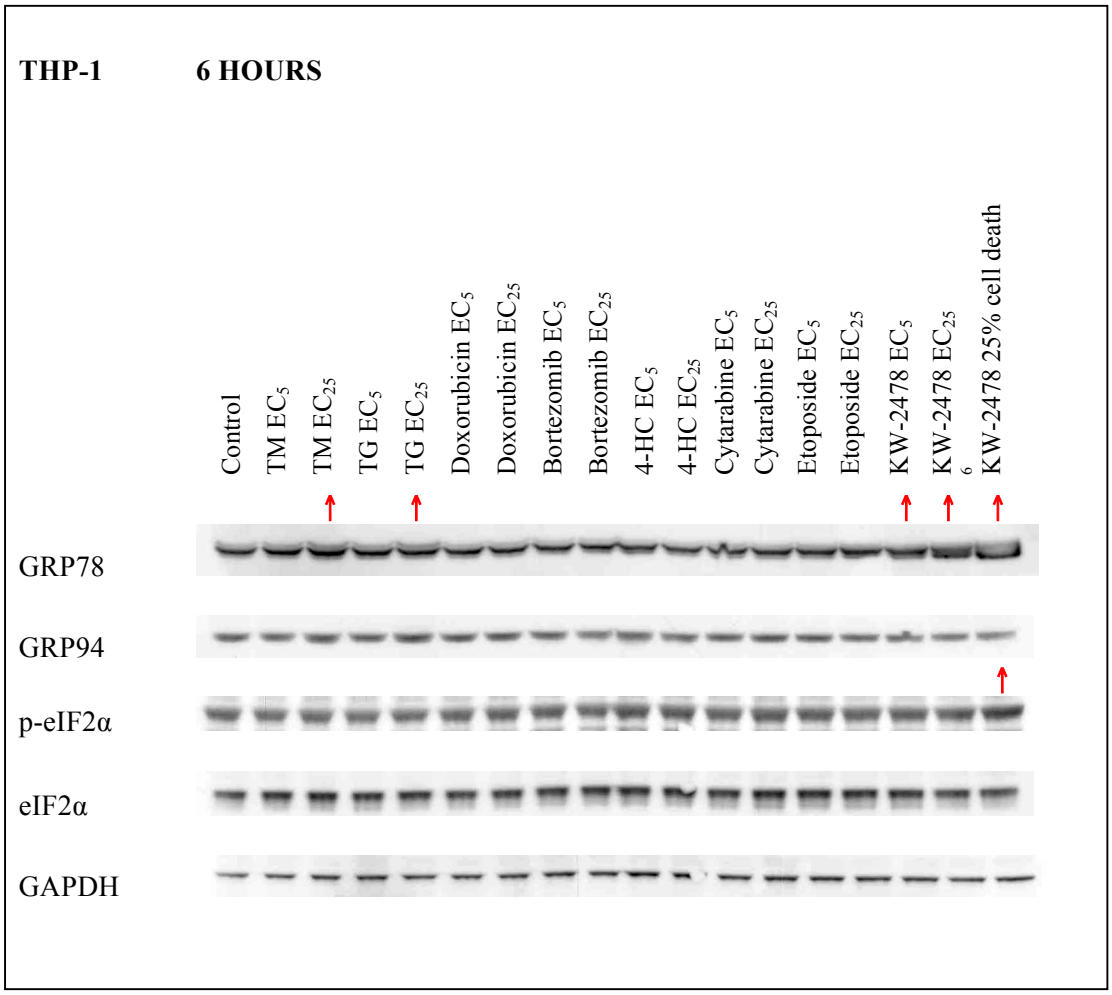

Figure 4.3. Western blotting experiments to investigate activation of unfolded protein response markers in the AML cell line THP1 after 6 hours of drug treatment. GAPDH is included as a loading control.

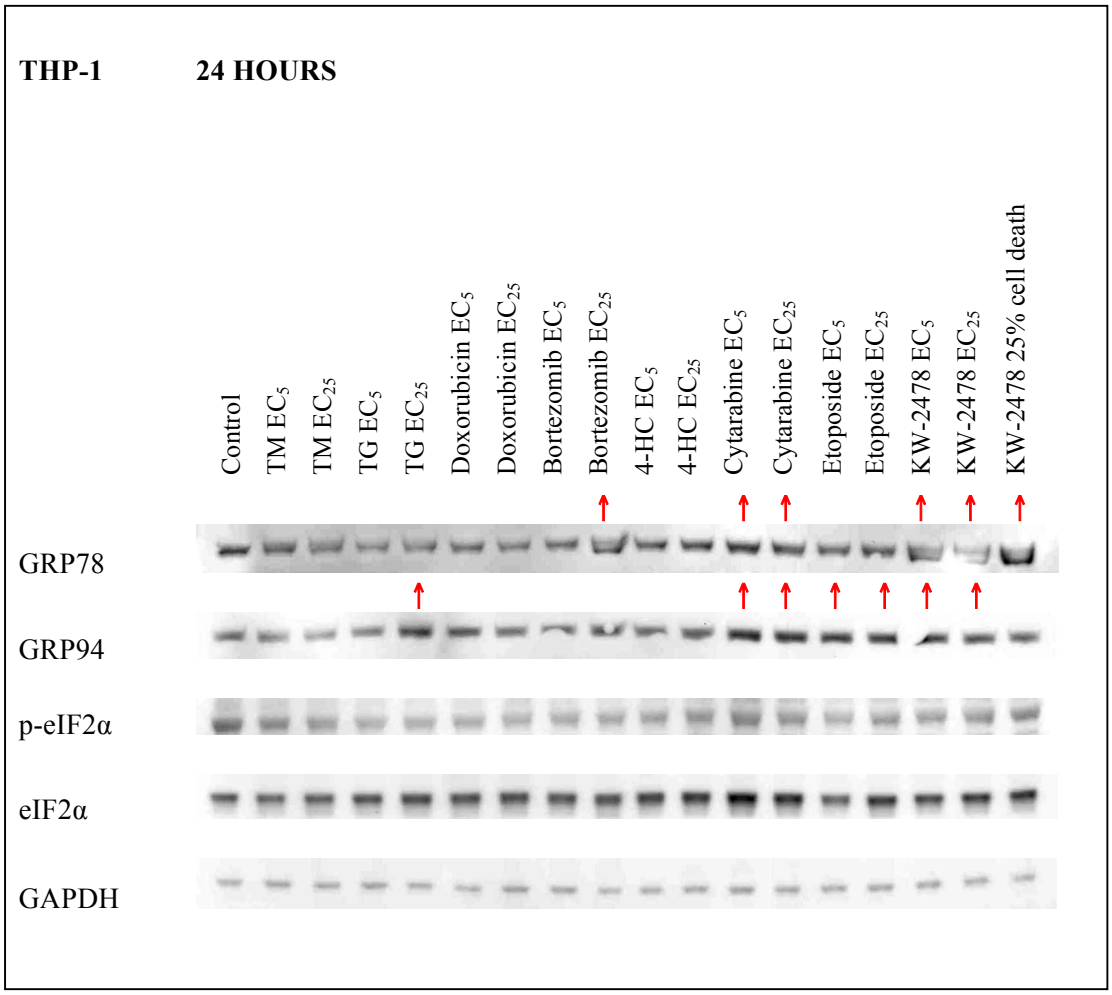

Figure 4.4. Western blotting experiments to investigate activation of unfolded protein response markers in the AML cell line THP1 after 24 hours of drug treatment. GAPDH is included as a loading control.

Figures 4.5 to 4.8 show expression of the UPR markers studied in the multiple myeloma cell lines after treatment with EC_5 and EC_{25} concentrations of drugs for 6 and 24 hours. After both 6 hours and 24 hours of drug treatment in the RPMI-8226 cell line, GRP78 protein was increased only in the highest KW-2478 concentration treated sample, with a marked increase after 24 hours (see figures 4.5 and 4.6 respectively). At 24 hours in this cell line, GRP94 protein levels were increased in the sample treated with the EC_{25} concentration of thapsigargin (see figure 4.6). Phosphorylated eIF2α expression was increased in the samples treated with EC_{25} concentrations of tunicamycin, thapsigargin,

bortezomib and KW-2478 for 6 hours (see figure 4.5). It was also increased in the samples treated with EC_5 concentrations of tunicamycin and thapsigargin for 24 hours, however a decrease in phosphorylation was seen following treatment with the highest KW-2478 concentration (see figure 4.6). Total IRE1 receptor protein levels were seen in all samples (including controls) to the same extent at 6 hours in RPMI-8226 cells (see figure 4.5). Total IRE1 protein was also visible in all samples at 24 hours, with increased levels seen in the EC_{25} tunicamycin and thapsigargin treated samples (see figure 4.6). Phosphorylated IRE1 protein was only visible in the EC_{25} tunicamycin and thapsigargin treated samples at both the 6 and 24 hour time points (figure 4.5 and 4.6 respectively).

In the U266 cell line, GRP78 protein was increased in the sample treated with the highest KW-2478 concentration, as shown in figure 4.7. In the 24 hour treated samples GRP78 protein levels were increased in the bortezomib (EC_{25}) and KW-2478 (at the two higher concentrations) treated samples (see figure 4.8). No changes were seen in the level of GRP94 protein after drug treatment in U266 cells at either time point. Phosphorylated eIF2α expression was increased in the thapsigargin (EC_5 and EC_{25}) treated samples after 6 hours treatment. At 24 hours phosphorylated eIF2α was increased in the samples treated with tunicamycin, thapsigargin and doxorubicin, whilst in the samples treated with the highest concentrations of bortezomib and KW-2478 there was a marked decrease in phosphorylated eIF2α, due mainly to a decrease in total eIF2α protein. GAPDH protein, used as a loading control, was present in both these samples. Total IRE1 protein was visible in all samples (including controls) after both 6 and 24 hours of drug treatment in U266 cells, but showed a clear increase with thapsigargin and KW-2478 (EC_5) treatment at 24 hours (see figure 4.7 and 4.8 respectively). Notably, total IRE1 protein decreased markedly after 24 hours treatment with the highest bortezomib and KW-2478 concentrations used (GAPDH was still present). The level of phosphorylated IRE1 protein in the EC_{25} treated bortezomib sample was very low in comparison to all other samples (see figure 4.8). As shown in both figures

4.7 and 4.8, no increase in the spliced isoform of XBP1 was seen at the protein level in response to any of the drug treatments used in the U266 cell line.

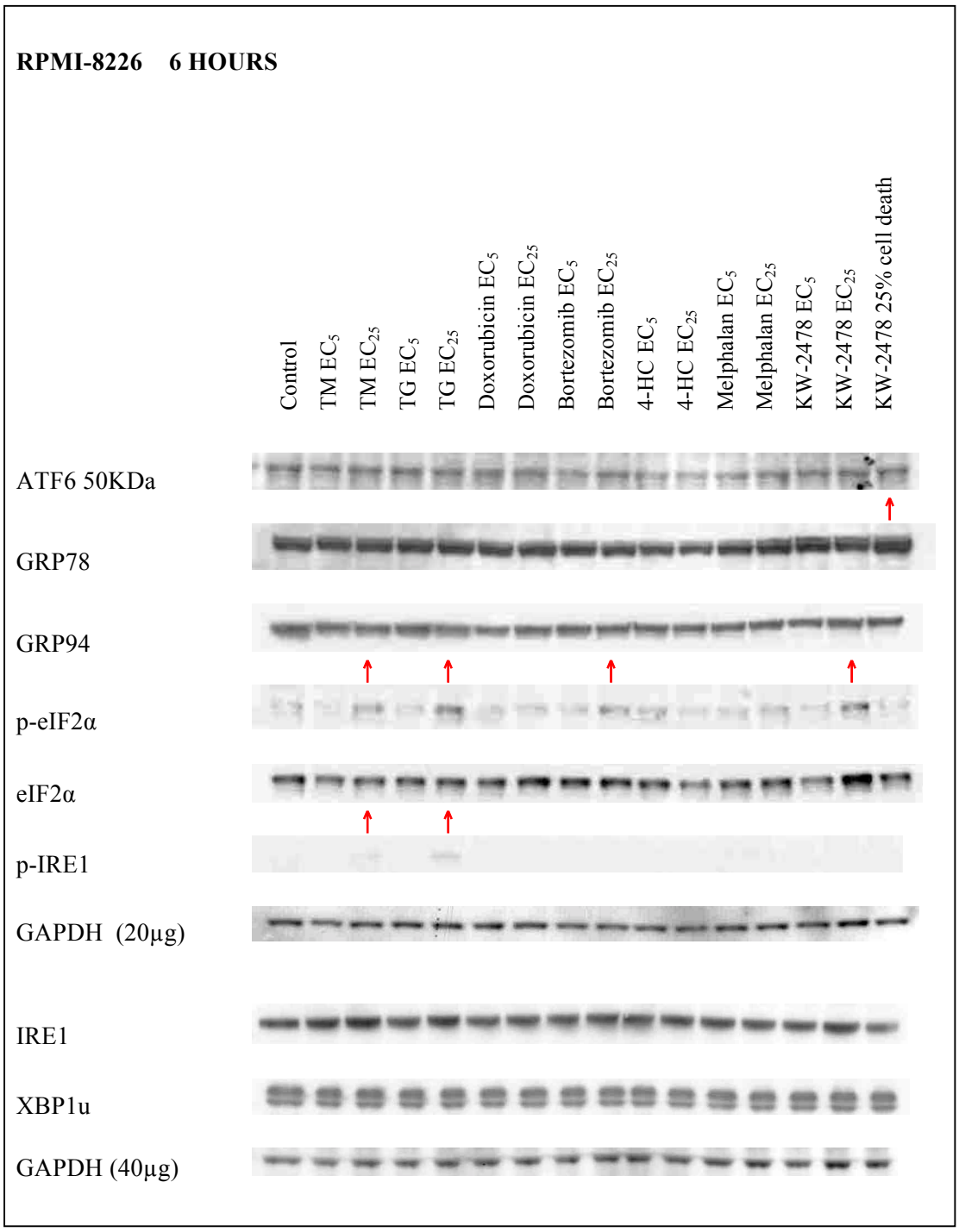

Figure 4.5. Western blotting experiments to investigate activation of unfolded protein response markers in the myeloma cell line RPMI-8226 after 6 hours of drug treatment. GAPDH is included as a loading control.

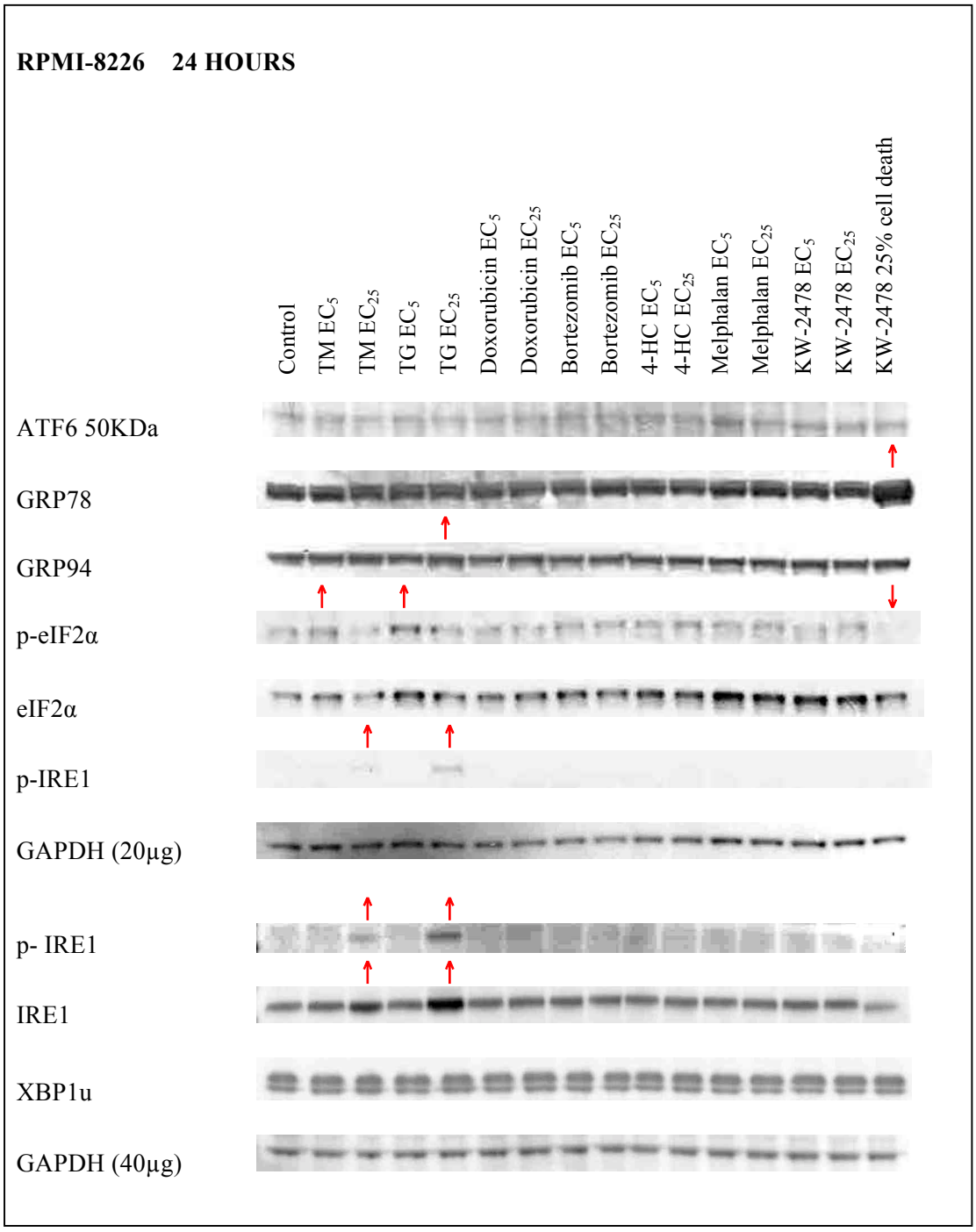

Figure 4.6. Western blotting experiments to investigate activation of unfolded protein response markers in the myeloma cell line RPMI-8226 after 24 hours of drug treatment. GAPDH is included as a loading control.

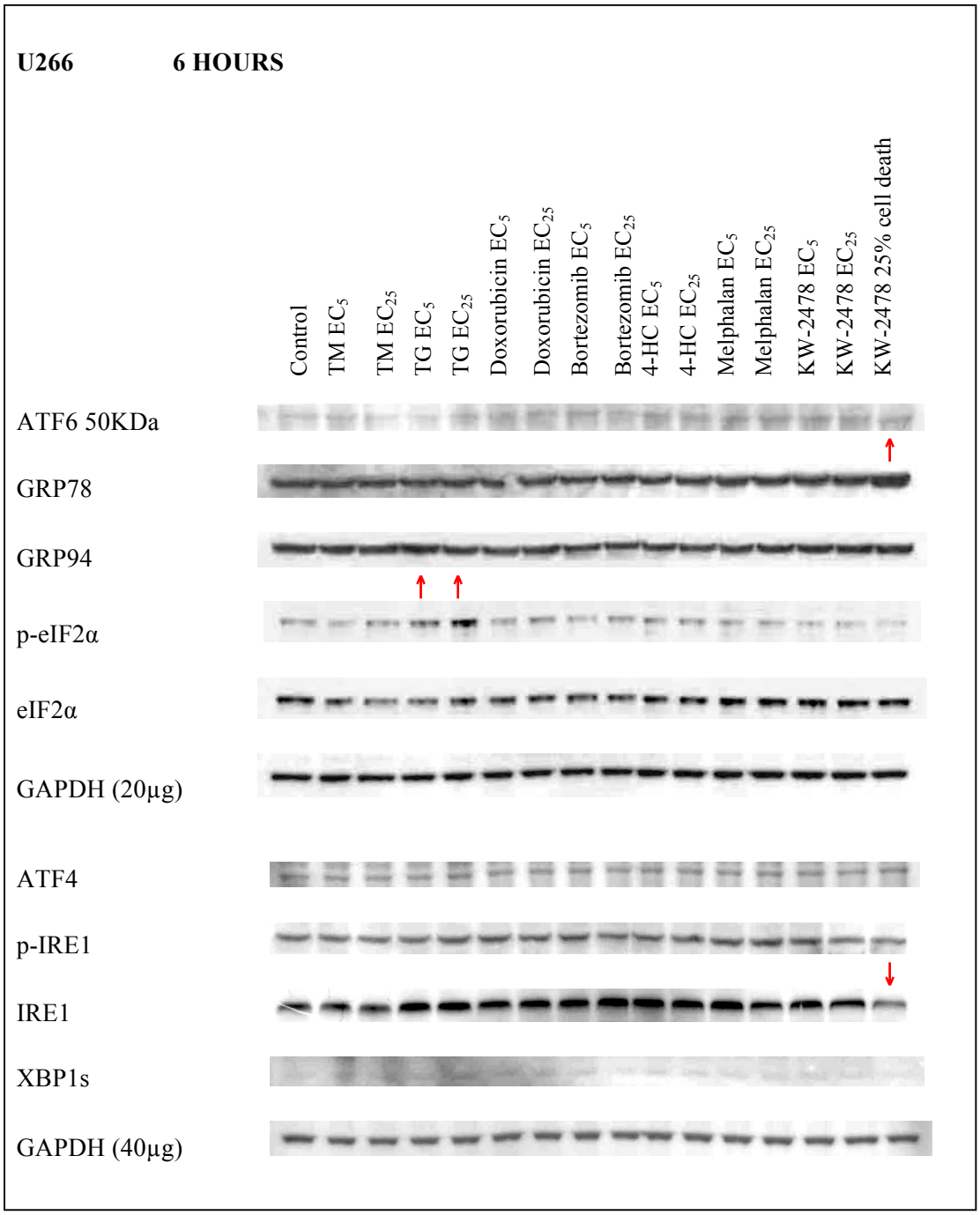

Figure 4.7. Western blotting experiments to investigate activation of unfolded protein response markers in the myeloma cell line U266 after 6 hours of drug treatment. GAPDH is included as a loading control.

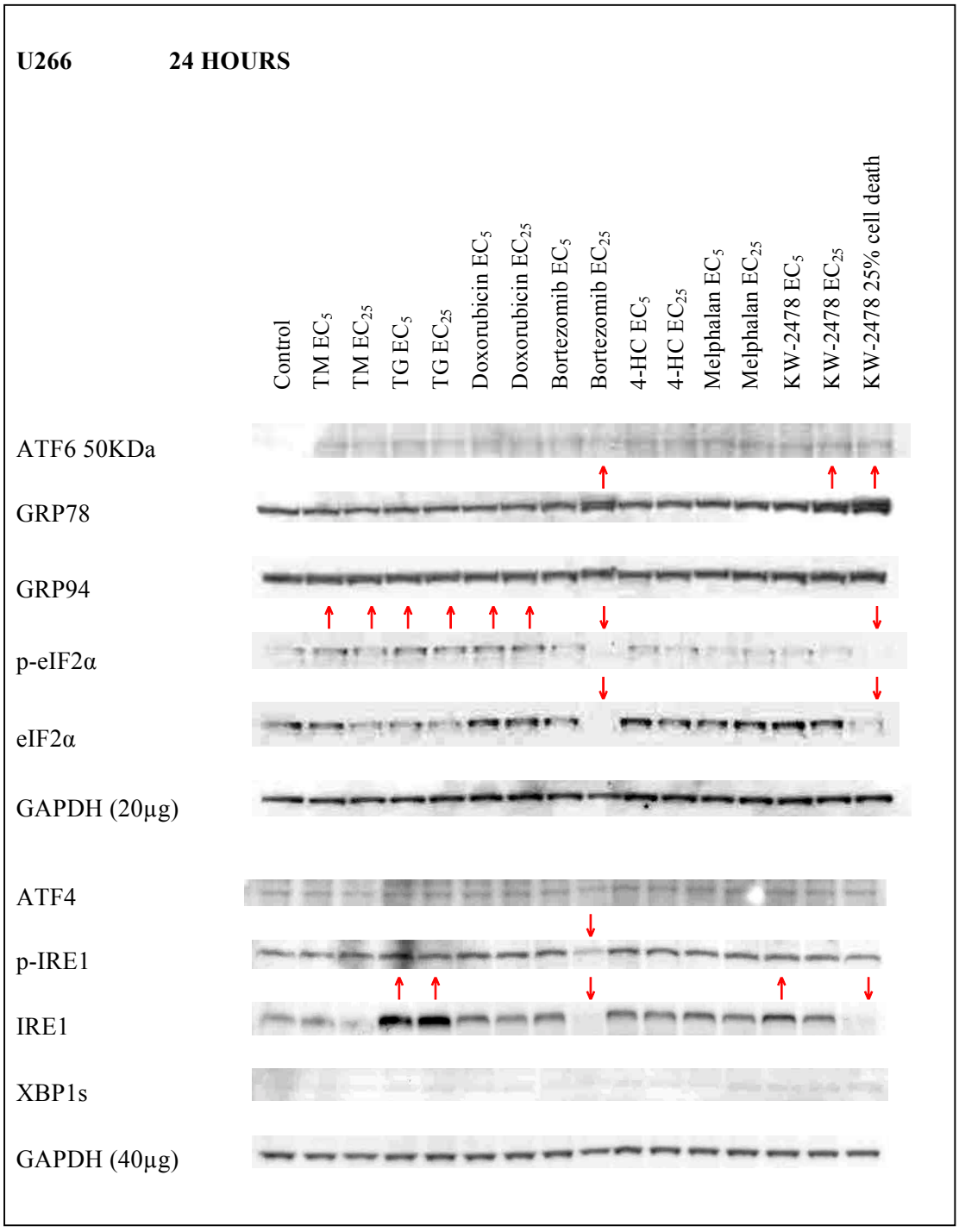

Figure 4.8. Western blotting experiments to investigate activation of unfolded protein response markers in the myeloma cell line U266 after 24 hours of drug treatment. GAPDH is included as a loading control.

Figures 4.9 to 4.12 show protein levels of the UPR markers studied in the lymphoma cell lines after treatment with EC_5 and EC_{25} concentrations of drugs for 6 and 24 hours. In the DOHH2 cell line, no changes were seen in the level of GRP78 or GRP94 following drug treatments for 6 hours (see figure 4.9). After 24 hours treatment with the two higher concentrations of KW-2478, GRP78 protein levels were shown to increase, however no changes were seen in GRP94 protein levels compared to the untreated control (see figure 4.10). In the DOHH2 cell line, no changes were found in phosphorylated eIF2α protein levels following drug treatments for 6 hours (see figure 4.9). After 6 hours of treatment, total eIF2α protein levels were increased with EC_{25} thapsigargin treatment, but decreased with all concentrations of KW-2478 studied, and remained decreased (relative to control) after 24 hours treatment with KW-2478 at the highest concentration studied (see figure 4.9 and 4.10 respectively). Phosphorylated eIF2α protein levels were also decreased following 24 hours treatment with KW-2478 at the highest concentration. Phosphorylated PERK receptor protein was increased in the sample treated with EC_{25} thapsigargin, but decreased in the samples treated with KW-2478, for 6 hours (see figure 4.9). At the 24 hour time point, both phosphorylated and total PERK receptor protein levels were decreased samples treated with KW-2478 at the highest concentration studied (see figure 4.10).

In the SUD4 cell line, GRP78 protein was shown to increase following both 6 hours and 24 hours of treatment with the highest concentration of KW-2478 used (figures 4.11 and 4.12 respectively). It was also shown that the level of GRP94 protein in this cell line was increased in all drug treated samples at 6 hours (see figure 4.11). Phosphorylated eIF2α protein was increased following 6 hours of treatment with tunicamycin, thapsigargin, 4-HC and KW-2478 EC_5 and EC_{25}, however a decrease was seen in the highest KW-2478 concentration treated sample (see figure 4.11). At the 24 hour time point, phosphorylated eIF2α protein was decreased in all KW-2478 treated samples (see figure 4.12). Phosphorylated PERK receptor protein was increased following 6 hours of treatment with

KW-2478 at the highest concentration studied (see figure 4.11). Blots for phosphorylated PERK protein at the 24 hour time point were quite faint when developed and any changes occurring following drug treatment were therefore hard to discern (see figure 4.12).

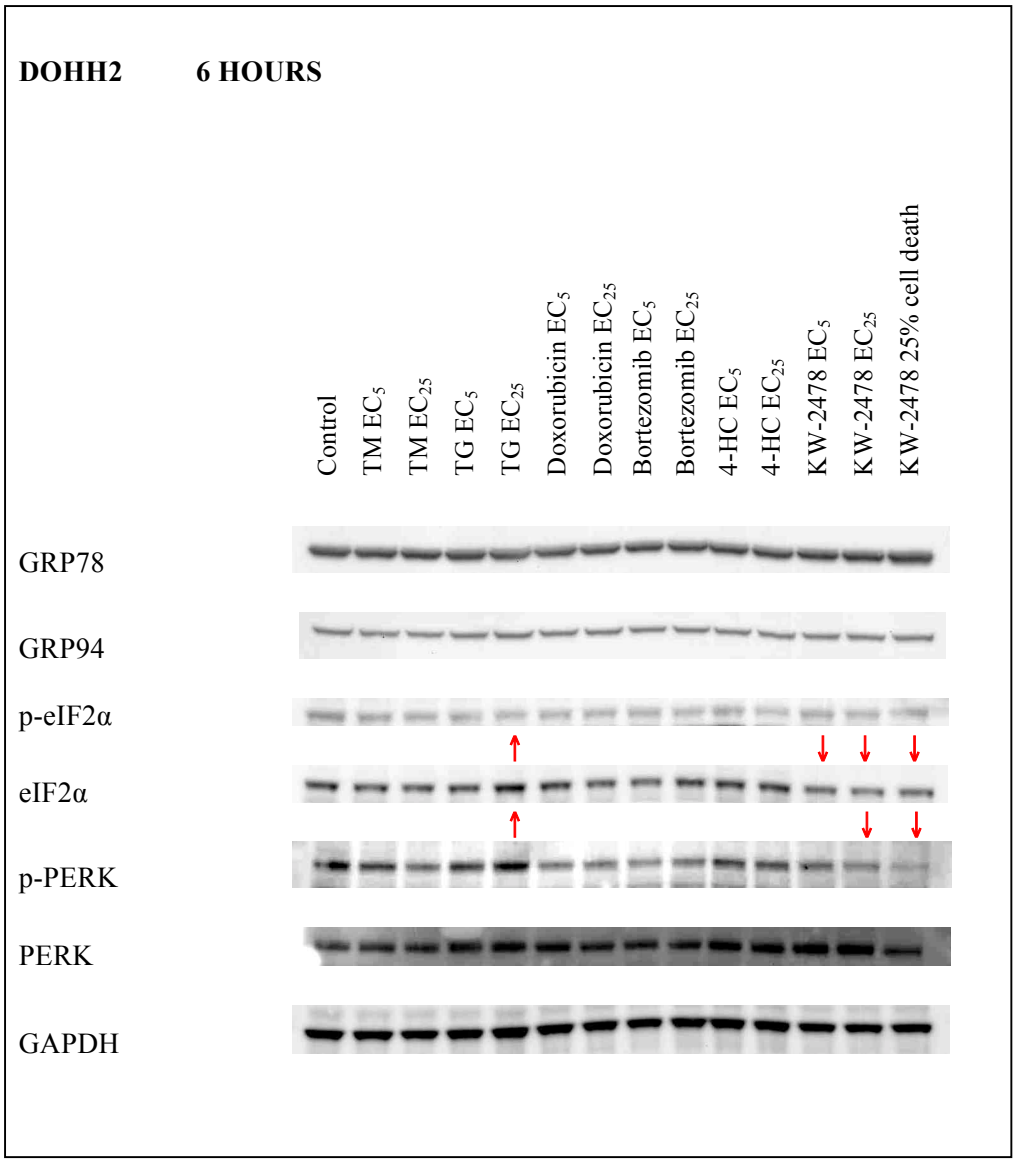

Figure 4.9. Western blotting experiments to investigate activation of unfolded protein response markers in the lymphoma cell line DOHH2 after 6 hours of drug treatment. GAPDH is included as a loading control.

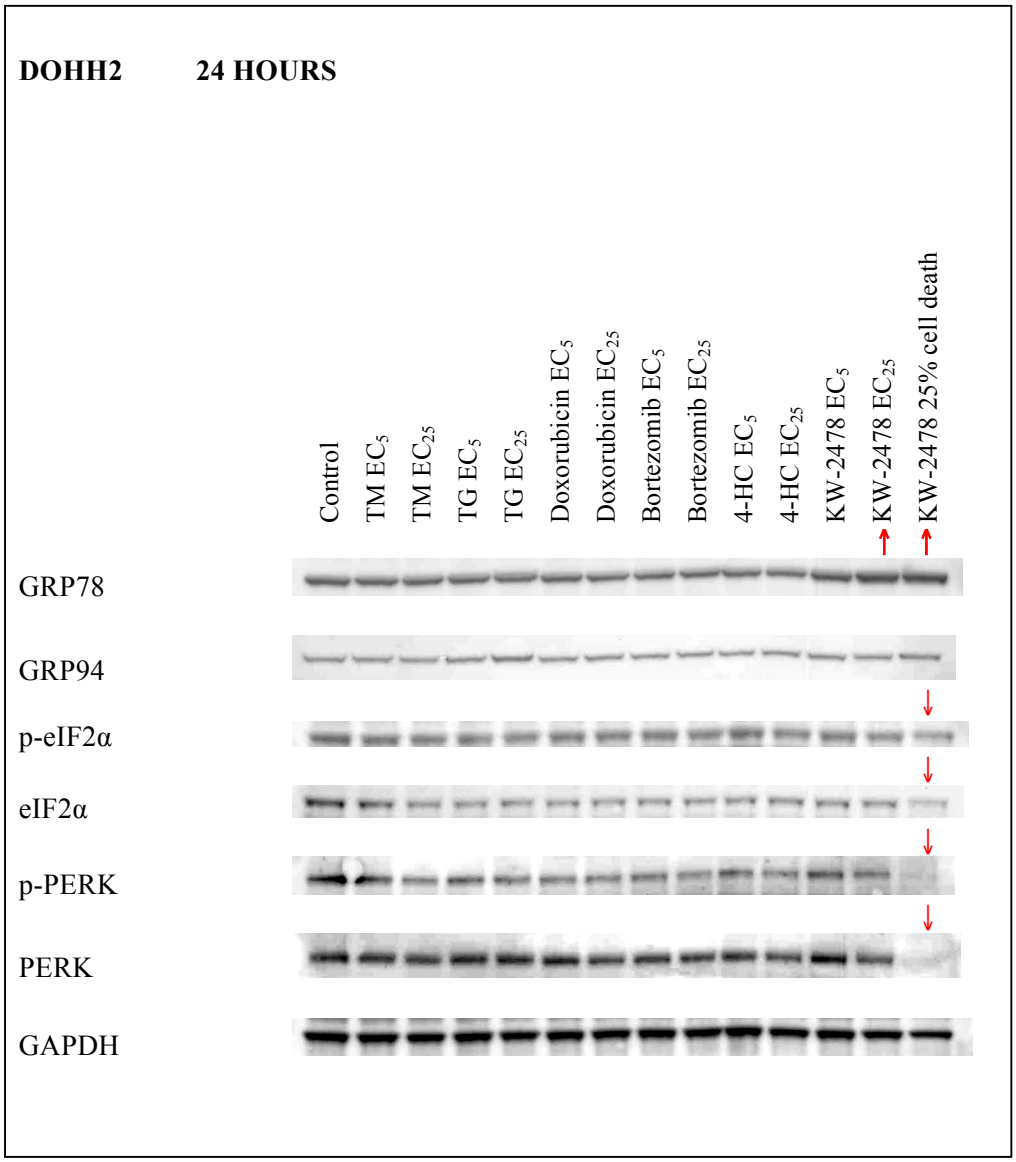

Figure 4.10. Western blotting experiments to investigate activation of unfolded protein response markers in the lymphoma cell line DOHH2 after 24 hours of drug treatment. GAPDH is included as a loading control.

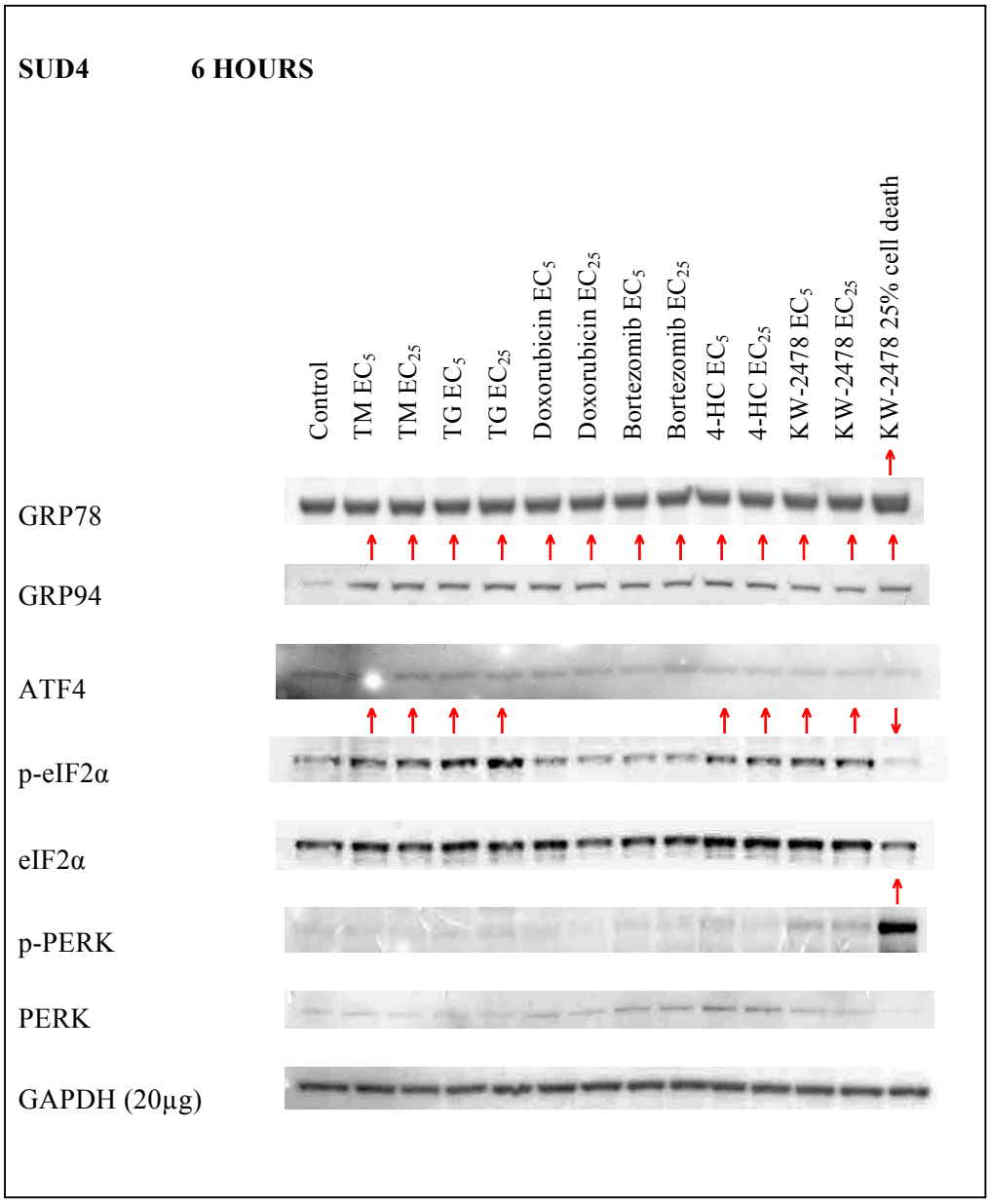

Figure 4.11. Western blotting experiments to investigate activation of unfolded protein response markers in the lymphoma cell line SUD4 after 6 hours of drug treatment. GAPDH is included as a loading control.

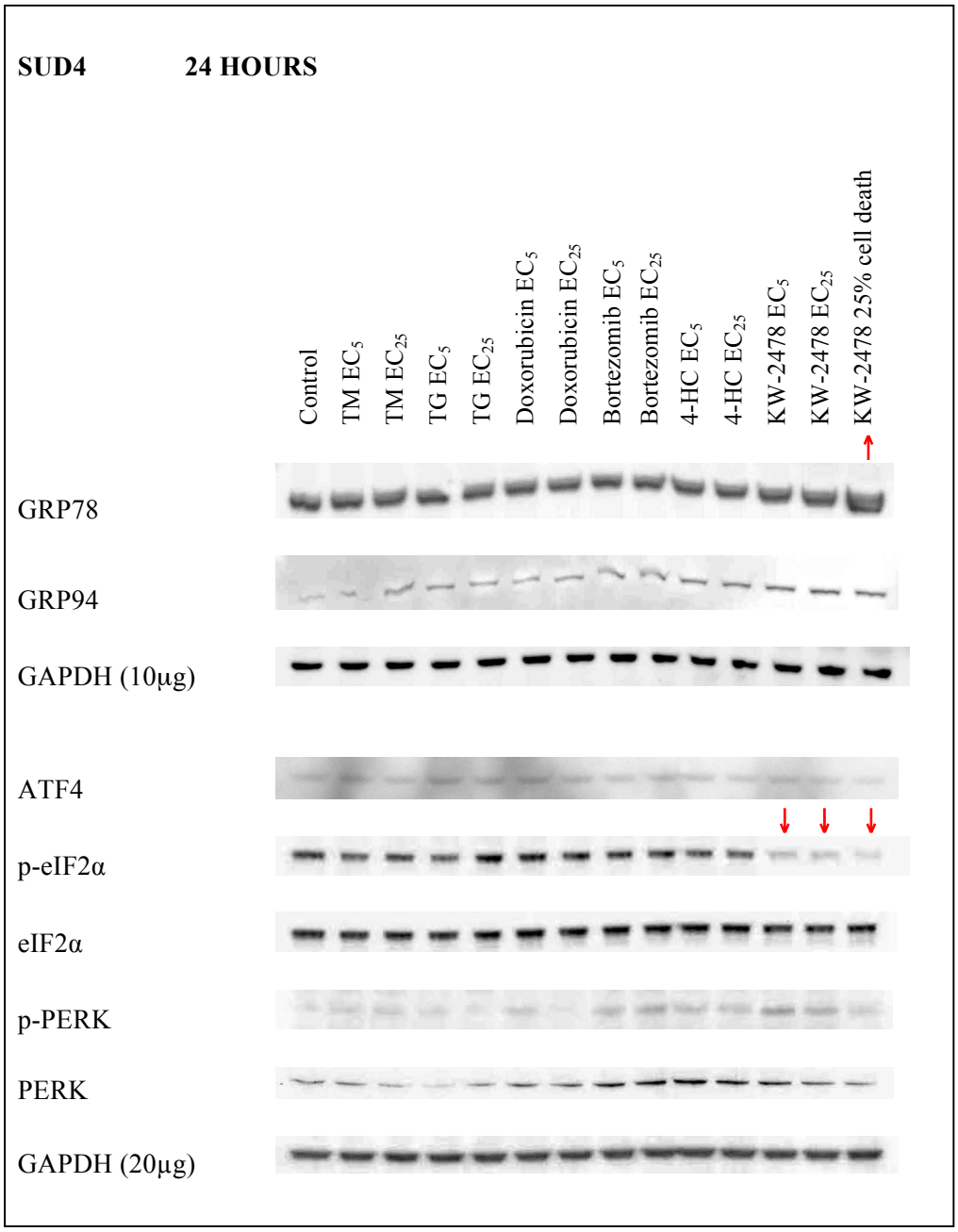

Figure 4.12. Western blotting experiments to investigate activation of unfolded protein response markers in the lymphoma cell line SUD4 after 24 hours of drug treatment. GAPDH is included as a loading control.

Because the changes seen with EC_5 and EC_{25} concentrations were relatively minimal, the experiments were repeated with EC_{50} concentrations of drugs in order to determine if these higher concentrations would cause a more pronounced increase in UPR activation. The fitted EC_{50} concentrations of each drug used on cell viability in each cell line

are as listed in chapter 3.3. Figures 4.13 to 4.18 shows the effect of treatment with EC_{50} drug concentrations on protein levels of various UPR markers in the haematological cell line panel studied. Clear changes observed in activation status of the UPR markers studied compared to untreated control cells are described below. Figure 4.13 shows the effect of treatment with EC_{50} drug concentrations for 6 and 24 hours on protein levels of UPR markers in the AML cell line HL60. GRP78 levels were only seen to increase in the KW-2478 treated sample at 24 hours. GRP94 protein levels showed a slight increase after 24 hours treatment with thapsigargin and a marked increase after 24 hours treatment with tunicamycin. A decrease in phosphorylated eIF2α protein was seen after 6 hours treatment with thapsigargin. It should be noted that a difference was also seen in eIF2α protein levels in the untreated control samples. At 6 hours there was low expression of eIF2α protein, however an increased protein level was seen in the 24 hour control sample.

In the THP1 cell line (see figure 4.14), a slight increase in GRP78 protein was seen after 24 hours treatment with both tunicamycin and thapsigargin, with a marked increase seen after 24 hours treatment with KW-2478. A slight increase in GRP94 protein was also seen following 24 hours of treatment with both tunicamycin and thapsigargin. Changes were seen in the levels of phosphorylated eIF2α protein between the two control samples, with a lower level seen at 6 hours compared with 24 hours. However, no corresponding changes were seen in the levels of total eIF2α protein. An increase in phosphorylated eIF2α protein was seen after treatment with tunicamycin and thapsigargin for 6 hours.

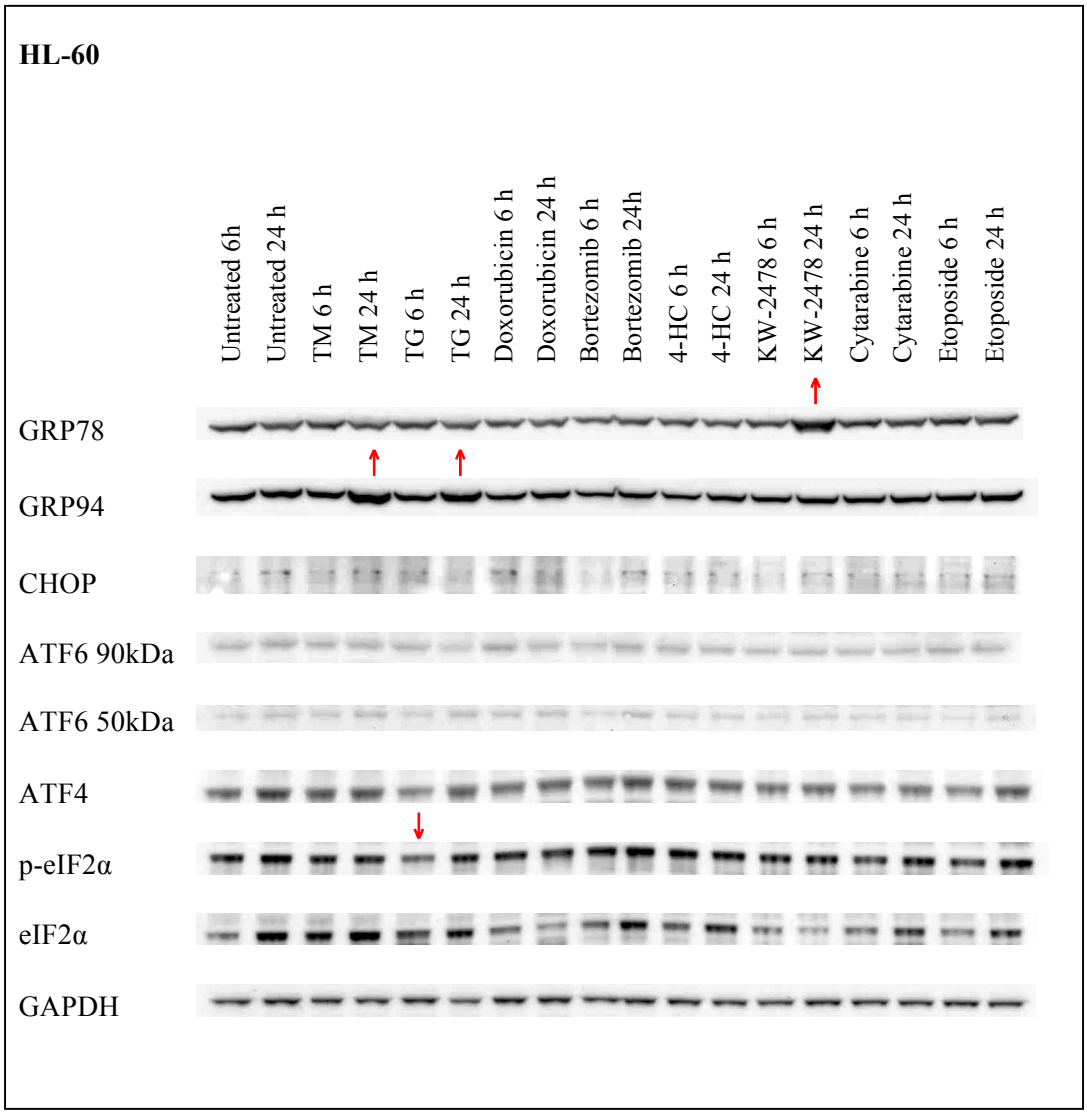

Figure 4.13. Western blotting experiments to investigate activation of unfolded protein response markers after treatment with EC_{50} concentrations of drug for 6 and 24 hours in the AML cell line HL-60. GAPDH is included as a loading control.

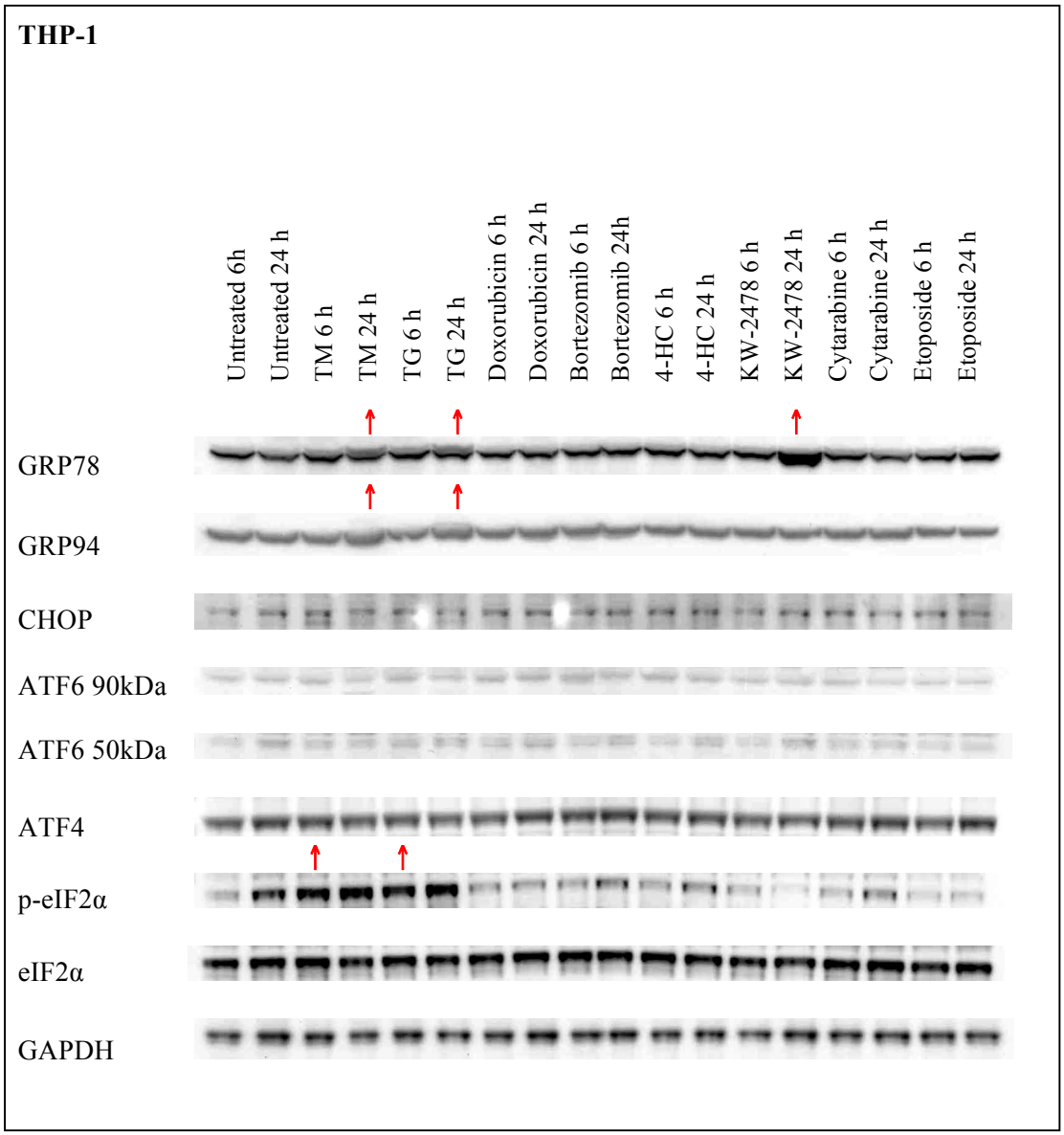

Figure 4.14. Western blotting experiments to investigate activation of unfolded protein response markers after treatment with EC_{50} concentrations of drug for 6 and 24 hours in the AML cell line THP1. GAPDH is included as a loading control.

In the RPMI-8226 cell line, the only changes in UPR activation seen after treatment with EC_{50} drug concentrations were in the levels of the ER molecular chaperone proteins (see figure 4.15). A clear increase in GRP78 protein levels were seen following treatment with tunicamycin and thapsigargin for 24 hours, and a marked increase seen following KW-2478 treatment at both 6 and 24 hours. An increase in the level of GRP94 protein was seen in the samples treated with tunicamycin and thapsigargin for 24 hours.

Figure 4.16 shows the effect of EC_{50} drug treatment on UPR protein levels in the U266 cell line. Again, the only changes seen following drug treatment were in the levels of the molecular chaperone proteins GRP78 and GRP94. GRP78 protein increased after treatment with thapsigargin, melphalan and bortezomib for 24 hours, with a marked increase seen after treatment with KW-2478 for 24 hours. GRP94 protein was observed to increase following treatment with thapsigargin, bortezomib and melphalan for 24 hours.

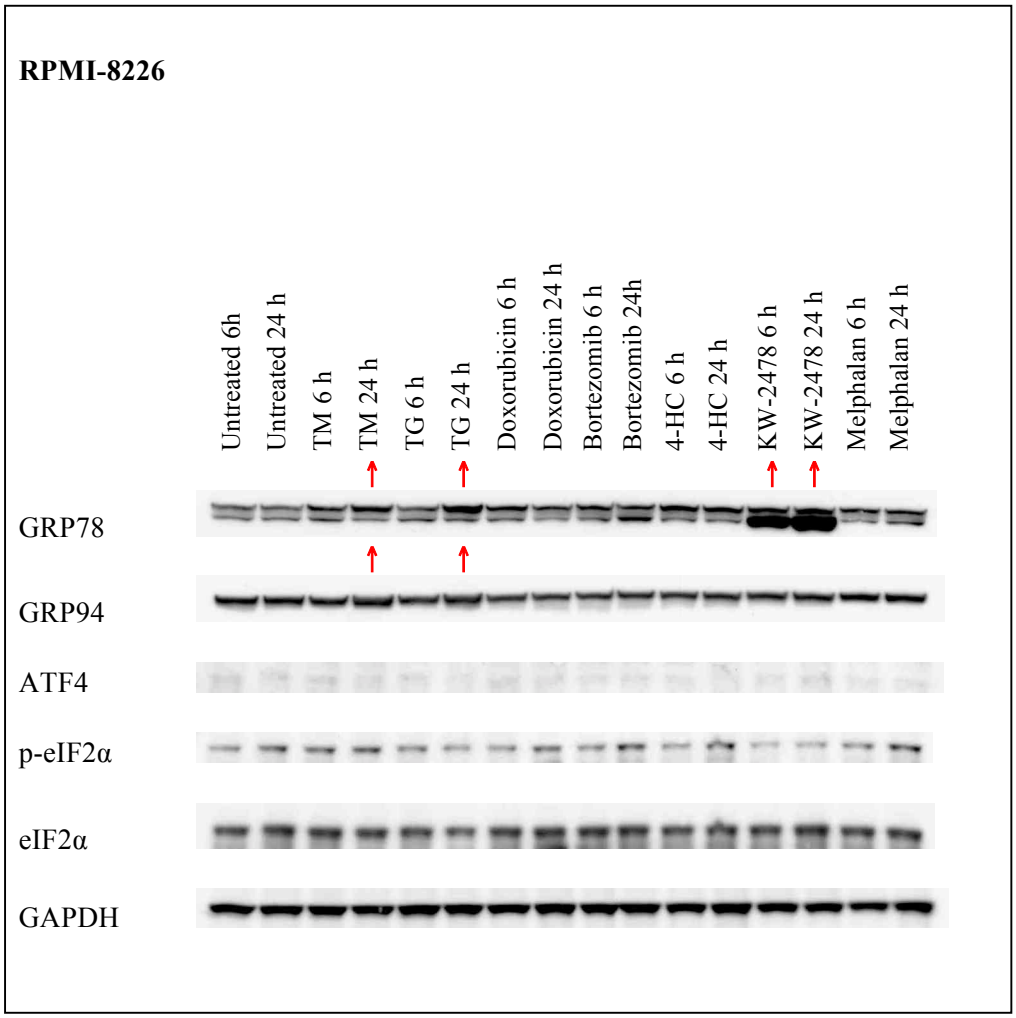

Figure 4.15. Western blotting experiments to investigate activation of unfolded protein response markers after treatment with EC_{50} concentrations of drug for 6 and 24 hours in the myeloma cell line RPMI-8226. GAPDH is included as a loading control.

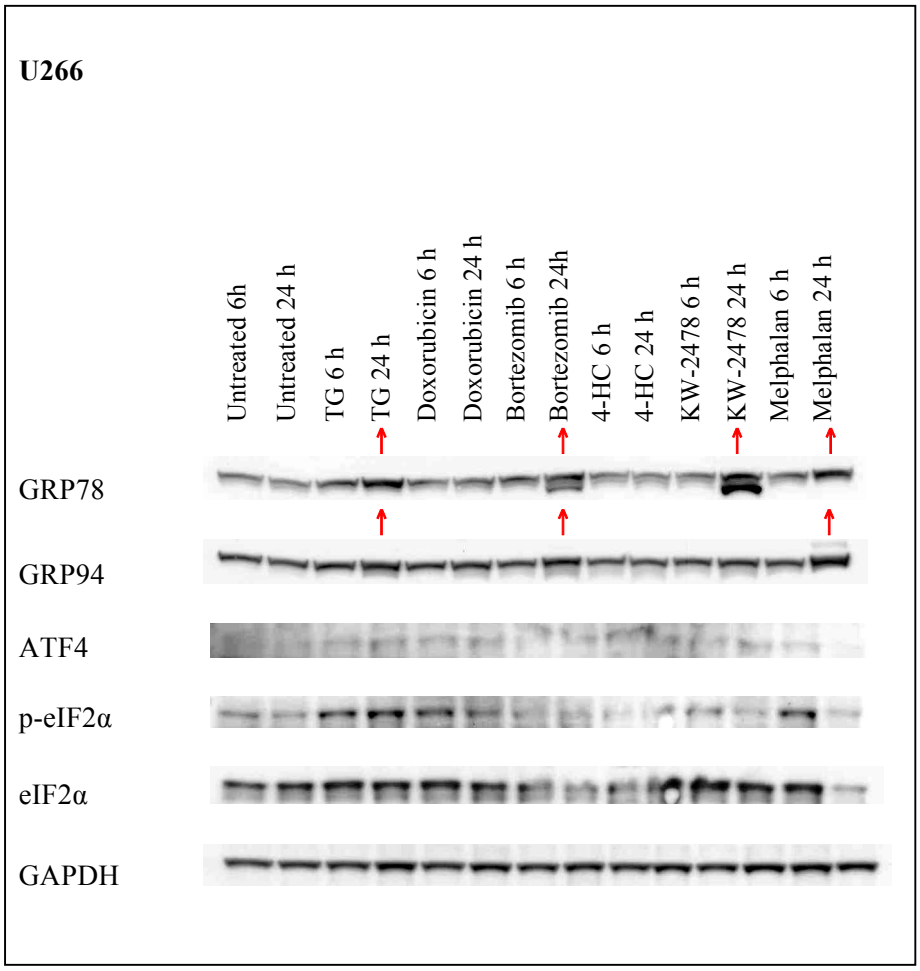

Figure 4.16. Western blotting experiments to investigate activation of unfolded protein response markers after treatment with EC_{50} concentrations of drug for 6 and 24 hours in the myeloma cell line U266. GAPDH is included as a loading control. The TM treated samples could not be included as the protein content of the samples was insufficient for western blotting.

Figures 4.17 and 4.18 show the effect of treatment with EC_{50} drug concentrations on protein levels of various UPR markers in the diffuse large B-cell lymphoma cell lines DOHH2 and SUD4 respectively. In the DOHH2 cell line, a clear increase in GRP78 protein was seen following KW-2478 treatment for 24 hours, relative to control (see figure 4.17). Treatment with KW-2478 for 24 hours led to a decrease in phosphorylated eIF2α protein levels. Western blots for PARP protein were also carried out in order to study the effect of drug treatment on apoptosis. In the DOHH2 cells, PARP cleavage was seen following treatment with tunicamycin (6 hours), doxorubicin (24 hours) and KW-2478 (24 hours).

Figure 4.18 shows that in the SUD4 cell line, GRP78 protein was increased following treatment with tunicamycin and KW-2478 at both time points. GRP94 protein levels were increased after treatment with tunicamycin and thapsigargin for 24 hours. Differences were also seen in activation of the PERK pathway of the unfolded protein response in this cell line. An increase in phosphorylated PERK was seen following 6 hours of treatment with tunicamycin. Phosphorylated eIF2α protein levels were shown to increase after 6 hours treatment with tunicamycin, whilst a decrease was seen with KW-2478 at both time points. An increase was also seen in the levels of eIF2α protein and the pro-apoptotic ATF4 protein after 6 hours treatment with tunicamycin. PARP cleavage was present after treatment with tunicamycin for both 6 and 24 hours (notably, there was no PARP cleavage visible after treatment with KW-2478 in this cell line).

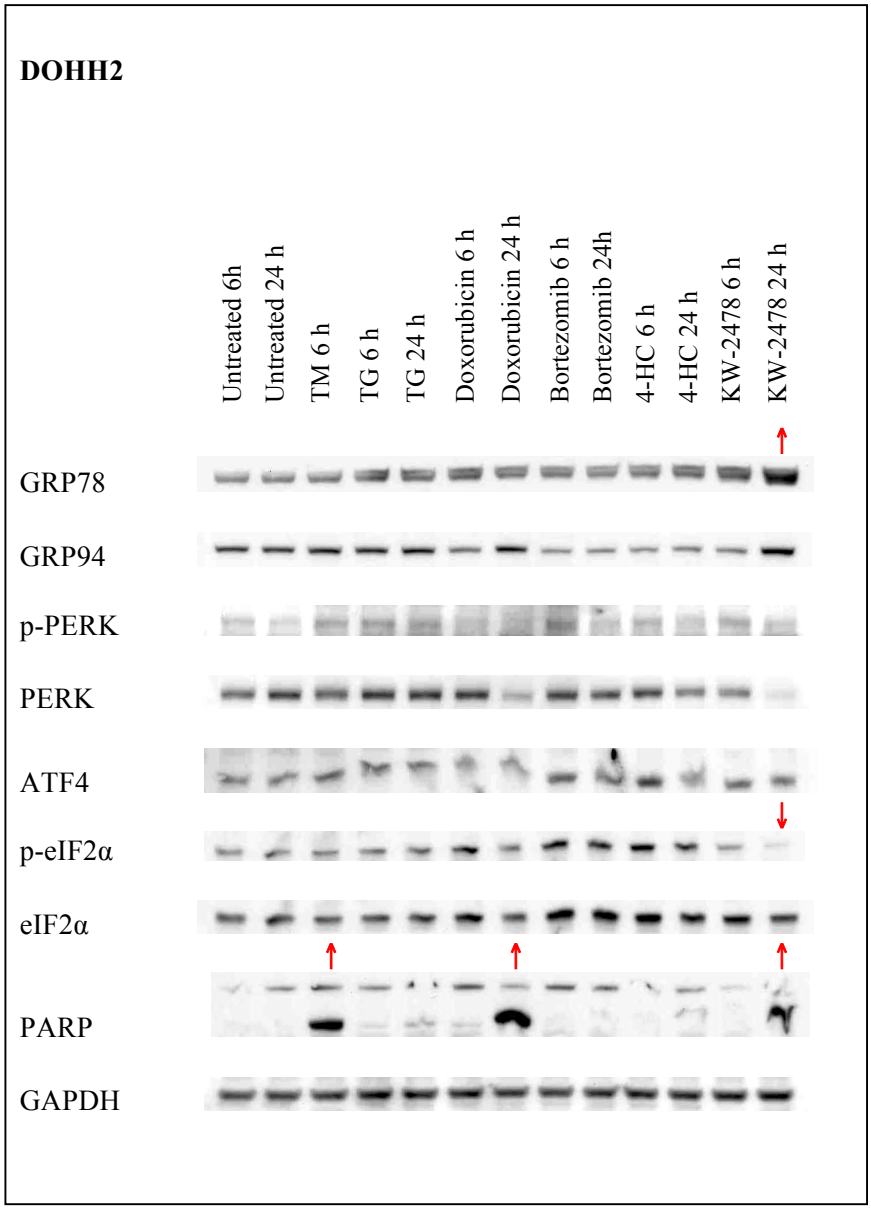

Figure 4.17. Western blotting experiments to investigate activation of unfolded protein response markers after treatment with EC_{50} concentrations of drug for 6 and 24 hours in the lymphoma cell line DOHH2. GAPDH is included as a loading control. The TM 24 hour treated sample could not be included as the protein content of the sample was insufficient for western blotting.

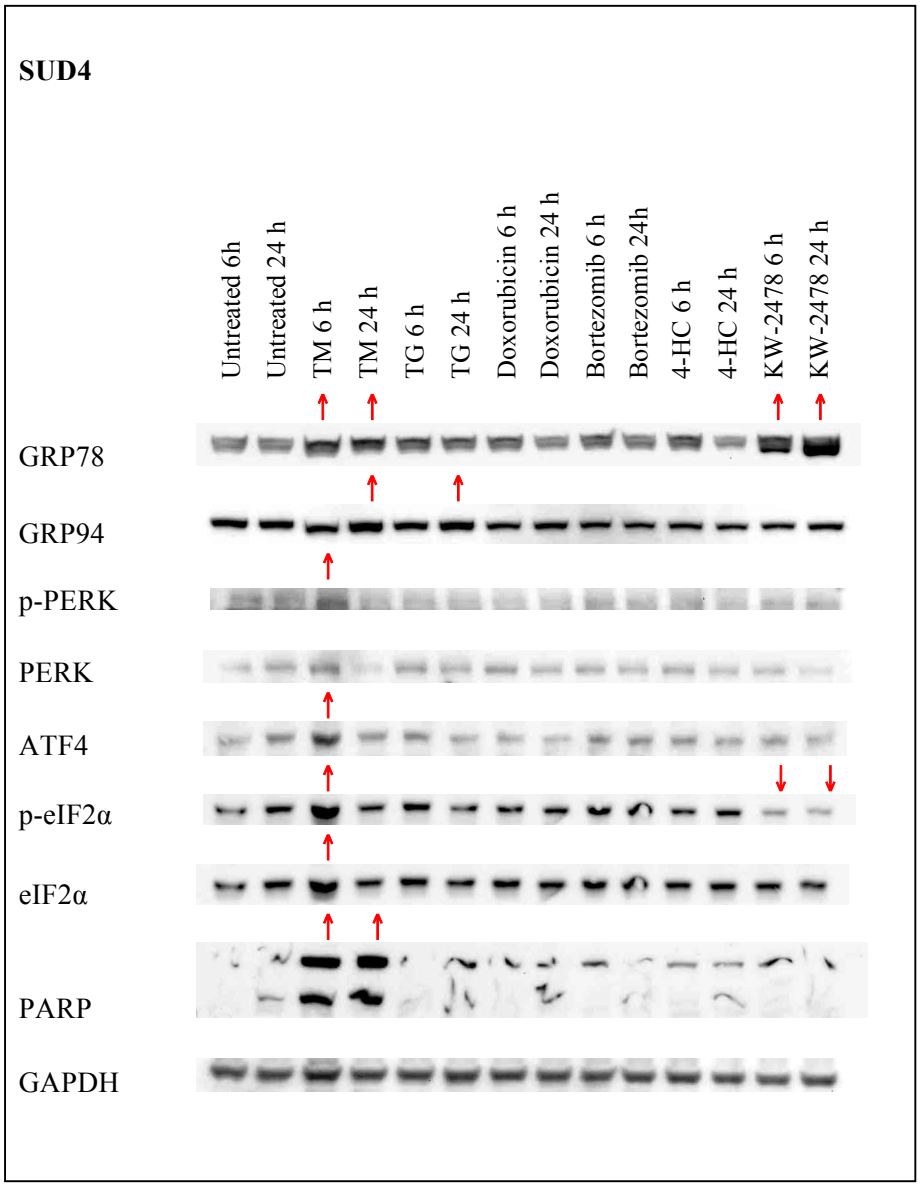

Figure 4.18. Western blotting experiments to investigate activation of unfolded protein response markers after treatment with EC_{50} concentrations of drug for 6 and 24 hours in the lymphoma cell line SUD4. GAPDH is included as a loading control.

Figures 4.19 to 4.27 show summaries of protein expression of key UPR markers after treatment with minimally toxic (EC_5) and cytotoxic (EC_{25} and EC_{50}) concentrations of each drug for 6 and 24 hours compared to the untreated control. This provides an overview of the effect of each drug at the various concentrations in the cell line panel studied. The proteins listed in each table highlight key findings and are not an exhaustive list of the

proteins studied in each cell line. Figures 4.19 and 4.20 summarise the data for the two ER stress inducing agents tunicamycin and thapsigargin. Figure 4.19 illustrates that tunicamycin treatment caused some increases in the protein levels of both molecular chaperones GRP78 and GRP94. Some increases in expression of PERK pathway proteins were also seen. At the EC_{25} concentration an increase in phosphorylated and total IRE1 protein was seen in the RPMI-8226 cell line compared to untreated control, but not in the U266 cell line.

Figure 4.20 shows that thapsigargin treatment caused some increases in the protein levels of the molecular chaperones GRP78 and GRP94. At minimally toxic concentrations the only increases in molecular chaperone protein levels were in the HL60 cell line (GRP78) and SUD4 cell line (GRP94). Phosphorylated eIF2α protein levels were increased in the myeloma cell lines. In the multiple myeloma cell lines there was no change in phosphorylated IRE1 protein at the minimally toxic thapsigargin concentration, however an increase was seen with the cytotoxic concentration in the RPMI-8226 cell line. An increase in total IRE1 receptor protein levels was seen in the U266 cell line at both minimally toxic and cytotoxic thapsigargin concentrations following 24 hours of treatment.

Cell line	Protein	TM EC_5 6 hr	TM EC_5 24 hr	TM EC_{25} 6 hr	TM EC_{25} 24 hr	TM EC_{50} 6 hr	TM EC_{50} 24 hr
HL60	GRP78						
THP1	GRP78						
RPMI8226	GRP78						
U266	GRP78						
DOHH2	GRP78						
SUD4	GRP78						
HL60	GRP94						
THP1	GRP94						
RPMI8226	GRP94						
U266	GRP94						
DOHH2	GRP94						
SUD4	GRP94						
HL60	p-eIF2α						
THP1	p-eIF2α						
RPMI8226	p-eIF2α						
U266	p-eIF2α						
DOHH2	p-eIF2α						
SUD4	p-eIF2α						
HL60	eIF2α						
THP1	eIF2α						
RPMI8226	eIF2α						
U266	eIF2α						
DOHH2	eIF2α						
SUD4	eIF2α						
DOHH2	p-PERK						
SUD4	p-PERK						
DOHH2	PERK						
SUD4	PERK						
RPMI8226	p-IRE1						
U266	p-IRE1						
RPMI8226	IRE1						
U266	IRE1						

Figure 4.19. Summary of protein levels of key UPR markers after treatment with minimally toxic (EC_5) and cytotoxic (EC_{25} and EC_{50}) concentrations of tunicamycin (TM) for 6 and 24 hours, where:

Increase in protein compared to untreated control
No change in protein compared to untreated control
Decrease in protein compared to untreated control

Cell line	Protein	TG EC_5 6 hr	TG EC_5 24 hr	TG EC_{25} 6 hr	TG EC_{25} 24 hr	TG EC_{50} 6 hr	TG EC_{50} 24 hr
HL60	GRP78						
THP1	GRP78						
RPMI8226	GRP78						
U266	GRP78						
DOHH2	GRP78						
SUD4	GRP78						
HL60	GRP94						
THP1	GRP94						
RPMI8226	GRP94						
U266	GRP94						
DOHH2	GRP94						
SUD4	GRP94						
HL60	p-eIF2α						
THP1	p-eIF2α						
RPMI8226	p-eIF2α						
U266	p-eIF2α						
DOHH2	p-eIF2α						
SUD4	p-eIF2α						
HL60	eIF2α						
THP1	eIF2α						
RPMI8226	eIF2α						
U266	eIF2α						
DOHH2	eIF2α						
SUD4	eIF2α						
DOHH2	p-PERK						
SUD4	p-PERK						
DOHH2	PERK						
SUD4	PERK						
RPMI8226	p-IRE1						
U266	p-IRE1						
RPMI8226	IRE1						
U266	IRE1						

Figure 4.20. Summary of protein levels of key UPR markers after treatment with minimally toxic (EC_5) and cytotoxic (EC_{25} and EC_{50}) concentrations of thapsigargin (TG) for 6 and 24 hours, where:

Increase in protein compared to untreated control
No change in protein compared to untreated control
Decrease in protein compared to untreated control

Figures 4.21 to 4.24 summarise the western blot data for the effect of doxorubicin, bortezomib, 4-HC and KW-2478 respectively on the activation of UPR marker proteins. These drugs were tested in all cell lines in the panel.

Few changes were observed in the UPR proteins studied following treatment with doxorubicin (see figure 4.25). Increases were seen in the molecular chaperone GRP78 in the AML cell line HL60, and GRP94 protein in the lymphoma cell line SUD4 after 6 hours. An increase in phosphorylated eIF2α was seen after treatment with the EC_5 and EC_{25} concentrations of doxorubicin for 24 hours in the U266 cell line. In the myeloma cell lines, no changes were seen in phosphorylated or total IRE1 receptor activation after doxorubicin treatment with minimally toxic or cytotoxic concentrations for 6 or 24 hours.

Cell line	Protein	Dox EC_5 6 hr	Dox EC_5 24 hr	Dox EC_{25} 6 hr	Dox EC_{25} 24 hr	Dox EC_{50} 6 hr	Dox EC_{50} 24 hr
HL60	GRP78						
THP1	GRP78						
RPMI8226	GRP78						
U266	GRP78						
DOHH2	GRP78						
SUD4	GRP78						
HL60	GRP94						
THP1	GRP94						
RPMI8226	GRP94						
U266	GRP94						
DOHH2	GRP94						
SUD4	GRP94						
HL60	p-eIF2α						
THP1	p-eIF2α						
RPMI8226	p-eIF2α						
U266	p-eIF2α						
DOHH2	p-eIF2α						
SUD4	p-eIF2α						
HL60	eIF2α						
THP1	eIF2α						
RPMI8226	eIF2α						
U266	eIF2α						
DOHH2	eIF2α						
SUD4	eIF2α						
DOHH2	p-PERK						
SUD4	p-PERK						
DOHH2	PERK						
SUD4	PERK						
RPMI8226	p-IRE1						
U266	p-IRE1						
RPMI8226	IRE1						
U266	IRE1						

Figure 4.21. Summary of protein levels of key UPR markers after treatment with minimally toxic (EC_5) and cytotoxic (EC_{25} and EC_{50}) concentrations of doxorubicin (dox) for 6 and 24 hours, where:

Increase in protein compared to untreated control
No change in protein compared to untreated control
Decrease in protein compared to untreated control

The effects of bortezomib treatment on UPR activation are summarised in figure 4.22. Some changes in levels of both GRP78 and GRP94 proteins were observed after bortezomib treatment. Increases were observed in the level of GRP78 protein in the AML cell lines, HL60 and THP1, and the myeloma cell line U266. In the SUD4 cell line, GRP94 protein levels increased after treatment with the minimally toxic and cytotoxic EC_{25} concentrations for 6 hours. The U266 myeloma cell line showed a decrease in the level of phosphorylated and total IRE1 protein after treatment with the cytotoxic EC_{25} bortezomib concentration for 24 hours, with no changes seen in the RPMI-8226 cell line.

Cell line	Protein	Bort EC_5 6 hr	Bort EC_5 24 hr	Bort EC_{25} 6 hr	Bort EC_{25} 24 hr	Bort EC_{50} 6 hr	Bort EC_{50} 24 hr
HL60	GRP78						
THP1	GRP78						
RPMI8226	GRP78						
U266	GRP78						
DOHH2	GRP78						
SUD4	GRP78						
HL60	GRP94						
THP1	GRP94						
RPMI8226	GRP94						
U266	GRP94						
DOHH2	GRP94						
SUD4	GRP94						
HL60	p-eIF2α						
THP1	p-eIF2α						
RPMI8226	p-eIF2α						
U266	p-eIF2α						
DOHH2	p-eIF2α						
SUD4	p-eIF2α						
HL60	eIF2α						
THP1	eIF2α						
RPMI8226	eIF2α						
U266	eIF2α						
DOHH2	eIF2α						
SUD4	eIF2α						
DOHH2	p-PERK						
SUD4	p-PERK						
DOHH2	PERK						
SUD4	PERK						
RPMI8226	p-IRE1						
U266	p-IRE1						
RPMI8226	IRE1						
U266	IRE1						

Figure 4.22. Summary of protein levels of key UPR markers after treatment with minimally toxic (EC_5) and cytotoxic (EC_{25} and EC_{50}) concentrations of bortezomib (bort) for 6 and 24 hours, where:

Increase in protein compared to untreated control
No change in protein compared to untreated control
Decrease in protein compared to untreated control

Similarly to doxorubicin, drug treatment with 4-HC did not result in UPR activation to the same extent as some of the other drugs tested. An increase in GRP78 protein was seen in the HL60 cell line after 6 hours of treatment with both the minimally toxic and EC_{25} cytotoxic concentrations. Changes in the level of GRP94 protein was only seen in the SUD4 cell line, with an increase in GRP94 protein was observed after treatment with the EC_5 and EC_{25} concentrations of 4-HC for 6 hours.

Cell line	Protein	4-HC EC_5 6 hr	4-HC EC_5 24 hr	4-HC EC_{25} 6 hr	4-HC EC_{25} 24 hr	4-HC EC_{50} 6 hr	4-HC EC_{50} 24 hr
HL60	GRP78						
THP1	GRP78						
RPMI8226	GRP78						
U266	GRP78						
DOHH2	GRP78						
SUD4	GRP78						
HL60	GRP94						
THP1	GRP94						
RPMI8226	GRP94						
U266	GRP94						
DOHH2	GRP94						
SUD4	GRP94						
HL60	p-eIF2α						
THP1	p-eIF2α						
RPMI8226	p-eIF2α						
U266	p-eIF2α						
DOHH2	p-eIF2α						
SUD4	p-eIF2α						
HL60	eIF2α						
THP1	eIF2α						
RPMI8226	eIF2α						
U266	eIF2α						
DOHH2	eIF2α						
SUD4	eIF2α						
DOHH2	p-PERK						
SUD4	p-PERK						
DOHH2	PERK						
SUD4	PERK						
RPMI8226	p-IRE1						
U266	p-IRE1						
RPMI8226	IRE1						
U266	IRE1						

Figure 4.23. Summary of protein levels of key UPR markers after treatment with minimally toxic (EC_5) and cytotoxic (EC_{25} and EC_{50}) concentrations of 4-HC for 6 and 24 hours, where:

Increase in protein compared to untreated control
No change in protein compared to untreated control
Decrease in protein compared to untreated control

A number of changes in UPR proteins were seen following treatment with the novel HSP90 inhibitor KW-2478 in the cell line panel studied, with the molecular chaperone protein GRP78 being particularly affected (see figure 4.24). Increases were seen in GRP78 protein following KW-2478 treatment in all cell lines. Marked increases in GRP78 protein levels were also seen at a number of KW-2478 concentrations and time points. The AML cell lines were most affected by HSP90 inhibitor treatment in terms of GRP78 changes, however, no changes were seen in GRP94 protein levels in these cell lines. In the HL60 and THP1 cell lines, GRP78 protein increased following all treatments except the EC_{50} concentration for 6 hours, with a marked increase observed after 24 hours treatment. Increased GRP78 protein was also seen in the RPMI-8226 myeloma cell line at the higher two concentrations, with a marked increase with 24 hours treatment with the 25% cell death concentration and the EC_{50} concentration at both 6 and 24 hours. In the U266 myeloma cell line, increased GRP78 protein was observed following treatment with the EC_{25} concentration for 24 hours, the 25% cell death concentration at both time points (marked increase after 24 hours) and a marked increase with 24 hours EC_{50} concentration treatment. DOHH2 cells treated KW-2478 for 24 hours resulted in increased GRP78 protein (with the exception of the EC_{25} concentration). The SUD4 cell line showed an increase in GRP78 protein at the two higher concentrations at both 6 and 24 hours, with a marked increase following the EC_{50} concentration for 24 hours. The only changes observed in GRP94 protein levels were in the SUD4 cell line, with an increase in the level of GRP94 protein after treatment with the three lower concentrations of KW-2478 at 6 hours, although no change was observed with the highest drug concentration studied.

Whilst there were some increases observed in phosphorylated eIF2α, there was a general trend towards decreased levels of this protein following KW-2478 treatment in the affected cell lines. There was also a difference in the effect of KW-2478 treatment on phosphorylated PERK protein levels between the lymphoma cell lines. In the DOHH2 cell line, there was no change at the minimally toxic concentration, a decrease in protein at the

EC_{25} concentration, a marked decrease in protein at the 25% cell death concentration. After treatment with the 25% cell death concentration of KW-2478 in the SUD4 cell line, there was an increase in phosphorylated PERK protein at 6 hours. There were no changes observed in the level of phosphorylated IRE1 protein in the myeloma cell lines. There was an increase in total IRE1 protein after treatment with the minimally toxic EC_5 concentration for 24 hours in the U266 cell line, with a decrease in IRE1 protein seen following treatment with the concentration resulting in 25% cell death at 6 and 24 hours.

Cell line	Protein	KW EC_5 6 h	KW EC_5 24 h	KW EC_{25} 6 h	KW EC_{25} 24 h	KW 25% cell death 6 h	KW 25% cell death 24 h	KW EC_{50} 6 h	KW EC_{50} 24 h
HL60	GRP78								
THP1	GRP78								
RPMI8226	GRP78								
U266	GRP78								
DOHH2	GRP78								
SUD4	GRP78								
HL60	GRP94								
THP1	GRP94								
RPMI8226	GRP94								
U266	GRP94								
DOHH2	GRP94								
SUD4	GRP94								
HL60	p-eIF2α								
THP1	p-eIF2α								
RPMI8226	p-eIF2α								
U266	p-eIF2α								
DOHH2	p-eIF2α								
SUD4	p-eIF2α								
HL60	eIF2α								
THP1	eIF2α								
RPMI8226	eIF2α								
U266	eIF2α								
DOHH2	eIF2α								
SUD4	eIF2α								
DOHH2	p-PERK								
SUD4	p-PERK								
DOHH2	PERK								
SUD4	PERK								
RPMI8226	p-IRE1								
U266	p-IRE1								
RPMI8226	IRE1								
U266	IRE1								

Figure 4.24. Summary of protein levels of key UPR markers after treatment with minimally toxic (EC_5) and cytotoxic (EC_{25}, $EC_{25\%\ cell\ death}$ and EC_{50}) concentrations of KW-2478 (KW) for 6 and 24 hours, where:

Increase in protein compared to untreated control
No change in protein compared to untreated control
Decrease in protein compared to untreated control

Figure 4.25 summarises the western blot data for the effect of cytarabine and etoposide respectively on the activation of UPR marker proteins. These drugs were tested in the AML cell lines HL60 and THP1. As with doxorubicin and 4-HC, few changes in UPR proteins were observed following cytarabine and etoposide treatment. Some increases were seen in the levels of the chaperone proteins GRP78 and GRP94 with both drugs at the minimally toxic and EC_{25} cytotoxic concentrations, although no such increases were seen with EC_{50} concentrations of either drug. No changes were seen in phosphorylated or total eIF2α protein levels in either cell line.

Cell line	Protein	Cyt EC_5 6 hr	Cyt EC_5 24 hr	Cyt EC_{25} 6 hr	Cyt EC_{25} 24 hr	Cyt EC_{50} 6 hr	Cyt EC_{50} 24 hr
HL60	GRP78						
THP1	GRP78						
HL60	GRP94						
THP1	GRP94						
HL60	p-eIF2α						
THP1	p-eIF2α						
HL60	eIF2α						
THP1	eIF2α						

Cell line	Protein	Etop EC_5 6 hr	Etop EC_5 24 hr	Etop EC_{25} 6 hr	Etop EC_{25} 24 hr	Etop EC_{50} 6 hr	Etop EC_{50} 24 hr
HL60	GRP78						
THP1	GRP78						
HL60	GRP94						
THP1	GRP94						
HL60	p-eIF2α						
THP1	p-eIF2α						
HL60	eIF2α						
THP1	eIF2α						

Figure 4.25. Summary of protein levels of key UPR markers after treatment with minimally toxic (EC_5) and cytotoxic (EC_{25} and EC_{50}) concentrations of cytarabine (cyt - top) and etoposide (etop - bottom) for 6 and 24 hours, where:

Increase in protein compared to untreated control
No change in protein compared to untreated control
Decrease in protein compared to untreated control

Figure 4.26 summarises the western blot data for the effect of melphalan on the activation of UPR marker proteins. These drugs were tested in the myeloma cell lines RPMI-8226 and U266. As can be seen from the figure, fewer changes were seen on UPR protein levels after melphalan treatment compared to the other agents investigated. At the highest concentration following 24 hours treatment, there was an increase in the levels of GRP78 and GRP94 proteins in the U266 cell line.

Cell line	Protein	Mel EC_5 6 hr	Mel EC_5 24 hr	Mel EC_{25} 6 hr	Mel EC_{25} 24 hr	Mel EC_{50} 6 hr	Mel EC_{50} 24 hr
RPMI8226	GRP78						
U266	GRP78						
RPMI8226	GRP94						
U266	GRP94						
RPMI8226	p-eIF2α						
U266	p-eIF2α						
RPMI8226	eIF2α						
U266	eIF2α						
RPMI8226	ATF6 50kDa						
U266	ATF6 50kDa						
RPMI8226	p-IRE1						
U266	p-IRE1						
RPMI8226	IRE1						
U266	IRE1						

Figure 4.26. Summary of protein levels of key UPR markers after treatment with minimally toxic (EC_5) and cytotoxic (EC_{25} and EC_{50}) concentrations of melphalan (mel) for 6 and 24 hours, where:

Increase in protein compared to untreated control
No change in protein compared to untreated control
Decrease in protein compared to untreated control

4.4 Discussion

The experiments described here established the extent of UPR activation in this haematological cell line panel as a result of treatment with a number of drugs. These experiments focus only on UPR activation occurring at the translational level, as opposed to

the transcriptional level (i.e. mRNA). This was in order to confirm that any changes in UPR markers observed were not just occurring at the transcriptional level, but were actually resulting in changes to protein translation. These translational changes were considered to be more relevant clinically, particularly in terms of chemosensitivity.

Due to the large scope of the work undertaken in this chapter, it was not possible to repeat every experiment multiple times, however, experiments with notable results were repeated, such as IRE1 activation in the myeloma cell lines. As a consequence, these experiments do not provide absolute or quantitative results, they do however provide a global snapshot of UPR activation in response to drug treatment at the time points studied. This overall view of the UPR as a whole was considered to be the most valuable to obtain, rather than looking in detail at only specific UPR components in isolation, hence the decision to approach the experiments in the manner described. Further experiments using densitometry software to analyse the results from three independent drug treatment and western blotting experiments would provide quantitative results and enable formal statistical analysis. This would provide a more robust analysis of UPR protein activation and allow for subsequent comparison and interpretation of the results obtained.

As in the previous chapter, it was decided to use a panel of anticancer drugs to study their effects on key UPR proteins, which included conventional cytotoxic drugs used in these tumour types, in addition to novel anticancer agents and ER stress inducing agents. Whilst there was some evidence of UPR activation after treatment with the conventional cytotoxic agents at the concentrations and time points studied, a far greater degree of UPR activation at the protein level was seen with the ER stress inducing drugs and novel anticancer agents. This finding suggests that the unfolded protein response is less significant with regard to treatment with conventional cytotoxic chemotherapy. This is also interesting as it suggests that in response to agents with a mechanism of action that differs from the conventional DNA damaging cytotoxicity, the unfolded protein response may play a greater role. For

example, the HSP90 inhibitor KW-2478 had little effect on cell viability in the majority of cell lines studied, with this compound appearing to exert its anticancer effect via its significant antiproliferative activity (see chapter 3). As a result of the experiments described in this chapter, it can be seen that UPR changes at the translational level in response to treatment with KW-2478 was more pronounced than with any of the other agents tested. In the case of the molecular chaperone GRP78, the increases seen were more marked (occurring even at minimally toxic concentrations in some cell lines) than with both ER stress inducing agents. This finding may be related to the action of this agent in binding to and inhibiting HSP90 (and its ER homologue GRP94) and suggests the possibility of a resulting compensatory increase in the key ER chaperone (and HSP70 family member) GRP78. This increase may be activated in an attempt to maintain ER protein homeostasis.

A number of other notable changes in UPR proteins were detected in response to drug treatment. One such change was activation of IRE1 receptor in response to drug treatment. It was described in chapter 3 that the multiple myeloma cell lines expressed higher levels of IRE1 protein than the leukaemia or lymphoma cell lines studied. In the drug activity studies described here, changes were observed in IRE1 protein levels in response to treatment. Differences were also seen between the multiple myeloma cell lines in their response to drug treatment. In the RPMI-8226 cell line, there was no phosphorylated (activated) IRE1 receptor protein visible in the untreated control samples, although total IRE1 protein was present. Phosphorylated IRE1 protein was only seen following treatment with EC_{25} concentrations of tunicamycin and thapsigargin (at both 6 and 24 hours) in this cell line. In contrast, phosphorylated IRE1 protein was observed in all U266 cell line samples, including the untreated control samples (at both time points). Experiments were carried out to look for IRE1 protein phosphorylation in the AML and DLBCL cell lines, but were unable to detect any protein under these experimental conditions. Experiments were also undertaken to detect the protein product of spliced XBP1 mRNA (this splicing of XBP1 mRNA occurs downstream of IRE activation). Spliced XBP1 protein product was detected

only in the myeloma cell lines, as evidenced by a faint band. However, no change in the protein was detected following treatment with any of the drug concentrations tested. Even in the presence of confirmed IRE1 receptor activation (phosphorylation), evidence of increased XBP1s protein levels was not seen in these experiments. This is most likely due to a problem with the antibody used, and further experiments using RT-PCR to detect XBP1s mRNA would therefore be valuable.

Some UPR proteins studied showed a mixed response to drug treatment, for example eIF2α protein. Phosphorylated and total eIF2α protein showed both increases and decreases in protein levels in response to drug treatment, although in general, there appeared to be a trend towards either increased protein levels, no change, or decreased protein levels following treatment with a particular drug, for example, after KW-2478 there was a pattern of decreased phosphorylated eIF2α protein.

In conclusion, it can be seen that KW-2478 treatment had the greatest effect on the activation of the UPR proteins studied, followed by the ER stress inducing agents and bortezomib. The conventional chemotherapy agents doxorubicin, 4-HC, cytarabine, etoposide and melphalan all had a minimal effect on the activation of the UPR proteins investigated here.

5. Treatment with Minimally Toxic Concentrations of ER Stress Inducing Agent and Effect on Chemosensitivity *in vitro*

5.1 Introduction

In addition to normal cellular stresses, a number of pharmacological agents have been shown to induce ER stress and trigger the ER stress response, thereby activating the unfolded protein response. One such agent is thapsigargin; a sesquiterpene lactone extracted from the plant, *Thapsia garganica*. It is an effective inhibitor of sarcoplasmic endoplasmic reticulum calcium ATPases (known as SERCA pumps). This inhibition leads to leakage of ER calcium, resulting in ER stress (Kijima *et al.*, 1991). Thapsigargin is a potent inducer of ER stress, with inhibition of the SERCA pumps at concentrations as low as 10^{-10}M (Sagara and Inesi, 1991). Along with tunicamycin, thapsigargin is commonly used by researchers to induce ER stress in order to study such stress and the resultant unfolded protein response.

Published research investigating the role of thapsigargin in modulating chemosensitivity have reported mixed results, with some studies describing sensitisation and others reporting resistance. Like tunicamycin, thapsigargin has been shown to sensitise melanoma cells to TRAIL-induced apoptosis by inducing ER stress and the unfolded protein response (Chen *et al.*, 2007). It has been reported that multidrug resistant cells deficient in the proapoptotic Bcl-2 family members Bax and Bak are sensitive to ER stress mediated cell death (caspase independent) following treatment with thapsigargin (Janssen *et al.*, 2009). Thapsigargin treatment was also shown to sensitise prostate cancer cells to the taxane chemotherapy agents paclitaxel and docetaxel (Wu *et al.*, 2009). However, thapsigargin has also been associated with chemoresistance. A study in rats revealed that thapsigargin treatment enhanced P-gp expression and transport function in liver cancer cells, known to be involved in the development of drug resistance. This effect was mediated by the endoplasmic reticulum stress response and involved MDR transcriptional induction through

c-Jun activation (Ledoux *et al.*, 2003). ER stress induction with tunicamycin has also been reported to lead to activation of p38 (via GRP78 upregulation and PERK activation) thereby protecting dormant tumor cells from chemotherapy and other stressors (Ranganathan *et al.*, 2006).

Another interesting area of research is the development of prodrugs of thapsigargin to inhibit SERCA pumps as a novel targeted treatment strategy in prostate cancer. The thapsigargin prodrug (thapsigargin coupled to a targeting peptide) is activated by the proteolytic enzyme prostate specific antigen (PSA) and has been shown to be selectively toxic to prostate cancer cells in preclinical studies *in vitro* and *in vivo* (Christensen *et al.*, 2009, Denmeade and Isaacs, 2005). If this approach proves succesful it would provide a solution to the important issue of thapsigargin cytotoxicity to normal cells and it may eventually be possible to apply this targeted strategy to other tumour types.

In this chapter, the effect of combining minimally toxic concentrations of the ER stress inducer thapsigargin on the activity of anticancer agents in haematological cell lines *in vitro* has been studied. Thapsigargin was chosen over tunicamycin as an ER stress inducing agent due to the high concentrations of tunicamycin necessary for ER stress induction and its associated toxicity. In contrast to other studies, minimally toxic concentrations of thapsigargin were used in an attempt to increase the relevance to clinical use of these agents, where treatment aims to minimise the potential toxicity to non-cancerous cells that would occur with higher concentrations. Two schedules of thapsigargin combinations were investigated; simultaneous treatment with thapsigargin and drug for 48 hours, and 6 hours of thapsigargin pretreatment followed by the addition of drugs for 48 hours. Previous experiments in this thesis have established that the UPR is activated in these cell lines following minimally toxic thapsigargin concentrations, with 6 hours of thapsigargin treatment sufficient to show UPR activation.

5.2 Materials and Methods

5.2.1 Cytotoxicity Studies

The effect of drug treatment on cell viability was investigated using a plate based adenosine triphosphate (ATP) cytotoxicity assay (see chapter 2.5). Cells in exponential growth phase were plated into 96 well plates (5000 cells per well in 100µl medium) and incubated for 24 hours. Cells were treated with thapsigargin (at two minimally toxic concentrations; approximate EC_5 and approximate EC_{15} based on previous cell viability experiments), and 2 concentrations each of doxorubicin (dox), bortezomib (bort), 17-AAG, and SAHA (approximate EC_{20} and EC_{50}). The concentrations of thapsigargin used in each cell line are shown in table 5.1 below.

Cell line	Approximate EC_5	Approximate EC_{15}
HL60	0.05nM	0.5nM
THP1	1nM	5nM
RPMI-8226	0.5nM	5nM
U266	1nM	5nM
DOHH2	0.05nM	0.5nM
SUD4	2nM (simultaneous) 1nM (pretreatment)	10nM

Table 5.1. Approximate EC_5 and EC_{15} concentrations of thapsigargin used in cytotoxicity studies.

The effects of both simultaneous drug treatment and pre-treatment for 6 hours with thapsigargin were investigated. Varying concentrations of drug were diluted in culture medium and then added to each well to obtain the required final concentration. Single agent treated wells, combination treated wells, and untreated control wells were present on each plate in the combination experiments. Control wells and single agent treatment wells were topped up with culture medium so that all wells of the plate contained a fixed volume of 120µl. Plates were then incubated for 48 hours at 37°C and 5% CO_2 in air, before analysis

using the ViaLight HS assay kit (Lonza Group Ltd, Switzerland) in conjunction with a BMG Labtech Polarstar Optima microplate reader (BMG Labtech, Germany).

Simultaneous treatment experiments were carried out in a cell line panel consisting of 2 AML cell lines (HL-60, THP1), 2 MM cell lines (RPMI-8226, U266) and 2 DLBCL cell lines (DOHH2, SUD4). Pretreatment experiments were carried out in 1 AML cell line (THP1), 1 MM cell line (U266) and 1 DLBCL cell line (SUD4). Experiments were repeated at least three times on separate occasions to ensure reproducibility, with the exception of the DOHH2 cell line where experiments were repeated twice. The effect of thapsigargin on the response to drug treatment was calculated using the fractional product method described by Webb (Webb, 1963) in order to determine if the effect of thapsigargin addition to drug treatment was additive, supra additive, or antagonistic. The ratio of the observed effect to the expected effect provides a measure of the interaction of two drugs used in a combination. If the ratio of the combination effect is 1 (i.e. the observed effect equals the expected effect), the combination is designated additive. If the ratio is less than 1 (i.e. the observed effect is greater than the expected effect), then the combination is considered to be supra-additive or synergistic. If the ratio is more than 1 (i.e. the observed effect is less than the expected effect), then the combination is said to be antagonistic.

5.2.2 Protein Analysis

Whole cell lysates were also prepared following drug treatments for use in western blotting experiments (see chapter 2.7). Western blotting was carried out as described in chapter 2.8, with 20μg of protein loaded in each lane of the gel. Blots were visualised using ECL (Amersham, UK) and a Fuji ImageQuant LAS 4000 camera (FujiFilm, Japan) used according to manufacturer's instructions.

5.2.3 Apoptosis Assay

The Guava Nexin assay (Guava Technologies Inc., USA) is a fluorescence based microplate apoptosis assay. Cells in exponential growth phase were plated into 96 well plates (10000 cells per well) and incubated at 37°C and 5% CO_2 in air for 24 hours before addition of drug solution. Cells were either pretreated with thapsigargin for 6 hours prior to the addition of drug, or treated only with drug for 48 hours. Cells were treated with the higher of the thapsigargin and drug concentrations used in the ATP cytotoxicity experiments in order to ensure detectable levels of apoptosis. The required amount of each drug was diluted in fresh culture medium and added to each well in order to achieve the desired molar concentration per well. Control wells and single agent treatment wells were topped up with culture medium so that all wells of the plate contained a fixed volume of 120µl. A positive control for apoptosis (doxorubicin 1µM) was included in all experiments. Cells were then returned to the incubator for a further 48 hours before addition of Guava Nexin Reagent to each plate well. Plates were incubated in the dark at room temperature for 20 minutes, then analysed using the Guava PCA – 96 System. All samples were run in triplicate and mean values and standard deviations used in subsequent data analysis. Data was presented as the percentage of cells per sample in each of the four cell populations. Total and viable cell number were also calculated for drug alone and drug with thapsigargin pretreatment (each normalised to its own control). As the concentrations of thapsigargin used were minimally toxic, the effect of thapsigargin pretreatment on chemosensitivity was also investigated using apoptosis assay at both higher thapsigargin and higher drug concentrations.

5.2.4 Statistical Analysis

Statistical analysis was performed using Microsoft Excel software, Microsoft Corporation, USA. The data obtained from the apoptosis assay was used to determine mean

and standard deviation values for each drug concentration. These values were then used for graphical representation and subsequent statistical analysis. Data was assumed to be normally distributed and parametric tests were therefore used throughout. Drug treatments were compared using a paired t-test, with a p value of less than 0.05 considered to be statistically significant.

5.3 Results

Cytotoxicity assay (ATP) results revealed a clear pattern of effect across all cell lines in the panel. The simultaneous administration of minimally toxic thapsigargin concentrations and chemotherapy resulted in additive to antagonistic effects in these haematological cancer cell lines. This effect was observed with both concentrations of thapsigargin used (i.e. EC_5 and EC_{15}), as seen in figures 5.1 to 5.4. Results are shown for the AML cell line THP1, myeloma cell line U266 and DLBCL cell line SUD4 (experimental data tables in appendix 2). These results are representative of all cell lines studied, with the results for the remaining cell lines given in appendix 2.

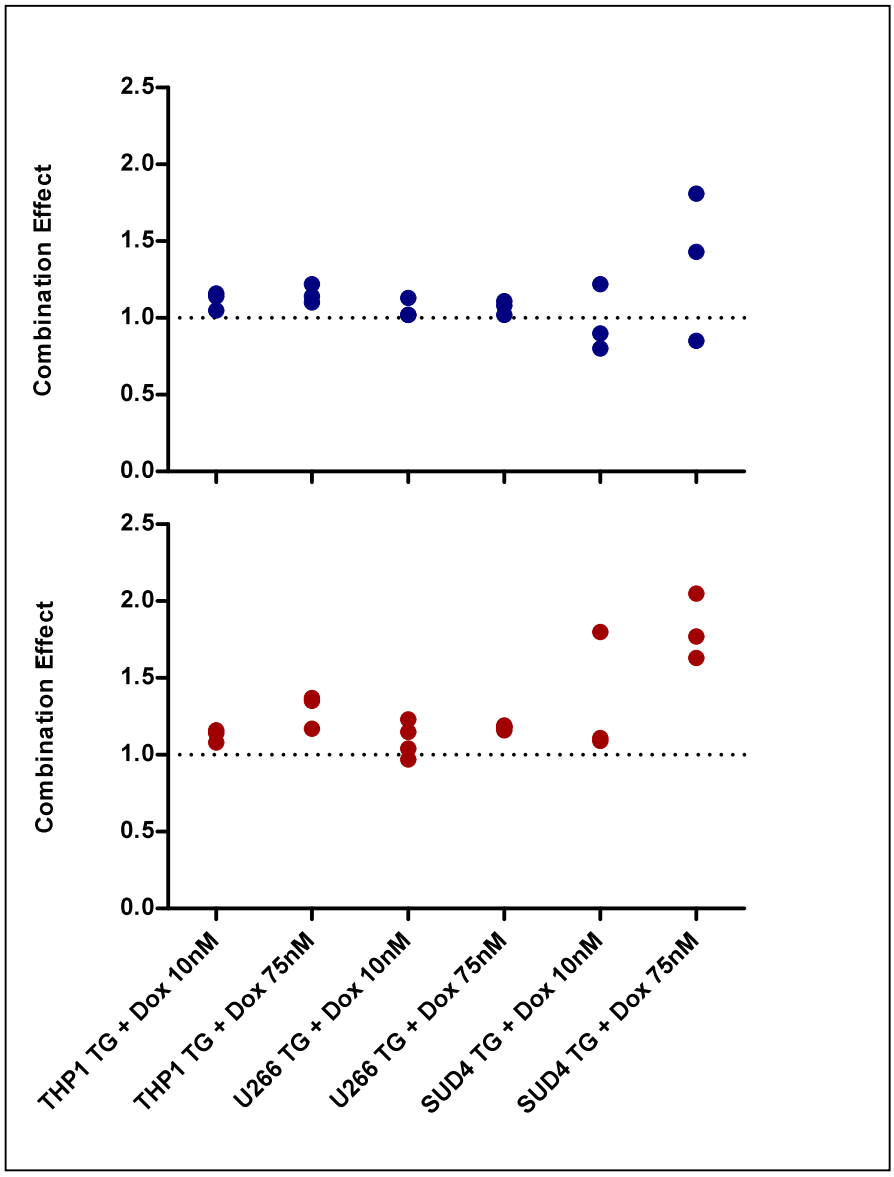

Figure 5.1. Effect of simultaneous treatment with EC_5 (top) and EC_{15} (bottom) thapsigargin (TG) concentrations and doxorubicin (Dox) for 48 hours on viable cell number (ATP content) in three haematological cancer cell lines. The combination effect compares the observed effect of the combination with the expected effect calculated using the fractional product method. Values ≈ 1 indicate an additive effect, values < 1 indicate synergy and values > 1 indicate antagonism. Results shown are from three separate experiments.

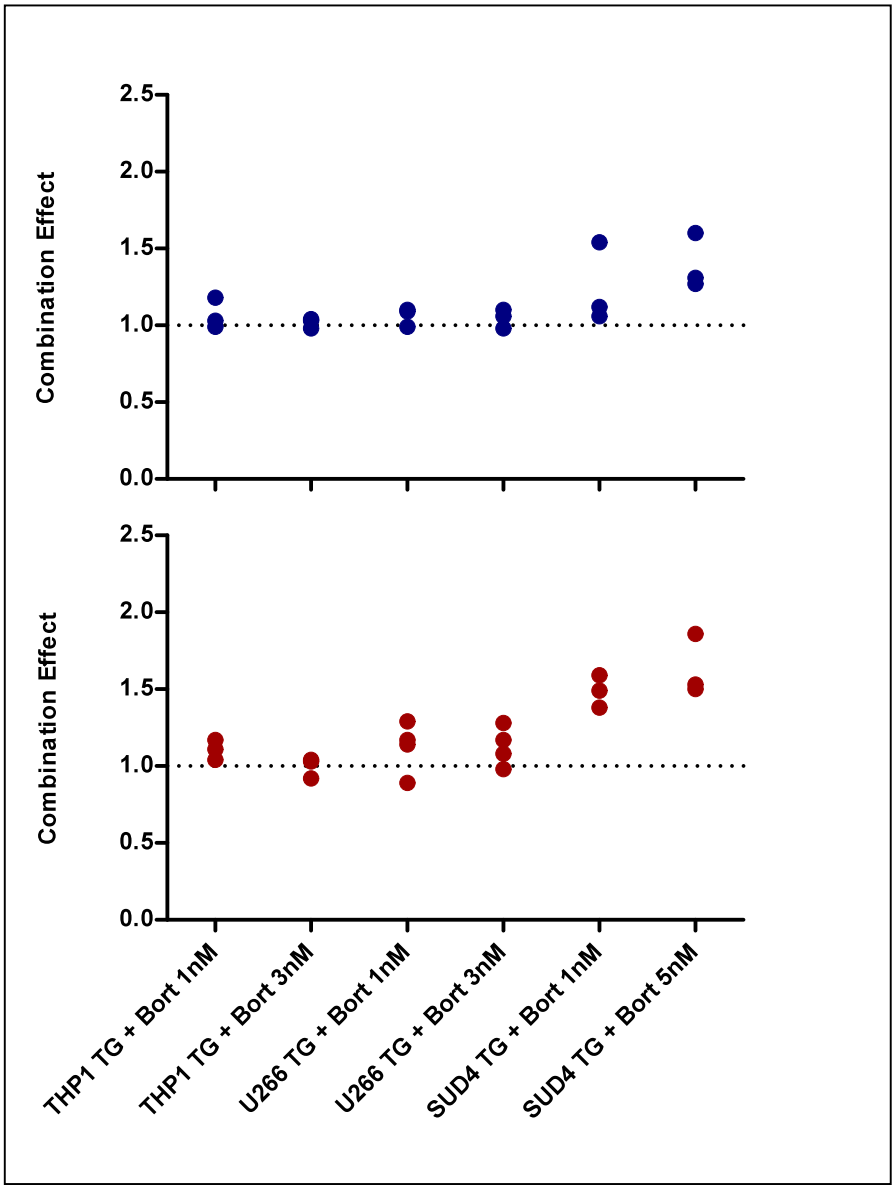

Figure 5.2. Effect of simultaneous treatment with EC_5 (top) and EC_{15} (bottom) thapsigargin (TG) concentrations and bortezomib (Bort) for 48 hours on viable cell number (ATP content) in three haematological cancer cell lines. The combination effect compares the observed effect of the combination with the expected effect calculated using the fractional product method. Values ≈ 1 indicate an additive effect, values < 1 indicate synergy and values > 1 indicate antagonism. Results shown are from three separate experiments.

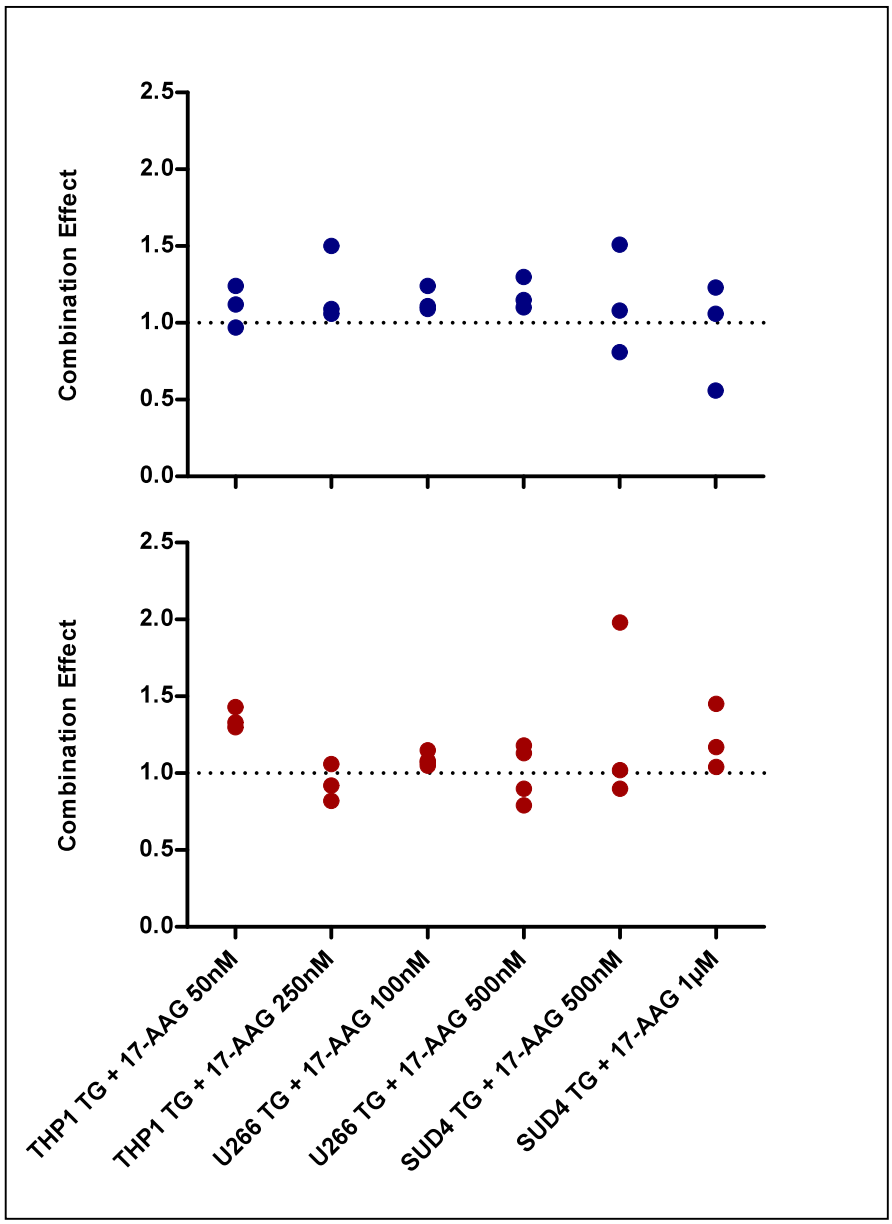

Figure 5.3. Effect of simultaneous treatment with EC_5 (top) and EC_{15} (bottom) thapsigargin (TG) concentrations and 17-AAG for 48 hours on viable cell number (ATP content) in three haematological cancer cell lines. The combination effect compares the observed effect of the combination with the expected effect calculated using the fractional product method. Values ≈ 1 indicate an additive effect, values < 1 indicate synergy and values > 1 indicate antagonism. Results shown are from three separate experiments.

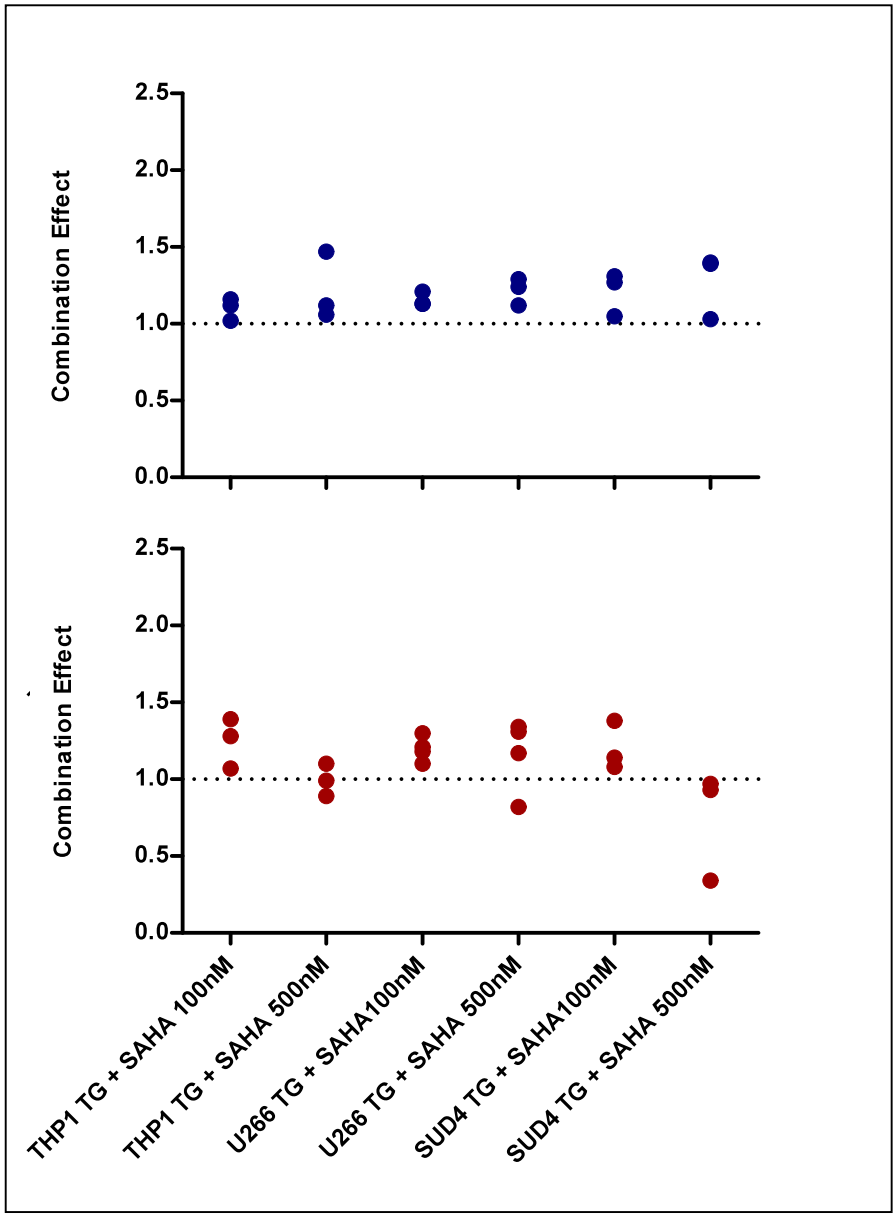

Figure 5.4. Effect of simultaneous treatment with EC_5 (top) and EC_{15} (bottom) thapsigargin (TG) concentrations and SAHA for 48 hours on viable cell number (ATP content) in three haematological cancer cell lines. The combination effect compares the observed effect of the combination with the expected effect calculated using the fractional product method. Values ≈ 1 indicate an additive effect, values < 1 indicate synergy and values > 1 indicate antagonism. Results shown are from three separate experiments.

The effect of pre-exposure, with minimally toxic concentrations of thapsigargin, was then investigated. As the pattern seen with simultaneous treatment was consistent across all cell lines in the panel, pre-exposure experiments were conducted in one cell line of each tumour type, namely THP1, U266 and SUD4. Figures 5.5 to 5.8 show the effect of 6 hours pretreatment with thapsigargin, followed by 48 hours further treatment with drug. Pre-exposure with minimally toxic thapsigargin concentrations resulted in chemoprotection, with antagonism of the effects of doxorubicin, bortezomib, 17-AAG and SAHA. Again, this effect was seen with both concentrations of thapsigargin, and in all cell lines studied.

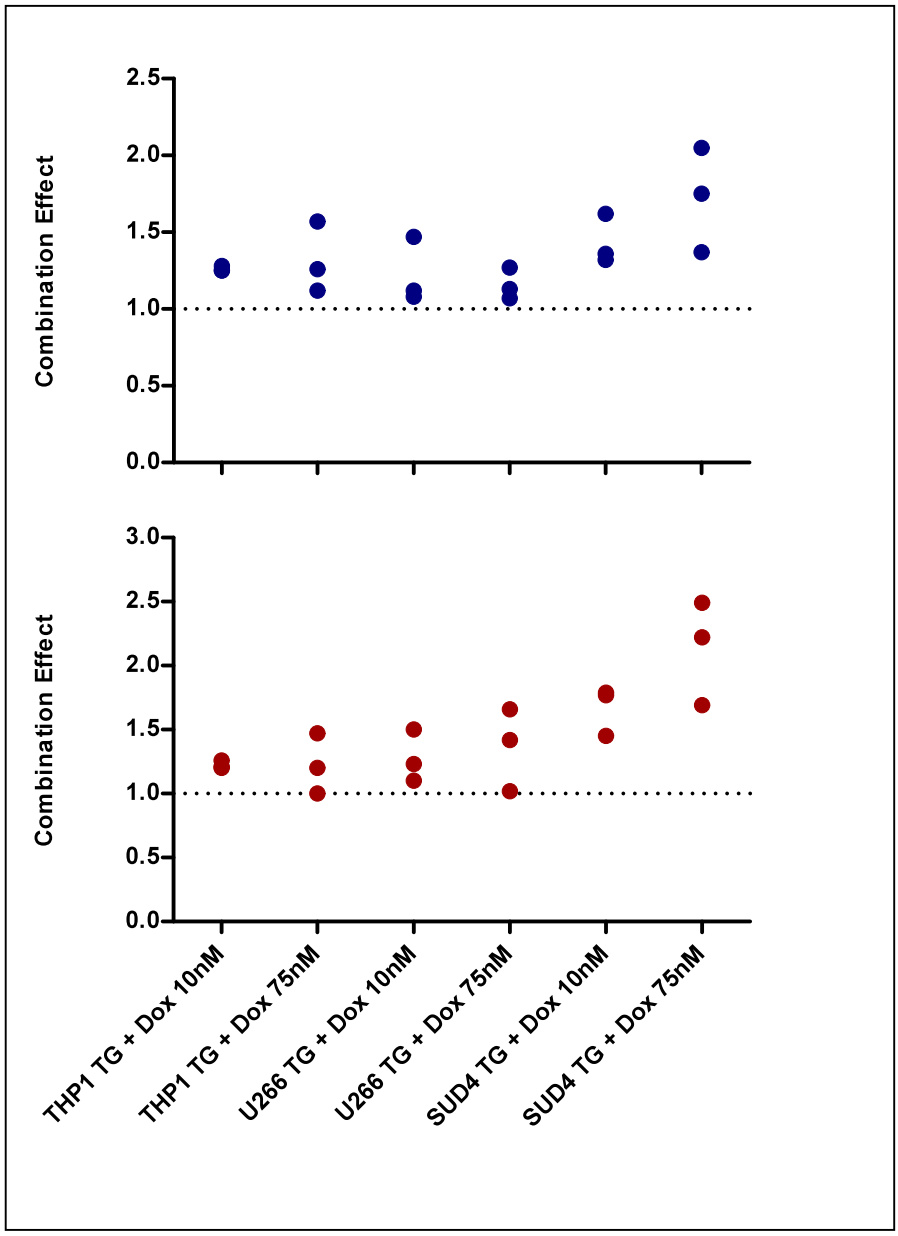

Figure 5.5. Effect of pretreatment with EC_5 (top) and EC_{15} (bottom) thapsigargin (TG) concentrations for 6 hours and doxorubicin (Dox) for a further 48 hours on viable cell number (ATP content) in three haematological cancer cell lines. The combination effect compares the observed effect of the combination with the expected effect calculated using the fractional product method. Values ≈ 1 indicate an additive effect, values < 1 indicate synergy and values > 1 indicate antagonism. Results shown are from three separate experiments.

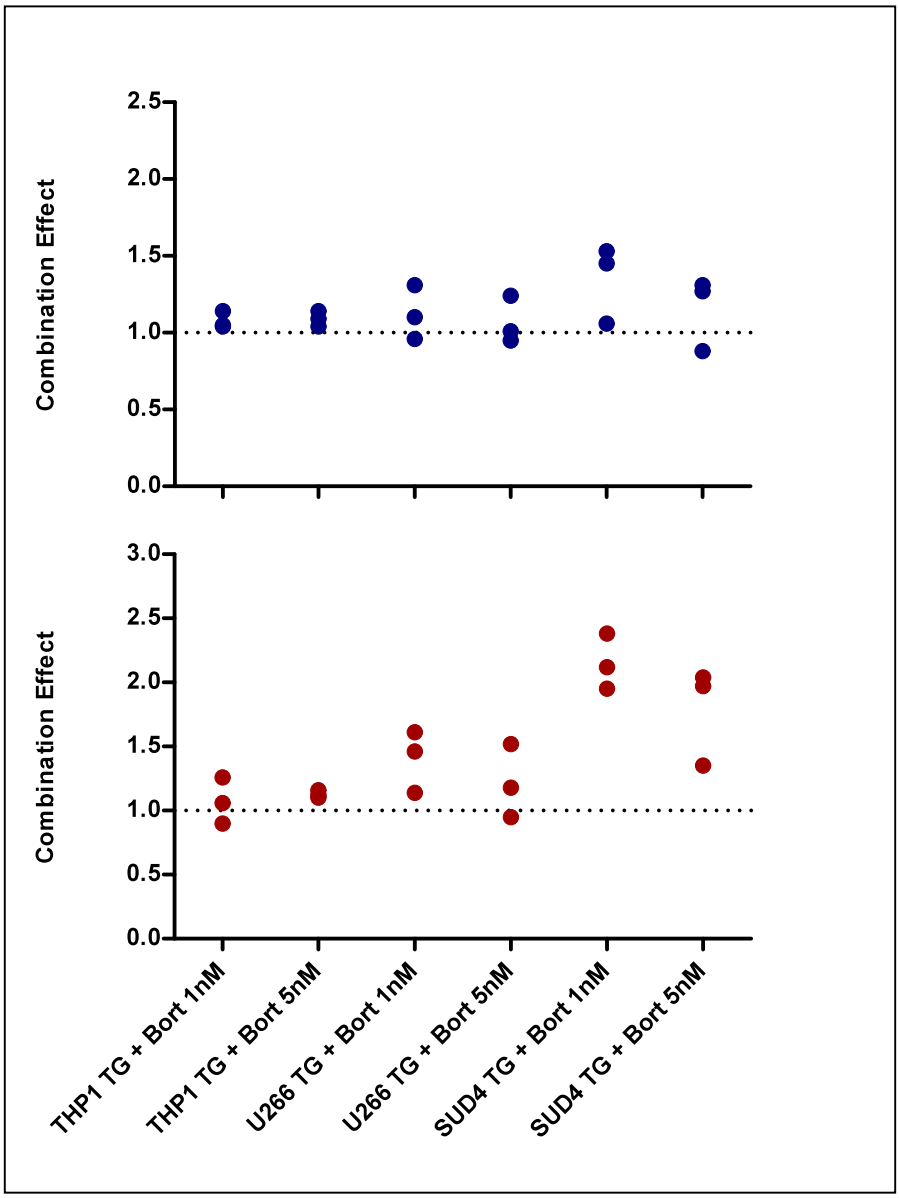

Figure 5.6. Effect of pretreatment with EC_5 (top) and EC_{15} (bottom) thapsigargin (TG) concentrations for 6 hours and bortezomib (Bort) for a further 48 hours on viable cell number (ATP content) in three haematological cancer cell lines. The combination effect compares the observed effect of the combination with the expected effect calculated using the fractional product method. Values ≈ 1 indicate an additive effect, values < 1 indicate synergy and values > 1 indicate antagonism. Results shown are from three separate experiments.

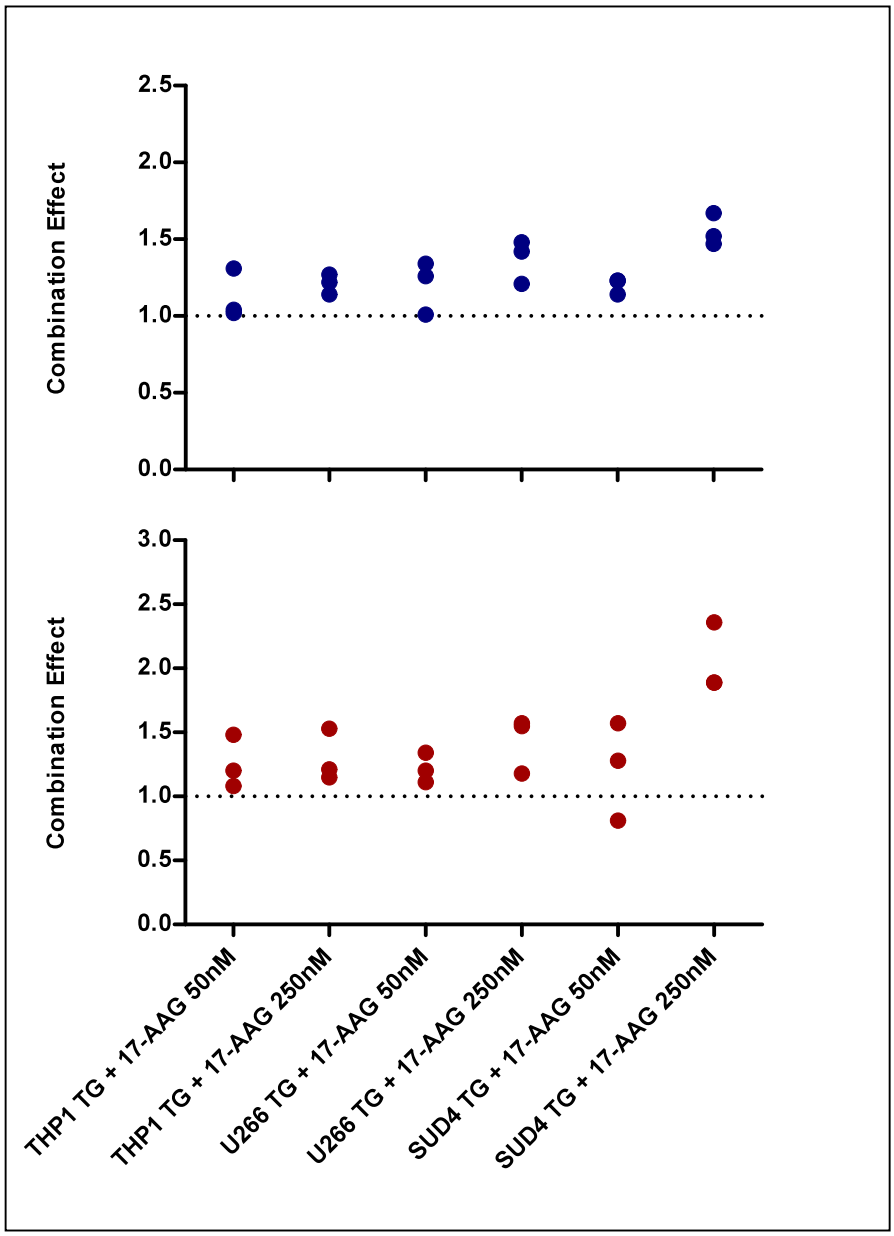

Figure 5.7. Effect of pretreatment with EC_5 (top) and EC_{15} (bottom) thapsigargin (TG) concentrations for 6 hours and 17-AAG for a further 48 hours on viable cell number (ATP content) in three haematological cancer cell lines. The combination effect compares the observed effect of the combination with the expected effect calculated using the fractional product method. Values ≈ 1 indicate an additive effect, values < 1 indicate synergy and values > 1 indicate antagonism. Results shown are from three separate experiments.

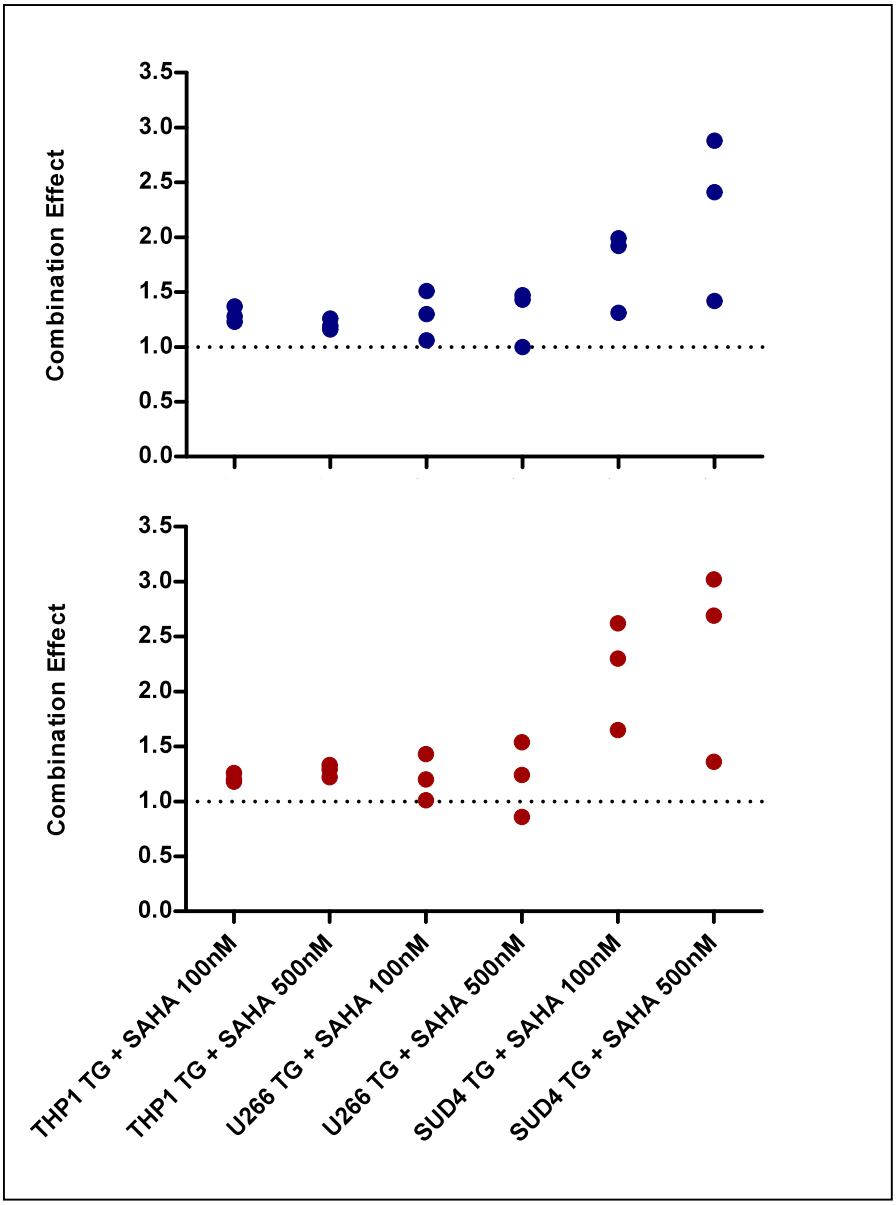

Figure 5.8. Effect of pretreatment with EC_5 (top) and EC_{15} (bottom) thapsigargin (TG) concentrations for 6 hours and SAHA for a further 48 hours on viable cell number (ATP content) in three haematological cancer cell lines. The combination effect compares the observed effect of the combination with the expected effect calculated using the fractional product method. Values ≈ 1 indicate an additive effect, values < 1 indicate synergy and values > 1 indicate antagonism. Results shown are from three separate experiments.

The next set of experiments were conducted to determine if this antagonism of drug was due to a decrease in apoptosis with the addition of thapsigargin to anticancer drug treatment in these cell lines. Apoptosis experiments were therefore carried out in the THP1, U266 and SUD4 cell lines after 6 hours pretreatment with the higher concentration of thapsigargin and 48 hours of further treatment with drug. The results are shown in figures 5.9 to 5.15. It can be seen that thapsigargin as a single agent at the minimally toxic concentrations used did not cause any increase in apoptosis compared to the untreated control in any of the cell lines studied. The proportion of THP1 cells that were apoptotic (early and late apoptosis) following TG pretreatment and 48 hour drug treatments can be seen in figure 5.9. At these concentrations the only samples with a large proportion of apoptotic cells were the doxorubicin treated THP1 cells. There was a small, but statistically significant, increase in apoptotic cells in the TG pretreated bortezomib sample ($p<0.05$). No antagonism of the proportion of apoptotic cells in each sample with TG pretreatment was observed.

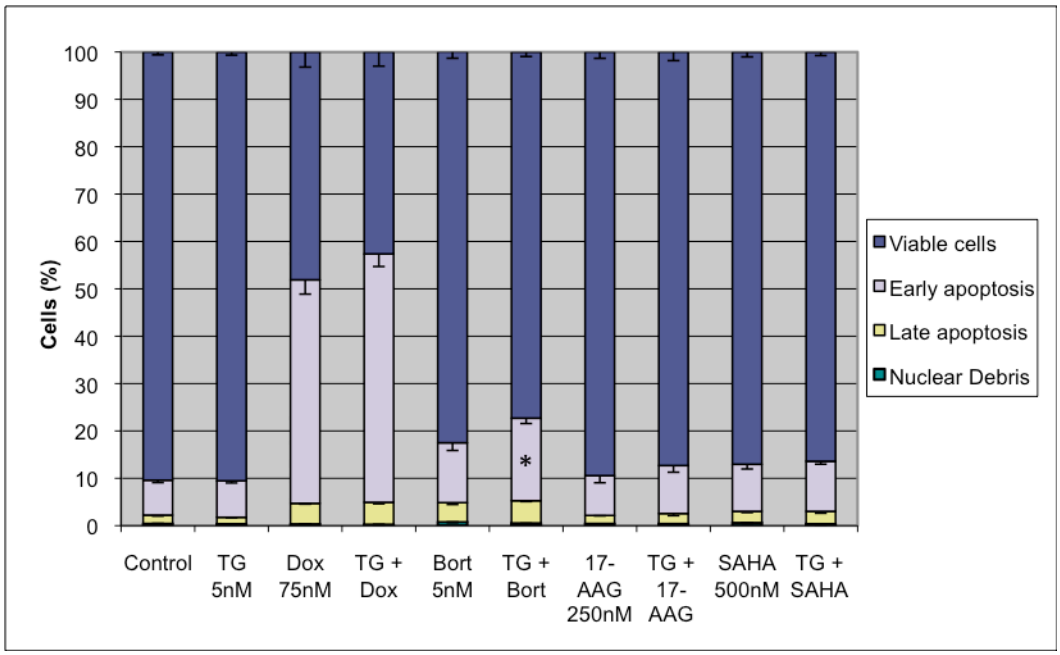

Figure 5.9. Percentage of cells in each category after treatment with drug alone for 48 hours, or 6 hours pretreatment with TG 5nM followed by addition of drug for a further 48 hours in the THP1 cell line. Error bars show mean ± SD. * denotes statistically significant increase in total apoptosis ($p < 0.05$) with TG pretreatment, compared to drug alone.

The apoptosis assay also provided data for total and viable cell number, which can be seen in figure 5.10. Thapsigargin treatment alone at this concentration was found to have an inhibitory effect on proliferation (data tables in appendix 2). Analysis of this data revealed a statistically significant protective effect on THP1 total cell proliferation when thapsigargin pretreatment was added to 48 hours of doxorubicin or SAHA treatment ($p<0.05$ and $p<0.01$ respectively). A statistically significant increase in viable cell number was also seen with the thapsigargin pretreated SAHA combination ($p<0.01$).

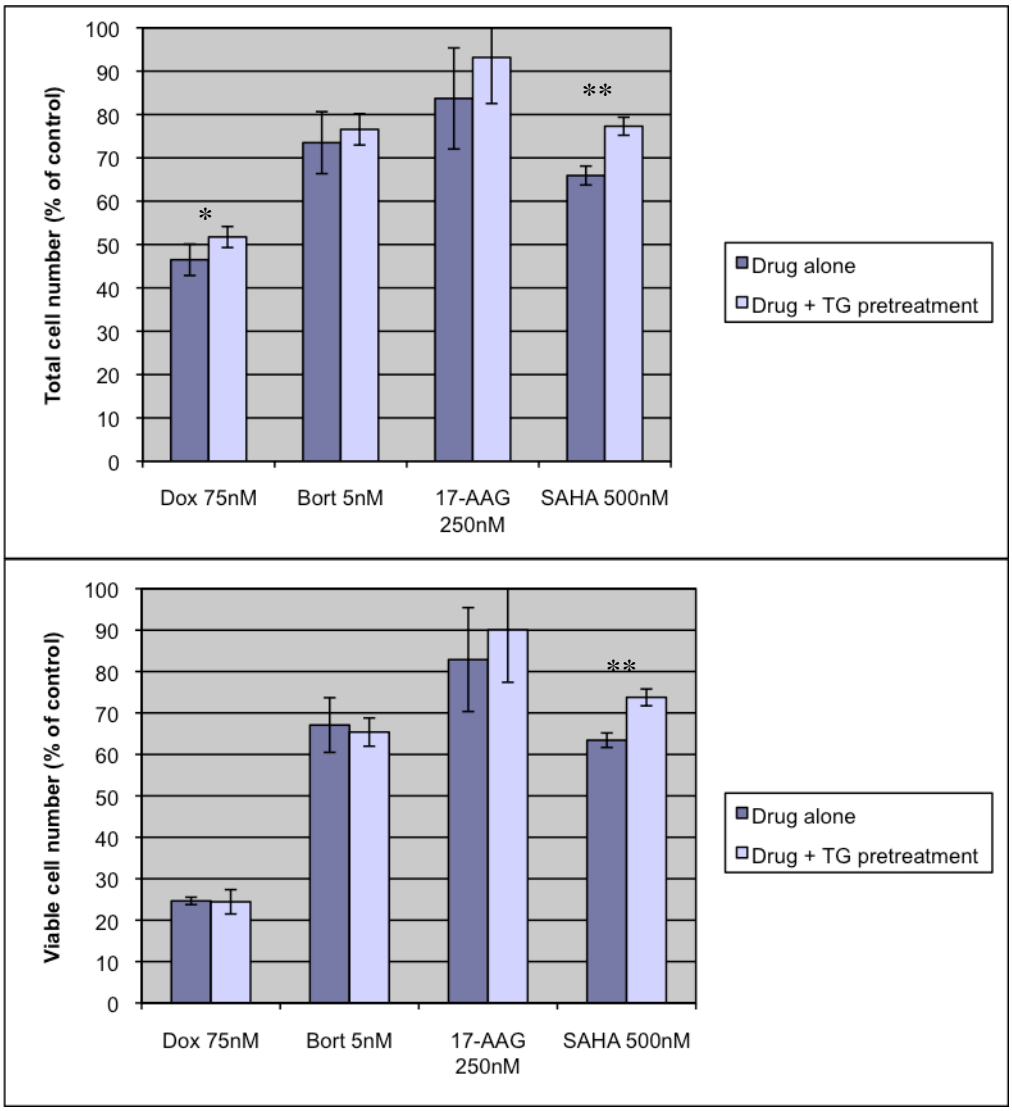

Figure 5.10. Cell number (top) and viable cell number (bottom) after 48 hours treatment with drug, with or without 6 hours of pretreatment with TG 5nM in THP1 cells (each value normalised to its own control). * or ** denotes statistically significant difference ($p < 0.05$ or $p<0.01$ respectively) between drug alone and drug with TG pretreatment.

Apoptosis assay results for the U266 cell line are shown in figures 5.11 and 5.12. As with the THP1 cell line, the addition of thapsigargin pretreatment to 48 hour drug incubation had little effect on the proportion of apoptotic cells, with no statistically significant differences seen (see figure 5.11).

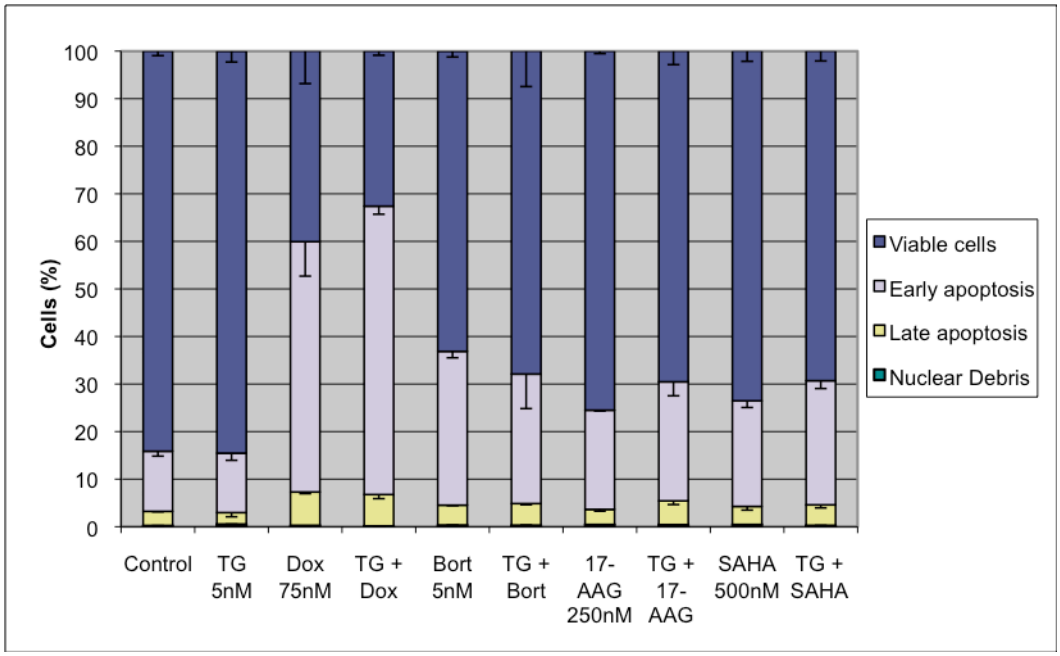

Figure 5.11. Percentage of cells in each category after treatment with drug alone for 48 hours, or 6 hours pretreatment with TG 5nM followed by addition of drug for a further 48 hours in the U266 cell line. Error bars show mean ± SD.

Some decreases in the antiproliferative effects of drugs were seen when combined with thapsigargin in the U266 cell line, as shown in figure 5.12. A small, but statistically significant, increase in total cell number was observed in the thapsigargin pretreated bortezomib sample ($p<0.01$), although an increase in viable cell number was not observed. A decrease in viable cell number was seen in the thapsigargin and doxorubicin combination sample ($p<0.05$). The increases in viable cell number observed in the bortezomib and SAHA combination treated samples were not statistically significant.

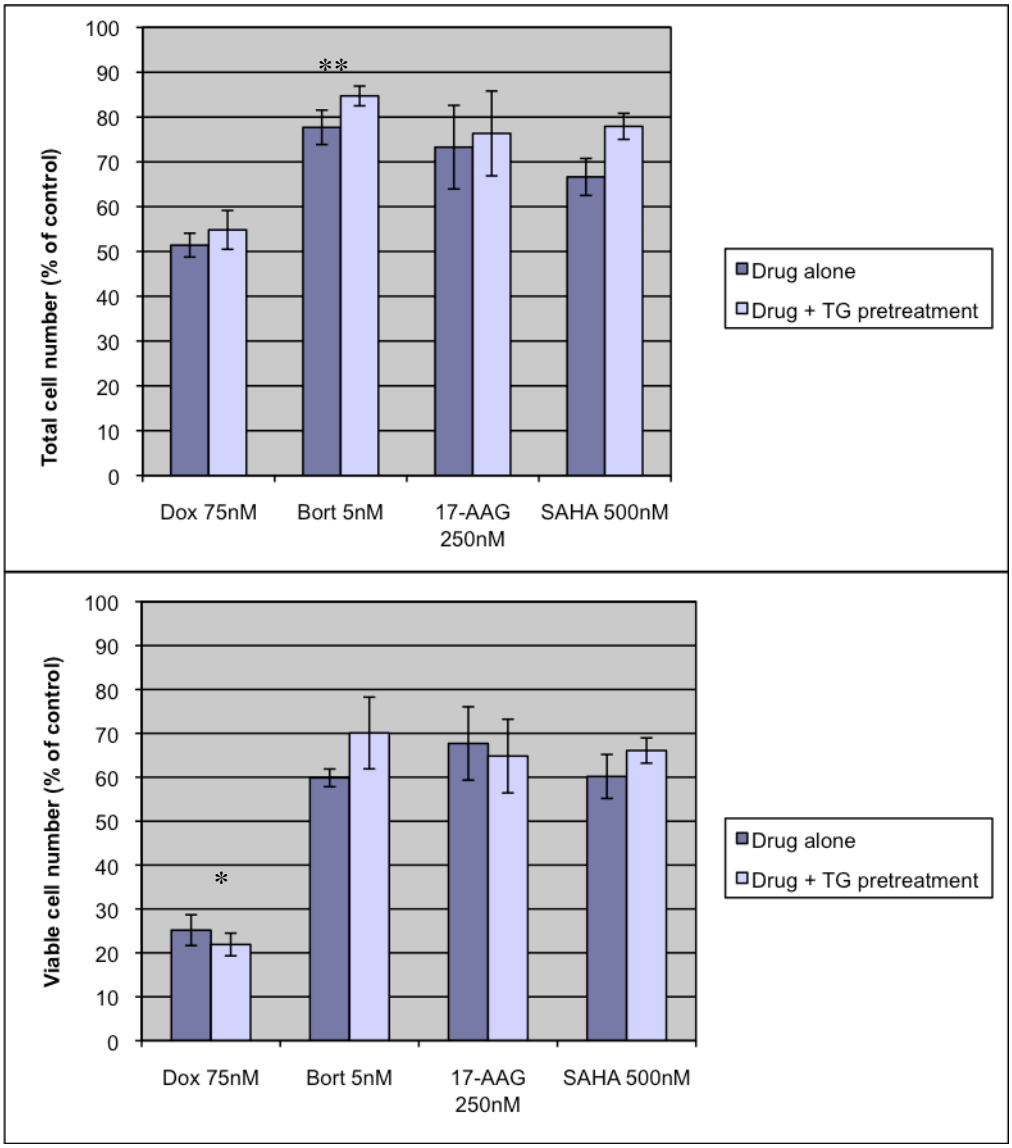

Figure 5.12. Cell number (top) and viable cell number (bottom) after 48 hours treatment with drug, with or without 6 hours of pretreatment with TG 5nM in U266 cells (each value normalised to its own control). * or ** denotes statistically significant difference ($p < 0.05$ or $p<0.01$ respectively) between drug alone and drug with TG pretreatment.

Apoptosis assay results for the SUD4 cell line are shown in figure 5.13. The addition of thapsigargin pretreatment to 48 hour drug incubation had little effect on the proportion of apoptotic cells, however a very small, but statistically significant, increase in apoptotic cells was seen in both the pretreated doxorubicin and SAHA samples ($p<0.05$ and $p<0.01$ respectively).

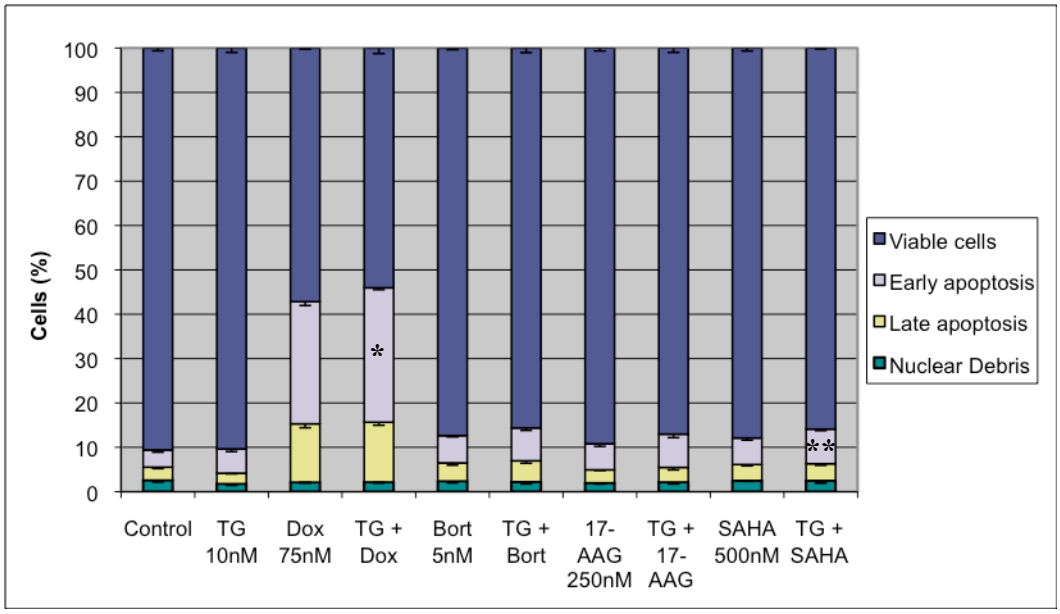

Figure 5.13. Percentage of cells in each category after treatment with drug alone for 48 hours, or 6 hours pretreatment with TG 10nM followed by addition of drug for a further 48 hours in the SUD4 cell line. Error bars show mean ± SD. * or ** denotes statistically significant difference ($p < 0.05$ or $p<0.01$ respectively) in total apoptosis with TG pretreatment,. compared to drug alone.

In the SUD4 cell line, some decreases in the antiproliferative effects of drugs were seen when combined with thapsigargin, with a trend towards increased viable and total cell number in the thapsigargin pretreated samples (see figure 5.14). Pretreatment with thapsigargin resulted in a statistically significant increase in total cell number after 17-AAG treatment ($p<0.01$), and this increase corresponded to a statistically significant increase in the number of viable cells in this sample ($p<0.05$).

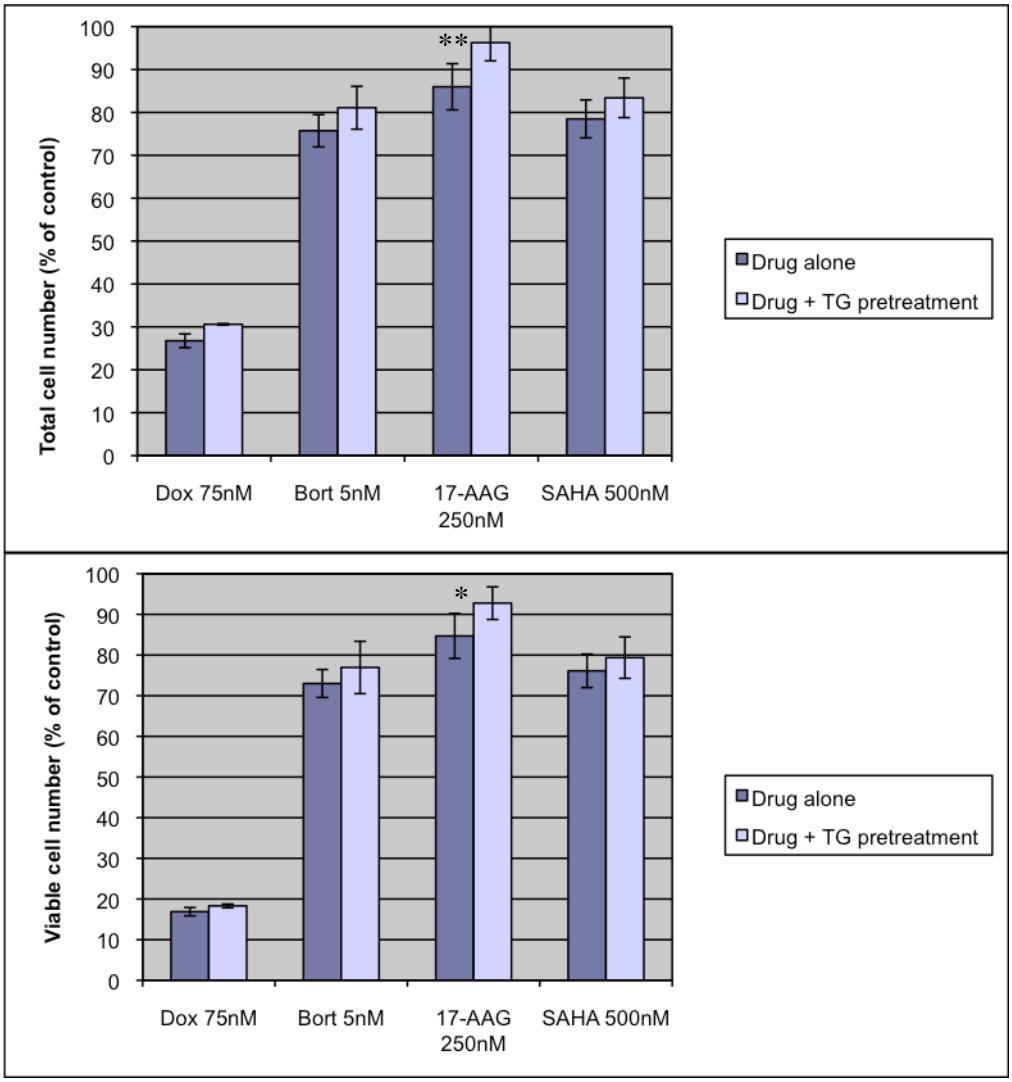

Figure 5.14. Cell number (top) and viable cell number (bottom) after 48 hours treatment with drug, with or without 6 hours of pretreatment with TG 10nM in SUD4 cells (each value normalised to its own control). * or ** denotes statistically significant difference ($p < 0.05$ or $p<0.01$ respectively) between drug alone and drug with TG pretreatment.

The apoptosis experiments were then repeated in the SUD4 cell line, in order to establish if the effect of TG pretreatment differed at higher cytotoxic drug concentrations. The proportion of apoptotic cells in the sample treated with this higher concentration of thapsigargin alone was not found to be statistically significant from that of the control sample. It can be seen from figure 5.15 that higher concentrations resulted in an increase in the proportion of apoptotic cells seen; specifically an increase in late apoptosis. There was a pattern of increased proportion of apoptotic cells observed when thapsigargin pretreatment was combined with all drugs studied compared to drug alone, and these increases were

statistically significant in the doxorubicin, bortezomib and 17-AAG treated samples ($p<0.05$). At these concentrations, no antagonism of the antiproliferative drug effects were seen following thapsigargin pretreatment, with no statistically significant changes observed in either total or viable cell number (data not shown).

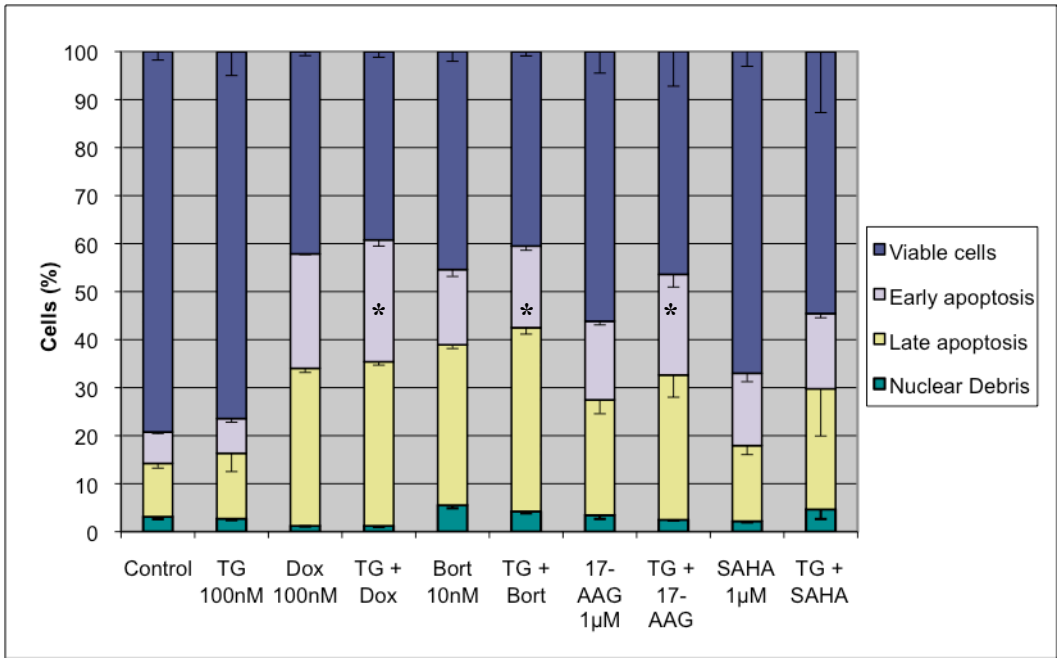

Figure 5.15. Percentage of cells in each category after treatment with drug alone for 48 hours, or 6 hours pretreatment with TG 100nM followed by addition of drug for a further 48 hours in the SUD4 cell line. Error bars show mean ± SD. * denotes statistically significant increase in total apoptosis ($p < 0.05$) with TG pretreatment, compared to drug alone.

In an attempt to further elucidate the mechanism of the antagonism observed when combining minimally toxic concentrations of thapsigargin and anticancer agents, western blotting was carried out to determine changes occurring at the protein level after 6 hours of thapsigargin pretreatment and a further 24 hours of drug treatment. In the THP1 cell line (see figure 5.16), a clear increase in GRP78 protein was seen following treatment with 17-AAG (with or without thapsigargin), however no other changes in the molecular chaperone proteins GRP78 and GRP94 were seen. LC3B protein cleavage is used as a marker of autophagy, and was visible at a low level in all samples. There appeared to be a subtle

increase in LC3B in the thapsigargin pretreated bortezomib sample, compared to bortezomib alone (indicating a possible increase in autophagy) and a decrease in the thapsigargin pretreated 17-AAG sample (indicating a possible reduction in autophagy). No clear difference was seen in the levels of the antiapoptotic protein BCL-2 or apoptosis mediated cleavage of PARP protein in this cell line, when comparing drug treatment alone with drug plus thapsigargin pretreatment.

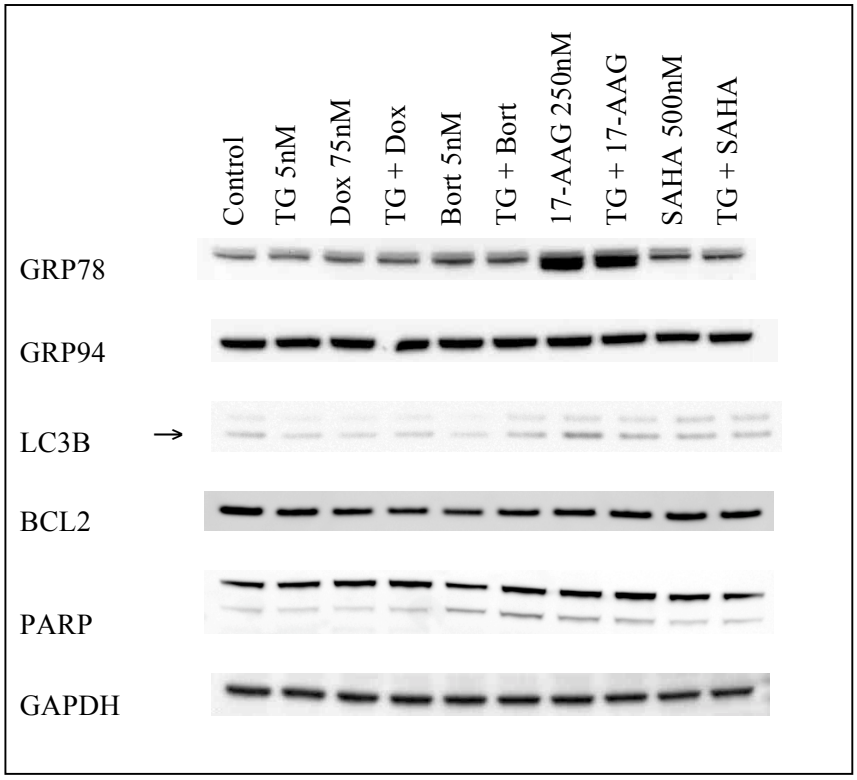

Figure 5.16. Western blotting experiments to investigate the effect of pretreatment with TG on chemosensitivity in THP1 cells. Markers of the unfolded protein response, autophagy and apoptosis were studied. GAPDH is included as a loading control.

In the U266 cell line (see figure 5.17), no clear changes in the levels of the molecular chaperone proteins GRP78 and GRP94 were observed when thapsigargin pretreatment was combined with chemotherapy. LC3B protein cleavage was clearly present in all samples, including untreated control, consistent with the basal level of autophagy reported to occur in this myeloma cell line. A decrease in LC3B protein cleavage was seen in the thapsigargin pretreated doxorubicin sample, compared to doxorubicin treatment alone, indicating a possible reduction in autophagy. No clear changes were observed in the levels of BCL2 and MCL1 proteins, or in the amount of parp cleavage seen, in the thapsigargin pretreated samples compared to chemotherapy drug alone.

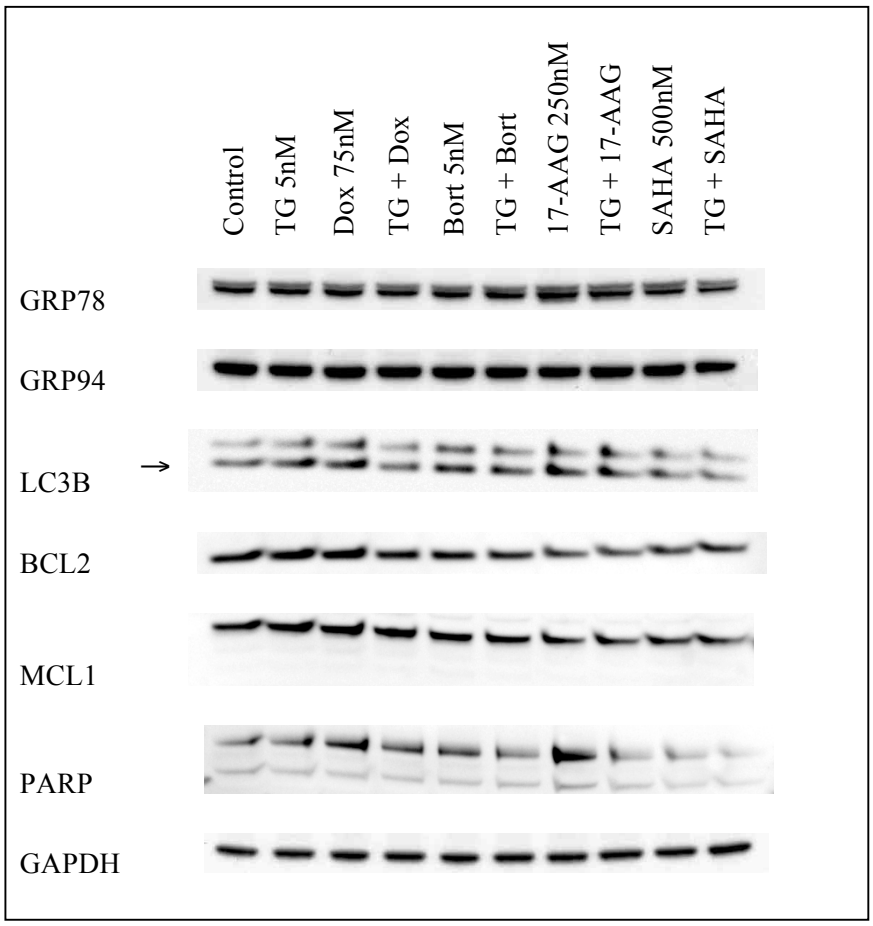

Figure 5.17. Western blotting experiments to investigate the effect of pretreatment with TG on chemosensitivity in U266 cells. Markers of the unfolded protein response, autophagy and apoptosis were studied. GAPDH is included as a loading control.

Western blotting results for the SUD4 cell line are shown in figure 5.18. Levels of the molecular chaperone proteins GRP78 and GRP94 did not appear to change following thapsigargin pretreatment prior to chemotherapy in the SUD4 cell line. The basal level of autophagy in the SUD4 cells was very low (as indicated by a very faint band representing LC3B cleavage on western blot). A small increase was seen in the level of LC3B protein cleavage in the thapsigargin pretreated doxorubicin sample, compared to doxorubicin alone and LC3B cleavage was present (but unchanged) in the bortezomib, 17-AAG and SAHA single agents and combinations. No clear changes were seen in BCL2 protein levels, although some changes were observed in the levels of MCL1 protein, with an increase seen in the thapsigargin single agent sample. The level of this antiapoptotic protein was seen to decrease in the thapsigargin pretreated doxorubicin and SAHA samples compared to each drug alone. This result is consistent with the statistically significant increase in apoptosis seen in the thapsigargin pretreated doxorubicin and SAHA samples compared to either drug alone in the apoptosis assay results (see figure 5.21). No changes in PARP cleavage were observed between the single agent and combination samples.

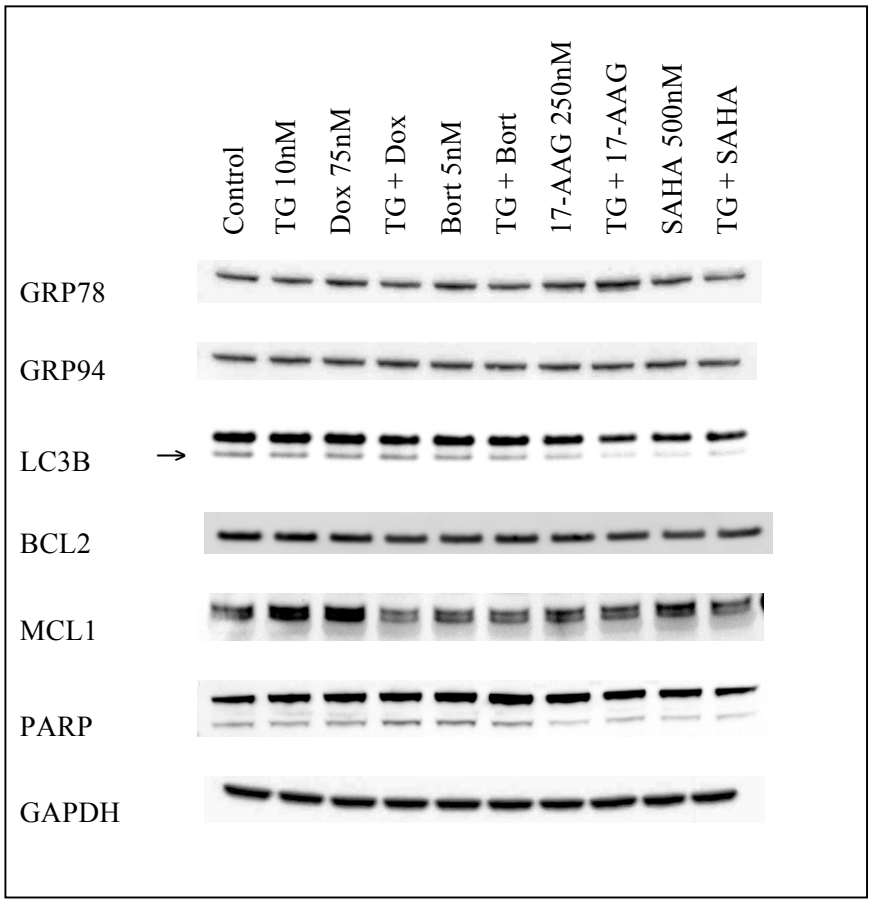

Figure 5.18. Western blotting experiments to investigate the effect of pretreatment with TG on chemosensitivity in SUD4 cells. Markers of the unfolded protein response, autophagy and apoptosis were studied. GAPDH is included as a loading control.

5.4 Discussion

Attempts to sensitise cancer cells to chemotherapy by inducing ER stress and activation of the unfolded protein response have been reported in the literature, with mixed results. It appears that whether such ER stress induction sensitises or protects cells from the effects of anticancer agents is dependent not only on the cell line and tumour type, but also on the particular anticancer agent used and the concentration of the ER stressor.

The results described in this chapter raise a number of important questions regarding the strategy of using ER stress induction to sensitise cancer cells to chemotherapy. Minimally toxic concentrations of thapsigargin were used here as an attempt to make these studies more relevant to anticancer treatment *in vivo*. It has long been known that compounds such as thapsigargin (and tunicamycin) are highly toxic to normal cells, as well as cancerous cells, due to their mechanism of action. Earlier experiments in this project have shown that ER stress and unfolded protein response activation does in fact occur with minimally toxic concentrations of ER stress inducing agents (see chapter 4) and experiments described here focused on investigating if this low level of ER stress and UPR activation was sufficient to affect the response of cancer cells to chemotherapeutic agents *in vitro*.

Cytotoxicity (ATP) assay results revealed a clear pattern of chemoprotection when minimally toxic thapsigargin pre-exposure was combined with the chemotherapy agents doxorubicin, bortezomib, 17-AAG or SAHA across all concentration ranges studied in these haematological cell lines. Whilst the effects of simultaneous administration for 48 hours had an additive to antagonistic effect in the cell lines studied, clear antagonism of the cytotoxic effects of the chemotherapeutic agents studied occurred following 6 hours pretreatment with thapsigargin prior to addition of drug treatment for a further 48 hours. Apoptosis assay data revealed that this protective effect did not occur as a result of a decrease in apoptosis on addition of thapsigargin treatment to chemotherapy, in contrast apoptosis actually increased in some combinations. However, analysis of cell proliferation suggested an increase in cell number and more importantly, the number of viable cells in thapsigargin pretreated samples. Western blotting experiments were conducted to investigate any changes occurring following the addition of thapsigargin pretreatment in these cells lines. Due to published reports suggesting an involvement of autophagy on myeloma cell cytotoxicity (Hoang *et al.*, 2009), determination of LC3B protein cleavage (a marker of autophagy) was also carried out. These experiments confirmed a basal level of autophagy was present in the myeloma

cell line U266, and to a lesser extent in the AML cell line THP1 (only very low protein levels were detectable in the DLBCL cell line SUD4).

No changes were seen in the protein levels of the molecular chaperones GRP78 and GRP94 in the thapsigargin pretreated samples compared to chemotherapy alone in any of the cell lines studied. Other markers of UPR activation were investigated, but protein levels were not detectable in these samples. This raises the possibility that the antagonism of chemotherapeutic drug effects seen following the addition of thapsigargin is not ER stress or UPR mediated, and is caused by another mechanism specific to the action of thapsigargin. Based on the experiments described in this chapter, it is possible that thapsigargin antagonises chemotherapy through effects on cell proliferation. Thapsigargin has been reported to induce growth arrest in prostate cancer cells due to an increase in intracellular calcium (occurring as a result of influx of extracellular calcium following depletion of ER calcium pools) (Lin *et al.*, 1997). Induction of growth arrest by low thapsigargin concentrations may decrease the effectiveness of chemotherapeutic agents and could explain why viable cell number is unaffected in the thapsigargin pretreated samples. Further experiments investigating cell cycle effects and intracellular calcium concentrations of thapsigargin combination treated cells and chemotherapy alone treated cells would determine if this calcium induced growth arrest is responsible for the antagonism observed.

As discussed in the introduction to this chapter, the development of thapsigargin prodrugs is another interesting area of cancer research. A thapsigargin prodrug (thapsigargin coupled to a targeting peptide) has now moved into a phase I clinical trial in solid tumours (clinical trials number: NCT01056029) (Ghantous *et al.*, 2010). Whilst this is an exciting development, the experiments described here would suggest a cautious approach to the combination of this thapsigargin prodrug with existing chemotherapy agents. The toxicity of such an agent to normal cells also remains to be determined.

6. Attenuation of the Unfolded Protein Response Using the Chemical Chaperone 4-Phenyl Butyric Acid and Effect on Chemosensitivity *in vitro*

6.1 Introduction

The small molecule compound 4-phenylbutyric acid (4-PBA) has been reported to act as a chemical chaperone, thereby relieving ER stress. 4-PBA is a simple molecule with a relative molecular mass of 164.2, and a chemical structure as shown in figure 6.1. 4-PBA is a short chain fatty acid derived from the first generation histone deacetylase (HDAC) inhibitor butyric acid. HDAC inhibitors have been discussed previously in chapter 1. 4-PBA has been reported to have weak HDAC inhibitory activity in addition to its action as a chemical chaperone (Lin *et al.*, 2009a).

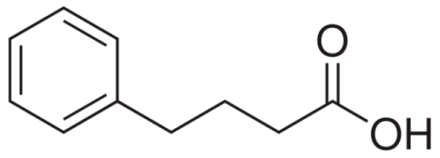

Figure 6.1. The chemical structure of 4-phenylbutyric acid (4-PBA)

4-PBA, as the sodium salt sodium phenylbutyrate, is clinically used for the treatment of urea cycle disorders, and is approved for use in both the USA and Europe. It is available as both oral and intravenous dosage forms and is well tolerated. It is oxidised *in vivo* to phenylacetic acid, which is conjugated with glutamine and excreted in the urine as phenylacetylglutamine. This results in the loss of two molecules of nitrogen for each molecule of PBA and is therefore effective in treating the hyperammonaemia seen in urea cycle disorders (Iannitti and Palmieri, 2011).

4-PBA has been used as a chemical chaperone in a number of studies. The function of a chemical chaperone is to reduce ER stress, both by stabilising protein conformation and by improving the folding capacity of the ER (Welch and Brown, 1996). It has been reported that pretreatment of liver cells with 4-PBA decreased PERK and eIF2α phosphorylation and JNK activation following tunicamycin treatment both in cell line and animal models. The authors also report that tunicamycin mediated XBP-1 mRNA splicing was reduced. This study found that 4-PBA was able to decrease ER stress and restore glucose homeostasis in a mouse diabetes model (Ozcan *et al.*, 2006). In a short term phase I/II clinical study, 4-PBA was shown to modulate heat shock protein expression and restore maturation of the ΔF508 CTFR mutant protein in cystic fibrosis patients (Zeitlin *et al.*, 2002) and this has also been shown in a number of *in vitro* studies (Rubenstein *et al.*, 1997, Brown *et al.*, 1996). Other chemical chaperone functions reported for 4-PBA include correction of temperature sensitive protein folding defects (Brown *et al.*, 1997) and enabling secretion of functionally active, but misfolded, mutant α1-antitrypsin protein, thereby providing a potential pharmacological strategy for prevention of liver injury and emphysema in α1-antitrypsin deficiency (Burrows *et al.*, 2000). The studies reported thus far using 4-PBA as a chemical chaperone support a role for the drug in reducing ER stress by preventing protein aggregation and increasing overall ER function, although 4-PBA has not been shown to alter the conformation of misfolded proteins themselves. These considerable effects are all the more surprising considering the simple chemical structure of 4-PBA.

The haematological cancer cell lines in this study have been shown to have an underlying degree of ER stress and a constitutively active UPR. The effect of the reported chemical chaperone 4-PBA on chemosensitivity has therefore been investigated in these cell lines in order to determine whether attenuation of ER stress by 4-PBA would alter the sensitivity of these cell lines to anticancer drugs and ER stress inducing agents.

6.2 Materials and Methods

6.2.1 Cytotoxicity Studies

Cytotoxicity experiments were carried out as described in chapter 2 (sections 2.4 to 2.6 inclusive). The effect of 4-PBA treatment on cell proliferation and viability was investigated using a plate based adenosine triphosphate (ATP) cytotoxicity assay. Four cancer cell lines were studied; three haematological cancer cell lines (THP1, U266 and DOHH2) and the colorectal cancer cell line HT-29 as an example of a solid tumour cell line. Cells in exponential growth phase were plated into 96 well plates (5000 cells per well in 100µl medium) and incubated for 24 hours. Varying concentrations of drug were diluted in culture medium and then added to each well to obtain the required final concentration (all drug additions were made in a fixed volume of 10µl per well). Control wells were topped up with culture medium so that all wells of the plate contained a fixed volume of 110µl. Plates were then incubated for 48 hours at 37°C and 5% CO_2 in air. 48 hours after addition of drug, plates were analysed using the ViaLight HS assay kit (Lonza Group Ltd, Switzerland) and read using a BMG Labtech Polarstar Optima microplate reader (BMG Labtech, Germany).

Each drug treatment was investigated in triplicate wells and experiments were repeated on three separate occasions. Effect of drug treatment was calculated from the assay data (expressed as a percentage of the control value). For each drug, the mean values and standard deviations of all experiments were determined for graphical representation. For concentration-effect modelling in GraphPad Prism, the mean values for each concentration in each experiment were used. Drug activity data was fitted using sigmoidal concentration effect curves to derive EC_{50} values (effective concentration 50 – i.e. the concentration required to exert 50% of maximum effect) with 95% confidence intervals, using non linear regression in GraphPad Prism software (GraphPad Software, San Diego, USA).

In the three haematological cancer cell lines, it was also possible to use the Guava ViaCount assay (Guava Technologies Inc., USA) to determine total cell number (total cell number per millilitre) and cell viability (percentage viable cells and percentage dead cells) of each sample (this assay is not suitable for use with adherent cell lines, such as the HT-29 cell line). Cells in exponential growth phase were plated into 96 well plates (5000 cells per well in 100µl medium) and incubated at 37°C and 5% CO_2 in air for 24 hours. Drug dilutions and addition to cells were as described for ATP assay above. Following 48 hours of incubation with drug, plates were analysed using the Guava PCA™ – 96 System, as described in chapter 2.4. All samples were run in triplicate and each experiment was repeated on three separate occasions to ensure reproducibility. The mean values and standard deviations of each data set were then calculated and used in subsequent data analysis. For concentration-effect modelling in GraphPad Prism, the mean values for each concentration in each experiment were used.

The effect of 4-PBA treatment combined with ER stress inducing agents and anticancer agents on cell proliferation and viability was investigated using ATP cytotoxicity assay as described above (see also chapter 2.5). Based on the results of initial experiments, cells were treated with 4-PBA 0.5mM and two concentrations each of tunicamycin (TM), thapsigargin (TG), doxorubicin (dox), bortezomib (bort), 17-AAG, and SAHA. The effects of both simultaneous drug treatment and pre-treatment for 24 hours with 4-PBA were investigated. Varying concentrations of drug were diluted in culture medium and then added to each well to obtain the required final concentration. Single agent treated wells, combination treated wells, and untreated control wells were present on each plate in the combination experiments. Control wells and single agent treatment wells were topped up with culture medium so that all wells of the plate contained a fixed volume of 120µl. Plates were then incubated for 48 hours at 37°C and 5% CO_2 in air, before analysis using the ViaLight HS assay kit (Lonza Group Ltd, Switzerland) in conjunction with a BMG Labtech Polarstar Optima microplate reader (BMG Labtech, Germany).

Each drug treatment was studied in triplicate and experiments were repeated three times on separate occasions. In the combination experiments, the effect of 4-PBA on the response to drug treatment was calculated using the fractional product method described by Webb (Webb, 1963). The ratio of the observed effect to the expected effect provides a measure of the interaction of two drugs used in a combination. If the ratio of the combination effect is 1 (i.e. the observed effect equals the expected effect), the combination is designated additive. If the ratio is less than 1 (i.e. the observed effect is greater than the expected effect), then the combination considered to be supra-additive or synergistic. If the ratio is more than 1 (i.e. the observed effect is less than the expected effect), then the combination is said to be antagonistic.

6.2.2 Apoptosis Assay

As the concentration of 4-PBA used in the ATP assay was minimally toxic, the effect of 4-PBA pretreatment on chemosensitivity was investigated using an apoptosis assay at the higher drug concentrations used in the cytotoxicity experiments. The Guava Nexin assay (Guava Technologies Inc., USA) is a fluorescence based microplate apoptosis assay (see chapter 2.9). Cells in exponential growth phase were plated into 96 well plates (10000 cells per well) and incubated at 37°C and 5% CO_2 in air for 24 hours before addition of drug solution. Cells were either pretreated with 4-PBA for 24 hours prior to the addition of drug for a further 48 hours, or treated only with drug for 48 hours. Control wells and single agent treatment wells were topped up with culture medium so that all wells of the plate contained a fixed volume of 120µl. All drug treatments were investigated in triplicate, with mean values and standard deviations used in subsequent data analysis. Data was presented as the percentage of cells per sample in each of the four cell populations. Total and viable cell number were also calculated for drug alone and drug with 4-PBA pretreatment (each normalised to its own control).

6.2.3 Protein Analysis

Whole cell lysates were also prepared following drug treatments for use in western blotting experiments (see chapter 2.7). Western blotting was carried out as described in chapter 2.8, with 20μg of protein loaded in each lane of the gel. Blots were visualised using ECL (Amersham, UK) and a Fuji ImageQuant LAS 4000 camera (FujiFilm, Japan) used according to manufacturer's instructions.

6.2.4 HDAC Activity

Inhibition of histone deacetylases (HDAC) by 4-PBA was evaluated using a HDAC Fluorimetric Assay/Drug Discovery Kit (BIOMOL, Enzo Life Sciences, UK) as per manufacturer's protocol (see chapter 2.10). Trichostatin A or test inhibitor was diluted in assay buffer and plated into wells of a 96-well plate. Diluted HeLa extract was added to all wells (except for no enzyme controls). Fluor de Lys Substrate was then added to the wells initiating HDAC reactions. The addition of Fluor de Lys Developer was used to stop the reactions and the plate was incubated in the dark at room temperature for 15 minutes. Samples were then read using a microplate reader (excitation wavelength 350 to 380nm and emission 440 to 460nm). Each sample was studied in duplicate, with the experiment performed on three separate occasions to ensure reproducibility. Values were expressed as percentage of control HDAC activity.

6.2.5 Statistical Analysis

Statistical analysis was performed using Microsoft Excel software, Microsoft Corporation, USA. The data obtained from the apoptosis assay was used to determine mean and standard deviation values for each drug concentration. These values were then used for graphical representation and subsequent statistical analysis. Data was assumed to be

normally distributed and parametric tests were therefore used throughout. Group means were analysed using a paired t-test, with a p value of less than 0.05 considered to be statistically significant.

6.3 Results

The reported chemical chaperone 4-PBA was found to have a cytotoxic effect in the cancer cell lines studied, with EC_{50} values in the low milimolar range following 48 hours of treatment (see figure 6.2). The lymphoma cell line DOHH2 was the most sensitive to the cytotoxic effects of 4-PBA, whilst the colorectal cancer cell line HT-29 was found to be the least sensitive. The AML cell line THP1 and the myeloma cell line U266 showed similar sensitivities to 4-PBA treatment.

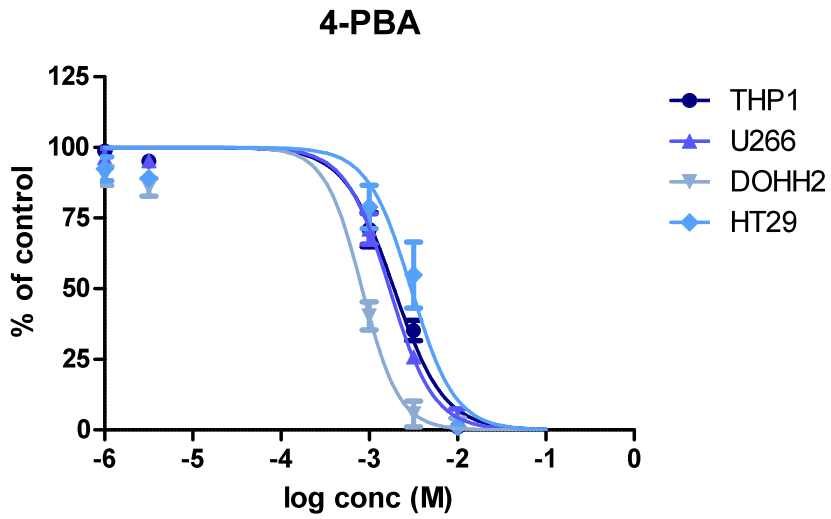

Drug	Cell line	EC_{50}	95% CI
4-PBA	THP-1	1.91mM	1.65mM to 2.20mM
	U266	1.70mM	1.52mM to 1.89mM
	DOHH2	0.83mM	0.61mM to 1.12mM
	HT-29	2.99mM	2.27mM to 3.92mM

Figure 6.2. Effect of treatment with 4-PBA for 48 hours on cell viability (ATP content) in three haematological cancer cell lines and the colorectal cancer cell line HT29 (error bars show mean ± SD). EC_{50} values, with 95% confidence intervals, for 4-PBA treatment are shown.

For the three haematological cancer (suspension) cell lines, the effect of 4-PBA on cell proliferation and cell viability was also determined. As illustrated in figure 6.3 A, treatment with 4-PBA had an antiproliferative effect across the concentration range studied, with the THP1 cell line being more sensitive to this antiproliferative effect, whilst the U266 and DOHH2 cell lines had similar sensitivities. It can be seen from figure 6.3 B that the cytotoxic effects of 4-PBA were observed at higher drug concentrations than the antiproliferative effects (as is often the case with anticancer agents). The DOHH2 cell line was found to be considerably more sensitive to the effect of 4-PBA in reducing cell viability, with the THP1 and U266 cell lines exhibiting similar sensitivities.

A

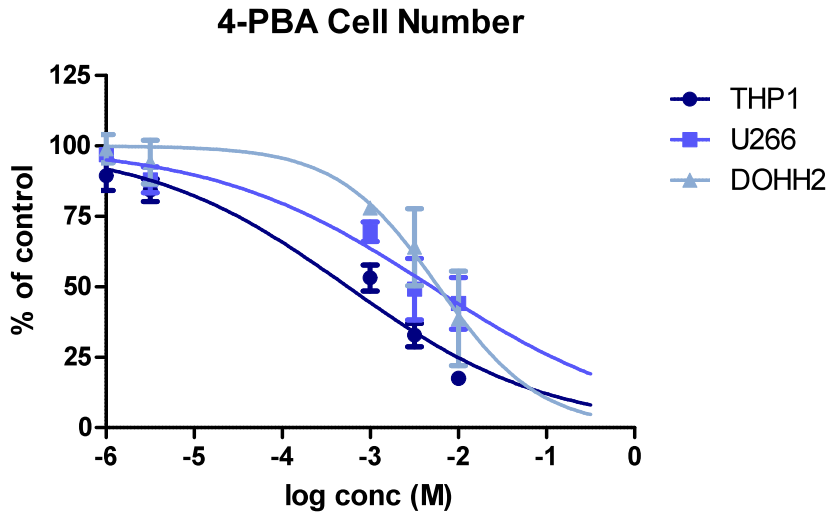

Drug	Cell line	EC_{50}	95% CI
4-PBA	THP-1	0.55mM	0.31mM to 1.00mM
	U266	4.98mM	2.52mM to 9.84mM
	DOHH2	5.92mM	3.71mM to 9.44mM

B

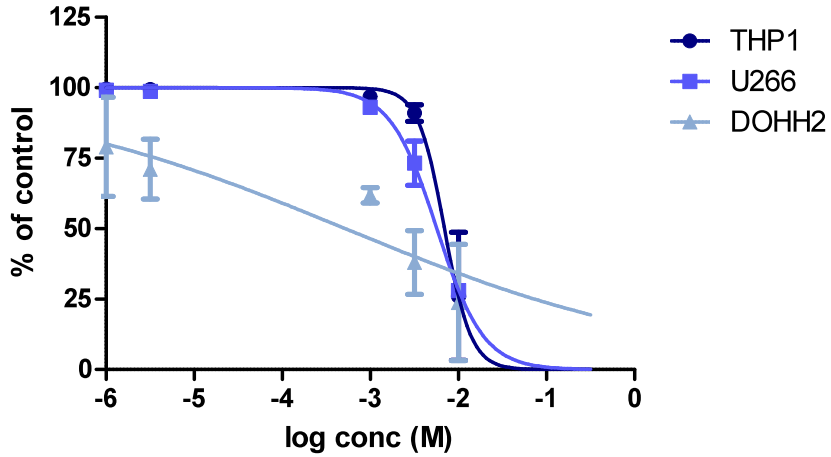

Drug	Cell line	EC_{50}	95% CI
4-PBA	THP-1	6.96mM	5.68mM to 8.54mM
	U266	5.70mM	5.21mM to 6.23mM
	DOHH2	0.52mM	0.09mM to 3.19mM

Figure 6.3. A - Effect of treatment with 4-PBA for 48 hours on cell number in three cancer cell lines (error bars show mean ± SD). EC_{50} values, with 95% confidence intervals, for 4-PBA treatment on cell number are shown. **B** - Effect of treatment with 4-PBA for 48 hours on cell viability in three cancer cell lines (error bars show mean ± SD). EC_{50} values, with 95% confidence intervals, for 4-PBA treatment on cell viability are shown

The effect of increasing concentrations of 4-PBA on UPR markers in the three haematological cancer cell lines was studied by western blotting, in an attempt to detect protein changes that may reflect its reported chemical chaperone activity (see figure 6.4). Levels of the antiapoptotic proteins BCL2 and MCL1 were also examined. A concentration dependent decrease in GRP78 was observed in the DOHH2 cell line following 4-PBA treatment, although this effect was subtle. No other changes in GRP78 or GRP94 protein levels were seen. No changes in either GADD153 protein or the spliced XBP1 protein product were detectable following 4-PBA treatment in this experiment. A concentration dependent decrease in the level of BCL2 protein was seen following treatment with increasing concentrations of 4-PBA in the THP1 and U266 cell lines, whilst no change was seen in the DOHH2 cell line. In the U266 cell line, a concentration dependent decrease in MCL1 protein was also observed after treatment with increasing 4-PBA concentrations. The THP1 and DOHH2 cell lines had lower basal expression of MCL1 protein than the U266 cell line. In these cell lines, treatment with lower concentrations of 4-PBA (0.5μM and 1μM) resulted in an increase in MCL1 protein, whilst treatment with the higher concentration (5mM) resulted in a decrease in MCL1 protein (this effect was more subtle in the THP1 cell line where a possible small decrease was seen at the higher concentration). GAPDH protein was included as a loading control, with equal protein loading seen within each cell line studied.

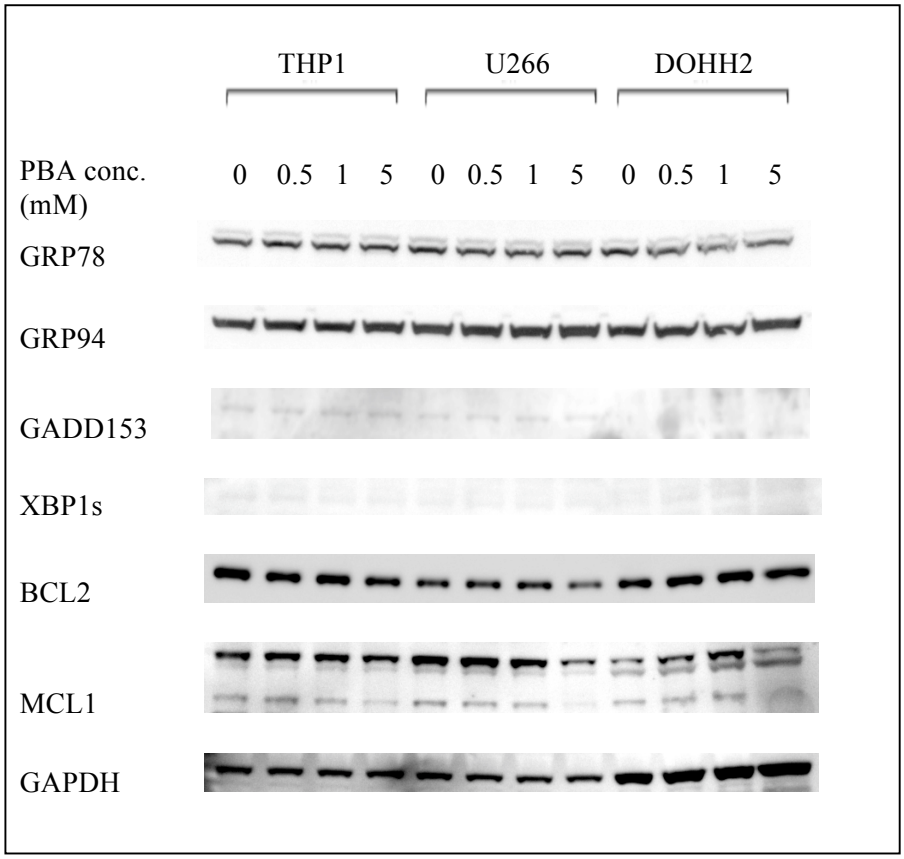

Figure 6.4. Western blotting experiments to investigate the effect of increasing concentrations of 4-PBA on markers of the unfolded protein response and apoptosis in three haematological cancer cell lines. GAPDH is included as a loading control.

Experiments next focused on establishing the effect of combining 4-PBA with other agents. Based on the results of the initial experiments described above, 4-PBA at a concentration of 0.5mM was chosen for use in further studies, as higher concentrations appeared too toxic in these haematological cell lines (particularly DOHH2). The effect of simultaneous treatment and pretreatment with 4-PBA on the cytotoxic effects of the ER stressors tunicamycin and thapsigargin, plus the anticancer agents doxorubicin, bortezomib, 17-AAG and SAHA were investigated in the three haematological cancer cell lines THP1, U266 and DOHH2. These experiments were also carried out in the colorectal cancer cell line HT-29, in order to determine if the effect of this chemical chaperone compound differed between the solid tumour cells and haematological cell lines.

Simultaneous treatment with 4-PBA had mixed effects in this cell line panel as shown in figures 6.5 to 6.8. Simultaneous treatment with 4-PBA and drugs for 48 hours in the THP1 cell line had a broadly additive effect, although a synergistic effect was seen with the combination of 4-PBA and tunicamycin 1μM (see figure 6.5).

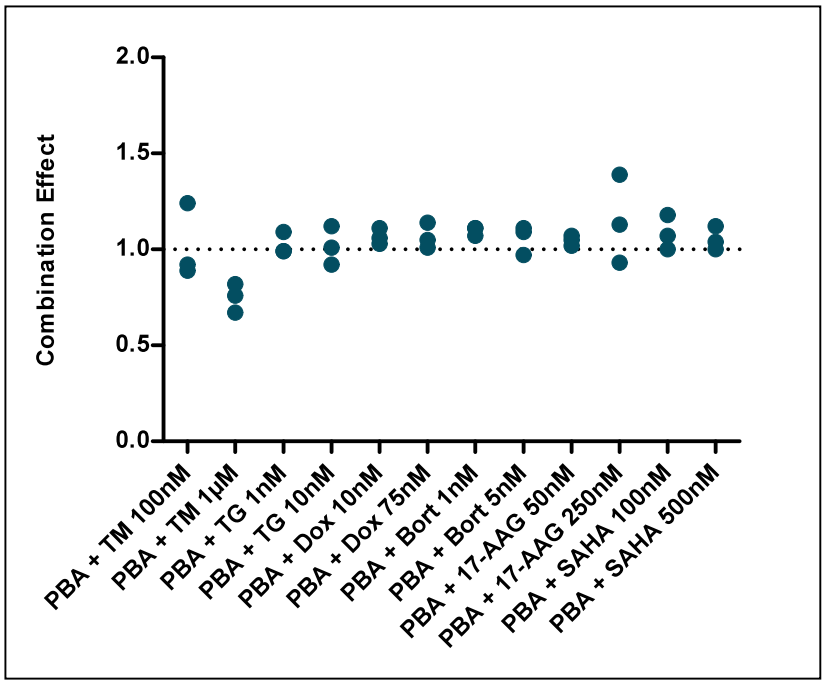

Figure 6.5. Effect of simultaneous treatment with 4-PBA 0.5mM and drug for 48 hours on viable cell number (ATP content) in THP1 cells. The combination effect compares the observed effect of the combination with the expected effect calculated using the fractional product method. Values ≈ 1 indicate an additive effect, values < 1 indicate synergy and values > 1 indicate antagonism. Results shown are from three separate experiments.

Figure 6.6 shows the result of simultaneous treatment with 4-PBA 0.5mM and drugs for 48 hours in the U266 cell line. In this cell line, concurrent treatment with 4-PBA and drugs was also broadly additive, although a synergistic effect was again seen with the combination of 4-PBA 0.5mM and tunicamycin at the 1μM concentration, and an antagonistic effect seen with 4-PBA combined with the higher concentrations of bortezomib and 17-AAG studied.

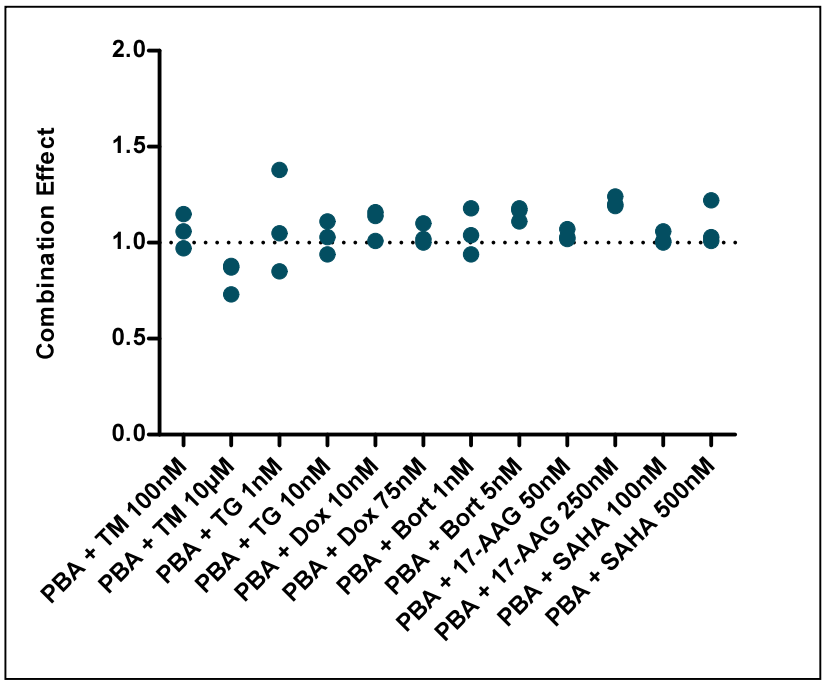

Figure 6.6. Effect of simultaneous treatment with 4-PBA 0.5mM and drug for 48 hours on viable cell number (ATP content) in U266 cells. The combination effect compares the observed effect of the combination with the expected effect calculated using the fractional product method. Values ≈ 1 indicate an additive effect, values < 1 indicate synergy and values > 1 indicate antagonism. Results shown are from three separate experiments.

In the DOHH2 cell line, mixed effects were seen when 4-PBA was combined with drug treatment for 48 hours (see figure 6.7). The combination of 4-PBA and the ER stress inducing drugs tunicamycin and thapsigargin was found to be broadly additive, whilst the combination of 4-PBA with anticancer agents was additive to antagonistic.

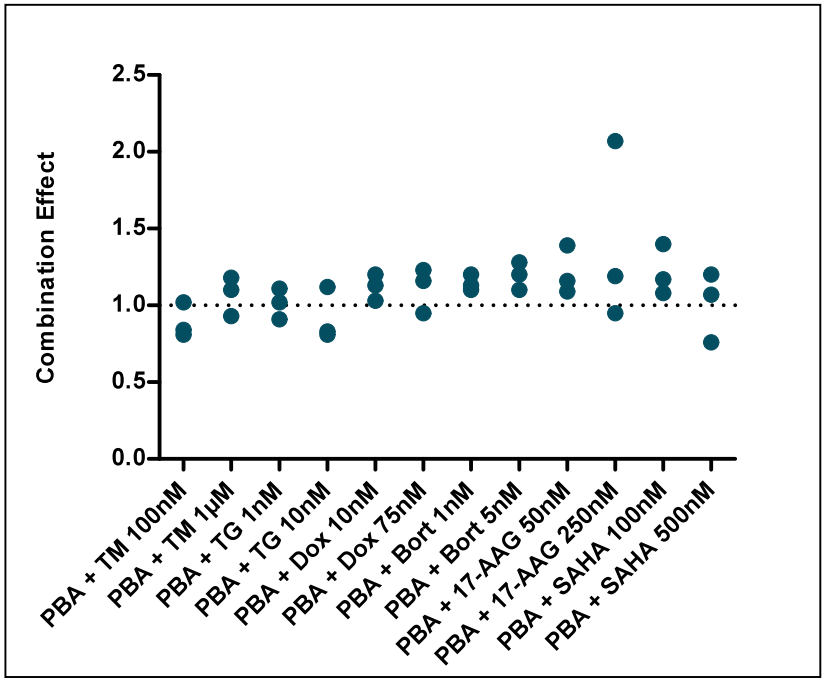

Figure 6.7. Effect of simultaneous treatment with 4-PBA 0.5mM and drug for 48 hours on viable cell number (ATP content) in DOHH2 cells. The combination effect compares the observed effect of the combination with the expected effect calculated using the fractional product method. Values ≈ 1 indicate an additive effect, values < 1 indicate synergy and values > 1 indicate antagonism. Results shown are from three separate experiments.

Figure 6.8 shows that in the colorectal cancer cell line HT29, the effect of simultaneous treatment with 4-PBA and drugs for 48 hours was broadly additive (additive to antagonistic).

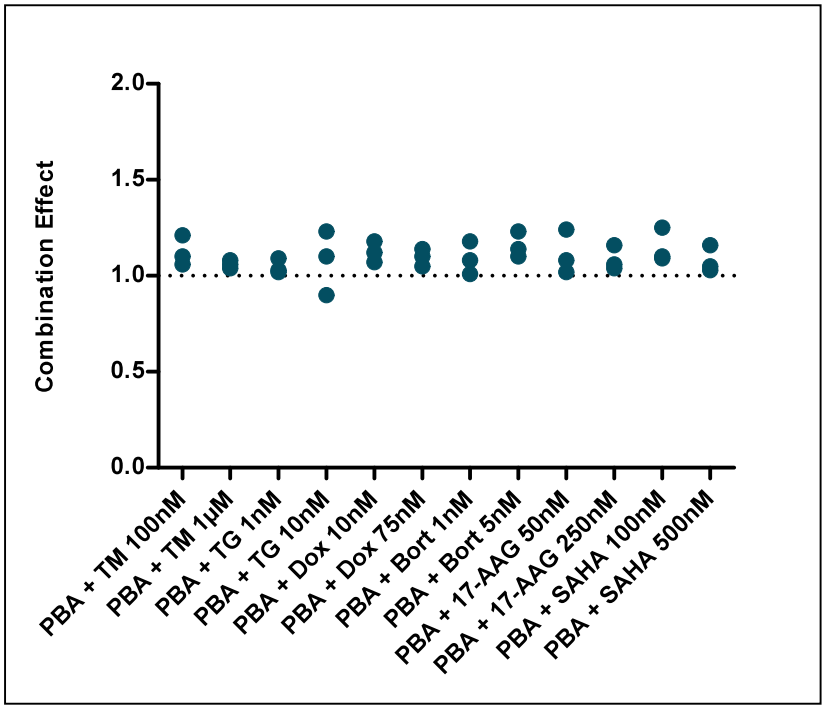

Figure 6.8. Effect of simultaneous treatment with 4-PBA 0.5mM and drug for 48 hours on viable cell number (ATP content) in HT29 cells. The combination effect compares the observed effect of the combination with the expected effect calculated using the fractional product method. Values ≈ 1 indicate an additive effect, values < 1 indicate synergy and values > 1 indicate antagonism. Results shown are from three separate experiments.

The effect of pre-treatment with 4-PBA 0.5mM for 24 hours followed by addition of drug for a further 48 hours was also investigated (see figures 6.9 to 6.12). Results were broadly additive in all four cancer cell lines studied. The additive effect of 4-PBA pretreatment in the THP1 cell line can be seen in figure 6.9.

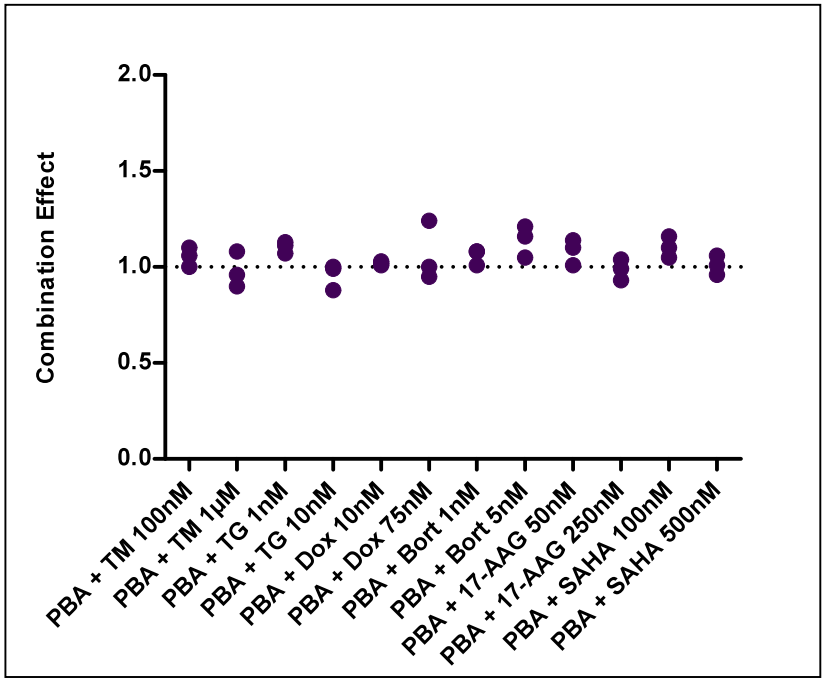

Figure 6.9. Effect of pretreatment with 4-PBA 0.5mM for 24 hours and drug for a further 48 hours on viable cell number (ATP content) in THP1 cells. The combination effect compares the observed effect of the combination with the expected effect calculated using the fractional product method. Values ≈ 1 indicate an additive effect, values < 1 indicate synergy and values > 1 indicate antagonism. Results shown are from three separate experiments.

In the U266 cell line (see figure 6.10), 4-PBA pretreatment also appeared to have a broadly additive effect when combined with all drugs studied, although a supra-additive effect was seen in the 4-PBA pretreated cells after 48 hours of treatment with thapsigargin 10nM.

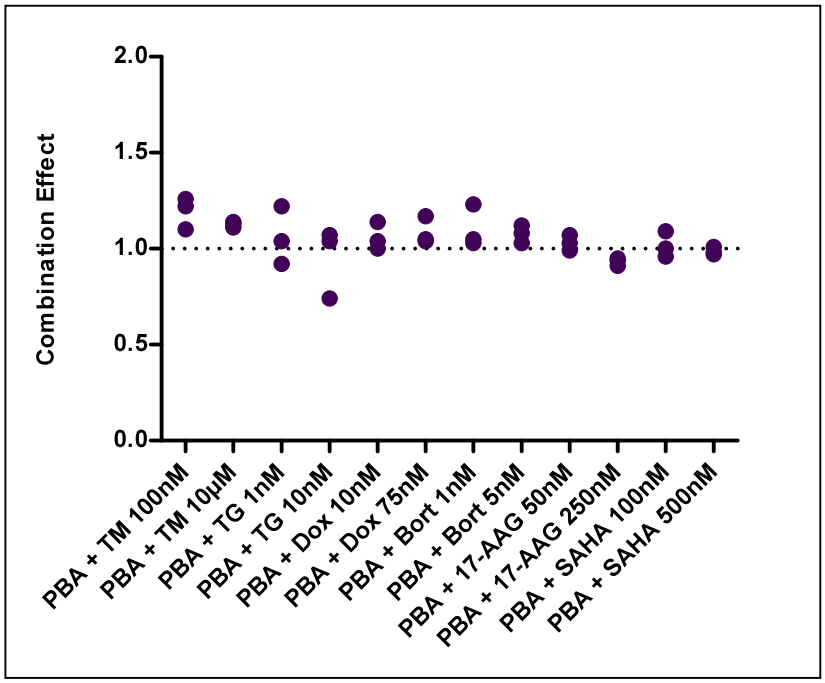

Figure 6.10. Effect of pretreatment with 4-PBA 0.5mM for 24 hours and drug for a further 48 hours on viable cell number (ATP content) in U266 cells. The combination effect compares the observed effect of the combination with the expected effect calculated using the fractional product method. Values ≈ 1 indicate an additive effect, values < 1 indicate synergy and values > 1 indicate antagonism. Results shown are from three separate experiments.

Pretreatment with 0.5mM 4-PBA for 24 hours prior to the addition of drugs was found to have an additive to antagonistic effect in the DOHH2 cell line, as shown in figure 6.11.

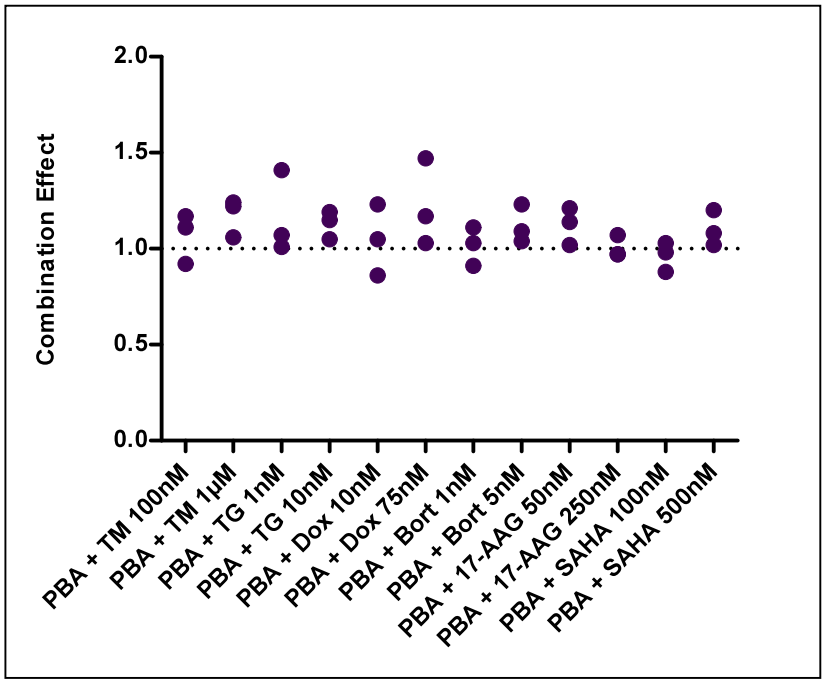

Figure 6.11. Effect of pretreatment with 4-PBA 0.5mM for 24 hours and drug for a further 48 hours on viable cell number (ATP content) in DOHH2 cells. The combination effect compares the observed effect of the combination with the expected effect calculated using the fractional product method. Values ≈ 1 indicate an additive effect, values < 1 indicate synergy and values > 1 indicate antagonism. Results shown are from three separate experiments.

Pretreatment with 4-PBA for 24 hours prior to drug treatment had a broadly additive effect in the colorectal cancer cell line HT29, as shown in figure 6.12.

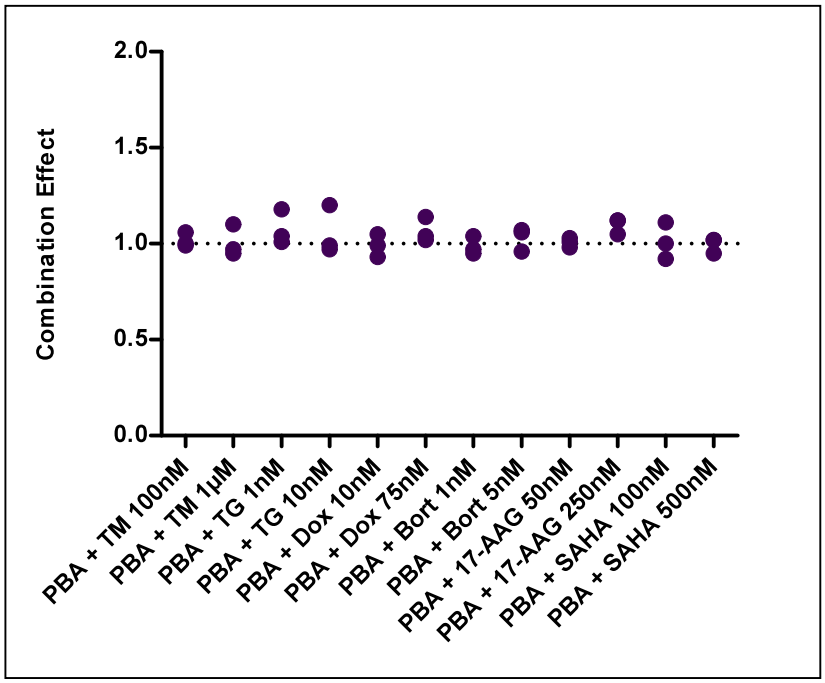

Figure 6.12. Effect of pretreatment with 4-PBA 0.5mM for 24 hours and drug for a further 48 hours on viable cell number (ATP content) in HT29 cells. The combination effect compares the observed effect of the combination with the expected effect calculated using the fractional product method. Values ≈ 1 indicate an additive effect, values < 1 indicate synergy and values > 1 indicate antagonism. Results shown are from three separate experiments.

Whilst the addition of 4-PBA to drug treatment appeared broadly additive using ATP cytotoxicity assay, the assay was not able to differentiate between cytotoxic and cytostatic effects that may be occurring as a result of 4-PBA addition to drug treatment. As a result, an apoptosis assay was carried out in order to investigate if 4-PBA pretreatment affected the level of apoptosis seen following treatment with the ER stress inducing agents tunicamycin and thapsigargin in the haematological cancer cell lines THP1 and U266. It was thought that use of this chemical chaperone might modulate the response to pharmacological ER stress inducers in these cell lines that have been shown in this thesis to have a

constitutively active UPR (as suggested by the supra-additive combination effects observed following treatment with 4-PBA tunicamycin and thapsigargin).

As can be seen from figure 6.13, a statistically significant increase in apoptotic cells was seen in the 4-PBA pretreated 1μM tunicamycin sample ($p<0.05$) and both thapsigargin samples ($p<0.01$) in the THP1 cell line, compared to samples treated with drug alone. This increase in apoptosis was manifested as both an increase in early apoptotic cells and an increase in late apoptotic (dead) cells.

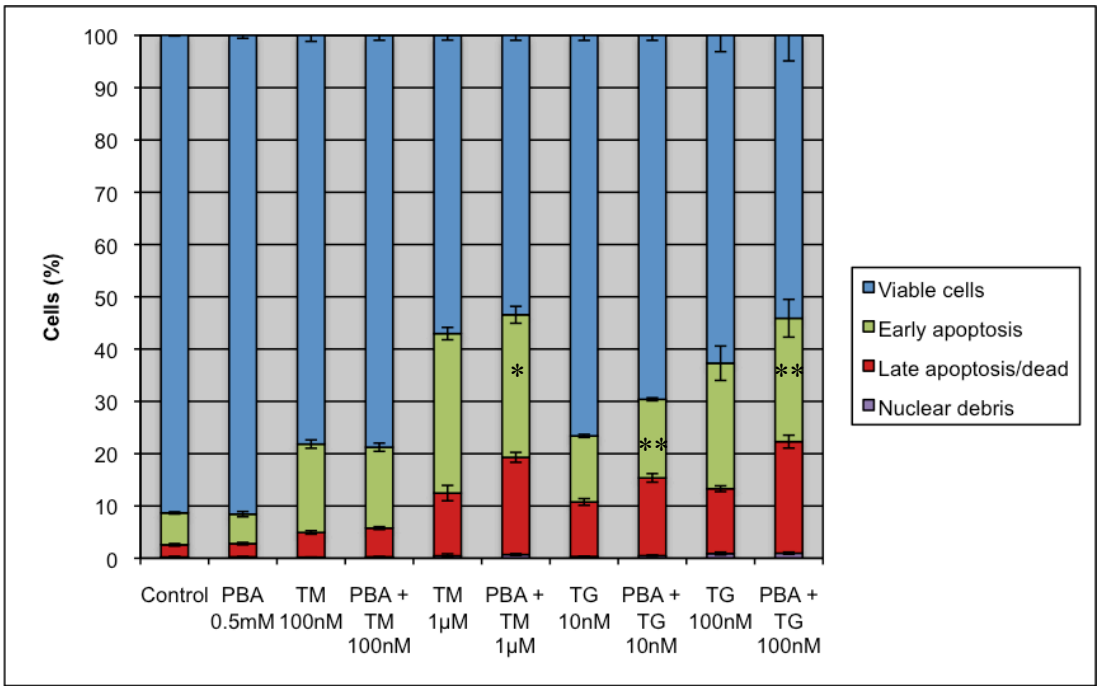

Figure 6.13. Percentage of cells in each category after treatment with drug alone for 48 hours, or 24 hours pretreatment with 4-PBA 0.5mM followed by addition of drug for a further 48 hours in the THP1 cell line. Error bars show mean ± SD. * or ** denotes statistically significant increase in total apoptosis ($p < 0.05$ or $p<0.01$ respectively) with 4-PBA pretreatment, compared to drug alone.

In addition to the percentage of apoptotic cells in each sample, this assay also provided counts of both total and viable cell number. It can be seen from figure 6.14 and 6.15 that there was little effect on cell proliferation in the tunicamycin treated samples,

however a statistically significant decrease in the number of viable cells was observed with 4-PBA pretreatment in the thapsigargin treated THP1 cells ($p<0.05$).

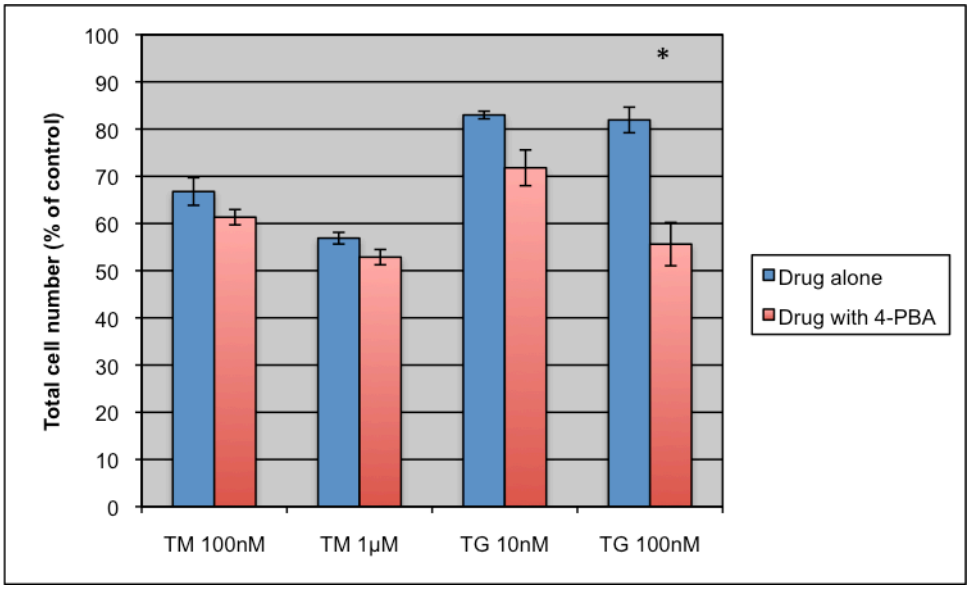

Figure 6.14. Cell number after 48 hours treatment with drug, with or without 24 hours of pretreatment with 4-PBA 0.5mM in THP1 cells (each value normalised to its own control). Error bars show mean ± SD. * denotes statistically significant difference ($p < 0.05$) between drug alone and drug with 4-PBA pretreatment.

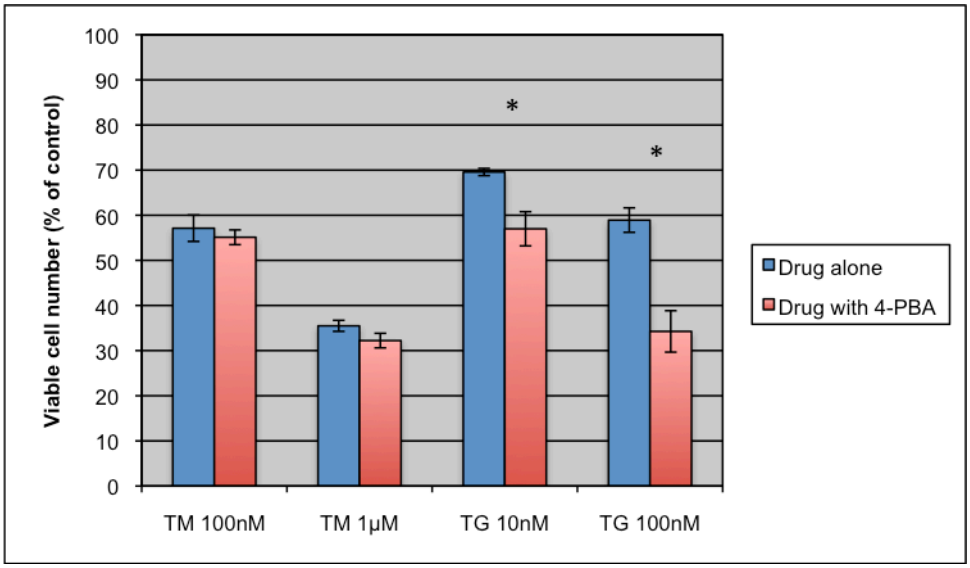

Figure 6.15. Viable cell number after 48 hours treatment with drug, with or without 24 hours of pretreatment with 4-PBA 0.5mM in THP1 cells (each value normalised to its own control). Error bars show mean ± SD. * denotes statistically significant difference ($p < 0.05$) between drug alone and drug with 4-PBA pretreatment.

Figure 6.16 shows the results of the apoptosis assay in the U266 cell line, where a statistically significant increase in apoptotic cells was seen in the 4-PBA pretreated thapsigargin samples, compared to samples treated with thapsigargin alone (10nM, $p<0.01$ and 100nM, $p<0.05$ respectively). This increase in apoptosis was manifested as both an increase in early apoptotic cells and an increase in late apoptotic (dead) cells. However, no significant differences were seen in the tunicamycin treated samples when 4-PBA pretreatment was added.

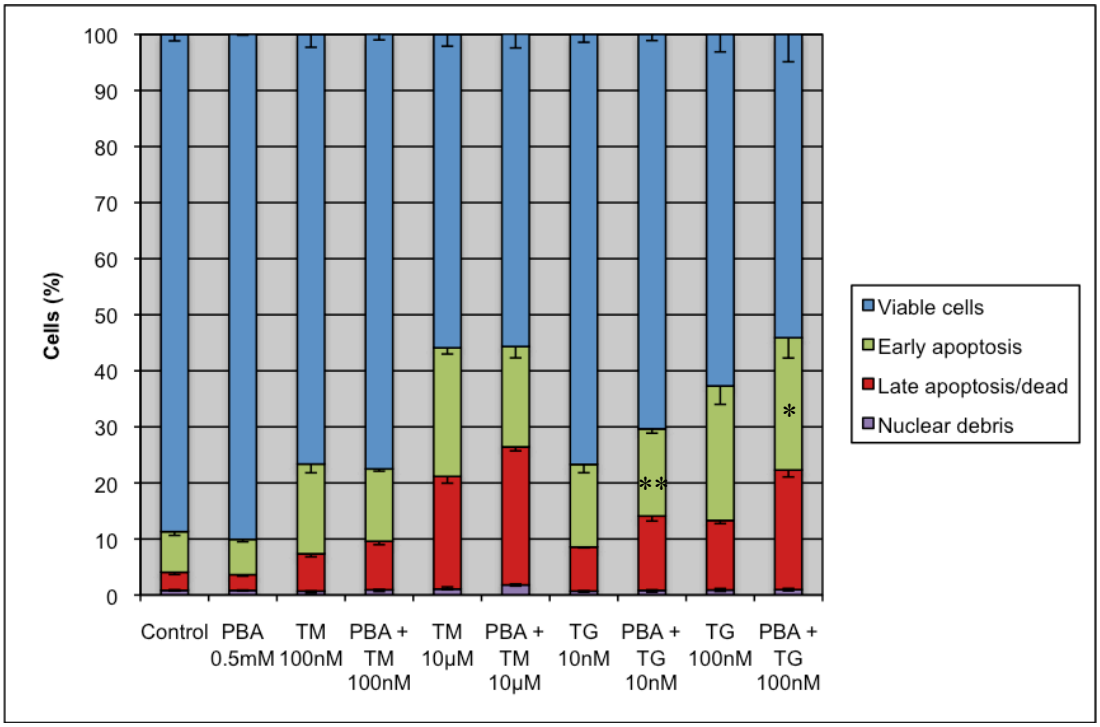

Figure 6.16. Percentage of cells in each category after treatment with drug alone for 48 hours, or 24 hours pretreatment with 4-PBA 0.5mM followed by addition of drug for a further 48 hours in the U266 cell line. Error bars show mean ± SD. * or * denotes statistically significant increase in total apoptosis ($p < 0.05$ or $p<0.01$ respectively) with 4-PBA pretreatment, compared to drug alone.

It can be seen from figures 6.17 and 6,18, that whilst there were no significant differences in total cell number with the addition of 4-PBA pretreatment, a statistically significant decrease in viable cell number was observed in the 4-PBA pretreated thapsigargin treated U266 cells ($p<0.05$).

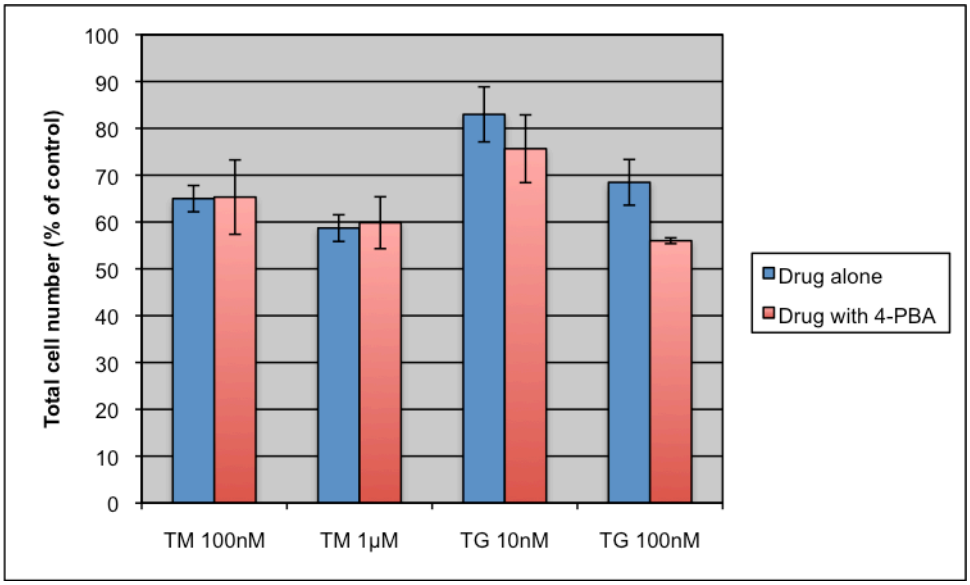

Figure 6.17. Cell number after 48 hours treatment with drug, with or without 24 hours of pretreatment with 4-PBA 0.5mM in U266 cells (each value normalised to its own control). Error bars show mean ± SD.

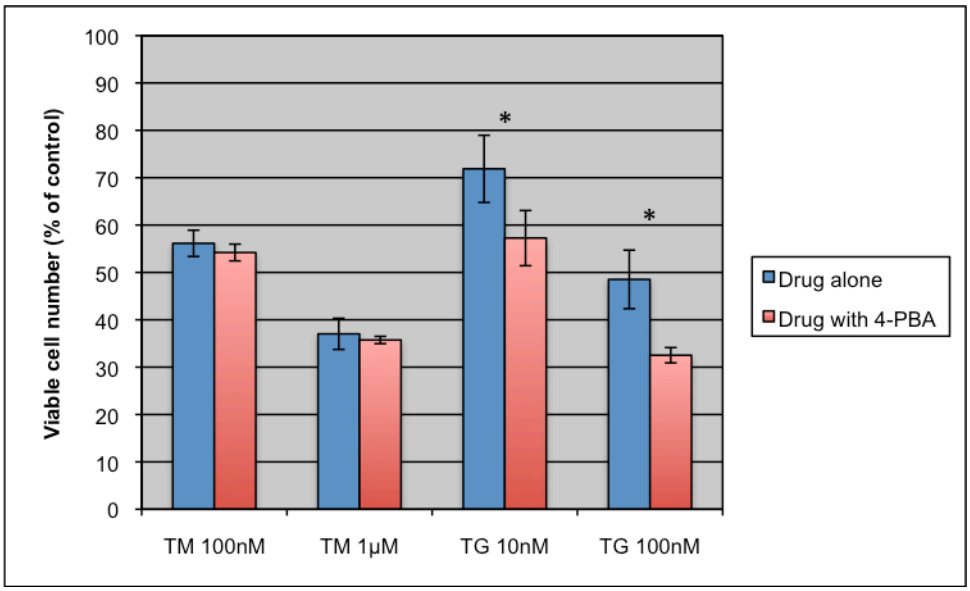

Figure 6.18. Viable cell number after 48 hours treatment with drug, with or without 24 hours of pretreatment with 4-PBA 0.5mM in U266 cells (each value normalised to its own control). Error bars show mean ± SD. * denotes statistically significant difference ($p < 0.05$) between drug alone and drug with 4-PBA pretreatment.

4-PBA has been reported to have weak HDAC inhibitory activity, as well as chaperone activity, therefore a HDAC activity assay was used to determine the extent of HDAC inhibition by 4-PBA. The results are shown in figures 6.19 to 6.21 and table 6.5.

Trichostatin A is the positive control HDAC inhibitor included in the assay kit, and figure 6.19 shows effective inhibition of HDAC activity by Trichostatin A with increasing concentration. The known HDAC inhibitor SAHA was also included in the assay as it had been used as an anticancer agent in these experiments, therefore comparison of its HDAC inhibitory activity at the concentrations used here would provide useful insight. Figure 6.20 shows that SAHA at a concentration of 0.5μM (500nM), which has been used in cytotoxicity experiments in this chapter, resulted in a decrease in HDAC activity of over 70 percent. This assay confirmed that 4-PBA does have HDAC inhibitory activity (see figure 6.21). At the concentration used in this experiment (0.5mM) 4-PBA inhibited HDAC activity by almost 25 percent, with around 70 percent inhibition seen at the 5mM concentration.

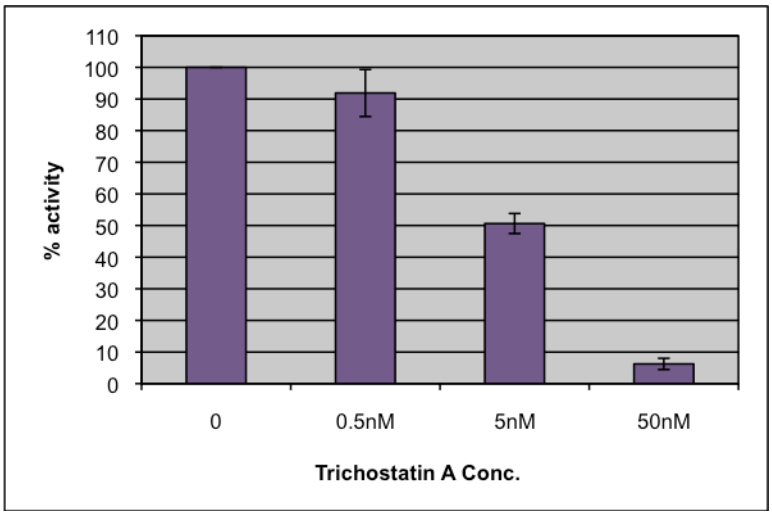

Figure 6.19. Trichostatin A inhibition of substrate deacetylation by HeLa nuclear extract. Error bars show mean ± SD

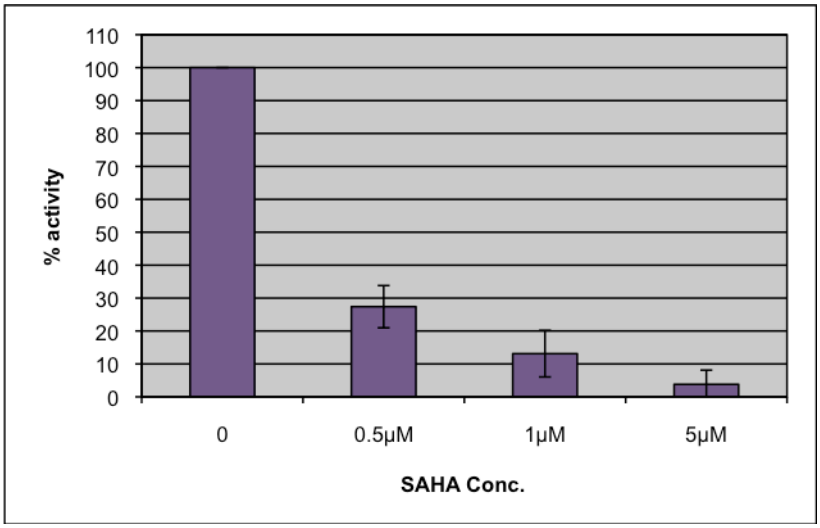

Figure 6.20. SAHA inhibition of substrate deacetylation by HeLa nuclear extract. Error bars show mean ± SD

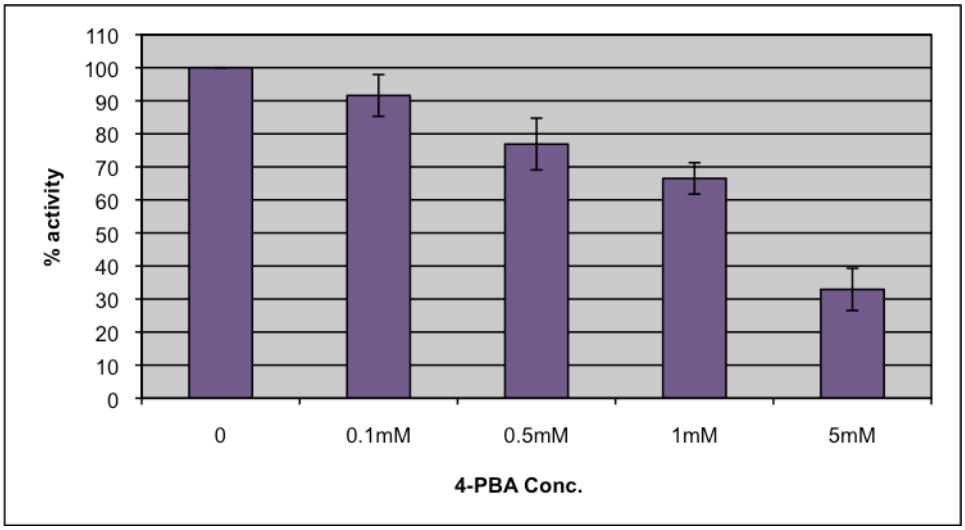

Figure 6.21. 4-PBA inhibition of substrate deacetylation by HeLa nuclear extract. Error bars show mean ± SD

Western blotting experiments were carried out to study the levels of various chaperone proteins and UPR markers following treatment with the ER stress inducing drugs tunicamycin and thapsigargin for 24 hours, with or without 4-PBA pretreatment for 24 hours. Experiments were conducted in the AML cell line THP1 and myeloma cell line U266 (figures 6.22 and 6.23 respectively). No clear changes in protein levels were seen between the 4-PBA pretreated samples and those treated with drug alone. Other UPR proteins were studied, but were undetectable under these experimental conditions.

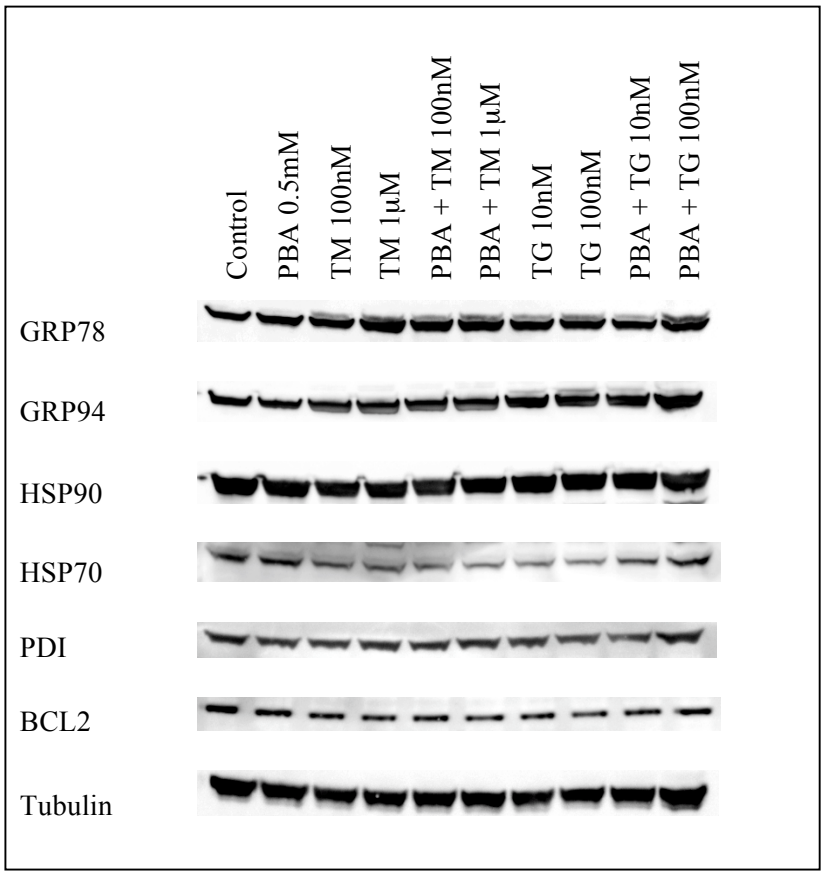

Figure 6.22. Western blotting experiments to investigate the effect of pretreatment with 4-PBA on chemosensitivity in THP1 cells. Tubulin is included as a loading control.

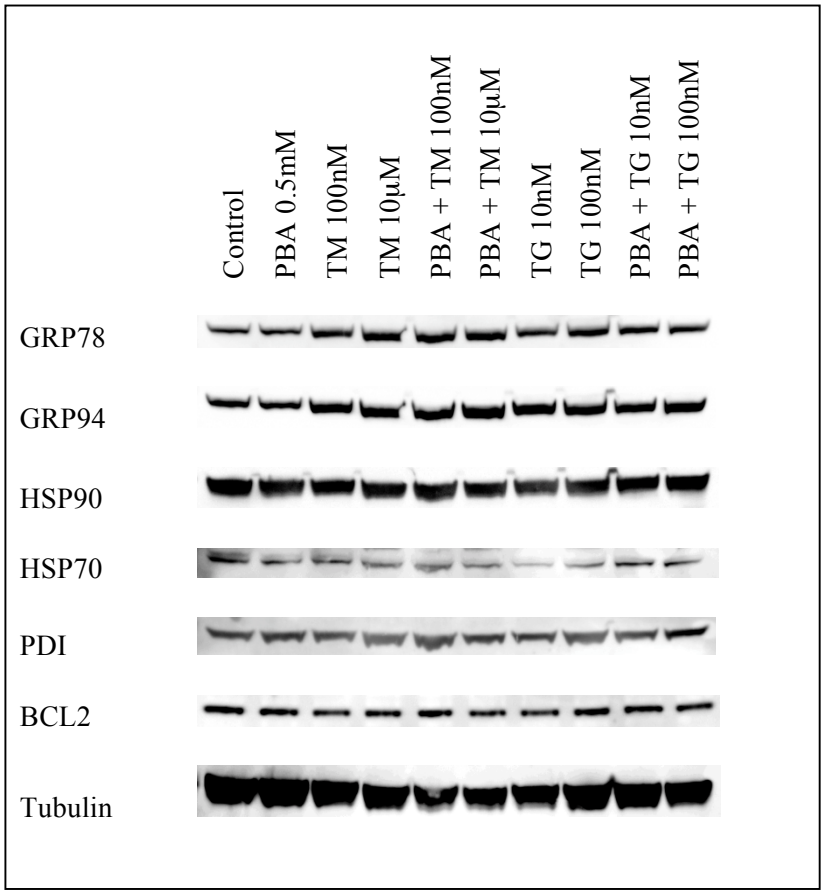

Figure 6.23. Western blotting experiments to investigate the effect of pretreatment with 4-PBA on chemosensitivity in U266 cells. Tubulin is included as a loading control.

6.4 Discussion

4-PBA is a small molecule that has been reported to act as a chemical chaperone. The experiments described here focused on the effect of this compound on the chemosensitivity of haematological cancer cell lines. The colorectal cancer cell line HT29 was used in the cytotoxicity studies as an example of a commonly used solid tumour cell line, in order to detect if any differences occurred between the solid tumour cell line and the haematological cancer cell lines, which have been shown in earlier experiments to have a constitutively active UPR.

The cytotoxic activity of 4-PBA as a single agent was confirmed, with EC_{50} values in the low milimolar range (the HT-29 cell line proved the least sensitive to 4-PBA treatment with an approximate 3-fold increase in EC_{50} compared to the most sensitive cell line DOHH2). Based on these initial cytotoxicity experiments, it was decided to use a concentration of 0.5mM in combination studies, as higher concentrations would prove too toxic in these cell lines. Other investigators have reported that 0.1mM and 2mM concentrations of 4-PBA are clinically relevant concentrations (Brusilow *et al*. 1991). In addition, two phase I clinical trials of sodium phenylbutyrate in refractory solid tumours have been conducted. These studies reported that the molecular effects of 4-PBA were noted at concentrations above 0.5mM, and that these concentrations were readily achievable *in vivo*. The recommended phase II doses (both intravenous and oral) from these trials aimed for plasma concentrations above this 0.5mM level (Carducci *et al.*, 2001, Gilbert *et al.*, 2001).

While mixed effects on drug sensitivity were observed following simultaneous administration of 4-PBA and drug for 48 hours in this study, the effect was broadly additive. This additive effect was confirmed in experiments using a 24 hour 4-PBA pretreatment, prior to the addition of drug for a further 48 hours.

An apoptosis assay was utilised to investigate the effect of 4-PBA pretreatment for 24 hours on the level of apoptosis seen following 48 hours of treatment with the pharmacological ER stress inducers tunicamycin and thapsigargin. These experiments were undertaken in the THP1 and U266 cell lines due to the supra-additive effects seen with these combinations using the ATP cytotoxicity in these cell lines. This assay revealed a statistically significant increase in apoptotic cells with both thapsigargin concentrations used following pretreatment with 0.5mM 4-PBA for 24 hours in the THP1 and U266 cell line. A statistically significant increase in apoptotic cells was also seen following tunicamycin treatment at the higher concentration in the 4-PBA pretreated THP1 cells. Interestingly,

these results suggest that pretreatment with 4-PBA sensitises these haematological cell lines to ER stress mediated apoptosis. The potential interaction with other anticancer agents remains to be determined. The apoptosis assay described here was the result of one experiment conducted in triplicate and as a result further confirmatory experiments would be needed before definite conclusions could be drawn from these results.

This study also investigated the mechanism of action of 4-PBA in these haematological cancer cell lines. At the protein level, decreases in the antiapoptotic proteins BCL2 and MCL1 were seen following 24 hours of treatment with the 5mM 4-PBA concentration, however no changes were detected in the UPR proteins studied. Whilst it is possible that the attenuation of ER stress is not visible at the protein level under these experimental conditions, it is also a possibility that the effect of 4-PBA is mediated by another mechanism, for example HDAC inhibition. Down regulation of antiapoptotic BCL2 family proteins is consistent with the mechanism of action of HDAC inhibitors (Zhang *et al.*, 2004).

4-PBA is a derivative of the first generation HDAC inhibitor butyric acid, and whilst investigators who have reported the chemical chaperone function of 4-PBA have generally overlooked its HDAC inhibitory activity, it may be significant in this context. The HDAC activity assay revealed that 4-PBA at the 0.5mM concentration used in this study did exhibit some HDAC inhibitory activity. At the 5mM concentration, this HDAC inhibitory activity was comparable to that of the clinically used HDAC inhibitor SAHA at the 0.5µM concentration used in these *in vitro* studies. It is therefore worth considering the HDAC inhibitory activity of this 4-PBA when discussing its other reported function as a chemical chaperone.

One other important issue relating to the use of 4-PBA as a chemical chaperone is the concentration of 4-PBA used. The studies of 4-PBA reported to date (see the

introduction to this chapter) routinely use concentrations 10 to 20-fold higher than those used in this experiment to show amelioration of ER stress and the UPR. No mention is made of the cytotoxicity of 4-PBA alone at this concentration in the experimental models used. For example, in the 2006 report in the journal Science by Ozcan and colleagues, 4-PBA concentrations of 10mM and 20mM were used in the *in vitro* studies (Ozcan *et al.*, 2006). In the experiments conducted as part of this project, 4-PBA proved extremely cytotoxic at these concentrations, hence the use of the lower 0.5mM concentration. In addition, 4-PBA at these higher concentrations has been shown in this project to be an effective HDAC inhibitor, which is important when considering the effects that have been ascribed to 4-PBA treatment. The lack of an ER stress relieving effect at lower concentrations observed in this project has been confirmed by other investigators, for example Basseri and colleagues showed a decrease in GRP78 and GRP94 protein levels following administration of 10mM 4-PBA, but no change compared to the control levels after treatment with 1mM 4-PBA (Basseri *et al.*, 2009). Taken together, these results suggest that 4-PBA is not acting as a chemical chaperone at these lower concentrations and the effects observed are mediated by other mechanisms (for example, HDAC inhibition).

Further experiments are needed to fully establish the relationship between 4-PBA treatment and increased sensitivity to the cytotoxic effects of ER stress inducing agents. Experiments investigating the effect of 4-PBA on cell cycle distribution (HDAC inhibitors are known to cause cell cycle arrest in G1/G2) and histone acetylation would further determine the importance of HDAC inhibition in the action of 4-PBA at the concentrations studied.

7. Downregulation of ER Resident Molecular Chaperones Using the Novel Small Molecule Compound Versipelostatin and the Effect on Chemosensitivity *in vitro*

7.1 Introduction

Molecular chaperones facilitate the correct folding of proteins, with the ER containing a number of resident molecular chaperones, such as the heat shock protein (HSP) 70 and HSP90 families, the lectins calnexin and calreticulin, and the HSP40 family of co-chaperones. HSPs have an affinity for, and bind to, exposed hydrophobic sites on unfolded proteins that would ordinarily be buried in the interior of the structure, using hydrolysis of ATP to provide the energy required to carry out their chaperone function. HSPs often require many cycles of ATP hydrolysis in order to fold a single polypeptide chain correctly (Ellgaard and Helenius, 2003, Alberts, 2002, Ma and Hendershot, 2004a).

Targeting molecular chaperones has been suggested as a therapeutic strategy in a number of different diseases and anticancer agents inhibiting the chaperone protein HSP90 have now progressed to clinical trials (Smith and Workman, 2007). The two molecular chaperones with the most direct effect on UPR activation and UPR signalling are GRP78 and GRP94. GRP78 is a member of the HSP70 family and GRP94 is a member of the HSP90 family of heat shock proteins (Lee, 2007). GRP78 recognises hydrophobic residues on unfolded or misfolded proteins and binds to them, thereby preventing their interaction with other molecules (Bole *et al.*, 1986). GRP94 is the ER resident isoform of cytosolic HSP90, however in contrast to HSP90 (which has a very large number of client proteins, a number of which are oncogenic), GRP94 appears to have a very limited number of client proteins. GRP94 has been shown to be involved in B-cell differentiation and is also involved in the immune response (Ni and Lee, 2007, Liu and Li, 2008). GRP78 is a vital mediator of the response to ER stress, being the main ER stress sensor whose dissociation from the three

transmembrane UPR receptors results in activation of the UPR. The role of this key ER molecular chaperone in the UPR and chemosensitivity have been described in detail in Chapter 1; brief highlights from the literature describing the importance of these ER molecular chaperones in cancer are discussed below.

Involvement of GRP78 (and to a lesser extent GRP94) in a number of different solid tumour types has been shown. In hepatocellular carcinoma GRP78 has been identified as a transformation associated gene, along with activation of the ATF6 and IRE1/XBP1 pathways (Shuda *et al.*, 2003). In colon cancer, GRP78 has been shown to be upregulated in colon cancer tissue and increased cytoplasmic GRP78 expression was associated with the transformation from normal tissue to adenoma and then carcinoma (Xing *et al.*, 2006). GRP78 has also been shown to be overexpressed in malignant breast tumours, but there was no overexpression seen in benign breast tumours (Fernandez *et al.*, 2000). Both GRP78 and GRP94 have been shown to be overexpressed in lung cancer tissues (Wang *et al.*, 2005), and GRP94 overexpression has been reported in oesophageal adenocarcinomas (Chen *et al.*, 2002). Activation of the UPR has also been shown in prostate cancer (Misra *et al.*, 2006) and GRP78 has been linked to prostate cancer metastasis. GRP78 has been shown to be weakly expressed in normal prostate tissue, however it is highly expressed in the bone metastases of prostate cancer patients (Mintz *et al.*, 2003). In another study in prostate cancer it was found that the intensity of GRP78 expression in prostate tissue was associated with survival and clinical recurrence (Daneshmand *et al.*, 2007).

A number of years before the elucidation of the mammalian UPR pathways and the vital role played by molecular chaperones such as GRP78, it was already known that the glucose related proteins were involved in resistance of tumours to treatment with traditional DNA-damaging chemotherapy drugs. In 1987, it was shown that exposure of chinese hamster ovary (CHO) cells to conditions that induced GRPs (e.g. glucose deprivation and anoxia) induced resistance to the topoisomerase II poison doxorubicin (Shen *et al.*, 1987).

These researchers then went on to attempt to identify a mechanism for this resistance. They found that following exposure of CHO cells to GRP inducing conditions (also including tunicamycin treatment) there was a rapid and selective depletion of topoisomeraase II from the nucleus of these cells and associated cell cycle effects (Shen *et al.*, 1989). GRP78 and drug resistance is discussed in more detail in chapter 1.5.

In light of the importance of these ER resident molecular chaperones in cancer, modulating the UPR by targeting these chaperones has been proposed as a novel anticancer strategy. Research has focused on modulating GRP78 (also known as BiP) function. However, work conducted in this area to date has consisted almost exclusively of studies in solid tumours, the vast majority of which have involved utilisation of molecular biology techniques such as gene silencing or overexpression in order to modulate GRP78 function (Kardosh *et al.*, 2008, Pyrko *et al.*, 2007b, Lee *et al.*, 2008). The search for more clinically viable strategies to target GRP78 is therefore ongoing. Strategies for targeting GRP78 currently being explored include the use of the cytokine interleukin-24 (IL-24 – also known as melanoma differentiation-associated gene-7 or MDA-7), a member of the interleukin-10 family of cytokines (Jiang *et al.*, 1995, Dent *et al.*, 2005).

One emerging therapeutic strategy to modulate GRP78 function is the use of the novel small molecule Versipelostatin (VST). This compound was discovered by Dr Shin-ya and colleagues at the National Institute of Advanced Industrial Science and Technology (AIST) in Japan, as a result of a screen for compounds with the potential to affect molecular chaperones. These researchers utilised a luciferase reporter gene assay to detect activation of the GRP78 promoter in their screen for inhibitors of GRP78 expression. Versipelostatin was isolated from the culture broth of *Streptomyces versipellis* 4083-SVS6. Its molecular formula was determined as $C_{61}H_{94}O_{17}$ and study of the NMR spectra revealed its structure to be a macrocyclic compound consisting of an α-acyltetronic acid and sugar moieties.

Versipelostatin has a relative molecular mass of 1099 (chemical structure is shown in figure 7.1) (Park *et al.*, 2002).

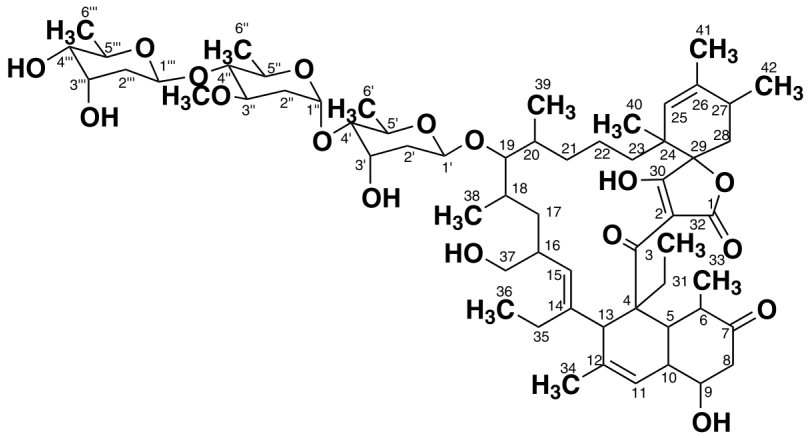

Figure 7.1. The structure of versipelostatin.
Reproduced from Park *et al.* (2002).

In the initial publication detailing the discovery and structure of versipelostatin, it was reported that the compound exhibited limited cytotoxicity alone *in vitro*, yet was able to inhibit the expression of GRP78 induced by ER stressors such as tunicamycin treatment or hypoglycaemic insult in the HeLa cell line (Park *et al.*, 2002). Research published by this group in 2004 further elucidated the mechanism of action of versipelostatin and its potential as an anticancer agent (Park *et al.*, 2004). This work confirmed that versipelostatin inhibited GRP78 expression in response to ER stress due to glucose deprivation, but not GRP78 expression resulting from ER stress induction with tunicamycin. At this time it was also reported that in addition to inhibiting GRP78 expression occurring as a result of glucose deprivation mediated ER stress, versipelostatin inhibited the expression of GRP94 under glucose deprivation conditions (Park *et al.*, 2004).

Versipelostatin is the only compound described to date that acts specifically to reduce the expression of the ER molecular chaperones GRP78 and GRP94 induced after ER stress. In order to test the specificity of versipelostatin for UPR molecular chaperones, the

authors examined the effect of versipelostatin on HSP70 mRNA expression and discovered that VST was unable to inhibit HSP70 gene expression under all experimental conditions studied. The authors propose that versipelostatin selectively inhibits the transcription of genes containing the endoplasmic reticulum stress response element (ERSE) in their promoter during glucose deprivation conditions. XBP1 splicing and ATF4 expression were both decreased by versipelostatin treatment during glucose deprivation, indicating UPR suppression, however no decrease in ATF6 cleavage (activation) was seen (Park *et al.*, 2004).

This study also examined the effect of versipelostatin treatment on cell viability. After 24 hours drug treatment in the colorectal cancer cell line HT-29, versipelostatin was found to have only a weak cytotoxic effect alone, but had a profound cytotoxic effect under glucose deprivation conditions with an approximately 30-fold lower $IC_{50.}$ The growth inhibitory effect of versipelostatin was characterised in a panel of 39 solid tumour cancer cell lines, with growth inhibition seen in the majority of cell lines following 48 hours treatment under normal growth conditions. The authors report that there was little apoptosis in the cell line panel under normal growth conditions, whilst extensive apoptosis was seen under glucose deprivation conditions (Park *et al.*, 2004). In a mouse xenograft model, the *in vivo* cytotoxic effect of versipelostatin was comparable to that of single agent cisplatin treatment, and the drug was well tolerated (Park *et al.*, 2004). These studies provided encouraging early results for this novel compound, however further research is required to fully elucidate the mechanism of versipelostatin downregulation of GRP78 and GRP94.

Differences in glucose metabolism between tumour cells and normal non-malignant cells have been known for many years. In a February 1956 issue of the journal Science, the nobel laureate Otto Warburg published his work “On the origin of cancer cells”, which outlined his observation that the increased glycolysis seen in cancer cells was due to a fundamental injury in cellular respiration. This metabolic shift from oxidative

phosphorylation for energy production in normal cells, to the less efficient aerobic glycolysis in tumour cells is known as the Warburg effect (Warburg, 1956). Whilst it has still not been definitively established whether this metabolic shift is the cause of cancer (as proposed by Warburg) or a by-product of tumour growth, the Warburg effect does highlight a potential difference between normal and cancer cells that may be exploited as a therapeutic target.

ER stress and the unfolded protein response can be provoked in a number of different ways; one example of which is glucose deprivation. As a tumour grows, increasing demands are placed on the microenvironment, eventually leading to glucose deprivation, low pH, poor vascular supply and hypoxia (Ma and Hendershot, 2004b). Aerobic glycolysis and increased glucose metabolism by tumours is the rationale behind the use of ^{18}fluorodeoxyglucose positron emission tomography (^{18}FDG-PET) imaging in the diagnosis of tumours (Gatenby and Gillies, 2004, Lopez-Lazaro, 2010). Similar to research on the UPR in cancer, research into targeting glycolysis in cancer cells has focused only on solid tumours. However, a recent review has highlighted that with ^{18}FDG-PET being utilised as a diagnostic tool in some haematological malignancies, targeting glycolysis does therefore represent a valid therapeutic approach in these haematological cancers (Shanmugam *et al.*, 2009). In the versipelostatin studies by the Shin-ya research group, glucose deprivation conditions were achieved either through the replacement of normal (glucose-containing) culture medium with glucose free medium, or the addition of 2-deoxyglucose (2-deoxy-D-glucose, 2-DG) to glucose-containing culture medium. 2-DG is an antimetabolite compound that is almost identical in structure to glucose. 2-DG is therefore imported into cells via glucose transporters and is phosphorylated by the enzyme hexokinase to 2-deoxyglucose-6-phosphate, which accumulates intracellularly, but importantly inhibits the activity of hexokinase, thereby inhibiting the metabolism of glucose. 2-DG treatment has been reported to potentiate the cytotoxic effects of both chemotherapy and radiotherapy in a number of tumour types (Yamada *et al.*, 1999, Maschek *et al.*, 2004, Hernlund *et al.*, 2008, Simons *et al.*, 2007). 2-DG has also been investigated as an anticancer agent in its own right and has

shown potency in vitro, however, after progressing to phase I clinical trials development appears to have been halted due to lack of efficacy in the clinic, with the dose administered limited by unacceptable toxicity at the concentrations required for activity (Shanmugam *et al.*, 2009).

In this chapter, the activity of the novel compound versipelostatin is established in haematological cancer cell lines, and its ability to downregulate the ER molecular chaperones GRP78 and GRP94 determined. The activity of versipelostatin and its effect on the UPR has not previously been reported in haematological cancer cells.

7.2 Materials and Methods

Versipelostatin (VST) was kindly provided by Dr K Shin-ya, National Institute of Advanced Industrial Science and Technology, Japan. VST stock solution was prepared in DMSO and stored at -20°C until use. 2-deoxyglucose (2-DG) was obtained from Sigma Aldrich, UK. Stock solution of 2-DG was prepared in purified water and stored at -20°C until use. All further dilutions of the stock solutions were prepared fresh in culture medium under sterile conditions immediately prior to use. The haematological cancer cell lines THP1, U266 and SUD4 were used for experiments in this chapter, along with the adherent colorectal cancer cell line HT-29 (the activity of versipelostatin in this solid tumour cell line has previously been reported (Park *et al.*, 2004)). Cell culture materials and conditions were as described in chapter 2.

Cytotoxicity experiments were carried out as described in chapter 2 (sections 2.4 to 2.6 inclusive). The effect of drug treatment on cell proliferation and viability was investigated using a plate based adenosine triphosphate (ATP) cytotoxicity assay. Cells in exponential growth phase were plated into 96 well plates (5000 cells per well in 100µl

medium) and incubated for 24 hours. Varying concentrations of drug were diluted in culture medium and then added to each well to obtain the required final concentration (all drug additions were made in a fixed volume of 10µl per well). Control wells were topped up with culture medium so that all wells of the plate contained a fixed volume of 110µl. Plates were then incubated for 48 hours at 37°C and 5% CO_2, before analysis using the ViaLight HS assay kit (Lonza Group Ltd, Switzerland) and a BMG Labtech Polarstar Optima microplate reader (BMG Labtech, Germany).

The effect of VST concentration was studied in triplicate wells with biological replicates studied on three separate occasions (expressed as a percentage of the control value). For each drug, the mean values and standard deviations of all experiments were determined for graphical representation. For concentration-effect modelling in GraphPad Prism, the mean values for each concentration in each experiment were used.

Further studies in two cell lines used the Guava ViaCount assay (Guava Technologies Inc., USA) to determine total cell number (total cell number per millilitre) and cell viability (percentage viable cells and percentage dead cells) of each sample. Cells were plated out and drug additions made as described above. 48 hours after addition of drug, plates were removed from the incubator and 100µl of diluted Guava ViaCount Flex Reagent was added to each well. Plates were then analysed using the Guava PCA™ – 96 System. All samples were run in triplicate and each experiment was repeated on two separate occasions. The mean values and standard deviations of each data set were then calculated and used in subsequent data analysis. For concentration-effect modelling in GraphPad Prism, the mean values for each concentration in each experiment were used.

Drug activity data was fitted using sigmoidal concentration effect curves to derive EC_{50} values (effective concentration 50 – i.e. the concentration required to exert 50% of

maximum effect) with 95% confidence intervals, using non linear regression in GraphPad Prism software (GraphPad Software, San Diego, USA) as described in chapter 2.6

For western blotting experiments, two million cells were plated out into each well of six-well culture plates and incubated for 24 hours at 37°C and 5% CO_2 in air. Drug dilutions were made as described in chapter 2.7. Cells were then incubated for a further 24 hours, after which time the cells were harvested and whole cell lysates prepared as described in chapter 2.7. All antibodies, reagents and experimental conditions for western blotting were as described in chapter 2.8. For some experiments, drug incubations were carried out in the absence of glucose. In these cases, glucose free RPMI-1640 medium was used, supplemented with 10% dialysed heat-inactivated foetal calf serum (FCS) and 1% penicillin-streptomycin. All western blotting experiments were repeated to ensure reproducibility.

In conjunction with the western blotting experiments, cytotoxicity experiments were carried out in order to establish the effect of versipelostatin treatment in combination with 2-DG treatment. The Guava ViaCount assay (Guava Technologies Inc., USA) was used to determine total cell number (total cell number per millilitre) and cell viability (percentage viable cells and percentage dead cells) of each sample as described above. Single agent treated wells, combination treated wells, and untreated control wells were present on each plate in the combination experiments. Control wells and single agent treatment wells were topped up with culture medium so that all wells of the plate contained a fixed volume. Plates were then incubated for 24 hours at 37°C and 5% CO_2 in air, before analysis. Each concentration was studied in duplicate, with mean values and standard deviations determined for graphical representation.

7.3 Results

The activity of versipelostatin has not previously been reported in haematological cancer cell lines. It was therefore necessary to initially determine the effect of this novel small molecule compound under normal cell culture conditions in these cell lines. The solid tumour cell line HT-29 was also included as a reference cell line in which the activity of versipelostatin has previously been reported. Figure 7.2 below shows an example of the data generated in these experiments. Cells were treated for 48 hours with increasing concentrations of versipelostatin and the effect on cell proliferation and viability was then assessed using an ATP cytotoxicity assay. This data was then used to plot concentration-effect curves and calculate EC_{50} values (see figure 7.3). The same was also done for 2-DG treatment in these cell lines (see figure 7.4).

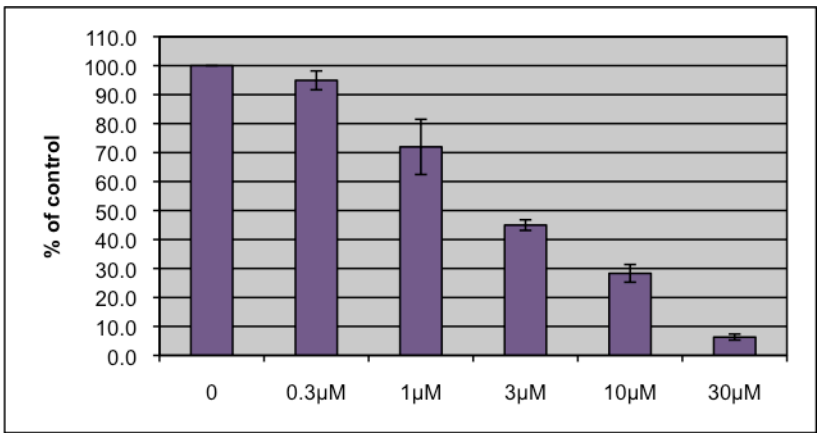

Figure 7.2. Effect of treatment with increasing concentrations of VST for 48 hours on viable cell number (ATP content) in the AML cell line THP1. Error bars show mean ± standard deviation (SD).

Figure 7.3 shows the cytotoxicity of versipelostatin in the three haematological cancer cell lines and the colorectal cancer cell line being studied. The haematological cancer cell lines were more sensitive to versipelostatin treatment than the solid tumour cell line. The AML cell line THP1 and the DLBCL cell line DOHH2 proved significantly more sensitive to versipelostatin treatment, with EC_{50} values of 2.9μM and 2.5μM respectively.

The U266 cell line was the least sensitive of the haematological cancer cell lines, with an EC_{50} of 7.5µM. The colorectal cancer cell line HT-29 was the least sensitive cell line overall to versipelostatin, with an EC_{50} of 19.0µM.

A

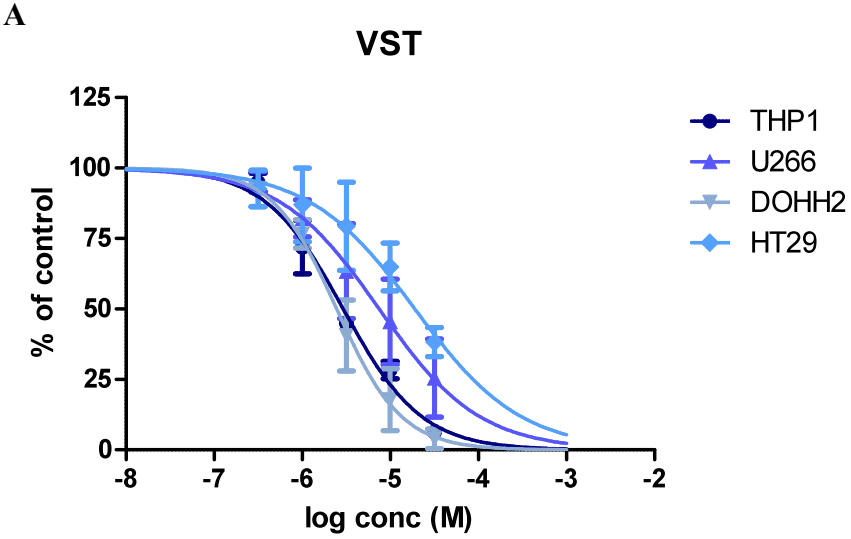

B

Drug	Cell line	EC_{50}	95% CI
VST	THP-1	2.9µM	2.4µM to 3.6µM
	U266	7.5µM	4.8µM to 11.6µM
	DOHH2	2.5µM	2.0µM to 3.1µM
	HT29	19.0µM	11.7µM to 30.7µM

Figure 7.3. A – Effect of treatment with VST for 48 hours on viable cell number (ATP content) in three haematological cancer cell lines and the colorectal cancer cell line HT29 (error bars show mean ± SD). **B –** EC_{50} values, with 95% confidence intervals, for VST treatment.

In order to further investigate the cytotoxicity of versipelostatin, experiments were conducted in the THP1 (AML) and U266 (MM) cell lines to determine the differential effects of this compound on cell proliferation and cell viability. Versipelostatin decreased cell proliferation in a concentration dependent manner in both cell lines studied after 48 hours of treatment. Cell viability data revealed that viability decreased with 48 hours of versipelostatin treatment, also in a concentration dependent manner. Similar sensitivity to versipelostatin was seen with both cell lines, with similar EC_{50} values.

A

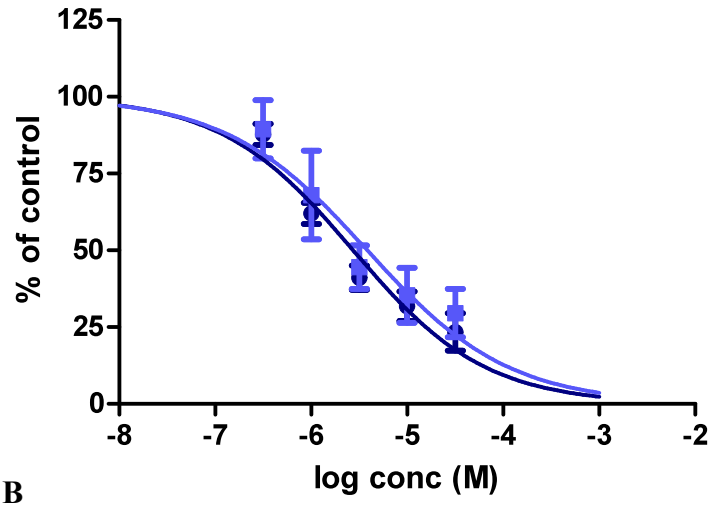

B

Drug	Cell line	EC_{50}	95% CI
VST	THP-1	2.7µM	1.8µM to 4.1µM
	U266	3.8µM	2.1µM to 7.2µM

C

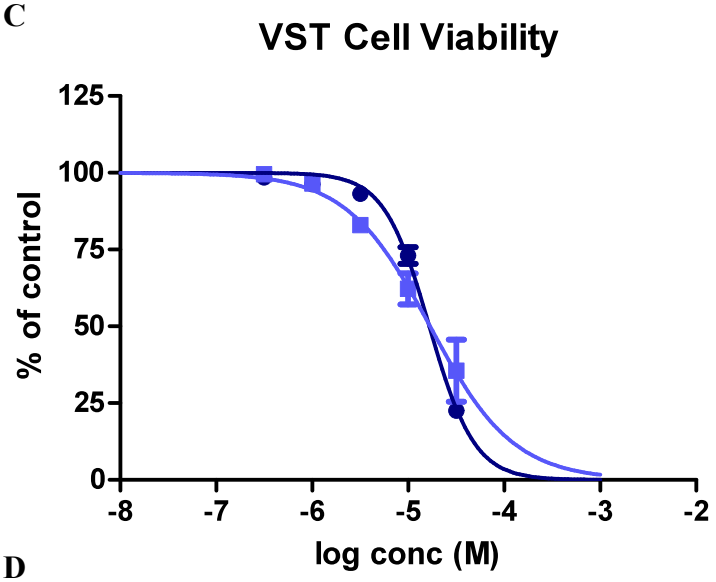

D

Drug	Cell line	EC_{50}	95% CI
VST	THP-1	16.6µM	15.3µM to 18.0µM
	U266	16.9µM	13.8µM to 20.8µM

Figure 7.5. **A –** Effect of treatment with VST for 48 hours on cell number in three cancer cell lines (error bars show mean ± SD). **B –** EC_{50} values, with 95% confidence intervals, for VST treatment on cell number. **C** - Effect of treatment with VST for 48 hours on cell viability in three cancer cell lines (error bars show standard deviation). **D –** EC_{50} values, with 95% confidence intervals, for VST treatment on cell viability

In order to induce hypoglycaemic (glucose deprivation) conditions *in vitro*, investigators commonly use the glycolysis inhibitor 2-DG. In higher concentrations, this compound can exert a cytotoxic effect in its own right, therefore in order to optimise its use in these cell lines, initial experiments were undertaken to study the cytotoxicity of increasing concentrations of 2-DG for 48 hours in these cell lines (see figure 7.4). It can be seen that in the milimolar range, 2-DG did in fact exhibit a concentration-dependent cytotoxic effect. The DOHH2 cell line appeared most sensitive to 2-DG treatment across the concentration range studied, followed by the THP1 and U266 cell lines. The colorectal cancer cell line HT-29 was least sensitive to treatment with 2-DG at the concentrations studied.

A

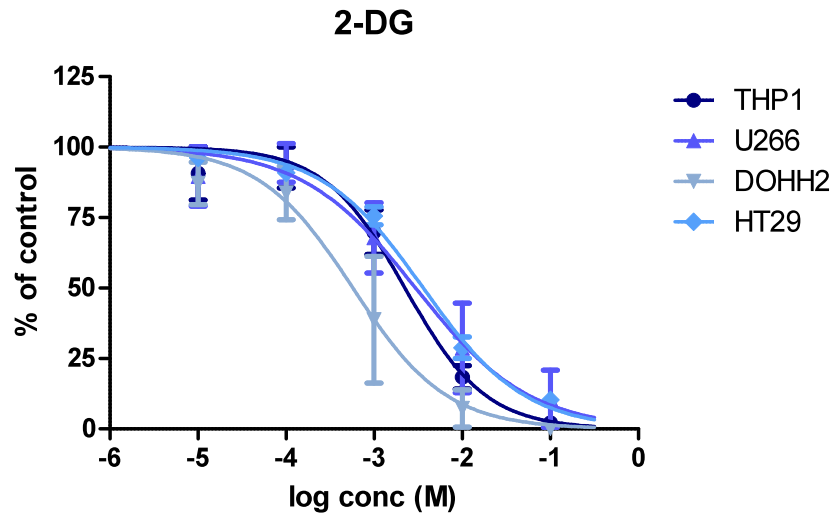

B

Drug	Cell line	EC_{50}	95% CI
2-DG	THP-1	2.2mM	1.6mM to 3.2mM
	U266	3.0mM	1.6mM to 5.6mM
	DOHH2	0.57mM	0.32mM to 1.0mM
	HT29	3.6mM	3.0mM to 4.4mM

Figure 7.4. A – Effect of treatment with 2-DG for 48 hours on viable cell number (ATP content) three haematological cancer cell lines and the colorectal cancer cell line HT29 (error bars show standard deviation). **B –** EC_{50} values, with 95% confidence intervals, for 2-DG treatment

As with versipelostatin treatment, experiments were carried out using the THP1 and U266 cell lines to determine the effects of 48 hours of 2-DG treatment on cell proliferation and cell viability. A similar pattern of sensitivity to that occurring with versipelostatin treatment was seen in each of the haematological cancer cell lines. 2-DG treatment was found to decrease cell proliferation in both cell lines studied after 48 hours of treatment. As with versipelostatin treatment, the antiproliferative effect seen was concentration dependent. Cell viability also decreased after 48 hours of 2-DG treatment in a concentration dependent manner in these cell lines.

A

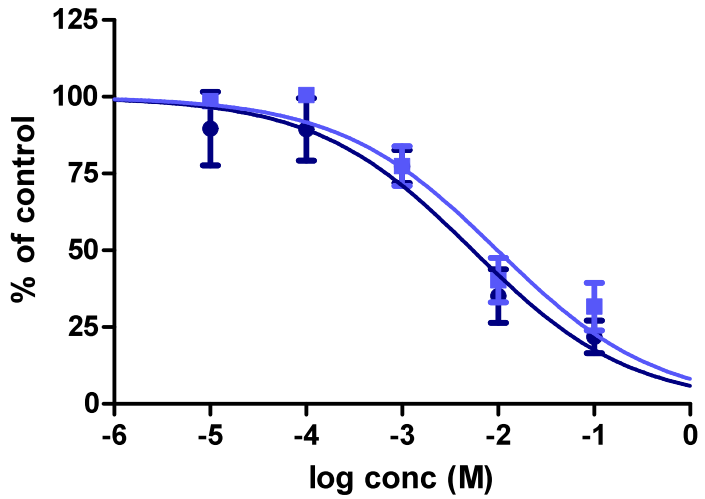

B

Drug	Cell line	EC_{50}	95% CI
2-DG	THP-1	5.5mM	2.5mM to 11.9mM
	U266	9.8mM	4.5mM to 21.5mM

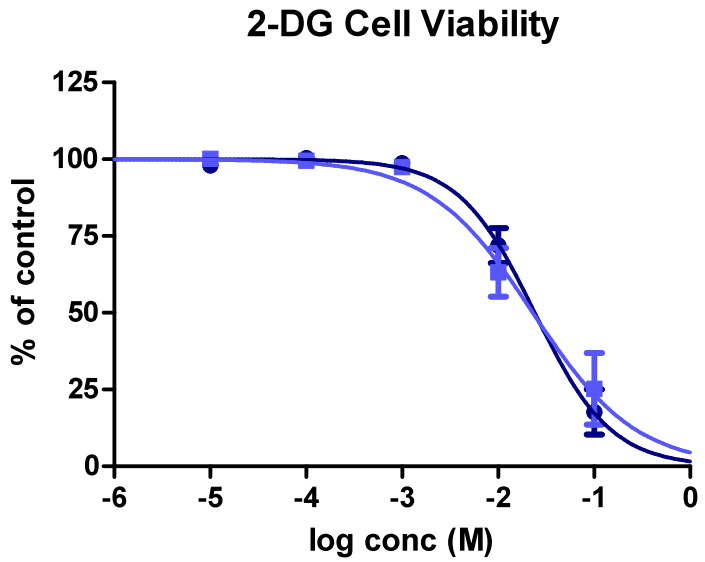

D

Drug	Cell line	EC_{50}	95% CI
2-DG	THP-1	24.1mM	19.3mM to 30.0mM
	U266	23.0mM	15.4mM to 34.4mM

Figure 7.6. A – Effect of treatment with 2-DG for 48 hours on cell number in three cancer cell lines (error bars show standard deviation). **B** – EC_{50} values, with 95% confidence intervals, for 2-DG treatment on cell number. **C** – Effect of treatment with 2-DG for 48 hours on cell viability in three cancer cell lines (error bars show standard deviation). **D** – EC_{50} values, with 95% confidence intervals, for 2-DG treatment on cell viability

The next set of experiments were carried out to investigate the effect of versipelostatin treatment under glucose deprivation conditions on ER molecular chaperone protein levels in the haematological cell lines THP1 and U266. The glycolysis inhibitor 2-DG was used to induce glucose deprivation conditions *in vitro*. As a result, the DOHH2 cell line was not used due to its extreme sensitivity to 2-DG treatment at concentrations required for glycolysis inhibition, as determined in the previous experiments. In conjunction with the western blotting experiments, cytotoxicity experiments were carried out to establish the effect of versipelostatin treatment in combination with 2-DG treatment on cell number and viability. Treatments with increasing concentrations of versipelostatin were carried out, alone or in the presence of 2-DG, for 24 hours before analysis.

After 24 hours of treatment, neither versipelostatin alone nor 2-DG alone exhibited any major effects on cell number in either the THP1 or U266 cell lines (see figures 7.7 and 7.9 respectively). The inhibition of cell proliferation seen with the combination of versipelostatin treatment and glucose deprivation conditions (mediated by 2-DG treatment) appeared to be broadly additive in both cell lines. In the THP1 cell line, only the 0.3μM versipelostatin concentration showing a statistically significant decrease in cell number with glucose deprivation compared with versipelostatin alone under normal growth conditions. In the U266 cell line, treatment with the highest versipelostatin concentration under glucose deprivation conditions led to a statistically significant increase in cell number compared to treatment under normal glucose conditions.

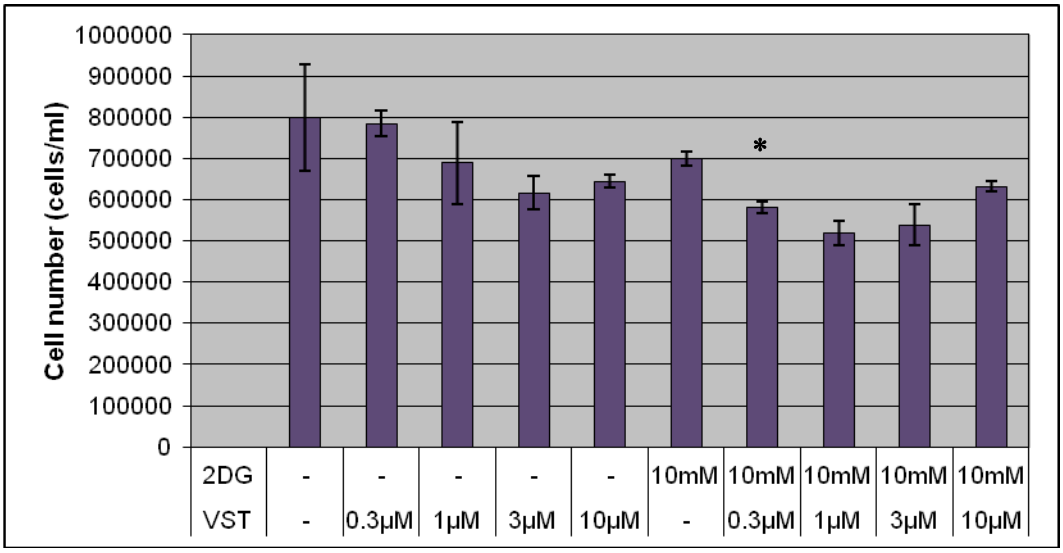

Figure 7.7. Effect of treatment with VST alone, or in combination with 2-DG, for 24 hours on cell number in THP1 cells. Error bars show standard deviation. * denotes statistically significant difference ($p < 0.05$) between treatment with VST alone and VST in combination with 2DG at that concentration.

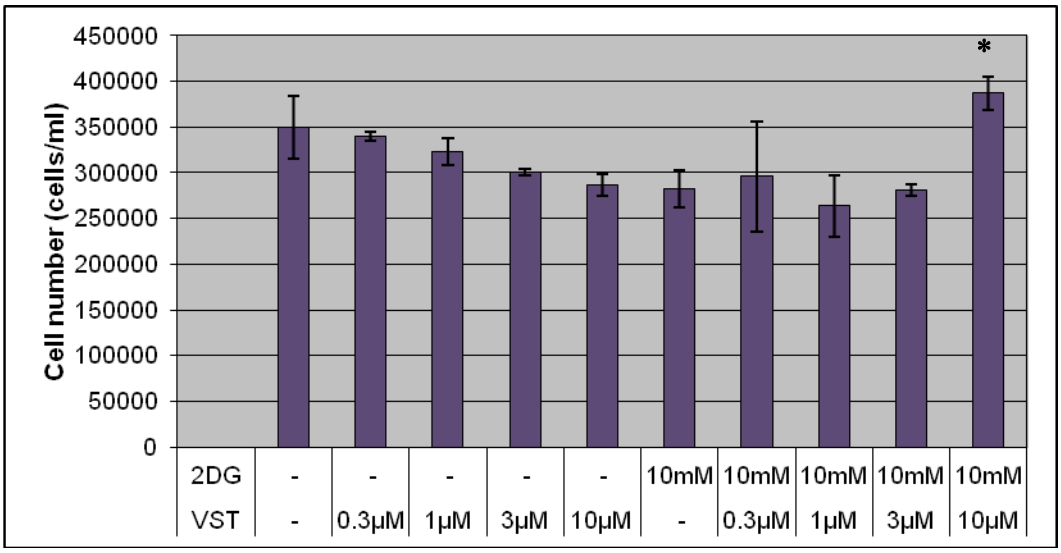

Figure 7.8. Effect of treatment with VST alone, or in combination with 2-DG, for 24 hours on cell number in U266 cells. Error bars show standard deviation. * denotes statistically significant difference ($p < 0.05$) between treatment with VST alone and VST in combination with 2DG at that concentration.

Following 24 hours of treatment, 2-DG had a minimal effect on cell viability in either the THP1 or U266 cell lines at the concentration studied (see figure 7.9 and 7.10 respectively), with the U266 cell line being slightly more sensitive. In the THP1 cell line, treatment with versipelostatin alone proved minimally toxic at all concentrations tested, as shown in figure 7.9. However, when cells were treated with versipelostatin together with 2-DG, there was a greater than additive decrease in cell viability compared to versipelostatin alone at all concentrations studied. This increased cytotoxicity of versipelostatin combined with 2-DG proved statistically significant at the highest versipelostatin concentration used (10μM). In the U266 cell line, versipelostatin treatment alone also had little effect on cell viability, with the highest concentration resulting in only a 13 percent decrease in viability compared to the untreated control (see figure 7.10). It can also be seen that the combination of versipelostatin and 2-DG for 24 hours whilst having an additive effect at the lowest versipelostatin concentration, caused a greater than additive decrease in viability compared with versipelostatin alone at the three higher versipelostatin concentrations studied. As with the THP1 cell line, this increased cytotoxic effect on U266 cell viability was statistically significant at the highest concentration studied.

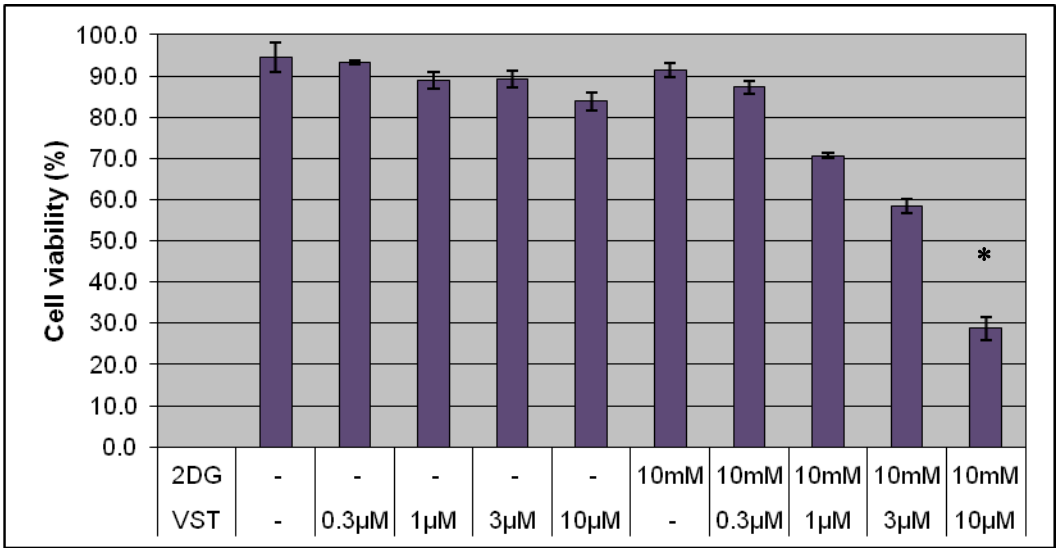

Figure 7.9. Effect of treatment with VST alone, or in combination with 2-DG, for 24 hours on cell viability in THP1 cells. Error bars show standard deviation. * denotes statistically significant difference ($p < 0.05$) between treatment with VST alone and VST in combination with 2DG at that concentration.

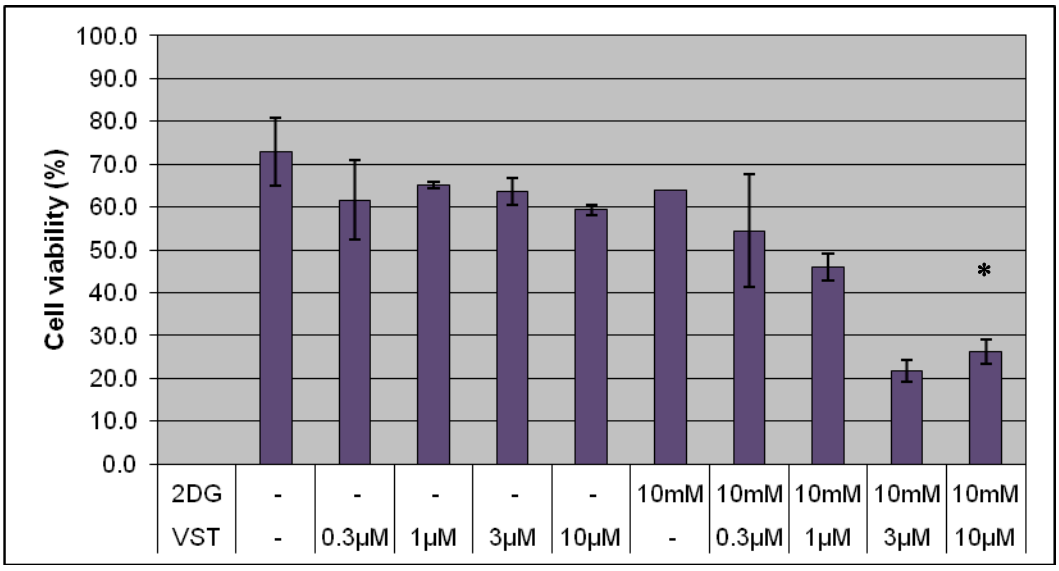

Figure 7.10. Effect of treatment with VST alone, or in combination with 2-DG, for 24 hours on cell viability in U266 cells. Error bars show standard deviation. * denotes statistically significant difference ($p < 0.05$) between treatment with VST alone and VST in combination with 2DG at that concentration.

By this point, experiments had established the cytotoxic effect of versipelostatin as a single agent and confirmed an increased cytotoxic effect when versipelostatin treatment occurred under 2-DG mediated glucose deprivation conditions. The next set of experiments were undertaken to investigate the ability of versipelostatin to downregulate GRP78 and GRP94 expression, both under normal cell culture conditions and glucose deprivation conditions. It was decided to use a 10mM concentration of 2-DG, as this concentration has been used for glycolysis inhibition by other researchers, and yet is not unduly toxic in the haematological cancer cell lines being studied. However, studies in solid tumours have used the higher concentration of 20mM 2-DG(Park *et al.*, 2004). A range of versipelostatin concentrations was then studied, as shown in figure 7.11, in order to identify any changes in protein levels of the molecular chaperones GRP78 and GRP94 after 24 hours treatment. In both the AML cell line THP1 and the myeloma cell line U266, versipelostatin treatment alone had no effect on the protein levels of GRP78 and GRP94 compared to the untreated control. There was a slight increase in both GRP78 and GRP94 protein levels with 2-DG treatment, although the effect was subtle, and the addition of versipelostatin to 2-DG treatment did not result in any change to the levels of these proteins. No downregulation of GRP78 or GRP94 protein levels with versipelostatin under 2-DG mediated glucose deprivation conditions was seen in either haematological cell line studied.

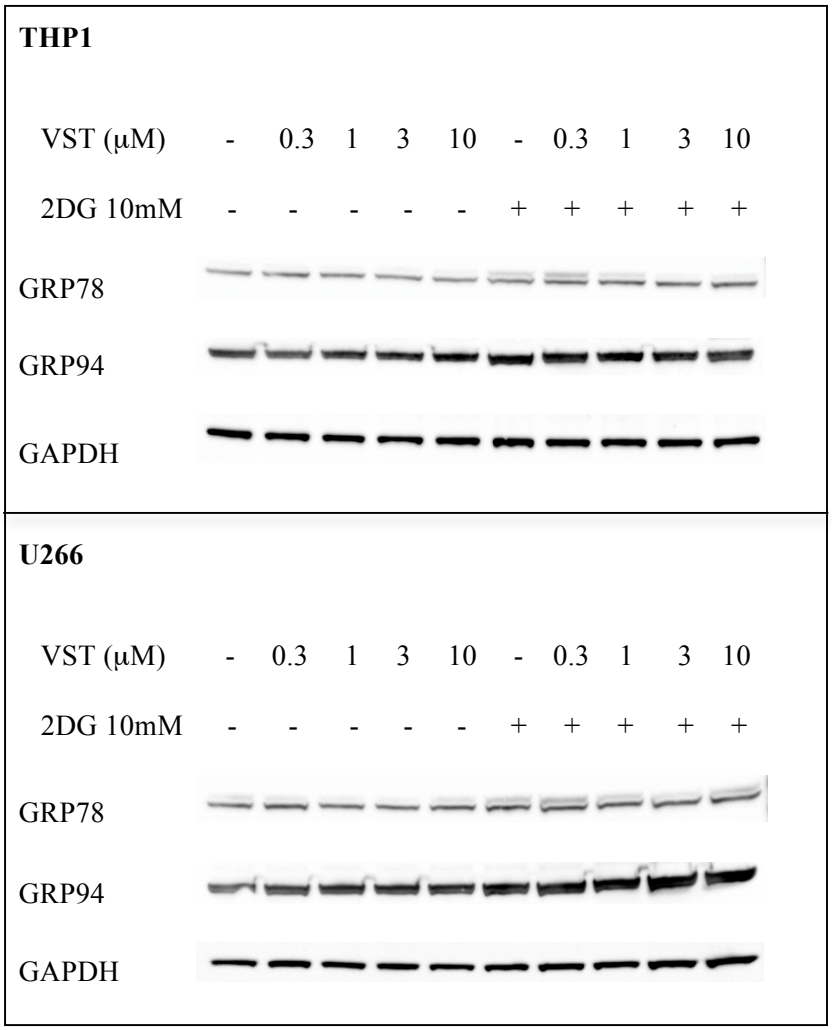

Figure 7.11. Effect of VST treatment, alone or in combination with 2-DG, for 24 hours on GRP78 and GRP94 protein expression in THP1 cells (top panel) and U266 cells (bottom panel). GAPDH included as a loading control.

Due to the inability of versipelostatin to downregulate GRP78 and GRP94 protein expression under glucose deprivation conditions in the haematological cell lines tested, the same experimental conditions were investigated in the colorectal cancer cell line HT-29, in which such downregulation has previously been reported in published studies. Versipelostatin treatment alone for 24 hours appeared to have little, if any, effect on the levels of the chaperone proteins studied. However, when combined with 2-DG treatment, a downregulation of GRP78 protein levels was seen with versipelostatin at the 1, 3 and 10μM concentrations. Effects on GRP94 protein were more subtle, although there did appear to be a decrease in protein with the 1μM versipelostatin concentration.

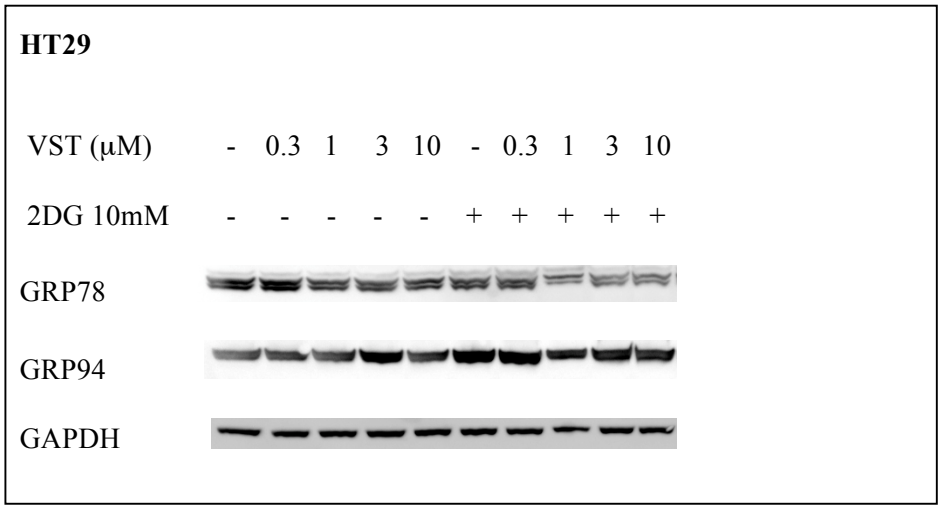

Figure 7.12. Effect of VST treatment alone, or VST in combination with 2-DG, for 24 hours on GRP78 and GRP94 protein expression in HT29 cells. GAPDH is included as a loading control.

7.4 Discussion

The two molecular chaperones with the most direct effect on UPR activation and UPR signalling are GRP78 and GRP94. Versipelostatin is a novel small molecule compound proposed to act via downregulation of GRP78 and GRP94 levels in glucose deprived cells (this glucose deprivation leads to ER stress and activation of the UPR). Studies of versipelostatin so far have been exclusively in solid tumours, and the activity of

this novel compound in haematological malignancies has not previously been reported. This is in line with other research concerning glycolysis and the Warburg effect in cancer, which has historically focused almost exclusively on solid tumours (Gatenby and Gillies, 2004). Whilst encouraging early studies of versipelostatin action have been reported, the detailed molecular mechanism underlying the effect of versipelostatin remains to be fully elucidated. The research group responsible for the initial discovery of versipelostatin have now synthesised a number of labelled derivatives of versipelostatin, with a view to developing a chemical biological method in order to identify the precise molecular target of this compound (Shin-Ya, 2005).

Versipelostatin has been reported to downregulate GRP78 and GRP94 only in response to glucose deprivation mediated ER stress, and not to UPR activation mediated through other known pharmacological inducers, such as tunicamycin. Therefore, it follows that this compound may have anticancer activity in tumours where hypoglycaemia is known to occur as a consequence of tumour growth (as is the case in a number of solid tumours). In theory, treatment with versipelostatin may offer a tumour selective anticancer effect, resulting in decreased toxicity to normal (unstressed, non-glucose deprived) cells. The glycolysis inhibitor 2-DG has long been used to induce glucose deprivation conditions *in vitro*, as has been done in the experiments in this chapter. 2-DG has also been investigated as an anticancer agent in its own right. After promising pre-clinical findings, 2-DG progressed to a phase I clinical trial in solid tumours (Raez *et al.*, 2006), however it has since been reported that development of 2-DG as a cancer therapeutic agent has been halted by the pharmaceutical company involved. This was apparently a consequence of unacceptable toxicities reported at concentrations that are required for glycolysis inhibition *in vivo* (Gatenby and Gillies, 2004). In the experiments described in this chapter, the effect of versipelostatin in downregulating ER molecular chaperone expression under glucose deprivation conditions was not observed in the haematological cancer cell lines studied. However, this downregulation was confirmed to occur when the same experiments were

carried out using the adherent solid tumour (colorectal cancer) cell line HT-29. This observation supports the hypothesis that glucose deprivation, though a phenomenon associated with the growth of solid tumours, may be of less significance in haematological malignancies.

It is also of note that the haematological cell lines proved more sensitive to the cytotoxic effects of versipelostatin treatment as a single agent than either the HT-29 cell line used in these experiments, or the solid tumour cell lines reported in other versipelostatin studies. Versipelostatin was cytotoxic in these leukaemia, lymphoma and myeloma cell lines at low micromolar concentrations, indicating a potency *in vitro* comparable to that of clinically used cytotoxic agents such as 4-HC (the active metabolite of cyclophosphamide) or melphalan in these cell lines. Further investigation may reveal that the increased potency of versipelostatin in these haematological cancers *in vitro* is mediated by a previously undescribed mechanism.

In recent years it has been reported that a number of drugs widely used in clinical practice have other, previously unknown, off target effects linked to the unfolded protein response. For example, the antidiabetic drug metformin (belonging to the biguanide class) is one of the most comment agents prescribed for the treatment of type 2 diabetes. It acts by inhibiting glucose production in the liver, delaying intestinal glucose absorption and increasing insulin sensitivity in muscle. It has been reported that metformin (and the other biguanide drugs buformin and phenformin) modulated the UPR under glucose deprivation conditions in a manner similar to that of versipelostatin (Saito *et al.*, 2009). Whilst a great deal more research is needed as regards metformin for cancer treatment, utilising drugs that are already in widespread clinical use for their UPR targeting effects is a particularly attractive treatment strategy. A drug such as metformin that is taken orally, has been used for many years, is considered safe and has a well known adverse effect profile would be an ideal therapeutic candidate, particularly in light of the toxicity associated with administration

of 2-DG at clinically relevant concentrations for glycolysis inhibition(Gatenby and Gillies, 2004). However, it may well prove to be the case that the activity of agents such as metformin that have been described to modulate the UPR in the same manner as versipelostatin are only clinically relevant in glucose deprived solid tumours, as the experiments described in this chapter with versipelostatin suggest.

One of the limitations of the agents mentioned above in targeting molecular chaperones is the possible lack of total selectivity for a given chaperone. However, these therapeutic targets and anticancer agents have only recently been identified and it is hoped that with continued research, agents with higher target selectivity (and therefore more potential to pass successfully through the drug development process and into the clinic) will be identified.

8. siRNA Mediated Gene Silencing of ER Resident Molecular Chaperones and the Effect on Chemosensitivity *in vitro*

8.1 Introduction

Molecular chaperones facilitate the correct folding of proteins, with the ER containing a number of resident molecular chaperones, such as the heat shock protein (HSP) 70 and HSP90 families, the lectins calnexin and calreticulin, and the HSP40 family of co-chaperones (Ellgaard and Helenius, 2003, Alberts, 2002, Ma and Hendershot, 2004a). The two molecular chaperones with the most direct effect on UPR activation and UPR signalling are the glucose related proteins (GRPs) GRP78 and GRP94. Molecular chaperones have been discussed extensively in chapters 1 and 7.

GRP94 is the most abundant glycoprotein found in the ER and regulation of GRP94 at the transcriptional level is linked to that of GRP78, as evidenced by conservation of elements of the regulatory promoter (Fu and Lee, 2006, Yang and Li, 2005). GRP94 is the ER resident isoform of the cytosolic chaperone protein HSP90 and is a member of the HSP90 family of heat shock proteins. Anticancer agents inhibiting HSP90 have now progressed to clinical trials (Smith and Workman, 2007). In contrast to HSP90 (which has a very large number of client proteins, many of which are oncogenic), GRP94 appears to have a very limited number of client proteins. The main roles of GRP94 described to date include involvement in B-cell differentiation and the immune response (Ni and Lee, 2007, Liu and Li, 2008). Oncogenic client proteins of GRP94 identified to date are limited to ErbB1 and ErbB2 (also designated EGFR and HER2 respectively). More recently it has been reported that insulin-like growth factor (IGF) 1 and 2 are also clients of GRP94. This has implications for cancer research as IGF-1 signalling activates AKT, whose activation is a feature of numerous cancers.

GRP78 is a member of the HSP70 family (Lee, 2007). GRP78 recognises hydrophobic residues on unfolded or misfolded proteins and binds to them, thereby preventing their interaction with other molecules (Bole *et al.*, 1986). GRP78 is a vital mediator of the response to ER stress; it is the main ER stress sensor and dissociation of GRP78 from the three transmembrane UPR receptors is necessary for activation of the UPR. GRP78 has also been implicated in resistance to anticancer agents, which is discussed in more detail in chapter 1.5.

The role of these key ER molecular chaperones in the UPR and chemosensitivity has been described in chapters 1 and 7. In light of the importance of these ER resident molecular chaperones in cancer, modulating the UPR by targeting these chaperones has been proposed as a novel anticancer strategy. Attempts to therapeutically target GRP78 and GRP94 in this project using small molecule approaches have not succeeded thus far. In light of the positive results published by groups that have targeted GRP78 using gene silencing *in vitro* in solid tumours, it was decided to adopt this approach in the haematological cell lines being studied. This would establish whether the lack of any chemosensitising effect was due to lack of target efficacy of the small molecules tested in these experiments, or the absence of such a chemosensitising effect occurring in these haematological cancer cell lines following downregulation of these ER chaperone proteins. Gene silencing, using small interfering RNA (siRNA) targeting GRP78 and GRP94 was therefore carried out and the resultant effect on chemosensitivity was determined using cytotoxicity assays and clonogenic assay.

8.2 Materials and Methods

8.2.1 siRNA Transfection

Experimental techniques used for transfection of small interfering RNA (siRNA) were as described in chapter 2.11. HP Validated siRNA and HiPerFect Transfection

Reagent were obtained from Qiagen, UK. The following siRNA duplexes were used: All Stars Negative Control siRNA Alexa Fluor 488 labelled (catalog no. 1027292), GRP78 siRNA (catalog no. SI02780554), GRP94 siRNA (catalog no. SI02663738), GFP siRNA (catalog no. 1022064) and the positive control MAPK1 siRNA (catalog no. 1022564). Sequences for the siRNA duplexes used are given in chapter 2.11. Positive control siRNA, negative control siRNA, mock transfected (transfection reagent without siRNA) and untransfected controls were included in all experiments.

Transfection was carried out as per the manufacturer's protocol for suspension cell lines. The day before transfection cells in exponential growth phase were seeded in flasks at a density of 3 x 10^5 cells/ml in RPMI-1640 containing 10% foetal bovine serum and 1% penicillin streptomycin. Cells were incubated under normal growth conditions for 24 hours before plating out at 2 x 10^5 cells per well of a 24-well plate in 100µl culture medium containing serum and antibiotics. 100µl of siRNA at a concentration of 200nM (diluted in serum free medium) was added to 3µl of HiPerFect transfection reagent (giving a siRNA to transfection reagent ratio of 500:1), mixed by vortexing and incubated at room temperature for 5 to 10 minutes to allow formation of transfection complexes. The transfection complexes were then added drop-wise onto the cells and mixed by swirling the plate. Cells were incubated under normal growth conditions for a further 6 hours before the addition of 400µl culture medium containing serum and antibiotics. Cells were then returned to the incubator until analysis of transfection efficiency (and toxicity) at 24 hours post transfection. Further culture medium was added as required.

8.2.2 Transfection Efficiency

The uptake of siRNA into cells was monitored by observation of Alexa Fluor 488 fluorescence after transfection with Alexa Fluor 488 labelled negative control siRNA (Qiagen, UK). The percentage of cells transfected with siRNA from the total cell population

(transfection efficiency) was determined at 24 hours post transfection for each siRNA transfection experiment. Transfection was carried out as previously described, after which aliquots of cell samples were removed and analysed by flow cytometry (see chapter 2.12). Cells were washed twice with PBS, then resuspended in 500µl PBS and run immediately using a BD FacsCalibur flow cytometer with BD CellQuest software used for acquisition (BD Biosciences, UK). Percent positive cells for fluorescence compared with mock transfected controls gave percentage uptake of siRNA, ie. transfection efficiency. In conjunction with the transfection efficiency experiments, an aliquot of cells was also removed at this time for analysis of the cytotoxicity of the transfection process. Cell number and viability was assessed using the Guava Viacount assay (methodology described in chapter 2.4).

A series of initial experiments were conducted to determine the optimum experimental conditions for transfection in the haematological cancer cell lines being studied, (i.e. effective delivery of siRNA into cells, with limited associated toxicity). Transfection reagents were tested using a range of siRNA concentrations, along with a range of dilution ratios of siRNA to transfection reagent. Transfection efficiency was determined at 24 hours post transfection and, in conjunction with cytotoxicity data, used to determine the final siRNA concentration and ratio of siRNA to transfection reagent to be used in subsequent experiments. All six cell lines in the haematological cell line panel (2 AML, 2 MM, and 2 DLBCL) were used in initial experiments, before the THP1 (AML) and U266 (MM) cell lines were chosen for further experiments.

8.2.3 Knockdown Efficiency

Knockdown efficiency following siRNA transfection was determined at 48 and 72 hours post transfection using reverse transcription real time polymerase chain reaction (RT-PCR) as described in chapter 2.13. All reagents for reverse transcription and real time RT-

PCR were obtained from Applied Biosystems, UK. TaqMan Fast Cells-to-CT Kit was used to prepare samples for use in real time (RT-PCR) according to manufacturer's protocol. Pilot experiments were carried out using the TaqMan Fast Cells-to-CT Kit in conjunction with the TaqMan Cells-to-CT Control Kit in order to optimise the procedure and determine the cell number to be used for each cell line. The prepared cell lysates were then reverse transcribed to cDNA using RT Enzyme Mix and buffer and run in a thermal cycler (37°C for 60 minutes, then 95°C for 5 minutes to inactivate the RT). Minus RT controls were included to demonstrate that the template for PCR was cDNA, not genomic DNA. Completed RT reactions were either used immediately or stored at -20°C until use.

The cDNA was amplified by fast-cycling real time PCR using Taqman Fast Universal PCR Master Mix and Taqman Gene Expression Assay. PCR Cocktail was added to cDNA samples and run in an Applied Biosystems 7900HD real time PCR instrument using fast settings (enzyme activation at 95°C for 20 seconds, PCR at 95°C for 1 second then 60°C for 20 seconds x 40 cycles). Gene expression assays were used for the target genes GRP78 (Assay ID: Hs00607129_gH) and GRP94 (Assay ID: Hs00427665_g1). Assays were also used for the endogenous control gene actin (Assay ID: Hs03023880_g1) and the positive control gene MAPK1 (Assay ID: Hs00177066_m1). Non-template control samples were included for each assay to ensure that any fluorescent signal generated in the assay was not due to DNA contamination.

Quantitative real-time PCR uses cycle threshold (C_T) values to quantify the amount of starting template. Knockdown of target mRNA following siRNA transfection was calculated using the delta delta C_T ($\Delta\Delta C_T$) method for relative quantitation as per the manufacturer's protocol. ΔC_T is the normalised expression value for the gene of interest, calculated as the difference in the C_T value of the targeted mRNA vs. the C_T of the endogenous control mRNA (any gene whose mRNA values do not change under the

experimental conditions). This ΔC_T value for the gene of interest is then compared to the ΔC_T value for the negative control siRNA transfected sample. Calculation of percentage knockdown was carried out as follows:

- Mean C_T and standard deviation of experimental replicates calculated
- ΔC_T (sample C_T – endogenous control C_T) for target siRNA transfected and control siRNA transfected samples calculated
- $\Delta\Delta C_T$ calculated ($\Delta\Delta C_T$ = ΔC_T target siRNA transfected sample – ΔC_T negative control siRNA transfected sample)
- Percentage knockdown (%KD) calculated using the formula

  $\%KD = (1–2^{-\Delta\Delta C}{}_T \times 100)$

8.2.4 Cytotoxicity Studies

For chemosensitivity experiments, cells were transfected with target siRNA (grp78 or grp94 siRNA) or control (non-targeting) siRNA (GFP siRNA). Addition of drugs to cells was made at 48 hours post transfection and cells were incubated under normal growth conditions for a further 48 hours. Cytotoxicity experiments were carried out at this time using the Guava Viacount assay, as described in section 2.4. In the cytotoxicity experiments, each drug treatment was studied in triplicate and experiments were carried out on three separate occasions (following three independent siRNA transfection experiments).

Colony formation assay was carried out as described in chapter 2.14. Cells were transfected with either target siRNA (grp78 or grp94 siRNA) or control siRNA (GFP siRNA) as described above. At 48 hours post transfection, drugs were added to the cells (at the higher concentrations used in the cytotoxicity assays) and incubated for a further 48 hours before medium containing drug was removed and cells resuspended in fresh medium. Cells were counted and viability determined before 500 cells per well were plated into 12-well plates in MethoCult methylcellulose-based media (StemCell Technologies, UK)

according to the manufacturer's instructions. All plates contained wells with water only, in order to maintain humidity and prevent the methylcellulose from drying out. The cells were then incubated under normal growth conditions and allowed to form colonies for 10 days. Each drug treated sample was grown in duplicate and each experiment was performed on two separate occasions (following two independent siRNA transfection experiments). Colonies were visualised for counting using an inverted microscope fitted with a camera. For each well, photographs were taken with the well viewed under 10x magnification from three different (randomly chosen) areas of the well. Representative photographs of each sample were shown for illustration purposes.

8.2.5 Statistical Analysis

Statistical analysis was performed using Microsoft Excel software, Microsoft Corporation, USA. The data obtained from cytotoxicity experiments and apoptosis assay was used to determine mean and standard deviation values for each drug concentration. These values were then used for graphical representation and subsequent statistical analysis. Data was assumed to be normally distributed and parametric tests were therefore used throughout. Group means were analysed using a paired t-test, with a p value of less than 0.05 considered to be statistically significant.

8.3 Results

The AML cell line THP1 and multiple myeloma cell line U266 were chosen from initial transfection experiments to be used for further study. For each transfection experiment, evaluation of transfection efficiency (percentage of transfected cells from the total cell population) and cytotoxicity and antiproliferative effects of the transfection process was determined at 24 hours post transfection. Untransfected cells, mock transfected (transfection reagent only), along with samples containing siRNA without transfection

reagent were subject to the same experimental conditions as the siRNA transfected sample and used as an experimental controls. The effect of the transfection process on cell number and viability is given in figure 8.1 below. It can be seen that the siRNA transfection process was not toxic to either the THP1 or U266 cell lines. A small antiproliferative effect was seen in the transfected samples in both cell lines.

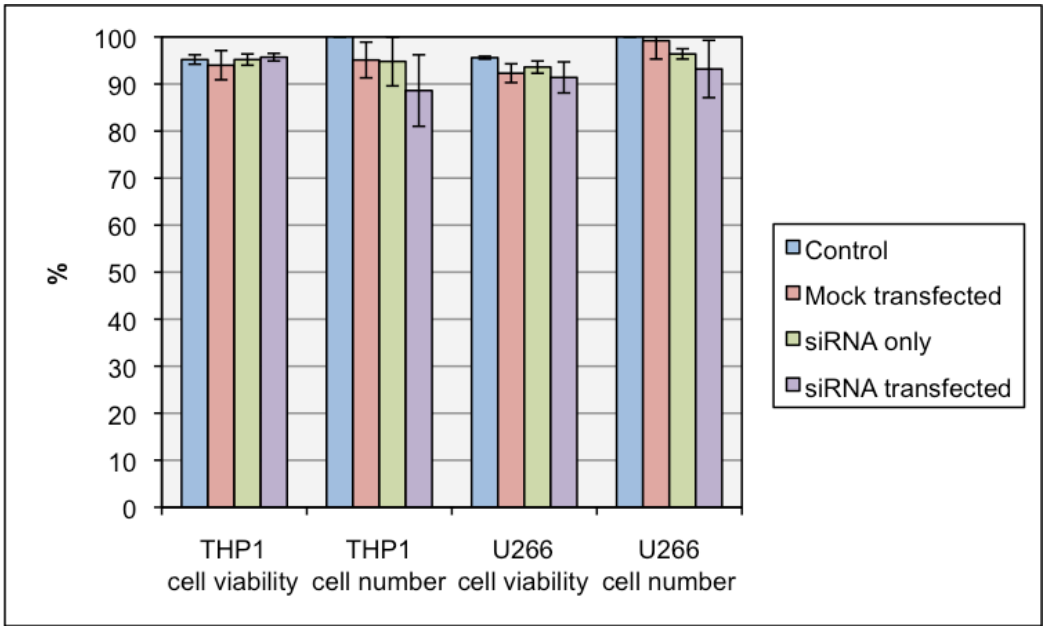

Figure 8.1. Cell viability and cell number of transfected cells at 24 hours post transfection in the THP1 and U266 cell lines. Values shown are mean ± SD of three separate experiments

Transfection efficiency was determined by uptake of fluorescently labelled siRNA using flow cytometry, the results are shown in figures 8.2 (THP1) and 8.3 (U266). Evaluation of transfection efficiency was carried out for each of the three transfection experiments in both cell lines studied. Transfection efficiency was highest in the THP1 cell line, followed by the U266 cell line. Representative histogram plots from the flow cytometry experiments are shown in figures 8.2 (THP1) and 8.3 (U266). In both cell lines, an increase in fluorescence, along with the characteristic change in peak shape can be observed in the siRNA transfected samples compared to controls.

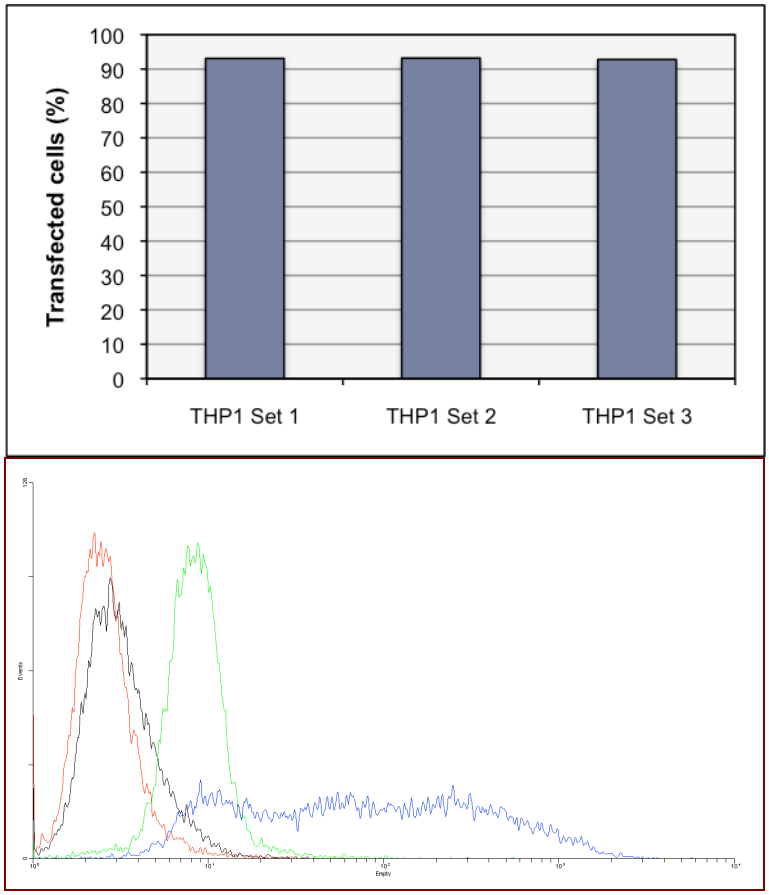

Figure 8.2. Transfection efficiency (percentage of transfected cells from the total cell population) for the THP1 cell line as determined by flow cytometry.
Top panel: Results from three separate transfection experiments
Bottom panel: Flow cytometry histogram plot of one transfection efficiency experiment.
KEY: Red = Untransfected control
Black = Mock transfected
Green = siRNA only
Blue = siRNA transfected

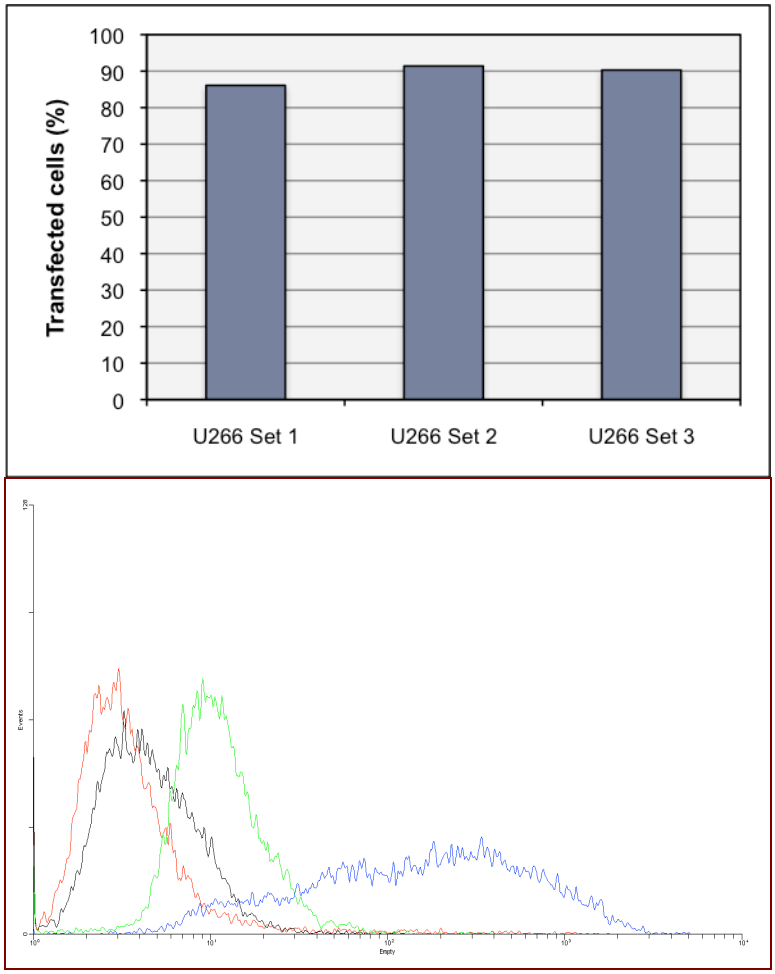

Figure 8.3. Transfection efficiency (percentage of transfected cells from the total cell population) for the U266 cell line as determined by flow cytometry.
Top panel: Results from three separate transfection experiments
Bottom panel: Flow cytometry histogram plot of one transfection efficiency experiment.
KEY: Red = Untransfected control
Black = Mock transfected
Green = siRNA only
Blue = siRNA transfected

Once successful uptake of siRNA by transfected cells was established, the next step in the gene silencing experiments was to evaluate the effect of siRNA transfection on the expression of the target (i.e. knockdown efficiency). Knockdown of the target gene was determined at both the transcriptional (mRNA) and translational (protein) levels at both 48 and 72 hours post transfection. Percentage GRP78 mRNA knockdown, as determined by

real time RT-PCR, is shown in table 8.1. Experiments to determine GRP94 mRNA knockdown could not be optimised in the time available. Knockdown of GRP78 and GRP94 at the protein level, determined by western blotting, is shown in figure 8.2 (blots shown are representative of three separate experiments). It can be seen that when siRNA targeting GRP78 was used, there appeared to be some upregulation of GRP94 at the protein level. This increase in GRP94 protein was most visible in the U266 cell line.

Cell line	siRNA	Knockdown (%) at 48 hours	Knockdown (%) at 72 hours
THP1	GRP78	63.1	96.8
U266	GRP78	72.5	71.9

Table 8.1. Knockdown efficiency as determined by real time RT-PCR in cells transfected with siRNA targeting GRP78 at 48 and 72 hours post transfection.

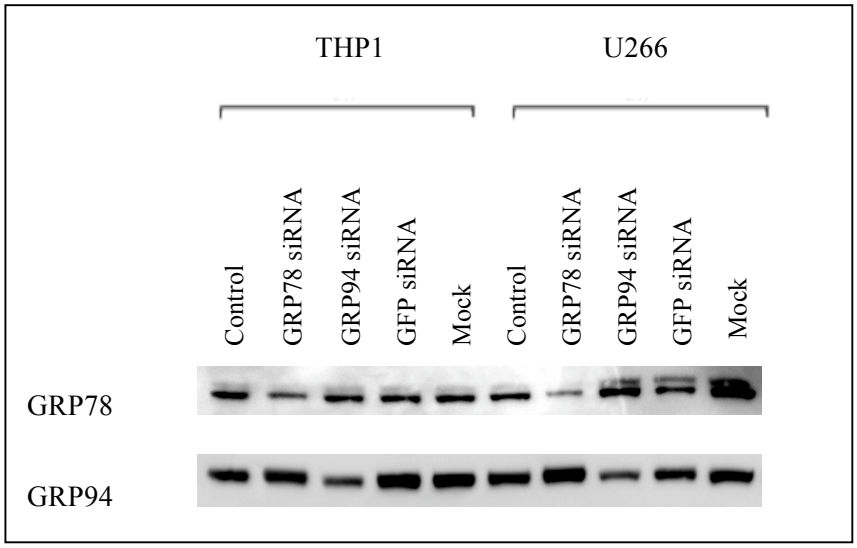

Figure 8.4. Westerns to show GRP78 and GRP94 protein expression in untransfected cells, mock transfected cells, and cells transfected with siRNA targeting GRP78, GRP94 or GFP at 72 hours post transfection.

After knockdown of the target gene had been achieved, the transfected cells were then used for further study. Chemosensitivity was investigated 48 hours after transfection with siRNA targeting GRP78 or GRP94. Cells transfected with siRNA targeting GFP were used as a control in the chemosensitivity experiments. At 48 hours post transfection,

assessment of cell number and viability was carried out prior to experimental set up, in order to confirm no excessive toxicity was observed from the transfection process. This was done for three separate transfection experiments and the mean values with standard deviations are shown in figure 8.5. It can be seen that the results at 48 hours post transfection do not reveal any excessive toxicity when compared to the results obtained 24 hours following transfection, but a small antiproliferative effect was apparent, particularly in U266 cells.

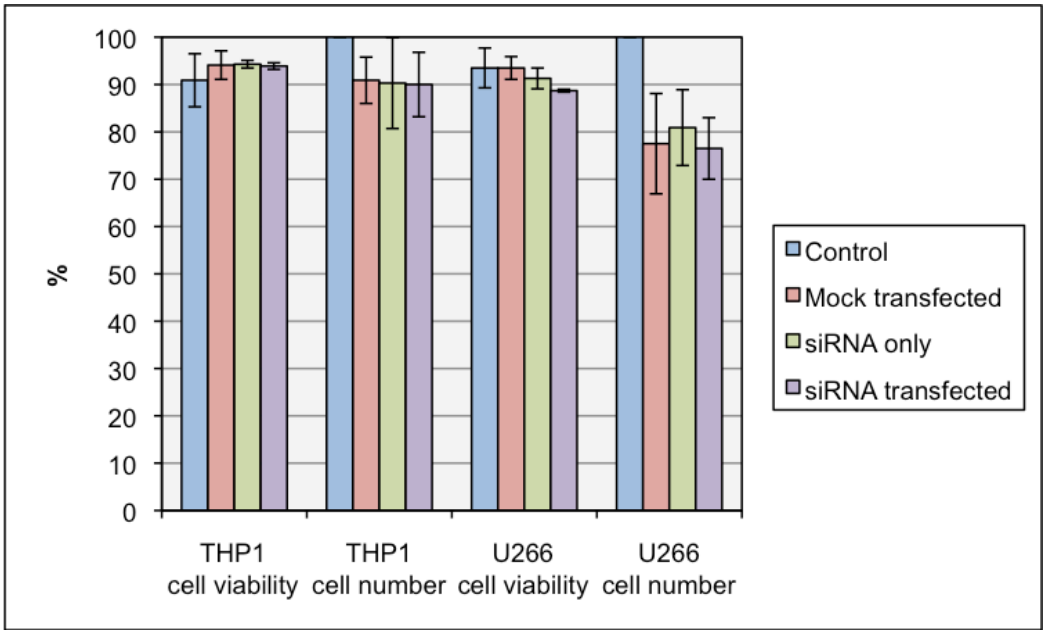

Figure 8.5. Cell viability and cell number of transfected cells at 48 hours post transfection in the THP1 and U266 cell lines. Values shown are mean ± SD of three separate experiments

Transfected cells were then treated with drugs for a further 48 hours, before analysis of the effect of GRP78 or GRP94 knockdown on chemosensitivity. This was done either by analysis of cell proliferation and viability using plate based cytotoxicity assays, or by washing the cells and plating out for colony formation assay to determine their ability to recover and form colonies in longer term culture. The results of the cell viability and proliferation experiments are shown in figures 8.6 to 8.9.

The effect of GRP78 and GRP94 knockdown on chemosensitivity was not marked, but overall there was a trend toward increased chemosensitivity in the THP1 cell line.

Following 48 hours of drug treatment, with all drugs at all concentrations studied, there was a decrease in cell number in the GRP78 and GRP94 knockdown cells compared to the control GFP siRNA transfected cells (see figure 8.6). This decrease in cell number following drug treatment with the GRP94 knockdown was statistically significant at the two higher tunicamycin concentrations (1μM, $p<0.001$ and 10μM, $p<0.05$) and the two lower thapsigargin concentrations (10nM, $p<0.05$ and 100nM, $p<0.05$). Although the effect was modest, GRP94 knockdown appeared to sensitise cells to a greater extent than GRP78 knockdown (exceptions being thapsigargin and SAHA at the highest concentration used).

This pattern was less apparent in the effect of GRP78 and GRP94 knockdown on cell viability in the THP1 cell line (see figure 8.7). With the majority of drugs and concentrations investigated, cell viability following 48 hours of drug treatment was not changed by GRP78 or GRP94 siRNA transfection. However, there was a statistically significant decrease in cell viability compared to control siRNA in the cells with GRP78 knockdown following treatment with tunicamycin 1μM and bortezomib 1nM for 48 hours ($p<0.05$ for both). The decreased viability in the GRP78 knockdown cells following bortezomib treatment, although statistically significant, was small and therefore unlikely to be of any clinical significance. The reduction in cell viability observed after drug treatment in the GRP94 knockdown cells was also statistically significant with the 10μM concentration of tunicamycin ($p<0.01$).

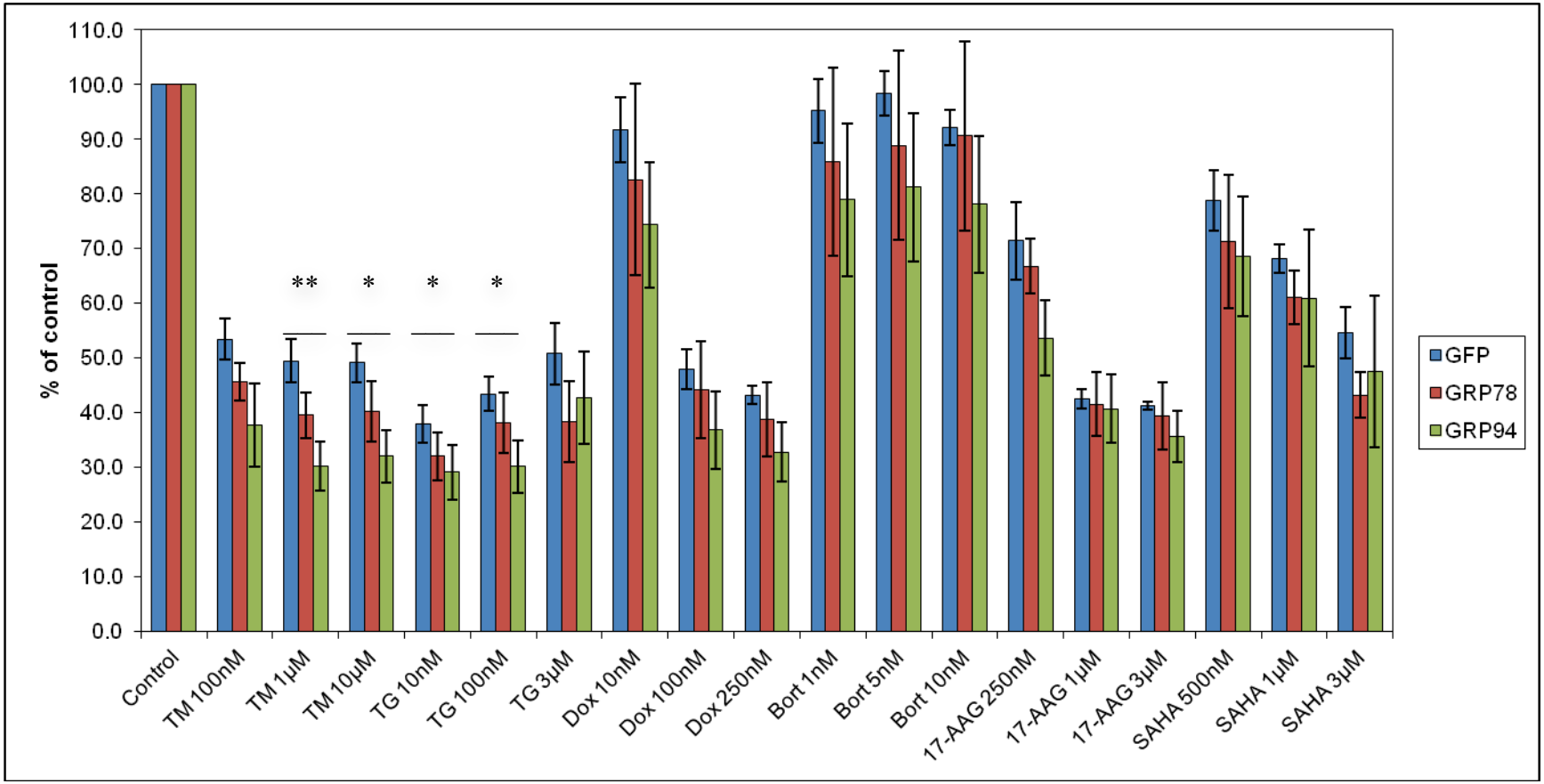

Figure 8.6. Effect of drug treatment for 48 hours on cell number in THP1 cells transfected with siRNA targeting GRP78, GRP94 and the control siRNA targeting GFP. Error bars show mean ± standard error of three separate experiments. * or ** denotes statistically significant difference between GRP94 siRNA and GFP control siRNA ($p<0.05$ and $p<0.01$ respectively).

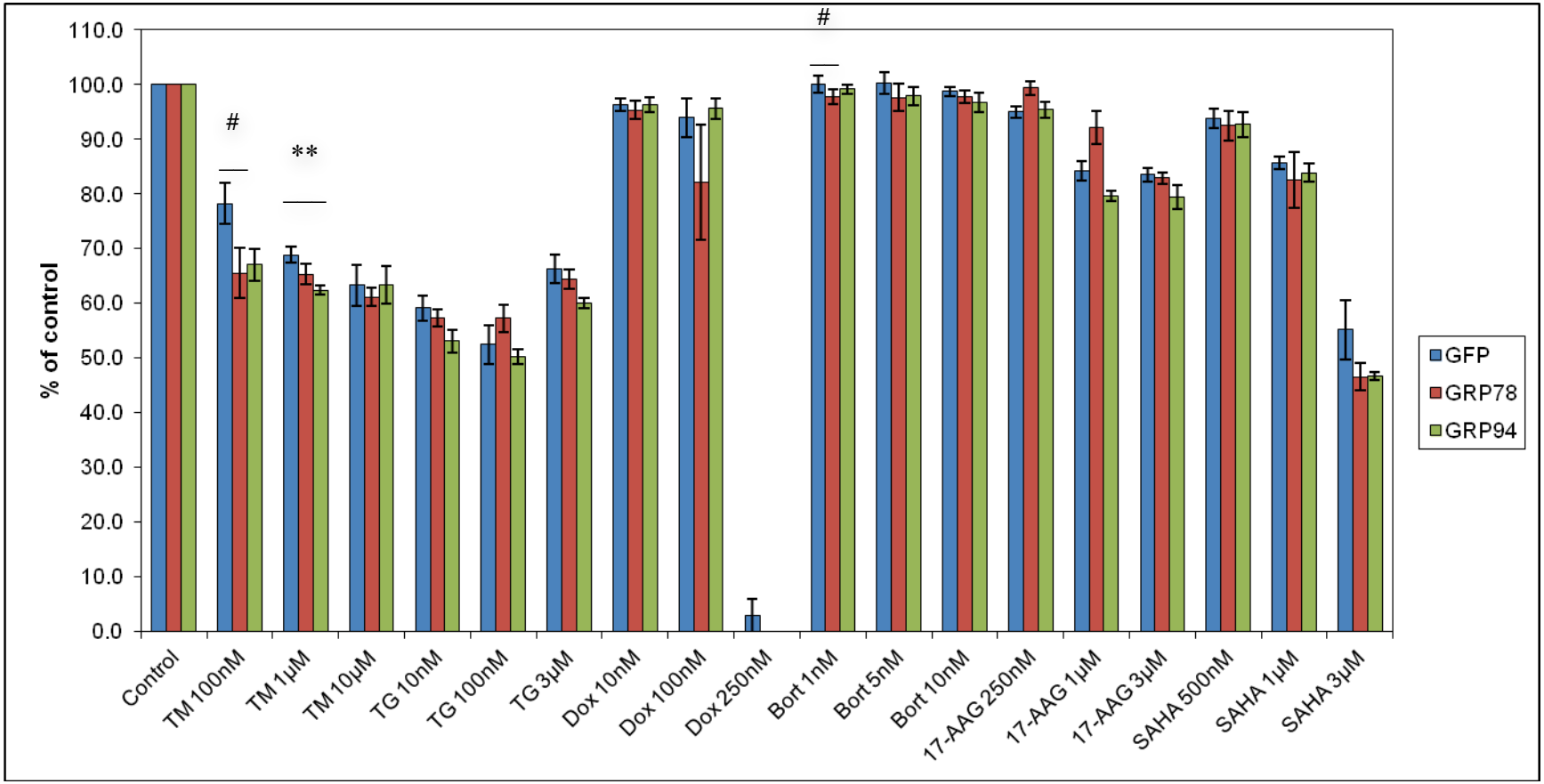

Figure 8.7. Effect of drug treatment for 48 hours on cell viability in THP1 cells transfected with siRNA targeting GRP78, GRP94 and the control siRNA targeting GFP. Error bars show mean ± standard error of three separate experiments. # denotes statistically significant difference between GRP78 siRNA and GFP control siRNA ($p<0.05$). ** denotes statistically significant difference between GRP94 siRNA and GFP control siRNA ($p<0.01$).

Figure 8.8 shows the effect of transfection with siRNA targeting GRP78, GRP94 or the control GFP, on cell number following 48 hours of drug treatment in the U266 cell line. There was little effect of GRP78 and GRP94 knockdown on chemosensitivity in U266 cells. There was a trend towards decreased cell number following 48 hours of drug treatment in the GRP94 knockdown cells compared to cells transfected with the control siRNA targeting GFP, however this was only statistically significant at the 3μM thapsigargin concentration ($p<0.01$). No statistically significant changes in cell number after drug treatment was observed in the GRP78 transfected cells compared to GFP transfected control.

The effect of transfection with siRNA targeting GRP78, GRP94 or the control GFP on cell viability following 48 hours drug treatment in the U266 cell line can be seen in figure 8.9. The only statistically significant changes in the target knockdown cells compared to the control were observed in the samples treated with 17-AAG. A statistically significant decrease in cell viability was seen following 17-AAG treatment in the GRP78 knockdown cells at the 3μM concentration and in the GRP94 knockdown cells at the 1μM concentration compared to cells transfected with non-targeting siRNA ($p<0.05$ for both).

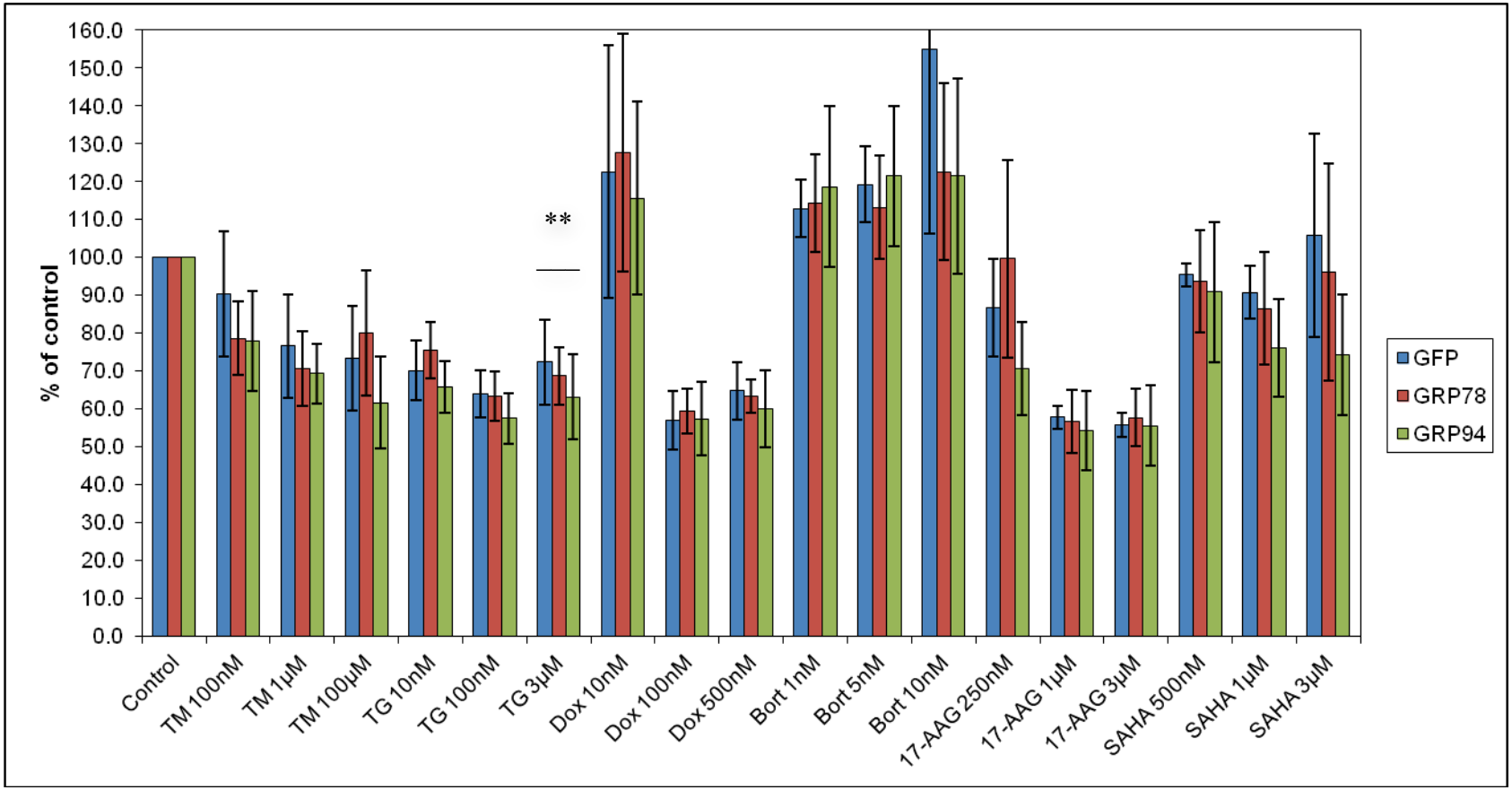

Figure 8.8. Effect of drug treatment for 48 hours on cell number in U266 cells transfected with siRNA targeting GRP78, GRP94 and the control siRNA targeting GFP. Error bars show mean ± standard error of three separate experiments. ** denotes statistically significant difference between GRP94 siRNA and GFP control siRNA ($p<0.01$)

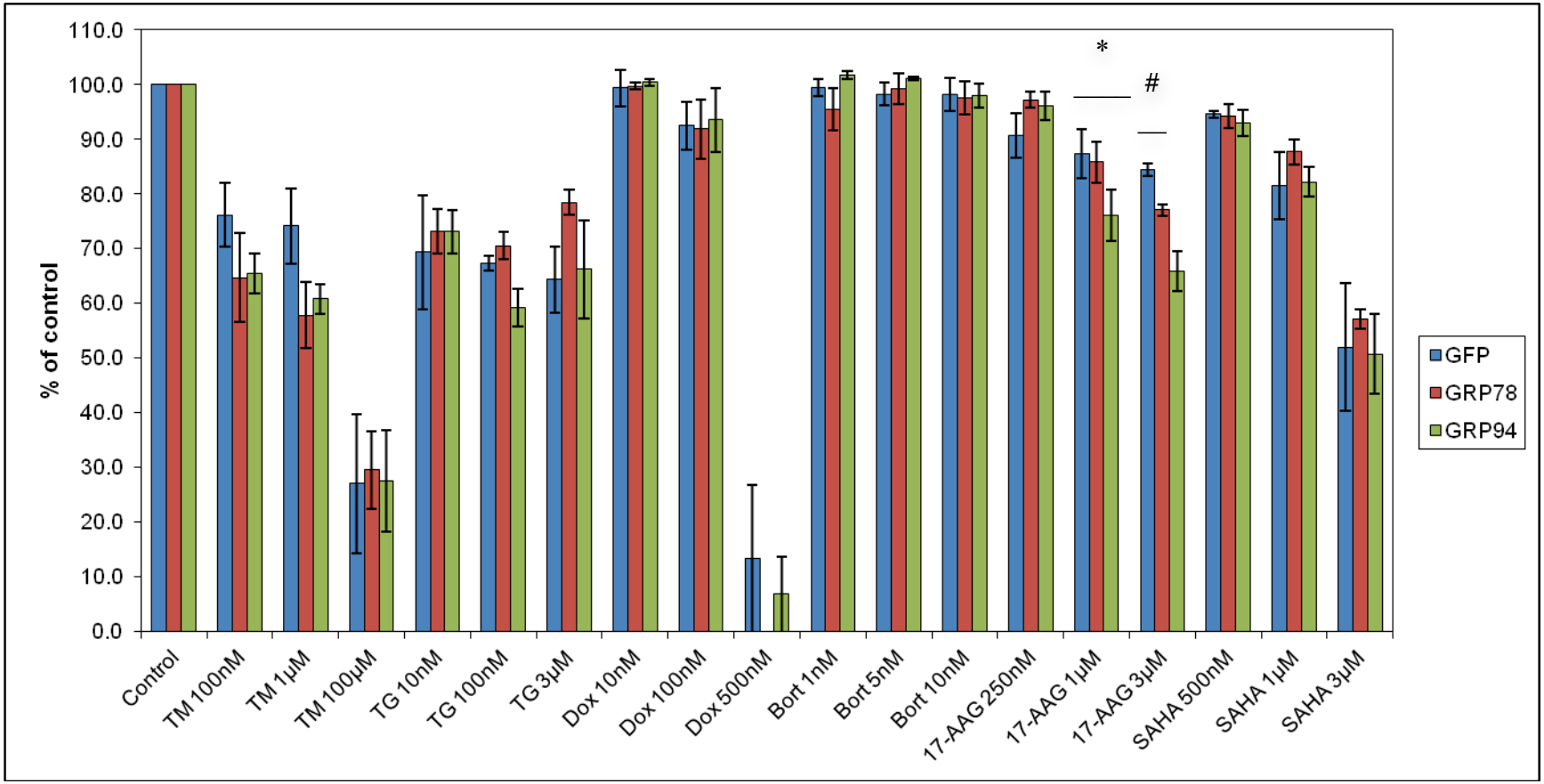

Figure 8.9. Effect of drug treatment for 48 hours on cell viability in U266 cells transfected with siRNA targeting GRP78, GRP94 and the control siRNA targeting GFP. Error bars show mean ± standard error of three separate experiments. # denotes statistically significant difference between GRP78 siRNA and GFP control siRNA ($p<0.05$). * denotes statistically significant difference between GRP94 siRNA and GFP control siRNA ($p<0.05$).

In addition to the cytotoxicity experiments with 48 hours of drug treatment in the cells transfected with target or control siRNA, colony formation assay was also conducted to determine the ability of these drug treated transfected cells to recover and grow as colonies in longer term culture conditions. In both the THP1 cell line and U266 cell line, colony growth in the non-drug treated GRP78 and GRP94 knockdown cells was comparable to that of the untreated GFP siRNA transfected cells as well as non-drug treated untransfected cells (see figures 8.8 and 8.9 respectively). Photographs of colonies formed in the THP1 and U266 transfected cells following drug treatment are shown in figures 8.10 and 8.11 respectively.

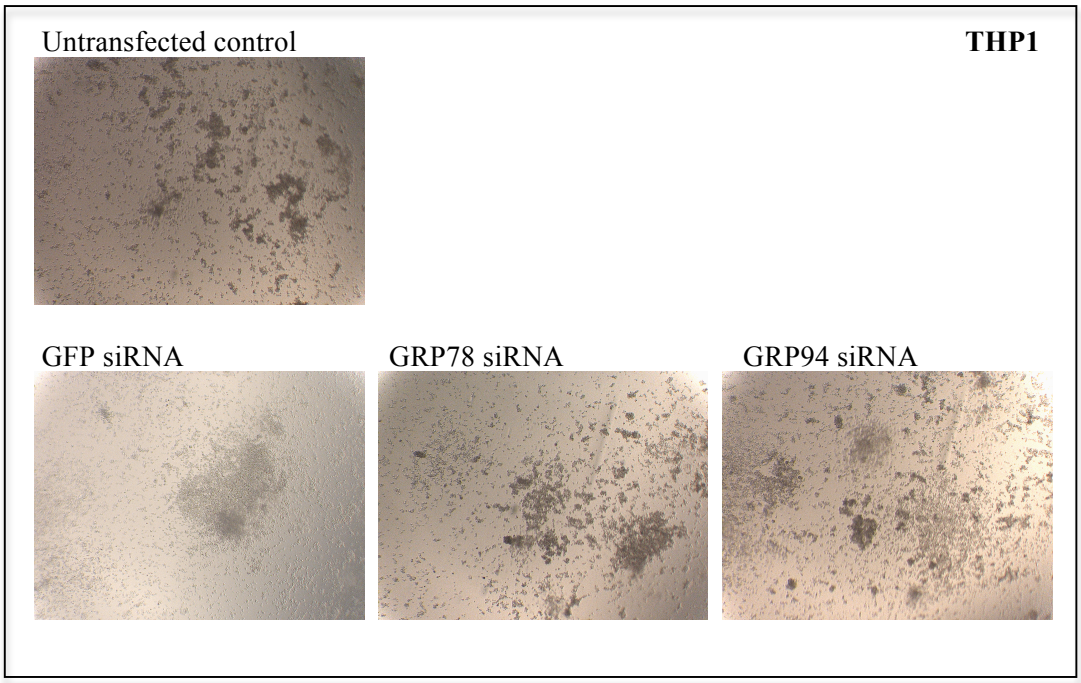

Figure 8.8. Colony formation assay in untransfected and siRNA transfected THP1 cells. Representative photographs are shown for each sample.

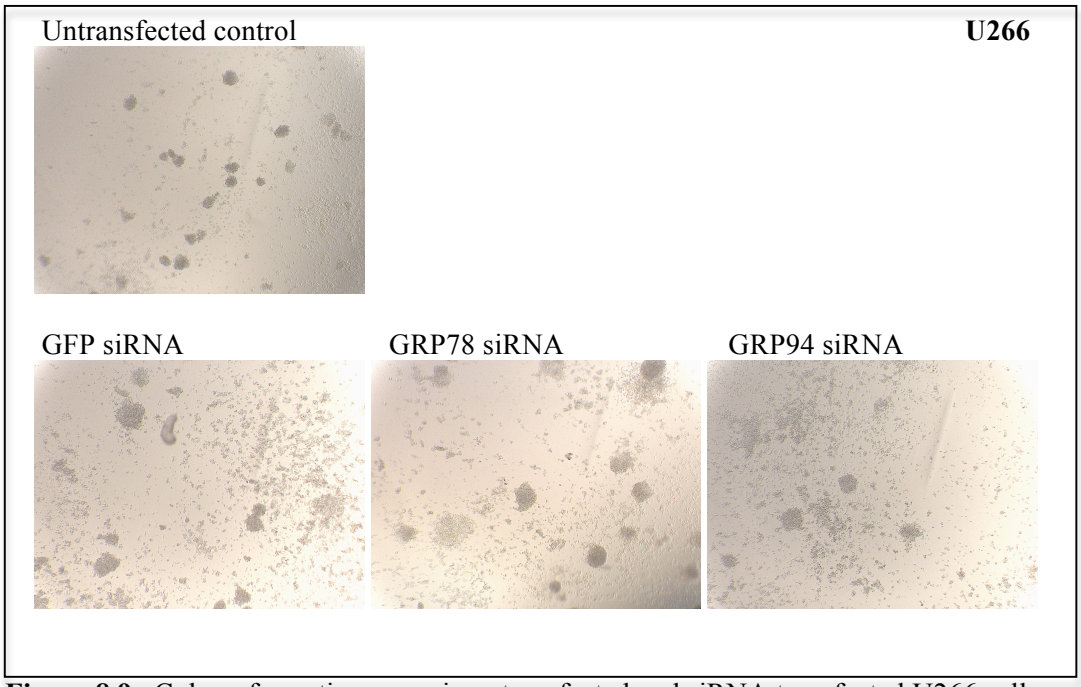

Figure 8.9. Colony formation assay in untransfected and siRNA transfected U266 cells. Representative photographs are shown for each sample.

In the THP1 cell line (see figure 8.10), transfection with siRNA targeting GRP78 or GRP94 rendered cells unable to recover and form colonies to the same extent as the cells transfected with control GFP siRNA following treatment with tunicamycin, doxorubicin, bortezomib and SAHA. Neither GRP78 nor GRP94 knockdown affected the colony growth observed following treatment with 17-AAG in this cell line. No colony growth was seen following thapsigargin treatment in either the cells transfected with target siRNA or control siRNA in the THP1 cell line.

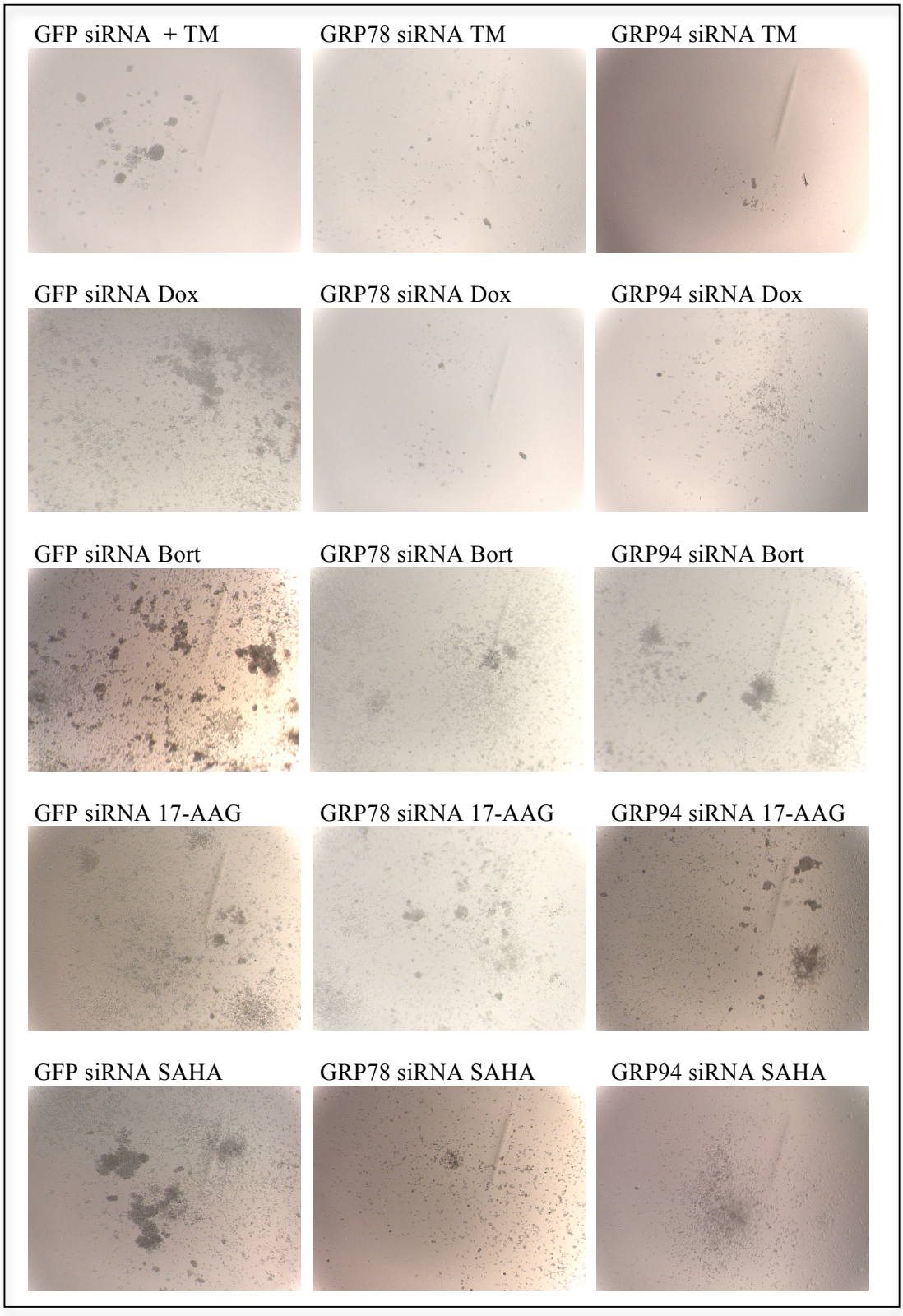

Figure 8.10. Colony formation assay following 48 hours of drug treatment in the THP1 cell line. Representative photographs are shown for each sample.

In the U266 cell line (see figure 8.11), transfection with either GRP78 or GRP94 siRNA led to a reduction in colony growth compared to the GFP transfected cells following treatment with SAHA. There also appeared to be a small decrease in colony growth following thapsigargin treatment. A reduction in colony formation was observed in the GRP78 siRNA transfected cells after treatment with 17-AAG, but not in the GRP94 siRNA transfected U266 cells. No colony growth was seen in either the control or target siRNA transfected cells following treatment with tunicamycin, doxorubicin or bortezomib in the U266 cell line.

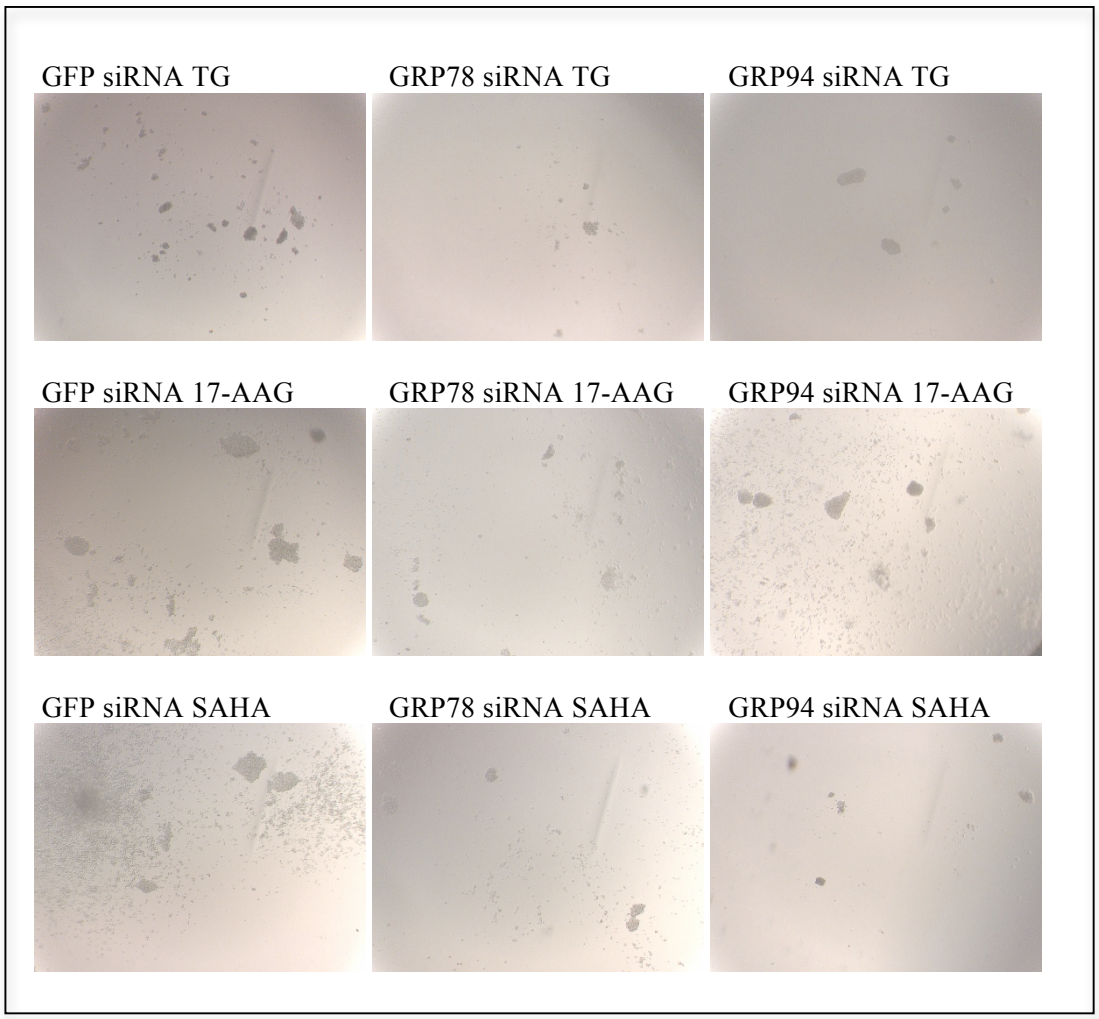

Figure 8.11. Colony formation assay following 48 hours of drug treatment in the U266 cell line. Representative photographs are shown for each sample.

8.4 Discussion

Previous studies conducted in solid tumours have reported that knockdown of GRP78 increases chemosensitivity (Pyrko *et al.*, 2007b, Dong *et al.*, 2005, Lee *et al.*, 2008). The experiments conducted here suggest that the role of ER molecular chaperone knockdown in chemosensitivity is less clear-cut in these haematological cell lines. However, it should also be noted that the transfection system used in these experiments did not result in a complete knockdown of the targeted protein, and further experiments using a lentiviral vector system to deliver short hairpin RNA (shRNA), resulting in stable transfection, could be utilised to achieve this and further investigate the effect of knockdown on chemosensitivity.

Results of cytotoxicity assay in cells with siRNA mediated GRP78 and GRP94 gene silencing revealed only a modest effect on chemosensitivity in these haematological cancer cell lines. In both cell lines, statistically significant sensitisation to the anticancer agents used occurred with only a minority of drug treatments studied. Sensitisation was more apparent in the THP1 cell line, in comparison with the U266 cell line. In the AML cell line THP1, knockdown of GRP94 sensitised cells to the antiproliferative effects of the two ER stress inducing agents tunicamycin and thapsigargin, although the effect was small. In the U266 cell line, GRP78 knockdown resulted in a decrease in sensitivity to the cytotoxic effect of treatment with 17-AAG, a HSP90 inhibitor. No consistent pattern was seen in the effect of knockdown on chemosensitivity in these cell lines, neither in terms of cell number, nor viability.

Other investigators have reported that knockdown of GRP78 in mouse models led to an increase in the levels of both GRP94 mRNA and protein (Luo *et al.*, 2006), and that this increase is a consequence of a novel compensatory feedback mechanism (Fu and Lee, 2006). Western blotting experiments in described in this chapter also suggest that when GRP78 is

silenced using a siRNA approach in the U266 cell line, an increase in GRP94 protein can be observed. It is possible that this is a compensatory mechanism, designed to protect ER molecular chaperone function and may influence the response to drug treatment after GRP78 knockdown. Interestingly, in the THP1 cell line the GRP78 knockdown resulted in a decrease in sensitivity to the cytotoxic effect of treatment with 17-AAG, an inhibitor of cytosolic HSP90, which has also been shown to bind to GRP94. Further investigation may reveal whether this antagonism is related to this possible compensatory feedback mechanism for these ER molecular chaperones.

When designing the colony formation experiments, it was intended that each well would be photographed (i.e. one picture of the entire well) enabling counting of the total number of colonies per well. Replicate wells could then be averaged and the mean of the two separate experiments could be calculated, along with standard deviation, with this data illustrated graphically. However, due to a fault with the microscope, the required objective was unavailable and this was unfortunately not possible. Therefore, representative photographs from each set of replicates are shown for illustration purposes. Further experiments conducted according to the originally planned methodology would provide quantitative results for the effect of chaperone knockdown on colony formation post drug treatment in these haematological cell lines.

The results of colony formation assay in the THP1 cell line confirmed the trend seen after the 48 hour cytotoxicity assay, with GRP78 or GRP94 knockdown enhancing the cytotoxic effects of drug treatment as shown by a decrease in the ability of these cells to recover and form colonies in longer term culture. The only exception to this was following treatment with 17-AAG in this cell line, where neither GRP78 nor GRP94 knockdown had any effect on colony formation. This may be related to the compensatory feedback loop suggested above, and further experiments would be needed to determine if this was in fact the case. In this cell line, no colony growth was seen following treatment with thapsigargin

in either the target or control (non-targeting) siRNA transfected cells. This may indicate that the THP1 cell line is particularly susceptible to ER stress induced cell death, mediated via SERCA inhibition, with cells being unable to recover upon removal of drug.

Whilst the cytotoxicity assay results in the U266 cell line showed limited effects of chaperone knockdown on chemosensitivity, colony formation assay did show a chemosensitising effect of molecular chaperone knockdown to treatment with SAHA, and to a lesser extent, thapsigargin. Chemosensitisation to 17-AAG treatment was only seen in the GRP78 knockdown cells, and further experiments would be required to establish the mechanism behind the differing responses seen with GRP78 or GRP94 knockdown cells following 17-AAG treatment. U266 cells proved particularly susceptible to the longer term effects of treatment with tunicamycin, doxorubicin and bortezomib, with no colony growth observed in any of the samples, including the transfection control samples.

In conclusion, some chemosensitisation effects were seen in these haematological cell lines, particularly in the AML cell line THP1. However, the chemosensitisation observed was modest and not present to same extent as that previously reported in solid tumours.

9. Discussion and Conclusions

At the time work began on this PhD project, ER stress and the unfolded protein response were generating a great deal of interest and excitement amongst cancer researchers. A considerable amount of research had already been published on the UPR and its role in cancer, however work in this emerging field almost exclusively related to solid tumours. This focus on solid tumours was understandable given that a number of the physiological conditions known to cause ER stress were more applicable to solid tumours, such as glucose deprivation or hypoxia. Very little research had been done at this point looking at the UPR in haematological malignancies, with the few studies that had been done looking at multiple myeloma. During the few years spent working on this project, the UPR has continued to be an area of intense study. More work has now been published on the UPR and haematological cancers, with a number of studies looking at the role of the UPR in drug treatment of cancers also being reported. The work presented in this thesis further contributes to the knowledge of this exciting area of cancer therapeutics.

Whilst there has been considerable progress in understanding the mammalian UPR in recent years, a number of important issues remain outstanding. One of the key issues is whether a therapeutic window exists in which modulating the UPR can be used as a therapeutic strategy in cancer and other diseases. As outlined in the introduction to this thesis, the UPR is a complex signalling pathway, initiated in response to a number of perturbations in ER homeostasis, with far reaching consequences for the cell (and the organism as a whole). Promising early results of modulating the UPR in solid tumours, such as glioblastoma, have been published (Pyrko *et al.*, 2007b, Dong *et al.*, 2005, Lee *et al.*, 2008). The work contained in this thesis focused on the potential of modulating the UPR in haematological malignancies. Research in this area is still in its infancy in comparison to the body of work published in solid tumours, and much remains to be determined. The data

presented here adds to the current knowledge of the UPR in haematological malignancies and the potential for targeting the UPR as a novel therapeutic strategy *in vitro*.

The first stage in this thesis was to establish the basal level of UPR activation in haematological cancer cells. This work was done in a panel of commonly used and well-characterised haematological cancer cell lines. Three cell lines were chosen, each representing one of three major types of haematological malignancy; AML, multiple myeloma and DLBCL. Basal activation of the UPR in cancer cell lines has not been described in this manner previously and novel insights into the role of the basal (physiological) UPR have been elucidated. It was observed that these haematological cell lines had a constitutively active UPR. It was particularly interesting to note the differences in protein expression of proteins in the three branches of UPR signalling; PERK, IRE1 and ATF6. Whilst small differences were seen between individual tumour types, in general, similar UPR protein activation was observed according to the tumour type studied, with the myeloma (and AML) cell lines exhibiting higher expression of IRE1 protein and the lymphoma cell lines showing higher expression of PERK pathway proteins. These findings suggest that different cell types have differences in their basal UPR activation. This agrees with established thought on the UPR, where it is believed that for certain types of cell, such as highly secretory cells, the UPR plays a more important role in maintaining protein homeostasis and normal cellular function (Glimcher and Hetz, 2008, Obeng *et al.*, 2006).

Interesting differences were also seen when basal UPR activation in the haematological cell line panel was compared with the solid tumour cell line HT29 and two samples of peripheral blood mononuclear cells (PBMC) from healthy donors. Increased expression of GRP78 was seen in the cancer cell lines compared to the healthy haematological cell PBMC samples. Although the number of normal samples was small, this finding highlights the potential value in targeting GRP78 as a cancer cell selective therapeutic strategy in these haematological malignancies.

The search for clinically meaningful *in vitro* models of haematological malignancies is ongoing, in an attempt to more closely reflect the complex tumour microenvironment of malignancies such as multiple myeloma. Whilst it would therefore have been preferable to confirm these cell line findings in primary tumour samples, the high demand and scarcity of supply of these patient tumour samples meant that this was not possible. Further experiments using a panel of primary tumour samples would be valuable in confirming whether UPR activation (and the differential pattern of activation seen across the various haematological cancer types studied) is also present in patient tumours *ex vivo*.

Analysis of cell proliferation and cell viability following drug treatment did not discover a direct relationship between basal UPR activation status and sensitivity to anticancer agents. However, these experiments did reveal that sensitivity to pharmacological ER stress inducers differed widely amongst the haematological cell lines studied, and sensitivity was dependent on the ER stressor used. This suggests that the sensitivity of cancer cells to ER stress inducing agents is specific to the mechanism of ER stress induction, and not as a result of general exposure to ER stress. This finding has implications for anticancer agents whose mechanism of action is related to ER stress induction, raising the possibility that efficacy may be cancer type specific. These experiments also established that novel anticancer agents and ER stress inducers did not always produce the characteristic cytotoxic effect expected from traditional cancer chemotherapy, with only antiproliferative effects seen in some of the cell lines studied.

Once basal UPR activation had been established, activation of the UPR following drug treatment was then studied. A number of potential approaches were available to undertake such studies, with the main strategies being either a detailed study of a limited number of UPR markers, or a snapshot of global UPR activation. It was decided to adopt the latter strategy, as this would identify potential areas of interest in these haematological cell lines that could then be studied in further detail. The UPR has not previously been

characterised in this way in haematological malignancies, so this was considered a suitable starting point for further investigation on the role of the UPR in chemosensitivity in these cell lines. Consequently, the results presented in chapter 4 represent a snapshot of global UPR activation following drug treatment for the purposes of highlighting potential areas of interest, and should not be viewed as quantitative or definitive results. With that in mind, whilst it was not possible to repeat all experiments presented due to the scope of the work undertaken, experiments were repeated to confirm notable results observed. In addition, only clear changes in protein levels were highlighted in the results observed. These changes are summarised in figures 4.19 to 4.26 inclusive. In general, it appeared that UPR activation was limited following treatment with conventional DNA damaging chemotherapy agents, with a greater degree of UPR activation seen after treatment with both the novel anticancer agents (bortezomib and KW-2478) and ER stress inducing agents (tunicamycin and thapsigargin) studied. The increase in UPR activation seen with the novel HSP90 inhibitor KW-2478 was more pronounced than any of the other agents studied, including the ER stress inducers tunicamycin and thapsigargin. These results support previous studies which have shown that treatment with the HSP90 inhibitior 17-AAG and the proteasome inhibitor bortezomib are associated with induction of ER stress and UPR activation in multiple myeloma cells (Davenport *et al*., 2007; Obeng *et al*., 2006). Future experiments providing more information on the functional significance of HSP90 inhibitors binding to the ER homologue of HSP90, GRP94, *in vivo* would further the current knowledge on the relationship between HSP90 inhibition and activation of the UPR.

The experiments presented in chapters 3 and 4 of this thesis provided some novel findings on basal UPR activation status in this haematological cancer cell line panel, sensitivity of these cell lines to both conventional and novel anticancer agents, as well as ER stress inducing agents, and UPR activation in response to treatment with these drugs. A number of potential strategies for targeting the UPR and studying chemosensitivity were identified, such as modulating the IRE1 pathway in AML and myeloma cell lines, or

targeting the PERK pathway in the lymphoma cell lines. It was observed that the key ER molecular chaperones GRP78 and GRP94 were implicated in all haematological cancer cell lines studied, with these chaperone proteins therefore considered good candidates for further study of the relationship between the UPR and chemosensitivity in these cell lines.

These haematological cancer cell lines had been shown in earlier experiments in this thesis to have a constitutively active UPR (see chapter 3), with evidence of UPR activation seen following even minimally toxic concentrations of ER stress inducing agents in some cell lines (see chapter 4). The effect of treatment with minimally toxic concentrations of an ER stress inducing agent on chemosensitivity was therefore investigated in the cell line panel. The rationale for adopting this approach was to investigate whether minimally toxic concentrations of ER stressors were sufficient to increase the apoptosis seen following anticancer drug treatment in these cells with a constitutively active UPR. If successful, this strategy would have the advantage of using much lower concentrations of ER stress inducing agents, which due to their mechanism of action are known to be highly toxic to normal cells, as well as cancer cells. Thapsigargin was chosen for these experiments as it is a much more potent inducer of ER stress than tunicamycin. The earlier drug activity experiments in chapter 3 had used the Guava Viacount assay to analyse both cell number and cell viability effects. However, the equipment being in high demand, combined with the sheer number of experiments to be undertaken meant that an alternative method of analysing cytotoxicity had to be used. A high sensitivity ATP cytotoxicity assay was therefore utilised for the experiments in chapters 5 and 6 of this thesis. Concentrations used with the ATP assay were lower than those used to see an effect on viability in the Guava Viacount assay, due to the cells beginning to lose ATP before there is loss of membrane permeability, therefore the ATP assay is more sensitive to changes in viability (with lower concentrations needed to see an effect).

There are a number of established methods of investigating and analysing the effect of combinations of drugs. Two of the most commonly used methods are to compare the combination effect with the single agent effect of either drug alone, or to compare the combination effect with an expected combination effect, based on the addition of the single agent effects of both drugs. Another widely used method is the combination index method of Chou and Talalay (Chou and Talalay, 1984). This method is particularly effective for analysis of combinations across a wide range of concentrations, where a constant ratio is maintained between the agents being studied, and for the study of more than two inhibitors. However, the purpose of these experiments was to act as an initial screen of only two concentrations used in combination, and if any synergy was seen the plan was to then carry out a more detailed set of experiments (for example, using the combination index method across a larger concentration range using constant ratios). For this reason, it was decided to use the fractional product method of Webb (Webb, 1963) to study the combination effect. As with the other combination analysis methods available the fractional product method also has its limitations. Whilst widely used by investigators, this method is considered most valid where the inhibitors obey first order kinetics, and where the inhibitors being tested have independent mechanisms of action. Whilst this method may not be ideal, it was considered the most appropriate in this case. In any event, treatment with minimally toxic thapsigargin concentrations was not found to have any synergistic effect with chemotherapy, with an antagonistic effect seen after pre-treatment with thapsigargin for 6 hours. This effect was consistent across all cell lines in the panel, and has interesting implications for the use of thapsigargin clinically. While experiments presented here suggest that the protective effect seen was due to changes in cell proliferation, further experiments are needed to fully elucidate the nature of this interaction and whether it occurs as a result of ER stress induction or rather as a result of thapsigargin mediated changes in intracellular calcium, or another as yet unidentified mechanism.

Another strategy utilised to modulate the UPR in these haematological cancer cell lines, was the use of the chemical chaperone 4-penylbutyric acid. This compound has been reported to act as a chemical chaperone, thereby reducing ER stress mediated cellular dysfunction (Welch and Brown, 1996). It was therefore hypothesised that if 4-PBA could reduce the levels of ER stress in these haematological cells where the UPR is constitutively active, then this may make the cells more sensitive to treatment with anticancer agents (particularly those known to induce ER stress). The apoptosis assay data for the combination of 4-PBA pre-treatment for 24 hours with the ER stressors tunicamycin and thapsigargin appears to support this hypothesis, although western blotting did not reveal any changes in the UPR proteins studied at these concentrations. However, analysis of HDAC activity showed that at the 0.5mM concentration used in these experiments, 4-PBA did possess weak HDAC inhibitory activity, with further experiments needed to determine if the results seen were due to chemical chaperone or HDAC inhibitory effects.

The activity of the novel small molecule versipelostatin was also studied. This promising small molecule is an inhibitor of both ER molecular chaperones GRP78 and GRP94. Inhibition occurs under glucose deprivation conditions, and although the previously published downregulation of these chaperones reported in solid tumours (Park *et al*., 2004) was confirmed in these experiments, downregulation was not observed in the haematological cell lines studied. This raises the possibility that glucose deprivation conditions have a more pronounced effect on solid tumour cells than haematological cells *in vitro*, and that versipelostatin may be of more value in the treatment of glucose starved solid tumours than haematological malignancies. However, versipelostatin is an anticancer agent in its own right with potency in the low micromolar range, and the haematological cell lines studied appearing more sensitive than the widely used solid tumour cell line HT-29. In addition, increased cytotoxicity was observed when versipelostatin was combined with 2-DG, compared to single agent versipelostatin treatment. Further investigation is needed to determine whether versipelostatin also acts via other, as yet undetermined, mechanisms.

With attempts to target the UPR in order to modulate chemosensitivity in this thesis using small molecules having had minimal success, siRNA mediated silencing of GRP78 and GRP94 was investigated to provide proof of concept that the UPR (and ER molecular chaperones in particular) are a valid therapeutic target in these haematological cancer cell lines. Earlier experiments in this thesis had shown that the molecular chaperones GRP78 and GRP94 were highly expressed in these haematological cell lines, and protein levels were seen to increase following treatment with ER stress inducing agents and novel anticancer agents. Other investigators have previously shown the potential benefit of GRP78 knockdown on chemosensitivity (Pyrko *et al.*, 2007b, Dong *et al.*, 2005, Lee *et al.*, 2008) and due to the high basal levels of GRP94 seen in these haematological cancer cells, GRP94 knockdown was also studied. Cytotoxicity experiments revealed minimal effects of GRP78 or GRP94 knockdown on chemosensitivity in the AML cell line THP1 and myeloma cell line U266. Whilst some decrease in proliferation was seen on the colony formation assay, this experiment did not provide quantitative data and further experiments would therefore be needed to confirm this effect. Previous reports in glioblastoma cell lines have shown that whilst transfection with siRNA targeting GRP78 is sufficient to decrease basal GRP78 levels, it does not prevent the induction of GRP78 protein seen upon induction of ER stress (Kardosh *et al*., 2008), suggesting the possibility that GRP78 induction following drug treatment may act to restore the silenced GRP78 function. Further experiments investigating the effect of GRP78 and GRP94 knockdown on chemosensitivity in these haematological malignancies are required to probe such an effect.

This thesis adds to the current knowledge of the UPR in haematological malignancies, an area that is continuing to provide novel discoveries and areas for further development in the search for new cancer treatments. One such area is the development of small molecule IRE inhibitors (Papandreou *et al*., 2011), which is of particular significance in multiple myeloma. Other important research areas include the discovery that GRP78 is found outside the ER, in locations including the nucleus, cytoplasm and mitochondria, and

what significance this may have on the viability of GRP78 as a therapeutic target (Ni *et al.*, 2011, Pfaffenbach and Lee, 2010, Zhang *et al.*, 2010). Studies also continue with versipelostatin and its derivatives. Recently, data on another GRP78 targeting compound NKP-1339 (developed by Niiki Pharma) was presented at the American Society of Clinical Oncology Annual Meeting 2011, with a phase I clinical trial of this agent in patients with metastatic solid tumours resistant to standard therapies initiated in the United States (ClinicalTrials.gov identifier: NCT01415297) (Dickson *et al.*, 2011). The UPR remains a promising area of cancer research, and the arrival of the first UPR targeted therapy to reach the clinic is eagerly awaited.

In conclusion, the UPR is activated in these haematological cancer cell lines and plays a complex role in chemosensitivity. In contrast to previous reports in solid tumour cells, modulating the UPR in these haematological malignancies had only a modest effect on chemosensitivity.

10. References

Abeloff, M. D. 2004. *Clinical oncology* [Online]. Philadelphia, Pa.: Elsevier Churchill Livingstone. [Accessed].

Abramson, J. S., Chen, W., Juszczynski, P., Takahashi, H., Neuberg, D., Kutok, J. L., Takeyama, K. & Shipp, M. A. 2008. The heat shock protein 90 inhibitor IPI-504 induces apoptosis of AKT-dependent diffuse large B-cell lymphomas. *Br J Haematol*.

Acosta-Alvear, D., Zhou, Y., Blais, A., Tsikitis, M., Lents, N. H., Arias, C., Lennon, C. J., Kluger, Y. & Dynlacht, B. D. 2007. XBP1 controls diverse cell type- and condition-specific transcriptional regulatory networks. *Mol Cell,* 27**,** 53-66.

Aebi, M., Bernasconi, R., Clerc, S. & Molinari, M. 2010. N-glycan structures: recognition and processing in the ER. *Trends Biochem Sci,* 35**,** 74-82.

Alberts, B. 2002. *Molecular biology of the cell,* New York, Garland Science.

Ali, M. M., Bagratuni, T., Davenport, E. L., Nowak, P. R., Silva-Santisteban, M. C., Hardcastle, A., Mcandrews, C., Rowlands, M. G., Morgan, G. J., Aherne, W., Collins, I., Davies, F. E. & Pearl, L. H. 2011. Structure of the Ire1 autophosphorylation complex and implications for the unfolded protein response. *Embo J*.

Auf, G., Jabouille, A., Guerit, S., Pineau, R., Delugin, M., Bouchecareilh, M., Magnin, N., Favereaux, A., Maitre, M., Gaiser, T., Von Deimling, A., Czabanka, M., Vajkoczy, P., Chevet, E., Bikfalvi, A. & Moenner, M. 2010. Inositol-requiring enzyme 1alpha is a key regulator of angiogenesis and invasion in malignant glioma. *Proc Natl Acad Sci U S A,* 107**,** 15553-8.

Bagratuni, T., Wu, P., Gonzalez De Castro, D., Davenport, E. L., Dickens, N. J., Walker, B. A., Boyd, K., Johnson, D. C., Gregory, W., Morgan, G. J. & Davies, F. E. 2010. XBP1s levels are implicated in the biology and outcome of myeloma mediating different clinical outcomes to thalidomide-based treatments. *Blood,* 116**,** 250-3.

Basseri, S., Lhotak, S., Sharma, A. M. & Austin, R. C. 2009. The chemical chaperone 4-phenylbutyrate inhibits adipogenesis by modulating the unfolded protein response. *J Lipid Res,* 50**,** 2486-501.

Baumeister, P., Dong, D., Fu, Y. & Lee, A. S. 2009. Transcriptional induction of GRP78/BiP by histone deacetylase inhibitors and resistance to histone deacetylase inhibitor-induced apoptosis. *Mol Cancer Ther,* 8**,** 1086-94.

Beers, M. H. & Merck Research Laboratories. 2006. *The Merck manual of diagnosis and therapy,* Whitehouse Station, N.J., Merck Research Laboratories.

Bennett, J. M., Catovsky, D., Daniel, M. T., Flandrin, G., Galton, D. A., Gralnick, H. R. & Sultan, C. 1976. Proposals for the classification of the acute leukaemias. French-American-British (FAB) co-operative group. *Br J Haematol,* 33**,** 451-8.

Bernales, S., Papa, F. R. & Walter, P. 2006. Intracellular signaling by the unfolded protein response. *Annu Rev Cell Dev Biol,* 22**,** 487-508.

Boden, G., Duan, X., Homko, C., Molina, E. J., Song, W., Perez, O., Cheung, P. & Merali, S. 2008. Increase in endoplasmic reticulum stress-related proteins and genes in adipose tissue of obese, insulin-resistant individuals. *Diabetes,* 57**,** 2438-44.

Bolden, J. E., Peart, M. J. & Johnstone, R. W. 2006. Anticancer activities of histone deacetylase inhibitors. *Nat Rev Drug Discov,* 5**,** 769-84.

Bole, D. G., Hendershot, L. M. & Kearney, J. F. 1986. Posttranslational association of immunoglobulin heavy chain binding protein with nascent heavy chains in nonsecreting and secreting hybridomas. *J Cell Biol,* 102**,** 1558-66.

Bommiasamy, H., Back, S. H., Fagone, P., Lee, K., Meshinchi, S., Vink, E., Sriburi, R., Frank, M., Jackowski, S., Kaufman, R. J. & Brewer, J. W. 2009. ATF6{alpha} induces XBP1-independent expansion of the endoplasmic reticulum. *J Cell Sci,* 122**,** 1626-36.

Braakman, I., Helenius, J. & Helenius, A. 1992. Role of ATP and disulphide bonds during protein folding in the endoplasmic reticulum. *Nature,* 356**,** 260-2.

Brewer, J. W. & Diehl, J. A. 2000. PERK mediates cell-cycle exit during the mammalian unfolded protein response. *Proc Natl Acad Sci U S A,* 97**,** 12625-30.

Brough, P. A., Aherne, W., Barril, X., Borgognoni, J., Boxall, K., Cansfield, J. E., Cheung, K. M., Collins, I., Davies, N. G., Drysdale, M. J., Dymock, B., Eccles, S. A., Finch, H., Fink, A., Hayes, A., Howes, R., Hubbard, R. E., James, K., Jordan, A. M., Lockie, A., Martins, V., Massey, A., Matthews, T. P., Mcdonald, E., Northfield, C. J., Pearl, L. H., Prodromou, C., Ray, S., Raynaud, F. I., Roughley, S. D., Sharp, S. Y., Surgenor, A., Walmsley, D. L., Webb, P., Wood, M., Workman, P. & Wright, L. 2008. 4,5-diarylisoxazole Hsp90 chaperone inhibitors: potential therapeutic agents for the treatment of cancer. *J Med Chem,* 51**,** 196-218.

Brown, C. R., Hong-Brown, L. Q., Biwersi, J., Verkman, A. S. & Welch, W. J. 1996. Chemical chaperones correct the mutant phenotype of the delta F508 cystic fibrosis transmembrane conductance regulator protein. *Cell Stress Chaperones,* 1**,** 117-25.

Brown, C. R., Hong-Brown, L. Q. & Welch, W. J. 1997. Correcting temperature-sensitive protein folding defects. *J Clin Invest,* 99**,** 1432-44.

Brunner, T. B., Geiger, M., Grabenbauer, G. G., Lang-Welzenbach, M., Mantoni, T. S., Cavallaro, A., Sauer, R., Hohenberger, W. & Mckenna, W. G. 2008. Phase I trial of the human immunodeficiency virus protease inhibitor nelfinavir and chemoradiation for locally advanced pancreatic cancer. *J Clin Oncol,* 26**,** 2699-706.

Buchberger, A., Bukau, B. & Sommer, T. 2010. Protein quality control in the cytosol and the endoplasmic reticulum: brothers in arms. *Mol Cell,* 40**,** 238-52.

Burrows, J. A., Willis, L. K. & Perlmutter, D. H. 2000. Chemical chaperones mediate increased secretion of mutant alpha 1-antitrypsin (alpha 1-AT) Z: A potential pharmacological strategy for prevention of liver injury and emphysema in alpha 1-AT deficiency. *Proc Natl Acad Sci U S A,* 97**,** 1796-801.

Cancerresearchuk 2010a. CancerStats report – Leukaemia UK, Cancer Research UK.

Cancerresearchuk 2010b. CancerStats report – Multiple Myeloma UK, Cancer Research UK.

Cancerresearchuk 2010c. CancerStats report – Non-Hodgkin Lymphoma UK, Cancer Research UK.

Canellos, G. P., Lister, T. A. & Young, B. D. 2006. *The lymphomas,* Philadelphia, Saunders Elsevier.

Carducci, M. A., Gilbert, J., Bowling, M. K., Noe, D., Eisenberger, M. A., Sinibaldi, V., Zabelina, Y., Chen, T. L., Grochow, L. B. & Donehower, R. C. 2001. A Phase I clinical and pharmacological evaluation of sodium phenylbutyrate on an 120-h infusion schedule. *Clin Cancer Res,* 7**,** 3047-55.

Carew, J. S., Nawrocki, S. T., Krupnik, Y. V., Dunner, K., Jr., Mcconkey, D. J., Keating, M. J. & Huang, P. 2006. Targeting endoplasmic reticulum protein transport: a novel strategy to kill malignant B cells and overcome fludarabine resistance in CLL. *Blood,* 107**,** 222-31.

Cavenagh, J. D., Yong, K., Byrne, J., Cavet, J., Johnson, P., Morgan, G., Williams, C., Akinaga, S., Francis, G. & Kilborn, J. 2008. The Safety, Pharmacokinetics and Pharmacodynamics of KW-2478, a Novel Hsp90 Antagonist, in Patients with B-Cell Malignancies: A First-in-Man, Phase I, Multicentre, Open-Label, Dose Escalation Study. *ASH Annual Meeting Abstracts,* 112**,** 2777-.

Chant, I. D., Rose, P. E. & Morris, A. G. 1996. Susceptibility of AML cells to in vitro apoptosis correlates with heat shock protein 70 (hsp 70) expression. *Br J Haematol,* 93**,** 898-902.

Chatterjee, S., Hirota, H., Belfi, C. A., Berger, S. J. & Berger, N. A. 1997. Hypersensitivity to DNA cross-linking agents associated with up-regulation of glucose-regulated stress protein GRP78. *Cancer Res,* 57**,** 5112-6.

Chavany, C., Mimnaugh, E., Miller, P., Bitton, R., Nguyen, P., Trepel, J., Whitesell, L., Schnur, R., Moyer, J. & Neckers, L. 1996. p185erbB2 binds to GRP94 in vivo. Dissociation of the p185erbB2/GRP94 heterocomplex by benzoquinone ansamycins precedes depletion of p185erbB2. *J Biol Chem,* 271**,** 4974-7.

Chen, L. H., Jiang, C. C., Kiejda, K. A., Wang, Y. F., Thorne, R. F., Zhang, X. D. & Hersey, P. 2007. Thapsigargin sensitizes human melanoma cells to TRAIL-induced apoptosis by up-regulation of TRAIL-R2 through the unfolded protein response. *Carcinogenesis,* 28**,** 2328-36.

Chen, X., Ding, Y., Liu, C. G., Mikhail, S. & Yang, C. S. 2002. Overexpression of glucose-regulated protein 94 (Grp94) in esophageal adenocarcinomas of a rat surgical model and humans. *Carcinogenesis,* 23**,** 123-30.

Cho, H. Y., Thomas, S., Golden, E. B., Gaffney, K. J., Hofman, F. M., Chen, T. C., Louie, S. G., Petasis, N. A. & Schonthal, A. H. 2009. Enhanced killing of chemo-resistant breast cancer cells via controlled aggravation of ER stress. *Cancer Lett*.

Choudhary, C., Kumar, C., Gnad, F., Nielsen, M. L., Rehman, M., Walther, T. C., Olsen, J. V. & Mann, M. 2009. Lysine acetylation targets protein complexes and co-regulates major cellular functions. *Science,* 325**,** 834-40.

Christensen, S. B., Skytte, D. M., Denmeade, S. R., Dionne, C., Moller, J. V., Nissen, P. & Isaacs, J. T. 2009. A Trojan horse in drug development: targeting of thapsigargins towards prostate cancer cells. *Anticancer Agents Med Chem,* 9**,** 276-94.

Cox, J. S., Shamu, C. E. & Walter, P. 1993. Transcriptional induction of genes encoding endoplasmic reticulum resident proteins requires a transmembrane protein kinase. *Cell,* 73**,** 1197-206.

Crosti, P., Malerba, M. & Bianchetti, R. 2001. Tunicamycin and Brefeldin A induce in plant cells a programmed cell death showing apoptotic features. *Protoplasma,* 216**,** 31-8.

Daneshmand, S., Quek, M. L., Lin, E., Lee, C., Cote, R. J., Hawes, D., Cai, J., Groshen, S., Lieskovsky, G., Skinner, D. G., Lee, A. S. & Pinski, J. 2007. Glucose-regulated protein GRP78 is up-regulated in prostate cancer and correlates with recurrence and survival. *Hum Pathol,* 38**,** 1547-52.

Dash, R., Richards, J. E., Su, Z. Z., Bhutia, S. K., Azab, B., Rahmani, M., Dasmahapatra, G., Yacoub, A., Dent, P., Dmitriev, I. P., Curiel, D. T., Grant, S., Pellecchia, M., Reed, J. C., Sarkar, D. & Fisher, P. B. 2010. Mechanism by which Mcl-1 regulates cancer-specific apoptosis triggered by mda-7/IL-24, an IL-10-related cytokine. *Cancer Res,* 70**,** 5034-45.

Davenport, E. L., Moore, H. E., Dunlop, A. S., Sharp, S. Y., Workman, P., Morgan, G. J. & Davies, F. E. 2007. Heat shock protein inhibition is associated with activation of the unfolded protein response pathway in myeloma plasma cells. *Blood,* 110**,** 2641-9.

Davies, F. E., Dring, A. M., Li, C., Rawstron, A. C., Shammas, M. A., O'connor, S. M., Fenton, J. A., Hideshima, T., Chauhan, D., Tai, I. T., Robinson, E., Auclair, D., Rees, K., Gonzalez, D., Ashcroft, A. J., Dasgupta, R., Mitsiades, C., Mitsiades, N., Chen, L. B., Wong, W. H., Munshi, N. C., Morgan, G. J. & Anderson, K. C. 2003. Insights into the multistep transformation of MGUS to myeloma using microarray expression analysis. *Blood,* 102**,** 4504-11.

De Almeida, S. F., Picarote, G., Fleming, J. V., Carmo-Fonseca, M., Azevedo, J. E. & De Sousa, M. 2007. Chemical chaperones reduce endoplasmic reticulum stress and prevent mutant HFE aggregate formation. *J Biol Chem,* 282**,** 27905-12.

Delepine, M., Nicolino, M., Barrett, T., Golamaully, M., Lathrop, G. M. & Julier, C. 2000. EIF2AK3, encoding translation initiation factor 2-alpha kinase 3, is mutated in patients with Wolcott-Rallison syndrome. *Nat Genet,* 25**,** 406-9.

Denic, V., Quan, E. M. & Weissman, J. S. 2006. A luminal surveillance complex that selects misfolded glycoproteins for ER-associated degradation. *Cell,* 126**,** 349-59.

Denmeade, S. R. & Isaacs, J. T. 2005. The SERCA pump as a therapeutic target: making a "smart bomb" for prostate cancer. *Cancer Biol Ther,* 4**,** 14-22.

Dent, P., Yacoub, A., Grant, S., Curiel, D. T. & Fisher, P. B. 2005. MDA-7/IL-24 regulates proliferation, invasion and tumor cell radiosensitivity: a new cancer therapy? *J Cell Biochem,* 95**,** 712-9.

Dick, L. R. & Fleming, P. E. 2010. Building on bortezomib: second-generation proteasome inhibitors as anti-cancer therapy. *Drug Discov Today,* 15**,** 243-9.

Dickson, N. R., Jones, S. F., Burris, H. A., Ramanathan, R. K., Weiss, G. J., Infante, J. R., Bendell, J. C., Mcculloch, W. & Von Hoff, D. D. 2011. A phase I dose-escalation study of NKP-1339 in patients with advanced solid tumors refractory to treatment. *ASCO Meeting Abstracts,* 29**,** 2607.

Ding, W. X., Ni, H. M., Gao, W., Yoshimori, T., Stolz, D. B., Ron, D. & Yin, X. M. 2007. Linking of autophagy to ubiquitin-proteasome system is important for the regulation of endoplasmic reticulum stress and cell viability. *Am J Pathol,* 171**,** 513-24.

Dong, D., Ko, B., Baumeister, P., Swenson, S., Costa, F., Markland, F., Stiles, C., Patterson, J. B., Bates, S. E. & Lee, A. S. 2005. Vascular targeting and antiangiogenesis agents induce drug resistance effector GRP78 within the tumor microenvironment. *Cancer Res,* 65**,** 5785-91.

Dorner, A. J., Bole, D. G. & Kaufman, R. J. 1987. The relationship of N-linked glycosylation and heavy chain-binding protein association with the secretion of glycoproteins. *J Cell Biol,* 105**,** 2665-74.

Drogat, B., Auguste, P., Nguyen, D. T., Bouchecareilh, M., Pineau, R., Nalbantoglu, J., Kaufman, R. J., Chevet, E., Bikfalvi, A. & Moenner, M. 2007. IRE1 signaling is essential for ischemia-induced vascular endothelial growth factor-A expression and contributes to angiogenesis and tumor growth in vivo. *Cancer Res,* 67**,** 6700-7.

Durie, B. G. & Salmon, S. E. 1975. A clinical staging system for multiple myeloma. Correlation of measured myeloma cell mass with presenting clinical features, response to treatment, and survival. *Cancer,* 36**,** 842-54.

Egger, L., Schneider, J., Rheme, C., Tapernoux, M., Hacki, J. & Borner, C. 2003. Serine proteases mediate apoptosis-like cell death and phagocytosis under caspase-inhibiting conditions. *Cell Death Differ,* 10**,** 1188-203.

Eizirik, D. L., Cardozo, A. K. & Cnop, M. 2008. The role for endoplasmic reticulum stress in diabetes mellitus. *Endocr Rev,* 29**,** 42-61.

Ellgaard, L. & Helenius, A. 2003. Quality control in the endoplasmic reticulum. *Nat Rev Mol Cell Biol,* 4**,** 181-91.

Fels, D. R., Ye, J., Segan, A. T., Kridel, S. J., Spiotto, M., Olson, M., Koong, A. C. & Koumenis, C. 2008. Preferential Cytotoxicity of Bortezomib toward Hypoxic Tumor Cells via Overactivation of Endoplasmic Reticulum Stress Pathways. *Cancer Res,* 68**,** 9323-30.

Felts, S. J., Owen, B. A., Nguyen, P., Trepel, J., Donner, D. B. & Toft, D. O. 2000. The hsp90-related protein TRAP1 is a mitochondrial protein with distinct functional properties. *J Biol Chem,* 275**,** 3305-12.

Fernandez, P. M., Tabbara, S. O., Jacobs, L. K., Manning, F. C., Tsangaris, T. N., Schwartz, A. M., Kennedy, K. A. & Patierno, S. R. 2000. Overexpression of the glucose-regulated stress gene GRP78 in malignant but not benign human breast lesions. *Breast Cancer Res Treat,* 59**,** 15-26.

Fersht, A. R. 2000. Transition-state structure as a unifying basis in protein-folding mechanisms: contact order, chain topology, stability, and the extended nucleus mechanism. *Proc Natl Acad Sci U S A,* 97**,** 1525-9.

Foyouzi-Youssefi, R., Arnaudeau, S., Borner, C., Kelley, W. L., Tschopp, J., Lew, D. P., Demaurex, N. & Krause, K. H. 2000. Bcl-2 decreases the free Ca2+ concentration within the endoplasmic reticulum. *Proc Natl Acad Sci U S A,* 97**,** 5723-8.

Fu, Y. & Lee, A. S. 2006. Glucose regulated proteins in cancer progression, drug resistance and immunotherapy. *Cancer Biol Ther,* 5**,** 741-4.

Fujita, E., Kouroku, Y., Jimbo, A., Isoai, A., Maruyama, K. & Momoi, T. 2002. Caspase-12 processing and fragment translocation into nuclei of tunicamycin-treated cells. *Cell Death Differ,* 9**,** 1108-14.

Garcia-Mata, R., Gao, Y. S. & Sztul, E. 2002. Hassles with taking out the garbage: aggravating aggresomes. *Traffic,* 3**,** 388-96.

Gass, J. N., Gunn, K. E., Sriburi, R. & Brewer, J. W. 2004. Stressed-out B cells? Plasma-cell differentiation and the unfolded protein response. *Trends Immunol,* 25**,** 17-24.

Gass, J. N., Jiang, H. Y., Wek, R. C. & Brewer, J. W. 2008. The unfolded protein response of B-lymphocytes: PERK-independent development of antibody-secreting cells. *Mol Immunol,* 45**,** 1035-43.

Gatenby, R. A. & Gillies, R. J. 2004. Why do cancers have high aerobic glycolysis? *Nat Rev Cancer,* 4**,** 891-9.

Gething, M. J. & Sambrook, J. 1992. Protein folding in the cell. *Nature,* 355**,** 33-45.

Ghantous, A., Gali-Muhtasib, H., Vuorela, H., Saliba, N. A. & Darwiche, N. 2010. What made sesquiterpene lactones reach cancer clinical trials? *Drug Discov Today,* 15**,** 668-78.

Gilbert, J., Baker, S. D., Bowling, M. K., Grochow, L., Figg, W. D., Zabelina, Y., Donehower, R. C. & Carducci, M. A. 2001. A phase I dose escalation and bioavailability study of oral sodium phenylbutyrate in patients with refractory solid tumor malignancies. *Clin Cancer Res,* 7**,** 2292-300.

Gills, J. J., Lopiccolo, J., Tsurutani, J., Shoemaker, R. H., Best, C. J., Abu-Asab, M. S., Borojerdi, J., Warfel, N. A., Gardner, E. R., Danish, M., Hollander, M. C., Kawabata, S., Tsokos, M., Figg, W. D., Steeg, P. S. & Dennis, P. A. 2007. Nelfinavir, A lead HIV protease inhibitor, is a broad-spectrum, anticancer agent that induces endoplasmic reticulum stress, autophagy, and apoptosis in vitro and in vivo. *Clin Cancer Res,* 13**,** 5183-94.

Glimcher, L. H. & Hetz, C. 2008. XBP-1 and the UPRosome: Mastering Secretory Cell Function. *Current Immunology Reviews,* 4**,** 1-10.

Goetz, M. P., Toft, D. O., Ames, M. M. & Erlichman, C. 2003. The Hsp90 chaperone complex as a novel target for cancer therapy. *Ann Oncol,* 14**,** 1169-76.

Gosky, D. & Chatterjee, S. 2003. Down-regulation of topoisomerase II alpha is caused by up-regulation of GRP78. *Biochem Biophys Res Commun,* 300**,** 327-32.

Gray, M. D., Mann, M., Nitiss, J. L. & Hendershot, L. M. 2005. Activation of the unfolded protein response is necessary and sufficient for reducing topoisomerase IIalpha protein levels and decreasing sensitivity to topoisomerase-targeted drugs. *Mol Pharmacol,* 68**,** 1699-707.

Greipp, P. R., San Miguel, J., Durie, B. G., Crowley, J. J., Barlogie, B., Blade, J., Boccadoro, M., Child, J. A., Avet-Loiseau, H., Kyle, R. A., Lahuerta, J. J., Ludwig, H., Morgan, G., Powles, R., Shimizu, K., Shustik, C., Sonneveld, P., Tosi, P., Turesson, I. & Westin, J. 2005. International staging system for multiple myeloma. *J Clin Oncol,* 23**,** 3412-20.

Guo, Q., Sopher, B. L., Furukawa, K., Pham, D. G., Robinson, N., Martin, G. M. & Mattson, M. P. 1997. Alzheimer's presenilin mutation sensitizes neural cells to apoptosis induced by trophic factor withdrawal and amyloid beta-peptide: involvement of calcium and oxyradicals. *J Neurosci,* 17**,** 4212-22.

Gupta, A. K., Li, B., Cerniglia, G. J., Ahmed, M. S., Hahn, S. M. & Maity, A. 2007. The HIV protease inhibitor nelfinavir downregulates Akt phosphorylation by inhibiting proteasomal activity and inducing the unfolded protein response. *Neoplasia,* 9**,** 271-8.

Gupta, P., Walter, M. R., Su, Z. Z., Lebedeva, I. V., Emdad, L., Randolph, A., Valerie, K., Sarkar, D. & Fisher, P. B. 2006. BiP/GRP78 is an intracellular target for MDA-7/IL-24 induction of cancer-specific apoptosis. *Cancer Res,* 66**,** 8182-91.

Haas, I. G. & Wabl, M. 1983. Immunoglobulin heavy chain binding protein. *Nature,* 306**,** 387-9.

Hamanaka, R. B., Bennett, B. S., Cullinan, S. B. & Diehl, J. A. 2005. PERK and GCN2 contribute to eIF2alpha phosphorylation and cell cycle arrest after activation of the unfolded protein response pathway. *Mol Biol Cell,* 16**,** 5493-501.

Hampton, R. Y. 2002. Proteolysis and sterol regulation. *Annu Rev Cell Dev Biol,* 18**,** 345-78.

Harding, H. P., Novoa, I., Zhang, Y., Zeng, H., Wek, R., Schapira, M. & Ron, D. 2000a. Regulated translation initiation controls stress-induced gene expression in mammalian cells. *Mol Cell,* 6**,** 1099-108.

Harding, H. P., Zhang, Y., Bertolotti, A., Zeng, H. & Ron, D. 2000b. Perk is essential for translational regulation and cell survival during the unfolded protein response. *Mol Cell,* 5**,** 897-904.

Harding, H. P., Zhang, Y. & Ron, D. 1999. Protein translation and folding are coupled by an endoplasmic-reticulum-resident kinase. *Nature,* 397**,** 271-4.

Harris, N. L., Jaffe, E. S., Diebold, J., Flandrin, G., Muller-Hermelink, H. K., Vardiman, J., Lister, T. A. & Bloomfield, C. D. 1999. World Health Organization classification of neoplastic diseases of the hematopoietic and lymphoid tissues: report of the Clinical Advisory Committee meeting-Airlie House, Virginia, November 1997. *J Clin Oncol,* 17**,** 3835-49.

Harris, N. L., Jaffe, E. S., Stein, H., Banks, P. M., Chan, J. K., Cleary, M. L., Delsol, G., De Wolf-Peeters, C., Falini, B., Gatter, K. C. & Et Al. 1994. A revised European-American classification of lymphoid neoplasms: a proposal from the International Lymphoma Study Group. *Blood,* 84**,** 1361-92.

Hartl, F. U. & Hayer-Hartl, M. 2002. Molecular chaperones in the cytosol: from nascent chain to folded protein. *Science,* 295**,** 1852-8.

Hasegawa, A., Osuga, Y., Hirota, Y., Hamasaki, K., Kodama, A., Harada, M., Tajima, T., Takemura, Y., Hirata, T., Yoshino, O., Koga, K., Yano, T. & Taketani, Y. 2008. Tunicamycin enhances the apoptosis induced by tumor necrosis factor-related apoptosis-inducing ligand in endometriotic stromal cells. *Hum Reprod*.

Haze, K., Yoshida, H., Yanagi, H., Yura, T. & Mori, K. 1999. Mammalian transcription factor ATF6 is synthesized as a transmembrane protein and activated by proteolysis in response to endoplasmic reticulum stress. *Mol Biol Cell,* 10**,** 3787-99.

Heifetz, A., Keenan, R. W. & Elbein, A. D. 1979. Mechanism of action of tunicamycin on the UDP-GlcNAc:dolichyl-phosphate Glc-NAc-1-phosphate transferase. *Biochemistry,* 18**,** 2186-92.

Helenius, A. 1994. How N-linked oligosaccharides affect glycoprotein folding in the endoplasmic reticulum. *Mol Biol Cell,* 5**,** 253-65.

Hernlund, E., Ihrlund, L. S., Khan, O., Ates, Y. O., Linder, S., Panaretakis, T. & Shoshan, M. C. 2008. Potentiation of chemotherapeutic drugs by energy metabolism inhibitors 2-deoxyglucose and etomoxir. *Int J Cancer,* 123**,** 476-83.

Hetz, C., Bernasconi, P., Fisher, J., Lee, A. H., Bassik, M. C., Antonsson, B., Brandt, G. S., Iwakoshi, N. N., Schinzel, A., Glimcher, L. H. & Korsmeyer, S. J. 2006. Proapoptotic BAX and BAK modulate the unfolded protein response by a direct interaction with IRE1alpha. *Science,* 312**,** 572-6.

Hideshima, T., Bradner, J. E., Wong, J., Chauhan, D., Richardson, P., Schreiber, S. L. & Anderson, K. C. 2005. Small-molecule inhibition of proteasome and aggresome function induces synergistic antitumor activity in multiple myeloma. *Proc Natl Acad Sci U S A,* 102**,** 8567-72.

Hirsch, C., Gauss, R., Horn, S. C., Neuber, O. & Sommer, T. 2009. The ubiquitylation machinery of the endoplasmic reticulum. *Nature,* 458**,** 453-60.

Hiss, D., Gabriels, G., Jacobs, P. & Folb, P. 1996. Tunicamycin potentiates drug cytotoxicity and vincristine retention in multidrug resistant cell lines. *Eur J Cancer,* 32A**,** 2164-72.

Hiss, D. C., Gabriels, G. A. & Folb, P. I. 2007. Combination of tunicamycin with anticancer drugs synergistically enhances their toxicity in multidrug-resistant human ovarian cystadenocarcinoma cells. *Cancer Cell Int,* 7**,** 5.

Hitomi, J., Katayama, T., Eguchi, Y., Kudo, T., Taniguchi, M., Koyama, Y., Manabe, T., Yamagishi, S., Bando, Y., Imaizumi, K., Tsujimoto, Y. & Tohyama, M. 2004. Involvement of caspase-4 in endoplasmic reticulum stress-induced apoptosis and Abeta-induced cell death. *J Cell Biol,* 165**,** 347-56.

Hoang, B., Benavides, A., Shi, Y., Frost, P. & Lichtenstein, A. 2009. Effect of autophagy on multiple myeloma cell viability. *Mol Cancer Ther,* 8**,** 1974-84.

Hsu, J. L., Chiang, P. C. & Guh, J. H. 2009. Tunicamycin induces resistance to camptothecin and etoposide in human hepatocellular carcinoma cells: role of cell-cycle arrest and GRP78. *Naunyn Schmiedebergs Arch Pharmacol,* 380**,** 373-82.

Iannitti, T. & Palmieri, B. 2011. Clinical and experimental applications of sodium phenylbutyrate. *Drugs R D,* 11**,** 227-49.

Imai, Y., Soda, M. & Takahashi, R. 2000. Parkin suppresses unfolded protein stress-induced cell death through its E3 ubiquitin-protein ligase activity. *J Biol Chem,* 275**,** 35661-4.

Inoue, S., Shanker, M., Miyahara, R., Gopalan, B., Patel, S., Oida, Y., Branch, C. D., Munshi, A., Meyn, R. E., Andreeff, M., Tanaka, F., Mhashilkar, A. M., Chada, S. & Ramesh, R. 2006. MDA-7/IL-24-based cancer gene therapy: translation from the laboratory to the clinic. *Curr Gene Ther,* 6**,** 73-91.

Iwakoshi, N. N., Lee, A. H., Vallabhajosyula, P., Otipoby, K. L., Rajewsky, K. & Glimcher, L. H. 2003. Plasma cell differentiation and the unfolded protein response intersect at the transcription factor XBP-1. *Nat Immunol,* 4**,** 321-9.

Iwawaki, T., Akai, R., Yamanaka, S. & Kohno, K. 2009. Function of IRE1 alpha in the placenta is essential for placental development and embryonic viability. *Proc Natl Acad Sci U S A,* 106**,** 16657-62.

Janssen, K., Horn, S., Niemann, M. T., Daniel, P. T., Schulze-Osthoff, K. & Fischer, U. 2009. Inhibition of the ER Ca2+ pump forces multidrug-resistant cells deficient in Bak and Bax into necrosis. *J Cell Sci,* 122**,** 4481-91.

Jiang, C. C., Chen, L. H., Gillespie, S., Kiejda, K. A., Mhaidat, N., Wang, Y. F., Thorne, R., Zhang, X. D. & Hersey, P. 2007a. Tunicamycin sensitizes human melanoma cells to tumor necrosis factor-related apoptosis-inducing ligand-induced apoptosis by up-regulation of TRAIL-R2 via the unfolded protein response. *Cancer Res,* 67**,** 5880-8.

Jiang, C. C., Chen, L. H., Gillespie, S., Wang, Y. F., Kiejda, K. A., Zhang, X. D. & Hersey, P. 2007b. Inhibition of MEK sensitizes human melanoma cells to endoplasmic reticulum stress-induced apoptosis. *Cancer Res,* 67**,** 9750-61.

Jiang, C. C., Yang, F., Thorne, R. F., Zhu, B. K., Hersey, P. & Zhang, X. D. 2009. Human melanoma cells under endoplasmic reticulum stress acquire resistance to microtubule-targeting drugs through XBP-1-mediated activation of Akt. *Neoplasia,* 11**,** 436-47.

Jiang, H., Lin, J. J., Su, Z. Z., Goldstein, N. I. & Fisher, P. B. 1995. Subtraction hybridization identifies a novel melanoma differentiation associated gene, mda-7, modulated during human melanoma differentiation, growth and progression. *Oncogene,* 11**,** 2477-86.

Johnson, A. J., Hsu, A. L., Lin, H. P., Song, X. & Chen, C. S. 2002. The cyclo-oxygenase-2 inhibitor celecoxib perturbs intracellular calcium by inhibiting endoplasmic reticulum Ca2+-ATPases: a plausible link with its anti-tumour effect and cardiovascular risks. *Biochem J,* 366**,** 831-7.

Jones, R. G., Bui, T., White, C., Madesh, M., Krawczyk, C. M., Lindsten, T., Hawkins, B. J., Kubek, S., Frauwirth, K. A., Wang, Y. L., Conway, S. J., Roderick, H. L., Bootman, M. D., Shen, H., Foskett, J. K. & Thompson, C. B. 2007. The proapoptotic factors Bax and Bak regulate T Cell proliferation through control of endoplasmic reticulum Ca(2+) homeostasis. *Immunity,* 27**,** 268-80.

Juliger, S., Nakashima, T., Maharaj, L., Ishii, T., Nakagawa, H., Kanda, Y., Oakervee, H., Cavenagh, J., Akinaga, S., Shiotsu, Y. & Joel, S. P. 2008. A Novel Heat Shock Protein (HSP) 90 Inhibitor KW-2478 shows Activity in B-Cell Malignancies in Vitro and in Vivo. *ASH Annual Meeting Abstracts,* 112**,** 1625-.

Kahali, S., Sarcar, B., Fang, B., Williams, E. S., Koomen, J. M., Tofilon, P. J. & Chinnaiyan, P. 2010. Activation of the unfolded protein response contributes toward the antitumor activity of vorinostat. *Neoplasia,* 12**,** 80-6.

Kamal, A., Thao, L., Sensintaffar, J., Zhang, L., Boehm, M. F., Fritz, L. C. & Burrows, F. J. 2003. A high-affinity conformation of Hsp90 confers tumour selectivity on Hsp90 inhibitors. *Nature,* 425**,** 407-10.

Kardosh, A., Golden, E. B., Pyrko, P., Uddin, J., Hofman, F. M., Chen, T. C., Louie, S. G., Petasis, N. A. & Schonthal, A. H. 2008. Aggravated endoplasmic reticulum stress as a basis for enhanced glioblastoma cell killing by bortezomib in combination with celecoxib or its non-coxib analogue, 2,5-dimethyl-celecoxib. *Cancer Res,* 68**,** 843-51.

Kaser, A., Lee, A. H., Franke, A., Glickman, J. N., Zeissig, S., Tilg, H., Nieuwenhuis, E. E., Higgins, D. E., Schreiber, S., Glimcher, L. H. & Blumberg, R. S. 2008. XBP1 links ER stress to intestinal inflammation and confers genetic risk for human inflammatory bowel disease. *Cell,* 134**,** 743-56.

Katayama, T., Imaizumi, K., Honda, A., Yoneda, T., Kudo, T., Takeda, M., Mori, K., Rozmahel, R., Fraser, P., George-Hyslop, P. S. & Tohyama, M. 2001. Disturbed activation of endoplasmic reticulum stress transducers by familial Alzheimer's disease-linked presenilin-1 mutations. *J Biol Chem,* 276**,** 43446-54.

Katayama, T., Imaizumi, K., Sato, N., Miyoshi, K., Kudo, T., Hitomi, J., Morihara, T., Yoneda, T., Gomi, F., Mori, Y., Nakano, Y., Takeda, J., Tsuda, T., Itoyama, Y., Murayama, O., Takashima, A., St George-Hyslop, P., Takeda, M. & Tohyama, M. 1999. Presenilin-1 mutations downregulate the signalling pathway of the unfolded-protein response. *Nat Cell Biol,* 1**,** 479-85.

Kaufman, R. J. 1999. Stress signaling from the lumen of the endoplasmic reticulum: coordination of gene transcriptional and translational controls. *Genes Dev,* 13**,** 1211-33.

Kaufman, R. J. 2002. Orchestrating the unfolded protein response in health and disease. *J Clin Invest,* 110**,** 1389-98.

Kaufman, R. J., Scheuner, D., Schroder, M., Shen, X., Lee, K., Liu, C. Y. & Arnold, S. M. 2002. The unfolded protein response in nutrient sensing and differentiation. *Nat Rev Mol Cell Biol,* 3**,** 411-21.

Keenan, R. J., Freymann, D. M., Stroud, R. M. & Walter, P. 2001. The signal recognition particle. *Annu Rev Biochem,* 70**,** 755-75.

Kern, J., Untergasser, G., Zenzmaier, C., Sarg, B., Gastl, G., Gunsilius, E. & Steurer, M. 2009. GRP-78 secreted by tumor cells blocks the antiangiogenic activity of bortezomib. *Blood,* 114**,** 3960-7.

Kijima, Y., Ogunbunmi, E. & Fleischer, S. 1991. Drug action of thapsigargin on the Ca2+ pump protein of sarcoplasmic reticulum. *J Biol Chem,* 266**,** 22912-8.

Kim, I., Xu, W. & Reed, J. C. 2008. Cell death and endoplasmic reticulum stress: disease relevance and therapeutic opportunities. *Nat Rev Drug Discov,* 7**,** 1013-30.

Kitamura, M. 2008. Endoplasmic reticulum stress in the kidney. *Clin Exp Nephrol,* 12**,** 317-25.

Korennykh, A. V., Egea, P. F., Korostelev, A. A., Finer-Moore, J., Zhang, C., Shokat, K. M., Stroud, R. M. & Walter, P. 2008. The unfolded protein response signals through high-order assembly of Ire1. *Nature*.

Korosec, B., Glavac, D., Volavsek, M. & Ravnik-Glavac, M. 2008. Alterations in genes encoding sarcoplasmic-endoplasmic reticulum Ca(2+) pumps in association with head and neck squamous cell carcinoma. *Cancer Genet Cytogenet,* 181**,** 112-8.

Koumenis, C., Naczki, C., Koritzinsky, M., Rastani, S., Diehl, A., Sonenberg, N., Koromilas, A. & Wouters, B. G. 2002. Regulation of protein synthesis by hypoxia via activation of the endoplasmic reticulum kinase PERK and phosphorylation of the translation initiation factor eIF2alpha. *Mol Cell Biol,* 22**,** 7405-16.

Kouroku, Y., Fujita, E., Tanida, I., Ueno, T., Isoai, A., Kumagai, H., Ogawa, S., Kaufman, R. J., Kominami, E. & Momoi, T. 2007. ER stress (PERK/eIF2alpha phosphorylation) mediates the polyglutamine-induced LC3 conversion, an essential step for autophagy formation. *Cell Death Differ,* 14**,** 230-9.

Kozutsumi, Y., Segal, M., Normington, K., Gething, M. J. & Sambrook, J. 1988. The presence of malfolded proteins in the endoplasmic reticulum signals the induction of glucose-regulated proteins. *Nature,* 332**,** 462-4.

Kraus, M., Malenke, E., Gogel, J., Muller, H., Ruckrich, T., Overkleeft, H., Ovaa, H., Koscielniak, E., Hartmann, J. T. & Driessen, C. 2008. Ritonavir induces endoplasmic reticulum stress and sensitizes sarcoma cells toward bortezomib-induced apoptosis. *Mol Cancer Ther,* 7**,** 1940-8.

Kumar, R., Azam, S., Sullivan, J. M., Owen, C., Cavener, D. R., Zhang, P., Ron, D., Harding, H. P., Chen, J. J., Han, A., White, B. C., Krause, G. S. & Degracia, D. J. 2001. Brain ischemia and reperfusion activates the eukaryotic initiation factor 2alpha kinase, PERK. *J Neurochem,* 77**,** 1418-21.

Kurtoglu, M., Philips, K., Liu, H., Boise, L. H. & Lampidis, T. J. 2010. High endoplasmic reticulum activity renders multiple myeloma cells hypersensitive to mitochondrial inhibitors. *Cancer Chemother Pharmacol,* 66**,** 129-40.

Kyle, R. A. & Rajkumar, S. V. 2008. Multiple myeloma. *Blood,* 111**,** 2962-72.

Lane, A. A. & Chabner, B. A. 2009. Histone deacetylase inhibitors in cancer therapy. *J Clin Oncol,* 27**,** 5459-68.

Laybutt, D. R., Preston, A. M., Akerfeldt, M. C., Kench, J. G., Busch, A. K., Biankin, A. V. & Biden, T. J. 2007. Endoplasmic reticulum stress contributes to beta cell apoptosis in type 2 diabetes. *Diabetologia,* 50**,** 752-63.

Lebedeva, I. V., Emdad, L., Su, Z. Z., Gupta, P., Sauane, M., Sarkar, D., Staudt, M. R., Liu, S. J., Taher, M. M., Xiao, R., Barral, P., Lee, S. G., Wang, D., Vozhilla, N., Park, E. S., Chatman, L., Boukerche, H., Ramesh, R., Inoue, S., Chada, S., Li, R., De Pass, A. L., Mahasreshti, P. J., Dmitriev, I. P., Curiel, D. T., Yacoub, A., Grant, S., Dent, P., Senzer, N., Nemunaitis, J. J. & Fisher, P. B. 2007. mda-7/IL-24, novel anticancer cytokine: focus on bystander antitumor, radiosensitization and antiangiogenic properties and overview of the phase I clinical experience (Review). *Int J Oncol,* 31**,** 985-1007.

Ledoux, S., Yang, R., Friedlander, G. & Laouari, D. 2003. Glucose depletion enhances P-glycoprotein expression in hepatoma cells: role of endoplasmic reticulum stress response. *Cancer Res,* 63**,** 7284-90.

Lee, A. S. 1987. Coordinated regulation of a set of genes by glucose and calcium ionophores in mammalian cells *Trends Biochem Sci,* 12**,** 20-23.

Lee, A. S. 2001. The glucose-regulated proteins: stress induction and clinical applications. *Trends Biochem Sci,* 26**,** 504-10.

Lee, A. S. 2007. GRP78 induction in cancer: therapeutic and prognostic implications. *Cancer Res,* 67**,** 3496-9.

Lee, E., Nichols, P., Spicer, D., Groshen, S., Yu, M. C. & Lee, A. S. 2006. GRP78 as a novel predictor of responsiveness to chemotherapy in breast cancer. *Cancer Res,* 66**,** 7849-53.

Lee, H. K., Xiang, C., Cazacu, S., Finniss, S., Kazimirsky, G., Lemke, N., Lehman, N. L., Rempel, S. A., Mikkelsen, T. & Brodie, C. 2008. GRP78 is overexpressed in glioblastomas and regulates glioma cell growth and apoptosis. *Neuro Oncol,* 10**,** 236-43.

Lee, K., Tirasophon, W., Shen, X., Michalak, M., Prywes, R., Okada, T., Yoshida, H., Mori, K. & Kaufman, R. J. 2002. IRE1-mediated unconventional mRNA splicing and S2P-mediated ATF6 cleavage merge to regulate XBP1 in signaling the unfolded protein response. *Genes Dev,* 16**,** 452-66.

Li, H., Korennykh, A. V., Behrman, S. L. & Walter, P. 2010. Mammalian endoplasmic reticulum stress sensor IRE1 signals by dynamic clustering. *Proc Natl Acad Sci U S A,* 107**,** 16113-8.

Lin, J., Gilbert, J., Rudek, M. A., Zwiebel, J. A., Gore, S., Jiemjit, A., Zhao, M., Baker, S. D., Ambinder, R. F., Herman, J. G., Donehower, R. C. & Carducci, M. A. 2009a. A phase I dose-finding study of 5-azacytidine in combination with sodium phenylbutyrate in patients with refractory solid tumors. *Clin Cancer Res,* 15**,** 6241-9.

Lin, J. H., Li, H., Yasumura, D., Cohen, H. R., Zhang, C., Panning, B., Shokat, K. M., Lavail, M. M. & Walter, P. 2007. IRE1 signaling affects cell fate during the unfolded protein response. *Science,* 318**,** 944-9.

Lin, J. H., Li, H., Zhang, Y., Ron, D. & Walter, P. 2009b. Divergent effects of PERK and IRE1 signaling on cell viability. *PLoS ONE,* 4**,** e4170.

Lin, X. S., Denmeade, S. R., Cisek, L. & Isaacs, J. T. 1997. Mechanism and role of growth arrest in programmed (apoptotic) death of prostatic cancer cells induced by thapsigargin. *Prostate,* 33**,** 201-7.

Lippincott-Schwartz, J., Bonifacino, J. S., Yuan, L. C. & Klausner, R. D. 1988. Degradation from the endoplasmic reticulum: disposing of newly synthesized proteins. *Cell,* 54**,** 209-20.

Liu, B. & Li, Z. 2008. Endoplasmic reticulum HSP90b1 (gp96, grp94) optimizes B-cell function via chaperoning integrin and TLR but not immunoglobulin. *Blood,* 112**,** 1223-30.

Liu, B. Q., Gao, Y. Y., Niu, X. F., Xie, J. S., Meng, X., Guan, Y. & Wang, H. Q. 2010. Implication of unfolded protein response in resveratrol-induced inhibition of K562 cell proliferation. *Biochem Biophys Res Commun,* 391**,** 778-82.

Lopez-Lazaro, M. 2010. A new view of carcinogenesis and an alternative approach to cancer therapy. *Mol Med,* 16**,** 144-53.

Lord, J. M., Roberts, L. M. & Lencer, W. I. 2005. Entry of protein toxins into mammalian cells by crossing the endoplasmic reticulum membrane: co-opting basic mechanisms of endoplasmic reticulum-associated degradation. *Curr Top Microbiol Immunol,* 300**,** 149-68.

Lovat, P. E., Corazzari, M., Armstrong, J. L., Martin, S., Pagliarini, V., Hill, D., Brown, A. M., Piacentini, M., Birch-Machin, M. A. & Redfern, C. P. 2008. Increasing melanoma cell death using inhibitors of protein disulfide isomerases to abrogate survival responses to endoplasmic reticulum stress. *Cancer Res,* 68**,** 5363-9.

Luo, S., Mao, C., Lee, B. & Lee, A. S. 2006. GRP78/BiP is required for cell proliferation and protecting the inner cell mass from apoptosis during early mouse embryonic development. *Mol Cell Biol,* 26**,** 5688-97.

Lust, S., Vanhoecke, B., M, V. A. N. G., Boelens, J., H, V. A. N. M., Kaileh, M., Vanden Berghe, W., Haegeman, G., Philippe, J., Bracke, M. & Offner, F. 2009. Xanthohumol activates the proapoptotic arm of the unfolded protein response in chronic lymphocytic leukemia. *Anticancer Res,* 29**,** 3797-805.

Lust, S., Vanhoecke, B., Van Gele, M., Philippe, J., Bracke, M. & Offner, F. 2010. The flavonoid tangeretin activates the unfolded protein response and synergizes with imatinib in the erythroleukemia cell line K562. *Mol Nutr Food Res,* 54**,** 823-32.

Ma, M. H., Yang, H. H., Parker, K., Manyak, S., Friedman, J. M., Altamirano, C., Wu, Z. Q., Borad, M. J., Frantzen, M., Roussos, E., Neeser, J., Mikail, A., Adams, J., Sjak-Shie, N., Vescio, R. A. & Berenson, J. R. 2003. The proteasome inhibitor PS-341 markedly enhances sensitivity of multiple myeloma tumor cells to chemotherapeutic agents. *Clin Cancer Res,* 9**,** 1136-44.

Ma, Y. & Hendershot, L. M. 2001. The unfolding tale of the unfolded protein response. *Cell,* 107**,** 827-30.

Ma, Y. & Hendershot, L. M. 2003. Delineation of a negative feedback regulatory loop that controls protein translation during endoplasmic reticulum stress. *J Biol Chem,* 278**,** 34864-73.

Ma, Y. & Hendershot, L. M. 2004a. ER chaperone functions during normal and stress conditions. *J Chem Neuroanat,* 28**,** 51-65.

Ma, Y. & Hendershot, L. M. 2004b. The role of the unfolded protein response in tumour development: friend or foe? *Nat Rev Cancer,* 4**,** 966-77.

Marcu, M. G., Doyle, M., Bertolotti, A., Ron, D., Hendershot, L. & Neckers, L. 2002. Heat shock protein 90 modulates the unfolded protein response by stabilizing IRE1alpha. *Mol Cell Biol,* 22**,** 8506-13.

Martinon, F., Chen, X., Lee, A. H. & Glimcher, L. H. 2010. TLR activation of the transcription factor XBP1 regulates innate immune responses in macrophages. *Nat Immunol,* 11**,** 411-8.

Martinon, F. & Glimcher, L. H. 2011. Regulation of innate immunity by signaling pathways emerging from the endoplasmic reticulum. *Curr Opin Immunol,* 23**,** 35-40.

Maschek, G., Savaraj, N., Priebe, W., Braunschweiger, P., Hamilton, K., Tidmarsh, G. F., De Young, L. R. & Lampidis, T. J. 2004. 2-deoxy-D-glucose increases the efficacy of adriamycin and paclitaxel in human osteosarcoma and non-small cell lung cancers in vivo. *Cancer Res,* 64**,** 31-4.

Mattson, M. P., Tomaselli, K. J. & Rydel, R. E. 1993. Calcium-destabilizing and neurodegenerative effects of aggregated beta-amyloid peptide are attenuated by basic FGF. *Brain Res,* 621**,** 35-49.

Mattson, M. P., Zhu, H., Yu, J. & Kindy, M. S. 2000. Presenilin-1 mutation increases neuronal vulnerability to focal ischemia in vivo and to hypoxia and glucose deprivation in cell culture: involvement of perturbed calcium homeostasis. *J Neurosci,* 20**,** 1358-64.

Mcconkey, D., Nawrocki, S. T. & Andtbacka, R. 2005. Velcade displays promising activity in primary effusion lymphoma cells. *Cancer Biol Ther,* 4**,** 491-2.

Mcconkey, D. J. & Zhu, K. 2008. Mechanisms of proteasome inhibitor action and resistance in cancer. *Drug Resist Updat*.

Mccracken, A. A. & Brodsky, J. L. 1996. Assembly of ER-associated protein degradation in vitro: dependence on cytosol, calnexin, and ATP. *J Cell Biol,* 132**,** 291-8.

Meister, S., Frey, B., Lang, V. R., Gaipl, U. S., Schett, G., Schlotzer-Schrehardt, U. & Voll, R. E. 2010. Calcium channel blocker verapamil enhances endoplasmic reticulum stress and cell death induced by proteasome inhibition in myeloma cells. *Neoplasia,* 12**,** 550-61.

Meusser, B., Hirsch, C., Jarosch, E. & Sommer, T. 2005. ERAD: the long road to destruction. *Nat Cell Biol,* 7**,** 766-72.

Mintz, P. J., Kim, J., Do, K. A., Wang, X., Zinner, R. G., Cristofanilli, M., Arap, M. A., Hong, W. K., Troncoso, P., Logothetis, C. J., Pasqualini, R. & Arap, W. 2003. Fingerprinting the circulating repertoire of antibodies from cancer patients. *Nat Biotechnol,* 21**,** 57-63.

Misra, U. K., Deedwania, R. & Pizzo, S. V. 2006. Activation and cross-talk between Akt, NF-kappaB, and unfolded protein response signaling in 1-LN prostate cancer cells consequent to ligation of cell surface-associated GRP78. *J Biol Chem,* 281**,** 13694-707.

Mitsiades, C. S., Mitsiades, N. S., Mcmullan, C. J., Poulaki, V., Kung, A. L., Davies, F. E., Morgan, G., Akiyama, M., Shringarpure, R., Munshi, N. C., Richardson, P. G., Hideshima, T., Chauhan, D., Gu, X., Bailey, C., Joseph, M., Libermann, T. A., Rosen, N. S. & Anderson, K. C. 2006. Antimyeloma activity of heat shock protein-90 inhibition. *Blood,* 107**,** 1092-100.

Mori, K., Ma, W., Gething, M. J. & Sambrook, J. 1993. A transmembrane protein with a cdc2+/CDC28-related kinase activity is required for signaling from the ER to the nucleus. *Cell,* 74**,** 743-56.

Mori, K., Sant, A., Kohno, K., Normington, K., Gething, M. J. & Sambrook, J. F. 1992. A 22 bp cis-acting element is necessary and sufficient for the induction of the yeast KAR2 (BiP) gene by unfolded proteins. *Embo J,* 11**,** 2583-93.

Munro, S. & Pelham, H. R. 1986. An Hsp70-like protein in the ER: identity with the 78 kd glucose-regulated protein and immunoglobulin heavy chain binding protein. *Cell,* 46**,** 291-300.

Munro, S. & Pelham, H. R. 1987. A C-terminal signal prevents secretion of luminal ER proteins. *Cell,* 48**,** 899-907.

Munshi, N. C., Hideshima, T., Carrasco, D., Shammas, M., Auclair, D., Davies, F., Mitsiades, N., Mitsiades, C., Kim, R. S., Li, C., Rajkumar, S. V., Fonseca, R., Bergsagel, L., Chauhan, D. & Anderson, K. C. 2004. Identification of genes modulated in multiple myeloma using genetically identical twin samples. *Blood,* 103**,** 1799-806.

Nakagawa, T., Zhu, H., Morishima, N., Li, E., Xu, J., Yankner, B. A. & Yuan, J. 2000. Caspase-12 mediates endoplasmic-reticulum-specific apoptosis and cytotoxicity by amyloid-beta. *Nature,* 403**,** 98-103.

Nakashima, T., Ishii, T., Tagaya, H., Seike, T., Nakagawa, H., Kanda, Y., Akinaga, S., Soga, S. & Shiotsu, Y. 2010. New molecular and biological mechanism of antitumor activities of

KW-2478, a novel nonansamycin heat shock protein 90 inhibitor, in multiple myeloma cells. *Clin Cancer Res,* 16**,** 2792-802.

Nawrocki, S. T., Carew, J. S., Dunner, K., Jr., Boise, L. H., Chiao, P. J., Huang, P., Abbruzzese, J. L. & Mcconkey, D. J. 2005a. Bortezomib inhibits PKR-like endoplasmic reticulum (ER) kinase and induces apoptosis via ER stress in human pancreatic cancer cells. *Cancer Res,* 65**,** 11510-9.

Nawrocki, S. T., Carew, J. S., Pino, M. S., Highshaw, R. A., Dunner, K., Jr., Huang, P., Abbruzzese, J. L. & Mcconkey, D. J. 2005b. Bortezomib sensitizes pancreatic cancer cells to endoplasmic reticulum stress-mediated apoptosis. *Cancer Res,* 65**,** 11658-66.

Neckers, L. 2002. Hsp90 inhibitors as novel cancer chemotherapeutic agents. *Trends Mol Med,* 8**,** S55-61.

Neckers, L. & Neckers, K. 2002. Heat-shock protein 90 inhibitors as novel cancer chemotherapeutic agents. *Expert Opin Emerg Drugs,* 7**,** 277-88.

Ni, M. & Lee, A. S. 2007. ER chaperones in mammalian development and human diseases. *FEBS Lett,* 581**,** 3641-51.

Ni, M., Zhang, Y. & Lee, A. S. 2011. Beyond the endoplasmic reticulum: atypical GRP78 in cell viability, signalling and therapeutic targeting. *Biochem J,* 434**,** 181-8.

Novoa, I., Zeng, H., Harding, H. P. & Ron, D. 2001. Feedback inhibition of the unfolded protein response by GADD34-mediated dephosphorylation of eIF2alpha. *J Cell Biol,* 153**,** 1011-22.

Novosyadlyy, R., Kurshan, N., Lann, D., Vijayakumar, A., Yakar, S. & Leroith, D. 2008. Insulin-like growth factor-I protects cells from ER stress-induced apoptosis via enhancement of the adaptive capacity of endoplasmic reticulum. *Cell Death Differ,* 15**,** 1304-17.

Obeng, E. A., Carlson, L. M., Gutman, D. M., Harrington, W. J., Jr., Lee, K. P. & Boise, L. H. 2006. Proteasome inhibitors induce a terminal unfolded protein response in multiple myeloma cells. *Blood,* 107**,** 4907-16.

Ogata, M., Hino, S., Saito, A., Morikawa, K., Kondo, S., Kanemoto, S., Murakami, T., Taniguchi, M., Tanii, I., Yoshinaga, K., Shiosaka, S., Hammarback, J. A., Urano, F. & Imaizumi, K. 2006. Autophagy is activated for cell survival after endoplasmic reticulum stress. *Mol Cell Biol,* 26**,** 9220-31.

Orlowski, R. Z. & Kuhn, D. J. 2008. Proteasome inhibitors in cancer therapy: lessons from the first decade. *Clin Cancer Res,* 14**,** 1649-57.

Ozcan, U., Cao, Q., Yilmaz, E., Lee, A. H., Iwakoshi, N. N., Ozdelen, E., Tuncman, G., Gorgun, C., Glimcher, L. H. & Hotamisligil, G. S. 2004. Endoplasmic reticulum stress links obesity, insulin action, and type 2 diabetes. *Science,* 306**,** 457-61.

Ozcan, U., Yilmaz, E., Ozcan, L., Furuhashi, M., Vaillancourt, E., Smith, R. O., Gorgun, C. Z. & Hotamisligil, G. S. 2006. Chemical chaperones reduce ER stress and restore glucose homeostasis in a mouse model of type 2 diabetes. *Science,* 313**,** 1137-40.

Papandreou, I., Denko, N. C., Olson, M., Van Melckebeke, H., Lust, S., Tam, A., Solow-Cordero, D. E., Bouley, D. M., Offner, F., Niwa, M. & Koong, A. C. 2011. Identification of

an Ire1alpha endonuclease specific inhibitor with cytotoxic activity against human multiple myeloma. *Blood,* 117**,** 1311-4.

Park, H. R., Furihata, K., Hayakawa, Y. & Shin-Ya, K. 2002. Versipelostatin, a novel GRP78/Bip molecular chaperone down-regulator of microbial origin. *Tetrahedron Letters,* 43**,** 6941-45.

Park, H. R., Tomida, A., Sato, S., Tsukumo, Y., Yun, J., Yamori, T., Hayakawa, Y., Tsuruo, T. & Shin-Ya, K. 2004. Effect on tumor cells of blocking survival response to glucose deprivation. *J Natl Cancer Inst,* 96**,** 1300-10.

Paschen, W. 2004. Endoplasmic reticulum dysfunction in brain pathology: critical role of protein synthesis. *Curr Neurovasc Res,* 1**,** 173-81.

Paschen, W., Aufenberg, C., Hotop, S. & Mengesdorf, T. 2003. Transient cerebral ischemia activates processing of xbp1 messenger RNA indicative of endoplasmic reticulum stress. *J Cereb Blood Flow Metab,* 23**,** 449-61.

Patil, C. & Walter, P. 2001. Intracellular signaling from the endoplasmic reticulum to the nucleus: the unfolded protein response in yeast and mammals. *Curr Opin Cell Biol,* 13**,** 349-55.

Patterson, J., Palombella, V. J., Fritz, C. & Normant, E. 2008. IPI-504, a novel and soluble HSP-90 inhibitor, blocks the unfolded protein response in multiple myeloma cells. *Cancer Chemother Pharmacol,* 61**,** 923-32.

Pfaffenbach, K. T. & Lee, A. S. 2010. The critical role of GRP78 in physiologic and pathologic stress. *Curr Opin Cell Biol*.

Pincus, D., Chevalier, M. W., Aragon, T., Van Anken, E., Vidal, S. E., El-Samad, H. & Walter, P. 2010. BiP binding to the ER-stress sensor Ire1 tunes the homeostatic behavior of the unfolded protein response. *PLoS Biol,* 8**,** e1000415.

Pootrakul, L., Datar, R. H., Shi, S. R., Cai, J., Hawes, D., Groshen, S. G., Lee, A. S. & Cote, R. J. 2006. Expression of stress response protein Grp78 is associated with the development of castration-resistant prostate cancer. *Clin Cancer Res,* 12**,** 5987-93.

Porter, K. R., Claude, A. And Fullam. E.F. 1945. A STUDY OF TISSUE CULTURE CELLS BY ELECTRON MICROSCOPY: METHODS AND PRELIMINARY OBSERVATIONS *J. Exp. Med.,* 81**,** 233-246.

Pyrko, P., Kardosh, A. & Schonthal, A. H. 2008. Celecoxib transiently inhibits cellular protein synthesis. *Biochem Pharmacol,* 75**,** 395-404.

Pyrko, P., Kardosh, A., Wang, W., Xiong, W., Schonthal, A. H. & Chen, T. C. 2007a. HIV-1 protease inhibitors nelfinavir and atazanavir induce malignant glioma death by triggering endoplasmic reticulum stress. *Cancer Res,* 67**,** 10920-8.

Pyrko, P., Schonthal, A. H., Hofman, F. M., Chen, T. C. & Lee, A. S. 2007b. The unfolded protein response regulator GRP78/BiP as a novel target for increasing chemosensitivity in malignant gliomas. *Cancer Res,* 67**,** 9809-16.

Pyrko, P., Soriano, N., Kardosh, A., Liu, Y. T., Uddin, J., Petasis, N. A., Hofman, F. M., Chen, C. S., Chen, T. C. & Schonthal, A. H. 2006. Downregulation of survivin expression and concomitant induction of apoptosis by celecoxib and its non-cyclooxygenase-2-

inhibitory analog, dimethyl-celecoxib (DMC), in tumor cells in vitro and in vivo. *Mol Cancer,* 5**,** 19.

Raez, L. E., Langmuir, V. K., Papadopoulus, K., Ricart, A., Rocha-Lima, C. M., Rosenblatt, J., Schlesselman, J., Colowick, A., Jung, D. & Lampidis, T. 2006. Phase I trial of glycolitic inhibition with 2-deoxyglucose and docetaxel for patients with solid tumors. *Proc Amer Assoc Cancer Res,* 47**,** Abstract no 515.

Rahmani, M., Davis, E. M., Crabtree, T. R., Habibi, J. R., Nguyen, T. K., Dent, P. & Grant, S. 2007. The kinase inhibitor sorafenib induces cell death through a process involving induction of endoplasmic reticulum stress. *Mol Cell Biol,* 27**,** 5499-513.

Rahmani, M., Mayo, M., Dash, R., Sokhi, U. K., Dmitriev, I. P., Sarkar, D., Dent, P., Curiel, D. T., Fisher, P. B. & Grant, S. 2010. Melanoma differentiation associated gene-7/interleukin-24 potently induces apoptosis in human myeloid leukemia cells through a process regulated by endoplasmic reticulum stress. *Mol Pharmacol,* 78**,** 1096-104.

Ranganathan, A. C., Ojha, S., Kourtidis, A., Conklin, D. S. & Aguirre-Ghiso, J. A. 2008. Dual function of pancreatic endoplasmic reticulum kinase in tumor cell growth arrest and survival. *Cancer Res,* 68**,** 3260-8.

Ranganathan, A. C., Zhang, L., Adam, A. P. & Aguirre-Ghiso, J. A. 2006. Functional coupling of p38-induced up-regulation of BiP and activation of RNA-dependent protein kinase-like endoplasmic reticulum kinase to drug resistance of dormant carcinoma cells. *Cancer Res,* 66**,** 1702-11.

Raven, J. F., Baltzis, D., Wang, S., Mounir, Z., Papadakis, A. I., Gao, H. Q. & Koromilas, A. E. 2008. PKR and PKR-like endoplasmic reticulum kinase induce the proteasome-dependent degradation of cyclin D1 via a mechanism requiring eukaryotic initiation factor 2alpha phosphorylation. *J Biol Chem,* 283**,** 3097-108.

Reddy, R. K., Mao, C., Baumeister, P., Austin, R. C., Kaufman, R. J. & Lee, A. S. 2003. Endoplasmic reticulum chaperone protein GRP78 protects cells from apoptosis induced by topoisomerase inhibitors: role of ATP binding site in suppression of caspase-7 activation. *J Biol Chem,* 278**,** 20915-24.

Reimold, A. M., Iwakoshi, N. N., Manis, J., Vallabhajosyula, P., Szomolanyi-Tsuda, E., Gravallese, E. M., Friend, D., Grusby, M. J., Alt, F. & Glimcher, L. H. 2001. Plasma cell differentiation requires the transcription factor XBP-1. *Nature,* 412**,** 300-7.

Riccioni, R., Senese, M., Diverio, D., Riti, V., Buffolino, S., Mariani, G., Boe, A., Cedrone, M., Lo-Coco, F., Foa, R., Peschle, C. & Testa, U. 2007. M4 and M5 acute myeloid leukaemias display a high sensitivity to Bortezomib-mediated apoptosis. *Br J Haematol,* 139**,** 194-205.

Richardson, P. G., Mitsiades, C., Hideshima, T. & Anderson, K. C. 2006. Bortezomib: proteasome inhibition as an effective anticancer therapy. *Annu Rev Med,* 57**,** 33-47.

Rodriguez-Gonzalez, A., Lin, T., Ikeda, A. K., Simms-Waldrip, T., Fu, C. & Sakamoto, K. M. 2008. Role of the aggresome pathway in cancer: targeting histone deacetylase 6-dependent protein degradation. *Cancer Res,* 68**,** 2557-60.

Romero-Ramirez, L., Cao, H., Nelson, D., Hammond, E., Lee, A. H., Yoshida, H., Mori, K., Glimcher, L. H., Denko, N. C., Giaccia, A. J., Le, Q. T. & Koong, A. C. 2004. XBP1 is

essential for survival under hypoxic conditions and is required for tumor growth. *Cancer Res,* 64**,** 5943-7.

Romero-Ramirez, L., Cao, H., Regalado, M. P., Kambham, N., Siemann, D., Kim, J. J., Le, Q. T. & Koong, A. C. 2009. X box-binding protein 1 regulates angiogenesis in human pancreatic adenocarcinomas. *Transl Oncol,* 2**,** 31-8.

Ron, D. 2002. Translational control in the endoplasmic reticulum stress response. *J Clin Invest,* 110**,** 1383-8.

Roue, G., Perez-Galan, P., Mozos, A., Lopez-Guerra, M., Xargay-Torrent, S., Rosich, L., Saborit-Villarroya, I., Normant, E., Campo, E. & Colomer, D. 2011. The Hsp90 inhibitor IPI-504 overcomes bortezomib resistance in mantle cell lymphoma in vitro and in vivo by down-regulation of the prosurvival ER chaperone BiP/Grp78. *Blood,* 117**,** 1270-9.

Rubenstein, R. C., Egan, M. E. & Zeitlin, P. L. 1997. In vitro pharmacologic restoration of CFTR-mediated chloride transport with sodium 4-phenylbutyrate in cystic fibrosis epithelial cells containing delta F508-CFTR. *J Clin Invest,* 100**,** 2457-65.

Rutkowski, D. T., Kang, S. W., Goodman, A. G., Garrison, J. L., Taunton, J., Katze, M. G., Kaufman, R. J. & Hegde, R. S. 2007. The role of p58IPK in protecting the stressed endoplasmic reticulum. *Mol Biol Cell,* 18**,** 3681-91.

Sagara, Y. & Inesi, G. 1991. Inhibition of the sarcoplasmic reticulum Ca2+ transport ATPase by thapsigargin at subnanomolar concentrations. *J Biol Chem,* 266**,** 13503-6.

Saito, S., Furuno, A., Sakurai, J., Sakamoto, A., Park, H. R., Shin-Ya, K., Tsuruo, T. & Tomida, A. 2009. Chemical genomics identifies the unfolded protein response as a target for selective cancer cell killing during glucose deprivation. *Cancer Res,* 69**,** 4225-34.

Sato, N., Imaizumi, K., Manabe, T., Taniguchi, M., Hitomi, J., Katayama, T., Yoneda, T., Morihara, T., Yasuda, Y., Takagi, T., Kudo, T., Tsuda, T., Itoyama, Y., Makifuchi, T., Fraser, P. E., St George-Hyslop, P. & Tohyama, M. 2001. Increased production of beta-amyloid and vulnerability to endoplasmic reticulum stress by an aberrant spliced form of presenilin 2. *J Biol Chem,* 276**,** 2108-14.

Schewe, D. M. & Aguirre-Ghiso, J. A. 2008. ATF6alpha-Rheb-mTOR signaling promotes survival of dormant tumor cells in vivo. *Proc Natl Acad Sci U S A,* 105**,** 10519-24.

Schroder, M. & Kaufman, R. J. 2005a. ER stress and the unfolded protein response. *Mutat Res,* 569**,** 29-63.

Schroder, M. & Kaufman, R. J. 2005b. The mammalian unfolded protein response. *Annu Rev Biochem,* 74**,** 739-89.

Schubert, U., Anton, L. C., Gibbs, J., Norbury, C. C., Yewdell, J. W. & Bennink, J. R. 2000. Rapid degradation of a large fraction of newly synthesized proteins by proteasomes. *Nature,* 404**,** 770-4.

Selkoe, D. J. 2003. Folding proteins in fatal ways. *Nature,* 426**,** 900-4.

Shanmugam, M., Mcbrayer, S. K. & Rosen, S. T. 2009. Targeting the Warburg effect in hematological malignancies: from PET to therapy. *Curr Opin Oncol,* 21**,** 531-6.

Shen, J., Hughes, C., Chao, C., Cai, J., Bartels, C., Gessner, T. & Subjeck, J. 1987. Coinduction of glucose-regulated proteins and doxorubicin resistance in Chinese hamster cells. *Proc Natl Acad Sci U S A,* 84**,** 3278-82.

Shen, J., Snapp, E. L., Lippincott-Schwartz, J. & Prywes, R. 2005. Stable binding of ATF6 to BiP in the endoplasmic reticulum stress response. *Mol Cell Biol,* 25**,** 921-32.

Shen, J. W., Subjeck, J. R., Lock, R. B. & Ross, W. E. 1989. Depletion of topoisomerase II in isolated nuclei during a glucose-regulated stress response. *Mol Cell Biol,* 9**,** 3284-91.

Shen, X., Ellis, R. E., Lee, K., Liu, C. Y., Yang, K., Solomon, A., Yoshida, H., Morimoto, R., Kurnit, D. M., Mori, K. & Kaufman, R. J. 2001. Complementary signaling pathways regulate the unfolded protein response and are required for C. elegans development. *Cell,* 107**,** 893-903.

Shi, Y., Vattem, K. M., Sood, R., An, J., Liang, J., Stramm, L. & Wek, R. C. 1998. Identification and characterization of pancreatic eukaryotic initiation factor 2 alpha-subunit kinase, PEK, involved in translational control. *Mol Cell Biol,* 18**,** 7499-509.

Shimura, H., Hattori, N., Kubo, S., Mizuno, Y., Asakawa, S., Minoshima, S., Shimizu, N., Iwai, K., Chiba, T., Tanaka, K. & Suzuki, T. 2000. Familial Parkinson disease gene product, parkin, is a ubiquitin-protein ligase. *Nat Genet,* 25**,** 302-5.

Shin-Ya, K. 2005. Novel antitumor and neuroprotective substances discovered by characteristic screenings based on specific molecular targets. *Biosci Biotechnol Biochem,* 69**,** 867-72.

Shiu, R. P., Pouyssegur, J. & Pastan, I. 1977. Glucose depletion accounts for the induction of two transformation-sensitive membrane proteinsin Rous sarcoma virus-transformed chick embryo fibroblasts. *Proc Natl Acad Sci U S A,* 74**,** 3840-4.

Shuda, M., Kondoh, N., Imazeki, N., Tanaka, K., Okada, T., Mori, K., Hada, A., Arai, M., Wakatsuki, T., Matsubara, O., Yamamoto, N. & Yamamoto, M. 2003. Activation of the ATF6, XBP1 and grp78 genes in human hepatocellular carcinoma: a possible involvement of the ER stress pathway in hepatocarcinogenesis. *J Hepatol,* 38**,** 605-14.

Simons, A. L., Ahmad, I. M., Mattson, D. M., Dornfeld, K. J. & Spitz, D. R. 2007. 2-Deoxy-D-glucose combined with cisplatin enhances cytotoxicity via metabolic oxidative stress in human head and neck cancer cells. *Cancer Res,* 67**,** 3364-70.

Sitia, R. & Braakman, I. 2003. Quality control in the endoplasmic reticulum protein factory. *Nature,* 426**,** 891-4.

Smith, J. R. & Workman, P. 2007. Targeting the cancer chaperone HSP90. *Drug Discov Today: Ther Strategies,* 4**,** 219-27.

Sommer, T. & Jentsch, S. 1993. A protein translocation defect linked to ubiquitin conjugation at the endoplasmic reticulum. *Nature,* 365**,** 176-9.

Sriburi, R., Jackowski, S., Mori, K. & Brewer, J. W. 2004. XBP1: a link between the unfolded protein response, lipid biosynthesis, and biogenesis of the endoplasmic reticulum. *J Cell Biol,* 167**,** 35-41.

Szegezdi, E., Logue, S. E., Gorman, A. M. & Samali, A. 2006. Mediators of endoplasmic reticulum stress-induced apoptosis. *EMBO Rep,* 7**,** 880-5.

Tannock, I. 2005. *The basic science of oncology,* New York, McGraw-Hill, Medical Pub. Division.

The_Non-Hodgkin's_Lymphoma_Classification_Project 1997. A clinical evaluation of the International Lymphoma Study Group classification of non-Hodgkin's lymphoma. The Non-Hodgkin's Lymphoma Classification Project. *Blood,* 89**,** 3909-18.

Thuerauf, D. J., Marcinko, M., Belmont, P. J. & Glembotski, C. C. 2007. Effects of the isoform-specific characteristics of ATF6 alpha and ATF6 beta on endoplasmic reticulum stress response gene expression and cell viability. *J Biol Chem,* 282**,** 22865-78.

Tirasophon, W., Welihinda, A. A. & Kaufman, R. J. 1998. A stress response pathway from the endoplasmic reticulum to the nucleus requires a novel bifunctional protein kinase/endoribonuclease (Ire1p) in mammalian cells. *Genes Dev,* 12**,** 1812-24.

Toth, A., Nickson, P., Mandl, A., Bannister, M. L., Toth, K. & Erhardt, P. 2007. Endoplasmic reticulum stress as a novel therapeutic target in heart diseases. *Cardiovasc Hematol Disord Drug Targets,* 7**,** 205-18.

Trepel, J., Mollapour, M., Giaccone, G. & Neckers, L. 2010. Targeting the dynamic HSP90 complex in cancer. *Nat Rev Cancer,* 10**,** 537-49.

Tsutsumi, S., Gotoh, T., Tomisato, W., Mima, S., Hoshino, T., Hwang, H. J., Takenaka, H., Tsuchiya, T., Mori, M. & Mizushima, T. 2004. Endoplasmic reticulum stress response is involved in nonsteroidal anti-inflammatory drug-induced apoptosis. *Cell Death Differ,* 11**,** 1009-16.

Tsutsumi, S., Namba, T., Tanaka, K. I., Arai, Y., Ishihara, T., Aburaya, M., Mima, S., Hoshino, T. & Mizushima, T. 2006. Celecoxib upregulates endoplasmic reticulum chaperones that inhibit celecoxib-induced apoptosis in human gastric cells. *Oncogene,* 25**,** 1018-29.

Uemura, A., Oku, M., Mori, K. & Yoshida, H. 2009. Unconventional splicing of XBP1 mRNA occurs in the cytoplasm during the mammalian unfolded protein response. *J Cell Sci,* 122**,** 2877-86.

Urano, F., Wang, X., Bertolotti, A., Zhang, Y., Chung, P., Harding, H. P. & Ron, D. 2000. Coupling of stress in the ER to activation of JNK protein kinases by transmembrane protein kinase IRE1. *Science,* 287**,** 664-6.

Van Huizen, R., Martindale, J. L., Gorospe, M. & Holbrook, N. J. 2003. P58IPK, a novel endoplasmic reticulum stress-inducible protein and potential negative regulator of eIF2alpha signaling. *J Biol Chem,* 278**,** 15558-64.

Vembar, S. S. & Brodsky, J. L. 2008. One step at a time: endoplasmic reticulum-associated degradation. *Nat Rev Mol Cell Biol,* 9**,** 944-57.

Vink, J., Cloos, J. & Kaspers, G. J. 2006. Proteasome inhibition as novel treatment strategy in leukaemia. *Br J Haematol,* 134**,** 253-62.

Volkmann, K., Lucas, J. L., Vuga, D., Wang, X., Brumm, D., Stiles, C., Kriebel, D., Der-Sarkissian, A., Krishnan, K., Schweitzer, C., Liu, Z., Malyankar, U. M., Chiovitti, D., Canny, M., Durocher, D., Sicheri, F. & Patterson, J. B. 2011. Potent and selective inhibitors of the inositol-requiring enzyme 1 endoribonuclease. *J Biol Chem*.

Wang, Q., He, Z., Zhang, J., Wang, Y., Wang, T., Tong, S., Wang, L., Wang, S. & Chen, Y. 2005. Overexpression of endoplasmic reticulum molecular chaperone GRP94 and GRP78 in human lung cancer tissues and its significance. *Cancer Detect Prev,* 29**,** 544-51.

Wang, X. Z., Harding, H. P., Zhang, Y., Jolicoeur, E. M., Kuroda, M. & Ron, D. 1998. Cloning of mammalian Ire1 reveals diversity in the ER stress responses. *Embo J,* 17**,** 5708-17.

Warburg, O. 1956. On the origin of cancer cells. *Science,* 123**,** 309-14.

Webb, J. L. 1963. *Enzyme and metabolic inhibitors : volume 1 general principles of inhibition,* [S.l.], Academic press.

Welch, W. J. & Brown, C. R. 1996. Influence of molecular and chemical chaperones on protein folding. *Cell Stress Chaperones,* 1**,** 109-15.

Wellen, K. E. & Thompson, C. B. 2010. Cellular metabolic stress: considering how cells respond to nutrient excess. *Mol Cell,* 40**,** 323-32.

Wouters, B. G. & Koritzinsky, M. 2008. Hypoxia signalling through mTOR and the unfolded protein response in cancer. *Nat Rev Cancer*.

Wu, J. & Kaufman, R. J. 2006. From acute ER stress to physiological roles of the Unfolded Protein Response. *Cell Death Differ,* 13**,** 374-84.

Wu, J., Rutkowski, D. T., Dubois, M., Swathirajan, J., Saunders, T., Wang, J., Song, B., Yau, G. D. & Kaufman, R. J. 2007. ATF6alpha optimizes long-term endoplasmic reticulum function to protect cells from chronic stress. *Dev Cell,* 13**,** 351-64.

Wu, Y., Fabritius, M. & Ip, C. 2009. Chemotherapeutic sensitization by endoplasmic reticulum stress: increasing the efficacy of taxane against prostate cancer. *Cancer Biol Ther,* 8**,** 146-52.

Xing, X., Lai, M., Wang, Y., Xu, E. & Huang, Q. 2006. Overexpression of glucose-regulated protein 78 in colon cancer. *Clin Chim Acta,* 364**,** 308-15.

Yaari-Stark, S., Shaked, M., Nevo-Caspi, Y., Jacob-Hircsh, J., Shamir, R., Rechavi, G. & Kloog, Y. 2010. Ras inhibits endoplasmic reticulum stress in human cancer cells with amplified Myc. *Int J Cancer,* 126**,** 2268-81.

Yacoub, A., Hamed, H. A., Allegood, J., Mitchell, C., Spiegel, S., Lesniak, M. S., Ogretmen, B., Dash, R., Sarkar, D., Broaddus, W. C., Grant, S., Curiel, D. T., Fisher, P. B. & Dent, P. 2010a. PERK-dependent regulation of ceramide synthase 6 and thioredoxin play a key role in mda-7/IL-24-induced killing of primary human glioblastoma multiforme cells. *Cancer Res,* 70**,** 1120-9.

Yacoub, A., Liu, R., Park, M. A., Hamed, H. A., Dash, R., Schramm, D. N., Sarkar, D., Dimitriev, I. P., Bell, J. K., Grant, S., Farrell, N. P., Curiel, D. T., Fisher, P. B. & Dent, P. 2010b. Cisplatin enhances protein kinase R-like endoplasmic reticulum kinase- and CD95-dependent melanoma differentiation-associated gene-7/interleukin-24-induced killing in ovarian carcinoma cells. *Mol Pharmacol,* 77**,** 298-310.

Yamada, M., Tomida, A., Yun, J., Cai, B., Yoshikawa, H., Taketani, Y. & Tsuruo, T. 1999. Cellular sensitization to cisplatin and carboplatin with decreased removal of platinum-DNA adduct by glucose-regulated stress. *Cancer Chemother Pharmacol,* 44**,** 59-64.

Yamaguchi, Y., Larkin, D., Lara-Lemus, R., Ramos-Castaneda, J., Liu, M. & Arvan, P. 2008. Endoplasmic reticulum (ER) chaperone regulation and survival of cells compensating for deficiency in the ER stress response kinase, PERK. *J Biol Chem,* 283**,** 17020-9.

Yamamoto, K., Sato, T., Matsui, T., Sato, M., Okada, T., Yoshida, H., Harada, A. & Mori, K. 2007. Transcriptional induction of mammalian ER quality control proteins is mediated by single or combined action of ATF6alpha and XBP1. *Dev Cell,* 13**,** 365-76.

Yan, W., Frank, C. L., Korth, M. J., Sopher, B. L., Novoa, I., Ron, D. & Katze, M. G. 2002. Control of PERK eIF2alpha kinase activity by the endoplasmic reticulum stress-induced molecular chaperone P58IPK. *Proc Natl Acad Sci U S A,* 99**,** 15920-5.

Yanagitani, K., Imagawa, Y., Iwawaki, T., Hosoda, A., Saito, M., Kimata, Y. & Kohno, K. 2009. Cotranslational targeting of XBP1 protein to the membrane promotes cytoplasmic splicing of its own mRNA. *Mol Cell,* 34**,** 191-200.

Yang, C., Tong, Y., Ni, W., Liu, J., Xu, W., Li, L., Liu, X., Meng, H. & Qian, W. 2010. Inhibition of autophagy induced by overexpression of mda-7/interleukin-24 strongly augments the antileukemia activity in vitro and in vivo. *Cancer Gene Ther,* 17**,** 109-19.

Yang, Y. & Li, Z. 2005. Roles of heat shock protein gp96 in the ER quality control: redundant or unique function? *Mol Cells,* 20**,** 173-82.

Yoshida, H. 2009. ER stress response, peroxisome proliferation, mitochondrial unfolded protein response and Golgi stress response. *IUBMB Life,* 61**,** 871-9.

Yoshida, H., Haze, K., Yanagi, H., Yura, T. & Mori, K. 1998. Identification of the cis-acting endoplasmic reticulum stress response element responsible for transcriptional induction of mammalian glucose-regulated proteins. Involvement of basic leucine zipper transcription factors. *J Biol Chem,* 273**,** 33741-9.

Yoshida, H., Matsui, T., Yamamoto, A., Okada, T. & Mori, K. 2001. XBP1 mRNA is induced by ATF6 and spliced by IRE1 in response to ER stress to produce a highly active transcription factor. *Cell,* 107**,** 881-91.

Yu, X., Guo, Z. S., Marcu, M. G., Neckers, L., Nguyen, D. M., Chen, G. A. & Schrump, D. S. 2002. Modulation of p53, ErbB1, ErbB2, and Raf-1 expression in lung cancer cells by depsipeptide FR901228. *J Natl Cancer Inst,* 94**,** 504-13.

Yun, J., Tomida, A., Andoh, T. & Tsuruo, T. 2004. Interaction between glucose-regulated destruction domain of DNA topoisomerase IIalpha and MPN domain of Jab1/CSN5. *J Biol Chem,* 279**,** 31296-303.

Yun, J., Tomida, A., Nagata, K. & Tsuruo, T. 1995. Glucose-regulated stresses confer resistance to VP-16 in human cancer cells through a decreased expression of DNA topoisomerase II. *Oncol Res,* 7**,** 583-90.

Zeitlin, P. L., Diener-West, M., Rubenstein, R. C., Boyle, M. P., Lee, C. K. & Brass-Ernst, L. 2002. Evidence of CFTR function in cystic fibrosis after systemic administration of 4-phenylbutyrate. *Mol Ther,* 6**,** 119-26.

Zhang, K., Wong, H. N., Song, B., Miller, C. N., Scheuner, D. & Kaufman, R. J. 2005. The unfolded protein response sensor IRE1alpha is required at 2 distinct steps in B cell lymphopoiesis. *J Clin Invest,* 115**,** 268-81.

Zhang, L. J., Chen, S., Wu, P., Hu, C. S., Thorne, R. F., Luo, C. M., Hersey, P. & Zhang, X. D. 2008. Inhibition of MEK blocks GRP78 up-regulation and enhances apoptosis induced by ER stress in gastric cancer cells. *Cancer Lett*.

Zhang, X. D., Gillespie, S. K., Borrow, J. M. & Hersey, P. 2004. The histone deacetylase inhibitor suberic bishydroxamate regulates the expression of multiple apoptotic mediators and induces mitochondria-dependent apoptosis of melanoma cells. *Mol Cancer Ther,* 3**,** 425-35.

Zhang, Y., Liu, R., Ni, M., Gill, P. & Lee, A. S. 2010. Cell surface relocalization of the endoplasmic reticulum chaperone and unfolded protein response regulator GRP78/BiP. *J Biol Chem,* 285**,** 15065-75.

Zhao, L. & Ackerman, S. L. 2006. Endoplasmic reticulum stress in health and disease. *Curr Opin Cell Biol,* 18**,** 444-52.

Zinszner, H., Kuroda, M., Wang, X., Batchvarova, N., Lightfoot, R. T., Remotti, H., Stevens, J. L. & Ron, D. 1998. CHOP is implicated in programmed cell death in response to impaired function of the endoplasmic reticulum. *Genes Dev,* 12**,** 982-95.

11. Appendices

Appendix 1

Additional data for chapter 3:

Cell line	Conc.	Cell no. (% of control)			Average	SD
		Set 1	Set 2	Set 3		
HL-60	**0**	100.0	100.0	100.0	**100.0**	**0.0**
HL-60	**10nM**	80.2	85.6	85.7	**83.8**	**3.1**
HL-60	**100nM**	84.4	87.7	80.8	**84.3**	**3.5**
HL-60	**1µM**	48.7	51.0	46.3	**48.7**	**2.4**
HL-60	**10µM**	49.2	47.0	44.4	**46.9**	**2.4**
HL-60	**100µM**	23.6	20.8	31.7	**25.4**	**5.7**
THP-1	**0**	100.0	100.0	100.0	**100.0**	**0.0**
THP-1	**10nM**	66.2	80.2	88.6	**78.3**	**11.3**
THP-1	**100nM**	43.8	53.9	58.3	**52.0**	**7.4**
THP-1	**1µM**	42.8	50.4	42.8	**45.3**	**4.4**
THP-1	**10µM**	49.4	44.7	40.4	**44.8**	**4.5**
THP-1	**100µM**	31.3	33.1	30.2	**31.5**	**1.5**
RPMI-8226	**0**	100.0	100.0	100.0	**100.0**	**0.0**
RPMI-8226	**10nM**	97.9	94.8	91.1	**94.6**	**3.4**
RPMI-8226	**100nM**	95.5	77.5	93.7	**88.9**	**9.9**
RPMI-8226	**1µM**	75.9	61.9	62.3	**66.7**	**8.0**
RPMI-8226	**10µM**	62.8	54.8	59.8	**59.1**	**4.0**
RPMI-8226	**100µM**	40.4	31.4	44.7	**38.8**	**6.8**
U266	**0**	100.0	100.0	100.0	**100.0**	**0.0**
U266	**10nM**	87.0	91.8	93.0	**90.6**	**3.2**
U266	**100nM**	86.3	85.9	89.6	**87.3**	**2.0**
U266	**1µM**	71.0	78.7	76.8	**75.5**	**4.0**
U266	**10µM**	63.6	62.2	68.0	**64.6**	**3.0**
U266	**100µM**	38.1	47.4	60.0	**48.5**	**11.0**
DOHH2	**0**	100.0	100.0	100.0	**100.0**	**0.0**
DOHH2	**10nM**	99.9	100.5	95.6	**98.7**	**2.7**
DOHH2	**100nM**	75.8	79.3	79.1	**78.1**	**2.0**
DOHH2	**1µM**	50.2	43.4	40.0	**44.5**	**5.2**
DOHH2	**10µM**	44.7	34.8	38.3	**39.3**	**5.0**
DOHH2	**100µM**	31.0	32.1	31.0	**31.4**	**0.6**
SUD4	**0**	100.0	100.0	100.0	**100.0**	**0.0**
SUD4	**10nM**	93.3	70.4	84.8	**82.8**	**11.6**
SUD4	**100nM**	61.0	56.4	56.1	**57.8**	**2.7**
SUD4	**1µM**	50.9	43.9	31.4	**42.1**	**9.9**
SUD4	**10µM**	33.3	46.4	31.9	**37.2**	**8.0**
SUD4	**100µM**	18.7	21.5	20.2	**20.1**	**1.4**

Table A1.1. Effect of tunicamycin treatment for 48 hours on cell number

Cell line	Conc.	Cell viability (%)			Average	SD
		Set 1	Set 2	Set 3		
HL-60	**0**	90.0	94.6	90.2	**91.6**	**2.6**
HL-60	**10nM**	82.1	84.7	89.4	**85.4**	**3.7**
HL-60	**100nM**	84.2	83.1	88.1	**85.1**	**2.6**
HL-60	**1µM**	52.6	68.6	70.0	**63.7**	**9.7**
HL-60	**10µM**	53.1	60.9	67.4	**60.5**	**7.1**
HL-60	**100µM**	83.0	81.7	95.2	**86.6**	**7.4**
THP-1	**0**	96.0	96.2	95.4	**95.9**	**0.5**
THP-1	**10nM**	92.2	95.5	94.2	**94.0**	**1.7**
THP-1	**100nM**	75.0	86.9	76.1	**79.3**	**6.6**
THP-1	**1µM**	74.3	76.5	63.0	**71.2**	**7.2**
THP-1	**10µM**	58.3	66.1	58.9	**61.1**	**4.4**
THP-1	**100µM**	47.3	60.6	79.1	**62.3**	**16.0**
RPMI-8226	**0**	91.1	90.7	85.5	**89.1**	**3.1**
RPMI-8226	**10nM**	84.4	90.2	86.6	**87.1**	**2.9**
RPMI-8226	**100nM**	78.3	89.3	85.7	**84.5**	**5.6**
RPMI-8226	**1µM**	51.4	59.3	57.5	**56.1**	**4.2**
RPMI-8226	**10µM**	40.2	35.9	25.2	**33.8**	**7.7**
RPMI-8226	**100µM**	8.2	28.7	15.6	**17.5**	**10.4**
U266	**0**	90.1	94.6	92.6	**92.4**	**2.3**
U266	**10nM**	89.2	94.2	93.2	**92.2**	**2.6**
U266	**100nM**	86.1	90.5	88.3	**88.3**	**2.2**
U266	**1µM**	80.9	83.7	92.1	**85.6**	**5.8**
U266	**10µM**	69.8	89.7	87.2	**82.2**	**10.8**
U266	**100µM**	35.3	40.4	54.2	**43.3**	**9.8**
DOHH2	**0**	83.6	88.5	80.1	**84.1**	**4.2**
DOHH2	**10nM**	74.9	88.8	84.4	**82.7**	**7.1**
DOHH2	**100nM**	57.5	64.1	67.9	**63.2**	**5.3**
DOHH2	**1µM**	21.2	22.7	21.7	**21.9**	**0.8**
DOHH2	**10µM**	24.0	23.5	22.4	**23.3**	**0.9**
DOHH2	**100µM**	25.8	23.4	24.9	**24.7**	**1.2**
SUD4	**0**	89.4	90.4	94.3	**91.4**	**2.6**
SUD4	**10nM**	90.8	95.0	93.9	**93.3**	**2.2**
SUD4	**100nM**	74.1	76.7	84.3	**78.4**	**5.3**
SUD4	**1µM**	51.4	54.5	58.4	**54.8**	**3.5**
SUD4	**10µM**	58.8	40.9	54.0	**51.2**	**9.2**
SUD4	**100µM**	5.9	0.0	31.5	**12.5**	**16.8**

Table A1.2. Effect of tunicamycin treatment for 48 hours on cell viability

Cell line	Conc.	Cell no. (% of control)			Average	SD
		Set 1	Set 2	Set 3		
HL-60	**0**	100.0	100.0	100.0	**100.0**	**0.0**
HL-60	**1nM**	67.0	69.4	82.0	**72.8**	**8.1**
HL-60	**10nM**	51.5	50.2	39.5	**47.1**	**6.6**
HL-60	**100nM**	53.7	49.8	37.6	**47.0**	**8.4**
HL-60	**1µM**	59.6	43.3	37.6	**46.8**	**11.4**
HL-60	**3µM**	31.7	50.4	39.4	**40.5**	**9.4**
HL-60	**10µM**	64.5	64.4	38.8	**55.9**	**14.8**
THP-1	**0**	100.0	100.0	100.0	**100.0**	**0.0**
THP-1	**1nM**	94.7	96.9	103.5	**98.4**	**4.6**
THP-1	**10nM**	47.8	49.9	60.5	**52.7**	**6.8**
THP-1	**100nM**	46.1	36.4	39.4	**40.6**	**5.0**
THP-1	**1µM**	40.0	52.0	34.4	**42.1**	**9.0**
THP-1	**3µM**	38.6	44.1	35.4	**39.4**	**4.4**
THP-1	**10µM**	29.6	37.2	33.9	**33.6**	**3.8**
RPMI-8226	**0**	100.0	100.0	100.0	**100.0**	**0.0**
RPMI-8226	**1nM**	89.8	83.3	92.9	**88.7**	**4.9**
RPMI-8226	**10nM**	48.0	46.3	54.2	**49.5**	**4.2**
RPMI-8226	**100nM**	52.4	46.1	60.1	**52.9**	**7.0**
RPMI-8226	**1µM**	70.3	60.3	58.8	**63.1**	**6.3**
RPMI-8226	**3µM**	82.4	54.8	40.9	**59.4**	**21.1**
RPMI-8226	**10µM**	49.6	40.6	41.9	**44.0**	**4.9**
U266	**0**	100.0	100.0	100.0	**100.0**	**0.0**
U266	**1nM**	96.3	86.8	97.7	**93.6**	**5.9**
U266	**10nM**	64.6	68.2	70.7	**67.8**	**3.1**
U266	**100nM**	59.5	61.5	58.2	**59.7**	**1.7**
U266	**1µM**	57.9	61.1	57.2	**58.7**	**2.1**
U266	**3µM**	55.9	57.4	53.2	**55.5**	**2.1**
U266	**10µM**	53.2	56.6	55.8	**55.2**	**1.8**
DOHH2	**0**	100.0	100.0	100.0	**100.0**	**0.0**
DOHH2	**1nM**	75.4	74.1	83.2	**77.6**	**4.9**
DOHH2	**10nM**	40.6	41.0	54.0	**45.2**	**7.6**
DOHH2	**100nM**	25.4	37.2	51.4	**38.0**	**13.0**
DOHH2	**1µM**	31.8	39.4	54.4	**41.9**	**11.5**
DOHH2	**3µM**	37.3	40.6	51.3	**43.1**	**7.3**
DOHH2	**10µM**	39.6	40.5	43.8	**41.3**	**2.2**
SUD4	**0**	100.0	100.0	100.0	**100.0**	**0.0**
SUD4	**1nM**	91.4	90.4	98.0	**93.3**	**4.1**
SUD4	**10nM**	66.3	50.9	53.7	**57.0**	**8.2**
SUD4	**100nM**	52.2	39.3	41.5	**44.3**	**6.9**
SUD4	**1µM**	57.4	35.2	39.9	**44.2**	**11.7**
SUD4	**3µM**	45.2	34.3	37.3	**38.9**	**5.6**
SUD4	**10µM**	45.2	33.2	31.8	**32.5**	**1.0**

Table A1.3. Effect of thapsigargin treatment for 48 hours on cell number

Cell line	Conc.	Cell viability (%)			Average	SD
		Set 1	Set 2	Set 3		
HL-60	**0**	90.0	90.2	89.5	**89.9**	**0.4**
HL-60	**1nM**	58.3	74.0	53.2	**61.8**	**10.9**
HL-60	**10nM**	65.2	50.2	28.9	**48.1**	**18.3**
HL-60	**100nM**	53.1	49.8	14.7	**39.2**	**21.3**
HL-60	**1µM**	51.1	42.2	18.7	**37.3**	**16.8**
HL-60	**3µM**	38.4	43.2	26.0	**35.9**	**8.9**
HL-60	**10µM**	27.9	34.0	35.1	**32.3**	**3.9**
THP-1	**0**	95.4	96.9	97.5	**96.6**	**1.1**
THP-1	**1nM**	95.2	97.8	97.6	**96.9**	**1.4**
THP-1	**10nM**	84.0	88.4	91.6	**88.0**	**3.8**
THP-1	**100nM**	63.0	61.8	71.4	**65.4**	**5.2**
THP-1	**1µM**	41.8	50.4	63.5	**51.9**	**10.9**
THP-1	**3µM**	28.0	49.9	47.9	**41.9**	**12.1**
THP-1	**10µM**	7.5	15.4	19.6	**14.1**	**6.2**
RPMI-8226	**0**	90.6	92.2	90.9	**91.2**	**0.8**
RPMI-8226	**1nM**	76.1	93.3	88.8	**86.1**	**8.9**
RPMI-8226	**10nM**	65.8	68.7	56.3	**63.6**	**6.5**
RPMI-8226	**100nM**	28.3	30.5	38.7	**32.5**	**5.5**
RPMI-8226	**1µM**	16.7	19.7	32.1	**22.8**	**8.1**
RPMI-8226	**3µM**	26.0	13.6	27.5	**22.4**	**7.6**
RPMI-8226	**10µM**	3.5	44.8	13.5	**20.6**	**21.5**
U266	**0**	94.3	94.2	94.6	**94.4**	**0.2**
U266	**1nM**	83.4	95.0	96.2	**91.5**	**7.1**
U266	**10nM**	78.7	91.2	94.6	**88.2**	**8.4**
U266	**100nM**	78.2	81.4	92.6	**84.1**	**7.5**
U266	**1µM**	61.4	85.7	89.7	**78.9**	**15.3**
U266	**3µM**	73.3	83.9	78.7	**78.6**	**5.3**
U266	**10µM**	45.0	32.2	56.0	**44.4**	**11.9**
DOHH2	**0**	86.6	88.5	78.5	**84.5**	**5.3**
DOHH2	**1nM**	84.9	73.9	70.1	**76.3**	**7.7**
DOHH2	**10nM**	26.3	11.5	15.2	**17.7**	**7.7**
DOHH2	**100nM**	9.5	12.3	10.6	**10.8**	**1.4**
DOHH2	**1µM**	9.5	19.1	9.6	**12.7**	**5.5**
DOHH2	**3µM**	9.8	15.4	17.9	**14.4**	**4.1**
DOHH2	**10µM**	16.4	13.2	12.4	**14.0**	**2.1**
SUD4	**0**	94.4	93.4	94.3	**94.1**	**0.6**
SUD4	**1nM**	91.8	92.2	94.2	**92.7**	**1.3**
SUD4	**10nM**	79.9	87.7	86.2	**84.6**	**4.1**
SUD4	**100nM**	70.0	81.4	69.4	**73.6**	**6.7**
SUD4	**1µM**	63.4	59.5	67.1	**63.3**	**3.8**
SUD4	**3µM**	28.0	30.1	51.1	**36.4**	**12.8**
SUD4	**10µM**	9.4	18.0	20.5	**15.9**	**5.8**

Table A1.4. Effect of thapsigargin treatment for 48 hours on cell viability

Cell line	Conc.	Cell no. (% of control)			Average	SD
		Set 1	Set 2	Set 3		
HL-60	**0**	100.0	100.0	100.0	**100.0**	**0.0**
HL-60	**1nM**	83.7	88.3	85.8	**85.9**	**2.3**
HL-60	**10nM**	79.5	81.4	76.5	**79.1**	**2.5**
HL-60	**100nM**	47.2	34.7	41.2	**41.0**	**6.3**
HL-60	**300nM**	45.2	37.0	38.8	**40.3**	**4.3**
HL-60	**1μM**	42.7	34.1	33.7	**36.8**	**5.1**
THP-1	**0**	100.0	100.0	100.0	**100.0**	**0.0**
THP-1	**1nM**	98.2	92.5	91.6	**94.1**	**3.6**
THP-1	**10nM**	96.1	82.7	80.9	**86.6**	**8.3**
THP-1	**100nM**	41.3	32.8	31.8	**35.3**	**5.2**
THP-1	**300nM**	41.2	31.0	37.1	**36.4**	**5.1**
THP-1	**1μM**	40.8	30.6	33.2	**34.9**	**5.3**
RPMI-8226	**0**	100.0	100.0	100.0	**100.0**	**0.0**
RPMI-8226	**1nM**	89.5	86.3	87.7	**87.8**	**1.6**
RPMI-8226	**10nM**	62.7	62.5	76.2	**67.1**	**7.9**
RPMI-8226	**100nM**	30.7	27.4	27.1	**28.4**	**2.0**
RPMI-8226	**300nM**	28.3	28.9	28.8	**28.7**	**0.3**
RPMI-8226	**1μM**	43.2	42.4	45.9	**43.8**	**1.8**
U266	**0**	100.0	100.0	100.0	**100.0**	**0.0**
U266	**1nM**	88.5	89.9	83.6	**87.3**	**3.3**
U266	**10nM**	65.2	86.6	80.6	**77.5**	**11.0**
U266	**100nM**	42.7	56.5	62.9	**54.0**	**10.3**
U266	**300nM**	52.2	48.7	58.5	**53.1**	**5.0**
U266	**1μM**	56.6	47.8	54.7	**53.0**	**4.6**
U266	**3μM**	67.3	60.3	59.3	**62.3**	**4.4**
DOHH2	**0**	100.0	100.0	100.0	**100.0**	**0.0**
DOHH2	**1nM**	82.7	84.5	85.7	**84.3**	**1.5**
DOHH2	**10nM**	63.8	62.1	54.0	**60.0**	**5.2**
DOHH2	**100nM**	36.4	35.1	43.2	**38.2**	**4.4**
DOHH2	**300nM**	35.0	30.3	30.8	**32.0**	**2.6**
DOHH2	**1μM**	37.6	26.9	29.7	**31.4**	**5.5**
SUD4	**0**	100.0	100.0	100.0	**100.0**	**0.0**
SUD4	**1nM**	80.7	71.9	66.5	**73.0**	**7.2**
SUD4	**10nM**	53.8	42.0	42.1	**46.0**	**6.8**
SUD4	**100nM**	33.7	21.3	27.7	**27.6**	**6.2**
SUD4	**300nM**	36.6	22.6	30.8	**30.0**	**7.0**
SUD4	**1μM**	31.5	24.9	31.0	**29.1**	**3.7**

Table A1.5. Effect of doxorubicin treatment for 48 hours on cell number

Cell line	Conc.	Cell viability (%)			Average	SD
		Set 1	Set 2	Set 3		
HL-60	**0**	94.0	90.2	85.6	**89.9**	**4.2**
HL-60	**1nM**	80.1	86.3	89.9	**85.4**	**5.0**
HL-60	**10nM**	86.4	85.0	91.2	**87.5**	**3.3**
HL-60	**100nM**	77.0	72.1	67.6	**72.2**	**4.7**
HL-60	**300nM**	11.1	24.6	32.7	**22.8**	**10.9**
HL-60	**1µM**	0.0	8.6	0.0	**2.9**	**5.0**
THP-1	**0**	95.0	95.5	97.5	**96.0**	**1.3**
THP-1	**1nM**	96.6	96.8	95.9	**96.4**	**0.5**
THP-1	**10nM**	97.6	96.5	94.6	**96.2**	**1.5**
THP-1	**100nM**	89.5	92.4	93.1	**91.7**	**1.9**
THP-1	**300nM**	0.0	5.1	0.0	**1.7**	**2.9**
THP-1	**1µM**	0.0	0.0	0.0	**0.0**	**0.0**
RPMI-8226	**0**	89.0	92.2	91.3	**90.8**	**1.6**
RPMI-8226	**1nM**	84.3	89.4	91.8	**88.5**	**3.8**
RPMI-8226	**10nM**	81.7	86.6	86.5	**84.9**	**2.8**
RPMI-8226	**100nM**	81.6	82.1	63.7	**75.8**	**10.5**
RPMI-8226	**300nM**	0.0	0.0	0.0	**0.0**	**0.0**
RPMI-8226	**1µM**	0.0	0.0	5.3	**1.8**	**3.0**
U266	**0**	96.8	94.6	93.2	**94.9**	**1.8**
U266	**1nM**	90.8	93.3	95.4	**93.2**	**2.3**
U266	**10nM**	93.3	93.2	93.7	**93.4**	**0.3**
U266	**100nM**	95.5	96.0	88.0	**93.2**	**4.5**
U266	**300nM**	95.1	76.3	89.6	**87.0**	**9.7**
U266	**1µM**	56.1	51.6	48.5	**52.1**	**3.9**
U266	**3µM**	0.0	0.0	0.0	**0.0**	**0.0**
DOHH2	**0**	85.5	85.1	88.5	**86.4**	**1.8**
DOHH2	**1nM**	71.9	91.5	87.3	**83.6**	**10.3**
DOHH2	**10nM**	76.7	71.3	70.6	**72.9**	**3.3**
DOHH2	**100nM**	29.0	27.3	27.7	**28.0**	**0.9**
DOHH2	**300nM**	17.0	21.9	35.7	**24.9**	**9.7**
DOHH2	**1µM**	16.5	16.5	20.1	**17.7**	**2.1**
SUD4	**0**	91.2	94.3	90.9	**92.1**	**1.9**
SUD4	**1nM**	94.6	90.8	92.6	**92.7**	**1.9**
SUD4	**10nM**	90.6	88.7	84.0	**87.7**	**3.4**
SUD4	**100nM**	74.2	73.5	71.4	**73.0**	**1.4**
SUD4	**300nM**	79.8	52.8	67.8	**66.8**	**13.5**
SUD4	**1µM**	0.0	0.0	11.7	**3.9**	**6.7**

Table A1.6. Effect of doxorubicin treatment for 48 hours on cell viability

Cell line	Conc.	Cell no. (% of control)			Average	SD
		Set 1	Set 2	Set 3		
HL-60	**0**	100.0	100.0	100.0	**100.0**	**0.0**
HL-60	**1nM**	95.5	80.9	82.9	**86.4**	**7.9**
HL-60	**3nM**	46.8	57.0	56.2	**53.3**	**5.7**
HL-60	**10nM**	49.2	37.1	36.8	**41.0**	**7.1**
HL-60	**30nM**	49.0	37.8	28.8	**38.5**	**10.1**
HL-60	**100nM**	45.0	35.0	29.1	**36.4**	**8.0**
HL-60	**300nM**	42.7	40.7	35.8	**39.7**	**3.6**
HL-60	**1µM**	45.7	40.4	34.3	**40.1**	**5.7**
THP-1	**0**	100.0	100.0	100.0	**100.0**	**0.0**
THP-1	**1nM**	97.6	79.0	89.1	**88.6**	**9.3**
THP-1	**3nM**	74.6	72.2	67.1	**71.3**	**3.8**
THP-1	**10nM**	45.2	32.4	30.8	**36.1**	**7.9**
THP-1	**30nM**	40.4	34.2	33.9	**36.2**	**3.7**
THP-1	**100nM**	42.2	29.9	34.4	**35.5**	**6.2**
THP-1	**300nM**	45.7	47.7	31.8	**41.7**	**8.7**
THP-1	**1µM**	49.7	35.3	32.0	**39.0**	**9.4**
RPMI-8226	**0**	100.0	100.0	100.0	**100.0**	**0.0**
RPMI-8226	**1nM**	98.8	89.7	86.8	**91.8**	**6.3**
RPMI-8226	**3nM**	66.9	57.8	51.5	**58.7**	**7.7**
RPMI-8226	**10nM**	55.7	48.0	45.5	**49.7**	**5.3**
RPMI-8226	**30nM**	51.3	46.8	50.8	**49.6**	**2.5**
RPMI-8226	**100nM**	57.8	56.4	55.7	**56.6**	**1.1**
RPMI-8226	**300nM**	70.1	76.1	72.2	**72.8**	**3.0**
RPMI-8226	**1µM**	73.3	79.8	58.2	**70.4**	**11.1**
U266	**0**	100.0	100.0	100.0	**100.0**	**0.0**
U266	**1nM**	79.1	84.9	82.2	**82.1**	**2.9**
U266	**3nM**	49.6	55.7	52.4	**52.6**	**3.1**
U266	**10nM**	42.6	50.6	45.1	**46.1**	**4.1**
U266	**30nM**	37.4	50.5	47.8	**45.2**	**6.9**
U266	**100nM**	44.4	55.0	49.9	**49.8**	**5.3**
U266	**300nM**	48.8	55.4	62.1	**55.4**	**6.7**
U266	**1µM**	54.2	61.1	53.8	**56.4**	**4.1**
U266	**3µM**	42.2	55.8	57.9	**52.0**	**8.5**
DOHH2	**0**	100.0	100.0	100.0	**100.0**	**0.0**
DOHH2	**1nM**	92.1	90.2	100.3	**94.2**	**5.4**
DOHH2	**3nM**	88.9	78.5	82.6	**83.3**	**5.2**
DOHH2	**10nM**	42.6	41.0	36.4	**40.0**	**3.2**
DOHH2	**30nM**	42.9	42.8	33.7	**39.8**	**5.3**
DOHH2	**100nM**	35.5	32.7	33.8	**34.0**	**1.4**
DOHH2	**300nM**	37.0	33.3	38.0	**36.1**	**2.5**
DOHH2	**1µM**	42.9	32.7	42.2	**39.3**	**5.7**
SUD4	**0**	100.0	100.0	100.0	**100.0**	**0.0**
SUD4	**1nM**	107.6	93.5	80.5	**93.9**	**13.6**
SUD4	**3nM**	99.1	90.5	75.7	**88.4**	**11.8**
SUD4	**10nM**	38.7	38.1	28.9	**35.2**	**5.5**
SUD4	**30nM**	38.0	35.7	28.3	**34.0**	**5.1**
SUD4	**100nM**	35.1	26.6	44.5	**35.4**	**9.0**
SUD4	**300nM**	33.0	46.6	44.3	**41.3**	**7.3**
SUD4	**1µM**	42.1	51.7	30.9	**41.6**	**10.4**

Table A1.7. Effect of bortezomib treatment for 48 hours on cell number

Cell line	Conc.	Cell viability (%)			Average	SD
		Set 1	Set 2	Set 3		
HL-60	**0**	90.0	90.2	90.2	**90.1**	**0.1**
HL-60	**1nM**	85.7	91.7	89.4	**88.9**	**3.0**
HL-60	**3nM**	66.1	75.8	80.1	**74.0**	**7.1**
HL-60	**10nM**	34.7	25.2	44.5	**34.8**	**9.6**
HL-60	**30nM**	15.5	25.7	30.5	**23.9**	**7.7**
HL-60	**100nM**	10.7	17.6	29.5	**19.3**	**9.5**
HL-60	**300nM**	8.3	16.8	35.1	**20.1**	**13.7**
HL-60	**1μM**	10.5	16.0	35.6	**20.7**	**13.2**
THP-1	**0**	97.9	97.3	97.5	**97.6**	**0.3**
THP-1	**1nM**	97.3	97.5	95.2	**96.6**	**1.3**
THP-1	**3nM**	90.6	85.6	78.6	**84.9**	**6.0**
THP-1	**10nM**	21.5	29.0	49.1	**33.2**	**14.3**
THP-1	**30nM**	8.7	17.4	7.7	**13.0**	**6.1**
THP-1	**100nM**	0.0	0.0	45.2	**15.1**	**26.1**
THP-1	**300nM**	3.5	2.8	37.1	**14.5**	**19.6**
THP-1	**1μM**	0.0	4.5	13.9	**6.1**	**7.1**
RPMI-8226	**0**	90.0	92.2	88.6	**90.3**	**1.8**
RPMI-8226	**1nM**	88.6	91.0	88.2	**89.3**	**1.5**
RPMI-8226	**3nM**	71.2	74.2	67.8	**71.0**	**3.2**
RPMI-8226	**10nM**	42.5	39.2	33.3	**38.3**	**4.7**
RPMI-8226	**30nM**	35.9	17.2	23.8	**25.6**	**9.5**
RPMI-8226	**100nM**	30.0	6.8	20.8	**19.2**	**11.7**
RPMI-8226	**300nM**	18.3	12.2	29.6	**20.0**	**8.8**
RPMI-8226	**1μM**	16.0	15.6	13.7	**15.1**	**1.2**
U266	**0**	92.8	94.6	93.9	**93.7**	**0.9**
U266	**1nM**	91.7	92.5	92.6	**92.3**	**0.5**
U266	**3nM**	78.8	82.7	79.9	**80.5**	**2.0**
U266	**10nM**	65.4	72.6	77.7	**71.9**	**6.2**
U266	**30nM**	62.7	77.8	75.7	**72.1**	**8.2**
U266	**100nM**	57.2	69.4	76.1	**67.6**	**9.6**
U266	**300nM**	60.5	63.8	65.3	**63.2**	**2.5**
U266	**1μM**	64.8	73.1	45.9	**61.3**	**13.9**
U266	**3μM**	58.0	71.9	30.6	**53.5**	**21.0**
DOHH2	**0**	82.2	88.5	80.8	**83.8**	**4.1**
DOHH2	**1nM**	73.6	85.1	83.7	**80.8**	**6.3**
DOHH2	**3nM**	74.3	81.1	82.7	**79.3**	**4.5**
DOHH2	**10nM**	18.0	16.4	18.6	**17.6**	**1.1**
DOHH2	**30nM**	12.4	13.2	16.1	**13.9**	**1.9**
DOHH2	**100nM**	22.8	7.6	10.4	**13.6**	**8.1**
DOHH2	**300nM**	38.6	25.5	14.8	**26.3**	**11.9**
DOHH2	**1μM**	13.8	10.0	12.2	**12.0**	**1.9**
SUD4	**0**	96.6	94.3	90.6	**93.8**	**3.0**
SUD4	**1nM**	91.2	92.8	91.3	**91.8**	**0.9**
SUD4	**3nM**	89.2	90.8	90.3	**90.1**	**0.8**
SUD4	**10nM**	31.0	28.9	29.5	**29.8**	**1.1**
SUD4	**30nM**	33.7	22.5	27.4	**27.8**	**5.6**
SUD4	**100nM**	26.6	23.6	17.9	**22.7**	**4.4**
SUD4	**300nM**	31.7	19.5	16.4	**22.5**	**8.1**
SUD4	**1μM**	22.8	17.8	6.9	**15.8**	**8.1**

Table A1.8. Effect of bortezomib treatment for 48 hours on cell viability

Cell line	Conc.	Cell no. (% of control)			Average	SD
		Set 1	Set 2	Set 3		
HL-60	**0**	100.0	100.0	100.0	**100.0**	**0.0**
HL-60	**1nM**	100.0	71.7	83.3	**85.0**	**14.2**
HL-60	**10nM**	112.4	78.2	70.1	**86.9**	**22.5**
HL-60	**100nM**	117.3	81.2	66.1	**88.2**	**26.3**
HL-60	**1µM**	77.7	76.0	58.1	**70.6**	**10.9**
HL-60	**10µM**	48.7	35.8	27.7	**37.4**	**10.6**
THP-1	**0**	100.0	100.0	100.0	**100.0**	**0.0**
THP-1	**1nM**	93.8	92.4	70.8	**85.7**	**12.9**
THP-1	**10nM**	93.5	91.5	85.6	**90.2**	**4.1**
THP-1	**100nM**	101.9	88.4	82.2	**90.8**	**10.1**
THP-1	**1µM**	83.4	77.9	71.2	**77.5**	**6.1**
THP-1	**10µM**	39.4	31.6	35.3	**35.4**	**3.9**
RPMI-8226	**0**	100.0	100.0	100.0	**100.0**	**0.0**
RPMI-8226	**1nM**	87.5	74.8	94.6	**85.6**	**10.0**
RPMI-8226	**10nM**	94.6	81.6	92.8	**89.7**	**7.0**
RPMI-8226	**100nM**	89.6	83.2	88.5	**87.1**	**3.4**
RPMI-8226	**1µM**	63.6	63.5	64.6	**63.9**	**0.6**
RPMI-8226	**10µM**	49.9	40.9	39.6	**43.5**	**5.6**
RPMI-8226	**100µM**	65.1	54.6	45.1	**54.9**	**10.0**
U266	**0**	100.0	100.0	100.0	**100.0**	**0.0**
U266	**1nM**	90.5	95.3	75.4	**87.1**	**10.4**
U266	**10nM**	97.3	87.6	84.9	**89.9**	**6.5**
U266	**100nM**	98.5	96.5	85.7	**93.6**	**6.9**
U266	**1µM**	76.1	74.9	73.5	**74.8**	**1.3**
U266	**10µM**	61.2	60.4	60.6	**60.7**	**0.4**
U266	**100µM**	63.2	50.9	53.4	**55.8**	**6.5**
DOHH2	**0**	100.0	100.0	100.0	**100.0**	**0.0**
DOHH2	**1nM**	100.0	100.0	88.4	**96.1**	**6.7**
DOHH2	**10nM**	92.4	71.7	69.7	**77.9**	**12.6**
DOHH2	**100nM**	88.6	75.0	67.5	**77.0**	**10.7**
DOHH2	**1µM**	40.2	34.7	40.6	**38.5**	**3.3**
DOHH2	**10µM**	41.7	27.6	23.1	**30.8**	**9.7**
SUD4	**0**	100.0	100.0	100.0	**100.0**	**0.0**
SUD4	**1nM**	100.0	100.0	74.9	**91.6**	**14.5**
SUD4	**10nM**	98.5	95.1	91.1	**94.9**	**3.7**
SUD4	**100nM**	99.8	95.1	90.0	**95.0**	**4.9**
SUD4	**1µM**	82.6	75.2	59.1	**72.3**	**12.0**
SUD4	**10µM**	36.1	29.4	40.1	**35.2**	**5.4**

Table A1.9. Effect of 4-HC treatment for 48 hours on cell number

Cell line	Conc.	Cell viability (%)			Average	SD
		Set 1	Set 2	Set 3		
HL-60	**0**	94.0	88.4	94.2	**92.2**	**3.3**
HL-60	**1nM**	85.0	75.7	93.7	**84.8**	**9.0**
HL-60	**10nM**	73.4	86.1	86.6	**82.0**	**7.5**
HL-60	**100nM**	79.3	83.7	81.9	**81.6**	**2.2**
HL-60	**1µM**	69.5	87.2	74.6	**77.1**	**9.1**
HL-60	**10µM**	16.6	16.8	10.3	**14.6**	**3.7**
THP-1	**0**	95.3	97.1	97.0	**96.5**	**1.0**
THP-1	**1nM**	96.5	97.7	95.7	**96.6**	**1.0**
THP-1	**10nM**	94.0	96.8	98.3	**96.4**	**2.2**
THP-1	**100nM**	97.2	96.3	96.8	**96.8**	**0.4**
THP-1	**1µM**	96.2	97.4	96.5	**96.7**	**0.6**
THP-1	**10µM**	28.4	19.5	38.2	**28.7**	**9.3**
RPMI-8226	**0**	89.0	92.2	91.3	**90.8**	**1.6**
RPMI-8226	**1nM**	87.1	84.8	86.5	**86.1**	**1.2**
RPMI-8226	**10nM**	80.7	89.2	82.2	**84.0**	**4.5**
RPMI-8226	**100nM**	87.2	91.7	81.6	**86.8**	**5.1**
RPMI-8226	**1µM**	67.7	87.5	76.8	**77.3**	**9.9**
RPMI-8226	**10µM**	45.2	51.8	40.2	**45.7**	**5.8**
RPMI-8226	**100µM**	3.0	0.0	0.0	**1.0**	**1.8**
U266	**0**	96.8	94.6	93.2	**94.9**	**1.8**
U266	**1nM**	86.4	88.9	83.7	**86.3**	**2.6**
U266	**10nM**	91.6	94.1	79.2	**88.3**	**8.0**
U266	**100nM**	85.3	91.1	76.1	**84.2**	**7.6**
U266	**1µM**	94.2	85.4	75.2	**85.0**	**9.5**
U266	**10µM**	64.2	62.2	63.0	**63.1**	**1.0**
U266	**100µM**	8.7	11.3	0.0	**6.7**	**5.9**
DOHH2	**0**	85.5	85.1	88.5	**86.4**	**1.8**
DOHH2	**1nM**	86.2	88.6	61.9	**78.9**	**14.8**
DOHH2	**10nM**	81.7	91.1	76.9	**83.2**	**7.2**
DOHH2	**100nM**	74.4	84.0	81.2	**79.9**	**4.9**
DOHH2	**1µM**	42.2	31.2	19.7	**31.1**	**11.2**
DOHH2	**10µM**	11.1	14.1	23.7	**16.3**	**6.6**
SUD4	**0**	91.2	93.2	90.9	**91.8**	**1.3**
SUD4	**1nM**	84.0	93.1	71.2	**82.7**	**11.0**
SUD4	**10nM**	81.7	93.5	92.6	**89.3**	**6.6**
SUD4	**100nM**	95.5	94.8	90.7	**93.7**	**2.6**
SUD4	**1µM**	94.5	86.4	93.7	**91.5**	**4.4**
SUD4	**10µM**	13.2	17.3	32.8	**21.1**	**10.3**

Table A1.10. Effect of 4-HC treatment for 48 hours on cell viability

Cell line	Conc.	Cell no. (% of control)			Average	SD
		Set 1	Set 2	Set 3		
HL-60	**0**	100.0	100.0	100.0	**100.0**	**0.0**
HL-60	**10nM**	69.4	75.9	76.5	**73.9**	**3.9**
HL-60	**100nM**	42.5	41.8	51.7	**45.3**	**5.5**
HL-60	**1µM**	36.5	34.3	31.1	**34.0**	**2.7**
HL-60	**10µM**	39.0	31.5	32.2	**34.2**	**4.1**
HL-60	**100µM**	41.8	31.9	31.5	**35.1**	**5.8**
THP-1	**0**	100.0	100.0	100.0	**100.0**	**0.0**
THP-1	**10nM**	90.3	82.9	85.2	**86.1**	**3.8**
THP-1	**100nM**	67.0	56.8	60.5	**61.4**	**5.2**
THP-1	**1µM**	35.3	34.5	33.5	**34.4**	**0.9**
THP-1	**10µM**	36.6	33.8	29.0	**33.1**	**3.8**
THP-1	**100µM**	35.7	35.7	30.6	**34.0**	**2.9**

Table A1.11. Effect of cytarabine treatment for 48 hours on cell number

Cell line	Conc.	Cell viability (%)			Average	SD
		Set 1	Set 2	Set 3		
HL-60	**0**	89.1	96.7	94.1	**93.3**	**3.9**
HL-60	**10nM**	87.8	96.1	94.3	**92.7**	**4.4**
HL-60	**100nM**	73.4	89.0	90.4	**84.3**	**9.5**
HL-60	**1µM**	38.7	51.5	34.7	**41.6**	**8.8**
HL-60	**10µM**	35.4	39.6	17.4	**30.8**	**11.8**
HL-60	**100µM**	26.7	32.9	13.1	**24.2**	**10.2**
THP-1	**0**	96.6	97.2	97.9	**97.2**	**0.7**
THP-1	**10nM**	96.9	96.8	97.6	**97.1**	**0.4**
THP-1	**100nM**	96.4	96.5	97.4	**96.8**	**0.6**
THP-1	**1µM**	93.2	91.9	95.5	**93.5**	**1.8**
THP-1	**10µM**	66.0	52.4	59.3	**59.2**	**6.8**
THP-1	**100µM**	60.6	43.9	27.5	**44.0**	**16.5**

Table A1.12. Effect of cytarabine treatment for 48 hours on cell viability

Cell line	Conc.	Cell no. (% of control)			Average	SD
		Set 1	Set 2	Set 3		
HL-60	**0**	100.0	100.0	100.0	**100.0**	**0.0**
HL-60	**10nM**	95.2	97.8	87.8	**93.6**	**5.2**
HL-60	**100nM**	69.4	61.9	64.1	**65.1**	**3.9**
HL-60	**1µM**	42.9	37.0	30.5	**36.8**	**6.2**
HL-60	**10µM**	42.5	31.7	28.1	**34.1**	**7.5**
HL-60	**30µM**	41.1	33.7	29.3	**34.7**	**6.0**
THP-1	**0**	100.0	100.0	100.0	**100.0**	**0.0**
THP-1	**10nM**	93.1	96.7	94.4	**94.7**	**1.8**
THP-1	**100nM**	56.7	56.5	55.9	**56.4**	**0.4**
THP-1	**1µM**	34.5	30.8	30.4	**31.9**	**2.3**
THP-1	**10µM**	36.8	30.9	26.1	**31.3**	**5.4**
THP-1	**30µM**	38.6	29.9	27.8	**32.1**	**5.7**

Table A1.13. Effect of etoposide treatment for 48 hours on cell number

Cell line	Conc.	Cell viability (%)			Average	SD
		Set 1	Set 2	Set 3		
HL-60	**0**	87.0	93.5	93.3	**91.3**	**3.7**
HL-60	**10nM**	88.0	95.2	92.2	**91.8**	**3.7**
HL-60	**100nM**	81.9	94.4	88.1	**88.1**	**6.2**
HL-60	**1µM**	43.8	67.6	37.9	**49.8**	**15.8**
HL-60	**10µM**	36.1	52.6	23.5	**37.4**	**14.6**
HL-60	**30µM**	17.0	43.1	26.6	**28.9**	**13.2**
THP-1	**0**	95.3	95.9	97.2	**96.1**	**1.0**
THP-1	**10nM**	96.2	96.8	97.2	**96.7**	**0.5**
THP-1	**100nM**	92.9	96.6	97.6	**95.7**	**2.5**
THP-1	**1µM**	72.7	56.1	53.2	**60.6**	**10.5**
THP-1	**10µM**	29.1	38.4	23.2	**30.2**	**7.7**
THP-1	**30µM**	17.2	25.1	32.3	**24.9**	**7.6**

Table A1.14. Effect of etoposide treatment for 48 hours on cell viability

Cell line	Conc.	Cell no. (% of control)			Average	SD
		Set 1	Set 2	Set 3		
HL-60	**0**	100.0	100.0	100.0	**100.0**	**0.0**
HL-60	**10nM**	97.3	91.9	91.1	**93.4**	**3.4**
HL-60	**100nM**	94.2	94.6	85.1	**91.3**	**5.4**
HL-60	**300nM**	88.9	90.2	80.2	**86.4**	**5.4**
HL-60	**1µM**	52.0	50.9	41.1	**48.0**	**6.0**
HL-60	**10µM**	37.6	29.7	27.7	**31.7**	**5.2**
THP-1	**0**	100.0	100.0	100.0	**100.0**	**0.0**
THP-1	**10nM**	94.4	89.0	89.1	**90.8**	**3.1**
THP-1	**100nM**	89.8	87.3	80.5	**85.9**	**4.8**
THP-1	**300nM**	75.3	74.9	66.7	**72.3**	**4.9**
THP-1	**1µM**	37.1	32.9	28.9	**33.0**	**4.1**
THP-1	**10µM**	32.7	29.4	25.5	**29.2**	**3.6**

Table A1.15. Effect of KW-2478 treatment for 48 hours on cell number

Cell line	Conc.	Cell viability (%)			Average	SD
		Set 1	Set 2	Set 3		
HL-60	**0**	96.4	91.8	93.8	**94.0**	**2.3**
HL-60	**10nM**	96.0	91.7	93.6	**93.8**	**2.2**
HL-60	**100nM**	95.7	92.6	92.5	**93.6**	**1.8**
HL-60	**300nM**	96.4	92.7	93.1	**94.1**	**2.0**
HL-60	**1µM**	88.7	82.8	79.6	**83.7**	**4.6**
HL-60	**10µM**	35.3	26.3	45.6	**35.7**	**9.6**
THP-1	**0**	97.5	98.2	97.3	**97.7**	**0.5**
THP-1	**10nM**	96.9	98.0	97.8	**97.6**	**0.6**
THP-1	**100nM**	96.9	98.4	97.9	**97.7**	**0.8**
THP-1	**300nM**	97.6	97.8	96.7	**97.4**	**0.6**
THP-1	**1µM**	89.2	91.3	86.7	**89.1**	**2.3**
THP-1	**10µM**	80.1	75.0	72.8	**76.0**	**3.7**

Table A1.16. Effect of KW-2478 treatment for 48 hours on cell viability

Cell line	Conc.	Cell no. (% of control)			Average	SD
		Set 1	Set 2	Set 3		
RPMI-8226	**0**	100.0	100.0	100.0	**100.0**	**0.0**
RPMI-8226	**10nM**	93.7	95.9	90.1	**93.2**	**2.9**
RPMI-8226	**100nM**	89.5	95.4	83.2	**89.4**	**6.1**
RPMI-8226	**1µM**	67.8	74.8	64.2	**68.9**	**5.4**
RPMI-8226	**10µM**	51.3	45.3	35.3	**44.0**	**8.1**
RPMI-8226	**100µM**	50.2	53.7	54.7	**52.9**	**2.4**
U266	**0**	100.0	100.0	100.0	**100.0**	**0.0**
U266	**10nM**	94.8	99.4	86.2	**93.5**	**6.7**
U266	**100nM**	97.2	93.1	79.2	**89.8**	**9.4**
U266	**1µM**	88.7	80.4	68.9	**79.3**	**9.9**
U266	**10µM**	84.2	58.0	55.4	**65.9**	**15.9**
U266	**100µM**	67.9	57.6	54.4	**60.0**	**7.1**

Table A1.17. Effect of melphalan treatment for 48 hours on cell number

Cell line	Conc.	Cell viability (%)			Average	SD
		Set 1	Set 2	Set 3		
RPMI-8226	**0**	83.1	87.8	83.2	**84.7**	**2.7**
RPMI-8226	**10nM**	72.0	92.8	83.6	**82.8**	**10.4**
RPMI-8226	**100nM**	69.4	88.7	83.2	**80.4**	**10.0**
RPMI-8226	**1µM**	82.6	85.7	83.4	**83.9**	**1.6**
RPMI-8226	**10µM**	60.6	85.6	68.5	**71.6**	**12.8**
RPMI-8226	**100µM**	34.2	27.3	18.4	**26.7**	**7.9**
U266	**0**	93.3	94.6	93.2	**93.7**	**0.8**
U266	**10nM**	77.4	93.4	83.5	**84.8**	**8.1**
U266	**100nM**	76.7	93.9	81.0	**83.9**	**9.0**
U266	**1µM**	81.6	93.2	79.3	**84.7**	**7.4**
U266	**10µM**	80.6	88.5	75.0	**81.4**	**6.8**
U266	**100µM**	55.5	44.2	39.0	**46.2**	**8.4**

Table A1.18. Effect of melphalan treatment for 48 hours on cell viability

Drug	Cell line	EC_{50} cell number	95% CI	EC_{50} cell viability	95% CI
Doxorubicin	HL-60	18.16nM	6.87nM to 47.96nM	191.60nM	163.60nM to 224.50nM
	THP-1	16.04nM	2.53nM to 101.70nM	161.10nM	147.10nM to 176.30nM
	RPMI-8226	8.49 nM	4.46nM to 16.17nM	115.4nM	1.5950e-026 to 8.3400e+011
	U266	9.62nM	2.00nM to 46.33nM	1.06µM	973.60nM to 1.16µM
	DOHH2	6.92nM	4.27nM to 11.21nM	64.13nM	39.75nM to 103.4nM
	SUD4	2.13nM	1.19nM to 3.80nM	420.50nM	324.30nM to 545.10nM
Bortezomib	HL-60	1.82nM	1.41nM to 2.36nM	5.45nM	4.02nM to 7.40nM
	THP-1	3.08nM	2.31nM to 4.10nM	6.24nM	4.28nM to 9.08nM
	RPMI-8226	1.17nM	1.7840e-021 to 763.1	5.85nM	4.54nM to 7.54nM
	U266	1.17nM	0.89nM to 1.55nM	5.95nM	1.81nM to 19.54nM
	DOHH2	4.29nM	3.56nM to 5.18nM	4.88nM	2.70nM to 8.83nM
	SUD4	3.79nM	7.1650e-013 to 2.0080e-005	6.11nM	4.81nM to 7.75nM
Tunicamycin	HL-60	1.23µM	61.70nM to 24.36µM	251.80nM	59.43nM to 1.07µM
	THP-1	22.58nM	8.96nM to 56.93nM	220.90nM	271.90nM to 1.79µM
	RPMI-8226	3.86µM	113.60nM to 131.00µM	1.68µM	702.60nM to 4.00µM
	U266	84.08µM	38.10µM to 185.50µM	85.78µM	52.81µM to 139.30µM
	DOHH2	198.40nM	138.60nM to 284.10nM	116.4nM	1.2400e-010 to 0.0001093
	SUD4	122.60nM	25.12nM to 598.10nM	4.87µM	2.05µM to 11.59µM
Thapsigargin	HL-60	0.99nM		1.00nM	0.085nM to 11.92nM
	THP-1	5.51nM	3.04nM to 9.99nM	922.90nM	534.80nM to 1.59µM
	RPMI-8226	1.26nM		16.22nM	7.29nM to 36.09nM
	U266	4.18nM	2.93nM to 5.96nM	10.6µM	5.59µM to 20.09µM
	DOHH2	1.43nM	0.80nM to 2.55nM	2.67nM	1.78nM to 3.99nM
	SUD4	4.80nM	2.70nM to 8.53nM	1.58µM	1.02µM to 2.44µM

Table A1.19. EC_{50} values, with 95% confidence intervals for doxorubicin, bortezomib, tunicamycin and thapsigargin on cell number and viability

Drug	Cell line	EC_{50} cell number	95% CI	EC_{50} cell viability	95% CI
4-HC	HL-60	4.62µM	913.2nM to 23.33µM	3.18µM	2.02µM to 4.99µM
	THP-1	4.65µM	2.34µM to 9.26µM	7.30µM	4.02µM to 13.25µM
	RPMI-8226	5.61µM	2.32µM to 13.55µM	9.13µM	6.22µM to 13.41µM
	U266	61.36µM	7.81µM to 482.20µM	18.35µM	10.62µM to 31.70µM
	DOHH2	726.60nM	311.20nM to1.70µM	642.90nM	329.60nM to 1.25µM
	SUD4	4.13µM	2.39µM to 7.16µM	5.55µM	3.01µM to 10.23µM
Cytarabine	HL-60	16.29nM	11.24nM to 23.60nM	396.90nM	203.70nM to 773.30nM
	THP-1	61.96nM	43.10nM to 89.06nM	5.63µM	2.84µM to 11.14µM
Etoposide	HL-60	88.23nM	59.68nM to 130.40nM	555.80nM	233.10nM to 1.33µM
	THP-1	66.05nM	53.05nM to 82.24nM	982.20nM	684.30nM to 1.41µM
KW-2478	HL-60	588.90nM	436.80nM to 794.10nM	2.01µM	353.60nM to 11.45µM
	THP-1	361.1nM	253.40nM to 514.60nM	1.16µM	897.30nM to 1.52µM
Melphalan	RPMI-8226	515.10nM	212.40nM to 1.25µM	46.19µM	28.64µM to 74.49µM
	U266	1.53µM	11.71nM to 199.7µM	107.4µM	52.43µM to 220.1µM

Table A1.20. EC_{50} values, with 95% confidence intervals for 4-HC, cytarabine, etoposide, KW-2478, and melphalan on cell number and viability

Appendix 2

Additional data for chapter 5:

TG Simultaneous treatment

HL-60	% of control				
	Set 1	**Set 2**	**Set 3**	**Average**	**SD**
Control	100.0	100.0	100.0	**100.0**	**0.0**
TG 0.05nM	92.2	89.0	85.0	**88.7**	**3.6**
Dox 5nM	95.1	75.6	88.6	**86.5**	**9.9**
Dox 75nM	66.2	59.2	36.7	**54.0**	**15.4**
TG 0.05nM + Dox 5nM	89.2	77.9	92.8	**86.6**	**7.8**
TG 0.05nM + Dox 75nM	47.1	55.0	48.0	**50.0**	**4.3**
Bort 1nM	94.0	88.6	87.8	**90.1**	**3.4**
Bort 3nM	93.9	83.5	84.2	**87.2**	**5.9**
TG 0.05nM + Bort 1nM	80.8	89.7	74.0	**81.5**	**7.8**
TG 0.05nM + Bort 3nM	83.0	88.3	73.9	**81.7**	**7.2**
17-AAG 50nM	62.9	57.2	80.4	**66.8**	**12.1**
17-AAG 250nM	46.8	42.7	53.6	**47.7**	**5.5**
TG 0.05nM + 17-AAG 50nM	74.3	66.1	76.4	**72.3**	**5.5**
TG 0.05nM + 17-AAG 250nM	48.5	40.4	50.9	**46.6**	**5.5**
SAHA 100nM	77.2	74.6	89.1	**80.3**	**7.7**
SAHA 500nM	46.1	50.2	58.7	**51.7**	**6.4**
TG 0.05nM + SAHA 100nM	72.3	58.7	77.3	**69.5**	**9.6**
TG 0.05nM + SAHA 500nM	66.8	42.2	63.4	**57.5**	**13.4**

Table A2.1. TG 0.05nM combined with drug treatment for 48 hours in the HL60 cell line

HL-60	% of control				
	Set 1	**Set 2**	**Set 3**	**Average**	**SD**
Control	100.0	100.0	100.0	**100.0**	**0.0**
TG 0.5nM	81.5	85.4	80.8	**82.6**	**2.5**
Dox 5nM	80.4	84.6	76.9	**80.6**	**3.9**
Dox 75nM	53.4	53.6	39.3	**48.8**	**8.2**
TG 0.5nM + Dox 5nM	75.0	88.9	78.4	**80.8**	**7.2**
TG 0.5nM + Dox 75nM	65.3	54.4	39.0	**52.9**	**13.2**
Bort 1nM	76.6	89.2	87.8	**84.5**	**6.9**
Bort 3nM	77.6	85.1	84.2	**82.3**	**4.1**
TG 0.5nM + Bort 1nM	68.3	70.4	69.6	**69.4**	**1.0**
TG 0.5nM + Bort 3nM	67.5	72.3	66.5	**68.8**	**3.1**
17-AAG 50nM	86.3	75.1	76.4	**79.2**	**6.1**
17-AAG 250nM	52.1	43.0	58.6	**51.2**	**7.8**
TG 0.5nM + 17-AAG 50nM	72.0	73.6	65.0	**70.2**	**4.5**
TG 0.5nM + 17-AAG 250nM	48.7	38.7	44.9	**44.1**	**5.0**
SAHA 100nM	63.1	73.6	79.6	**72.1**	**8.3**
SAHA 500nM	51.4	52.1	59.8	**54.4**	**4.7**
TG 0.5nM + SAHA 100nM	78.4	65.5	67.8	**70.6**	**6.9**
TG 0.5nM + SAHA 500nM	57.7	37.0	60.4	**51.7**	**12.8**

Table A2.2. TG 0. 5nM combined with drug treatment for 48 hours in the HL60 cell line

THP1	% of control				
	Set 1	Set 2	Set 3	Average	SD
Control	100.0	100.0	100.0	**100.0**	**0.0**
TG 1nM	91.0	87.6	87.2	**88.6**	**2.1**
Dox 10nM	89.2	86.4	99.0	**91.5**	**6.6**
Dox 75nM	54.0	36.3	30.5	**40.3**	**12.3**
TG 1nM + Dox 10nM	85.1	87.7	98.6	**90.5**	**7.1**
TG 1nM + Dox 75nM	56.1	35.1	32.6	**41.3**	**12.9**
Bort 1nM	89.4	87.7	96.2	**91.1**	**4.5**
Bort 3nM	88.6	82.6	91.0	**87.4**	**4.3**
TG 1nM + Bort 1nM	83.5	90.7	82.9	**85.7**	**4.3**
TG 1nM + Bort 3nM	83.9	74.9	77.6	**78.8**	**4.6**
17-AAG 50nM	54.8	63.2	54.3	**57.4**	**5.0**
17-AAG 250nM	17.4	18.6	21.0	**19.0**	**1.8**
TG 1nM + 17-AAG 50nM	55.7	53.8	58.5	**56.0**	**2.4**
TG 1nM + 17-AAG 250nM	17.2	17.3	27.4	**20.7**	**5.9**
SAHA 100nM	90.2	89.3	92.7	**90.7**	**1.8**
SAHA 500nM	63.1	65.6	62.2	**63.6**	**1.8**
TG 1nM + SAHA 100nM	83.7	91.0	90.4	**88.4**	**4.1**
TG 1nM + SAHA 500nM	61.0	64.6	79.5	**68.3**	**9.8**

Table A2.3. TG 1nM combined with drug treatment for 48 hours in the THP1 cell line

THP1	% of control				
	Set 1	Set 2	Set 3	Average	SD
Control	100.0	100.0	100.0	**100.0**	**0.0**
TG 5nM	84.8	75.1	79.5	**79.8**	**4.9**
Dox 10nM	89.1	89.1	89.0	**89.1**	**0.1**
Dox 75nM	52.4	36.1	33.2	**40.6**	**10.4**
TG 5nM + Dox 10nM	86.2	77.7	76.7	**80.2**	**5.2**
TG 5nM + Dox 75nM	60.1	37.3	30.8	**42.7**	**15.4**
Bort 1nM	84.7	91.0	87.4	**87.7**	**3.1**
Bort 3nM	84.8	89.8	81.8	**85.5**	**4.0**
TG 5nM + Bort 1nM	74.5	80.0	77.5	**77.3**	**2.8**
TG 5nM + Bort 3nM	74.9	69.2	60.1	**68.1**	**7.4**
17-AAG 50nM	52.8	61.0	57.8	**57.2**	**4.1**
17-AAG 250nM	17.2	19.3	25.9	**20.8**	**4.5**
TG 5nM + 17-AAG 50nM	58.2	61.1	65.6	**61.6**	**3.7**
TG 5nM + 17-AAG 250nM	11.9	13.4	21.8	**15.7**	**5.3**
SAHA 100nM	84.5	83.4	79.1	**82.3**	**2.9**
SAHA 500nM	63.8	71.2	65.5	**66.8**	**3.9**
TG 5nM + SAHA 100nM	76.9	80.2	87.6	**81.6**	**5.5**
TG 5nM + SAHA 500nM	53.5	47.7	57.3	**52.8**	**4.8**

Table A2.4. TG 5nM combined with drug treatment for 48 hours in the THP1 cell line

RPMI-8226	% of control				
	Set 1	Set 2	Set 3	Average	SD
Control	100.0	100.0	100.0	**100.0**	**0.0**
TG 0.5nM	88.3	92.2	89.1	**89.8**	**2.0**
Dox 5nM	88.9	94.0	85.7	**89.5**	**4.2**
Dox 75nM	78.1	91.6	76.5	**82.0**	**8.3**
TG 0.5nM + Dox 5nM	84.1	87.1	86.6	**85.9**	**1.6**
TG 0.5nM + Dox 75nM	79.0	86.7	80.1	**81.9**	**4.2**
Bort 1nM	86.6	92.3	94.9	**91.2**	**4.2**
Bort 3nM	87.5	91.8	86.3	**88.5**	**2.9**
TG 0.5nM + Bort 1nM	80.2	88.3	86.0	**84.9**	**4.2**
TG 0.5nM + Bort 3nM	83.6	87.5	83.6	**84.9**	**2.2**
17-AAG 100nM	62.5	94.7	66.7	**74.6**	**17.5**
17-AAG 500nM	44.3	51.3	36.9	**44.2**	**7.2**
TG 0.5nM + 17-AAG 100nM	58.6	92.3	58.8	**69.9**	**19.4**
TG 0.5nM + 17-AAG 500nM	39.0	49.8	35.5	**41.4**	**7.5**
SAHA 100nM	84.3	73.8	74.9	**77.7**	**5.8**
SAHA 500nM	52.5	24.0	54.7	**43.7**	**17.1**
TG 0.5nM + SAHA 100nM	73.3	71.8	79.4	**74.8**	**4.1**
TG 0.5nM + SAHA 500nM	48.4	22.7	53.8	**41.6**	**16.6**

Table A2.5. TG 0.5nM combined with drug treatment for 48 hours in the RPMI8226 cell line

RPMI-8226	% of control				
	Set 1	Set 2	Set 3	Average	SD
Control	100.0	100.0	100.0	**100.0**	**0.0**
TG 5nM	65.4	40.0	46.5	**50.6**	**13.2**
Dox 5nM	89.4	85.2	93.0	**89.2**	**3.9**
Dox 75nM	88.6	76.6	90.8	**85.3**	**7.6**
TG 5nM + Dox 5nM	47.3	43.9	49.4	**46.9**	**2.8**
TG 5nM + Dox 75nM	63.3	53.7	48.9	**55.3**	**7.3**
Bort 1nM	86.8	90.6	91.3	**89.6**	**2.4**
Bort 3nM	88.2	88.4	85.9	**87.5**	**1.4**
TG 5nM + Bort 1nM	60.6	41.2	41.2	**47.6**	**11.2**
TG 5nM + Bort 3nM	64.9	38.0	35.7	**46.2**	**16.2**
17-AAG 100nM	98.8	61.8	62.0	**74.2**	**21.3**
17-AAG 500nM	48.2	38.0	50.2	**45.5**	**6.6**
TG 5nM + 17-AAG 100nM	71.5	35.9	44.0	**50.5**	**18.7**
TG 5nM + 17-AAG 500nM	49.6	23.4	33.0	**35.4**	**13.3**
SAHA 100nM	73.4	83.9	91.3	**82.9**	**9.0**
SAHA 500nM	20.7	55.0	57.8	**44.5**	**20.6**
TG 5nM + SAHA 100nM	42.7	39.9	42.9	**41.8**	**1.7**
TG 5nM + SAHA 500nM	14.0	24.4	26.4	**21.6**	**6.7**

Table A2.6. TG 5nM combined with drug treatment for 48 hours in the RPMI8226 cell line

U266	% of control				
	Set 1	Set 2	Set 3	Average	SD
Control	100.0	100.0	100.0	**100.0**	**0.0**
TG 1nM	87.8	87.9	90.8	**88.8**	**1.7**
Dox 10nM	90.9	85.9	87.7	**88.2**	**2.5**
Dox 75nM	88.8	84.9	82.2	**85.3**	**3.3**
TG 1nM + Dox 10nM	81.6	85.3	81.2	**82.7**	**2.2**
TG 1nM + Dox 75nM	79.7	80.5	83.0	**81.1**	**1.7**
Bort 1nM	89.2	84.8	86.9	**86.9**	**2.2**
Bort 3nM	85.6	80.8	66.8	**77.7**	**9.7**
TG 1nM + Bort 1nM	77.4	81.4	87.0	**81.9**	**4.8**
TG 1nM + Bort 3nM	73.6	77.8	64.3	**71.9**	**6.9**
17-AAG 100nM	67.5	82.0	69.9	**73.1**	**7.8**
17-AAG 500nM	22.1	36.4	26.4	**28.3**	**7.3**
TG 1nM + 17-AAG 100nM	64.6	80.3	78.7	**74.5**	**8.6**
TG 1nM + 17-AAG 500nM	22.3	41.7	26.4	**30.2**	**10.2**
SAHA 100nM	78.0	89.5	80.4	**82.6**	**6.0**
SAHA 500nM	63.1	70.1	66.6	**66.6**	**3.5**
TG 1nM + SAHA100nM	77.8	88.6	88.1	**84.8**	**6.1**
TG 1nM + SAHA 500nM	68.8	69.2	78.2	**72.1**	**5.3**

Table A2.7. TG 1nM combined with drug treatment for 48 hours in the U266 cell line

U266	% of control					
	Set 1	Set 2	Set 3	Set 4	Average	SD
Control	100.0	100.0	100.0	100.0	**100.0**	**0.0**
TG 5nM	77.0	80.0	62.2	79.0	**74.6**	**8.3**
Dox 10nM	90.0	82.6	90.7	88.2	**87.9**	**3.6**
Dox 75nM	83.3	73.5	87.7	77.7	**80.6**	**6.2**
TG 5nM + Dox 10nM	67.4	68.9	65.1	85.4	**71.7**	**9.3**
TG 5nM + Dox 75nM	75.9	68.0	65.0	72.2	**70.3**	**4.8**
Bort 1nM	96.3	77.3	91.1	87.2	**87.9**	**8.0**
Bort 3nM	78.4	73.9	69.3	79.1	**75.2**	**4.6**
TG 5nM + Bort 1nM	65.7	79.8	64.4	80.5	**72.6**	**8.8**
TG 5nM + Bort 3nM	65.4	75.6	42.3	72.9	**64.1**	**15.1**
17-AAG 100nM	64.8	82.8	84.0	81.3	**78.2**	**9.0**
17-AAG 500nM	23.4	31.7	26.8	24.8	**26.6**	**3.6**
TG 5nM + 17-AAG 100nM	57.2	70.6	56.4	67.7	**63.0**	**7.2**
TG 5nM + 17-AAG 500nM	21.2	28.6	14.9	15.4	**20.0**	**6.4**
SAHA 100nM	83.3	74.4	86.0	90.3	**83.5**	**6.7**
SAHA 500nM	66.1	57.5	72.0	69.4	**66.2**	**6.3**
TG 5nM + SAHA100nM	70.4	70.3	69.3	86.2	**74.0**	**8.1**
TG 5nM + SAHA 500nM	59.6	37.6	58.5	73.4	**57.3**	**14.8**

Table A2.8. TG 5nM combined with drug treatment for 48 hours in the U266 cell line

DOHH2	% of control			
	Set 1	Set 2	Average	SD
Control	100.0	100.0	**100.0**	**0.0**
TG 0.05nM	84.4	84.4	**84.4**	**0.1**
Dox 5nM	46.5	44.2	**45.4**	**1.6**
Dox 50nM	2.3	2.1	**2.2**	**0.2**
TG 0.05nM + Dox 5nM	48.7	45.3	**47.0**	**2.4**
TG 0.05nM + Dox 50nM	1.0	1.1	**1.0**	**0.0**
Bort 1nM	95.0	80.0	**87.5**	**10.6**
Bort 3nM	91.4	78.2	**84.8**	**9.3**
TG 0.05nM + Bort 1nM	85.3	83.0	**84.1**	**1.6**
TG 0.05nM + Bort 3nM	91.3	76.6	**84.0**	**10.4**
17-AAG 50nM	76.1	80.2	**78.2**	**2.9**
17-AAG 250nM	58.8	54.8	**56.8**	**2.8**
TG 0.05nM + 17-AAG 50nM	72.9	70.2	**71.6**	**1.9**
TG 0.05nM + 17-AAG 250nM	62.9	53.2	**58.0**	**6.9**
SAHA 100nM	89.6	86.5	**88.1**	**2.2**
SAHA 500nM	63.5	66.2	**64.8**	**1.8**
TG 0.05nM + SAHA 100nM	88.6	80.1	**84.3**	**6.0**
TG 0.05nM + SAHA 500nM	69.7	62.2	**65.9**	**5.3**

Table A2.9. TG 0.05nM combined with drug treatment for 48 hours in the DOHH2 cell line

DOHH2	% of control			
	Set 1	Set 2	Average	SD
Control	100.0	100.0	**100.0**	**0.0**
TG 0.5nM	81.5	79.8	**80.6**	**1.2**
Dox 5nM	44.0	40.5	**42.3**	**2.5**
Dox 50nM	2.3	2.3	**2.3**	**0.1**
TG 0.5nM + Dox 5nM	41.2	42.8	**42.0**	**1.1**
TG 0.5nM + Dox 50nM	0.9	0.9	**0.9**	**0.0**
Bort 1nM	80.2	77.8	**79.0**	**1.7**
Bort 3nM	79.5	77.3	**78.4**	**1.5**
TG 0.5nM + Bort 1nM	84.6	89.3	**87.0**	**3.3**
TG 0.5nM + Bort 3nM	81.1	99.2	**90.1**	**12.8**
17-AAG 50nM	77.0	91.8	**84.4**	**10.5**
17-AAG 250nM	61.6	65.7	**63.6**	**2.9**
TG 0.5nM + 17-AAG 50nM	76.0	88.8	**82.4**	**9.1**
TG 0.5nM + 17-AAG 250nM	56.3	63.9	**60.1**	**5.4**
SAHA 100nM	86.4	91.7	**89.1**	**3.8**
SAHA 500nM	63.9	60.7	**62.3**	**2.3**
TG 0.5nM + SAHA 100nM	78.6	91.7	**85.1**	**9.3**
TG 0.5nM + SAHA 500nM	55.3	69.5	**62.4**	**10.0**

Table A2.10. TG 0.5nM combined with drug treatment for 48 hours in the DOHH2 cell line

SUD4	% of control				
	Set 1	Set 2	Set 3	Average	SD
Control	100.0	100.0	100.0	**100.0**	**0.0**
TG 2nM	82.4	92.1	84.2	**86.2**	**5.1**
Dox 10nM	64.4	84.4	77.9	**75.6**	**10.2**
Dox 75nM	65.5	61.3	45.7	**57.5**	**10.4**
TG 2nM + Dox 10nM	64.5	62.5	58.9	**62.0**	**2.9**
TG 2nM + Dox 75nM	77.3	48.2	69.5	**65.0**	**15.1**
Bort 1nM	73.0	75.5	89.8	**79.4**	**9.0**
Bort 5nM	63.2	70.7	59.2	**64.4**	**5.9**
TG 2nM + Bort 1nM	92.5	77.8	80.4	**83.6**	**7.9**
TG 2nM + Bort 5nM	83.5	82.7	65.3	**77.2**	**10.3**
17-AAG 500nM	24.0	13.0	8.6	**15.2**	**7.9**
17-AAG 1μM	11.5	5.8	6.3	**7.9**	**3.2**
TG 2nM + 17-AAG 500nM	16.0	12.9	10.9	**13.3**	**2.6**
TG 2nM + 17-AAG 1μM	5.4	6.6	5.6	**5.9**	**0.6**
SAHA 100nM	65.9	62.8	70.8	**66.5**	**4.0**
SAHA 500nM	38.3	27.2	28.2	**31.2**	**6.1**
TG 2nM + SAHA100nM	71.3	73.3	62.4	**69.0**	**5.8**
TG 2nM + SAHA 500nM	44.1	25.9	33.1	**34.3**	**9.2**

Table A2.11. TG 2nM combined with drug treatment for 48 hours in the SUD4 cell line

SUD4	% of control				
	Set 1	Set 2	Set 3	Average	SD
Control	100.0	100.0	100.0	**100.0**	**0.0**
TG 10nM	53.1	50.4	49.6	**51.1**	**1.8**
Dox 10nM	81.6	86.1	66.9	**78.2**	**10.0**
Dox 75nM	65.0	56.7	57.4	**59.7**	**4.6**
TG 10nM + Dox 10nM	48.1	47.1	59.7	**51.6**	**7.0**
TG 10nM + Dox 75nM	56.2	50.7	58.4	**55.1**	**4.0**
Bort 1nM	89.3	86.4	95.2	**90.3**	**4.5**
Bort 5nM	69.2	75.8	70.8	**71.9**	**3.5**
TG 10nM + Bort 1nM	70.9	60.0	75.1	**68.7**	**7.8**
TG 10nM + Bort 5nM	56.3	57.3	65.3	**59.6**	**4.9**
17-AAG 500nM	16.2	20.9	30.7	**22.6**	**7.4**
17-AAG 1μM	8.4	8.5	23.2	**13.4**	**8.5**
TG 10nM + 17-AAG 500nM	7.7	10.8	30.1	**16.2**	**12.1**
TG 10nM + 17-AAG 1μM	5.2	4.5	16.7	**8.8**	**6.8**
SAHA 100nM	65.8	91.9	58.9	**72.2**	**17.4**
SAHA 500nM	33.1	30.8	26.1	**30.0**	**3.6**
TG 10nM + SAHA100nM	39.8	50.2	40.3	**43.5**	**5.8**
TG 10nM + SAHA 500nM	17.0	14.4	4.3	**11.9**	**6.7**

Table A2.12. TG 10nM combined with drug treatment for 48 hours in the SUD4 cell line

HL60	Combination Effect		
	Set 1	Set 2	Set 3
TG 0.05nM + Dox 5nM	1.02	1.16	1.23
TG 0.05nM + Dox 75nM	0.77	1.04	1.54
TG 0.05nM + Bort 1nM	0.93	1.14	0.99
TG 0.05nM + Bort 3nM	0.96	1.19	1.03
TG 0.05nM + 17-AAG 50nM	1.28	1.30	1.12
TG 0.05nM + 17-AAG 250nM	1.12	1.06	1.12
TG 0.05nM + SAHA 100nM	1.02	0.88	1.02
TG 0.05nM + SAHA 500nM	1.57	0.94	1.27
TG 0.5nM + Dox 5nM	1.15	1.23	1.26
TG 0.5nM + Dox 75nM	1.50	1.19	1.23
TG 0.5nM + Bort 1nM	1.10	0.92	0.98
TG 0.5nM + Bort 3nM	1.07	0.99	0.98
TG 0.5nM + 17-AAG 50nM	1.02	1.15	1.05
TG 0.5nM + 17-AAG 250nM	1.15	1.05	0.95
TG 0.5nM + SAHA 100nM	1.52	1.04	1.05
TG 0.5nM + SAHA 500nM	1.38	0.83	1.25

Table A2.13. Combination effect of TG combined with drug treatment for 48 hours in the HL60 cell line (calculated using the fractional product method).

THP1	Combination Effect		
	Set 1	Set 2	Set 3
TG 1nM + Dox 10nM	1.05	1.16	1.14
TG 1nM + Dox 75nM	1.14	1.10	1.22
TG 1nM + Bort 1nM	1.03	1.18	0.99
TG 1nM + Bort 3nM	1.04	1.03	0.98
TG 1nM + 17-AAG 50nM	1.12	0.97	1.24
TG 1nM + 17-AAG 250nM	1.09	1.06	1.50
TG 1nM + SAHA 100nM	1.02	1.16	1.12
TG 1nM + SAHA 500nM	1.06	1.12	1.47
TG 5nM + Dox 10nM	1.14	1.16	1.08
TG 5nM + Dox 75nM	1.35	1.37	1.17
TG 5nM + Bort 1nM	1.04	1.17	1.11
TG 5nM + Bort 3nM	1.04	1.03	0.92
TG 5nM + 17-AAG 50nM	1.30	1.33	1.43
TG 5nM + 17-AAG 250nM	0.82	0.92	1.06
TG 5nM + SAHA 100nM	1.07	1.28	1.39
TG 5nM + SAHA 500nM	0.99	0.89	1.10

Table A2.14. Combination effect of TG combined with drug treatment for 48 hours in the THP1 cell line (calculated using the fractional product method).

RPMI8226	Combination Effect		
	Set 1	Set 2	Set 3
TG 0.5nM + Dox 5nM	1.07	1.01	1.13
TG 0.5nM + Dox 75nM	1.15	1.03	1.18
TG 0.5nM + Bort 1nM	1.05	1.04	1.02
TG 0.5nM + Bort 3nM	1.08	1.03	1.09
TG 0.5nM + 17-AAG 100nM	1.06	1.06	0.99
TG 0.5nM + 17-AAG 500nM	1.00	1.05	1.08
TG 0.5nM + SAHA 100nM	0.98	1.06	1.19
TG 0.5nM + SAHA 500nM	1.04	1.03	1.11
TG 5nM + Dox 5nM	0.81	1.29	1.14
TG 5nM + Dox 75nM	1.09	1.75	1.16
TG 5nM + Bort 1nM	1.07	1.14	0.97
TG 5nM + Bort 3nM	1.12	1.07	0.89
TG 5nM + 17-AAG 100nM	1.11	1.45	1.52
TG 5nM + 17-AAG 500nM	1.58	1.54	1.41
TG 5nM + SAHA 100nM	0.89	1.19	1.01
TG 5nM + SAHA 500nM	1.03	1.11	0.98

Table A2.15. Combination effect of TG combined with drug treatment for 48 hours in the RPMI8226 cell line (calculated using the fractional product method).

U266	Combination Effect			
	Set 1	Set 2	Set 3	Set 4
TG 1nM + Dox 10nM	1.02	1.13	1.02	
TG 1nM + Dox 75nM	1.02	1.08	1.11	
TG 1nM + Bort 1nM	0.99	1.09	1.10	
TG 1nM + Bort 3nM	0.98	1.10	1.06	
TG 1nM + 17-AAG 100nM	1.09	1.11	1.24	
TG 1nM + 17-AAG 500nM	1.15	1.30	1.10	
TG 1nM + SAHA100nM	1.13	1.13	1.21	
TG 1nM + SAHA 500nM	1.24	1.12	1.29	
TG 5nM + Dox 10nM	0.97	1.04	1.15	1.23
TG 5nM + Dox 75nM	1.18	1.16	1.19	1.18
TG 5nM + Bort 1nM	0.89	1.29	1.14	1.17
TG 5nM + Bort 3nM	1.08	1.28	0.98	1.17
TG 5nM + 17-AAG 100nM	1.15	1.07	1.08	1.05
TG 5nM + 17-AAG 500nM	1.18	1.13	0.90	0.79
TG 5nM + SAHA100nM	1.10	1.18	1.30	1.21
TG 5nM + SAHA 500nM	1.17	0.82	1.31	1.34

Table A2.16. Combination effect of TG combined with drug treatment for 48 hours in the U266 cell line (calculated using the fractional product method).

DOHH2	Combination Effect	
	Set 1	Set 2
TG 0.05nM + Dox 5nM	1.24	1.21
TG 0.05nM + Dox 50nM	0.53	0.60
TG 0.05nM + Bort 1nM	1.06	1.23
TG 0.05nM + Bort 3nM	1.18	1.16
TG 0.05nM + 17-AAG 50nM	1.13	1.04
TG 0.05nM + 17-AAG 250nM	1.27	1.15
TG 0.05nM + SAHA 100nM	1.17	1.10
TG 0.05nM + SAHA 500nM	1.30	1.11
TG 0.5nM + Dox 5nM	1.15	1.32
TG 0.5nM + Dox 50nM	0.48	0.49
TG 0.5nM + Bort 1nM	1.29	1.44
TG 0.5nM + Bort 3nM	1.25	1.61
TG 0.5nM + 17-AAG 50nM	1.21	1.21
TG 0.5nM + 17-AAG 250nM	1.12	1.22
TG 0.5nM + SAHA 100nM	1.12	1.25
TG 0.5nM + SAHA 500nM	1.06	1.44

Table A2.17. Combination effect of TG combined with drug treatment for 48 hours in the DOHH2 cell line (calculated using the fractional product method).

SUD4	Combination Effect		
	Set 1	Set 2	Set 3
TG 2nM + Dox 10nM	1.22	0.80	0.90
TG 2nM + Dox 75nM	1.43	0.85	1.81
TG 2nM + Bort 1nM	1.54	1.12	1.06
TG 2nM + Bort 5nM	1.60	1.27	1.31
TG 2nM + 17-AAG 500nM	0.81	1.08	1.51
TG 2nM + 17-AAG 1μM	0.56	1.23	1.06
TG 2nM + SAHA100nM	1.31	1.27	1.05
TG 2nM + SAHA 500nM	1.40	1.03	1.39
TG 10nM + Dox 10nM	1.11	1.09	1.80
TG 10nM + Dox 75nM	1.63	1.77	2.05
TG 10nM + Bort 1nM	1.49	1.38	1.59
TG 10nM + Bort 5nM	1.53	1.50	1.86
TG 10nM + 17-AAG 500nM	0.90	1.02	1.98
TG 10nM + 17-AAG 1μM	1.17	1.04	1.45
TG 10nM + SAHA100nM	1.14	1.08	1.38
TG 10nM + SAHA 500nM	0.97	0.93	0.34

Table A2.18. Combination effect of TG combined with drug treatment for 48 hours in the SUD4 cell line (calculated using the fractional product method).

TG Pre-treatment

THP1	% of control				
	Set 1	**Set 2**	**Set 3**	**Average**	**SD**
Control	100.0	100.0	100.0	**100.0**	**0.0**
TG 1nM	86.7	85.4	82.7	**84.9**	**2.0**
Dox 10nM	81.8	86.5	80.6	**83.0**	**3.1**
Dox 75nM	20.9	14.2	14.2	**16.4**	**3.8**
TG 1nM + Dox 10nM	88.4	94.9	83.6	**88.9**	**5.7**
TG 1nM + Dox 75nM	28.3	13.6	14.9	**18.9**	**8.2**
Bort 1nM	88.5	84.3	76.4	**83.1**	**6.1**
Bort 5nM	45.2	33.5	30.9	**36.5**	**7.6**
TG 1nM + Bort 1nM	79.9	81.9	66.1	**76.0**	**8.6**
TG 1nM + Bort 5nM	40.7	31.2	29.2	**33.7**	**6.2**
17-AAG 50nM	46.2	72.2	70.8	**63.1**	**14.6**
17-AAG 250nM	21.8	37.6	35.4	**31.6**	**8.6**
TG 1nM + 17-AAG 50nM	52.5	64.1	59.8	**58.8**	**5.9**
TG 1nM + 17-AAG 250nM	21.5	39.2	37.2	**32.6**	**9.7**
SAHA 100nM	82.9	79.3	73.8	**78.7**	**4.6**
SAHA 500nM	72.6	72.4	71.0	**72.0**	**0.9**
TG 1nM + SAHA 100nM	98.6	83.4	78.4	**86.8**	**10.5**
TG 1nM + SAHA 500nM	75.0	71.8	73.7	**73.5**	**1.6**

Table A2.19. TG 1nM pretreatment for 6 hours combined with drug treatment for a further 48 hours in the THP1 cell line.

THP1	% of control				
	Set 1	**Set 2**	**Set 3**	**Average**	**SD**
Control	100.0	100.0	100.0	**100.0**	**0.0**
TG 5nM	80.2	83.1	81.1	**81.5**	**1.5**
Dox 10nM	79.9	81.3	80.0	**80.4**	**0.8**
Dox 75nM	24.0	14.5	13.0	**17.2**	**5.9**
TG 5nM + Dox 10nM	80.7	81.6	77.7	**80.0**	**2.1**
TG 5nM + Dox 75nM	23.0	12.1	15.5	**16.9**	**5.6**
Bort 1nM	76.1	82.8	80.0	**79.6**	**3.4**
Bort 5nM	38.1	30.2	33.2	**33.8**	**4.0**
TG 5nM + Bort 1nM	77.0	72.9	58.1	**69.3**	**10.0**
TG 5nM + Bort 5nM	34.2	29.2	29.6	**31.0**	**2.8**
17-AAG 50nM	52.8	57.5	67.5	**59.3**	**7.5**
17-AAG 250nM	19.6	31.9	37.3	**29.6**	**9.0**
TG 5nM + 17-AAG 50nM	45.9	70.6	65.6	**60.7**	**13.1**
TG 5nM + 17-AAG 250nM	18.1	40.5	36.5	**31.7**	**12.0**
SAHA 100nM	76.2	78.1	72.3	**75.5**	**2.9**
SAHA 500nM	61.8	66.7	64.1	**64.2**	**2.4**
TG 5nM + SAHA 100nM	72.2	81.5	70.3	**74.7**	**6.0**
TG 5nM + SAHA 500nM	64.1	73.6	63.4	**67.0**	**5.7**

Table A2.20. TG 5nM pretreatment for 6 hours combined with drug treatment for a further 48 hours in the THP1 cell line.

U266	% of control				
	Set 1	Set 2	Set 3	Average	SD
Control	100.0	100.0	100.0	**100.0**	**0.0**
TG 1nM	72.3	79.3	83.8	**78.5**	**5.8**
Dox 10nM	73.1	80.4	82.7	**78.7**	**5.0**
Dox 75nM	70.4	75.4	79.5	**75.1**	**4.6**
TG 1nM + Dox 10nM	77.8	68.8	77.8	**74.8**	**5.2**
TG 1nM + Dox 75nM	64.7	63.8	75.4	**68.0**	**6.5**
Bort 1nM	74.3	75.5	84.7	**78.2**	**5.7**
Bort 5nM	5.1	5.7	6.3	**5.7**	**0.6**
TG 1nM + Bort 1nM	70.1	65.9	68.3	**68.1**	**2.1**
TG 1nM + Bort 5nM	4.6	4.2	5.3	**4.7**	**0.5**
17-AAG 50nM	71.1	66.0	76.6	**71.2**	**5.3**
17-AAG 250nM	44.8	61.0	73.9	**59.9**	**14.6**
TG 1nM + 17-AAG 50nM	69.0	65.9	64.6	**66.5**	**2.3**
TG 1nM + 17-AAG 250nM	47.8	68.9	75.3	**64.0**	**14.3**
SAHA 100nM	66.9	71.0	80.3	**72.7**	**6.9**
SAHA 500nM	59.8	58.9	76.1	**65.0**	**9.7**
TG 1nM + SAHA 100nM	73.1	73.3	71.4	**72.6**	**1.0**
TG 1nM + SAHA 500nM	61.9	68.7	64.0	**64.9**	**3.5**

Table A2.21. TG 1nM pretreatment for 6 hours combined with drug treatment for a further 48 hours in the U266 cell line.

U266	% of control				
	Set 1	Set 2	Set 3	Average	SD
Control	100.0	100.0	100.0	**100.0**	**0.0**
TG 5nM	65.8	73.9	77.6	**72.4**	**6.0**
Dox 10nM	67.8	74.4	82.3	**74.8**	**7.2**
Dox 75nM	60.3	69.1	63.6	**64.3**	**4.5**
TG 5nM + Dox 10nM	67.1	67.6	70.0	**68.3**	**1.5**
TG 5nM + Dox 75nM	65.7	52.3	70.3	**62.8**	**9.3**
Bort 1nM	64.4	70.6	63.4	**66.1**	**3.9**
Bort 5nM	4.6	5.0	4.7	**4.8**	**0.2**
TG 5nM + Bort 1nM	68.5	59.3	71.9	**66.5**	**6.5**
TG 5nM + Bort 5nM	3.6	3.5	5.5	**4.2**	**1.2**
17-AAG 50nM	68.0	61.4	81.0	**70.2**	**10.0**
17-AAG 250nM	42.4	59.7	67.9	**56.6**	**13.0**
TG 5nM + 17-AAG 50nM	60.0	54.4	69.9	**61.4**	**7.8**
TG 5nM + 17-AAG 250nM	43.9	68.4	61.9	**58.1**	**12.7**
SAHA 100nM	62.5	67.0	72.1	**67.2**	**4.8**
SAHA 500nM	54.4	62.8	67.4	**61.5**	**6.6**
TG 5nM + SAHA 100nM	58.9	59.6	56.7	**58.4**	**1.5**
TG 5nM + SAHA 500nM	55.2	40.0	64.9	**53.4**	**12.6**

Table A2.22. TG 5nM pretreatment for 6 hours combined with drug treatment for a further 48 hours in the U266 cell line.

SUD4	% of control				
	Set 1	Set 2	Set 3	Average	SD
Control	100.0	100.0	100.0	**100.0**	**0.0**
TG 1nM	74.0	78.7	75.2	**76.0**	**2.5**
Dox 10nM	56.7	47.2	41.1	**48.4**	**7.9**
Dox 75nM	30.0	30.7	23.0	**27.9**	**4.2**
TG 1nM + Dox 10nM	67.9	49.0	42.1	**53.0**	**13.3**
TG 1nM + Dox 75nM	45.5	33.1	30.2	**36.3**	**8.1**
Bort 1nM	70.9	76.6	63.3	**70.3**	**6.7**
Bort 5nM	73.4	83.0	65.5	**74.0**	**8.7**
TG 1nM + Bort 1nM	75.8	64.0	73.0	**70.9**	**6.2**
TG 1nM + Bort 5nM	68.8	57.4	64.3	**63.5**	**5.8**
17-AAG 50nM	67.8	70.8	70.4	**69.7**	**1.6**
17-AAG 250nM	44.6	57.9	55.2	**52.5**	**7.0**
TG 1nM + 17-AAG 50nM	61.6	63.7	64.8	**63.3**	**1.7**
TG 1nM + 17-AAG 250nM	55.0	67.1	63.1	**61.7**	**6.2**
SAHA 100nM	58.2	63.3	49.5	**57.0**	**7.0**
SAHA 500nM	36.2	47.7	27.8	**37.3**	**10.0**
TG 1nM + SAHA 100nM	85.4	65.6	71.6	**74.2**	**10.2**
TG 1nM + SAHA 500nM	64.7	53.5	60.1	**59.4**	**5.6**

Table A2.23. TG 1nM pretreatment for 6 hours combined with drug treatment for a further 48 hours in the SUD4 cell line.

SUD4	% of control				
	Set 1	Set 2	Set 3	Average	SD
Control	100.0	100.0	100.0	**100.0**	**0.0**
TG 10nM	59.0	60.3	61.9	**60.4**	**1.4**
Dox 10nM	47.3	55.2	38.4	**46.9**	**8.4**
Dox 75nM	28.2	24.3	22.7	**25.1**	**2.8**
TG 10nM + Dox 10nM	49.4	48.2	42.5	**46.7**	**3.7**
TG 10nM + Dox 75nM	41.5	24.8	31.2	**32.5**	**8.4**
Bort 1nM	69.8	57.5	57.6	**61.6**	**7.1**
Bort 5nM	53.6	51.8	65.3	**56.9**	**7.3**
TG 10nM + Bort 1nM	87.5	82.7	69.4	**79.9**	**9.4**
TG 10nM + Bort 5nM	62.3	63.7	54.3	**60.1**	**5.0**
17-AAG 50nM	72.5	53.2	68.7	**64.8**	**10.3**
17-AAG 250nM	37.9	14.9	43.6	**32.2**	**15.2**
TG 10nM + 17-AAG 50nM	34.6	50.3	54.3	**46.4**	**10.4**
TG 10nM + 17-AAG 250nM	42.4	21.3	50.9	**38.2**	**15.3**
SAHA 100nM	47.1	52.3	39.5	**46.3**	**6.4**
SAHA 500nM	27.9	22.0	30.6	**26.8**	**4.4**
TG 10nM + SAHA 100nM	73.0	52.0	56.3	**60.4**	**11.1**
TG 10nM + SAHA 500nM	49.7	18.0	50.9	**39.5**	**18.6**

Table A2.24. TG 10nM pretreatment for 6 hours combined with drug treatment for a further 48 hours in the SUD4 cell line.

THP1	Combination Effect		
	Set 1	Set 2	Set 3
TG 1nM + Dox 10nM	1.25	1.28	1.25
TG 1nM + Dox 75nM	1.57	1.12	1.26
TG 1nM + Bort 1nM	1.04	1.14	1.05
TG 1nM + Bort 5nM	1.04	1.09	1.14
TG 1nM + 17-AAG 50nM	1.31	1.04	1.02
TG 1nM + 17-AAG 250nM	1.14	1.22	1.27
TG 1nM + SAHA 100nM	1.37	1.23	1.28
TG 1nM + SAHA 500nM	1.19	1.16	1.26
TG 5nM + Dox 10nM	1.26	1.21	1.20
TG 5nM + Dox 75nM	1.20	1.00	1.47
TG 5nM + Bort 1nM	1.26	1.06	0.90
TG 5nM + Bort 5nM	1.12	1.16	1.10
TG 5nM + 17-AAG 50nM	1.08	1.48	1.20
TG 5nM + 17-AAG 250nM	1.15	1.53	1.21
TG 5nM + SAHA 100nM	1.18	1.26	1.20
TG 5nM + SAHA 500nM	1.29	1.33	1.22

Table A2.25. Combination effect of TG pretreatment for 6 hours combined with drug treatment for a further 48 hours in the THP1 cell line (calculated using the fractional product method).

U266	Combination Effect		
	Set 1	Set 2	Set 3
TG 1nM + Dox 10nM	1.47	1.08	1.12
TG 1nM + Dox 75nM	1.27	1.07	1.13
TG 1nM + Bort 1nM	1.31	1.10	0.96
TG 1nM + Bort 5nM	1.24	0.95	1.01
TG 1nM + 17-AAG 50nM	1.34	1.26	1.01
TG 1nM + 17-AAG 250nM	1.48	1.42	1.21
TG 1nM + SAHA 100nM	1.51	1.30	1.06
TG 1nM + SAHA 500nM	1.43	1.47	1.00
TG 5nM + Dox 10nM	1.50	1.23	1.10
TG 5nM + Dox 75nM	1.66	1.02	1.42
TG 5nM + Bort 1nM	1.61	1.14	1.46
TG 5nM + Bort 5nM	1.18	0.95	1.52
TG 5nM + 17-AAG 50nM	1.34	1.20	1.11
TG 5nM + 17-AAG 250nM	1.57	1.55	1.18
TG 5nM + SAHA 100nM	1.43	1.20	1.01
TG 5nM + SAHA 500nM	1.54	0.86	1.24

Table A2.26. Combination effect of TG pretreatment for 6 hours combined with drug treatment for a further 48 hours in the U266 cell line (calculated using the fractional product method).

SUD4	Combination Index		
	Set 1	Set 2	Set 3
TG 1nM + Dox 10nM	1.62	1.32	1.36
TG 1nM + Dox 75nM	2.05	1.37	1.75
TG 1nM + Bort 1nM	1.45	1.06	1.53
TG 1nM + Bort 5nM	1.27	0.88	1.31
TG 1nM + 17-AAG 50nM	1.23	1.14	1.23
TG 1nM + 17-AAG 250nM	1.67	1.47	1.52
TG 1nM + SAHA 100nM	1.99	1.31	1.92
TG 1nM + SAHA 500nM	2.41	1.42	2.88
TG 10nM + Dox 10nM	1.77	1.45	1.79
TG 10nM + Dox 75nM	2.49	1.69	2.22
TG 10nM + Bort 1nM	2.12	2.38	1.95
TG 10nM + Bort 5nM	1.97	2.04	1.35
TG 10nM + 17-AAG 50nM	0.81	1.57	1.28
TG 10nM + 17-AAG 250nM	1.89	2.36	1.89
TG 10nM + SAHA 100nM	2.62	1.65	2.30
TG 10nM + SAHA 500nM	3.02	1.36	2.69

Table A2.27. Combination effect of TG pretreatment for 6 hours combined with drug treatment for a further 48 hours in the SUD4 cell line (calculated using the fractional product method).

THP1		Cells In Each Region (%)			Average	SD
Control	nuclear debris	0.5	0.4	0.5	**0.5**	**0.1**
	late apoptosis/dead cells	1.6	2.0	1.7	**1.8**	**0.2**
	viable cells	91.1	90.1	90.0	**90.4**	**0.6**
	early apoptosis	6.8	7.5	7.8	**7.4**	**0.5**
TG 5nM	nuclear debris	0.3	0.5	0.4	**0.4**	**0.1**
	late apoptosis/dead cells	1.3	1.4	1.4	**1.4**	**0.1**
	viable cells	91.2	90.3	90.0	**90.5**	**0.6**
	early apoptosis	7.2	7.8	8.1	**7.7**	**0.5**
Dox 1μM	nuclear debris	0.1	0.1	0.0	**0.1**	**0.1**
(positive control)	late apoptosis/dead cells	62.2	59.9	62.4	**61.5**	**1.4**
	viable cells	13.5	13.7	13.3	**13.5**	**0.2**
	early apoptosis	24.2	26.3	24.3	**24.9**	**1.2**
Dox 75nM	nuclear debris	0.3	0.4	0.4	**0.4**	**0.1**
	late apoptosis/dead cells	4.3	4.2	4.5	**4.3**	**0.2**
	viable cells	51.4	47.7	45.1	**48.1**	**3.2**
	early apoptosis	44.0	47.6	50.0	**47.2**	**3.0**
TG + Dox	nuclear debris	0.4	0.3	0.2	**0.3**	**0.1**
	late apoptosis/dead cells	4.9	4.7	4.3	**4.6**	**0.3**
	viable cells	39.2	44.0	44.7	**42.6**	**3.0**
	early apoptosis	55.5	51.0	50.8	**52.4**	**2.7**
Bort 5nM	nuclear debris	0.8	0.9	0.7	**0.8**	**0.1**
	late apoptosis/dead cells	4.3	4.3	3.6	**4.1**	**0.4**
	viable cells	84.1	81.7	81.8	**82.5**	**1.4**
	early apoptosis	10.8	13.2	13.9	**12.6**	**1.6**
TG + Bort	nuclear debris	0.6	0.7	0.4	**0.6**	**0.2**
	late apoptosis/dead cells	4.6	4.9	4.6	**4.7**	**0.2**
	viable cells	77.7	77.9	76.2	**77.3**	**0.9**
	early apoptosis	17.1	16.5	18.7	**17.4**	**1.1**
17-AAG 250nM	nuclear debris	0.6	0.3	0.5	**0.5**	**0.2**
	late apoptosis/dead cells	1.8	1.7	1.6	**1.7**	**0.1**
	viable cells	90.4	87.9	90.0	**89.4**	**1.3**
	early apoptosis	7.2	10.1	7.9	**8.4**	**1.5**
TG + 17-AAG	nuclear debris	0.4	0.6	0.3	**0.4**	**0.2**
	late apoptosis/dead cells	2.1	2.6	1.7	**2.1**	**0.5**
	viable cells	86.1	86.4	89.4	**87.3**	**1.8**
	early apoptosis	11.4	10.4	8.6	**10.1**	**1.4**
SAHA 500nM	nuclear debris	0.6	0.6	0.7	**0.6**	**0.1**
	late apoptosis/dead cells	2.6	2.1	2.5	**2.4**	**0.3**
	viable cells	88.0	87.0	86.0	**87.0**	**1.0**
	early apoptosis	8.8	10.3	10.7	**9.9**	**1.0**
TG + SAHA	nuclear debris	0.2	0.4	0.6	**0.4**	**0.2**
	late apoptosis/dead cells	3.1	2.4	2.4	**2.6**	**0.4**
	viable cells	86.0	87.2	85.9	**86.4**	**0.7**
	early apoptosis	10.7	9.9	11.1	**10.6**	**0.6**

Table A2.28. Apoptosis assay results for cells in each region (%) following 48 hours of drug treatment in the THP1 cell line

THP1		Cell No. By Region (cells/mL)			Average	SD
Control	nuclear debris	2671	2510	2533	**2571**	**87**
	late apoptosis/dead cells	8546	11391	8779	**9572**	**1579**
	viable cells	486576	522047	455680	**488101**	**33210**
	early apoptosis	36320	43247	39507	**39691**	**3467**
TG 5nM	nuclear debris	1453	2206	1839	**1832**	**377**
	late apoptosis/dead cells	6295	6775	6590	**6553**	**242**
	viable cells	441604	426643	413958	**427402**	**13839**
	early apoptosis	34864	37024	37396	**36428**	**1367**
Dox 1μM	nuclear debris	271	142	0	**138**	**136**
(positive control)	late apoptosis/dead cells	126380	127753	137800	**130644**	**6235**
	viable cells	27512	29219	29386	**28706**	**1037**
	early apoptosis	49129	56163	53765	**53019**	**3576**
Dox 75nM	nuclear debris	629	1121	1112	**954**	**282**
	late apoptosis/dead cells	10215	10863	11635	**10904**	**711**
	viable cells	121166	123455	115664	**120095**	**4005**
	early apoptosis	103722	123196	128239	**118386**	**12947**
TG + Dox	nuclear debris	952	820	579	**784**	**189**
	late apoptosis/dead cells	11586	11484	10753	**11274**	**455**
	viable cells	93324	108280	110838	**104148**	**9460**
	early apoptosis	132209	125507	125975	**127897**	**3742**
Bort 5nM	nuclear debris	3122	3342	2731	**3065**	**310**
	late apoptosis/dead cells	16911	16453	14882	**16082**	**1064**
	viable cells	328212	314921	334914	**326016**	**10176**
	early apoptosis	42018	50901	57071	**49997**	**7567**
TG + Bort	nuclear debris	2447	2677	1448	**2191**	**653**
	late apoptosis/dead cells	17642	17886	15485	**17004**	**1321**
	viable cells	300171	284352	254672	**279731**	**23099**
	early apoptosis	66061	60107	62610	**62926**	**2990**
17-AAG 250nM	nuclear debris	3009	1222	2325	**2185**	**902**
	late apoptosis/dead cells	8551	6925	7596	**7691**	**817**
	viable cells	429311	357939	418574	**401941**	**38483**
	early apoptosis	34206	41280	36586	**37357**	**3600**
TG + 17-AAG	nuclear debris	1568	2298	1292	**1719**	**520**
	late apoptosis/dead cells	8981	10546	8234	**9254**	**1180**
	viable cells	368206	350448	433174	**383943**	**43550**
	early apoptosis	48895	42319	41654	**44289**	**4002**
SAHA 500nM	nuclear debris	2165	2403	2536	**2368**	**188**
	late apoptosis/dead cells	8772	7840	8761	**8458**	**535**
	viable cells	300637	330030	297414	**309361**	**17973**
	early apoptosis	30189	39073	37119	**35460**	**4668**
TG + SAHA	nuclear debris	741	1551	2075	**1456**	**672**
	late apoptosis/dead cells	11604	8591	8912	**9702**	**1655**
	viable cells	318368	312256	314714	**315112**	**3075**
	early apoptosis	39626	35557	40530	**38571**	**2649**

Table A2.29. Apoptosis assay results for cells number by region following 48 hours of drug treatment in the THP1 cell line.

THP1	Apoptotic cells (%)						p value
	Drug alone			Drug with TG pretreatment			
Dox 75nM	48.3	51.8	54.5	60.4	55.7	55.1	0.24843
Bort 5nM	15.1	17.5	17.6	21.7	21.4	23.4	0.02071
17-AAG 250nM	9.0	11.8	9.5	13.5	13.0	10.3	0.20709
SAHA 500nM	11.4	12.4	13.3	13.8	12.3	13.5	0.37811

Table 2.30. Apoptotic cells (as a percentage of total cells) after 48 hours treatment with drug, with or without 6 hours of thapsigargin pretreatment, in the THP1 cell line.

THP1	Total cell number (%)						p value
	Drug alone			Drug with TG pretreatment			
Dox 75nM	44.1	44.7	50.7	49.2	52.1	54.0	0.04796
Bort 5nM	73.1	66.6	80.9	79.8	77.2	72.7	0.64672
17-AAG 250nM	88.9	70.3	91.8	88.3	85.8	105.3	0.20341
SAHA 500nM	64.0	65.5	68.3	76.5	75.7	79.7	0.00327

Table 2.31. Total cell number (%) after 48 hours treatment with drug, with or without 6 hours of thapsigargin pretreatment, in the THP1 cell line (each normalised to its own control).

THP1	Viable cell number (%)						p value
	Drug alone			Drug with TG pretreatment			
Dox 75nM	24.9	23.6	25.4	21.1	25.4	26.8	0.91491
Bort 5nM	67.5	60.3	73.5	68.0	66.6	61.5	0.78136
17-AAG 250nM	88.2	68.6	91.9	83.4	82.1	104.6	0.35554
SAHA 500nM	61.8	63.2	65.3	72.1	73.2	76.0	0.00049

Table 2.32. Viable cell number (%) after 48 hours treatment with drug, with or without 6 hours of thapsigargin pretreatment, in the THP1 cell line (each normalised to its own control).

U266		Cells In Each Region (%)			Average	SD
Control	nuclear debris	0.2	0.4	0.2	**0.3**	**0.1**
	late apoptosis/dead cells	3.1	2.9	2.9	**3.0**	**0.1**
	viable cells	83.8	85.2	83.4	**84.1**	**0.9**
	early apoptosis	12.9	11.5	13.5	**12.6**	**1.0**
TG 5nM	nuclear debris	0.5	0.5	0.7	**0.6**	**0.1**
	late apoptosis/dead cells	3.4	1.7	2.1	**2.4**	**0.9**
	viable cells	81.9	85.8	85.8	**84.5**	**2.3**
	early apoptosis	14.2	12.0	11.3	**12.5**	**1.5**
Dox 1μM	nuclear debris	0.0	0.0	0.0	**0.0**	**0.0**
(positive control)	late apoptosis/dead cells	34.8	41.2	46.2	**40.7**	**5.7**
	viable cells	5.7	4.1	3.1	**4.3**	**1.3**
	early apoptosis	59.5	54.8	50.7	**55.0**	**4.4**
Dox 75nM	nuclear debris	0.6	0.1	0.2	**0.3**	**0.3**
	late apoptosis/dead cells	7.3	7.1	6.6	**7.0**	**0.4**
	viable cells	47.1	33.4	39.8	**40.1**	**6.9**
	early apoptosis	45.0	59.4	53.5	**52.6**	**7.2**
TG + Dox	nuclear debris	0.3	0.1	0.1	**0.2**	**0.1**
	late apoptosis/dead cells	7.6	6.0	6.2	**6.6**	**0.9**
	viable cells	33.2	31.6	33.0	**32.6**	**0.9**
	early apoptosis	58.9	62.3	60.7	**60.6**	**1.7**
Bort 5nM	nuclear debris	0.5	0.3	0.3	**0.4**	**0.1**
	late apoptosis/dead cells	4.3	4.1	4.1	**4.2**	**0.1**
	viable cells	64.3	61.9	63.1	**63.1**	**1.2**
	early apoptosis	30.9	33.6	32.5	**32.3**	**1.4**
TG + Bort	nuclear debris	0.3	0.3	0.4	**0.3**	**0.1**
	late apoptosis/dead cells	4.8	4.3	4.5	**4.5**	**0.3**
	viable cells	59.3	72.0	72.5	**67.9**	**7.5**
	early apoptosis	35.6	23.5	22.6	**27.2**	**7.3**
17-AAG 250nM	nuclear debris	0.6	0.2	0.6	**0.5**	**0.2**
	late apoptosis/dead cells	3.5	2.8	3.2	**3.2**	**0.4**
	viable cells	75.2	76.1	75.2	**75.5**	**0.5**
	early apoptosis	20.7	21.0	20.9	**20.9**	**0.2**
TG + 17-AAG	nuclear debris	0.3	0.3	0.7	**0.4**	**0.2**
	late apoptosis/dead cells	4.6	4.5	5.9	**5.0**	**0.8**
	viable cells	66.9	72.6	69.2	**69.6**	**2.9**
	early apoptosis	28.3	22.6	24.2	**25.0**	**2.9**
SAHA 500nM	nuclear debris	0.7	0.5	0.2	**0.5**	**0.3**
	late apoptosis/dead cells	4.7	3.4	3.3	**3.8**	**0.8**
	viable cells	71.5	73.4	75.9	**73.6**	**2.2**
	early apoptosis	23.2	22.8	20.6	**22.2**	**1.4**
TG + SAHA	nuclear debris	0.2	0.4	0.3	**0.3**	**0.1**
	late apoptosis/dead cells	5.0	3.7	4.2	**4.3**	**0.7**
	viable cells	67.7	71.7	68.6	**69.3**	**2.1**
	early apoptosis	27.2	24.2	26.9	**26.1**	**1.7**

Table A2.33. Apoptosis assay results for cells in each region (%) following 48 hours of drug treatment in the U266 cell line.

U266		Cell No. By Region (cells/mL)			Average	SD
Control	nuclear debris	577	1008	446	**677**	**294**
	late apoptosis/dead cells	7337	7059	7496	**7297**	**221**
	viable cells	199746	206990	215066	**207267**	**7664**
	early apoptosis	30832	27901	34892	**31208**	**3511**
TG 5nM	nuclear debris	1271	992	1620	**1294**	**315**
	late apoptosis/dead cells	8897	3739	4705	**5780**	**2742**
	viable cells	216619	188553	189515	**198229**	**15934**
	early apoptosis	37677	26402	24914	**29664**	**6979**
Dox 1μM	nuclear debris	0	0	0	**0**	**0**
(positive control)	late apoptosis/dead cells	43836	51235	61712	**52261**	**8982**
	viable cells	7235	5044	4177	**5486**	**1576**
	early apoptosis	75063	68118	67640	**70274**	**4154**
Dox 75nM	nuclear debris	699	183	267	**383**	**277**
	late apoptosis/dead cells	8926	9659	8720	**9101**	**493**
	viable cells	57833	45592	52809	**52078**	**6153**
	early apoptosis	55200	81205	71005	**69137**	**13103**
TG + Dox	nuclear debris	489	160	121	**257**	**202**
	late apoptosis/dead cells	12219	7129	7484	**8944**	**2842**
	viable cells	53762	37607	39713	**43694**	**8782**
	early apoptosis	95305	74052	72948	**80769**	**12601**
Bort 5nM	nuclear debris	952	688	663	**767**	**160**
	late apoptosis/dead cells	8058	8460	7953	**8157**	**268**
	viable cells	121315	126907	123802	**124008**	**2802**
	early apoptosis	58246	68991	63889	**63709**	**5374**
TG + Bort	nuclear debris	597	525	795	**639**	**140**
	late apoptosis/dead cells	10592	8275	8876	**9248**	**1202**
	viable cells	131428	140022	142750	**138067**	**5909**
	early apoptosis	78991	45777	44382	**56383**	**19592**
17-AAG 250nM	nuclear debris	1210	316	1071	**865**	**481**
	late apoptosis/dead cells	6923	5240	5354	**5839**	**940**
	viable cells	150356	143000	126351	**139902**	**12299**
	early apoptosis	41471	39459	35166	**38699**	**3220**
TG + 17-AAG	nuclear debris	613	481	1118	**737**	**337**
	late apoptosis/dead cells	10414	8053	8896	**9121**	**1196**
	viable cells	152301	130110	104566	**128992**	**23887**
	early apoptosis	64320	40565	36550	**47145**	**15009**
SAHA 500nM	nuclear debris	1022	880	425	**776**	**312**
	late apoptosis/dead cells	7101	5869	5893	**6288**	**705**
	viable cells	108867	128464	137613	**124981**	**14686**
	early apoptosis	35250	39907	37304	**37487**	**2334**
TG + SAHA	nuclear debris	368	706	524	**533**	**169**
	late apoptosis/dead cells	10975	6474	7219	**8223**	**2413**
	viable cells	148498	125942	119231	**131224**	**15332**
	early apoptosis	59591	42491	46749	**49610**	**8902**

Table A2.34. Apoptosis assay results for cell number by region following 48 hours of drug treatment in the U266 cell line.

U266	Apoptotic cells (%)						p value
	Drug alone			Drug with TG pretreatment			
Dox 75nM	52.0	66.2	59.7	66.0	67.6	66.6	0.17874
Bort 5nM	34.8	37.5	36.1	40.0	27.4	26.8	0.44107
17-AAG 250nM	24.0	23.6	24.0	32.5	27.0	29.8	0.05820
SAHA 500nM	27.6	26.0	23.7	31.9	27.7	30.9	0.10782

Table A2.35. Apoptotic cells (as a percentage of total cells) after 48 hours treatment with drug, with or without 6 hours of thapsigargin pretreatment, in the U266 cell line.

U266	Total cell number (%)						p value
	Drug alone			Drug with TG pretreatment			
Dox 75nM	49.9	54.5	49.9	59.8	52.5	52.2	0.42980
Bort 5nM	77.0	81.8	74.3	82.2	86.1	85.9	0.09422
17-AAG 250nM	81.5	75.1	63.2	84.3	78.8	65.9	0.00850
SAHA 500nM	62.0	69.8	68.1	81.1	77.1	75.5	0.10334

Table A2.36. Total cell number (%) after 48 hours treatment with drug, with or without 6 hours of thapsigargin pretreatment, in the U266 cell line (each normalised to its own control).

U266	Viable cell number (%)						p value
	Drug alone			Drug with TG pretreatment			
Dox 75nM	29.0	22.0	24.6	24.8	19.9	21.0	0.03356
Bort 5nM	60.7	61.3	57.6	60.7	74.3	75.3	0.19496
17-AAG 250nM	75.3	69.1	58.7	70.3	69.0	55.2	0.18655
SAHA 500nM	54.5	62.1	64.0	68.6	66.8	62.9	0.31215

Table A2.37. Viable cell number (%) after 48 hours treatment with drug, with or without 6 hours of thapsigargin pretreatment, in the U266 cell line (each normalised to its own control).

SUD4		Cells In Each Region (%)			Average	SD
Control	nuclear debris	2.9	2.2	2.7	**2.6**	**0.4**
	late apoptosis/dead cells	3.3	2.7	2.8	**2.9**	**0.3**
	viable cells	90.3	91.3	90.2	**90.6**	**0.6**
	early apoptosis	3.4	3.8	4.4	**3.9**	**0.5**
TG 10nM	nuclear debris	1.8	1.5	2.1	**1.8**	**0.3**
	late apoptosis/dead cells	2.5	2.2	2.4	**2.4**	**0.2**
	viable cells	89.8	91.5	89.8	**90.4**	**1.0**
	early apoptosis	5.9	4.8	5.7	**5.5**	**0.6**
Dox 1μM	nuclear debris	0.3	0.5	0.5	**0.4**	**0.1**
(positive control)	late apoptosis/dead cells	40.6	39.3	42.6	**40.8**	**1.7**
	viable cells	18.5	18.3	15.5	**17.4**	**1.7**
	early apoptosis	40.5	41.9	41.4	**41.3**	**0.7**
Dox 75nM	nuclear debris	2.2	2.2	2.0	**2.1**	**0.1**
	late apoptosis/dead cells	14.2	12.7	12.6	**13.2**	**0.9**
	viable cells	57.0	57.4	57.1	**57.2**	**0.2**
	early apoptosis	26.6	27.7	28.3	**27.5**	**0.9**
TG + Dox	nuclear debris	2.0	2.2	2.3	**2.2**	**0.2**
	late apoptosis/dead cells	13.1	13.1	14.3	**13.5**	**0.7**
	viable cells	54.8	54.7	52.6	**54.0**	**1.2**
	early apoptosis	30.1	30.0	30.8	**30.3**	**0.4**
Bort 5nM	nuclear debris	2.6	2.6	2.0	**2.4**	**0.3**
	late apoptosis/dead cells	3.7	3.9	4.7	**4.1**	**0.5**
	viable cells	87.4	87.7	87.0	**87.4**	**0.4**
	early apoptosis	6.3	5.8	6.3	**6.1**	**0.3**
TG + Bort	nuclear debris	1.8	2.3	2.6	**2.2**	**0.4**
	late apoptosis/dead cells	4.2	5.3	4.7	**4.7**	**0.6**
	viable cells	86.5	84.5	85.9	**85.6**	**1.0**
	early apoptosis	7.5	7.9	6.8	**7.4**	**0.6**
17-AAG 250nM	nuclear debris	2.2	1.8	2.0	**2.0**	**0.2**
	late apoptosis/dead cells	2.8	3.1	2.9	**2.9**	**0.2**
	viable cells	88.7	90.0	89.0	**89.2**	**0.7**
	early apoptosis	6.3	5.2	6.1	**5.9**	**0.6**
TG + 17-AAG	nuclear debris	2.5	1.8	2.2	**2.2**	**0.4**
	late apoptosis/dead cells	2.8	3.9	3.2	**3.3**	**0.6**
	viable cells	88.2	86.3	86.7	**87.1**	**1.0**
	early apoptosis	6.6	8.0	7.9	**7.5**	**0.8**
SAHA 500nM	nuclear debris	2.6	2.4	2.5	**2.5**	**0.1**
	late apoptosis/dead cells	3.7	3.9	3.3	**3.6**	**0.3**
	viable cells	88.0	87.2	88.5	**87.9**	**0.7**
	early apoptosis	5.7	6.5	5.7	**6.0**	**0.5**
TG + SAHA	nuclear debris	2.8	1.9	2.8	**2.5**	**0.5**
	late apoptosis/dead cells	3.7	4.2	3.5	**3.8**	**0.4**
	viable cells	86.0	85.7	86.1	**85.9**	**0.2**
	early apoptosis	7.6	8.2	7.6	**7.8**	**0.3**

Table A2.38. Apoptosis assay results for cells in each region (%) following 48 hours of drug treatment in the SUD4 cell line.

SUD4		Cell No. By Region (cells/mL)			Average	SD
Control	nuclear debris	24034	16918	19754	**20235**	**3582**
	late apoptosis/dead cells	27311	20507	20495	**22771**	**3932**
	viable cells	740126	702370	667941	**703479**	**36105**
	early apoptosis	27857	29223	32595	**29891**	**2438**
TG 10nM	nuclear debris	12555	10573	14213	**12447**	**1822**
	late apoptosis/dead cells	18003	14940	16243	**16396**	**1537**
	viable cells	637932	630939	607760	**625544**	**15793**
	early apoptosis	42166	33098	38577	**37947**	**4566**
Dox 1μM	nuclear debris	783	1253	1036	**1024**	**235**
(positive control)	late apoptosis/dead cells	95423	92265	94610	**94099**	**1640**
	viable cells	43445	43078	34471	**40331**	**5079**
	early apoptosis	95188	98374	91799	**95120**	**3288**
Dox 75nM	nuclear debris	4439	4522	4239	**4400**	**146**
	late apoptosis/dead cells	29090	26507	26267	**27288**	**1565**
	viable cells	116768	119803	119035	**118536**	**1578**
	early apoptosis	54560	57884	58927	**57124**	**2281**
TG + Dox	nuclear debris	4450	4689	4685	**4608**	**137**
	late apoptosis/dead cells	28598	27434	29623	**28552**	**1095**
	viable cells	119935	114777	108778	**114496**	**5583**
	early apoptosis	65876	63057	63586	**64173**	**1499**
Bort 5nM	nuclear debris	15219	15241	11827	**14095**	**1965**
	late apoptosis/dead cells	21657	23356	27337	**24117**	**2915**
	viable cells	511772	520766	505838	**512792**	**7516**
	early apoptosis	36681	34441	36644	**35922**	**1283**
TG + Bort	nuclear debris	10633	11781	14639	**12351**	**2063**
	late apoptosis/dead cells	25480	27547	26650	**26559**	**1037**
	viable cells	520833	439191	483645	**481223**	**40875**
	early apoptosis	44941	41234	38099	**41424**	**3425**
17-AAG 250nM	nuclear debris	14630	11764	13826	**13407**	**1478**
	late apoptosis/dead cells	18399	20043	19492	**19311**	**837**
	viable cells	590095	587992	605392	**594493**	**9497**
	early apoptosis	41896	33768	41251	**38972**	**4518**
TG + 17-AAG	nuclear debris	16213	11627	15017	**14286**	**2379**
	late apoptosis/dead cells	18404	25667	21616	**21896**	**3640**
	viable cells	579505	568189	591821	**579838**	**11819**
	early apoptosis	43162	52651	54154	**49989**	**5960**
SAHA 500nM	nuclear debris	15632	15189	15181	**15334**	**258**
	late apoptosis/dead cells	22447	24344	19776	**22189**	**2295**
	viable cells	529097	544096	530348	**534514**	**8322**
	early apoptosis	34071	40573	33958	**36201**	**3787**
TG + SAHA	nuclear debris	15957	10525	16609	**14364**	**3340**
	late apoptosis/dead cells	21148	23081	21011	**21747**	**1158**
	viable cells	496016	474923	517079	**496006**	**21078**
	early apoptosis	43642	45424	45625	**44897**	**1092**

Table A2.39. Apoptosis assay results for cell number by region following 48 hours of drug treatment in the SUD4 cell line.

SUD4	Apoptotic cells (%)						p value
	Drug alone			Drug with TG pretreatment			
Dox 75nM	40.8	40.4	40.9	43.2	43.1	45.1	0.03436
Bort 5nM	10.0	9.7	11.0	11.7	13.2	11.5	0.15934
17-AAG 250nM	9.1	8.2	8.9	9.4	11.9	11.1	0.17062
SAHA 500nM	9.4	10.4	9.0	11.2	12.4	11.1	0.00192

Table A2.40. Apoptotic cells (as a percentage of total cells) after 48 hours treatment with drug, with or without 6 hours of thapsigargin pretreatment, in the SUD4 cell line.

SUD4	Total cell number (%)						p value
	Drug alone			Drug with TG pretreatment			
Dox 75nM	25.0	27.1	28.1	30.8	30.4	30.5	0.06359
Bort 5nM	71.4	77.2	78.5	84.7	75.4	83.2	0.34470
17-AAG 250nM	81.2	85.0	91.8	92.5	95.4	100.9	0.00405
SAHA 500nM	73.4	81.2	80.9	81.2	80.3	88.7	0.22936

Table A2.41. Total cell number (%) after 48 hours treatment with drug, with or without 6 hours of thapsigargin pretreatment, in the SUD4 cell line (each normalised to its own control).

SUD4	Viable cell number (%)						p value
	Drug alone			Drug with TG pretreatment			
Dox 75nM	15.8	17.1	17.8	18.8	18.2	17.9	0.24308
Bort 5nM	69.1	74.1	75.7	81.6	69.6	79.6	0.50735
17-AAG 250nM	79.7	83.7	90.6	90.8	90.1	97.4	0.03408
SAHA 500nM	71.5	77.5	79.4	77.8	75.3	85.1	0.35553

Table A2.42. Viable cell number (%) after 48 hours treatment with drug, with or without 6 hours of thapsigargin pretreatment, in the SUD4 cell line (each normalised to its own control).

SUD4		Cells In Each Region (%)			Average	SD
Control	nuclear debris	3.0	3.7	2.7	**3.1**	**0.5**
	late apoptosis/dead cells	10.3	12.2	10.8	**11.1**	**1.0**
	viable cells	80.4	77.2	80.1	**79.2**	**1.8**
	early apoptosis	6.3	6.9	6.4	**6.5**	**0.3**
TG 100nM	nuclear debris	2.5	2.6	3.1	**2.7**	**0.3**
	late apoptosis/dead cells	11.5	11.3	18.0	**13.6**	**3.8**
	viable cells	78.9	79.5	70.7	**76.4**	**4.9**
	early apoptosis	7.0	6.6	8.1	**7.2**	**0.8**
Dox 1μM	nuclear debris	0.3	0.3	0.2	**0.3**	**0.1**
(positive control)	late apoptosis/dead cells	50.3	52.5	55.0	**52.6**	**2.4**
	viable cells	16.2	14.0	11.8	**14.0**	**2.2**
	early apoptosis	33.2	33.2	32.9	**33.1**	**0.2**
Dox 100nM	nuclear debris	1.4	1.2	1.1	**1.2**	**0.2**
	late apoptosis/dead cells	32.3	33.8	32.3	**32.8**	**0.9**
	viable cells	42.3	41.2	42.8	**42.1**	**0.8**
	early apoptosis	24.0	23.8	23.7	**23.8**	**0.2**
TG + Dox	nuclear debris	1.5	1.2	1.0	**1.2**	**0.3**
	late apoptosis/dead cells	34.3	34.8	33.4	**34.2**	**0.7**
	viable cells	40.3	38.0	39.3	**39.2**	**1.2**
	early apoptosis	23.9	26.0	26.2	**25.4**	**1.3**
Bort 10nM	nuclear debris	6.0	5.8	4.8	**5.5**	**0.6**
	late apoptosis/dead cells	32.5	33.8	33.9	**33.4**	**0.8**
	viable cells	46.9	43.1	46.2	**45.4**	**2.0**
	early apoptosis	14.6	17.3	15.1	**15.7**	**1.4**
TG + Bort	nuclear debris	4.3	4.6	3.8	**4.2**	**0.4**
	late apoptosis/dead cells	36.9	39.6	38.3	**38.3**	**1.4**
	viable cells	40.7	39.5	41.2	**40.5**	**0.9**
	early apoptosis	18.0	16.3	16.7	**17.0**	**0.9**
17-AAG 1μM	nuclear debris	3.6	2.6	4.2	**3.5**	**0.8**
	late apoptosis/dead cells	23.8	21.2	27.0	**24.0**	**2.9**
	viable cells	56.3	60.5	51.6	**56.1**	**4.5**
	early apoptosis	16.2	15.7	17.2	**16.4**	**0.8**
TG + 17-AAG	nuclear debris	2.6	2.3	2.6	**2.5**	**0.2**
	late apoptosis/dead cells	28.7	26.4	35.3	**30.1**	**4.6**
	viable cells	47.3	53.2	38.8	**46.4**	**7.2**
	early apoptosis	21.5	18.1	23.3	**21.0**	**2.6**
SAHA 1μM	nuclear debris	2.5	2.0	2.1	**2.2**	**0.3**
	late apoptosis/dead cells	13.7	17.4	16.1	**15.7**	**1.9**
	viable cells	69.7	63.6	67.9	**67.1**	**3.1**
	early apoptosis	14.1	17.1	14.0	**15.1**	**1.8**
TG + SAHA	nuclear debris	2.4	5.3	6.3	**4.7**	**2.0**
	late apoptosis/dead cells	14.9	25.9	34.5	**25.1**	**9.8**
	viable cells	67.9	52.8	42.8	**54.5**	**12.6**
	early apoptosis	14.7	15.9	16.4	**15.7**	**0.9**

Table A2.43. Apoptosis assay results for cells in each region (%) following 48 hours of drug treatment with higher drug concentrations in the SUD4 cell line.

SUD4		Cell No. By Region (cells/mL)			Average	SD
Control	nuclear debris	10933	11732	10280	**10982**	**727**
	late apoptosis/dead cells	37005	38233	41119	**38786**	**2112**
	viable cells	289911	242598	304839	**279116**	**32495**
	early apoptosis	22587	21683	24494	**22921**	**1435**
TG 100nM	nuclear debris	8624	8207	7827	**8219**	**399**
	late apoptosis/dead cells	39263	36131	45048	**40147**	**4524**
	viable cells	268710	254306	176696	**233237**	**49493**
	early apoptosis	23830	21103	20234	**21722**	**1876**
Dox 1μM	nuclear debris	455	416	272	**381**	**96**
(positive control)	late apoptosis/dead cells	76232	81995	74875	**77700**	**3780**
	viable cells	24568	21903	16100	**20857**	**4330**
	early apoptosis	50400	51767	44807	**48991**	**3688**
Dox 100nM	nuclear debris	2101	1681	1895	**1892**	**210**
	late apoptosis/dead cells	48414	48699	54061	**50391**	**3181**
	viable cells	63519	59409	71617	**64848**	**6212**
	early apoptosis	36011	34291	39626	**36643**	**2723**
TG + Dox	nuclear debris	2589	2015	1565	**2056**	**513**
	late apoptosis/dead cells	57916	58428	50632	**55659**	**4361**
	viable cells	68047	63856	59567	**63824**	**4240**
	early apoptosis	40299	43597	39678	**41191**	**2106**
Bort 10nM	nuclear debris	11768	10673	9602	**10681**	**1083**
	late apoptosis/dead cells	63741	62134	67817	**64564**	**2930**
	viable cells	92048	79309	92357	**87905**	**7446**
	early apoptosis	28569	31895	30274	**30246**	**1663**
TG + Bort	nuclear debris	7872	8167	6912	**7650**	**656**
	late apoptosis/dead cells	67093	69860	69123	**68692**	**1433**
	viable cells	73936	69566	74232	**72578**	**2613**
	early apoptosis	32759	28672	30053	**30495**	**2079**
17-AAG 1μM	nuclear debris	6405	5047	6694	**6049**	**879**
	late apoptosis/dead cells	42015	40567	43430	**42004**	**1431**
	viable cells	99308	115889	82897	**99365**	**16496**
	early apoptosis	28558	30154	27632	**28782**	**1276**
TG + 17-AAG	nuclear debris	4722	4081	4193	**4332**	**343**
	late apoptosis/dead cells	63299	47588	46226	**52371**	**9488**
	viable cells	69575	95717	76220	**80504**	**13587**
	early apoptosis	41721	32646	34616	**36328**	**4774**
SAHA 1μM	nuclear debris	5969	4949	4992	**5303**	**577**
	late apoptosis/dead cells	33231	42973	38807	**38337**	**4888**
	viable cells	168575	157294	164004	**163291**	**5674**
	early apoptosis	34199	42231	33735	**36722**	**4777**
TG + SAHA	nuclear debris	5825	10911	12198	**9644**	**3370**
	late apoptosis/dead cells	35668	53386	66733	**51929**	**15584**
	viable cells	162620	108763	82932	**118105**	**40657**
	early apoptosis	35269	32800	31753	**33274**	**1805**

Table A2.44. Apoptosis assay results for cell number by region following 48 hours of drug treatment with higher drug concentrations in the SUD4 cell line.

SUD4	Apoptotic cells (%)						p value
	Drug alone			Drug with TG pretreatment			
Dox 100nM	56.3	57.6	56.0	58.2	60.8	59.6	0.02978
Bort 10nM	47.1	51.1	49.0	55.0	55.9	55.0	0.02046
17-AAG 1μM	40.0	36.9	44.2	50.1	44.6	58.6	0.03157
SAHA 1μM	27.9	34.4	30.0	29.6	41.9	50.9	0.21858

Table A2.45. Apoptotic cells (as a percentage of total cells) after 48 hours treatment with drug, with or without 6 hours of thapsigargin pretreatment, in the SUD4 cell line.

SUD4	Total cell number (%)						p value
	Drug alone			Drug with TG pretreatment			
Dox 100nM	41.6	45.8	43.9	49.6	52.5	60.6	0.08031
Bort 10nM	49.6	52.5	60.6	54.4	58.6	52.5	0.56162
17-AAG 1μM	54.4	58.6	52.5	53.4	55.1	72.2	0.46539
SAHA 1μM	53.4	55.1	72.2	48.9	61.0	42.2	0.91803

Table A2.46. Total cell number (%) after 48 hours treatment with drug, with or without 6 hours of thapsigargin pretreatment, in the SUD4 cell line (each normalised to its own control).

SUD4	Viable cell number (%)						p value
	Drug alone			Drug with TG pretreatment			
Dox 100nM	21.9	24.5	23.5	25.3	25.1	33.7	0.23741
Bort 10nM	25.3	25.1	33.7	31.8	32.7	30.3	0.90872
17-AAG 1μM	31.8	32.7	30.3	27.5	27.4	42.0	0.92869
SAHA 1μM	27.5	27.4	42.0	34.3	47.8	27.2	0.33991

Table A2.47. Viable cell number (%) after 48 hours treatment with drug, with or without 6 hours of thapsigargin pretreatment, in the SUD4 cell line (each normalised to its own control).

Appendix 3

ADDITIONAL DATA FOR CHAPTER 6

ATP ASSAY:

Cell line	Conc.	Set 1	Set 2	Set 3	Average	SD
THP1	**0**	100.0	100.0	100.0	**100.0**	**0.0**
THP1	**100µM**	100.8	96.5	98.8	**98.7**	**2.2**
THP1	**300µM**	95.6	92.7	97.3	**95.2**	**2.3**
THP1	**1mM**	78.0	67.6	67.3	**71.0**	**6.1**
THP1	**3mM**	37.9	36.6	31.1	**35.2**	**3.6**
THP1	**10mM**	0.5	2.5	0.0	**1.0**	**1.3**

Table A3.1. Effect of 4-PBA treatment for 48 hours on cell viability (ATP content)

Cell line	Conc.	Set 1	Set 2	Set 3	Average	SD
U266	**0**	100.0	100.0	100.0	**100.0**	**0.0**
U266	**100µM**	97.4	92.8	99.1	**96.4**	**3.3**
U266	**300µM**	96.2	92.6	96.9	**95.2**	**2.4**
U266	**1mM**	71.2	65.7	76.5	**71.1**	**5.4**
U266	**3mM**	26.3	25.8	25.7	**25.9**	**0.3**
U266	**10mM**	1.4	8.1	0.0	**3.2**	**4.3**

Table A3.2. Effect of 4-PBA treatment for 48 hours on cell viability (ATP content)

Cell line	Conc.	Set 1	Set 2	Set 3	Average	SD
DOHH2	**0**	100.0	100.0	100.0	**100.0**	**0.0**
DOHH2	**100µM**	86.6	89.8	93.3	**89.9**	**3.3**
DOHH2	**300µM**	83.8	84.4	89.5	**85.9**	**3.2**
DOHH2	**1mM**	36.5	46.0	38.6	**40.3**	**5.0**
DOHH2	**3mM**	4.1	10.8	2.1	**5.7**	**4.6**
DOHH2	**10mM**	0.0	4.6	0.0	**1.5**	**2.7**

Table A3.3. Effect of 4-PBA treatment for 48 hours on cell viability (ATP content)

Cell line	Conc.	Set 1	Set 2	Set 3	Average	SD
HT29	**0**	100.0	100.0	100.0	**100.0**	**0.0**
HT29	**100µM**	95.0	94.7	87.5	**92.4**	**4.2**
HT29	**300µM**	86.5	90.2	90.7	**89.1**	**2.3**
HT29	**1mM**	87.5	72.8	76.5	**78.9**	**7.7**
HT29	**3mM**	68.2	50.0	46.4	**54.9**	**11.7**
HT29	**10mM**	1.3	0.9	1.0	**1.1**	**0.2**

Table A3.4. Effect of 4-PBA treatment for 48 hours on cell viability (ATP content)

GUAVA VIACOUNT ASSAY:

Cell line	Conc.	Set 1	Set 2	Set 3	Average	SD
THP1	**0**	100.0	100.0	100.0	**100.0**	**0.0**
THP1	**100µM**	83.7	90.6	93.9	**89.4**	**5.2**
THP1	**300µM**	81.1	83.0	88.8	**84.3**	**4.0**
THP1	**1mM**	54.1	48.1	57.2	**53.1**	**4.6**
THP1	**3mM**	35.5	28.1	35.1	**32.9**	**4.2**
THP1	**10mM**	16.8	17.7	18.2	**17.6**	**0.7**

Table A3.5. Effect of 4-PBA treatment for 48 hours on cell number (% of control)

Cell line	Conc.	Set 1	Set 2	Set 3	Average	SD
THP1	**0**	100.0	100.0	100.0	**100.0**	**0.0**
THP1	**100µM**	98.7	100.2	99.8	**99.6**	**0.8**
THP1	**300µM**	97.6	100.1	100.2	**99.3**	**1.4**
THP1	**1mM**	94.3	98.8	97.3	**96.8**	**2.3**
THP1	**3mM**	91.5	87.8	93.6	**90.9**	**2.9**
THP1	**10mM**	0.0	42.1	35.8	**26.0**	**22.7**

Table A3.6. Effect of 4-PBA treatment for 48 hours on cell viability (% of control)

Cell line	Conc.	Set 1	Set 2	Set 3	Average	SD
U266	**0**	100.0	100.0	100.0	100.0	**100.0**
U266	**100µM**	95.0	97.0	98.8	102.3	**97.0**
U266	**300µM**	88.3	83.2	92.4	95.0	**88.0**
U266	**1mM**	71.9	71.2	65.6	65.8	**69.6**
U266	**3mM**	61.4	45.7	40.5	38.4	**49.2**
U266	**10mM**	54.0	42.5	35.9	29.2	**44.1**

Table A3.7. Effect of 4-PBA treatment for 48 hours on cell number (% of control)

Cell line	Conc.	Set 1	Set 2	Set 3	Average	SD
U266	**0**	100.0	100.0	100.0	**100.0**	**0.0**
U266	**100µM**	99.3	98.4	99.7	**99.1**	**0.7**
U266	**300µM**	99.3	97.5	99.3	**98.7**	**1.0**
U266	**1mM**	93.7	92.0	93.6	**93.1**	**0.9**
U266	**3mM**	79.0	64.3	76.4	**73.3**	**7.8**
U266	**10mM**	26.5	28.3	29.3	**28.0**	**1.4**

Table A3.8. Effect of 4-PBA treatment for 48 hours on cell viability (% of control)

Cell line	Conc.	Set 1	Set 2	Set 3	Average	SD
DOHH2	**0**	100.0	100.0	100.0	**100.0**	**0.0**
DOHH2	**100µM**	93.6	103.4	100.0	**99.0**	**5.0**
DOHH2	**300µM**	86.6	102.1	94.0	**94.2**	**7.8**
DOHH2	**1mM**	79.6	75.9	78.5	**78.0**	**1.9**
DOHH2	**3mM**	71.5	48.3	72.5	**64.1**	**13.7**
DOHH2	**10mM**	57.3	34.5	24.6	**38.8**	**16.8**

Table A3.9. Effect of 4-PBA treatment for 48 hours on cell number (% of control)

Cell line	Conc.	Set 1	Set 2	Set 3	Average	SD
DOHH2	**0**	100.0	100.0	100.0	**100.0**	**0.0**
DOHH2	**100µM**	58.7	90.1	88.3	**79.0**	**17.7**
DOHH2	**300µM**	61.2	69.7	82.4	**71.1**	**10.6**
DOHH2	**1mM**	58.9	64.3	62.3	**61.8**	**2.7**
DOHH2	**3mM**	46.1	25.1	42.9	**38.0**	**11.3**
DOHH2	**10mM**	37.3	0.0	34.1	**23.8**	**20.7**

Table A3.10. Effect of 4-PBA treatment for 48 hours on cell number (% of control)

4-PBA Simultaneous treatment

THP1	% of control				
	Set 1	**Set 2**	**Set 3**	**Average**	**SD**
Control	100.0	100.0	100.0	**100.0**	**0.0**
PBA 0.5mM	93.1	81.0	89.3	**87.8**	**6.2**
TM 100nM	26.1	55.1	17.4	**32.9**	**19.8**
TM 1μM	7.5	10.1	10.2	**9.3**	**1.5**
PBA 0.5mM + TM 100nM	21.6	55.4	14.2	**30.4**	**22.0**
PBA 0.5mM + TM 1μM	5.7	6.2	6.1	**6.0**	**0.3**
TG 1nM	60.5	55.8	97.7	**71.3**	**23.0**
TG 10nM	32.0	33.2	44.3	**36.5**	**6.8**
PBA 0.5mM + TG 1nM	55.8	49.4	86.5	**63.9**	**19.9**
PBA 0.5mM + TG 10nM	27.4	27.2	44.3	**33.0**	**9.8**
Control	100.0	100.0	100.0	**100.0**	**0.0**
PBA 0.5mM	91.2	80.6	83.2	**85.0**	**5.5**
Dox 10nM	92.3	91.3	66.6	**83.4**	**14.6**
Dox 75nM	85.5	83.5	68.1	**79.0**	**9.5**
PBA 0.5mM + Dox 10nM	87.1	78.2	61.6	**75.6**	**12.9**
PBA 0.5mM + Dox 75nM	78.6	70.5	64.9	**71.3**	**6.9**
Bort 1nM	92.9	87.0	70.5	**83.5**	**11.6**
Bort 5nM	92.4	89.4	69.7	**83.8**	**12.3**
PBA 0.5mM + Bort 1nM	90.9	77.5	65.1	**77.8**	**12.9**
PBA 0.5mM + Bort 5nM	81.4	78.4	64.2	**74.7**	**9.2**
Control	100.0	100.0	100.0	**100.0**	**0.0**
PBA 0.5mM	89.2	80.2	90.1	**86.5**	**5.5**
17-AAG 50nM	87.6	89.9	98.0	**91.8**	**5.5**
17-AAG 250nM	70.1	61.2	77.5	**69.6**	**8.2**
PBA 0.5mM + 17-AAG 50nM	83.4	75.7	90.1	**83.0**	**7.2**
PBA 0.5mM + 17-AAG 250nM	70.6	68.5	64.6	**67.9**	**3.0**
SAHA 100nM	77.9	81.0	99.4	**86.1**	**11.7**
SAHA 500nM	73.5	72.8	91.6	**79.3**	**10.7**
PBA 0.5mM + SAHA 100nM	74.1	76.7	89.3	**80.0**	**8.1**
PBA 0.5mM + SAHA 500nM	68.1	65.2	82.3	**71.9**	**9.2**

Table A3.11. 4-PBA 0.5mM combined with drug treatment for 48 hours in the THP1 cell line

U266	% of control				
	Set 1	**Set 2**	**Set 3**	**Average**	**SD**
Control	100.0	100.0	100.0	**100.0**	**0.0**
PBA 0.5mM	94.4	84.7	89.9	**89.7**	**4.9**
TM 100nM	24.0	55.7	22.5	**34.1**	**18.8**
TM 10μM	10.6	11.2	13.1	**11.6**	**1.3**
PBA 0.5mM + TM 100nM	23.9	54.2	19.6	**32.5**	**18.8**
PBA 0.5mM + TM 10μM	8.8	8.2	8.5	**8.5**	**0.3**
TG 1nM	98.4	57.3	97.3	**84.3**	**23.4**
TG 10nM	46.0	39.6	46.0	**43.9**	**3.7**
PBA 0.5mM + TG 1nM	97.2	66.9	74.6	**79.6**	**15.8**
PBA 0.5mM + TG 10nM	41.0	37.3	42.7	**40.3**	**2.8**
Control	100.0	100.0	100.0	**100.0**	**0.0**
PBA 0.5mM	94.2	82.2	85.9	**87.4**	**6.1**
Dox 10nM	95.7	92.4	94.7	**94.3**	**1.7**
Dox 75nM	98.5	82.2	92.3	**91.0**	**8.2**
PBA 0.5mM + Dox 10nM	91.0	88.1	92.7	**90.6**	**2.3**
PBA 0.5mM + Dox 75nM	92.8	74.3	81.1	**82.7**	**9.3**
Bort 1nM	100.8	83.8	99.6	**94.7**	**9.5**
Bort 5nM	74.4	82.5	93.2	**83.4**	**9.4**
PBA 0.5mM + Bort 1nM	89.0	81.1	88.7	**86.3**	**4.4**
PBA 0.5mM + Bort 5nM	82.2	80.3	89.0	**83.8**	**4.6**
Control	100.0	100.0	100.0	**100.0**	**0.0**
PBA 0.5mM	93.6	85.0	88.2	**88.9**	**4.3**
17-AAG 50nM	98.5	97.7	96.1	**97.4**	**1.3**
17-AAG 250nM	87.6	77.0	75.2	**79.9**	**6.7**
PBA 0.5mM + 17-AAG 50nM	95.2	88.9	86.1	**90.1**	**4.6**
PBA 0.5mM + 17-AAG 250nM	98.1	80.9	78.8	**85.9**	**10.6**
SAHA 100nM	95.7	97.0	95.7	**96.1**	**0.8**
SAHA 500nM	80.0	84.1	84.8	**83.0**	**2.6**
PBA 0.5mM + SAHA 100nM	90.1	87.2	84.7	**87.3**	**2.7**
PBA 0.5mM + SAHA 500nM	91.5	72.5	76.9	**80.3**	**9.9**

Table A3.12. 4-PBA 0.5mM combined with drug treatment for 48 hours in the U266 cell line

DOHH2	% of control				
	Set 1	**Set 2**	**Set 3**	**Average**	**SD**
Control	100.0	100.0	100.0	**100.0**	**0.0**
PBA 0.5mM	72.4	81.5	82.5	**78.8**	**5.6**
TM 100nM	97.6	96.4	96.6	**96.9**	**0.7**
TM 1μM	60.6	46.3	37.8	**48.2**	**11.5**
PBA 0.5mM + TM 100nM	72.2	66.1	64.6	**67.6**	**4.0**
PBA 0.5mM + TM 1μM	48.2	35.0	36.8	**40.0**	**7.2**
TG 1nM	91.2	90.8	84.0	**88.7**	**4.1**
TG 10nM	80.8	82.7	91.2	**84.9**	**5.5**
PBA 0.5mM + TG 1nM	67.4	67.2	76.9	**70.5**	**5.6**
PBA 0.5mM + TG 10nM	65.3	55.9	60.8	**60.7**	**4.7**
Control	100.0	100.0	100.0	**100.0**	**0.0**
PBA 0.5mM	73.8	72.2	76.3	**74.1**	**2.1**
Dox 5nM	96.1	79.6	86.4	**87.4**	**8.3**
Dox 50nM	71.5	70.7	67.3	**69.8**	**2.2**
PBA 0.5mM + Dox 5nM	85.1	64.9	68.2	**72.7**	**10.8**
PBA 0.5mM + Dox 50nM	64.9	48.3	59.6	**57.6**	**8.5**
Bort 1nM	83.1	78.3	83.2	**81.5**	**2.8**
Bort 5nM	74.1	70.3	75.5	**73.3**	**2.7**
PBA 0.5mM + Bort 1nM	69.4	67.7	70.1	**69.1**	**1.2**
PBA 0.5mM + Bort 5nM	70.0	60.7	63.1	**64.6**	**4.8**
Control	100.0	100.0	100.0	**100.0**	**0.0**
PBA 0.5mM	75.0	66.8	69.2	**70.3**	**4.2**
17-AAG 50nM	72.4	70.5	64.5	**69.2**	**4.1**
17-AAG 250nM	52.7	15.2	31.8	**33.3**	**18.8**
PBA 0.5mM + 17-AAG 50nM	63.1	51.1	62.0	**58.7**	**6.6**
PBA 0.5mM + 17-AAG 250nM	47.0	21.1	20.8	**29.6**	**15.0**
SAHA 100nM	73.5	74.5	73.7	**73.9**	**0.5**
SAHA 500nM	46.2	45.2	62.7	**51.4**	**9.8**
PBA 0.5mM + SAHA 100nM	59.5	58.3	71.5	**63.1**	**7.3**
PBA 0.5mM + SAHA 500nM	36.9	36.4	33.0	**35.4**	**2.1**

Table A3.13. 4-PBA 0.5mM combined with drug treatment for 48 hours in the DOHH2 cell line

HT29	% of control				
	Set 1	**Set 2**	**Set 3**	**Average**	**SD**
Control	100.0	100.0	100.0	**100.0**	**0.0**
PBA 0.5mM	87.1	93.7	89.5	**90.1**	**3.4**
TM 100nM	87.2	82.9	87.8	**85.9**	**2.6**
TM 1μM	75.4	44.8	46.3	**55.5**	**17.2**
PBA 0.5mM + TM 100nM	92.2	82.2	86.7	**87.0**	**5.0**
PBA 0.5mM + TM 1μM	70.7	43.8	43.8	**52.8**	**15.5**
TG 1nM	80.7	93.8	91.0	**88.5**	**6.9**
TG 10nM	28.7	70.2	84.1	**61.0**	**28.8**
PBA 0.5mM + TG 1nM	72.1	89.8	88.7	**83.5**	**9.9**
PBA 0.5mM + TG 10nM	30.9	72.5	67.6	**57.0**	**22.8**
Control	100.0	100.0	100.0	**100.0**	**0.0**
PBA 0.5mM	88.9	88.3	92.4	**89.8**	**2.2**
Dox 10nM	89.1	93.5	97.5	**93.3**	**4.2**
Dox 75nM	88.8	94.2	96.3	**93.1**	**3.9**
PBA 0.5mM + Dox 10nM	88.3	97.1	96.0	**93.8**	**4.8**
PBA 0.5mM + Dox 75nM	90.2	91.8	93.4	**91.8**	**1.6**
Bort 1nM	93.7	93.6	96.8	**94.7**	**1.8**
Bort 5nM	92.3	90.5	92.0	**91.6**	**1.0**
PBA 0.5mM + Bort 1nM	98.3	89.7	89.8	**92.6**	**4.9**
PBA 0.5mM + Bort 5nM	100.5	91.3	93.3	**95.0**	**4.8**
Control	100.0	100.0	100.0	**100.0**	**0.0**
PBA 0.5mM	90.5	92.7	94.3	**92.5**	**1.9**
17-AAG 50nM	81.9	96.4	93.0	**90.4**	**7.6**
17-AAG 250nM	32.4	57.2	56.6	**48.7**	**14.2**
PBA 0.5mM + 17-AAG 50nM	91.6	91.0	95.0	**92.5**	**2.1**
PBA 0.5mM + 17-AAG 250nM	33.8	55.0	56.4	**48.4**	**12.7**
SAHA 100nM	87.7	95.5	96.4	**93.2**	**4.8**
SAHA 500nM	78.7	91.1	90.1	**86.6**	**6.9**
PBA 0.5mM + SAHA 100nM	98.8	96.7	99.8	**98.5**	**1.6**
PBA 0.5mM + SAHA 500nM	82.7	86.6	89.0	**86.1**	**3.2**

Table A3.14. 4-PBA 0.5mM combined with drug treatment for 48 hours in the HT29 cell line

Cell line	Drug concentrations	Combination Effect		
		Set 1	Set 2	Set 3
THP1	PBA 0.5mM + TM 100nM	0.89	1.24	0.92
THP1	PBA 0.5mM + TM 1μM	0.82	0.76	0.67
THP1	PBA 0.5mM + TG 1nM	0.99	1.09	0.99
THP1	PBA 0.5mM + TG 10nM	0.92	1.01	1.12
THP1	PBA 0.5mM + Dox 10nM	1.03	1.06	1.11
THP1	PBA 0.5mM + Dox 75nM	1.01	1.05	1.14
THP1	PBA 0.5mM + Bort 1nM	1.07	1.11	1.11
THP1	PBA 0.5mM + Bort 5nM	0.97	1.09	1.11
THP1	PBA 0.5mM + 17-AAG 50nM	1.07	1.05	1.02
THP1	PBA 0.5mM + 17-AAG 250nM	1.13	1.39	0.93
THP1	PBA 0.5mM + SAHA 100nM	1.07	1.18	1.00
THP1	PBA 0.5mM + SAHA 500nM	1.04	1.12	1.00

Table A3.15. Combination effect of 4-PBA combined with drug treatment for 48 hours in the THP1 cell line (calculated using the fractional product method).

Cell line	Drug concentrations	Combination Effect		
		Set 1	Set 2	Set 3
U266	PBA 0.5mM + TM 100nM	1.06	1.15	0.97
U266	PBA 0.5mM + TM 10μM	0.88	0.87	0.73
U266	PBA 0.5mM + TG 1nM	1.05	1.38	0.85
U266	PBA 0.5mM + TG 10nM	0.94	1.11	1.03
U266	PBA 0.5mM + Dox 10nM	1.01	1.16	1.14
U266	PBA 0.5mM + Dox 75nM	1.00	1.10	1.02
U266	PBA 0.5mM + Bort 1nM	0.94	1.18	1.04
U266	PBA 0.5mM + Bort 5nM	1.17	1.18	1.11
U266	PBA 0.5mM + 17-AAG 50nM	1.03	1.07	1.02
U266	PBA 0.5mM + 17-AAG 250nM	1.20	1.24	1.19
U266	PBA 0.5mM + SAHA 100nM	1.01	1.06	1.00
U266	PBA 0.5mM + SAHA 500nM	1.22	1.01	1.03

Table A3.16. Combination effect of 4-PBA combined with drug treatment for 48 hours in the U266 cell line (calculated using the fractional product method).

Cell line	Drug concentrations	Combination Effect		
		Set 1	Set 2	Set 3
DOHH2	PBA 0.5mM + TM 100nM	1.02	0.84	0.81
DOHH2	PBA 0.5mM + TM 1μM	1.10	0.93	1.18
DOHH2	PBA 0.5mM + TG 1nM	1.02	0.91	1.11
DOHH2	PBA 0.5mM + TG 10nM	1.12	0.83	0.81
DOHH2	PBA 0.5mM + Dox 5nM	1.20	1.13	1.03
DOHH2	PBA 0.5mM + Dox 50nM	1.23	0.95	1.16
DOHH2	PBA 0.5mM + Bort 1nM	1.13	1.20	1.10
DOHH2	PBA 0.5mM + Bort 5nM	1.28	1.20	1.10
DOHH2	PBA 0.5mM + 17-AAG 50nM	1.16	1.09	1.39
DOHH2	PBA 0.5mM + 17-AAG 250nM	1.19	2.07	0.95
DOHH2	PBA 0.5mM + SAHA 100nM	1.08	1.17	1.40
DOHH2	PBA 0.5mM + SAHA 500nM	1.07	1.20	0.76

Table A3.17. Combination effect of 4-PBA combined with drug treatment for 48 hours in the DOHH2 cell line (calculated using the fractional product method).

Cell line	Drug concentrations	Combination Effect		
		Set 1	Set 2	Set 3
HT29	PBA 0.5mM + TM 100nM	1.21	1.06	1.10
HT29	PBA 0.5mM + TM 1μM	1.08	1.04	1.06
HT29	PBA 0.5mM + TG 1nM	1.03	1.02	1.09
HT29	PBA 0.5mM + TG 10nM	1.23	1.10	0.90
HT29	PBA 0.5mM + Dox 10nM	1.12	1.18	1.07
HT29	PBA 0.5mM + Dox 75nM	1.14	1.10	1.05
HT29	PBA 0.5mM + Bort 1nM	1.18	1.08	1.01
HT29	PBA 0.5mM + Bort 5nM	1.23	1.14	1.10
HT29	PBA 0.5mM + 17-AAG 50nM	1.24	1.02	1.08
HT29	PBA 0.5mM + 17-AAG 250nM	1.16	1.04	1.06
HT29	PBA 0.5mM + SAHA 100nM	1.25	1.09	1.10
HT29	PBA 0.5mM + SAHA 500nM	1.16	1.03	1.05

Table A3.18. Combination effect of 4-PBA combined with drug treatment for 48 hours in the HT29 cell line (calculated using the fractional product method).

4-PBA Pre-treatment

THP1	% of control				
	Set 1	**Set 2**	**Set 3**	**Average**	**SD**
Control	100.0	100.0	100.0	**100.0**	**0.0**
PBA 0.5mM	82.6	88.2	88.0	**86.2**	**3.2**
TM 100nM	26.8	33.6	47.8	**36.1**	**10.7**
TM 1μM	15.2	21.5	24.9	**20.5**	**4.9**
PBA 0.5mM + TM 100nM	24.3	29.5	44.4	**32.7**	**10.4**
PBA 0.5mM + TM 1μM	12.1	17.0	23.5	**17.5**	**5.7**
TG 1nM	99.1	98.8	88.8	**95.6**	**5.9**
TG 10nM	54.0	56.3	38.8	**49.7**	**9.5**
PBA 0.5mM + TG 1nM	90.8	93.5	88.0	**90.8**	**2.8**
PBA 0.5mM + TG 10nM	44.8	43.5	33.7	**40.7**	**6.1**
Control	100.0	100.0	100.0	**100.0**	**0.0**
PBA 0.5mM	77.9	87.5	87.3	**84.2**	**5.5**
Dox 10nM	99.7	98.3	92.2	**96.7**	**4.0**
Dox 75nM	86.8	78.4	48.8	**71.3**	**20.0**
PBA 0.5mM + Dox 10nM	78.4	88.2	82.9	**83.2**	**4.9**
PBA 0.5mM + Dox 75nM	64.0	68.8	52.8	**61.9**	**8.2**
Bort 1nM	97.7	99.4	91.9	**96.3**	**3.9**
Bort 5nM	90.2	98.7	87.7	**92.2**	**5.8**
PBA 0.5mM + Bort 1nM	82.2	88.1	86.7	**85.7**	**3.1**
PBA 0.5mM + Bort 5nM	84.7	91.0	88.8	**88.2**	**3.2**
Control	100.0	100.0	100.0	**100.0**	**0.0**
PBA 0.5mM	73.4	89.2	88.5	**83.7**	**9.0**
17-AAG 50nM	89.2	91.2	87.1	**89.2**	**2.0**
17-AAG 250nM	70.1	75.2	68.5	**71.2**	**3.5**
PBA 0.5mM + 17-AAG 50nM	72.1	82.3	88.2	**80.9**	**8.2**
PBA 0.5mM + 17-AAG 250nM	51.1	62.4	62.8	**58.7**	**6.7**
SAHA 100nM	88.5	89.4	90.8	**89.6**	**1.1**
SAHA 500nM	85.8	86.1	84.1	**85.3**	**1.0**
PBA 0.5mM + SAHA 100nM	75.5	83.7	88.3	**82.5**	**6.5**
PBA 0.5mM + SAHA 500nM	66.5	73.7	75.3	**71.9**	**4.7**

Table A3.19. 4-PBA 0.5mM pretreatment for 24 hours combined with drug treatment for a further 48 hours in the THP1 cell line.

U266	% of control				
	Set 1	**Set 2**	**Set 3**	**Average**	**SD**
Control	100.0	100.0	100.0	**100.0**	**0.0**
PBA 0.5mM	80.5	88.4	83.5	**84.1**	**4.0**
TM 100nM	30.3	40.9	50.7	**40.6**	**10.2**
TM 10μM	14.5	18.9	25.8	**19.7**	**5.7**
PBA 0.5mM + TM 100nM	30.7	39.9	51.5	**40.7**	**10.4**
PBA 0.5mM + TM 10μM	12.9	18.8	24.6	**18.8**	**5.9**
TG 1nM	99.1	99.3	85.8	**94.7**	**7.7**
TG 10nM	59.5	68.8	50.6	**59.6**	**9.1**
PBA 0.5mM + TG 1nM	82.7	80.5	87.1	**83.4**	**3.3**
PBA 0.5mM + TG 10nM	49.9	45.0	45.1	**46.7**	**2.8**
Control	100.0	100.0	100.0	**100.0**	**0.0**
PBA 0.5mM	80.2	87.0	86.3	**84.5**	**3.8**
Dox 10nM	97.5	92.3	94.2	**94.7**	**2.6**
Dox 75nM	81.1	69.4	47.9	**66.1**	**16.8**
PBA 0.5mM + Dox 10nM	78.1	83.9	92.6	**84.9**	**7.3**
PBA 0.5mM + Dox 75nM	67.9	63.4	48.5	**60.0**	**10.2**
Bort 1nM	94.6	93.5	87.6	**91.9**	**3.8**
Bort 5nM	90.8	94.7	89.7	**91.7**	**2.6**
PBA 0.5mM + Bort 1nM	78.1	85.6	93.0	**85.6**	**7.5**
PBA 0.5mM + Bort 5nM	78.8	85.0	87.1	**83.6**	**4.3**
Control	100.0	100.0	100.0	**100.0**	**0.0**
PBA 0.5mM	79.3	83.3	84.0	**82.2**	**2.5**
17-AAG 50nM	93.7	98.5	92.5	**94.9**	**3.2**
17-AAG 250nM	74.6	82.6	68.6	**75.3**	**7.0**
PBA 0.5mM + 17-AAG 50nM	73.5	87.7	80.3	**80.5**	**7.1**
PBA 0.5mM + 17-AAG 250nM	53.7	65.4	54.1	**57.8**	**6.7**
SAHA 100nM	92.8	98.2	87.4	**92.8**	**5.4**
SAHA 500nM	81.6	93.6	78.2	**84.4**	**8.1**
PBA 0.5mM + SAHA 100nM	73.5	89.3	70.3	**77.7**	**10.2**
PBA 0.5mM + SAHA 500nM	62.6	76.5	66.3	**68.5**	**7.2**

Table A3.20. 4-PBA 0.5mM pretreatment for 24 hours combined with drug treatment for a further 48 hours in the U266 cell line.

DOHH2	% of control				
	Set 1	**Set 2**	**Set 3**	**Average**	**SD**
Control	100.0	100.0	100.0	**100.0**	**0.0**
PBA 0.5mM	71.5	75.8	83.1	**76.8**	**5.8**
TM 100nM	94.2	79.7	90.1	**88.0**	**7.5**
TM 1μM	54.6	35.2	34.8	**41.5**	**11.3**
PBA 0.5mM + TM 100nM	62.0	66.7	87.6	**72.1**	**13.7**
PBA 0.5mM + TM 1μM	47.6	28.3	35.8	**37.2**	**9.7**
TG 1nM	81.1	76.6	52.5	**70.1**	**15.4**
TG 5nM	63.9	60.1	49.6	**57.9**	**7.4**
PBA 0.5mM + TG 1nM	58.6	62.3	61.3	**60.7**	**1.9**
PBA 0.5mM + TG 5nM	48.0	52.2	48.9	**49.7**	**2.2**
Control	100.0	100.0	100.0	**100.0**	**0.0**
PBA 0.5mM	71.1	71.5	86.4	**76.3**	**8.7**
Dox 10nM	86.5	79.2	70.4	**78.7**	**8.0**
Dox 75nM	42.8	42.2	19.4	**34.8**	**13.4**
PBA 0.5mM + Dox 5nM	52.8	59.3	74.8	**62.3**	**11.3**
PBA 0.5mM + Dox 50nM	31.3	35.2	24.6	**30.4**	**5.4**
Bort 1nM	96.0	95.7	95.4	**95.7**	**0.3**
Bort 5nM	78.3	90.8	87.0	**85.4**	**6.4**
PBA 0.5mM + Bort 1nM	61.8	70.7	91.7	**74.7**	**15.3**
PBA 0.5mM + Bort 5nM	60.7	67.7	92.3	**73.6**	**16.6**
Control	100.0	100.0	100.0	**100.0**	**0.0**
PBA 0.5mM	69.7	76.1	81.0	**75.6**	**5.6**
17-AAG 50nM	54.7	89.5	93.8	**79.3**	**21.5**
17-AAG 250nM	29.8	54.8	69.2	**51.3**	**20.0**
PBA 0.5mM + 17-AAG 50nM	46.3	69.8	86.5	**67.5**	**20.2**
PBA 0.5mM + 17-AAG 250nM	22.3	40.4	54.3	**39.0**	**16.0**
SAHA 100nM	91.5	75.7	91.1	**86.1**	**9.0**
SAHA 500nM	59.8	41.7	47.7	**49.7**	**9.2**
PBA 0.5mM + SAHA 100nM	56.3	59.3	72.7	**62.8**	**8.7**
PBA 0.5mM + SAHA 500nM	42.3	34.4	46.2	**41.0**	**6.0**

Table A3.21. 4-PBA 0.5mM pretreatment for 24 hours combined with drug treatment for a further 48 hours in the DOHH2 cell line.

HT29	% of control				
	Set 1	**Set 2**	**Set 3**	**Average**	**SD**
Control	100.0	100.0	100.0	**100.0**	**0.0**
PBA 0.5mM	81.3	91.8	88.3	**87.2**	**5.3**
TM 100nM	92.8	88.7	92.2	**91.2**	**2.2**
TM 1μM	57.8	60.9	65.4	**61.3**	**3.8**
PBA 0.5mM + TM 100nM	80.2	81.0	80.3	**80.5**	**0.5**
PBA 0.5mM + TM 1μM	44.5	61.3	56.1	**54.0**	**8.6**
TG 1nM	92.0	83.1	91.6	**88.9**	**5.0**
TG 10nM	69.5	47.6	37.7	**51.6**	**16.3**
PBA 0.5mM + TG 1nM	88.5	79.6	82.1	**83.4**	**4.6**
PBA 0.5mM + TG 10nM	55.8	42.3	40.0	**46.0**	**8.5**
Control	100.0	100.0	100.0	**100.0**	**0.0**
PBA 0.5mM	85.3	93.2	92.6	**90.4**	**4.4**
Dox 10nM	98.1	98.8	93.8	**96.9**	**2.7**
Dox 75nM	92.4	97.0	91.9	**93.7**	**2.8**
PBA 0.5mM + Dox 10nM	83.3	85.9	91.3	**86.8**	**4.1**
PBA 0.5mM + Dox 75nM	89.9	94.3	87.1	**90.4**	**3.6**
Bort 1nM	98.2	97.3	95.3	**96.9**	**1.5**
Bort 5nM	93.7	97.8	87.5	**93.0**	**5.2**
PBA 0.5mM + Bort 1nM	87.3	88.3	83.5	**86.4**	**2.5**
PBA 0.5mM + Bort 5nM	86.0	87.6	86.2	**86.6**	**0.9**
Control	100.0	100.0	100.0	**100.0**	**0.0**
PBA 0.5mM	86.1	91.4	91.3	**89.6**	**3.0**
17-AAG 50nM	90.9	92.3	94.9	**92.7**	**2.0**
17-AAG 250nM	66.7	72.2	69.8	**69.6**	**2.7**
PBA 0.5mM + 17-AAG 50nM	76.7	85.3	89.5	**83.8**	**6.5**
PBA 0.5mM + 17-AAG 250nM	64.6	73.7	66.6	**68.3**	**4.8**
SAHA 100nM	87.8	99.4	92.4	**93.2**	**5.8**
SAHA 500nM	83.1	92.6	82.3	**86.0**	**5.7**
PBA 0.5mM + SAHA 100nM	84.1	84.0	84.1	**84.0**	**0.1**
PBA 0.5mM + SAHA 500nM	73.2	80.4	76.9	**76.9**	**3.6**

Table A3.22. 4-PBA 0.5mM pretreatment for 24 hours combined with drug treatment for a further 48 hours in the HT29 cell line.

Cell line	Drug concentrations	Combination Effect		
		Set 1	Set 2	Set 3
THP1	PBA 0.5mM + TM 100nM	1.10	1.00	1.06
THP1	PBA 0.5mM + TM 1μM	0.96	0.90	1.08
THP1	PBA 0.5mM + TG 1nM	1.11	1.07	1.13
THP1	PBA 0.5mM + TG 10nM	1.00	0.88	0.99
THP1	PBA 0.5mM + Dox 10nM	1.01	1.02	1.03
THP1	PBA 0.5mM + Dox 75nM	0.95	1.00	1.24
THP1	PBA 0.5mM + Bort 1nM	1.08	1.01	1.08
THP1	PBA 0.5mM + Bort 5nM	1.21	1.05	1.16
THP1	PBA 0.5mM + 17-AAG 50nM	1.10	1.01	1.14
THP1	PBA 0.5mM + 17-AAG 250nM	0.99	0.93	1.04
THP1	PBA 0.5mM + SAHA 100nM	1.16	1.05	1.10
THP1	PBA 0.5mM + SAHA 500nM	1.06	0.96	1.01

Table A3.23. Combination effect of 4-PBA pretreatment for 24 hours combined with drug treatment for a further 48 hours in the THP1 cell line (calculated using the fractional product method).

Cell line	Drug concentrations	Combination Effect		
		Set 1	Set 2	Set 3
U266	PBA 0.5mM + TM 100nM	1.26	1.10	1.22
U266	PBA 0.5mM + TM 10μM	1.11	1.13	1.14
U266	PBA 0.5mM + TG 1nM	1.04	0.92	1.22
U266	PBA 0.5mM + TG 10nM	1.04	0.74	1.07
U266	PBA 0.5mM + Dox 10nM	1.00	1.04	1.14
U266	PBA 0.5mM + Dox 75nM	1.04	1.05	1.17
U266	PBA 0.5mM + Bort 1nM	1.03	1.05	1.23
U266	PBA 0.5mM + Bort 5nM	1.08	1.03	1.12
U266	PBA 0.5mM + 17-AAG 50nM	0.99	1.07	1.03
U266	PBA 0.5mM + 17-AAG 250nM	0.91	0.95	0.94
U266	PBA 0.5mM + SAHA 100nM	1.00	1.09	0.96
U266	PBA 0.5mM + SAHA 500nM	0.97	0.98	1.01

Table A3.24. Combination effect of 4-PBA pretreatment for 24 hours combined with drug treatment for a further 48 hours in the U266 cell line (calculated using the fractional product method).

Cell line	Drug concentrations	Combination Effect		
		Set 1	Set 2	Set 3
DOHH2	PBA 0.5mM + TM 100nM	0.92	1.11	1.17
DOHH2	PBA 0.5mM + TM 1μM	1.22	1.06	1.24
DOHH2	PBA 0.5mM + TG 1nM	1.01	1.07	1.41
DOHH2	PBA 0.5mM + TG 10nM	1.05	1.15	1.19
DOHH2	PBA 0.5mM + Dox 5nM	0.86	1.05	1.23
DOHH2	PBA 0.5mM + Dox 50nM	1.03	1.17	1.47
DOHH2	PBA 0.5mM + Bort 1nM	0.91	1.03	1.11
DOHH2	PBA 0.5mM + Bort 5nM	1.09	1.04	1.23
DOHH2	PBA 0.5mM + 17-AAG 50nM	1.21	1.02	1.14
DOHH2	PBA 0.5mM + 17-AAG 250nM	1.07	0.97	0.97
DOHH2	PBA 0.5mM + SAHA 100nM	0.88	1.03	0.98
DOHH2	PBA 0.5mM + SAHA 500nM	1.02	1.08	1.20

Table A3.25. Combination effect of 4-PBA pretreatment for 24 hours combined with drug treatment for a further 48 hours in the DOHH2 cell line (calculated using the fractional product method).

Cell line	Drug concentrations	Combination Effect		
		Set 1	Set 2	Set 3
HT29	PBA 0.5mM + TM 100nM	1.06	1.00	0.99
HT29	PBA 0.5mM + TM 1μM	0.95	1.10	0.97
HT29	PBA 0.5mM + TG 1nM	1.18	1.04	1.01
HT29	PBA 0.5mM + TG 10nM	0.99	0.97	1.20
HT29	PBA 0.5mM + Dox 10nM	0.99	0.93	1.05
HT29	PBA 0.5mM + Dox 75nM	1.14	1.04	1.02
HT29	PBA 0.5mM + Bort 1nM	1.04	0.97	0.95
HT29	PBA 0.5mM + Bort 5nM	1.07	0.96	1.06
HT29	PBA 0.5mM + 17-AAG 50nM	0.98	1.01	1.03
HT29	PBA 0.5mM + 17-AAG 250nM	1.12	1.12	1.05
HT29	PBA 0.5mM + SAHA 100nM	1.11	0.92	1.00
HT29	PBA 0.5mM + SAHA 500nM	1.02	0.95	1.02

Table A3.26. Combination effect of 4-PBA pretreatment for 24 hours combined with drug treatment for a further 48 hours in the HT29 cell line (calculated using the fractional product method).

THP1		Cells In Each Region (%)			Average	SD
Control	nuclear debris	0.1	0.3	0.3	**0.2**	**0.1**
	late apoptosis/dead cells	2.2	2.2	2.6	**2.3**	**0.2**
	viable cells	91.4	91.5	91.2	**91.4**	**0.2**
	early apoptosis	6.3	6.1	5.9	**6.1**	**0.2**
PBA 0.5mM	nuclear debris	0.2	0.3	0.3	**0.3**	**0.1**
	late apoptosis/dead cells	2.8	2.4	2.4	**2.5**	**0.2**
	viable cells	91.3	92.2	91.2	**91.6**	**0.6**
	early apoptosis	5.7	5.1	6.1	**5.6**	**0.5**
TM 100nM	nuclear debris	0.2	0.2	0.2	**0.2**	**0.0**
	late apoptosis/dead cells	4.5	4.6	5.1	**4.7**	**0.3**
	viable cells	79.3	78.2	77.0	**78.2**	**1.2**
	early apoptosis	16.1	16.9	17.7	**16.9**	**0.8**
PBA + TM 100nM	nuclear debris	0.2	0.3	0.3	**0.3**	**0.1**
	late apoptosis/dead cells	5.8	5.3	5.4	**5.5**	**0.3**
	viable cells	77.9	79.7	78.6	**78.7**	**0.9**
	early apoptosis	16.1	14.6	15.7	**15.5**	**0.8**
TM 1µM	nuclear debris	0.2	0.3	0.9	**0.5**	**0.4**
	late apoptosis/dead cells	10.3	12.8	12.9	**12.0**	**1.5**
	viable cells	57.6	57.4	56.0	**57.0**	**0.9**
	early apoptosis	31.8	29.5	30.2	**30.5**	**1.2**
PBA + TM 1µM	nuclear debris	0.9	0.6	0.6	**0.7**	**0.2**
	late apoptosis/dead cells	18.5	19.6	17.7	**18.6**	**1.0**
	viable cells	52.5	54.4	53.4	**53.4**	**1.0**
	early apoptosis	28.1	25.4	28.3	**27.3**	**1.6**
TG 10nM	nuclear debris	0.3	0.3	0.4	**0.3**	**0.1**
	late apoptosis/dead cells	10.7	9.7	10.9	**10.4**	**0.6**
	viable cells	76.2	77.7	75.9	**76.6**	**1.0**
	early apoptosis	12.8	12.3	12.8	**12.6**	**0.3**
PBA + TG 10nM	nuclear debris	0.5	0.6	0.4	**0.5**	**0.1**
	late apoptosis/dead cells	15.8	14.5	14.3	**14.9**	**0.8**
	viable cells	68.5	70.2	70.1	**69.6**	**1.0**
	early apoptosis	15.2	14.7	15.2	**15.0**	**0.3**
TG 100nM	nuclear debris	1.0	0.6	1.1	**0.9**	**0.3**
	late apoptosis/dead cells	13.0	12.3	11.9	**12.4**	**0.6**
	viable cells	63.1	59.4	65.6	**62.7**	**3.1**
	early apoptosis	22.9	27.7	21.4	**24.0**	**3.3**
PBA + TG 100nM	nuclear debris	0.9	1.2	0.8	**1.0**	**0.2**
	late apoptosis/dead cells	21.0	22.7	20.3	**21.3**	**1.2**
	viable cells	53.1	49.8	59.4	**54.1**	**4.9**
	early apoptosis	25.0	26.3	19.5	**23.6**	**3.6**

Table A3.27. Apoptosis assay results for cells in each region (%) following 48 hours of drug treatment in the THP1 cell line.

THP1		Cell No. By Region (cells/mL)			Average	SD
Control	nuclear debris	1148	2255	2284	**1896**	**648**
	late apoptosis/dead cells	19231	18322	21986	**19846**	**1908**
	viable cells	786751	773465	781500	**780572**	**6691**
	early apoptosis	53962	51583	50825	**52123**	**1637**
PBA 0.5mM	nuclear debris	3142	1943	1935	**2340**	**694**
	late apoptosis/dead cells	20159	19983	19628	**19923**	**270**
	viable cells	716032	765723	766043	**749266**	**28782**
	early apoptosis	46077	44961	41744	**44261**	**2250**
TM 100nM	nuclear debris	926	1297	1201	**1141**	**193**
	late apoptosis/dead cells	24805	25574	30613	**26997**	**3155**
	viable cells	440204	434941	462395	**445847**	**14571**
	early apoptosis	89411	94141	106045	**96532**	**8571**
PBA + TM 100nM	nuclear debris	1212	1753	1580	**1515**	**276**
	late apoptosis/dead cells	29957	27880	28611	**28816**	**1053**
	viable cells	404854	419433	413899	**412729**	**7359**
	early apoptosis	83464	76978	82499	**80980**	**3500**
TM 1µM	nuclear debris	1155	1407	4283	**2282**	**1738**
	late apoptosis/dead cells	51156	59885	63916	**58319**	**6522**
	viable cells	285154	269248	276748	**277050**	**7957**
	early apoptosis	157594	138533	149246	**148457**	**9555**
PBA + TM 1µM	nuclear debris	3808	2985	2664	**3152**	**590**
	late apoptosis/dead cells	81150	92224	78582	**83985**	**7250**
	viable cells	230852	256248	237226	**241442**	**13213**
	early apoptosis	123629	119876	125494	**123000**	**2862**
TG 10nM	nuclear debris	1905	2126	2816	**2282**	**475**
	late apoptosis/dead cells	76663	68742	76978	**74127**	**4667**
	viable cells	544020	550877	534149	**543016**	**8409**
	early apoptosis	91662	86931	90120	**89571**	**2413**
PBA + TG 10nM	nuclear debris	3056	3843	2155	**3018**	**845**
	late apoptosis/dead cells	96584	93083	84050	**91239**	**6467**
	viable cells	418737	449401	412218	**426785**	**19855**
	early apoptosis	92917	94150	89340	**92136**	**2498**
TG 100nM	nuclear debris	2862	3333	3113	**3103**	**236**
	late apoptosis/dead cells	104934	94890	116156	**105327**	**10638**
	viable cells	469816	440896	469173	**459962**	**16515**
	early apoptosis	137845	127558	130046	**131816**	**5367**
PBA + TG 100nM	nuclear debris	2829	3501	2822	**3051**	**390**
	late apoptosis/dead cells	109323	101984	95016	**102107**	**7154**
	viable cells	275053	241565	251180	**255933**	**17243**
	early apoptosis	111985	109595	121357	**114312**	**6217**

Table A3.28. Apoptosis assay results for cell number by region following 48 hours of drug treatment in the THP1 cell line.

THP1	Apoptotic cells (%)						p value
	Drug alone			Drug with 4-PBA pretreatment			
TM 100nM	20.6	21.5	22.8	21.8	19.9	21.1	0.53810
TM 1µM	42.2	42.3	43.1	46.6	45.0	46.0	0.02494
TG 10nM	23.6	22.0	23.7	31.0	29.2	29.5	0.00543
TG 100nM	33.9	33.4	34.3	44.3	46.3	46.0	0.00381

Table A3.29. Apoptotic cells (as a percentage of total cells) after 48 hours treatment with drug, with or without 24 hours of 4-PBA pretreatment, in the THP1 cell line.

THP1	Total cell number (%)						p value
	Drug alone			Drug with TG pretreatment			
TM 100nM	64.5	65.7	70.1	66.1	63.2	63.5	0.40327
TM 1µM	57.5	55.5	57.7	56.0	56.6	53.5	0.42482
TG 10nM	82.9	83.8	82.2	77.8	76.9	70.9	0.05206
TG 100nM	83.1	78.8	83.9	63.6	54.8	56.7	0.00871

Table A3.30. Total cell number (%) after 48 hours treatment with drug, with or without 24 hours of 4-PBA pretreatment, in the THP1 cell line (each normalised to its own control).

THP1	Viable cell number (%)						p value
	Drug alone			Drug with TG pretreatment			
TM 100nM	56.0	56.2	59.2	56.5	54.8	54.0	0.35466
TM 1µM	36.2	34.8	35.4	32.2	33.5	31.0	0.07778
TG 10nM	69.1	71.2	68.3	58.5	58.7	53.8	0.00780
TG 100nM	59.7	57.0	60.0	38.4	31.5	32.8	0.00505

Table A3.31. Viable cell number (%) after 48 hours treatment with drug, with or without 24 hours of 4-PBA pretreatment, in the THP1 cell line (each normalised to its own control).

U266		Cells In Each Region (%)			Average	SD
Control	nuclear debris	0.9	0.7	0.9	**0.8**	**0.1**
	late apoptosis/dead cells	3.0	3.0	3.7	**3.2**	**0.4**
	viable cells	89.1	89.5	87.4	**88.7**	**1.1**
	early apoptosis	6.9	6.8	8.0	**7.2**	**0.7**
PBA 0.5mM	nuclear debris	0.9	0.7	0.9	**0.8**	**0.1**
	late apoptosis/dead cells	3.1	2.7	2.6	**2.8**	**0.3**
	viable cells	90.3	90.0	90.0	**90.1**	**0.2**
	early apoptosis	5.8	6.5	6.6	**6.3**	**0.4**
TM 100nM	nuclear debris	0.6	0.4	1.1	**0.7**	**0.4**
	late apoptosis/dead cells	6.4	6.3	7.3	**6.7**	**0.6**
	viable cells	76.0	79.1	74.7	**76.6**	**2.3**
	early apoptosis	17.0	14.2	16.8	**16.0**	**1.6**
PBA + TM 100nM	nuclear debris	1.3	0.8	0.7	**0.9**	**0.3**
	late apoptosis/dead cells	8.8	8.0	9.2	**8.7**	**0.6**
	viable cells	77.0	78.7	76.9	**77.5**	**1.0**
	early apoptosis	12.9	12.5	13.3	**12.9**	**0.4**
TM 10µM	nuclear debris	1.0	1.2	1.0	**1.1**	**0.1**
	late apoptosis/dead cells	21.4	19.0	19.9	**20.1**	**1.2**
	viable cells	53.5	56.9	57.2	**55.9**	**2.1**
	early apoptosis	24.1	22.8	21.9	**22.9**	**1.1**
PBA + TM 10µM	nuclear debris	2.0	1.6	1.8	**1.8**	**0.2**
	late apoptosis/dead cells	24.0	24.5	25.4	**24.6**	**0.7**
	viable cells	58.4	55.3	53.5	**55.7**	**2.5**
	early apoptosis	15.6	18.7	19.4	**17.9**	**2.0**
TG 10nM	nuclear debris	0.5	0.8	0.8	**0.7**	**0.2**
	late apoptosis/dead cells	7.7	8.0	7.9	**7.9**	**0.2**
	viable cells	75.7	76.1	78.3	**76.7**	**1.4**
	early apoptosis	16.0	15.1	13.1	**14.7**	**1.5**
PBA + TG 10nM	nuclear debris	1.1	0.9	0.5	**0.8**	**0.3**
	late apoptosis/dead cells	14.3	12.7	12.8	**13.3**	**0.9**
	viable cells	69.5	70.0	71.6	**70.4**	**1.1**
	early apoptosis	15.1	16.4	15.1	**15.5**	**0.8**
TG 100nM	nuclear debris	1.1	1.0	0.6	**0.9**	**0.3**
	late apoptosis/dead cells	11.9	13.0	12.3	**12.4**	**0.6**
	viable cells	65.6	63.1	59.4	**62.7**	**3.1**
	early apoptosis	21.4	22.9	27.7	**24.0**	**3.3**
PBA + TG 100nM	nuclear debris	0.8	0.9	1.2	**1.0**	**0.2**
	late apoptosis/dead cells	20.3	21.0	22.7	**21.3**	**1.2**
	viable cells	59.4	53.1	49.8	**54.1**	**4.9**
	early apoptosis	19.5	25.0	26.3	**23.6**	**3.6**

Table A3.32. Apoptosis assay results for cells in each region (%) following 48 hours of drug treatment in the U266 cell line.

U266		Cell No. By Region (cells/mL)			Average	SD
Control	nuclear debris	5705	4318	5247	**5090**	**706**
	late apoptosis/dead cells	18337	19648	21765	**19916**	**1730**
	viable cells	544801	579942	509330	**544691**	**35306**
	early apoptosis	42378	43830	46638	**44282**	**2166**
PBA 0.5mM	nuclear debris	5674	4362	4984	**5007**	**656**
	late apoptosis/dead cells	20079	17034	14762	**17292**	**2668**
	viable cells	591016	561094	517619	**556576**	**36906**
	early apoptosis	37975	40716	37767	**38819**	**1646**
TM 100nM	nuclear debris	2278	1828	4343	**2816**	**1341**
	late apoptosis/dead cells	24170	26580	28950	**26567**	**2390**
	viable cells	288518	333723	295031	**305757**	**24437**
	early apoptosis	64663	59769	66454	**63629**	**3461**
PBA + TM 100nM	nuclear debris	5299	3165	2525	**3663**	**1452**
	late apoptosis/dead cells	35732	30386	34722	**33613**	**2840**
	viable cells	313848	298924	291156	**301309**	**11533**
	early apoptosis	52716	47352	50378	**50148**	**2689**
TM 10µM	nuclear debris	3587	4581	3613	**3927**	**566**
	late apoptosis/dead cells	74401	70565	71891	**72286**	**1949**
	viable cells	185598	211447	206641	**201229**	**13748**
	early apoptosis	83542	84801	79116	**82487**	**2986**
PBA + TM 10µM	nuclear debris	7129	5556	6236	**6307**	**789**
	late apoptosis/dead cells	87120	86891	89652	**87888**	**1532**
	viable cells	211698	196008	188716	**198808**	**11744**
	early apoptosis	56550	66203	68357	**63703**	**6288**
TG 10nM	nuclear debris	2720	4150	4133	**3668**	**821**
	late apoptosis/dead cells	39270	39675	40642	**39863**	**705**
	viable cells	386243	378824	404355	**389808**	**13133**
	early apoptosis	81771	75366	67507	**74881**	**7144**
PBA + TG 10nM	nuclear debris	4867	4050	2467	**3795**	**1220**
	late apoptosis/dead cells	65248	55253	59051	**59851**	**5045**
	viable cells	317264	303604	331181	**317350**	**13789**
	early apoptosis	68898	71019	69844	**69920**	**1063**
TG 100nM	nuclear debris	2291	4223	4751	**3755**	**1295**
	late apoptosis/dead cells	49854	55033	51396	**52095**	**2659**
	viable cells	240110	266300	283182	**263197**	**21703**
	early apoptosis	111970	96695	92570	**100412**	**10220**
PBA + TG 100nM	nuclear debris	2340	3326	4136	**3267**	**899**
	late apoptosis/dead cells	62059	74839	78117	**71672**	**8485**
	viable cells	181395	189235	171628	**180752**	**8821**
	early apoptosis	59414	88975	90754	**79714**	**17603**

Table A3.33. Apoptosis assay results for cell number by region following 48 hours of drug treatment in the U266 cell line.

U266	Apoptotic cells (%)						p value
	Drug alone			Drug with 4-PBA pretreatment			
TM 100nM	23.4	20.5	24.2	21.7	20.5	22.5	0.18350
TM 10µM	45.5	41.8	41.8	39.6	43.2	44.8	0.87199
TG 10nM	23.7	23.1	20.9	29.4	29.1	27.9	0.00395
TG 100nM	33.3	35.9	40.0	39.8	46.0	49.0	0.01522

Table A3.34. Apoptotic cells (as a percentage of total cells) after 48 hours treatment with drug, with or without 24 hours of 4-PBA pretreatment, in the U266 cell line.

U266	Total cell number (%)						p value
	Drug alone			Drug with TG pretreatment			
TM 100nM	62.1	65.1	67.7	74.5	60.4	61.0	0.96215
TM 10µM	56.8	57.3	62.0	66.2	56.4	56.9	0.81610
TG 10nM	83.4	76.9	88.6	83.4	69.0	74.5	0.21233
TG 100nM	66.1	65.2	74.1	55.8	56.7	55.5	0.05634

Table A3.35. Total cell number (%) after 48 hours treatment with drug, with or without 24 hours of 4-PBA pretreatment, in the U266 cell line (each normalised to its own control).

U266	Viable cell number (%)						p value
	Drug alone			Drug with TG pretreatment			
TM 100nM	53.0	57.5	57.9	53.1	53.3	56.2	0.27017
TM 10µM	34.1	36.5	40.6	35.8	34.9	36.5	0.52491
TG 10nM	70.9	65.3	79.4	53.7	54.1	64.0	0.01449
TG 100nM	44.1	45.9	55.6	30.7	33.7	33.2	0.03855

Table A3.36. Viable cell number (%) after 48 hours treatment with drug, with or without 24 hours of 4-PBA pretreatment, in the U266 cell line (each normalised to its own control).

Drug	Conc.	Set 1	Set 2	Set 3	Average	SD	p value
Trichostatin A	**0**	100.0	100.0	100.0	**100.0**	**0.0**	
	0.5nM	91.1	99.7	84.9	**91.9**	**7.4**	0.19969
	5nM	51.9	53.0	47.0	**50.6**	**3.2**	0.00438
	50nM	5.0	8.3	5.4	**6.2**	**1.8**	0.00161
4-PBA	**0**	100.0	100.0	100.0	**100.0**	**0.0**	
	0.1mM	91.7	97.9	85.2	**91.6**	**6.3**	0.14906
	0.5mM	75.8	85.2	69.6	**76.9**	**7.8**	0.03634
	1mM	63.6	72.0	64.0	**66.5**	**4.7**	0.00661
	5mM	31.6	39.9	27.3	**32.9**	**6.4**	0.00302
SAHA	**0**	100.0	100.0	100.0	**100.0**	**0.0**	
	0.5µM	24.0	34.8	23.4	**27.4**	**6.4**	0.00259
	1µM	11.2	21.0	7.2	**13.1**	**7.1**	0.00222
	5µM	3.0	8.5	0.0	**3.8**	**4.3**	0.00066

Table A3.37. Results of HDAC activity assay for 4-PBA expressed as percentage of control. Trichostatin A is used as the positive control for HDAC inhibition in this assay. SAHA, a known HDAC inhibitor used in this project, is included for comparison purposes. P value from paired t-test comparing drug treated sample to control sample is shown ($p<0.05$ considered statistically significant).

Appendix 4

ADDITIONAL DATA FOR CHAPTER 7

ATP ASSAY:

Cell line	Conc.	Set 1	Set 2	Set 3	Average	SD
THP1	**0**	100.0	100.0	100.0	**100.0**	**0.0**
THP1	**0.3µM**	92.6	98.6	93.5	**94.9**	**3.3**
THP1	**1µM**	65.8	67.1	82.9	**72.0**	**9.5**
THP1	**3µM**	44.3	43.6	47.0	**45.0**	**1.8**
THP1	**10µM**	28.8	25.1	31.1	**28.3**	**3.1**
THP1	**30µM**	7.4	6.2	5.4	**6.3**	**1.0**
Cell line	**Conc.**	**Set 1**	**Set 2**	**Set 3**	**Average**	**SD**
U266	**0**	100.0	100.0	100.0	**100.0**	**0.0**
U266	**0.3µM**	92.0	94.0	99.1	**95.0**	**3.7**
U266	**1µM**	80.1	76.8	89.5	**82.1**	**6.6**
U266	**3µM**	58.8	49.4	82.1	**63.4**	**16.9**
U266	**10µM**	47.0	29.6	59.8	**45.5**	**15.1**
U266	**30µM**	40.7	13.6	22.2	**25.5**	**13.9**
Cell line	**Conc.**	**Set 1**	**Set 2**	**Set 3**	**Average**	**SD**
DOHH2	**0**	100.0	100.0	100.0	**100.0**	**0.0**
DOHH2	**0.3µM**	94.9	87.0	89.4	**90.4**	**4.0**
DOHH2	**1µM**	78.5	80.4	70.9	**76.6**	**5.1**
DOHH2	**3µM**	29.4	54.3	38.0	**40.6**	**12.6**
DOHH2	**10µM**	5.3	26.1	22.0	**17.8**	**11.0**
DOHH2	**30µM**	0.3	4.3	7.2	**3.9**	**3.5**
Cell line	**Conc.**	**Set 1**	**Set 2**	**Set 3**	**Average**	**SD**
HT29	**0**	100.0	100.0	100.0	**100.0**	**0.0**
HT29	**0.3µM**	85.4	98.0	94.7	**92.7**	**6.5**
HT29	**1µM**	94.3	94.6	71.8	**86.9**	**13.1**
HT29	**3µM**	86.9	89.8	61.4	**79.4**	**15.6**
HT29	**10µM**	72.8	66.0	55.9	**64.9**	**8.5**
HT29	**30µM**	44.0	34.2	36.5	**38.3**	**5.1**

Table A4.1. Effect of versipelostatin treatment for 48 hours on cell viability (ATP content)

Cell line	Conc.	Set 1	Set 2	Set 3	Average	SD
THP1	**0**	100.0	100.0	100.0	**100.0**	**0.0**
THP1	**10µM**	80.0	98.0	94.1	**90.7**	**9.5**
THP1	**100µM**	88.0	101.2	89.2	**92.8**	**7.3**
THP1	**1mM**	67.6	78.6	63.3	**69.9**	**7.9**
THP1	**10mM**	20.2	21.2	13.6	**18.3**	**4.1**
THP1	**100mM**	2.9	2.4	1.2	**2.2**	**0.9**
Cell line	**Conc.**	**Set 1**	**Set 2**	**Set 3**	**Average**	**SD**
U266	**0**	100.0	100.0	100.0	**100.0**	**0.0**
U266	**10µM**	77.4	95.8	95.6	**89.6**	**10.6**
U266	**100µM**	87.6	101.4	94.3	**94.4**	**6.9**
U266	**1mM**	78.1	71.4	54.0	**67.9**	**12.4**
U266	**10mM**	46.3	24.6	15.3	**28.7**	**15.9**
U266	**100mM**	22.1	7.6	2.5	**10.8**	**10.1**
Cell line	**Conc.**	**Set 1**	**Set 2**	**Set 3**	**Average**	**SD**
DOHH2	**0**	100.0	100.0	100.0	**100.0**	**0.0**
DOHH2	**10µM**	80.5	95.2	85.7	**87.1**	**7.5**
DOHH2	**100µM**	72.9	87.6	90.7	**83.7**	**9.5**
DOHH2	**1mM**	16.1	61.0	39.2	**38.8**	**22.4**
DOHH2	**10mM**	0.3	13.5	8.1	**7.3**	**6.6**
DOHH2	**100mM**	0.0	0.3	0.2	**0.2**	**0.2**
Cell line	**Conc.**	**Set 1**	**Set 2**	**Set 3**	**Average**	**SD**
HT29	**0**	100.0	100.0	100.0	**100.0**	**0.0**
HT29	**10µM**	96.9	96.7	95.0	**96.2**	**1.0**
HT29	**100µM**	92.4	89.2	91.2	**90.9**	**1.6**
HT29	**1mM**	76.7	72.0	78.1	**75.6**	**3.2**
HT29	**10mM**	31.9	24.6	30.0	**28.8**	**3.8**
HT29	**100mM**	8.6	10.0	12.4	**10.4**	**1.9**

Table A4.2. Effect of 2-DG treatment for 48 hours on cell viability (ATP content)

GUAVA VIACOUNT:

THP1	Cell viability (% of control)				Cell no (% of control)			
VST	**Set 1**	**Set 2**	**Average**	**SD**	**Set 1**	**Set 2**	**Average**	**SD**
0	100.0	100.0	**100.0**	**0.0**	100.0	100.0	**100.0**	**0.0**
0.3µM	97.8	99.1	**98.4**	**0.9**	85.3	90.2	**87.7**	**3.5**
1µM	95.5	97.2	**96.3**	**1.2**	64.5	59.6	**62.0**	**3.5**
3µM	93.5	92.9	**93.2**	**0.4**	43.9	38.3	**41.1**	**4.0**
10µM	75.0	71.2	**73.1**	**2.7**	35.2	28.4	**31.8**	**4.8**
30µM	22.4	22.8	**22.6**	**0.3**	27.7	19.1	**23.4**	**6.1**

Table A4.3. Effect of versipelostatin treatment for 48 hours on cell viability and cell number (% of control) in the THP1 cell line.

U266	Cell viability (% of control)				Cell no (% of control)			
VST	**Set 1**	**Set 2**	**Average**	**SD**	**Set 1**	**Set 2**	**Average**	**SD**
0	100.0	100.0	**100.0**	**0.0**	100.0	100.0	**100.0**	**0.0**
0.3µM	100.1	98.9	**99.5**	**0.8**	82.7	96.1	**89.4**	**9.5**
1µM	96.8	96.2	**96.5**	**0.5**	57.8	78.2	**68.0**	**14.4**
3µM	83.3	82.7	**83.0**	**0.4**	39.5	49.5	**44.5**	**7.1**
10µM	58.6	65.8	**62.2**	**5.0**	29.0	41.7	**35.3**	**8.9**
30µM	28.4	42.7	**35.5**	**10.1**	24.0	35.1	**29.6**	**7.9**

Table A4.4. Effect of versipelostatin treatment for 48 hours on cell viability and cell number (% of control) in the U266 cell line.

THP1	Cell viability (% of control)				Cell no (% of control)			
2DG	**Set 1**	**Set 2**	**Average**	**SD**	**Set 1**	**Set 2**	**Average**	**SD**
0	100.0	100.0	**100.0**	**0.0**	100.0	100.0	**100.0**	**0.0**
10µM	96.7	99.2	**98.0**	**1.7**	81.2	98.1	**89.6**	**11.9**
100µM	101.3	99.4	**100.3**	**1.4**	82.2	96.6	**89.4**	**10.2**
1mM	99.1	98.3	**98.7**	**0.6**	73.5	81.1	**77.3**	**5.4**
10mM	75.9	67.9	**71.9**	**5.7**	41.3	29.0	**35.2**	**8.7**
100mM	22.9	12.5	**17.7**	**7.3**	25.6	18.1	**21.9**	**5.3**

Table A4.5. Effect of 2-DG treatment for 48 hours on cell viability and cell number (% of control) in the THP1 cell line.

U266	Cell viability (% of control)				Cell no (% of control)			
2DG	**Set 1**	**Set 2**	**Average**	**SD**	**Set 1**	**Set 2**	**Average**	**SD**
0	100.0	100.0	**100.0**	**0.0**	100.0	100.0	**100.0**	**0.0**
10µM	99.6	100.8	**100.2**	**0.9**	97.0	100.2	**98.6**	**2.2**
100µM	99.8	99.3	**99.5**	**0.3**	100.7	100.5	**100.6**	**0.1**
1mM	96.1	98.7	**97.4**	**1.9**	72.9	82.0	**77.4**	**6.5**
10mM	57.6	68.8	**63.2**	**7.9**	35.2	45.4	**40.3**	**7.2**
100mM	17.0	33.5	**25.3**	**11.7**	26.2	37.2	**31.7**	**7.8**

Table A4.6. Effect of 2-DG treatment for 48 hours on cell viability and cell number (% of control) in the U266 cell line.

VST	2DG	Cell viability		Average	SD
-	-	97.1	92.0	**94.5**	**3.6**
0.3µM	-	93.5	92.9	**93.2**	**0.4**
1µM	-	90.3	87.4	**88.8**	**2.0**
3µM	-	90.8	87.8	**89.3**	**2.1**
10µM	-	85.4	82.2	**83.8**	**2.3**
-	10mM	90.1	92.5	**91.3**	**1.7**
0.3µM	10mM	86.2	88.3	**87.2**	**1.5**
1µM	10mM	70.3	71.1	**70.7**	**0.5**
3µM	10mM	57.1	59.5	**58.3**	**1.7**
10µM	10mM	26.8	30.7	**28.7**	**2.8**

Table A4.7. Effect of versipelostatin treatment alone, or in combination with 2-DG, for 24 hours on cell viability in the THP1 cell line.

VST	2DG	Cell no (cells/ml)		Average	SD	% of control
-	-	889689	707392	**798540**	**128903**	**100.0**
0.3µM	-	806851	762872	**784862**	**31098**	**98.3**
1µM	-	760234	619425	**689830**	**99567**	**86.4**
3µM	-	644482	588766	**616624**	**39397**	**77.2**
10µM	-	656243	633392	**644818**	**16158**	**80.7**
-	10mM	688069	712145	**700107**	**17024**	**87.7**
0.3µM	10mM	590664	571170	**580917**	**13784**	**72.7**
1µM	10mM	540449	498328	**519389**	**29785**	**65.0**
3µM	10mM	502605	574478	**538541**	**50822**	**67.4**
10µM	10mM	640289	623932	**632111**	**11566**	**79.2**

Table A4.8. Effect of versipelostatin treatment alone, or in combination with 2-DG, for 24 hours on cell number in the THP1 cell line.

VST	2DG	Cell viability		**Average**	**SD**
-	-	67.3	78.4	**72.9**	**7.9**
0.3µM	-	68.2	55.0	**61.6**	**9.3**
1µM	-	65.6	64.5	**65.1**	**0.8**
3µM	-	61.3	65.8	**63.6**	**3.2**
10µM	-	60.1	58.5	**59.3**	**1.1**
-	10mM	63.7	63.9	**63.8**	**0.1**
0.3µM	10mM	45.2	63.7	**54.4**	**13.1**
1µM	10mM	43.8	48.3	**46.0**	**3.2**
3µM	10mM	23.7	20.0	**21.8**	**2.6**
10µM	10mM	28.3	24.3	**26.3**	**2.8**

Table A4.9. Effect of versipelostatin treatment alone, or in combination with 2-DG, for 24 hours on cell viability in the U266 cell line.

VST	2DG	Cell no (cells/ml)		**Average**	**SD**	**% of control**
-	-	325256	374052	**349654**	**34504**	**100.0**
0.3µM	-	343343	336693	**340018**	**4702**	**97.2**
1µM	-	312498	333890	**323194**	**15127**	**92.4**
3µM	-	298541	302682	**300611**	**2928**	**86.0**
10µM	-	278002	294754	**286378**	**11845**	**81.9**
-	10mM	268610	297413	**283011**	**20367**	**80.9**
0.3µM	10mM	253603	338982	**296293**	**60372**	**84.7**
1µM	10mM	240202	287366	**263784**	**33350**	**75.4**
3µM	10mM	285477	276225	**280851**	**6542**	**80.3**
10µM	10mM	374155	399623	**386889**	**18008**	**110.6**

Table A4.10. Effect of versipelostatin treatment alone, or in combination with 2-DG, for 24 hours on cell number in the U266 cell line.

Appendix 5

ADDITIONAL DATA FOR CHAPTER 8

Cell line	Transfection efficiency (%)		
	Set 1	Set 2	Set 3
THP1	93.1	93.2	92.8
U266	86.1	91.4	90.3
DOHH2	80.0	75.0	77.0

Table A5.1. Transfection efficiency (percentage of transfected cells from the total cell population) for each cell line as determined by flow cytometry. Values shown are results from three separate experiments

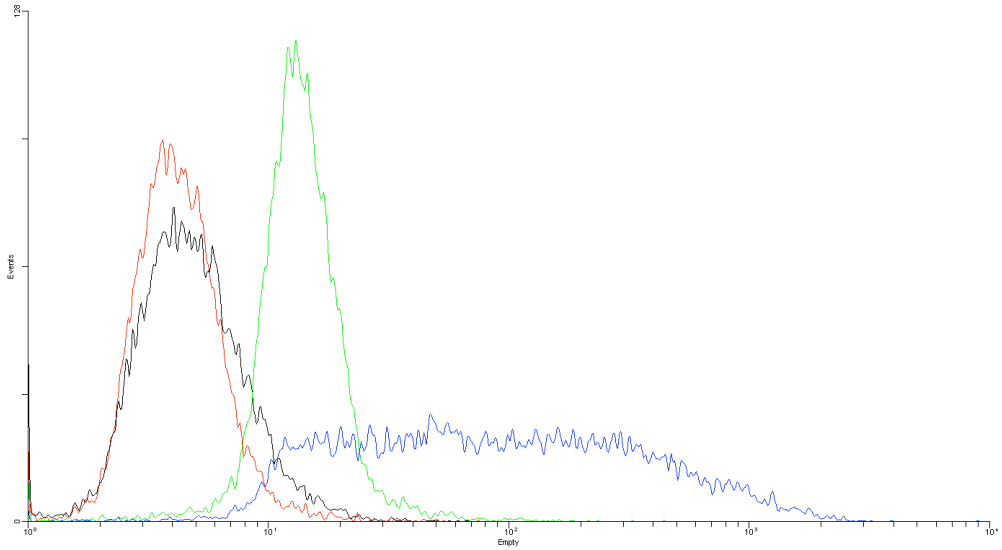

Figure A5.1. Flow cytometry histogram plot of the second transfection efficiency experiment in the THP1 cell line.

KEY: Red = Untransfected control
Black = Mock transfected
Green = siRNA only
Blue = siRNA transfected

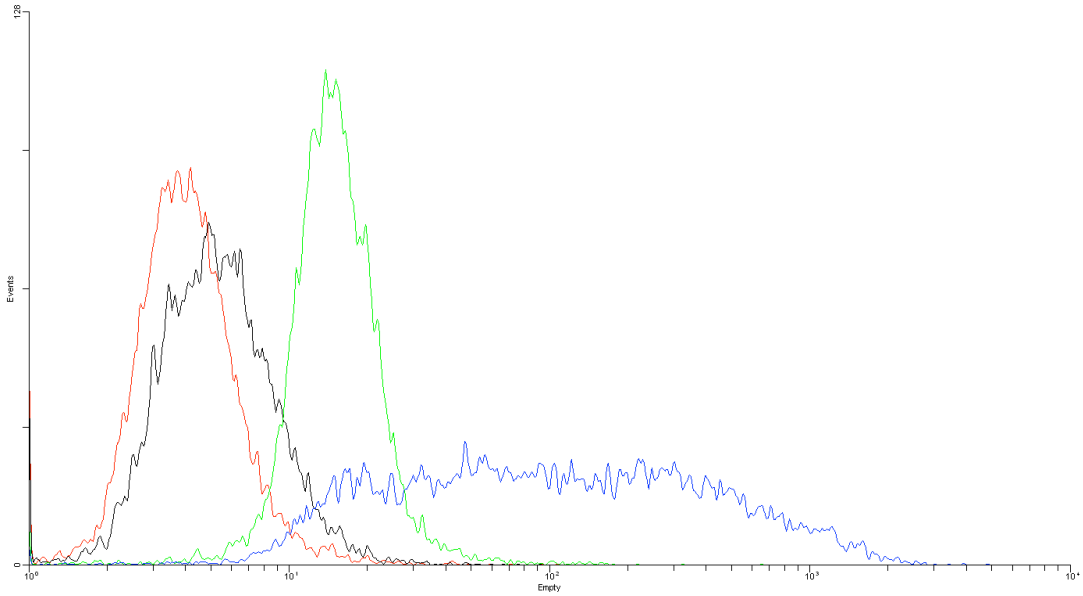

Figure A5.2. Flow cytometry histogram plot of the third transfection efficiency experiment in the THP1 cell line.

KEY: Red = Untransfected control
Black = Mock transfected
Green = siRNA only
Blue = siRNA transfected

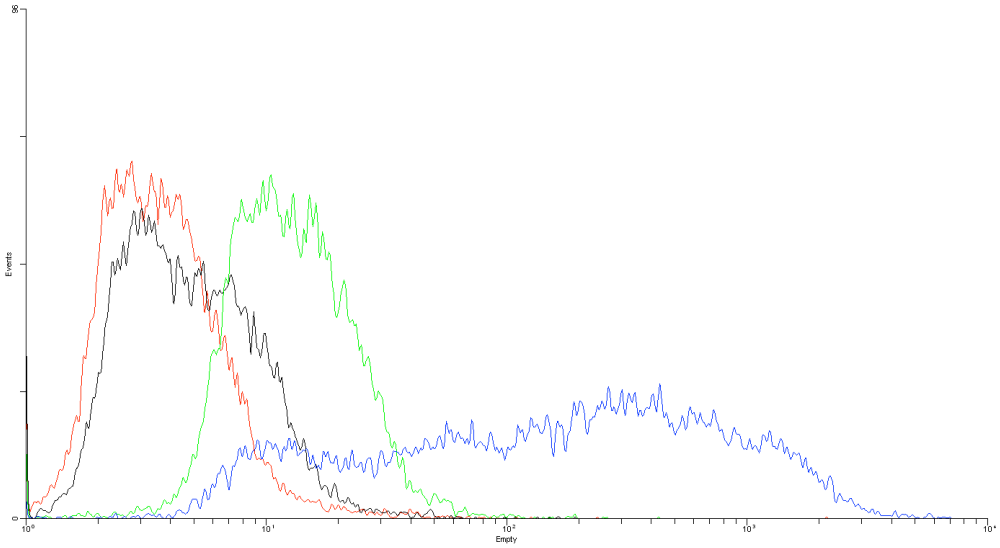

Figure A5.3. Flow cytometry histogram plot of the second transfection efficiency experiment in the U266 cell line.

KEY: Red = Untransfected control
Black = Mock transfected
Green = siRNA only
Blue = siRNA transfected

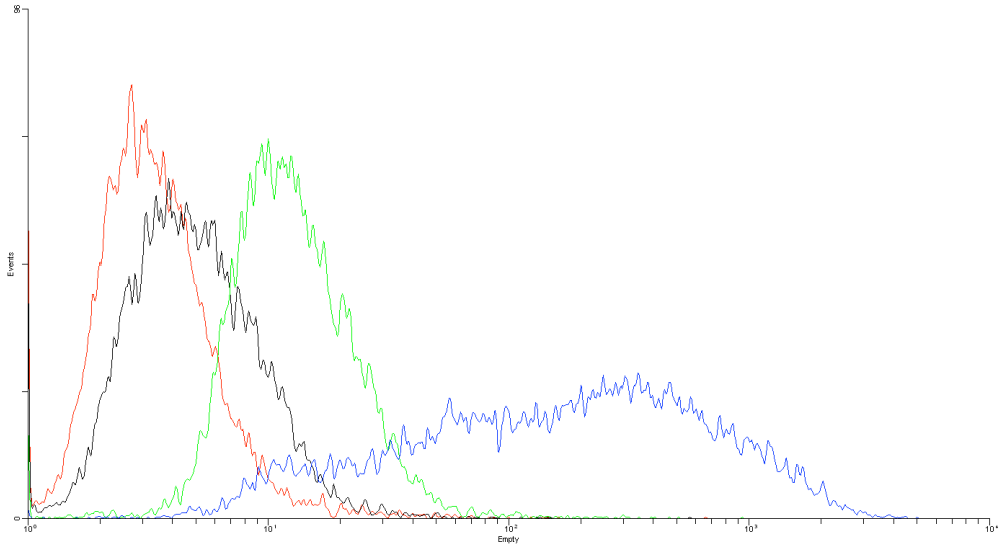

Figure A5.4. Flow cytometry histogram plot of the third transfection efficiency experiment in the U266 cell line.
KEY: Red = Untransfected control
Black = Mock transfected
Green = siRNA only
Blue = siRNA transfected

Cell line	Sample	Cell viability	SD	Cell number (% of control)	SD
THP1	Control	95.2	1.0	100.0	0.0
THP1	Mock transfected	94.0	3.1	95.1	3.8
THP1	siRNA only	95.2	1.2	94.8	5.2
THP1	siRNA transfected	95.7	0.8	88.6	7.6
U266	Control	95.6	0.3	100.0	0.0
U266	Mock transfected	92.3	2.0	99.2	3.9
U266	siRNA only	93.6	1.3	96.4	1.1
U266	siRNA transfected	91.4	3.3	93.2	6.1

Table A5.2. Cell viability and cell number of transfected cells at 24 hours post transfection in each cell line. Values shown are mean and standard deviation of three separate experiments

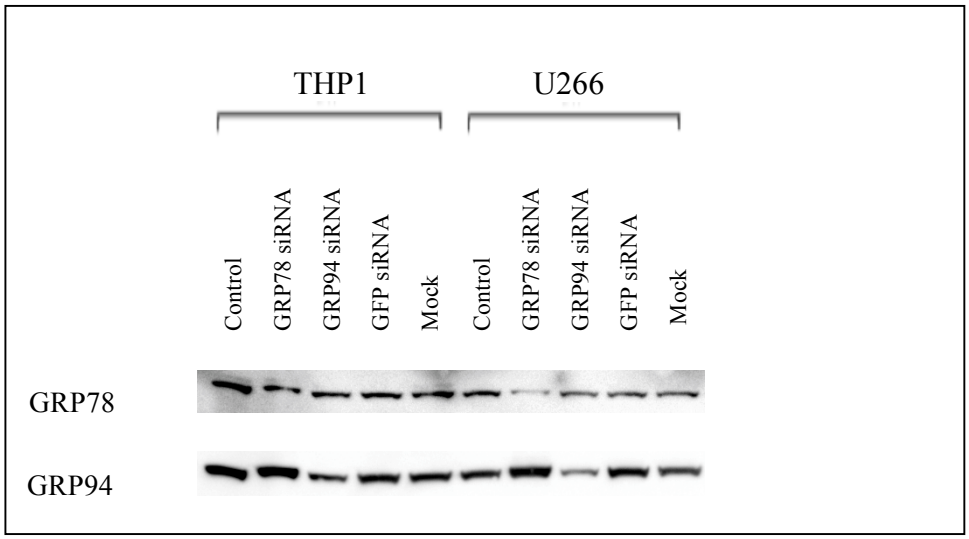

Figure A5.5. Western blot to show GRP78 and GRP94 protein expression in untransfected cells, mock transfected cells, and cells transfected with siRNA targeting GRP78, GRP94 or GFP at 72 hours post transfection.

Cell line	Sample	Cell viability	SD	Cell number (% of control)	SD
THP1	Control	90.9	5.6	100.0	0.0
THP1	Mock transfected	94.1	3.0	90.9	4.9
THP1	siRNA only	94.3	0.8	90.3	9.6
THP1	siRNA transfected	93.9	0.7	90.0	6.8
U266	Control	93.5	4.2	100.0	0.0
U266	Mock transfected	93.5	2.4	77.5	10.6
U266	siRNA only	91.3	2.2	80.9	8.0
U266	siRNA transfected	88.7	0.3	76.5	6.5

Table A5.3. Cell viability and cell number of transfected cells at 48 hours post transfection in each cell line. Values shown are mean and standard deviation of three separate experiments.

THP1	GRP78					GRP94					GFP				
	Set 1	Set 2	Set 3	**Average**	**SEM**	Set 1	Set 2	Set 3	**Average**	**SEM**	Set 1	Set 2	Set 3	**Average**	**SEM**
Control	100.0	100.0	100.0	**100.0**	**0.0**	100.0	100.0	100.0	**100.0**	**0.0**	100.0	100.0	100.0	**100.0**	**0.0**
TM 100nM	52.3	44.2	40.4	**45.6**	**3.5**	52.6	33.3	27.5	**37.8**	**7.6**	60.4	47.2	52.8	**53.5**	**3.8**
TM 1µM	46.8	39.6	32.3	**39.6**	**4.2**	39.3	24.9	26.7	**30.3**	**4.5**	57.5	45.0	46.1	**49.5**	**4.0**
TM 10µM	49.1	41.5	30.2	**40.3**	**5.5**	41.6	26.3	28.4	**32.1**	**4.8**	54.2	42.5	50.8	**49.2**	**3.5**
TG 10nM	39.1	33.0	24.1	**32.1**	**4.4**	39.2	24.8	23.5	**29.1**	**5.0**	44.7	35.0	34.1	**37.9**	**3.4**
TG 100nM	46.9	39.6	28.0	**38.1**	**5.5**	39.7	25.2	25.6	**30.2**	**4.8**	49.0	38.3	43.0	**43.4**	**3.1**
TG 3µM	49.2	41.5	24.2	**38.3**	**7.4**	59.4	37.6	31.4	**42.8**	**8.5**	61.5	48.2	42.6	**50.8**	**5.6**
Dox 10nM	79.0	114.7	54.2	**82.6**	**17.6**	82.4	89.0	51.8	**74.4**	**11.5**	83.2	103.2	88.6	**91.7**	**6.0**
Dox 100nM	47.6	57.5	27.5	**44.2**	**8.8**	44.6	43.0	22.8	**36.8**	**7.0**	52.6	50.6	40.6	**47.9**	**3.7**
Dox 250nM	41.7	49.0	25.7	**38.8**	**6.9**	39.2	37.4	21.9	**32.8**	**5.5**	43.7	45.7	40.1	**43.2**	**1.7**
Bort 1nM	79.0	118.7	60.2	**86.0**	**17.2**	90.8	95.0	51.1	**79.0**	**14.0**	94.2	105.7	85.7	**95.2**	**5.8**
Bort 5nM	82.2	121.6	63.0	**88.9**	**17.2**	93.7	95.9	54.2	**81.3**	**13.5**	99.0	105.1	91.2	**98.4**	**4.0**
Bort 10nM	99.4	115.3	57.2	**90.6**	**17.3**	91.1	90.2	53.2	**78.1**	**12.5**	91.7	97.9	86.9	**92.2**	**3.2**
17-AAG 250nM	72.0	71.4	56.9	**66.8**	**4.9**	62.8	57.9	40.2	**53.7**	**6.9**	77.8	57.3	79.2	**71.5**	**7.1**
17-AAG 1µM	43.1	50.7	30.7	**41.5**	**5.8**	49.2	44.4	28.7	**40.7**	**6.2**	43.7	38.9	44.9	**42.5**	**1.8**
17-AAG 3µM	38.7	50.4	29.1	**39.4**	**6.2**	40.0	40.5	26.4	**35.6**	**4.6**	40.7	40.5	42.7	**41.3**	**0.7**
SAHA 500nM	61.9	95.5	56.5	**71.3**	**12.2**	75.7	83.1	47.2	**68.7**	**10.9**	69.2	78.7	88.3	**78.8**	**5.5**
SAHA 1µM	53.2	69.8	60.3	**61.1**	**4.8**	81.5	63.2	38.3	**61.0**	**12.5**	63.5	68.7	72.4	**68.2**	**2.6**
SAHA 3µM	50.2	43.8	35.7	**43.3**	**4.2**	74.5	40.3	27.8	**47.5**	**13.9**	63.4	47.7	52.9	**54.7**	**4.6**

Table A5.4. Effect of drug treatment for 48 hours on cell number (% of control) in THP1 cells transfected with siRNA targeting GRP78, GRP94 and the control siRNA targeting GFP.

THP1	GRP78					GRP94					GFP				
	Set 1	Set 2	Set 3	**Average**	**SEM**	Set 1	Set 2	Set 3	**Average**	**SEM**	Set 1	Set 2	Set 3	**Average**	**SEM**
Control	100.0	100.0	100.0	**100.0**	**0.0**	100.0	100.0	100.0	**100.0**	**0.0**	100.0	100.0	100.0	**100.0**	**0.0**
TM 100nM	60.7	74.7	61.3	**65.6**	**4.6**	71.4	68.3	61.4	**67.1**	**3.0**	83.9	79.5	71.2	**78.2**	**3.7**
TM 1µM	63.0	69.1	63.9	**65.3**	**1.9**	61.3	62.0	64.0	**62.4**	**0.8**	67.0	71.7	67.7	**68.8**	**1.5**
TM 10µM	57.7	62.5	63.4	**61.2**	**1.8**	57.9	69.6	62.5	**63.4**	**3.4**	55.9	67.2	66.9	**63.3**	**3.7**
TG 10nM	60.5	56.4	55.3	**57.4**	**1.6**	57.3	51.6	50.4	**53.1**	**2.1**	63.1	55.3	59.1	**59.2**	**2.3**
TG 100nM	52.4	59.2	60.4	**57.3**	**2.5**	51.0	47.7	52.0	**50.3**	**1.3**	57.6	45.8	54.1	**52.5**	**3.5**
TG 3µM	67.1	65.3	61.1	**64.5**	**1.8**	58.6	61.8	59.6	**60.0**	**1.0**	71.6	64.3	63.1	**66.3**	**2.6**
Dox 10nM	92.5	98.0	95.6	**95.4**	**1.6**	93.6	97.3	98.0	**96.3**	**1.4**	94.6	98.5	95.7	**96.3**	**1.2**
Dox 100nM	87.1	97.6	62.1	**82.2**	**10.5**	97.7	97.4	91.8	**95.6**	**1.9**	99.7	94.9	87.5	**94.0**	**3.5**
Dox 250nM	0.0	0.0	0.0	**0.0**	**0.0**	0.0	0.0	0.0	**0.0**	**0.0**	0.0	0.0	8.9	**3.0**	**3.0**
Bort 1nM	95.0	99.5	98.7	**97.7**	**1.4**	99.3	100.5	97.6	**99.2**	**0.8**	97.3	102.6	100.5	**100.1**	**1.5**
Bort 5nM	92.8	100.9	99.3	**97.7**	**2.5**	95.5	101.2	97.2	**97.9**	**1.7**	99.1	104.2	97.6	**100.3**	**2.0**
Bort 10nM	97.3	100.1	95.9	**97.8**	**1.2**	96.1	100.1	93.9	**96.7**	**1.8**	99.8	99.5	97.0	**98.7**	**0.9**
17-AAG 250nM	97.4	99.0	101.8	**99.4**	**1.3**	93.0	98.2	95.0	**95.4**	**1.5**	96.4	92.8	95.8	**95.0**	**1.1**
17-AAG 1µM	86.3	96.8	93.3	**92.1**	**3.1**	78.6	78.7	81.4	**79.6**	**0.9**	80.9	84.5	87.2	**84.2**	**1.8**
17-AAG 3µM	81.0	84.4	83.3	**82.9**	**1.0**	79.7	83.1	75.6	**79.5**	**2.1**	81.1	84.7	84.8	**83.5**	**1.2**
SAHA 500nM	87.5	96.8	93.2	**92.5**	**2.7**	89.2	97.0	91.9	**92.7**	**2.3**	90.3	94.7	96.4	**93.8**	**1.8**
SAHA 1µM	74.7	81.1	92.1	**82.6**	**5.1**	80.6	86.3	84.8	**83.9**	**1.7**	85.5	87.9	83.9	**85.8**	**1.2**
SAHA 3µM	49.8	41.6	48.2	**46.5**	**2.5**	47.7	45.3	47.3	**46.8**	**0.7**	55.5	45.5	64.5	**55.2**	**5.5**

Table A5.5. Effect of drug treatment for 48 hours on cell viability (% of control) in THP1 cells transfected with siRNA targeting GRP78, GRP94 and the control siRNA targeting GFP.

U266	GRP78					GRP94					GFP				
	Set 1	Set 2	Set 3	**Average**	**SEM**	Set 1	Set 2	Set 3	**Average**	**SEM**	Set 1	Set 2	Set 3	**Average**	**SEM**
Control	100.0	100.0	100.0	**100.0**	**0.0**	100.0	100.0	100.0	**100.0**	**0.0**	100.0	100.0	100.0	**100.0**	**0.0**
TM 100nM	91.2	85.3	59.4	**78.7**	**9.8**	104.1	67.2	62.7	**78.0**	**13.1**	120.8	86.7	63.6	**90.3**	**16.6**
TM 1µM	87.1	72.3	52.8	**70.7**	**9.9**	85.0	59.2	63.8	**69.3**	**8.0**	98.6	79.9	51.4	**76.6**	**13.7**
TM 100µM	103.8	88.3	48.2	**80.1**	**16.6**	85.9	50.5	48.4	**61.6**	**12.1**	97.4	72.7	50.1	**73.4**	**13.7**
TG 10nM	74.5	89.1	63.2	**75.6**	**7.5**	79.4	57.4	61.0	**65.9**	**6.8**	84.8	67.7	57.8	**70.1**	**7.9**
TG 100nM	65.4	73.3	51.4	**63.4**	**6.4**	70.8	51.2	50.5	**57.5**	**6.6**	74.0	65.3	52.5	**63.9**	**6.2**
TG 3µM	74.3	78.4	53.6	**68.8**	**7.7**	85.5	55.5	48.6	**63.2**	**11.3**	94.5	63.9	58.8	**72.4**	**11.1**
Dox 10nM	182.5	126.8	73.7	**127.7**	**31.4**	166.8	90.1	90.2	**115.7**	**25.5**	186.5	107.1	74.3	**122.6**	**33.3**
Dox 100nM	64.6	65.9	47.5	**59.4**	**5.9**	76.8	47.9	47.5	**57.4**	**9.7**	71.8	54.2	45.3	**57.1**	**7.8**
Dox 500nM	66.5	68.7	54.9	**63.4**	**4.3**	80.6	49.4	50.3	**60.1**	**10.2**	79.2	60.7	54.4	**64.8**	**7.5**
Bort 1nM	123.1	131.1	88.8	**114.3**	**13.0**	161.0	101.3	93.8	**118.7**	**21.3**	122.1	118.8	97.9	**112.9**	**7.6**
Bort 5nM	129.5	124.1	86.1	**113.2**	**13.6**	158.3	107.5	98.7	**121.5**	**18.6**	136.5	120.0	101.5	**119.3**	**10.1**
Bort 10nM	162.6	123.3	81.8	**122.6**	**23.3**	173.0	99.4	92.1	**121.5**	**25.8**	249.8	123.8	90.8	**154.8**	**48.4**
17-AAG 250nM	151.8	74.9	72.5	**99.7**	**26.1**	94.5	64.7	52.8	**70.7**	**12.4**	108.9	64.1	87.5	**86.8**	**12.9**
17-AAG 1µM	71.6	55.9	42.9	**56.8**	**8.3**	75.1	43.8	44.1	**54.3**	**10.4**	62.4	51.9	59.1	**57.8**	**3.1**
17-AAG 3µM	71.1	57.3	44.8	**57.7**	**7.6**	76.7	45.4	44.9	**55.6**	**10.5**	58.1	49.5	59.9	**55.8**	**3.2**
SAHA 500nM	117.0	94.0	70.5	**93.8**	**13.4**	127.8	74.9	70.0	**90.9**	**18.5**	90.8	94.2	101.3	**95.4**	**3.1**
SAHA 1µM	115.7	77.5	66.4	**86.6**	**14.9**	101.9	60.4	66.1	**76.1**	**13.0**	100.2	77.2	95.1	**90.8**	**7.0**
SAHA 3µM	153.6	67.1	68.2	**96.3**	**28.7**	105.3	51.9	65.6	**74.3**	**16.0**	158.7	71.0	87.9	**105.8**	**26.9**

Table A5.6. Effect of drug treatment for 48 hours on cell number (% of control) in U266 cells transfected with siRNA targeting GRP78, GRP94 and the control siRNA targeting GFP.

U266	GRP78					GRP94					GFP				
	Set 1	Set 2	Set 3	**Average**	**SEM**	Set 1	Set 2	Set 3	**Average**	**SEM**	Set 1	Set 2	Set 3	**Average**	**SEM**
Control	100.0	100.0	100.0	**100.0**	**0.0**	100.0	100.0	100.0	**100.0**	**0.0**	100.0	100.0	100.0	**100.0**	**0.0**
TM 100nM	59.6	80.7	53.9	**64.7**	**8.2**	66.4	71.1	58.7	**65.4**	**3.6**	70.2	87.9	70.3	**76.1**	**5.9**
TM 1µM	46.5	67.0	60.0	**57.8**	**6.0**	66.3	57.4	58.8	**60.8**	**2.7**	78.5	83.3	60.7	**74.2**	**6.9**
TM 100µM	31.6	40.7	16.4	**29.6**	**7.1**	45.6	21.8	15.1	**27.5**	**9.2**	52.2	16.8	12.0	**27.0**	**12.7**
TG 10nM	65.3	79.0	74.9	**73.1**	**4.1**	80.0	73.1	66.3	**73.1**	**4.0**	85.3	72.9	49.9	**69.3**	**10.4**
TG 100nM	74.6	65.9	71.2	**70.6**	**2.6**	64.3	60.5	52.7	**59.2**	**3.4**	68.4	64.6	69.0	**67.3**	**1.4**
TG 3µM	81.5	74.0	79.8	**78.4**	**2.3**	83.4	62.2	53.2	**66.3**	**8.9**	71.4	69.3	52.4	**64.4**	**6.0**
Dox 10nM	98.7	99.5	100.9	**99.7**	**0.7**	101.4	100.7	99.3	**100.5**	**0.6**	105.3	99.4	93.4	**99.4**	**3.4**
Dox 100nM	94.6	99.7	81.4	**91.9**	**5.4**	101.4	97.2	82.0	**93.5**	**5.9**	96.3	97.6	83.7	**92.5**	**4.4**
Dox 500nM	0.0	0.0	0.0	**0.0**	**0.0**	20.7	0.0	0.0	**6.9**	**6.9**	40.2	0.0	0.0	**13.4**	**13.4**
Bort 1nM	88.2	101.7	96.5	**95.5**	**3.9**	100.7	103.2	101.6	**101.8**	**0.7**	98.7	102.5	97.3	**99.5**	**1.6**
Bort 5nM	93.9	103.5	100.3	**99.2**	**2.8**	100.9	101.8	100.8	**101.2**	**0.3**	94.9	102.1	97.9	**98.3**	**2.1**
Bort 10nM	93.5	103.5	96.0	**97.7**	**3.0**	100.1	100.3	93.7	**98.0**	**2.2**	99.1	102.8	92.7	**98.2**	**2.9**
17-AAG 250nM	96.0	95.5	100.3	**97.2**	**1.5**	101.4	94.3	92.8	**96.2**	**2.7**	98.0	84.0	90.1	**90.7**	**4.1**
17-AAG 1µM	89.4	78.3	89.9	**85.9**	**3.8**	85.1	74.5	68.9	**76.2**	**4.7**	96.4	82.1	83.6	**87.3**	**4.6**
17-AAG 3µM	75.5	78.9	77.0	**77.1**	**1.0**	73.1	60.9	63.6	**65.9**	**3.7**	82.9	83.7	86.8	**84.5**	**1.2**
SAHA 500nM	89.8	97.3	95.6	**94.2**	**2.3**	94.6	95.9	88.2	**92.9**	**2.4**	94.8	93.4	95.6	**94.6**	**0.6**
SAHA 1µM	86.6	92.0	84.5	**87.7**	**2.2**	86.0	83.6	77.1	**82.2**	**2.7**	93.0	71.9	79.5	**81.5**	**6.2**
SAHA 3µM	57.5	53.8	60.0	**57.1**	**1.8**	65.3	42.8	44.1	**50.8**	**7.3**	72.4	32.3	51.3	**52.0**	**11.6**

Table A5.7. Effect of drug treatment for 48 hours on cell viability (% of control) in U266 cells transfected with siRNA targeting GRP78, GRP94 and the control siRNA targeting GFP.

	THP1		U266	
	GRP78	**GRP94**	**GRP78**	**GRP94**
	p value	**p value**	**p value**	**p value**
TM 100nM	0.10067	0.09281	0.32186	0.16662
TM 1μM	0.05540	0.00087	0.26258	0.54469
TM 10μM	0.27611	0.02683	0.31551	0.18466
TG 10nM	0.12733	0.03236	0.60970	0.39946
TG 100nM	0.39786	0.03018	0.91694	0.23855
TG 3μM	0.06707	0.11147	0.75224	0.00301
Dox 10nM	0.57142	0.24219	0.56450	0.60464
Dox 100nM	0.58472	0.07898	0.71902	0.93983
Dox 250nM	0.48943	0.12597	0.83846	0.32963
Bort 1nM	0.50668	0.22615	0.84099	0.76674
Bort 5nM	0.55186	0.22783	0.39438	0.84965
Bort 10nM	0.92494	0.29859	0.36309	0.28425
17-AAG 250nM	0.70154	0.26197	0.52215	0.25438
17-AAG 1μM	0.90502	0.82781	0.90803	0.71644
17-AAG 3μM	0.80705	0.39843	0.84891	0.98535
SAHA 500nM	0.64922	0.58273	0.93118	0.84963
SAHA 1μM	0.22771	0.67857	0.77313	0.24106
SAHA 3μM	0.10156	0.56590	0.20036	0.10196

Table A5.8. P value from paired t-test comparing cell number following drug treatment in cells transfected with target siRNA (GRP78 or GRP94) and control siRNA (GFP) ($p<0.05$ considered statistically significant).

	THP1		U266	
	GRP78	**GRP94**	**GRP78**	**GRP94**
	p value	**p value**	**p value**	**p value**
TM 100nM	0.14661	0.00486	0.05220	0.10346
TM 1μM	0.01399	0.06914	0.21365	0.19411
TM 10μM	0.40246	0.98980	0.86113	0.90557
TG 10nM	0.35035	0.05318	0.80087	0.61901
TG 100nM	0.46346	0.46198	0.16334	0.18304
TG 3μM	0.35821	0.20033	0.17672	0.76650
Dox 10nM	0.27077	0.98755	0.93670	0.73529
Dox 100nM	0.28492	0.47762	0.69190	0.68184
Dox 250nM	0.42265	0.42265	0.42265	0.42265
Bort 1nM	0.02534	0.58775	0.34070	0.15265
Bort 5nM	0.37066	0.13337	0.45923	0.25360
Bort 10nM	0.40682	0.27255	0.85698	0.89523
17-AAG 250nM	0.12182	0.89247	0.26929	0.15395
17-AAG 1μM	0.06768	0.05694	0.74528	0.03237
17-AAG 3μM	0.30095	0.25292	0.03530	0.05128
SAHA 500nM	0.52625	0.64221	0.90306	0.62368
SAHA 1μM	0.64326	0.38706	0.50504	0.91161
SAHA 3μM	0.15485	0.22891	0.67944	0.84997

Table A5.9. P value from paired t-test comparing cell viability following drug treatment in cells transfected with target siRNA (GRP78 or GRP94) and control siRNA (GFP) ($p<0.05$ considered statistically significant).